UNIVERSITAT DE BARCELONA

Optimization of induced denitrification strategies in polluted water bodies from agricultural sources

Rosanna Margalef Marti

OPTIMIZATION OF INDUCED DENITRIFICATION STRATEGIES IN POLLUTED WATER BODIES FROM AGRICULTURAL SOURCES Rosanna Margalef Marti | 2020

PhD THESIS

Rosanna
Margalef Marti

2020

OPTIMIZATION OF INDUCED DENITRIFICATION STRATEGIES IN POLLUTED WATER BODIES FROM AGRICULTURAL SOURCES

Supervisors:
Dra. Neus Otero Pérez
Dr. Raúl Carrey Labarta

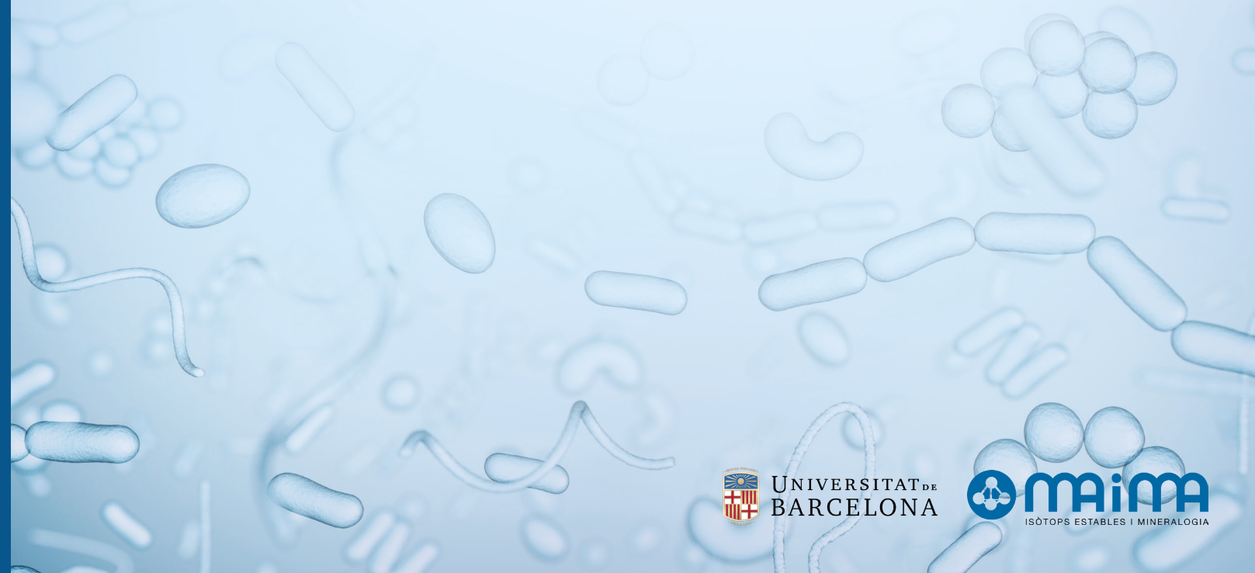

UNIVERSITAT DE BARCELONA

MAiMA ISÒTOPS ESTABLES I MINERALOGIA

Universitat de Barcelona

Facultat de Ciències de la Terra

Departament de Mineralogia, Petrologia i Dipòsits Minerals

OPTIMIZATION OF INDUCED DENITRIFICATION STRATEGIES IN POLLUTED WATER BODIES FROM AGRICULTURAL SOURCES

by

Rosanna Margalef Marti

Thesis submitted in partial fulfillment of the requirements to obtain the degree of:

Doctor of Philosophy in Earth Sciences

This work was conducted in the MAiMA research group, SGR Mineralogia Aplicada, Geoquímica i Geomicrobiologia (MAG), under the supervision of:

Dra. Neus Otero Pérez

Departament de Mineralogia, Petrologia i Geologia Aplicada, Universitat de Barcelona

Dr. Raúl Carrey Labarta

Departament de Mineralogia, Petrologia i Geologia Aplicada, Universitat de Barcelona

Barcelona, January 2020

MAiMA ISÒTOPS ESTABLES I MINERALOGIA

UNIVERSITAT DE BARCELONA

This work has been financed by the following projects: REMEDIATION (CGL2014-57215-C4), AGRO-SOS (CGL2015-66016-R) and PACE-ISOTEC (CGL2017-87216-C4-1-R), financed by the Spanish Government and AEI/FEDER from the UE; MAG (2017-SGR-1733) financed by the Catalan Government and LIFE Project InSiTrate (LIFE12 ENV/ES/000651). Rosanna Margalef Marti is grateful to the Spanish Government for the Ph.D. grant BES-2015-072882.

AGRAÏMENTS

Començar i acabar aquesta tesi no hauria estat possible sense el recolzament, ajuda i col·laboració de moltes persones. Arribat el moment de finalitzar aquest període de desenvolupament tant professional com personal, vull agrair les seves contribucions ja sigui directa o indirectament en el transcurs d'aquest treball.

En primer lloc, gràcies als meus directors i tutor, la Dra. Neus Otero, el Dr. Raúl Carrey i el Dr. Albert Soler, per donar-me l'oportunitat de realitzar aquesta tesi al grup MAiMA/MAG i per l'acompanyament, ajuda i formació rebuts al llarg d'aquets 4 anys. Gràcies també a tot l'equip de maimons amb qui he pogut compartir dinars, cafès, còctels, cerveses i xerrades, a banda de moltes hores de feina al 131, al 120 i als laboratoris: Marta, Clara, Dídac, Mònica, Sara, Cristina, Roger, Jordi, Manuela, Carme, Àngels, Marc, Pedro, Mercè, Alba, Diana, Edson, Martí, Àlex i Sergio.

Gràcies a tots els co-autors i persones involucrades en les publicacions derivades d'aquesta tesi (veure annex). Ja sigui a nivell experimental o de discussió de resultats, sense la vostra col·laboració aquests 6 articles no haurien estat possibles. Vull fer menció especial al Jesús, el Robert, el Francesco i l'Elina, amb qui he pogut compartir directament hores de feina ja sigui al camp o al laboratori. Agraeixo també l'ajuda rebuda pels tècnics dels Centres Científics i Tecnològics de la Universitat de Barcelona: Rosa Maria Marimón, Pilar Teixidó, Alejandra, Sandra, Eva, Anna, Pilar Rubio, Lourdes. Ells han fet possibles la majoria dels anàlisis gràcies al temps dedicat a resoldre els problemes analítics que han sorgit durant la tesi. D'altra banda, gràcies a la Sandra i l'Elisenda per la seva ajuda amb les tasques administratives.

I would like to acknowledge Dr. Mathieu Sebilo and Veronique Vaury for their help and dedication and for the knowledge provided during my stay at Institut d'Ecologie et des Sciences de l'Environnement de Paris, at the half way point of this thesis. From my last days being a PhD student, I'm thankful to Dr. Thomas Aiglsperger, Dr. Bernhard Dold and Dr. Johan Ingri for their help, hospitality and fruitful discussions at Lulea University of Technology; and to Dr. Emma Engstström, Dr. Ilia Rodushkin, Dr. Cora Paulukat, Simon and Isabella for all the help and knowledge provided at ALS Scandinavia. I'm also grateful to all the people that I met both inside and outside these institutions, for the shared experiences.

Finalment, gràcies al meu entorn més pròxim. Estar envoltada de persones que m'han fet costat des de molt abans de començar aquesta tesi, és una de les principals raons que m'han permès arribar fins aquí. Afortunadament la llista és llarga. Pel que fa als amics, ho podria resumir en micros, biotecs, companys de pis, els del Perelló i afins. Vull destacar a l'Alba Boyer no només per estar inclosa en aquesta llista sinó també pel disseny de la portada d'aquesta tesi. Finalment, gràcies a tota la família. Sobretot, a la Maria i als meus pares, Josep i Carme. Ells s'han esforçat sempre per proporcionar-me una bona educació i valors.

ABSTRACT

The worldwide persistence of nitrate (NO_3^-) in groundwater is worrying since this compound has been related to human illnesses and to eutrophication of aquatic ecosystems. The main sources of pollution are linked to intensive use of fertilizers and septic system leakage. Since 1991, European directives have been applied to mitigate NO_3^- pollution by limiting N application in agricultural lands. However, due to the long residence time of N in the soil organic matter pool, the outcome of the implemented management practices can be delayed for decades. Consequently, remediation strategies must be developed and optimized. The NO_3^- reduction to innocuous dinitrogen gas (N_2), can occur intrinsically in many environments due to the ubiquity of denitrifying microorganisms. However, the electron donor presence is usually a limiting factor in the contaminated aquifers. Hence, one feasible treatment involves inducing the denitrification by application of an external electron donor.

During the implementation of bioremediation strategies, the contaminant removal can be estimated by monitoring its concentrations before and after the treatment. However, this method does not reveal the specific processes involved in the attenuation, making it challenging to focus on the improvement of the remediation approach. Isotopic analyses have proved to be a powerful tool in identifying the sources and transformation processes of groundwater contaminants. During the enzymatic NO_3^- reduction, the unreacted residual substrate becomes enriched in the heavy isotopes ^{15}N and ^{18}O, allowing to distinguish the biotic reduction from processes such as dilution with non-polluted water that could also lead to a concentration decrease without influencing the isotopic signature.

The present thesis focusses on investigating the use of low-cost electron donors to promote the denitrification, and on using isotopic tools to evaluate the denitrification efficiency at field-scale. The tested materials in batch and flow-through experiments were: whey, corn stubble, wheat hay, animal compost, magnetite, siderite and olivine. Different parameters that could affect the biotic NO_3^- reduction efficiency were evaluated (e.g., temperature, ratio between electron donor and acceptor, harmful by-product accumulation, abiotic reactivity or coexistence of other contaminants) and the isotopic fractionation values ($\varepsilon^{15}N$ and $\varepsilon^{18}O$) were determined for all tested conditions. At field-scale, three different polluted water bodies were studied, in which the determined $\varepsilon^{15}N$ and $\varepsilon^{18}O$ at the laboratory were applied to quantify the natural and/or induced denitrification. In a polluted aquifer in Spain, the NO_3^- attenuation was evaluated during a long-term induced denitrification strategy by acetic acid injections. In a polluted aquifer in Argentina, the natural NO_3^- attenuation was evaluated

considering changes in the reactivity and isotopic fractionation due to the simultaneous presence of NO_3^- and Cr^{6+}. Finally, in a constructed wetland (CW) treating agricultural runoff water, the NO_3^- attenuation was evaluated before and after application of an electron donor both in the autumn-winter and spring-summer seasons.

The laboratory experiments demonstrated that magnetite nanoparticles, corn stubble, wheat hay, animal compost and whey could efficiently promote the denitrification in polluted water bodies. In these biotic experiments, the complete NO_3^- reduction to N_2 was demonstrated by transient or negligible accumulation of other nitrogen compounds such as nitrite (NO_2^-), ammonium (NH_4^+) or nitrous oxide (N_2O). However, the N_2O was found to be the end-product of the abiotic NO_2^- reduction, which can be mediated by ferrous iron, if present. The $\varepsilon^{15}N_{NO3/N2}$ and $\varepsilon^{18}O_{NO3/N2}$ values were calculated for all the batch experiments and for the periods of the flow-through experiment that allowed complete denitrification. For the non-complete denitrification periods, the NO_3^- isotopic characterization showed a mix of denitrified and non-denitrified water at the outflow. The isotopic characterization of NO_2^- and N_2O allowed to distinguish the biotic from the abiotic NO_2^- reduction by ferrous iron at the laboratory-scale. A two-stage isotopic fractionation pattern was found for Cr^{6+}, which can be reduced simultaneously to NO_3^-. Also, the carbon compounds isotopic analysis allowed to assess the fate of the studied organic carbon materials to be used as electron donors.

In the field-scale studies, the chemical and isotopic characterization allowed to trace the extent of the natural or induced denitrification and to evaluate the safety of the treatments. In a pilot plant to remediate groundwater NO_3^- pollution (Spain), acetic acid was injected by pulses to an alluvial aquifer for 22 months. According to the isotopic results, the induced denitrification achieved at least 50 % NO_3^- attenuation. The isotopic analyses also allowed to identify the reoxidation of NO_2^- to NO_3^- during the treatment and to recognize a mixture between the denitrified and partially or non-denitrified groundwater in one of the sampling points. In a polluted aquifer with both NO_3^- and Cr^{6+} (Argentina), the calculated natural attenuation was 20 % for NO_3^- and 60 % for Cr^{6+}. For this calculation, the two stage trend observed for the $\varepsilon^{53}Cr$ was considered. The attenuation of Cr^{6+} in a few samples was found to be due by both reduction and dilution. In a CW treating agricultural runoff water, a slight natural NO_3^- attenuation was only observed when the flow was below 5.5 L/s. According to the isotopic results, after the biostimulation by stubble application, at least 60 % NO_3^- was removed at 16 L/s. The biostimulation treatment in autumn lasted in one month, while in spring the attenuation remained for three months.

RESUM

La persistència del nitrat (NO_3^-) en aigües subterrànies és preocupant ja que aquest, pot provocar malalties en humans i eutrofització d'ecosistemes aquàtics. Els principals orígens de contaminació són l'ús intensiu de fertilitzants i les pèrdues dels sistemes sèptics. Tot i que els darrers anys s'ha limitat la quantitat de N aplicat en zones agrícoles, degut al llarg temps de residència del N en la matèria orgànica del sòl, el resultat de les pràctiques implementades, es pot ajornar fins dècades. Per tant, és necessari desenvolupar i optimitzar estratègies de remediació. La reducció del NO_3^- a dinitrogen gas (N_2), que és un gas innocu, es dona intrínsecament en molts ambients degut a la ubiqüitat dels microorganismes amb capacitat de desnitrificar. Malauradament, la presència de donadors d'electrons sol ser un factor limitant en aqüífers contaminats per NO_3^-. Per això, un possible tractament consisteix en induir la desnitrificació gràcies a l'aplicació d'un donador d'electrons extern.

Durant la implementació d'estratègies de bioremediació, l'eliminació del contaminant es pot determinar mitjançant la monitorització de les seves concentracions abans i després del tractament. Però aquest mètode no mostra el procés específic involucrat en l'atenuació i això dificulta l'optimització de l'estratègia de remediació. Els anàlisis isotòpics resulten útils per identificar fonts i processos de transformació de diversos contaminants en aigües subterrànies. Durant la reducció enzimàtica del NO_3^-, el substrat residual es va enriquint en els isòtops pesats ^{15}N i ^{18}O. Això permet distingir la reducció biòtica d'altres processos com la dilució amb aigua no contaminada que també podria donar lloc a una disminució de la concentració del NO_3^- però sense influenciar la seva signatura isotòpica.

Aquesta tesi es centra en investigar l'ús de donadors d'electrons de baix cost (sèrum làctic, restes vegetals (blat i panís), compost animal, magnetita, siderita i olivina) per induir la desnitrificació i l'ús d'eines isotòpiques per avaluar l'eficiència de desnitrificació a escala de camp. Durant els experiments al laboratori s'han avaluat diferents paràmetres que poden afectar l'eficiència de la reducció biòtica del NO_3^- (ex. temperatura, ràtio entre el donador i acceptor d'electrons, acumulació de productes intermedis tòxics, reactivitat abiòtica o coexistència d'altres contaminants) i s'han calculat els valors de fraccionament isotòpic ($\varepsilon^{15}N$ i $\varepsilon^{18}O$) per totes les condicions investigades. A escala de camp, s'han estudiat tres masses d'aigua contaminades en les que s'han aplicat els valors de $\varepsilon^{15}N$ i $\varepsilon^{18}O$ determinats al laboratori per quantificar la desnitrificació natural o induïda. En un aqüífer contaminat a Espanya, l'atenuació del NO_3^- s'ha avaluat durant una estratègia de desnitrificació induïda mitjançant la injecció d'àcid acètic. En un aqüífer contaminat a Argentina, l'atenuació natural

del NO_3^- s'ha avaluat considerant canvis en la reactivitat i el fraccionament isotòpic degut a la presencia simultània de NO_3^- i Cr^{6+}. En un aiguamoll construït en el qual es tracta aigua d'escorrentia agrícola, l'atenuació del NO_3^- s'ha avaluat abans i després de l'aplicació d'un donador d'electrons tant a la tardor-hivern com a la primavera-estiu.

Els experiments de laboratori han demostrat que les nanopartícules de magnetita, les restes vegetals (blat i panís), el compost animal i el sèrum làctic poden induir la desnitrificació en aigües contaminades. En aquests experiments biòtics, la reducció completa del NO_3^- a N_2 ha estat demostrada per una acumulació transient o negligible d'altres compostos nitrogenats com el nitrit (NO_2^-), l'amoni (NH_4^+) o l'òxid nitrós (N_2O). Tot i això, s'ha vist que el N_2O és el producte final de la reducció abiòtica del NO_2^- provocada per l'oxidació de Fe^{2+}, si és present en l'aigua. Els valors de $\varepsilon^{15}N_{NO3/N2}$ i $\varepsilon^{18}O_{NO3/N2}$ s'han calculat pels experiments de tipus batch i pels períodes d'un experiment de tipus flux continu durant els que es va assolir una desnitrificació completa. La caracterització isotòpica del NO_2^- i el N_2O ha permès distingir la reducció del NO_2^- biòtica de l'abiòtica per oxidació de Fe^{2+} al laboratori. Per al Cr^{6+}, un contaminant que es pot reduir simultàniament al NO_3^-, s'ha observat un fraccionament isotòpic en dos estadis. A més, l'anàlisi isotòpic dels compostos de carboni ha permès avaluar el consum dels donadors d'electrons de carboni orgànic estudiats.

En els estudis a escala de camp, la caracterització química i isotòpica ha permès traçar l'eficiència de la desnitrificació natural i/o induïda i avaluar la seguretat dels tractaments. En una planta pilot per remeiar la contaminació de NO_3^- d'aigües subterrànies (Espanya), s'ha injectat àcid acètic a l'aqüífer durant 22 mesos. D'acord amb els resultats isotòpics, la desnitrificació induïda ha assolit almenys un 50% d'atenuació del NO_3^-. La caracterització isotòpica també ha permès identificar la reoxidació de NO_2^- a NO_3^- durant el tractament i reconèixer una barreja entre aigua desnitrificada i aigua parcialment o no desnitrifricada en un dels punts de mostreig. En un altre aqüífer contaminat amb NO_3^- i Cr^{6+} (Argentina), l'atenuació natural calculada ha estat del 20% per al NO_3^- i del 60 % per al Cr^{6+}. Per a aquest càlcul s'ha tingut en compte el fraccionament isotòpic en dos estadis observat pel Cr^{6+} en els experiments de laboratori. L'atenuació del Cr^{6+} en algunes mostres ha estat deguda en part a dilució i en part a reducció. En l'aiguamoll construït, l'atenuació natural del NO_3^- només es dona quan el flux és inferior a 5.5 L/s. D'acord amb els resultats isotòpics, després de la bioestimulació per aplicació de restes vegetals (panís), s'ha aconseguit una reducció del 60 % del NO_3^-, a un flux de 16 L/s. El tractament de bioestimulació a l'octubre-hivern ha durat un mes, mentre que a la primavera-estiu s'ha mantingut durant tres mesos.

TABLE OF CONTENTS

LIST OF FIGURES

LIST OF TABLES

LIST OF ABBREVIATIONS

Acetic acid (CH_3COOH)

Agricultural runoff water (ARW)

Ammonium (NH_4^+)

Anaerobic NH_4^+ oxidation (anammox)

Aqueous (aq)

Assimilatory NO_3^- reductase (NAS)

Atmospheric N_2 (AIR)

Bacterial SO_4^{2-} reduction (BSR)

Centres Científics i Tecnològics of the Universitat de Barcelona (CCiT-UB)

Constructed Wetlands (CWs)

Deionized water (DIW)

Dinitrogen gas (N_2)

Dissimilatory nitrate reduction to ammonium (DNRA)

Ethanol (C_2H_6O)

Ethylene glycol ($C_2H_6O_2$)

Ferric iron (Fe^{3+})

Ferrous oxide (Fe^{2+})

Greenhouse Gas (GHG)

Groundwater (GW)

Hydrazine (N_2H_4)

Hydrogen (H_2)

Hydrogen sulfide (H_2S)

Hydroxylamine (NH_2OH)

Magnetite (Mag)

Manganese (Mn^{2+})

Manganese dioxide (MnO_2)

Matanza-Riachuelo basin (MRB)

Membrane-bound NO_3^- reductase (NAR)

Nanoparticles (NP)

Nitrate (NO_3^-)

Nitrate vulnerable zones (NVZ)

Nitric oxide (NO)

Nitric oxide reductases (NOR)

Nitrite (NO_2^-)

Nitrite reductases (NIR)

Nitrous oxide (N_2O)

Nitrous oxide reductases (NOS)

Periplasmic NO_3^- reductase (NAP)

Permeable reactive barrier (PRB)

Phenol (C_6H_5OH)

Seawater (SW)

Sulfate (SO_4^{2-})

Sulfide (S^{2-})

Sulfur (S^0)

Synthetic groundwater (SGW)

Synthetic sea water (SSW)

Urea ($CO(NH_2)_2$)

Vienna Canyon Diablo Troillite (V-CDT)

Vienna Peedee Belemnite (V-PDB)

Vienna Standard Mean Oceanic Water (V-SMOW)

Zero valent iron (ZVI)

1. INTRODUCTION

1.1. Anthropogenic impact on nitrogen cycling

The nitrogen biogeochemical cycle involves diverse complex and interconnected reactions such as:

I) The N fixation, which is the reduction of dinitrogen gas (N_2) to ammonium (NH_4^+) by free-living or symbiotic bacteria and archaea that contain the nitrogenase enzyme (Gaby and Buckley, 2011; Hoppe et al., 2014; Sapountzis et al., 2016; Zahran, 1999). The N fixation is essential for life since the N_2 bioavailability is only limited to a few microorganisms. Nevertheless, although the biological N fixation is the main N_2 sink, lightning can also mediate the oxidation of N_2 to N oxides (Fowler et al., 2013; Hill et al., 1980).

II) The nitrification, during which NH_4^+ is oxidized to hydroxylamine (NH_2OH), nitrite (NO_2^-) and finally, nitrate (NO_3^-) by bacteria and archaea (Beeckman et al., 2018; Heil et al., 2016; Sharma and Ahlert, 1977).

III) The denitrification, during which NO_3^- is reduced to NO_2^-, nitric oxide (NO), nitrous oxide (N_2O) and finally, N_2 (Knowles, 1982) by bacteria, archaea, fungi or foraminifera (Cabello et al., 2004; Glock et al., 2019; Moreno-vivián et al., 1999; Shoun et al., 1992).

IV) The dissimilatory NO_3^- reduction to NH_4^+ (DNRA), during which NO_3^- is reduced to NO_2^- and finally, NH_4^+ by bacteria, fungi and diatoms (Kamp et al., 2015; Rütting et al., 2011).

V) The bacterial anaerobic NH_4^+ oxidation to N_2 (anammox) while using NO_3^- and NO_2^- as electron acceptors (Kuenen et al., 1995; Kuypers et al., 2003).

VI) The N assimilation (or N immobilization). Inorganic N compounds such as NH_4^+, NO_2^- or NO_3^- can be converted to organic matter N by bacteria (Lin and Stewart, 1997), archaea (Cabello et al., 2004), fungi (Emmerton et al., 2001; Myrold and Posavatz, 2007), algae (Sanz-Luque et al., 2015; Waser et al., 1998), and plants (Emmerton et al., 2001; Masclaux-Daubresse et al., 2010).

VII) The N mineralization. When organic N is degraded by bacteria and fungi, NH_4^+ is released (Högberg et al., 2007).

Apart from all these well-known processes (**Figure 1.1**), biotic reactions involving the hydrazine (N_2H_4) synthesis from NH_4^+ and NO, which is then oxidized to N_2, have been

identified (Kuypers et al., 2018 and references therein). Furthermore, abiotic reactions involving N compounds have recently gained attraction. For example, NO_2^- can be easily reduced to N_2O by oxidation of ferrous iron (Fe^{2+}), or NH_2OH can be oxidized to N_2O by reduction of manganese dioxide (MnO_2) (Heil et al., 2016; Melton et al., 2014). All the above-mentioned processes occur naturally in the environment. However, human activities such as fertilizer and explosive manufacturing, combustion of fossil fuel, and industrial activities, have triggered an increased transformation of innocuous N_2 to reactive N compounds (e.g., NO_3^-, NO_2^-, NO, N_2O, NH_4^+) compared to the natural N fixation produced biotically or by lightning (Fowler et al., 2013; Howarth et al., 1997). The scope of this anthropogenic disturbance of the N cycle is conspicuous. Although N is essential for life, many compounds such as the oxidized forms NO_3^-, NO_2^- and N_2O have been recognized to produce detrimental effects on human health and the environment (Badr and Probert, 1993; Rivett et al., 2008; Vitousek et al., 1997; Ward et al., 2005). For this reason, the excessive accumulation of these reactive N compounds in the biosphere and the atmosphere raises concerns.

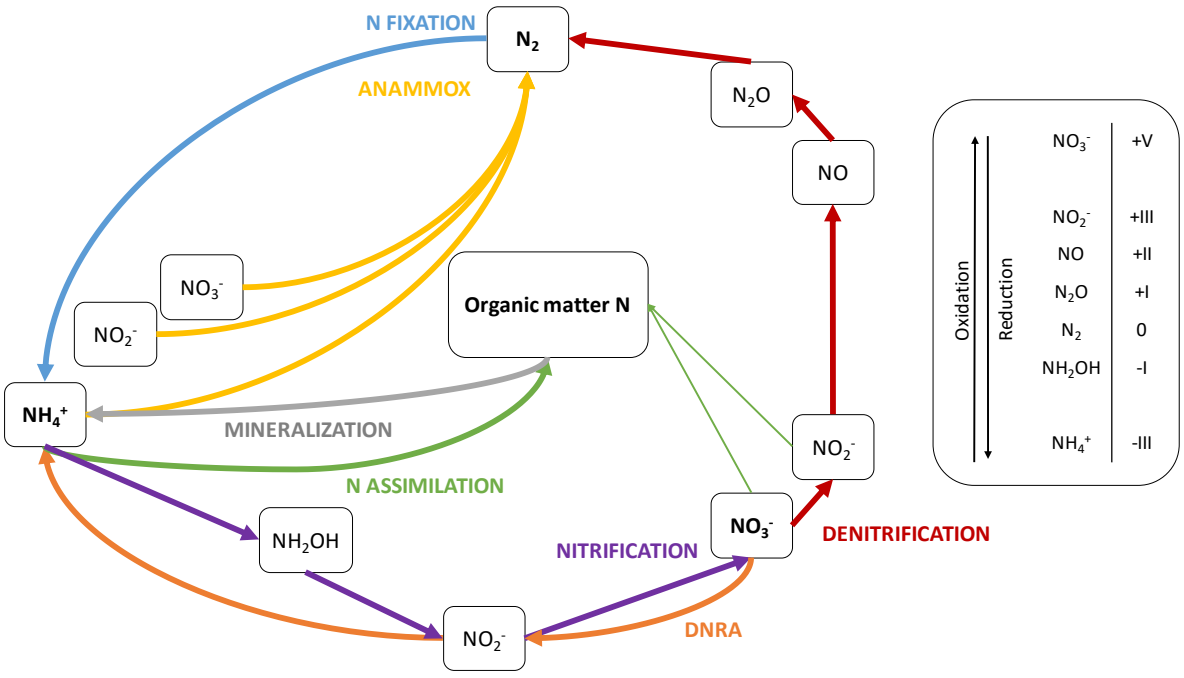

Figure 1.1. Simplified nitrogen cycle diagram. Adapted from: Kuypers et al., 2018 and Waser et al., 1998.

1.2. Nitrate pollution in aquifers

The worldwide persistence of NO_3^- in groundwater due to human activities is worrying since this compound has been related to illnesses such as cancer and methemoglobinemia (Fan and Steinberg, 1996; Volkmer et al., 2005; Ward et al., 2005) and to eutrophication of aquatic ecosystems (Camargo and Alonso, 2006; Justic et al., 2009). The main sources of groundwater NO_3^- pollution are linked to intensive use of synthetic and organic fertilizers (e.g., manure) and septic system leakage (Vitòria et al., 2008; Wassenaar, 1995). These N inputs into soil or water bodies are mainly in the form of NO_3^-, NH_4^+ or urea ($CO(NH_2)_2$). After nitrification and urea hydrolysis, all excess NO_3^- that cannot be uptaken by crops, can be leached to surface and groundwater bodies. For this reason, some of the European directives that have been applied since 1991 aiming to mitigate groundwater NO_3^- pollution, have focused on reducing the N inputs into the soil (e.g., 91/676/EEC; 2000/60/EC; 2006/118/EC).

As stated in the European directive 91/676/EEC, those areas of land which drain into polluted waters or waters at risk of NO_3^- pollution are designated as NO_3^- vulnerable zones (NVZ) (**Figure 1.2**). In these NVZ, action programs have to be implemented by farmers on a compulsory basis such as limitation of fertilizer application. Furthermore, a concentration of 50 mg/L NO_3^- was the threshold established by the Groundwater Framework Directive (2006/118/EC) as a goal to achieve good groundwater quality status and also the threshold value for consumption set in the European Drinking Water Directive (98/83/EC) and the World Health Organization guidelines for drinking water (WHO, 2011). Although the implementation of these directives started in 1991, according to the last available report from the European Environmental Agency, the total area of NVZ increased from 1,951,898 km^2 in 2012 to about 2,175,861 km^2 in 2015 (EC, 2018a). Also, for the period 2004-2015, a diminution of the water bodies presenting NO_3^- concentrations above 25 mg/L was observed for surface water but not for groundwater (**Figure 1.3**). One of the reasons is that, due to the long residence time of N in the soil organic matter pool, the outcome of the agricultural management practices influencing the NO_3^- loading to aquifers can be delayed for more than three decades (Sebilo et al., 2013). Consequently, developing remediation strategies and improving their effectiveness and economics is fundamental both to reach good groundwater quality standards according to the European directives and to obtain safe drinking water supplies.

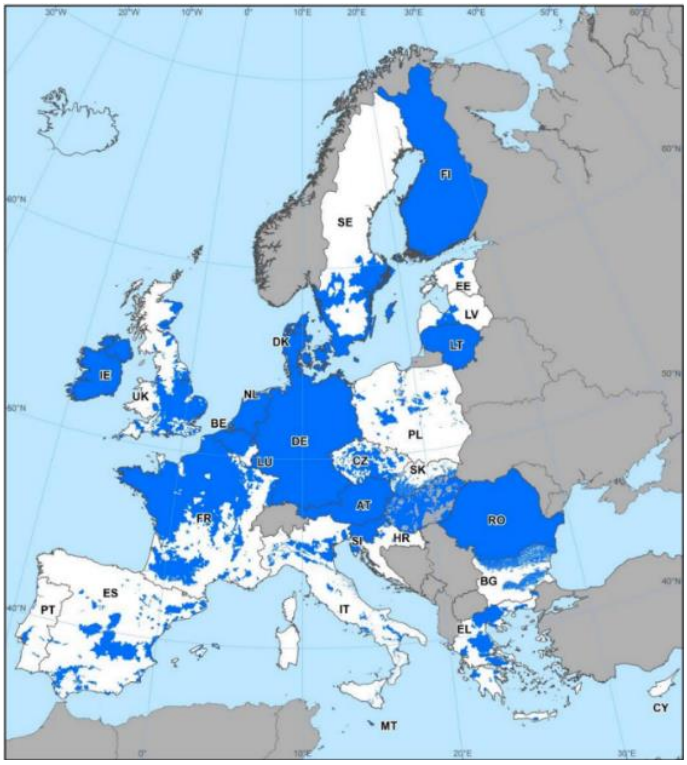

Figure 1.2. Nitrate vulnerable zones in the European Union. Designated nitrate vulnerable zones in the European Union countries until 2015 are marked in blue. Source: EC, 2018b.

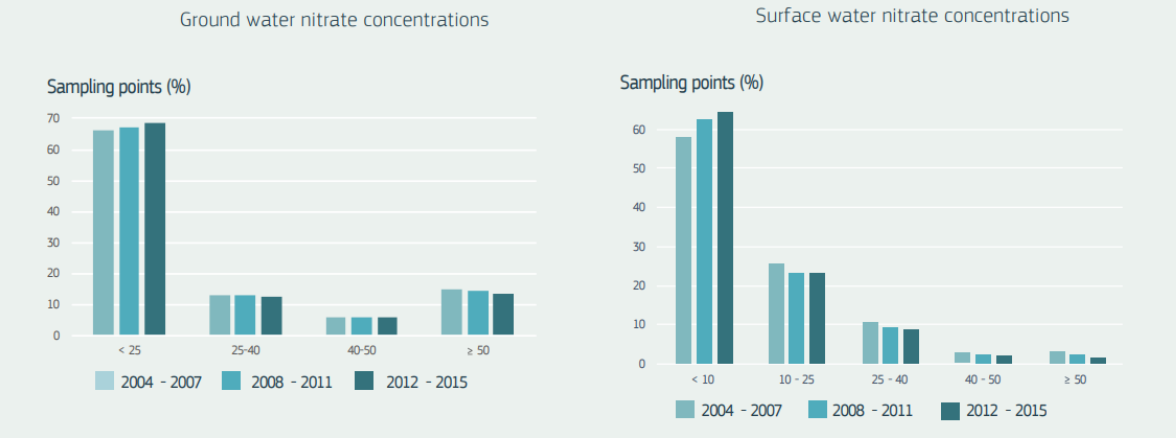

Figure 1.3. Groundwater and surface water nitrate concentration evolution in the European Union between 2004 and 2015. The nitrate concentration (x axis) is given as mg/L. Source: EC, 2018c.

1.3. How can we treat water polluted with nitrate?

Different strategies allow removing NO_3^- from water by using different mechanisms:

I) Physical treatments involving the separation of NO_3^- from water such as ion exchange, reverse osmosis, electrodialysis or adsorption onto different materials (Jensen et al., 2012; Öztürk and Bektaş, 2004).
II) Chemical treatments involving the conversion of NO_3^- to N_2 such as selective catalytic hydrogenation, abiotic NO_3^- reduction by metals (e.g., zero valent iron (ZVI)) or electrochemical systems (Jensen et al., 2012; Li et al., 2010; Pintar and Batista, 1999).
III) Biological treatments involving inducing the denitrification such as bioagumentation, biostimulation or microbial fuel cells (Dybas et al., 2002; Jensen et al., 2012; Virdis et al., 2010).
IV) Accumulation of N in biomass after the NO_3^- uptake by plants (Bachand and Horne, 1999).

The strategies consisting on the separation of NO_3^- from water are disadvantageous since the polluted residues must be managed afterwards. Also, in the case of plant uptake, the N sequestered as biomass can get back to the soil after plant litter decomposition. Therefore, the strategies involving the conversion of NO_3^- to N_2 are preferred, since they represent a real N sink from water. Furthermore, focusing on groundwater treatments, the in-situ application is usually advantageous since it might decrease implementation costs compared to ex-situ treatments. The in-situ biostimulation, which consists on the application of a substrate (electron donor) to induce the denitrification, has already been recognized to provide excellent remediation efficiencies while requiring low operation and maintenance costs during long-term treatments (Critchley et al., 2014; Gierczak et al., 2007; Khan and Spalding, 2004; Robertson et al., 2008).

The denitrification has been shown to occur intrinsically throughout many environments, including aquifers, due to the ubiquity of the denitrifying microorganisms (Kraft et al., 2011; Philippot et al., 2007; Richardson and Watmough, 1999). The microorganisms can use NO_3^- as the N source for growth and as the terminal electron acceptor for respiration. Three types of enzymes can catalyze the NO_3^- reduction: the eukaryotic assimilatory NO_3^- reductases and the prokaryotic assimilatory NO_3^- reductase (NAS), the membrane-bound respiratory NO_3^- reductase (NAR) and the periplasmic dissimilatory NO_3^- reductase (NAP)

(Kraft et al., 2011; Moreno-vivián et al., 1999). To complete the denitrification, the activity of the NO_2^- reductases (NIR), NO reductases (NOR) and N_2O reductases (NOS) is also needed (Kuypers et al., 2018; Moreno-vivián et al., 1999; Philippot et al., 2007). In the case of bacteria and archaea, depending on whether the NO_3^- respiration is coupled to the oxidation of an organic carbon (C), an inorganic compound (e.g., sulfur, hydrogen or iron) or both, it is distinguished between chemoorganotrophic (e.g., **Equation 1.1**), chemolithotrophic (e.g., **Equation 1.2**) or mixotrophic denitrification, respectively.

Equation 1.1. $5CH_2O + 4NO_3^- + 4H^+ \rightarrow 2N_2 + 5CO_2 + 7H_2O$

Equation 1.2. $5FeS_2 + 15NO_3^- + 5H_2O \rightarrow 10SO_4^{2-} + 7.5N_2 + 5FeOOH + 5H^+$

The mandatory conditions for denitrification, such as electron acceptor availability and low oxygen (O_2) concentration, are commonly encountered in contaminated aquifers, but the electron donor presence is usually a limiting factor (Rivett et al., 2008). Hence, one of the feasible treatments for NO_3^- removal involves inducing the denitrification by supplying an external electron donor (**Figure 1.4**). The specific electron donor employed, and its supply strategy play a critical role in the resulting execution efficiency. Among other parameters, it influences the NO_3^- reduction rates and the by-product accumulation (Hallin and Pell, 1998; Wilderer et al., 1987), which is undesirable, given that intermediates, such as NO_2^- or N_2O, could be even more harmful than NO_3^- itself (Badr and Probert, 1993; De Beer et al., 1997; Rivett et al., 2008). In addition, biomass accumulation and the promotion of other biotic processes such as the bacterial SO_4^{2-} reduction (BSR) or DNRA due to excess electron donor application could decrease the water quality (production of H_2S and NH_4^+, respectively) and should also be avoided (Rodríguez-Escales et al., 2016). Denitrification and BSR can occur simultaneously, especially at high C/N ratios (Laverman et al., 2012), and the DNRA is also favored at high C/N ratios, when NO_3^- is limited instead of the electron donor (Giles et al., 2012; Jones et al., 2017; Kelso et al., 1997). Hence, before field-scale application, laboratory experiments must be performed to assess the viability of using a specific electron donor to promote denitrification while avoiding the occurrence of adverse effects.

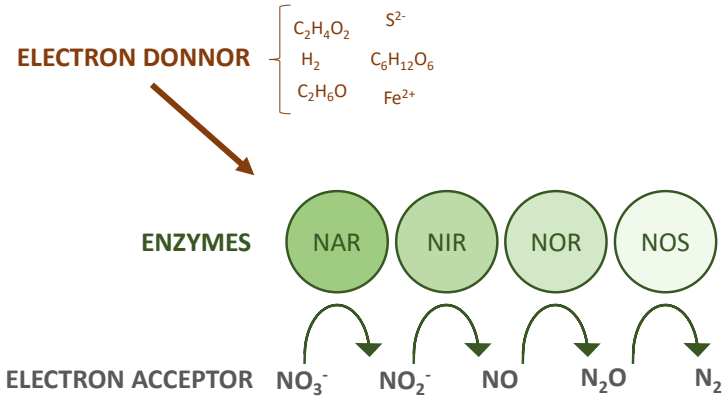

Figure 1.4. Induced denitrification by the addition of an electron donor. Only a few examples of possible organic C and inorganic compounds that can be used by microorganisms as electron donors to reduce nitrate are given.

1.3.1. Electron donors to promote denitrification

To induce the chemoorganotrophic denitrification, pure organic C compounds, such as glucose, acetate, ethanol or methanol have been widely proved to be appropriate (Akunna et al., 1993; Carrey et al., 2014; Peng et al., 2007). However, since the use of pure compounds might become expensive in long-term treatments, there has been an increasing interest in using alternative organic C sources. The potential use of animal or vegetal waste has already been verified (Grau-Martínez et al., 2017; Trois et al., 2010). If liquid compounds are preferred, products such as wine industry residues can also be useful (Carrey et al., 2018). On the other hand, inorganic compounds such as hydrogen (H_2), sulfur (S^0), sulfide (S^{2-}), Fe^{2+}, ZVI or manganese (Mn^{2+}), have been related to the chemolithotrophic denitrification (Di Capua et al., 2019). Few laboratory studies testing minerals such as pyrite, pyrrhotite or biotite have also shown potential to be used in low-cost biostimulation strategies aiming to attenuate NO_3^- pollution (Aquilina et al., 2018; Bosch et al., 2012; Torrentó et al., 2011; Yang et al., 2017). Furthermore, since the mineral nanoparticles (NP) are usually more reactive than macroparticles, their potential use to remediate polluted water bodies has recently gained attraction (Braunschweig et al., 2013). Regarding NO_3^-, NP of pyrite, Fe/Ni supported onto zeolite or mixed ZVI/Mag have been observed to attenuate the pollution (Bosch et al., 2012; Cho et al., 2015b, 2015a; He et al., 2018).

When applied at field-scale, all these electron donors could promote the reduction of other contaminants simultaneously to NO_3^- reduction. For example, the organic C electron donors have been shown to promote the reduction of compounds such as hexavalent chromium (Cr^{6+}), hexavalent uranium (U^{6+}) or chlorinated hydrocarbons (Innemanová et al., 2015; Lovley and Phillips, 1992; Mclean et al., 2015; Nancharaiah et al., 2010; Němeček et al., 2015; Orozco et al., 2010). While at laboratory-scale, NP of ZVI, ferric iron (Fe^{3+}) oxides, magnetite or mixed Mag/maghemite have been found to remove organic and inorganic contaminants such as uranium U^{6+}, Cr^{6+}, arsenic, ethylene glycol ($C_2H_6O_2$) and phenol (C_6H_5OH) (Chowdhury and Yanful, 2010; Crane et al., 2011; Zelmanov and Semiat, 2008). The presence of other contaminants simultaneously to NO_3^- has to be considered when assessing the induced denitrification strategies, since these compounds could also act as electron acceptors and therefore, compete with NO_3^- for the applied electron donors.

Regarding the accumulation of intermediate products during denitrification, in the aforementioned chemoorganotrophic and chemolithotrophic denitrification studies, a transient NO_2^- accumulation was observed (Ge et al., 2012; Torrentó et al., 2011; Yang et al., 2017). This transient NO_2^- accumulation occurs both at laboratory (Calderer et al., 2010; Carrey et al., 2013; Her and Huang, 1995) and field-scale (Critchley et al., 2014; Gierczak et al., 2007; Vidal-Gavilan et al., 2013). The NO_2^- usually accumulates until the bacterial communities adapt to the new redox conditions caused by the electron donor addition. One of the reasons is an earlier induction of the NO_3^- reductases with respect to the NO_2^- reductases (Zumft, 1997 and references therein). Thus, the NO_2^- accumulation might depend on the relative rates of NO_3^- and NO_2^- reduction (Betlach and Tiedje, 1981), as well as on the type of C source and C/N ratios employed (Akunna et al., 1993; Ge et al., 2012), among other parameters. Furthermore, although the gas emissions are not usually measured, the N_2O accumulation can never be discarded since this greenhouse gas (GHG) has also been detected during the NO_3^- reduction both at laboratory and field-scale (Jurado et al., 2017; Weymann et al., 2010), especially in the presence of dissolved O_2 (Morley et al., 2008). In induced denitrification strategies, parameters such as the water O_2 concentration, the C/N ratio and the temperature might play an important role in GHG emissions (Miettinen et al., 2015; Spoelstra et al., 2010; Teiter and Mander, 2005). Consequently, the remediation approach must avoid pollution swapping to ensure the safety of the treatment.

During the last years, numerous studies have pointed that abiotic reactions involving the N and Fe biogeochemical cycles occur simultaneously to the biotic denitrification (Carlson et al., 2013; Klueglein and Kappler, 2013; Matocha and Coyne, 2007; Melton et al., 2014). The NO_2^- reduction by Fe^{2+} oxidation has been well documented (Buchwald et al., 2016; Dhakal et al., 2013; Grabb et al., 2017; Rakshit et al., 2016) and might be advantageous in denitrification treatments to avoid a water quality decrease due to NO_2^- accumulation. However, N_2O has been proposed as the final product of this abiotic NO_2^- reduction by Fe^{2+} oxidation (Buchwald et al., 2016; Chen et al., 2018; Coby and Picardal, 2005; Wang et al., 2016). Hence, supplying NO_3^- polluted water bodies with Fe^{2+}-containing minerals to induce the denitrification might promote N_2O generation from both the biotic and the abiotic NO_2^- reduction. In fact, in laboratory experiments, Cooper et al. (2003) found a larger N_2O production during denitrification in the presence of Fe compared to absence. Nevertheless, the accumulated N_2O by both the biotic and abiotic pathways could be further reduced to N_2 biotically in the presence of electron donors. In induced denitrification studies, the relative contribution of the two pathways on N_2O production should be carefully assessed since this GHG is currently a focus of attention in climate change research (Reay et al., 2012).

1.3.2. Biostimulation strategies to promote denitrification

To induce NO_3^- attenuation in polluted water bodies from agricultural sources, the biostimulation strategies could be applied either directly to the polluted aquifers or to the agricultural runoff water before draining into larger water bodies. The advantages and disadvantages of each strategy must be carefully evaluated, and previous hydrogeochemical characterization at field is crucial to succeed in the operational design.

To remediate NO_3^- polluted aquifers, liquid electron donors can be easily injected through already installed or newly constructed wells. Systems involving an electron donor injection or cross-injection through wells placed across the path of the contaminant plume (Critchley et al., 2014; Gierczak et al., 2007; Tartakovsky et al., 2002), through a daisy-like wells system (Khan and Spalding, 2004) or through infiltration galleries (Salminen et al., 2014), have demonstrated to be effective. Also, the treatment can be performed by pumping groundwater outside the aquifer, mixing it with the electron donor in a tank and reinjecting it through wells (Vidal-Gavilan et al., 2013). On the other hand, solid electron donors can

be applied through passive systems, such as permeable reactive barriers (PRB) (Gibert et al., 2008; Huang et al., 2015; Robertson et al., 2008). The PRB consists of a porous material that is placed in the path of a groundwater plume to remove contaminants as the plume flows through it. This porous material can be filled with an electron donor to induce the denitrification. The PRB installation might involve important costs but the long-treatments might become cost-effective due to low operating and maintenance costs (Robertson et al., 2005, 2000). The PRB can also be installed in ponds for artificial recharge of groundwater (Barba et al., 2019; Grau-Martínez et al., 2018). Surface infiltration through ponds is commonly used for managed aquifer recharge (Bouwer, 2002; Wade Miller, 2006). Although these ponds usually aim to introduce water to the aquifer to recover groundwater levels or to become water reservoirs, they can also be used to remove contaminants from the water that has to be infiltrated.

Alternatively, the denitrification treatment can be applied to remediate NO_3^- polluted agricultural runoff water. For example, directing streams through constructed wetlands (CWs) can be useful to minimize further surface and/or groundwater pollution. The CWs are other promising, low cost and easy operation systems for the remediation of diverse water pollutants (Wu et al., 2015). The surface flow CWs consist of free surface water flowing horizontally through an artificial pond containing floating and/or emergent rooted vegetation and a high diversity of microorganisms (Ilyas and Masih, 2017; Sirivedhin and Gray, 2006; Vymazal, 2007). In surface flow CWs, not only denitrification but also plant uptake might contribute to NO_3^- pollution mitigation (Rogers et al., 1991). Parameters such as temperature, dissolved O_2, NO_3^- loading, the source and amount of organic C, microbial species, the type and density of macrophytes, wetland age, and hydraulic conditions play key roles in the NO_3^- removal efficiency (Bachand and Horne, 1999; Beutel et al., 2009; Kong et al., 2009; Sirivedhin and Gray, 2006). Different approaches can be implemented to enhance water remediation, but strategies directed towards the induction of bacterial NO_3^- respiration are preferred since denitrification is an authentic N sink in water, unlike biomass sequestration (Scott et al., 2008). N storage by plants is generally considered temporary, because organic N returns to the system after the death and decay of plants if they are not harvested (Cooper and Cooke, 1984; Gumbricht, 1993). In CWs, macrophytes are able not only to assimilate NO_3^-, but also to promote denitrification efficiently. Plants exert an influence on the diversity of microbial species and their enzymatic activities by releasing exudates and O_2 to the rhizosphere (Kong et al., 2009, and references therein), and decomposed plant material can be used by microbes as a source of organic C. For

this reason, increased NO_3^- removal is usually found in vegetated CWs relative to that in non-vegetated systems (Jacobs and Harrison, 2014; Soana et al., 2017). If the CW cannot provide enough organic C to support complete denitrification (e.g., from inlet water, soil, plant root exudates, and decomposed vegetal material), the addition of an external electron donors both in liquid or solid forms could enhance the denitrification efficiency (Lu et al., 2009; Si et al., 2018).

1.4. Isotopic tools to identify sources and transformation processes of contaminants

During the implementation of strategies to remediate water pollution, the contaminant removal can be estimated by monitoring its concentrations before and after the treatment. However, this method does not reveal the specific processes involved in the attenuation, making it challenging to focus on the improvement of the remediation approach. The isotopic characterization of the involved compounds can provide advantageous information. Isotope tracers have proven to be a powerful tool in identifying NO_3^- sources in groundwater as well as the sources of diverse compounds such as SO_4^{2-}, Cr^{6+} or organochlorides, among many others (Clark and Fritz, 1997; Ellis et al., 2002; Palau et al., 2014; Wassenaar, 1995). Taking NO_3^- as an example, different kinds of N synthetic fertilizers present different isotopic composition, which is also different from the isotopic composition of N from manure and septic systems discharges (**Figure 1.5**). Therefore, analyzing the isotopic composition of dissolved NO_3^-, allows identifying the sources of pollution (Puig et al., 2017; Vitòria et al., 2008; Widory et al., 2005). In addition, due to the different reaction rates between the light and heavy isotopes, the isotopic characterization allows tracing the natural and induced transformation processes occurring to diverse water contaminants (Aravena and Robertson, 1998; Audí-Miró et al., 2015; Berna et al., 2010; Hunkeler et al., 1999; Otero et al., 2007; Vidal-Gavilan et al., 2013).

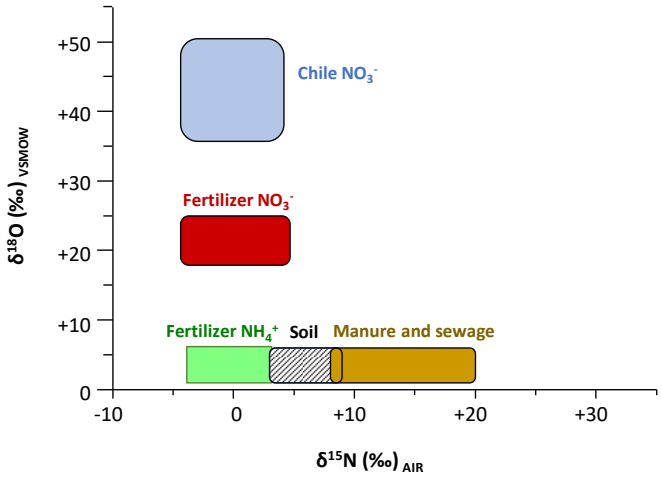

Figure 1.5. Nitrate sources and isotopic composition. The $\delta^{18}O$ values might depend on the isotopic composition of the oxygen from the water in the studied region. Source: Vitoria et al., 2004.

1.4.1. Isotopes to trace nitrate transformation processes

In the course of the enzymatic NO_3^- reduction, the unreacted residual substrate becomes enriched in the heavy isotopes ^{15}N and ^{18}O, since the lighter isotopes (^{14}N and ^{16}O) react preferentially (Aravena and Robertson, 1998; Böttcher et al., 1990; Fukada et al., 2003; Mariotti et al., 1981). The same pattern might be observed throughout the biotic and abiotic reduction of the intermediate products such as NO_2^- or N_2O (Buchwald et al., 2016; Grabb et al., 2017; Jones et al., 2015; Martin and Casciotti, 2016). These intermediate products will be initially depleted in ^{15}N and ^{18}O with respect to the substrate until reaction is completed, then the ultimate product will reach the substrate initial isotopic composition. Therefore, the isotopic characterization allows to distinguish the NO_3^- reduction from other processes, such as dilution due to non-polluted water inputs (e.g., from rainfall), that could also lead to a concentration decrease without influencing the isotopic signature. The isotopic fractionation determined during the reduction of NO_3^- and/or its intermediate compounds ($\varepsilon^{15}N$ and $\varepsilon^{18}O$) in laboratory experiments, performed under controlled conditions, can be later applied at field-scale to quantify the pollutant intrinsic or induced reduction by a specific electron donor (Böttcher et al., 1990; Mariotti et al., 1988).

Although the NO_3^- isotopic evolution through the chemoorganotrophic denitrification has been widely studied (Carrey et al., 2014; Granger et al., 2008; Grau-Martínez et al., 2017; Wunderlich et al., 2012), the characterization during the chemolithotrophic denitrification is scarce (Torrentó et al., 2011, 2010). Furthermore, the information on the dual isotope systematics of intermediates such as NO_2^- and N_2O throughout its biotic or abiotic reduction is also limited (Buchwald et al., 2016; Chen et al., 2018; Grabb et al., 2017; Jones et al., 2015). The range of $\varepsilon^{15}N$ and $\varepsilon^{18}O$ values reported in the literature up to date for the denitrification and the abiotic NO_2^- reduction is presented in **Table 1.1**. Several factors affect the isotopic fractionation under closed system conditions (laboratory):

I) The type of electron donor source might influence the $\varepsilon^{15}N_{NO3/N2}$ and $\varepsilon^{18}O_{NO3/N2}$ results by changing the ratio between the NO_3^- transport across the cell and the intracellular enzymatic reduction (Wunderlich et al., 2012).

II) As previously mentioned, throughout the denitrification the NAR or NAP catalyze the NO_3^- reduction to NO_2^-. Then, the haem-containing cd1 nitrite reductase (Fe-NIR) or the Cu-containing nitrite reductase (Cu-NIR) catalyze the NO_2^- reduction to NO. The use of these different types of NO_3^- and NO_2^- reductases have shown to

produce different $\varepsilon^{15}N/\varepsilon^{18}O$ values (Granger et al., 2008; Martin and Casciotti, 2016).

III) In the case of the NO_2^- abiotic reduction, lower $\varepsilon^{15}N_{NO2/N2O}$ and $\varepsilon^{18}O_{NO2/N2O}$ values have been generally related to higher NO_2^- reduction rates (Buchwald et al., 2016; Grabb et al., 2017).

When using $\varepsilon^{15}N$ and $\varepsilon^{18}O$ values determined at laboratory to evaluate the efficiency of the natural or induced denitrification at field-scale, attention must be focused on biological and hydrogeochemical effects, which could hinder the results interpretation. For this reason, coupling isotopic analysis with all possible data obtained throughout the characterization process will provide a more accurate evaluation. Apart from denitrification, three important processes can affect the NO_3^- isotopic composition at field-scale:

I) The NO_2^- reoxidation to NO_3^- after equilibration of the $\delta^{18}O\text{-}NO_2^-$ with the $\delta^{18}O\text{-}H_2O$ might modify the $\varepsilon^{18}O_{NO3/N2}$ and consequently, the $\varepsilon^{15}N/\varepsilon^{18}O$ (Wunderlich et al., 2013). For this reason, $\varepsilon^{15}N/\varepsilon^{18}O$ values close to 2 are common in field-scale freshwater denitrification studies where O_2 inputs are usual (Critchley et al., 2014; Granger and Wankel, 2016; Otero et al., 2009), while values remain close to 1 in laboratory experiments (Carrey et al., 2013; Grau-Martínez et al., 2017). Apart from abiotically (due to O_2 inputs), the NO_2^- can be reoxidated to NO_3^- by microorganisms performing the second step of the nitrification. In the first step, the ammonia monooxygenase (AMO) catalyzes the NH_4^+ oxidation to NO_2^- and then NO_2^- is oxidized to NO_3^- by the NO_2^- oxidoreductase (NXR). During the nitrification, the $\delta^{15}N$ of the residual NH_4^+ and NO_2^- increases (Högberg, 1997; Mariotti et al., 1981), while the isotopic composition of the $O\text{-}NO_3^-$ is controlled by the $O\text{-}H_2O$ (2/3) and the $O\text{-}O_2$ (1/3) (Andersson and Hooper, 1983).

II) Mixing of denitrified water with non-polluted water (e.g., rainfall events), could decrease the NO_3^- concentration without producing a further enrichment in the heavy isotopes ^{15}N and ^{18}O, while mixing of waters with NO_3^- from different sources could modify both the NO_3^- concentration and isotopic composition (Puig et al., 2013).

III) The NO_3^- assimilation by plants or other organisms might also cause an isotopic fractionation. Significant enrichment in both ^{15}N and ^{18}O has been observed in the NO_3^- extracted from leaves relative to the NO_3^- from water after plant uptake, but the changes in the NO_3^- isotopic composition in the water are ususally minor

(Estrada et al., 2017; Spoelstra et al., 2010). A higher ^{15}N of the intracellular NO_3^- compared to the NO_3^- from water has been also observed during assimilation by marine diatoms (Needoba et al., 2004). In another study investigating the NO_3^- isotope effects due to assimilation by different species of prokaryotes and eukaryotes, low $\varepsilon^{15}N$ and $\varepsilon^{18}O$ for the NO_3^- in water (from -0.4 to -2 ‰) were found for a heterotrophic α-proteobacteria, while higher values (-2 to -9 ‰) were found for marine cyanobacteria, chlorophytes and diatoms (Granger et al., 2010). Nevertheless, in NO_3^- remediation studies, the observed isotopic fractionation is usually attributed to denitrification since it is the process accounting for most of the NO_3^- removal, at least after the initial period of biomass increase due to the biostimulation.

1.4.2. Isotopic characterization of other compounds involved in the denitrification

The isotopic characterization of the applied electron donor (e.g., $\delta^{13}C$ or $\delta^{56}Fe$) and the produced dissolved inorganic carbon (and $\delta^{13}C$-DIC) during denitrification might provide knowledge on the fate of the added electron donor (Carrey et al., 2018; Nascimento and Krishnamurthy, 1997; Swanner et al., 2017). Furthermore, taking into consideration the intrinsic characteristics of the studied water bodies, the isotopic characterization of diverse compounds can be used to determine the existence of processes concurring with denitrification. For example, similarly to the case of NO_3^-, the isotopic composition of S and O from dissolved SO_4^{2-} allows to identify the occurrence of bacterial SO_4^{2-} reduction (Laverman et al., 2012; Strebel et al., 1990), or the isotopic composition of Cr^{6+} allows to identify its biotic or abiotic reduction (Basu et al., 2014; Chen et al., 2018; Ellis et al., 2002). Both the SO_4^{2-} and Cr^{6+} can be reduced simultaneously to NO_3^- in the presence of an electron donor.

Table 1.1. Range of $\varepsilon^{15}N$, $\varepsilon^{18}O$ and $\varepsilon^{15}N/\varepsilon^{18}O$ determined in laboratory-scale studies. Both the biotic and abiotic reduction of NO_3^- and NO_2^- are included. The end product of the biotic reduction was considered to be N_2 while for the abiotic reduction N_2O. For pure culture experiments, enzymes are specified inside the parentheses (if reported). Legend: GW = groundwater, SGW = synthetic groundwater, SSW = synthetic seawater, GM = growth medium, μ = microorganisms, aq = dissolved, ads = adsorbed on mineral surfaces.

CATALYST	STUDY TYPE	ELECTRON ACCEPTOR	ELECTRON DONOR	MEDIUM	$\varepsilon^{15}N$	$\varepsilon^{18}O$	$\varepsilon^{15}N/\varepsilon^{18}O$	REFERENCE
Paracoccus denitrificans, *Pseudomonas Chloraphis* (NAR)	Batch	NO_3^-	C_{org}	SSW	-16.9 to -26.6	-16.4 to -22.6	1.0 to 1.1	(Granger et al., 2008)
Ochrobactrum sp., *Pseudomonas stutzeri* (NAR)	Batch	NO_3^-	C_{org}	SSW	-5.4 to -22.9	-4.8 to -22.8	1.0 to 1.2	
Rhodobacter sphaeroides (NAP)	Batch	NO_3^-	C_{org}	SSW	-12.6 to -19.9	-7.9 to -13.1	1.5 to 1.8	
Pseudomonas pseudoalcaligenes	Batch	NO_3^-	Succinate	GM	-11.4 to -16.2	-5.5 to -6.2	2.0 to 3.0	(Knöller et al., 2011)
Azoarcus sp.	Batch	NO_3^-	Succinate	GM	-8.6 to -14.7	-5.7 to -6.8	1.3 to 2.3	
Azoarcus sp.	Batch	NO_3^-	Toluene	GM	-10.1 to -12.6	-4.0 to -7.3	1.7 to 2.5	
Thauera aromatica, *Aromatoleum aromaticum*	Batch	NO_3^-	Toluene	GM	-17.3 to -18.1	-16.1 to -16.5	1.1	(Wunderlich et al., 2012)
Thauera aromatica	Batch	NO_3^-	Benzoate	GM	-18.9	-15.9	1.2	
Thauera aromatica, *Aromatoleum aromaticum*	Batch	NO_3^-	Acetate	GM	-22.1 to -23.5	-19.9 to -23.7	1.0 to 1.1	
μ from sediment and GW (hypersaline lake)	Batch + column	NO_3^-	Compounds from sediment and GW (hypersaline lake)	GW	-14.7	-14.5	1.0	(Carrey et al., 2014)
μ from sediment and GW	Column	NO_3^-	Ethanol	GW	-6.5	-6.0	1.1	(Vidal-Gavilan et al., 2014)
μ from riparian sediments and GW	Column	NO_3^-	Compounds from riparian sediments and GW	GW	-32.9 to -34.1	-	-	(Tsushima et al., 2006)
μ from organic and pyrite rich sediments and GW	Column	NO_3^-	Compounds from organic and pyrite rich sediments and GW	GW	-11.6 to -15.7	-12.1 to -13.8	1.0 to 1.1	(Carrey et al., 2013)
Thiobacillus denitrificans	Batch	NO_3^-	Pyrite	GM	-12.6	-8.8	1.4	(Hosono et al., 2015)
Thiobacillus denitrificans	Batch	NO_3^-	Pyrite	GM	-15.0 to -22.9	-13.5 to -19.0	1.1 to 1.2	(Torrentó et al., 2010)
μ from sediments and GW	Batch	NO_3^-	Pyrite	GW	-27.6	-21.3	1.3	(Torrentó et al., 2011)
μ from sediments and GW and *Thiobacillus denitrificans*	Batch	NO_3^-	Pyrite	GW	-25.0	-19.5	1.3	
Pseudomonas aeruginosa, *Pseudomonas chlororaphis*, *Pseudomonas stutzeri* (Fe-NIR)	Batch	NO_2^-	C_{org}	GM	-3 to -11	-2 to -12	0.7 to 3.3	(Martin and Casciotti, 2016)
Achrombacter xylosoxidans, *Ochrobactrum* sp., *Pseudomonas aureofaciens* (Cu-NIR)	Batch	NO_2^-	C_{org}	GM	-19 to -26	0 to -6	3.1 to 22.0	
Abiotic	Batch	NO_2^-	Nontronite	SSW	-11.1	-10.4	1.1	(Grabb et al., 2017)
Abiotic	Batch	NO_2^-	Synthetic Fe^{2+} (aq+ads)	SSW	-2.3	-4.5	0.5	
Abiotic	Batch	NO_2^-	Green rust	SSW	-4.2 to -9.4	-4.1 to -9.4	0.8 to 1.1	
Abiotic	Batch	NO_2^-	Synthetic Fe^{2+} (aq)	SSW	-6.1 to -33.9	-5.7 to -24.8	0.8 to 1.6	(Buchwald et al., 2016)
Abiotic	Batch	NO_2^-	Synthetic Fe^{2+} (aq+ads)	SSW	-5.9 to -44.8	-5.2 to -33.0	1.0 to 1.4	
Abiotic	Batch	NO_2^-	Synthetic Fe^{2+} (aq)	SGW	-12.9	-9.8	1.3	(Jones et al., 2015)

1.5. Goals of the thesis

Since in many of the local and regional aquifers in Europe, the NO_3^- concentration still exceeds the threshold for human consumption of 50 mg/L (2006/118/EC), the optimization of the implementation and evaluation of remediation strategies is crucial. In this context, the main goal of this thesis is to improve the knowledge on the mechanisms based on biostimulation to remediate groundwater polluted with NO_3^-. According to this general objective, several specific goals were determined:

I) To evaluate the suitability of using Fe^{2+}-containing minerals (magnetite, siderite, olivine) to promote the NO_3^- attenuation in polluted water bodies; to quantify the changes in the NO_3^- reduction rate when the Fe^{2+}-containing minerals are nano-sized compared to micro-sized; to evaluate the possible abiotic reactivity between the Fe^{2+}-containing minerals or dissolved Fe^{2+} and NO_3^- or NO_2^-; and to quantify the ε values for all the tested conditions.

II) To evaluate the suitability of using a dairy industry residue to promote denitrification when injected into NO_3^- polluted aquifers; to find the best injection strategy to reduce NO_3^- values below the threshold fixed by European Directives while achieving complete whey consumption; and to quantify the ε values for all the tested conditions.

III) To evaluate the suitability of using rural waste products (animal compost, wheat hay, corn stubble) to promote denitrification if applied in a surface flow CW; to evaluate the influence of temperature on the induced denitrification efficiency; and to quantify the ε values for all the tested conditions.

IV) To test the usefulness of the isotopic tools to trace the induced denitrification efficiency during a long-term in-situ attenuation strategy at a pilot-plant to produce safe drinking water from NO_3^--polluted groundwater by acetic acid injections.

V) To trace the natural NO_3^- attenuation in a polluted aquifer with Cr^{6+} by using isotopic tools taking into account changes in the reactivity and isotopic fractionation due to the simultaneous presence of NO_3^- and Cr^{6+}.

VI) To trace the NO_3^- attenuation before and after the implementation of a biostimulation strategy in a CW both in the autumn-winter and spring-summer seasons by using isotopic tools.

1.6. Thesis outline

In order to accomplish the goals, several tasks were developed including both laboratory and field-scale research. At laboratory-scale, batch and flow-through experiments were performed by using the following electron donors to promote the denitrification: acetic acid, ethanol, whey, wheat hay, corn stubble, animal compost, magnetite (Mag), siderite (Sd), olivine (Ol). At field-scale the natural and induced denitrification was evaluated in two polluted aquifers and in a CW. During the studies, samples were collected and characterized chemically and isotopically. If needed, some analytical techniques were implemented and/or optimized. In the laboratory experiments, the ε values were determined for all tested conditions. The ε values obtained for acetic acid, ethanol and corn stubble were applied to determine the efficiency of denitrification in the field-scale studies (two polluted aquifers and a CW). The other values can be used in future field-scale studies if the tested electron donors are intrinsically present or applied to remediate polluted water bodies. Both at laboratory and field-scale, special attention was directed on the generation of harmful by-products throughout the induced denitrification from biostimulation strategies.

A total number of six scientific articles have resulted from the tasks performed during this thesis. Four of them have been already published in international peer-reviewed science citation index (SCI) journals with high impact factors, one has been recently submitted for publication and another one is still in preparation. These articles are listed below, including the information on the SCI journals rank according to Web Of Science (WOS, Thomson Reuters). A scheme of the relationship between the different published papers derived from the present thesis is found in **Figure 1.6**. The full text of the publications can be found in the **Annex** of this document.

I) Rosanna Margalef-Marti, Raúl Carrey, Albert Soler, Neus Otero. Induced nitrate attenuation by ferrous iron containing minerals. Submitted to Chemosphere. Q1 in Environmental Sciences, IF = 5.1 (2018).

II) Francesco Offfedu, Robert Benaiges-Fernandez, Rosanna Margalef-Marti, Jordi Palau, Jordi Urmeneta, Raúl Carrey, Neus Otero, Albert Soler, Jordi Cama. Geochemical and isotopic study of abiotic nitrite reduction coupled to bio-produced Fe(II) oxidation in marine environments. In preparation.

III) Rosanna Margalef-Marti, Raúl Carrey, Albert Soler, Neus Otero. 2019. Evaluating the potential use of a dairy industry residue to induce denitrification in polluted water bodies: A flow-through experiment. Journal of Environmental Management, 245, pp. 86-94. DOI: 10.1016/j.jenvman.2019.03.086. Q1 in Environmental Sciences, IF = 4.9 (2018).

IV) Rosanna Margalef-Marti, Raúl Carrey, Daniel Merchán, Albert Soler, Jesús Causapé, Neus Otero. 2019. Feasibility of using rural waste products to increase the denitrification efficiency in a surface flow constructed wetland. Journal of Hydrology, 578, 124035. DOI: 10.1016/j.jhydrol.2019.124035. Q1 in Civil Engineering, Geosciences Multidisciplinary and Water resources, IF = 4.4 (2018).

V) Rosanna Margalef-Marti, Raúl Carrey, Marta Viladés, Irene Jubany, Ester Vilanova, Roser Grau, Albert Soler, Neus Otero. 2019. Use of nitrogen and oxygen isotopes of dissolved nitrate to trace field-scale induced denitrification efficiency throughout an in-situ groundwater remediation strategy. Science of the Total Environment, 686, pp. 709-718. DOI: 10.1016/j.scitotenv.2019.06.003. Q1 in Environmental Sciences, IF = 5.6 (2018).

VI) Elina Ceballos, Rosanna Margalef-Marti, Raul Carrey, Robert Frei, Neus Otero, Albert Soler, Carlos Ayora. 2020. Characterization of the natural attenuation of chromium contamination in the presence of nitrate using isotopic methods. A case study from the Matanza-Riachuelo river basin, Argentina. Science of the Total Environment, 699, 134331. DOI: 10.1016/j.scitotenv.2019.134331. Q1 in Environmental Sciences, IF = 5.6 (2018).

While the tasks involving the articles I, III, IV and V where fully developed in the context of the present thesis, the tasks involving the articles II and VI where performed with the collaboration of researchers from the Institute of Environmental Assessment and Water Research (IDAEA) of the “Consejo Superior de Investigaciones Científicas (CSIC)” and the “Instituto de Hidrología de Llanuras *Eduardo J. Usunof”* of the “Consejo Nacional de Investigaciones Científicas (CONICET)”. The contribution of this thesis to paper II was: supporting the experimental design, isotope analysis, results interpretation of the isotopic data coupled to chemical data and writing of the isotope results and discussion section of the paper. The contribution to paper VI was: supporting the laboratory experiments design and set-up, isotope analysis, results interpretation of the isotopic data coupled to chemical data, writing of the isotope results and discussion section of the paper and general revision of the paper.

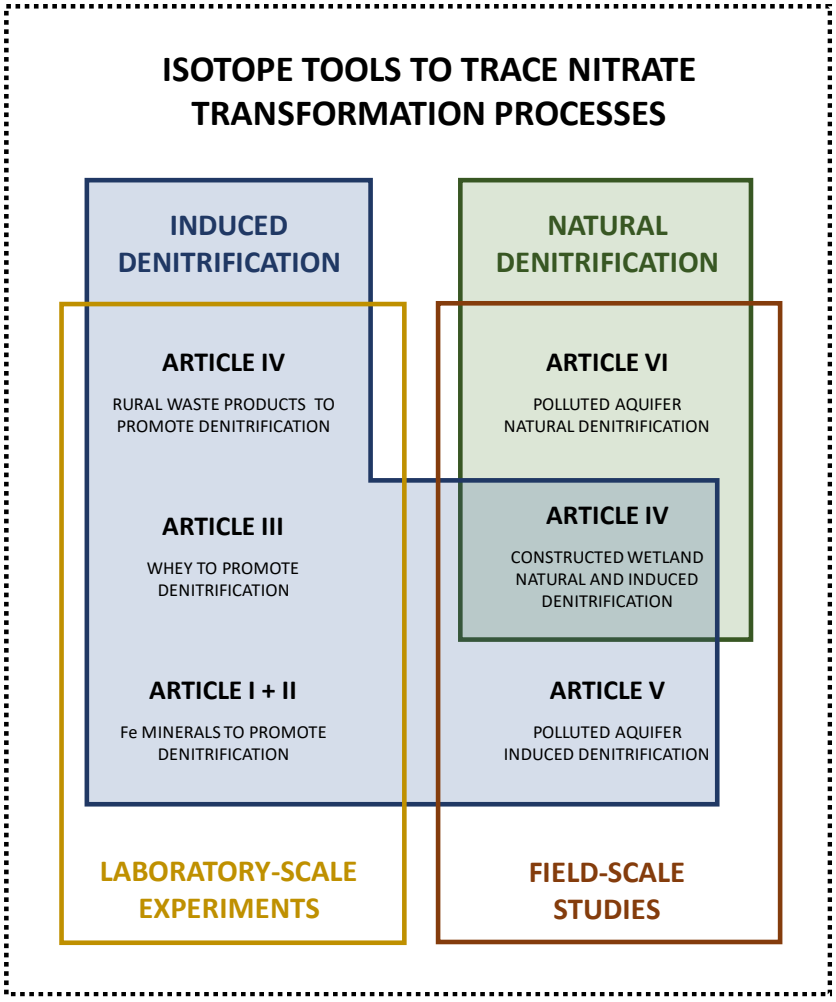

Figure 1.6. Relationship between the articles derived from this thesis. The title of each article is specified in the introduction section 1.6 and the full texts can be found in the Annex of this document. The articles V and VI also included laboratory experiments but as the methodology needed to calculate the isotopic fractionation values to be later applied at field-scale.

Apart from these articles, other contributions related with this thesis were presented in conferences:

I) Margalef Marti, R.; Offedu, F.; Benaiges-Fernandez, R.; Palau, J.; Urmeneta, J.; Carrey, R.; Otero, N.; Soler, A.; Cama, J. Isotopic analysis of nitrite during abiotic reduction by bio-produced Fe(II). Potential insight into the fate of nitrite in marine environments. Goldschmidt (international), August 2019, Barcelona, Spain. Oral communication.

II) Margalef-Marti, R.; Carrey, R.; Soler, A.; Otero, N. Isotopic fractionation associated to nitrate attenuation by ferrous iron containing minerals. 6th International Symposium on Water-Rock Interaction, 13th International Symposium on Applied Isotope Geochemistry and 1st IAGC International Conference (international), July 2019, Tomsk, Russia. Oral communication.

III) Martí, V.; Benito, J.A.; Jubany, I.; Ribas, D.; Margalef-Marti, R.; Carrey, R.; Otero, N.; Soler, A. Study of the elimination of phosphate and nitrate in water by using iron oxides nanoparticles obtained by top to down approach. 7th European Bioremediation Conference and 11th International Society for Environmental Biotechnology conference (international), June 2018, Chania, Greece. Oral communication.

IV) Margalef-Marti, R.; Carrey, R.; Merchán, D.; Otero, N.; Soler, A.; Causapé, J. Use of rural waste products to induce Denitrification in a constructed wetland: Batch experiments. Wetland Systems for Water Pollution Control (international), October 2018, Valencia, Spain. Poster.

V) Carrey, R.; Margalef-Marti, R.; Merchán, D.; Otero, N.; Soler, A.; Causapé, J. Feasibility of corn stubble to promote denitrification in a surface flow constructed wetland: Isotopic approach. Wetland Systems for Water Pollution Control (international), October 2018, Valencia, Spain. Oral communication.

VI) Soler, A.; Margalef-Marti, R.; Carrey, R.; Otero, N.; Vilades, M., Jubany, J.; Vilanova, E.; Grau, R. Nitrogen and oxygen isotopes of dissolved nitrate to evaluate the efficiency of induced groundwater denitrification at field-scale. Flowpath, National Meeting on Hydrogeology (national), June 2017, Cagliari, Italy. Invited talk.

VII) Margalef-Marti, R.; Carrey, R.; Otero, N.; Domenech, C.; Soler, A. Nitrate and nitrite attenuation by Fe(II) minerals: biotic and abiotic reactions. XXXVI Reunión Científica de la Sociedad Española de Mineralogía (national), June 2017, Oviedo, Spain. Oral communication.

VIII) Carrey, R.; Margalef-Marti, R.; Viladés, M.; Jubany, I.; Vilanova, E.; Grau, R.; Soler, A.; Otero, N. Stable isotope characterization to evaluate the efficiency of induced denitrification at field-scale. Goldschmidt (international), August 2017, Paris, France. Oral communication.

IX) Soler, A.; Margalef-Marti, R.; Carrey, R.; Otero, N.; Viladés, M.; Jubany, I.; Vilanova, E.; Grau, R. Nitrogen and oxygen isotopes of dissolved nitrate to

evaluate the efficiency of induced groundwater denitrification at field-scale. Isótopos Estables, Metodologías y Aplicaciones - Reunión de Usuarios IRMS (national), October 2017, Sevilla, Spain. Invited talk.

X) Carrey, R.; Margalef-Marti, R.; Merchán, D.; Otero, N.; Soler, A.; Causapé, J. Use of stable isotopes ($\delta^{15}N$ and $\delta^{18}O$) to evaluate nitrate reduction processes in a surface flow artificial wetland. IsoCycles (international), October 2017, Ascona, Switzerland. Oral communication.

XI) Margalef-Marti, R.; Carrey, R.; Otero, N.; Domenech, C.; Soler, A. Induced biodenitrification by a dairy industry by-product as an electron donor source: flow-through experiment. Joint European Stable Isotope Users group Meeting JESIUM (international), September 2016, Gent, Belgium. Poster. Awarded as the best student poster.

Furthermore, two short research stays abroad were performed during the thesis. The first one in the Ecogeochemistry team of the “Institut d'Ecologie et des Sciences de l'Environnement de Paris” (Université Pierre et Marie Curie), with the objective of learning the analytical techniques needed for the N_2O isotopic characterization. The second one in the Division of Geosciences and Environmental engineering of the Lulea University of Technology in collaboration with the company ALS Scandinavia, with the objective of learning the analytical techniques needed for the Fe isotopic characterization. The knowledge gained during these two stays is expected to be implemented in future projects related to the work developed in this thesis.

In the following chapters, the employed methodologies and obtained results during the present thesis are summarized and briefly described. A global discussion of the results is also provided along with the results.

REFERENCES

2000/60/EC, 2000. Water Framework Directive [WWW Document]. Off. J. Eur. Comm. URL http://ec.europa.eu/environment/index_en.htm (accessed 4.9.17).

2006/118/EC, 2006. Groundwater Directive. Council Directive 2006/118/EC, of 12 December 2006, on the protection of groundwater against pollution and deterioration [WWW Document]. Off. J. Eur. Comm. URL http://ec.europa.eu/environment/index_en.htm (accessed 4.9.17).

91/676/EEC, 1991. Nitrates Directive. Council Directive 91/676/EEC of 12 December 1991, concerning the protection of waters against pollution caused by nitrates from agricultural sources. [WWW Document]. Off. J. Eur. Comm. URL http://ec.europa.eu/environment/index_en.htm (accessed 4.9.17).

98/83/EC, 1998. Drinking Water Directive. Council Directive 98/83/EC, of 3 November 1998, on the quality of water intended for human consumption. [WWW Document]. Off. J. Eur. Comm. URL http://ec.europa.eu/environment/index_en.htm (accessed 4.9.17).

Akunna, J.C., Bizeau, C., Moletta, R., 1993. Nitrate and nitrite reductions with anaerobic sludge using various carbon sources: Glucose, glycerol, acetic acid, lactic acid and methanol. Water Res. 27, 1303–1312. https://doi.org/10.1016/0043-1354(93)90217-6

Andersson, K.K., Hooper, A.B., 1983. O_2 and H_2O are each the source of one O in NO_2^- produced from NH_3 by Nitrosomonas: ^{15}N-NMR evidence. FEBS Lett. 164, 236–240. https://doi.org/10.1016/0014-5793(83)80292-0

Aquilina, L., Roques, C., Boisson, A., Vergnaud-Ayraud, V., Labasque, T., Pauwels, H., Pételet-Giraud, E., Pettenati, M., Dufresne, A., Bethencourt, L., Bour, O., 2018. Autotrophic denitrification supported by biotite dissolution in crystalline aquifers (1): New insights from short-term batch experiments. Sci. Total Environ. 619–620, 842–853. https://doi.org/10.1016/j.scitotenv.2017.11.079

Aravena, R., Robertson, W.D., 1998. Use of multiple isotope tracers to evaluate denitrification in ground water: study of nitrate from a large-flux septic system plume. Ground Water 36, 975–982.

Audí-Miró, C., Cretnik, S., Torrentó, C., Rosell, M., Shouakar-Stash, O., Otero, N., Palau, J., Elsner, M., Soler, A., 2015. C, Cl and H compound-specific isotope analysis to assess natural versus Fe(0) barrier-induced degradation of chlorinated ethenes at a contaminated site. J. Hazard. Mater. 299, 747–754. https://doi.org/10.1016/j.jhazmat.2015.06.052

Bachand, P.A.M., Horne, A.J., 1999. Denitrification in constructed free-water surface wetlands: II. Effects of vegetation and temperature. Ecol. Eng. 14, 17–32. https://doi.org/10.1016/S0925-8574(99)00017-8

Badr, O., Probert, S.D., 1993. Environmental impacts of atmospheric nitrous oxide. Appl. Energy 44, 197–231. https://doi.org/10.1016/0306-2619(93)90018-K

Barba, C., Folch, A., Gaju, N., Sanchez-Vila, X., Carrasquilla, M., Grau-Martínez, A., Martínez-Alonso, M., 2019. Microbial community changes induced by Managed Aquifer Recharge activities: Linking hydrogeological and biological processes. Hydrol. Earth Syst. Sci. 23, 139–154. https://doi.org/10.5194/hess-23-139-2019

Basu, A., Johnson, T.M., Sanford, R.A., 2014. Cr isotope fractionation factors for Cr(VI) reduction by a metabolically diverse group of bacteria. Geochim. Cosmochim. Acta 142, 349–361. https://doi.org/10.1016/j.gca.2014.07.024

Beeckman, F., Motte, H., Beeckman, T., 2018. Nitrification in agricultural soils: impact, actors and mitigation. Curr. Opin. Biotechnol. 50, 166–173. https://doi.org/10.1016/j.copbio.2018.01.014

Berna, E.C., Johnson, T.M., Makdisi, R.S., Basu, A., 2010. Cr Stable Isotopes As Indicators of Cr(VI) Reduction in Groundwater: A Detailed Time-Series Study of a Point-Source Plume. Environ. Sci. Technol. 44, 1043–1048. https://doi.org/10.1021/es902280s

Betlach, M.R., Tiedje, J.M., 1981. Kinetic Explanation for Accumulation of Nitrite, Nitric Oxide, and Nitrous Oxide during Bacterial Denitrification. Appl. Environ. Microbiol. 42, 1074–1084.

Beutel, M.W., Newton, C.D., Brouillard, E.S., Watts, R.J., 2009. Nitrate removal in surface-flow constructed

wetlands treating dilute agricultural runoff in the lower Yakima Basin, Washington. Ecol. Eng. 35, 1538–1546. https://doi.org/10.1016/j.ecoleng.2009.07.005

Bosch, J., Lee, K.Y., Jordan, G., Kim, K.W., Meckenstock, R.U., 2012. Anaerobic, nitrate-dependent oxidation of pyrite nanoparticles by thiobacillus denitrificans. Environ. Sci. Technol. 46, 2095–2101. https://doi.org/10.1021/es2022329

Böttcher, J., Strebel, O., Voerkelius, S., Schmidt, H.L., 1990. Using isotope fractionation of nitrate-nitrogen and nitrate-oxygen for evaluation of microbial denitrification in a sandy aquifer. J. Hydrol. 114, 413–424. https://doi.org/10.1016/0022-1694(90)90068-9

Bouwer, H., 2002. Artificial recharge of groundwater: Hydrogeology and engineering. Hydrogeol. J. 10, 121–142. https://doi.org/10.1007/s10040-001-0182-4

Braunschweig, J., Bosch, J., Meckenstock, R.U., 2013. Iron oxide nanoparticles in geomicrobiology: from biogeochemistry to bioremediation. N. Biotechnol. 30, 793–802. https://doi.org/10.1016/j.nbt.2013.03.008

Buchwald, C., Grabb, K., Hansel, C.M., Wankel, S.D., 2016. Constraining the role of iron in environmental nitrogen transformations: Dual stable isotope systematics of abiotic NO_2^- reduction by Fe(II) and its production of N2O. Geochim. Cosmochim. Acta. https://doi.org/10.1016/j.gca.2016.04.041

Cabello, P., Roldán, M.D., Moreno-Vivián, C., 2004. Nitrate reduction and the nitrogen cycle in archaea. Microbiology 150, 3527–3546. https://doi.org/10.1099/mic.0.27303-0

Calderer, M., Gibert, O., Martí, V., Rovira, M., De Pablo, J., Jordana, S., Duro, L., Guimerá, J., Bruno, J., 2010. Denitrification in presence of acetate and glucose for bioremediation of nitrate-contaminated groundwater. Environ. Technol. 31, 799–814. https://doi.org/10.1080/09593331003667741

Camargo, J.A., Alonso, Á., 2006. Ecological and toxicological effects of inorganic nitrogen pollution in aquatic ecosystems: A global assessment. Environ. Int. 32, 831–849. https://doi.org/10.1016/j.envint.2006.05.002

Capua, F. Di, Pirozzi, F., Lens, P.N.L., Esposito, G., 2019. Electron donors for autotrophic denitrification. Chem. Eng. J. 362, 922–937.

Carlson, H.K., Clark, I.C., Blazewicz, S.J., Iavarone, A.T., Coates, J.D., 2013. Fe(II) oxidation is an innate capability of nitrate-reducing bacteria that involves abiotic and biotic reactions. J. Bacteriol. 195, 3260–3268. https://doi.org/10.1128/JB.00058-13

Carrey, R., Otero, N., Soler, A., Gómez-Alday, J.J., Ayora, C., 2013. The role of Lower Cretaceous sediments in groundwater nitrate attenuation in central Spain: Column experiments. Appl. Geochemistry 32, 142–152. https://doi.org/10.1016/j.apgeochem.2012.10.009

Carrey, R., Otero, N., Vidal-Gavilan, G., Ayora, C., Soler, A., Gómez-Alday, J.J., 2014. Induced nitrate attenuation by glucose in groundwater: Flow-through experiment. Chem. Geol. 370, 19–28. https://doi.org/10.1016/j.chemgeo.2014.01.016

Carrey, R., Rodríguez-Escales, P., Soler, A., Otero, N., 2018. Tracing the role of endogenous carbon in denitrification using wine industry by-product as an external electron donor: Coupling isotopic tools with mathematical modeling. J. Environ. Manage. 207, 105–115. https://doi.org/10.1016/j.jenvman.2017.10.063

Chen, D., Liu, T., Li, X., Li, F., Luo, X., Wu, Y., Wang, Y., 2018. Biological and chemical processes of microbially mediated nitrate-reducing Fe(II) oxidation by *Pseudogulbenkiania* sp. strain 2002. Chem. Geol. 476, 59–69. https://doi.org/10.1016/j.chemgeo.2017.11.004

Chen, G., Qin, L., Han, J., Mu, Y., Yu, H., 2018. Two-stage chromium isotope fractionation during microbial Cr(VI) reduction. Water Res. 148, 10–18. https://doi.org/10.1016/j.watres.2018.09.034

Cho, D.W., Song, H., Kim, B., Schwartz, F.W., Jeon, B.H., 2015a. Reduction of nitrate in groundwater by Fe(0)/Magnetite nanoparticles entrapped in Ca-Alginate beads. Water. Air. Soil Pollut. 226. https://doi.org/10.1007/s11270-015-2467-6

Cho, D.W., Song, H., Schwartz, F.W., Kim, B., Jeon, B.H., 2015b. The role of magnetite nanoparticles in the reduction of nitrate in groundwater by zero-valent iron. Chemosphere 125, 41–49. https://doi.org/10.1016/j.chemosphere.2015.01.019

Chowdhury, S.R., Yanful, E.K., 2010. Arsenic and chromium removal by mixed magnetite-maghemite nanoparticles and the effect of phosphate on removal. J. Environ. Manage. 91, 2238–2247. https://doi.org/10.1016/j.jenvman.2010.06.003

Clark, I., Fritz, P., 1997. Environmental Isotopes in Hydrogeology. Eos, Trans. Am. Geophys. Union 80, 217–217. https://doi.org/10.1029/99EO00169

Coby, A.J., Picardal, F.W., 2005. Inhibition of NO_3^- and NO_2^- reduction by microbial Fe(III) reduction: Evidence of a reaction between NO_2^- and cell surface-bound Fe^{2+}. Appl. Environ. Microbiol. 71, 5267–5274. https://doi.org/10.1128/AEM.71.9.5267-5274.2005

Cooper, A.B., Cooke, J.G., 1984. Nitrate loss and transformation in 2 vegetated headwater streams. New Zeal. J. Mar. Freshw. Res. 18, 441–450. https://doi.org/10.1080/00288330.1984.9516065

Cooper, D.C., Picardal, F.W., Schimmelmann, A., Coby, A.J., 2003. Chemical and Biological Interactions during Nitrate and Goethite Reduction by Shewanella putrefaciens 200 Chemical and Biological Interactions during Nitrate and Goethite Reduction by Shewanella putrefaciens 200. Appl. Environ. Microbiol. 69, 3517–3525. https://doi.org/10.1128/AEM.69.6.3517

Crane, R.A., Dickinson, M., Popescu, I.C., Scott, T.B., 2011. Magnetite and zero-valent iron nanoparticles for the remediation of uranium contaminated environmental water. Water Res. 45, 2931–2942. https://doi.org/10.1016/j.watres.2011.03.012

Critchley, K., Rudolph, D.L., Devlin, J.F., Schillig, P.C., 2014. Stimulating in situ denitrification in an aerobic, highly permeable municipal drinking water aquifer. J. Contam. Hydrol. 171, 66–80. https://doi.org/10.1016/j.jconhyd.2014.10.008

De Beer, D., Schramm, A., Santegoeds, C.M., Kühl, M., 1997. A nitrite microsensor for profiling environmental biofilms. Appl. Environ. Microbiol. 63, 973–977.

Dhakal, P., Matocha, C.J., Huggins, F.E., Vandiviere, M.M., 2013. Nitrite reactivity with magnetite. Environ. Sci. Technol. 47, 6206–6213. https://doi.org/10.1021/es304011w

Dybas, M.J., Hyndman, D.W., Heine, R., Tiedje, J., Linning, K., Wiggert, D., Voice, T., Zhao, X., Dybas, L., Criddle, C.S., 2002. Development, operation, and long-term performance of a full-scale biocurtain utilizing bioaugmentation. Environ. Sci. Technol. 36, 3635–3644. https://doi.org/10.1021/es0114557

EC, 2018a. Report from the Comission to the Council and the European Parliament on the implementation of Council Directive 91/676/EEC concerning the protection of waters against pollution caused by nitrates from agricultural sources based on Member State reports for [WWW Document]. URL http://ec.europa.eu/environment/water/water-nitrates/pdf/nitrates_directive_implementation_report.pdf (accessed 6.27.19).

EC, 2018b. Comission staff working document. Report from the Commission to the Council and the European Parliament on the implementation of Council Directive 91/676/EEC concerning the protection of waters against polllution caused by nitrates from agricultural sourc [WWW Document]. URL https://eur-lex.europa.eu/resource.html?uri=cellar:dab860df-4f7e-11e8-be1d-01aa75ed71a1.0001.02/DOC_6&format=PDF (accessed 6.27.19).

EC, 2018c. Water quality in the EU. Directive 91/676/EEC infographic for the period 2004-2015. [WWW Document]. URL http://ec.europa.eu/environment/water/water-nitrates/pdf/nitrates_directive_water_quality_infographic.pdf (accessed 6.27.19).

Ellis, A.S., Johnson, T.M., Bullen, T.D., 2002. Chromium isotopes and the fate of hexavalent chromium in the environment. Science (80), 295, 2060–2062. https://doi.org/10.1126/science.1068368

Emmerton, K.S., Jones, H.E., Leake, J.R., Michelsen, A., Read, D.J., Callaghan, T. V, 2001. Assimilation and isotopic fractionation of nitrogen by mycorrhizal fungi. New Phytol. 513–524.

Estrada, N.L., Böhlke, J.K., Sturchio, N.C., Gu, B., Harvey, G., Burkey, K.O., Grantz, D.A., McGrath, M.T., Anderson, T.A., Rao, B., Sevanthi, R., Hatzinger, P.B., Jackson, W.A., 2017. Stable isotopic composition of perchlorate and nitrate accumulated in plants: Hydroponic experiments and field data. Sci. Total Environ. 595, 556–566. https://doi.org/10.1016/j.scitotenv.2017.03.223

Fan, A.M., Steinberg, V.E., 1996. Health implications of nitrate and nitrite in drinking water: An update on methemoglobinemia occurrence and reproductive and developmental toxicity. Regul. Toxicol.

Pharmacol. 23, 35–43. https://doi.org/10.1006/rtph.1996.0006

Fowler, D., Coyle, M., Skiba, U., Sutton, M., Cape, J.N., Reis, S., Sheppard, L., Jenkins, A., Grizetti, B., Galloway, J.N., Vitousek, P., Leach, A., Bouwman, L., Butterbach-Bahl, K., Dentener, F., Stevenson, D., Amann, M., Voss, M., 2013. The global nitrogen cycle in the 21th century. Philisophical Trans. R. Soc. London, B Biol. Sci. 368, 20130165. https://doi.org/http://dx.doi.org/10.1098/rstb.2013.0164

Fukada, T., Hiscock, K.M., Dennis, P.F., Grischek, T., 2003. A dual isotope approach to identify denitrification in groundwater at a river-bank infiltration site. Water Res. 37, 3070–3078. https://doi.org/10.1016/S0043-1354(03)00176-3

Gaby, J.C., Buckley, D.H., 2011. A global census of nitrogenase diversity. Environ. Microbiol. 13, 1790–1799. https://doi.org/10.1111/j.1462-2920.2011.02488.x

Ge, S., Peng, Y., Wang, S., Lu, C., Cao, X., Zhu, Y., 2012. Nitrite accumulation under constant temperature in anoxic denitrification process: The effects of carbon sources and COD/NO_3-N. Bioresour. Technol. 114, 137–143. https://doi.org/10.1016/j.biortech.2012.03.016

Gibert, O., Pomierny, S., Rowe, I., Kalin, R.M., 2008. Selection of organic substrates as potential reactive materials for use in a denitrification permeable reactive barrier (PRB). Bioresour. Technol. 99, 7587–7596. https://doi.org/10.1016/j.biortech.2008.02.012

Gierczak, R., Devlin, J.F., Rudolph, D.L., 2007. Field test of a cross-injection scheme for stimulating in situ denitrification near a municipal water supply well. J. Contam. Hydrol. 89, 48–70. https://doi.org/10.1016/j.jconhyd.2006.08.001

Giles, M., Morley, N., Baggs, E.M., Daniell, T.J., 2012. Soil nitrate reducing processes - Drivers, mechanisms for spatial variation, and significance for nitrous oxide production. Front. Microbiol. 3, 1–16. https://doi.org/10.3389/fmicb.2012.00407

Glock, N., Roy, A.-S., Romero, D., Wein, T., Weissenbach, J., Revsbech, N.P., Høgslund, S., Clemens, D., Sommer, S., Dagan, T., 2019. Metabolic preference of nitrate over oxygen as an electron acceptor in foraminifera from the Peruvian oxygen minimum zone. Proc. Natl. Acad. Sci. 116, 2860–2865. https://doi.org/10.1073/pnas.1813887116

Grabb, K.C., Buchwald, C., Hansel, C.M., Wankel, S.D., 2017. A dual nitrite isotopic investigation of chemodenitrification by mineral-associated Fe(II) and its production of nitrous oxide. Geochim. Cosmochim. Acta 196, 388–402. https://doi.org/10.1016/j.gca.2016.10.026

Granger, J., Sigman, D.M., Lehmann, M.F., Tortell, P.D., 2008. Nitrogen and oxygen isotope fractionation during dissimilatory nitrate reduction by denitrifying bacteria. Limnol. Oceanogr. 53, 2533–2545. https://doi.org/10.4319/lo.2008.53.6.2533

Granger, J., Sigman, D.M., Rohde, M.M., Maldonado, M.T., Tortell, P.D., 2010. N and O isotope effects during nitrate assimilation by unicellular prokaryotic and eukaryotic plankton cultures. Geochim. Cosmochim. Acta 74, 1030–1040. https://doi.org/10.1016/j.gca.2009.10.044

Granger, J., Wankel, S.D., 2016. Isotopic overprinting of nitrification on denitrification as a ubiquitous and unifying feature of environmental nitrogen cycling. Proc. Natl. Acad. Sci. 113, E6391–E6400. https://doi.org/10.1073/pnas.1601383113

Grau-Martínez, A., Folch, A., Torrentó, C., Valhondo, C., Barba, C., Domènech, C., Soler, A., Otero, N., 2018. Monitoring induced denitrification during managed aquifer recharge in an infiltration pond. J. Hydrol. 561, 123–135. https://doi.org/10.1016/j.jhydrol.2018.03.044

Grau-Martínez, A., Torrentó, C., Carrey, R., Rodríguez-Escales, P., Domènech, C., Ghiglieri, G., Soler, A., Otero, N., 2017. Feasibility of two low-cost organic substrates for inducing denitrification in artificial recharge ponds: Batch and flow-through experiments. J. Contam. Hydrol. 198, 48–58. https://doi.org/10.1016/j.jconhyd.2017.01.001

Gumbricht, T., 1993. Nutrient removal capacity in submersed macrophyte pond systems in a temperature climate. Ecol. Eng. 2, 49–61. https://doi.org/10.1016/0925-8574(93)90026-C

Hallin, S., Pell, M., 1998. Metabolic properties of denitrifying bacteria adapting to methanol and ethanol in activated sludge. Water Res. 32, 13–18. https://doi.org/10.1016/S0043-1354(97)00199-1

He, Y., Lin, H., Dong, Y., Li, B., Wang, L., Chu, S., Luo, M., Liu, J., 2018. Zeolite supported Fe/Ni bimetallic nanoparticles for simultaneous removal of nitrate and phosphate: Synergistic effect and mechanism. Chem. Eng. J. 347, 669–681. https://doi.org/10.1016/j.cej.2018.04.088

Heil, J., Vereecken, H., Brüggemann, N., 2016. A review of chemical reactions of nitrification intermediates and their role in nitrogen cycling and nitrogen trace gas formation in soil. Eur. J. Soil Sci. 67, 23–39. https://doi.org/10.1111/ejss.12306

Her, J.J., Huang, J.S., 1995. Influences of carbon source and C/N ratio on nitrate/nitrite denitrification and carbon breakthrough. Bioresour. Technol. 54, 45–51. https://doi.org/10.1016/0960-8524(95)00113-1

Hill, R.D., Rinker, R.G., Dale Wilson, H., 1980. Atmospheric Nitrogen Fixation by Lighning. J. Atmos. Sci. 37, 179–192.

Högberg, M.N., Chen, Y., Högberg, P., 2007. Gross nitrogen mineralisation and fungi-to-bacteria ratios are negatively correlated in boreal forests. Biol. Fertil. Soils 44, 363–366. https://doi.org/10.1007/s00374-007-0215-9

Högberg, P., 1997. Tansley review no. 95 natural abundance in soil-plant systems. New Phytol. https://doi.org/10.1046/j.1469-8137.1997.00808.x

Hoppe, B., Kahl, T., Karasch, P., Wubet, T., Bauhus, J., Buscot, F., Krüger, D., 2014. Network analysis reveals ecological links between N-fixing bacteria and wood-decaying fungi. PLoS One 9. https://doi.org/10.1371/journal.pone.0088141

Hosono, T., Alvarez, K., Lin, I.T., Shimada, J., 2015. Nitrogen, carbon, and sulfur isotopic change during heterotrophic (Pseudomonas aureofaciens) and autotrophic (*Thiobacillus denitrificans*) denitrification reactions. J. Contam. Hydrol. 183, 72–81. https://doi.org/10.1016/j.jconhyd.2015.10.009

Howarth, R.W., Schlesinger, W.H., Vitousek, P.M., Aber, J.D., Likens, G.E., Matson, P.A., Schindler, D.W., Tilman, D.G., 1997. Human alteration of the global nitrogen cycle: sources and consequences. Ecol. Appl. 7, 737–750.

Huang, G., Huang, Y., Hu, H., Liu, F., Zhang, Y., Deng, R., 2015. Remediation of nitrate-nitrogen contaminated groundwater using a pilot-scale two-layer heterotrophic-autotrophic denitrification permeable reactive barrier with spongy iron/pine bark. Chemosphere 130, 8–16. https://doi.org/10.1016/j.chemosphere.2015.02.029

Hunkeler, D., Aravena, R., Butler, B.J., 1999. Monitoring Microbial Dechlorination of Tetrachloroethene (PCE) in Groundwater Using Compound-Specific Stable Carbon Isotope Ratios: Microcosm and Field Studies. Environ. Sci. Technol. 33, 2733-2738. https://doi.org/10.1021/es981282u

Ilyas, H., Masih, I., 2017. The performance of the intensified constructed wetlands for organic matter and nitrogen removal: A review. J. Environ. Manage. 198, 372–383. https://doi.org/10.1016/j.jenvman.2017.04.098

Innemanová, P., Velebová, R., Filipová, A., Čvančarová, M., Pokorný, P., Němeček, J., Cajthaml, T., 2015. Anaerobic in situ biodegradation of TNT using whey as an electron donor: a case study. N. Biotechnol. 32, 701–709. https://doi.org/10.1016/j.nbt.2015.03.014

Jacobs, A.E., Harrison, J.A., 2014. Effects of floating vegetation on denitrification, nitrogen retention, and greenhouse gas production in wetland microcosms. Biogeochemistry 119, 51–66. https://doi.org/10.1007/s10533-013-9947-9

Jensen, V.B., Darby, J.L., Seidel, C., Gorman, C., 2012. Drinking Water Treatment for Nitrate. Technical Report 6 in Addressing NItrate in Califronia's Drinking Water with a Foucs on Tulare Lake Basin and Salinas Valley Groundwater. Report for the State Water Resources Control Board Report to the Legislature. Addressing NItrate Califronia's Drink. Water with a Foucs Tulare Lake Basin Salinas Val. Groundwater. Rep. State Water Resour. Control Board Rep. to Legis.

Jones, L.C., Peters, B., Lezama Pacheco, J.S., Casciotti, K.L., Fendorf, S., 2015. Stable Isotopes and Iron Oxide Mineral Products as Markers of Chemodenitrification. Environ. Sci. Technol. 49, 3444–3452. https://doi.org/10.1021/es504862x

Jones, Z.L., Jasper, J.T., Sedlak, D.L., Sharp, J.O., 2017. Sulfide-Induced Dissimilatory Nitrate Reduction to Ammonium Supports Anaerobic Ammonium Oxidation (Anammox) in an Open-Water Unit Process

Wetland 83, 1–14.

Jurado, A., Borges, A. V., Brouyère, S., 2017. Dynamics and emissions of N_2O in groundwater: A review. Sci. Total Environ. 584–585, 207–218. https://doi.org/10.1016/j.scitotenv.2017.01.127

Justic, D., Rabalais, N., Turner, R.E., Dıaz, R.J., 2009. Global change and eutrophication of coastal waters. ICES J. Mar. Sci. 1528–1537.

Kamp, A., Høgslund, S., Risgaard-Petersen, N., Stief, P., 2015. Nitrate storage and dissimilatory nitrate reduction by eukaryotic microbes. Front. Microbiol. 6, 1–15. https://doi.org/10.3389/fmicb.2015.01492

Kelso, B.H.L., Smith, R. V., Laughlin, R.J., Lennox, S.D., 1997. Dissimilatory nitrate reduction in anaerobic sediments leading to river nitrite accumulation. Appl. Environ. Microbiol. 63, 4679–4685.

Khan, I.A., Spalding, R.F., 2004. Enhanced in situ denitrification for a municipal well. Water Res. 38, 3382–3388. https://doi.org/10.1016/j.watres.2004.04.052

Klueglein, N., Kappler, A., 2013. Abiotic oxidation of Fe(II) by reactive nitrogen species in cultures of the nitrate-reducing Fe(II) oxidizer Acidovorax sp. BoFeN1 - questioning the existence of enzymatic Fe(II) oxidation. Geobiology 11, 180–190. https://doi.org/10.1111/gbi.12019

Knöller, K., Vogt, C., Haupt, M., Feisthauer, S., Richnow, H.H., 2011. Experimental investigation of nitrogen and oxygen isotope fractionation in nitrate and nitrite during denitrification. Biogeochemistry 103, 371–384. https://doi.org/10.1007/s10533-010-9483-9

Knowles, R., 1982. Denitrification. Microbiol. Rev. 46, 43–70.

Kong, L., Wang, Y. Bin, Zhao, L.N., Chen, Z.H., 2009. Enzyme and root activities in surface-flow constructed wetlands. Chemosphere 76, 601–608. https://doi.org/10.1016/j.chemosphere.2009.04.056

Kraft, B., Strous, M., Tegetmeyer, H.E., 2011. Microbial nitrate respiration - Genes, enzymes and environmental distribution. J. Biotechnol. 155, 104–117. https://doi.org/10.1016/j.jbiotec.2010.12.025

Kuenen, J.G., van de Graaf, a a, Mulder, a, de Bruijn, P., Jetten, M.S., Robertson, L. a, 1995. Anaerobic oxidation of ammonium is a biologically mediated process. Appl. Environ. Microbiol. 61, 1246–51.

Kuypers, M.M.M., Marchant, H.K., Kartal, B., 2018. The microbial nitrogen-cycling network. Nat. Rev. Microbiol. 16, 263–276. https://doi.org/10.1038/nrmicro.2018.9

Kuypers M.M.M., Sliekers A.O., Lavik G., Schmid M., Jorgensen B.B., Kuenen J.G., Sinnenghe Damste J.S., Strous M., Jetten M.S.M., 2003. Anaerobic ammonium oxidation by anammox bacteria in the Black Sea. Nature 422, 608–611. https://doi.org/10.1038/nature01526.1.

Laverman, A.M., Pallud, C., Abell, J., Cappellen, P. Van, 2012. Comparative survey of potential nitrate and sulfate reduction rates in aquatic sediments. Geochim. Cosmochim. Acta 77, 474–488. https://doi.org/10.1016/j.gca.2011.10.033

Li, M., Feng, C., Zhang, Z., Yang, S., Sugiura, N., 2010. Treatment of nitrate contaminated water using an electrochemical method. Bioresour. Technol. 101, 6553–6557. https://doi.org/10.1016/j.biortech.2010.03.076

Lin, J.T., Stewart, V., 1997. Nitrate Assimilation by Bacteria 39, 1–30. https://doi.org/10.1016/S0065-2911(08)60014-4

Lovley, D.R., Phillips, E.J.P., 1992. Reduction of uranium by Desulfovibrio desulfuricans. Appl. Environ. Microbiol.

Lu, S., Hu, H., Sun, Y., Yang, J., 2009. Effect of carbon source on the denitrification in constructed wetlands. J. Environ. Sci. 21, 1036–1043. https://doi.org/10.1016/S1001-0742(08)62379-7

Mariotti, A., Germon, J.C., Hubert, P., Kaiser, P., Letolle, R., Tardieux, A., Tardieux, P., 1981. Experimental determination of nitrogen kinetic isotope fractionation: Some principles; illustration for the denitrification and nitrification processes. Plant Soil 62, 413–430. https://doi.org/10.1007/BF02374138

Mariotti, A., Landreau, A., Simon, B., 1988. ^{15}N isotope biogeochemistry and natural denitrification process in groundwater: Application to the chalk aquifer of northern France. Geochim. Cosmochim. Acta 52, 1869–1878. https://doi.org/10.1016/0016-7037(88)90010-5

Martin, T.S., Casciotti, K.L., 2016. Nitrogen and oxygen isotopic fractionation during microbial nitrite reduction. Limnol. Oceanogr. 61, 1134–1143. https://doi.org/10.1002/lno.10278

Masclaux-Daubresse, C., Daniel-Vedele, F., Dechorgnat, J., Chardon, F., Gaufichon, L., Suzuki, A., 2010. Nitrogen uptake, assimilation and remobilization in plants: Challenges for sustainable and productive agriculture. Ann. Bot. 105, 1141–1157. https://doi.org/10.1093/aob/mcq028

Matocha, C.J., Coyne, M.S., 2007. Short-term Response of Soil Iron to Nitrate Addition. Soil Sci. Soc. Am. J. 71, 108. https://doi.org/10.2136/sssaj2005.0170

Mclean, J.E., Ervin, J., Zhou, J., Sorensen, D.L., Dupont, R.R., 2015. Biostimulation and Bioaugmentation to Enhance Reductive Dechlorination of TCE in a Long-Term Flow Through Column Study. Groundw. Monit. Remediat. 35, 76–88. https://doi.org/10.1111/gwmr.12113

Melton, E.D., Swanner, E.D., Behrens, S., Schmidt, C., Kappler, A., 2014. The interplay of microbially mediated and abiotic reactions in the biogeochemical Fe cycle. Nat. Rev. Microbiol. 12, 797–808. https://doi.org/10.1038/nrmicro3347

Miettinen, H., Pumpanen, J., Heiskanen, J.J., 2015. Towards a more comprehensive understanding of lacustrine greenhouse gas dynamics - two-year measurements of concentrations and fluxes of CO_2, CH_4 and N_2O in a typical boreal lake surrounded by managed forests. Boreal Environ. Res. 20, 75–89.

Moreno-vivián, C., Cabello, P., Blasco, R., Castillo, F., Cabello, N., Marti, M., Moreno-vivia, C., 1999. Prokaryotic Nitrate Reduction : Molecular Properties and Functional Distinction among Bacterial Nitrate Reductases MINIREVIEW Prokaryotic Nitrate Reduction : Molecular Properties and Functional Distinction among Bacterial Nitrate Reductases 181, 6573–6584.

Morley, N., Baggs, E.M., Dörsch, P., Bakken, L., 2008. Production of NO, N_2O and N_2 by extracted soil bacteria, regulation by NO_2^- and O_2 concentrations. FEMS Microbiol. Ecol. 65, 102–112. https://doi.org/10.1111/j.1574-6941.2008.00495.x

Myrold, D.D., Posavatz, N.R., 2007. Potential importance of bacteria and fungi in nitrate assimilation in soil. Soil Biol. Biochem. 39, 1737–1743. https://doi.org/10.1016/j.soilbio.2007.01.033

Nancharaiah, Y. V., Dodge, C., Venugopalan, V.P., Narasimhan, S. V., Francis, A.J., 2010. Immobilization of Cr(VI) and Its reduction to Cr(III) phosphate by granular biofilms comprising a mixture of microbes. Appl. Environ. Microbiol. 76, 2433–2438. https://doi.org/10.1128/AEM.02792-09

Nascimento, C., Krishnamurthy, R. V, 1997. Inorganic Carbon in Denitrifying Environments Investigation. Geophys. Res. Lett. 24, 1511–1514.

Needoba, J.A., Sigman, D.M., Harrison, P.J., 2004. The mechanism of isotope fractionation during algal nitrate assimilation as illuminated by the $^{15}N/^{14}N$ of intracellular nitrate. J. Phycol. 40, 517–522. https://doi.org/10.1111/j.1529-8817.2004.03172.x

Němeček, J., Pokorný, P., Lacinová, L., Černík, M., Masopustová, Z., Lhotský, O., Filipová, A., Cajthaml, T., 2015. Combined abiotic and biotic in-situ reduction of hexavalent chromium in groundwater using nZVI and whey: A remedial pilot test. J. Hazard. Mater. 300, 670–679. https://doi.org/10.1016/j.jhazmat.2015.07.056

Orozco, A.M.F., Contreras, E.M., Zaritzky, N.E., 2010. Cr(VI) reduction capacity of activated sludge as affected by nitrogen and carbon sources, microbial acclimation and cell multiplication. J. Hazard. Mater. 176, 657–665. https://doi.org/10.1016/j.jhazmat.2009.11.082

Otero, N., Canals, À., Soler, A., 2007. Using dual-isotope data to trace the origin and processes of dissolved sulphate: A case study in Calders stream (Llobregat basin, Spain). Aquat. Geochemistry 13, 109–126. https://doi.org/10.1007/s10498-007-9010-3

Otero, N., Torrentó, C., Soler, A., Menció, A., Mas-Pla, J., 2009. Monitoring groundwater nitrate attenuation in a regional system coupling hydrogeology with multi-isotopic methods: The case of Plana de Vic (Osona, Spain). Agric. Ecosyst. Environ. 133, 103–113. https://doi.org/10.1016/j.agee.2009.05.007

Öztürk, N., Bektaş, T.E., 2004. Nitrate removal from aqueous solution by adsorption onto various materials. J. Hazard. Mater. 112, 155–162. https://doi.org/10.1016/j.jhazmat.2004.05.001

Palau, J., Marchesi, M., Chambon, J.C.C., Aravena, R., Canals, À., Binning, P.J., Bjerg, P.L., Otero, N., Soler,

A., 2014. Multi-isotope (carbon and chlorine) analysis for fingerprinting and site characterization at a fractured bedrock aquifer contaminated by chlorinated ethenes. Sci. Total Environ. 475, 61–70. https://doi.org/10.1016/j.scitotenv.2013.12.059

Peng, Y.Z., Ma, Y., Wang, S.Y., 2007. Denitrification potential enhancement by addition of external carbon sources in a pre-denitrification process. J. Environ. Sci. 19, 284–289. https://doi.org/10.1016/S1001-0742(07)60046-1

Philippot, L., Hallin, S., Schloter, M., 2007. Ecology of Denitrifying Prokaryotes in Agricultural Soil, in: Advances in Agronomy. pp. 249–305. https://doi.org/10.1016/S0065-2113(07)96003-4

Pintar, A., Batista, J., 1999. Catalytic hydrogenation of aqueous nitrate solutions in fixed-bed reactors. Catal. Today 53, 35–50. https://doi.org/10.1016/S0920-5861(99)00101-7

Puig, R., Folch, A., Menció, A., Soler, A., Mas-Pla, J., 2013. Multi-isotopic study (^{15}N, ^{34}S, ^{18}O, ^{13}C) to identify processes affecting nitrate and sulfate in response to local and regional groundwater mixing in a large-scale flow system. Appl. Geochemistry 32, 129–141. https://doi.org/10.1016/j.apgeochem.2012.10.014

Puig, R., Soler, A., Widory, D., Mas-Pla, J., Domènech, C., Otero, N., 2017. Characterizing sources and natural attenuation of nitrate contamination in the Baix Ter aquifer system (NE Spain) using a multi-isotope approach. Sci. Total Environ. 580, 518–532. https://doi.org/10.1016/j.scitotenv.2016.11.206

Rakshit, S., Matocha, C.J., Coyne, M.S., Sarkar, D., 2016. Nitrite reduction by Fe(II) associated with kaolinite. Int. J. Environ. Sci. Technol. 13, 1329–1334. https://doi.org/10.1007/s13762-016-0971-x

Reay, D.S., Davidson, E.A., Smith, K.A., Smith, P., Melillo, J.M., Dentener, F., Crutzen, P.J., 2012. Global agriculture and nitrous oxide emissions. Nat. Clim. Chang. 2, 410–416. https://doi.org/10.1038/nclimate1458

Richardson, D.J., Watmough, N.J., 1999. Inorganic nitrogen metabolism in bacteria. Curr. Opin. Chem. Biol. 3, 207–219. https://doi.org/10.1016/S1367-5931(99)80034-9

Rivett, M.O., Buss, S.R., Morgan, P., Smith, J.W.N., Bemment, C.D., 2008. Nitrate attenuation in groundwater: A review of biogeochemical controlling processes. Water Res. 42, 4215–4232. https://doi.org/10.1016/j.watres.2008.07.020

Robertson, W.D., Blowes, D.W., Ptacek, C.J., Cherry, J.A., 2000. Long-Term Performance of In Situ Reactive Barriers for Nitrate Remediation. Ground Water 38, 689–695.

Robertson, W.D., Vogan, J.L., Lombardo, P.S., 2008. Nitrate Removal Rates in a 15 Year Old Permeable Reactive Barrier Treating Septic System Nitrate. Ground Water Monit. Remediat. 28, 65–72.

Robertson, W.D., Yeung, N., VanDriel, P.W., Lombardo, P.S., 2005. High-permeability layers for remediation of ground water; go wide, not deep. Ground Water 43, 574–581. https://doi.org/10.1111/j.1745-6584.2005.0062.x

Rodríguez-Escales, P., Folch, A., Vidal-Gavilan, G., van Breukelen, B.M., 2016. Modeling biogeochemical processes and isotope fractionation of enhanced in situ biodenitrification in a fractured aquifer. Chem. Geol. 425, 52–64. https://doi.org/10.1016/j.chemgeo.2016.01.019

Rogers, K.H., Breen, P.F., Chick, A.J., 1991. Nitrogen Removal in Experimental Wetland Treatment Systems: Evidence for the Role of Aquatic Plants. Res. J. Water Pollut. Control Fed. 63, 934–941.

Rütting, T., Boeckx, P., Müller, C., Klemedtsson, L., 2011. Assessment of the importance of dissimilatory nitrate reduction to ammonium for the terrestrial nitrogen cycle. Biogeosciences 8, 1779–1791. https://doi.org/10.5194/bg-8-1779-2011

Salminen, J.M., Petäjäjärvi, S.J., Tuominen, S.M., Nystén, T.H., 2014. Ethanol-based in situ bioremediation of acidified, nitrate-contaminated groundwater. Water Res. 63, 306–315. https://doi.org/10.1016/j.watres.2014.06.013

Sanz-Luque, E., Chamizo-Ampudia, A., Llamas, A., Galvan, A., Fernandez, E., 2015. Understanding nitrate assimilation and its regulation in microalgae. Front. Plant Sci. 6. https://doi.org/10.3389/fpls.2015.00899

Sapountzis, P., de Verges, J., Rousk, K., Cilliers, M., Vorster, B.J., Poulsen, M., 2016. Potential for nitrogen fixation in the fungus-growing termite symbiosis. Front. Microbiol. 7, 1–5.

https://doi.org/10.3389/fmicb.2016.01993

Scott, J.T., McCarthy, M.J., Gardner, W.S., Doyle, R.D., 2008. Denitrification, dissimilatory nitrate reduction to ammonium, and nitrogen fixation along a nitrate concentration gradient in a created freshwater wetland. Biogeochemistry 87, 99–111. https://doi.org/10.1007/s10533-007-9171-6

Sebilo, M., Mayer, B., Nicolardot, B., Pinay, G., Mariotti, A., 2013. Long-term fate of nitrate fertilizer in agricultural soils. Proc. Natl. Acad. Sci. U. S. A. 110, 18185–9. https://doi.org/10.1073/pnas.1305372110

Sharma, B., Ahlert, R.C., 1977. Nitrification and nitrogen removal. Water Res. 11, 897–925. https://doi.org/10.1016/0043-1354(77)90078-1

Shoun, H., Kim, D.H., Uchiyama, H., Sugiyama, J., 1992. Denitrification by fungi. FEMS Microbiol. Lett. 94, 277–281. https://doi.org/10.1016/0378-1097(92)90643-3

Si, Z., Song, X., Wang, Y., Cao, X., Zhao, Y., Wang, B., Chen, Y., Arefe, A., 2018. Intensified heterotrophic denitrification in constructed wetlands using four solid carbon sources: Denitrification efficiency and bacterial community structure. Bioresour. Technol. 267, 416–425. https://doi.org/10.1016/j.biortech.2018.07.029

Sirivedhin, T., Gray, K.A., 2006. Factors affecting denitrification rates in experimental wetlands: Field and laboratory studies. Ecol. Eng. 26, 167–181. https://doi.org/10.1016/j.ecoleng.2005.09.001

Soana, E., Balestrini, R., Vincenzi, F., Bartoli, M., Castaldelli, G., 2017. Mitigation of nitrogen pollution in vegetated ditches fed by nitrate-rich spring waters. Agric. Ecosyst. Environ. 243, 74–82. https://doi.org/10.1016/j.agee.2017.04.004

Spoelstra, J., Schiff, S.L., Semkin, R.G., Jeffries, D.S., Elgood, R.J., 2010. Nitrate attenuation in a small temperate wetland following forest harvest. For. Ecol. Manage. 259, 2333–2341. https://doi.org/10.1016/j.foreco.2010.03.006

Strebel, O., Böttcher, J., Fritz, P., 1990. Use of isotope fractionation of sulfate-sulfur and sulfate-oxygen to assess bacterial desulfurication in a sandy aquifer. J. Hydrol. 121, 155–172. https://doi.org/10.1016/0022-1694(90)90230-U

Swanner, E.D., Bayer, T., Wu, W., Hao, L., Obst, M., Sundman, A., Byrne, J.M., Michel, F.M., Kleinhanns, I.C., Kappler, A., Schoenberg, R., 2017. Iron Isotope Fractionation during Fe(II) Oxidation Mediated by the Oxygen-Producing Marine Cyanobacterium Synechococcus PCC 7002. Environ. Sci. Technol. 51, 4897–4906. https://doi.org/10.1021/acs.est.6b05833

Tartakovsky, B., Millette, D., Del Isle, S., Guiot, S.R., 2002. Ethanol-stimulated bioremediation of nitrate-contaminated ground water. Gr. Water Monit. Remediat. https://doi.org/10.1111/j.1745-6592.2002.tb00656.x

Teiter, S., Mander, Ü., 2005. Emission of N_2O, N_2, CH_4, and CO_2 from constructed wetlands for wastewater treatment and from riparian buffer zones. Ecol. Eng. 25, 528–541. https://doi.org/10.1016/j.ecoleng.2005.07.011

Torrentó, C., Cama, J., Urmeneta, J., Otero, N., Soler, A., 2010. Denitrification of groundwater with pyrite and Thiobacillus denitrificans. Chem. Geol. 278, 80–91. https://doi.org/10.1016/j.chemgeo.2010.09.003

Torrentó, C., Urmeneta, J., Otero, N., Soler, A., Viñas, M., Cama, J., 2011. Enhanced denitrification in groundwater and sediments from a nitrate-contaminated aquifer after addition of pyrite. Chem. Geol. 287, 90–101. https://doi.org/10.1016/j.chemgeo.2011.06.002

Trois, C., Pisano, G., Oxarango, L., 2010. Alternative solutions for the bio-denitrification of landfill leachates using pine bark and compost. J. Hazard. Mater. 178, 1100–1105. https://doi.org/10.1016/j.jhazmat.2010.01.054

Tsushima, K., Ueda, S., Ohno, H., Ogura, N., Katase, T., Watanabe, K., 2006. Nitrate decrease with isotopic fractionation in riverside sediment column during infiltration experiment. Water. Air. Soil Pollut. 174, 47–61. https://doi.org/10.1007/s11270-005-9024-7

Vidal-Gavilan, G., Folch, A., Otero, N., Solanas, A.M., Soler, A., 2013. Isotope characterization of an in situ biodenitrification pilot-test in a fractured aquifer. Appl. Geochemistry 32, 153–163. https://doi.org/10.1016/j.apgeochem.2012.10.033

Vidal-Gavilan, G., Carrey, R., Solanas, A., Soler, A., 2014. Feeding strategies for groundwater enhanced biodenitrification in an alluvial aquifer: Chemical, microbial and isotope assessment of a 1D flow-through experiment. Sci. Total Environ. 494–495, 241–251. https://doi.org/10.1016/j.scitotenv.2014.06.100

Virdis, B., Rabaey, K., Rozendal, R.A., Yuan, Z., Keller, J., 2010. Simultaneous nitrification, denitrification and carbon removal in microbial fuel cells. Water Res. 44, 2970–2980. https://doi.org/10.1016/j.watres.2010.02.022

Vitoria, L., Otero, N., Soler, A., Canals, À., 2004. Fertilizer Characterization: Isotopic Data (N, S, O, C, and Sr). Environ. Sci. Technol. 38, 3254–3262. https://doi.org/10.1021/es0348187

Vitòria, L., Soler, A., Canals, À., Otero, N., 2008. Environmental isotopes (N, S, C, O, D) to determine natural attenuation processes in nitrate contaminated waters: Example of Osona (NE Spain). Appl. Geochemistry 23, 3597–3611. https://doi.org/10.1016/j.apgeochem.2008.07.018

Vitousek, P.M., Aber, J.D., Howarth, R.W., Likens, G.E., Matson, P.A., Schindler, D.W., Schlesinger, W.H., Tilman, D.G., 1997. Summary for Policymakers, in: Intergovernmental Panel on Climate Change (Ed.), Climate Change 2013 - The Physical Science Basis. Cambridge University Press, Cambridge, pp. 1–30. https://doi.org/10.1017/CBO9781107415324.004

Volkmer, B.G., Ernst, B., Simon, J., Kuefer, R., Bartsch, G., Bach, D., Gschwend, J.E., 2005. Influence of nitrate levels in drinking water on urological malignancies: A community-based cohort study. BJU Int. 95, 972–976. https://doi.org/10.1111/j.1464-410X.2005.05450.x

Vymazal, J., 2007. Removal of nutrients in various types of constructed wetlands. Sci. Total Environ. 380, 48–65. https://doi.org/10.1016/j.scitotenv.2006.09.014

Wade Miller, G., 2006. Integrated concepts in water reuse: Managing global water needs. Desalination 187, 65–75. https://doi.org/10.1016/j.desal.2005.04.068

Wang, M., Hu, R., Zhao, J., Kuzyakov, Y., Liu, S., 2016. Iron oxidation affects nitrous oxide emissions via donating electrons to denitrification in paddy soils. Geoderma 271, 173–180. https://doi.org/10.1016/j.geoderma.2016.02.022

Ward, M.H., DeKok, T.M., Levallois, P., Brender, J., Gulis, G., Nolan, B.T., VanDerslice, J., 2005. Workgroup Report: Drinking-Water Nitrate and Health - Recent Findings and Research Needs. Environ. Health Perspect. 113, 1607–1614. https://doi.org/10.1289/ehp.8043

Waser, N.A.D., Harrison, P.J., Nielsen, B., Calvert, S.E., Turpin, D.H., 1998. Nitrogen isotope fractionation during the uptake and assimilation of nitrate, nitrite, ammonium, and urea by a marine diatom. Limnol. Oceanogr. 43, 215–224. https://doi.org/10.4319/lo.1998.43.2.0215

Wassenaar, L.I., 1995. Evaluation of the origin and fate of nitrate in the Abbotsford Aquifer using the isotopes of ^{15}N and ^{18}O in NO_3^-. Appl. Geochemistry 10, 391–405. https://doi.org/10.1016/0883-2927(95)00013-A

Weymann, D., Geistlinger, H., Well, R., Von Der Heide, C., Flessa, H., 2010. Kinetics of N_2O production and reduction in a nitrate-contaminated aquifer inferred from laboratory incubation experiments. Biogeosciences 7, 1953–1972. https://doi.org/10.5194/bg-7-1953-2010

WHO, 2011. Guidelines for Drinking-water Quality 4th ed., WHO, Geneva, p. 340. World Heal. Organ. https://doi.org/10.1016/S1462-0758(00)00006-6

Widory, D., Pételet-Giraud, E., Négrel, P., Ladouche, B., 2005. Tracking the sources of nitrate in groundwater using coupled nitrogen and boron isotopes: a synthesis. Environ. Sci. Technol. 39, 539–548. https://doi.org/10.1021/es0493897

Wilderer, P.A., Jones, W.L., Dau, U., 1987. Competition in denitrification systems affecting reduction rate and accumulation of nitrite. Water Res. 21, 239–245. https://doi.org/10.1016/0043-1354(87)90056-X

Wu, H., Zhang, J., Ngo, H.H., Guo, W., Hu, Z., Liang, S., Fan, J., Liu, H., 2015. A review on the sustainability of constructed wetlands for wastewater treatment: Design and operation. Bioresour. Technol. 175, 594–601. https://doi.org/10.1016/j.biortech.2014.10.068

Wunderlich, A., Meckenstock, R., Einsiedl, F., 2012. Effect of different carbon substrates on nitrate stable isotope fractionation during microbial denitrification. Environ. Sci. Technol. 46, 4861–4868. https://doi.org/10.1021/es204075b

Wunderlich, A., Meckenstock, R.U., Einsiedl, F., 2013. A mixture of nitrite-oxidizing and denitrifying microorganisms affects the $\delta^{18}O$ of dissolved nitrate during anaerobic microbial denitrification depending on the $\delta^{18}O$ of ambient water. Geochim. Cosmochim. Acta 119, 31–45. https://doi.org/10.1016/j.gca.2013.05.028

Yang, Y., Chen, T., Morrison, L., Gerrity, S., Collins, G., Porca, E., Li, R., Zhan, X., 2017. Nanostructured pyrrhotite supports autotrophic denitrification for simultaneous nitrogen and phosphorus removal from secondary effluents. Chem. Eng. J. 328, 511–518. https://doi.org/10.1016/j.cej.2017.07.061

Zahran, H.H., 1999. Rhizobium-legume symbiosis and nitrogen fixation under severe conditions and in an arid climate. Microbiol. Mol. Biol. Rev. 63, 968–89, table of contents.

Zelmanov, G., Semiat, R., 2008. Iron(3) oxide-based nanoparticles as catalysts in advanced organic aqueous oxidation. Water Res. 42, 492–498. https://doi.org/10.1016/j.watres.2007.07.045

Zumft, W.G., 1997. Cell biology and molecular basis of denitrification. Microbiol. Mol. Biol. Rev. 61, 533–616.

2. STUDY SITES

2.1. Nitrate polluted aquifer in Sant Andreu de Llavaneres (Spain)

In Catalunya (north-east Spain), twelve areas have been designated as NVZ (DECRET 136/2009; DECRET 283/1998) (**Figure 2.1**). During the last decade, more than 50 % of the wells monitored by the Catalan Water Agency in the Maresme area (NVZ number 2 in **Figure 2.1**) presented NO_3^- concentrations above 50 mg/L (ACA, 2019), the threshold value for consumption set by the directive 98/83/EC. Despite the Maresme was designated a NVZ in 1998 and good agricultural practices were implemented, NO_3^- is still exceeding 200 mg/L in a number of wells (ACA, 2019).

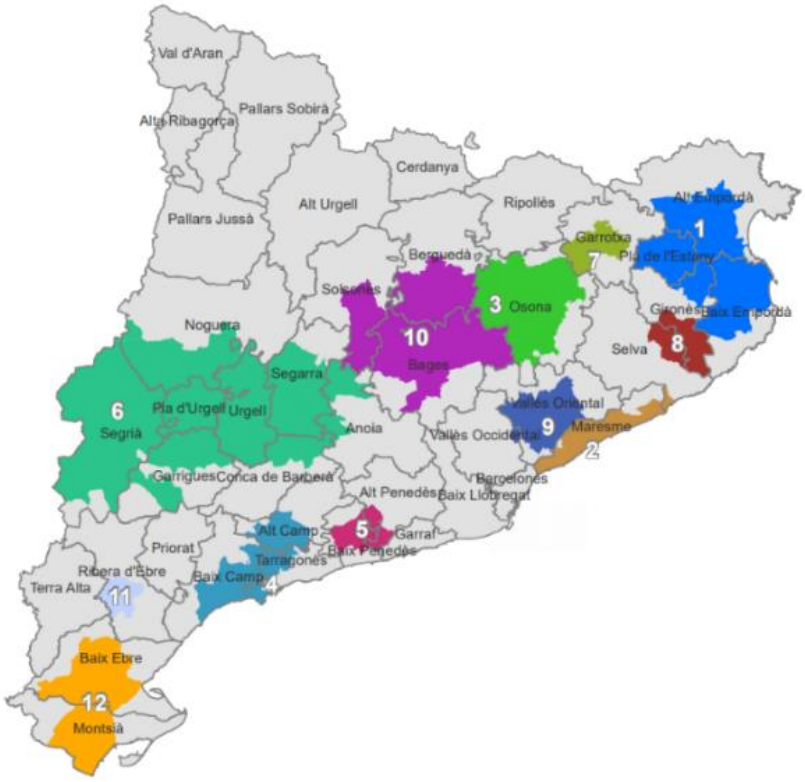

Figure 2.1. Designated nitrate vulnerable zones in Catalunya. Source: Generalitat de Catalunya, Departament d'Agricultura, Ramaderia, Pesca, 2015.

In the framework of the Life+ InSiTrate project, a pilot-plant was set up in Sant Andreu de Llavaneres (Maresme) to produce safe drinking water from NO_3^--polluted groundwater by inducing in-situ denitrification by acetic acid injections (2015-2017). The pilot-plant

consisted of two electron donor injection wells (I1 and I2), one treated water extraction well (EW) at an approximate distance of 30 m from the two injection wells, three monitoring piezometers (PZ1, PZ2 and PZ3) between the injection and the extraction wells, and one monitoring well (MW) downstream, located out of the area affected by the biostimulation (**Figure 2.2**).

The project site is located 10 m nearby the San Andreu de Llavaneres Creek. The pilot plant is placed in an alluvial aquifer, formed by Quaternary (Holocene) coarse sand and silt sediments overlying an altered Paleozoic granite formation located at 40 m depth (IGC, 2011). Before the biostimulation, the area was characterized by means of pumping and tracing assays. The obtained permeability was between 70 and 100 m/d, transmissivity was between 800 and 1000 m^2/d and the average porosity was 0.5. The average aquifer temperature was 20.3 ºC (SD = 1.4). Prior to the treatment, the aquifer showed aerobic conditions and natural NO_3^- attenuation was not observed, discarding the availability of electron donors in the aquifer that could promote denitrification intrinsically.

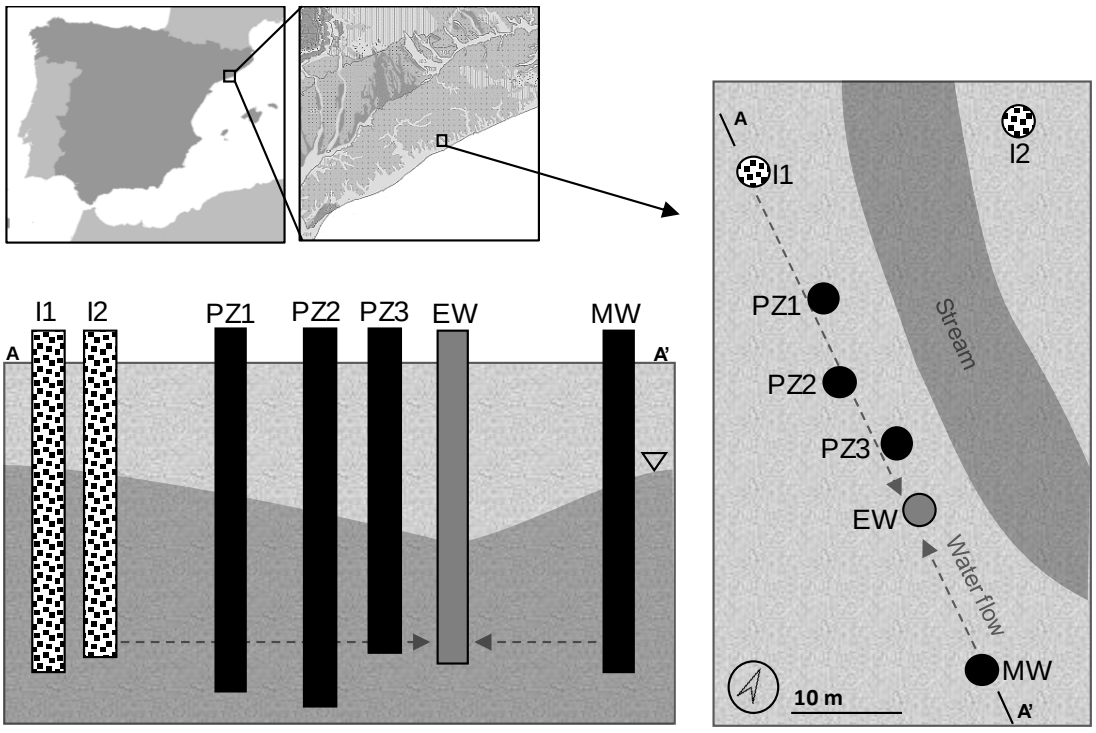

Figure 2.2. Pilot-plant scheme. Location, schematic map and cross-section of the pilot-plant. I1 and I2 are the injection wells; PZ1, PZ2 and PZ3 the monitoring piezometers; EW the extraction well and MW the monitoring well. I2 is projected on the cross-section. Arrows depict the flow direction when the EW is operating. Natural flow direction is from I1 to MW.

2.2. Nitrate polluted aquifer in the Matanza-Riachuelo basin (Argentina)

The Matanza-Riachuelo River Basin (MRB), located to the NE of the Buenos Aires province (**Figure 2.3.A**) is the most populated (>4 million people), industrialized and polluted basin in Argentina (Zabala et al., 2016). Groundwater, in some areas within the MRB, is affected by both Cr^{6+} (up to 5 mg/L) and NO_3^- (>100 mg/L) pollution (Sanci et al., 2018). The main source of Cr^{6+} contamination is related to a chemical industry plant that operated from 1968 to 1990, producing bichromates, chromic acid, sulfuric acid and tannery products. During the operation period, the processing residues containing Cr^{6+} salts were disposed untreated into nearby unlined piles where the dissolution of these waste salts promoted the migration of Cr^{6+} through the vadose zone into groundwater. In the case of NO_3^-, the pollution is likely due to septic system leakage, which could also be a source of organic carbon in the groundwater. The study area is located near this chemical industry, in the San Ignacio neighborhood (Jagüel town), at the lowest stretch of the Ortega Stream sub basin, a tributary of the Matanza-Riachuelo River (**Figure 2.3.B**). A few monitoring wells belonging to the basin authority ACUMAR (P13, P28 and P29) and private supply wells (P15, P16, P21, P22, P26, P27, P31, P33 and P34) are accessible for sampling within this area.

The MRB contains two aquifer systems, the Upper aquifer of medium to low productivity and a variable water quality, and the Puelche Aquifer, of medium to high productivity and good water quality (Zabala et al., 2016). The Upper Aquifer holds the water table and receives natural recharge by infiltration of rainfall. Its thickness is approximately 40 m (Mancino et al., 2013), and consists of sandy-clayey-silts loess (Holocene), homogeneous fine-grained loess and sandy loess (Pleistocene), and interbedded carbonate (tosca). The Puelche Aquifer has a maximum thickness of 60 m and consist of quartz sands in the lower sandy section and silts and clay that are interbedded towards the top (Upper Pliocene to Pleistocene). These silty clay sediments behave as an aquitard of heterogeneous thickness but in some sectors of the lower basin this aquitard does not exist because the sediments of the Upper Aquifer are in direct contact with the sands of the Puelche Aquifer. Due to the Puelche Aquifer not outcropping in the MRB, its recharge occurs directly from the Upper Aquifer by vertical filtration (Vives et al., 2013). The regional groundwater flow in the two aquifers is SW to NE (Vives et al., 2013).

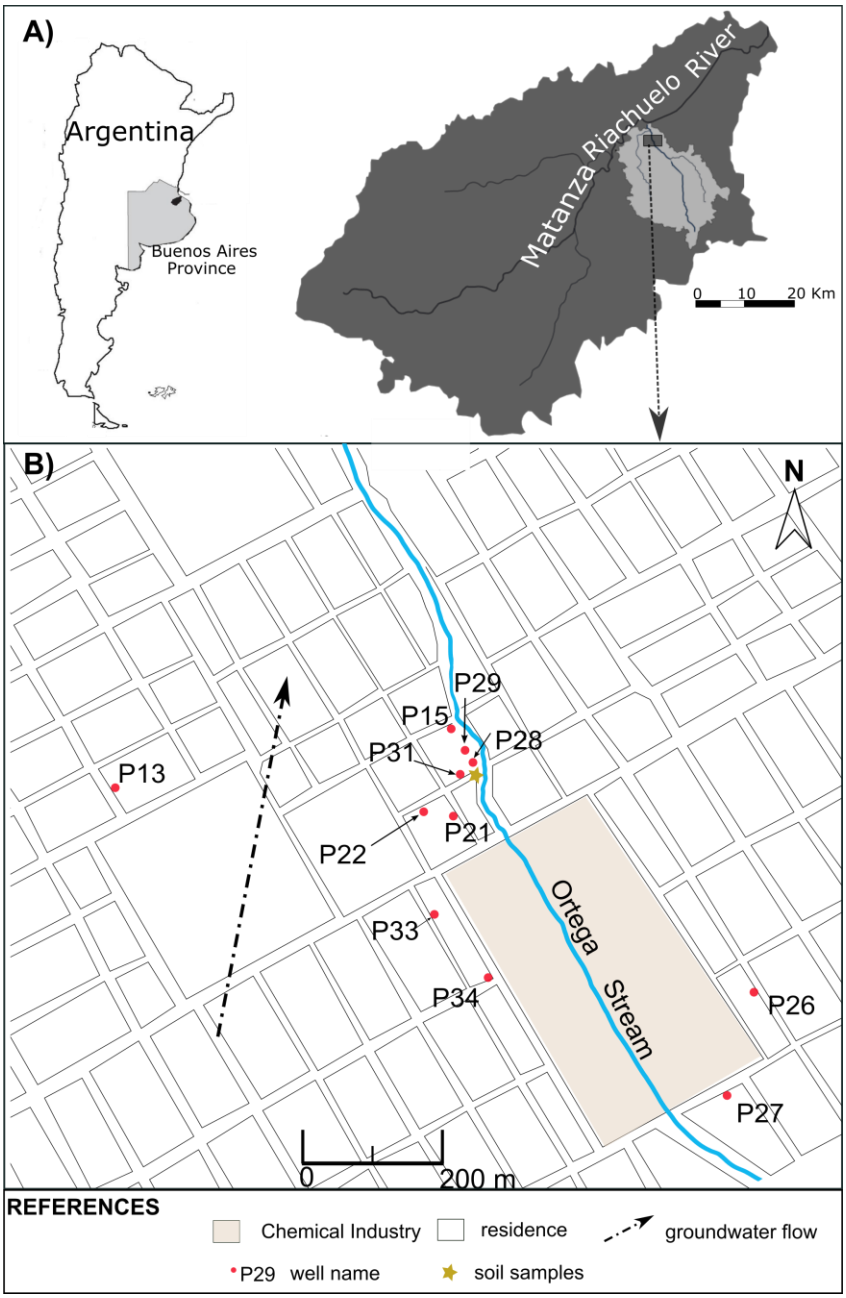

Figure 2.3. Scheme of the San Ignacio neighborhood study site. A) Location of the Matanza-Riachuelo River Basin (MRB), and Ortega stream sub basin. B) Site of study in the San Ignacio neighbourhood.

2.3. Nitrate polluted agricultural runoff water in the Lerma basin (Spain)

In the 2000s, approximately 20,000 ha of rainfed croplands were transformed into irrigated agricultural land in the Arba River Basin (Zaragoza, Spain). The Lerma basin (**Figure 2.4**), a small watershed representative of the area, was monitored to assess the effects of this transformation on the water balance and the salt and NO_3^--N exports (Merchán et al., 2015, 2014, 2013). In general, the implementation of irrigation implied a three-fold increase in N export to the receiving water bodies, in this case the Arba River, which was the first surface water body in the Ebro River Basin to be declared affected by NO_3^- pollution according to the BOA 91 (2014) in response to the Real Decreto 261/1996 (1996) established after the publication of the Nitrates Directive 91/676/EEC in 1991.

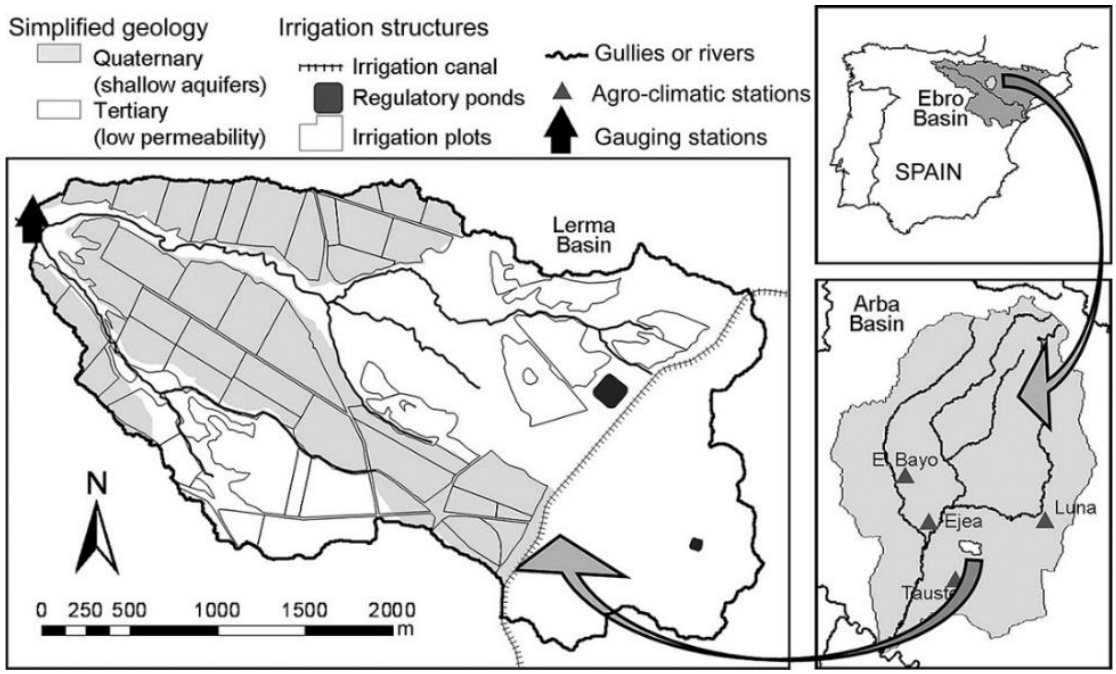

Figure 2.4. Scheme of the Lerma basin. Lerma basin situation and main characteristics. Source: (Merchán et al., 2013).

In order to diminish the release of NO_3^- from the Lerma Basin to the Arba River, a surface flow CW was constructed in October 2015, initially covering an area of ~1500 m^2, and was enlarged in June 2017, covering a final area of ~2500 m^2 with a depth of ~40 cm (**Figure 2.5**). The surface water of the Lerma gully can be totally or partially diverted towards the

CW. Water flow in the Lerma gully varies between 15 and 60 L/s. The CW is fully automated, with high frequency monitoring (every 10 minutes) of the water flow rate and NO_3^- concentration at both the inlet and the outlet. Emergent macrophytes (*Typha* and *Phragmites*) started growing since its construction.

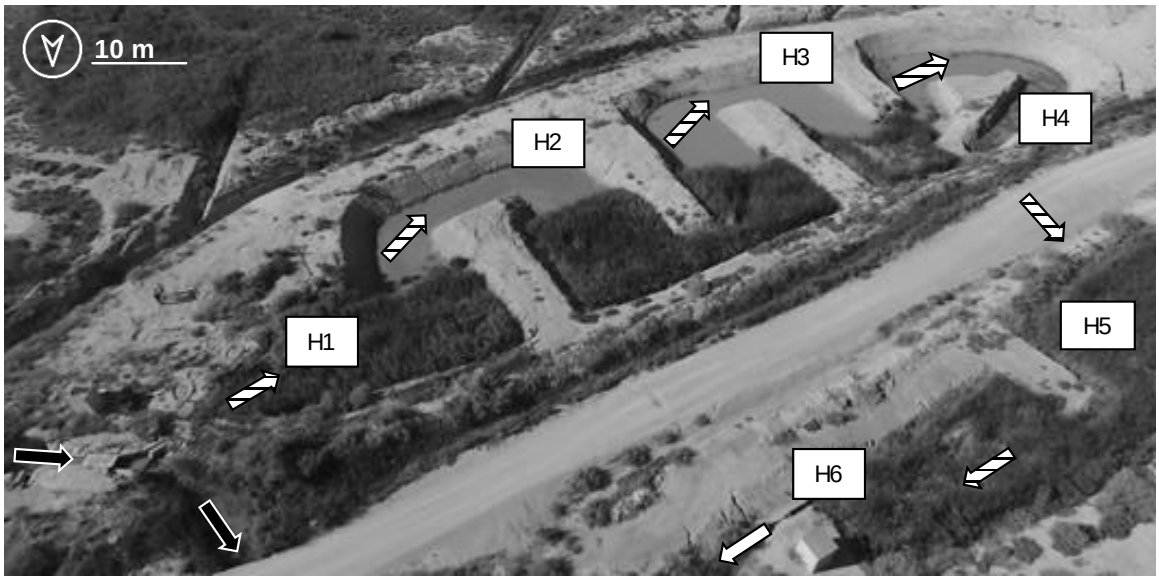

Figure 2.5. Constructed wetland design. Photograph of the surface flow CW with emergent macrophytes. The sampling points are depicted by white squares (H1 to H6), and the water flow within the CW with striped arrows. Non-treated water flow discharging to the Lerma gully is depicted with black arrows, and that of treated water with a white arrow.

REFERENCES

91/676/EEC, 1991. Nitrates Directive. Council Directive 91/676/EEC of 12 December 1991, concerning the protection of waters against pollution caused by nitrates from agricultural sources. [WWW Document]. Off. J. Eur. Comm. URL http://ec.europa.eu/environment/index_en.htm (accessed 4.9.17).

98/83/EC, 1998. Drinking Water Directive. Council Directive 98/83/EC, of 3 November 1998, on the quality of water intended for human consumption. [WWW Document]. Off. J. Eur. Comm. URL http://ec.europa.eu/environment/index_en.htm (accessed 4.9.17).

ACA, 2019. Consulta de dades de control de la qualitat i la quantitat de l'aigua al medi de l'Agència Catalana de l'Aigua (ACA). [WWW Document]. URL http://aca.gencat.cat/ca/laigua/estat-del-medi-hidric/estat-de-les-masses-daigua/subterranies/ (accessed 10.18.19).

BOA 91, 2014. ORDEN de 19 de julio de 2004, del Departamento de Agricultura y Alimentación, por la que designan las siguientes nuevas Zonas Vulnerables a la contaminación de las aguas por los nitratos procedentes de fuentes agrarias en la Comunidad Autónoma de Aragón y [WWW Document]. BOA num. 91. URL https://www.camarazaragoza.com/medioambiente/docs/leyes/leyes298.pdf (accessed 10.18.19).

DECRET 136/2009, 2009. DECRET 136/2009, d'1 de setembre, d'aprovació del programa d'actuació aplicable a les zones vulnerables en relació amb la contaminació de nitrats que procedeixen de fonts agràries i de gestió de les dejeccions ramaderes [WWW Document]. URL https://portaljuridic.gencat.cat/ca/pjur_ocults/pjur_resultats_fitxa/?action=fitxa&documentId=478701&language=ca_ES (accessed 5.2.19).

DECRET 283/1998, 1998. DECRET 283/1998, de 21 d'octubre, de designació de les zones vulnerables en relació amb la contaminació de nitrats procedents de fonts agràries. [WWW Document]. URL https://dogc.gencat.cat/ca/pdogc_canals_interns/pdogc_resultats_fitxa/?documentId=179342&language=ca_ES&action=fitxa (accessed 2.5.19).

Generalitat de Catalunya, Departament d'Agricultura, Ramaderia, Pesca, A. i M.N., 2015. Designació i ampliacions de les zones vulnerables establertes a: Decret 283/1998, Decret 476/2004, Acord GOV/128/2009 i Acord GOV/13/2015. Cartografia SIGPAC. [WWW Document]. URL http://agricultura.gencat.cat/ca/ambits/ramaderia/dar_dejeccions_ramaderes_fertilitzants_nitrogenats/dar_zones_vulnerables/ (accessed 7.11.19).

Mancino, C., Vives, L., Funes, A., Zarate, M., Martínez, S., Hidrología, I. De, Eduardo, D.L., Uncpba, J.U., Municipalidad, C.I.C., 2013. Modelación del flujo subterráneo en la cuenca Matanza-Riachuelo, provincia de Buenos Aires. 1. Geología y geometría del subsuelo. Temas actuales la Hidrol. subterránea.

Merchán, D., Causapé, J., Abrahão, R., 2013. Impact of irrigation implementation on hydrology and water quality in a small agricultural basin in Spain. Hydrol. Sci. J. 58, 1400–1413. https://doi.org/10.1080/02626667.2013.829576

Merchán, D., Causapé, J., Abrahão, R., García-Garizábal, I., 2015. Assessment of a newly implemented irrigated area (Lerma Basin, Spain) over a 10-year period. II: Salts and nitrate exported. Agric. Water Manag. 158, 288–296. https://doi.org/10.1016/j.agwat.2015.04.019

Merchán, D., Otero, N., Soler, A., Causapé, J., 2014. Main sources and processes affecting dissolved sulphates and nitrates in a small irrigated basin (Lerma Basin, Zaragoza, Spain): Isotopic characterization. Agric. Ecosyst. Environ. 195, 127–138. https://doi.org/10.1016/j.agee.2014.05.011

Real Decreto 261/1996, 1996. Real Decreto 261/1996 De 16 De Febrero, Sobre Protección De Las Aguas Contra La Contaminación Producida Por Los Nitratos Procedentes De Fuentes Agrarias [WWW Document]. BOE num. 61. URL https://www.boe.es/buscar/pdf/1996/BOE-A-1996-5618-consolidado.pdf (accessed 10.18.19).

Sanci, R., Bea, S.A., Ceballos, E., 2018. Applying reactive transport modelling in a chromium-contaminated site in the Matanza-Riachuelo basin, Buenos Aires, Argentina. Int. J. Environ. Heal. 9, 16. https://doi.org/10.1504/IJENVH.2018.10011987

Vives, L., Scioli, C., Mancino, C., Martínez, S., 2013. Modelación del flujo subterráneo e n la cuenca Matanza -

Riachuelo, Provincia de Buenos Aires. 3. Modelo numérico de flujo, in: Temas Actuales de La Hidrología Subterránea 2013.

Zabala, M.E., Martínez, S., Manzano, M., Vives, L., 2016. Groundwater chemical baseline values to assess the Recovery Plan in the Matanza-Riachuelo River basin, Argentina. Sci. Total Environ. https://doi.org/10.1016/j.scitotenv.2015.10.006

3. SUMMARY OF METHODS

3.1. Laboratory batch and column experiments

The laboratory experiments included several sets of batch and column tests aiming to evaluate the feasibility of using different low-cost materials as electron donors to induce the denitrification and to determine the resulting $\varepsilon^{18}O$ and $\varepsilon^{15}N$ values (Fe^{2+} containing minerals, vegetal and animal waste products and whey). Furthermore, two sets of batch experiments with acetic acid (CH_3COOH) or ethanol (C_2H_6O) were set up aiming to determine the $\varepsilon^{18}O$ and $\varepsilon^{15}N$ needed to calculate the efficiency of the denitrification in two polluted aquifers, one in Spain and one in Argentina (see **Section 2.1** and **Section 2.2**).

The batch experiments methodology was shared for all tested materials. The microcosms were set in different volume flasks and incubated under an Ar atmosphere, in the darkness with constant agitation. Different series of experiments were performed according to the tested electron donors: the Fe^{2+} containing minerals magnetite (Mag), olivine (Ol) and siderite (Sd) (**Table 3.1**), the pure organic carbon compounds acetic acid (CH_3COOH) and ethanol (C_2H_6O) (**Table 3.2**), and the complex organic carbon sources corn stubble, wheat hay and animal compost (**Table 3.2**). The biostimulated microcosms were sacrificed by turns at time intervals depending on the denitrification dynamics until a complete NO_3^- and NO_2^- removal was achieved. The control microcosms were sacrificed at the end of the experiments. These controls aimed to assess the intrinsic potential of the employed materials to attenuate the NO_3^- or NO_2^- or to act as a N supply. All series included replicates.

Table 3.1. Batch experiments with ferrous iron minerals. The different types of water sources used were: groundwater (GW) from Roda de Ter (Barcelona, Spain), deionized water (DIW) with NO_3^- or NO_2^-, MilliQ water (MilliQ) and synthetic sea water (SSW). In the Roda de Ter aquifer, lithotrophic denitrification occurrence have been previously reported (Hernández-del Amo et al., 2018; Otero et al., 2009; Vitòria et al., 2008). The sediment used in these experiments was milled limestone. The incubation was performed at 22-23ºC.

Reactor Type	Code	Water source	Sediment	Electron donor	Electron acceptor
Biostimulated	BioSedGW-Mag	GW	Yes	Mag	NO_3^-
Biostimulated	BioSedGW-Ol	GW	Yes	Ol	NO_3^-
Biostimulated	BioSedGW-Sd	GW	Yes	Sd	NO_3^-
Biostimulated	BioSedGW-Mag-NP	GW	Yes	Mag-NP	NO_3^-
Biotic control	BioSedGW-C	GW	Yes	-	NO_3^-
Biotic control	BioSedDIW-Mag	DIW	Yes	Mag	NO_3^-
Biotic control	BioSedDIW-Ol	DIW	Yes	Ol	NO_3^-
Biotic control	BioSedDIW-Sd	DIW	Yes	Sd	NO_3^-
Biotic control	BioSedDIW-Mag-NP	DIW	Yes	Mag-NP	NO_3^-
Biotic control	BioSedDIW-C	DIW	Yes	-	NO_3^-
Biotic control	Blank	MilliQ	Yes	-	-
Abiotic control	AbFeNO_3-Mag	DIW	No	Mag+Fe^{2+}	NO_2^-
Abiotic control	AbFeNO_3-Ol	DIW	No	Ol+Fe^{2+}	NO_2^-
Abiotic control	AbFeNO_3-Sd	DIW	No	Sd+Fe^{2+}	NO_2^-
Abiotic control	AbFeNO_2-Mag	DIW	No	Mag+Fe^{2+}	NO_2^-
Abiotic control	AbFeNO_2-Ol	DIW	No	Ol+Fe^{2+}	NO_2^-
Abiotic control	AbFeNO_2-Sd	DIW	No	Sd+Fe^{2+}	NO_2^-
Abiotic control	AbFeNO_2-C	DIW	No	Fe^{2+}	NO_2^-
Abiotic control	AbNO_2-Mag	DIW	No	Mag	NO_2^-
Abiotic control	AbNO_2-Ol	DIW	No	Ol	NO_2^-
Abiotic control	AbNO_2-Sd	DIW	No	Sd	NO_2^-
Abiotic control	AbseaNO_2-StFe_{aq}	SSW	No	Synthetic Fe^{2+} (aqueous)	NO_2^-
Abiotic control	AbseaNO_2-StFe_s	SSW	No	Synthetic Fe^{2+} (solid-bound)	NO_2^-
Abiotic control	AbseaNO_2-StFe_{aq+s}	SSW	No	Synthetic Fe^{2+} (aq+s)	NO_2^-
Abiotic control	AbseaNO_2-BioFe_{aq+s}	SSW	No	Biotic Fe^{2+} (aq+s)	NO_2^-
Biotic control	BioseaNO_2-Acetate	SSW	No	Acetate	NO_2^-
Biotic control	BioseaNO_2-Lactate	SSW	No	Lactate	NO_2^-

Table 3.2. Batch experiments with organic carbon sources. Content of the batch experiments either using pure organic carbon compounds or complex materials and temperature of incubation. All these experiments were performed using NO_3^- as de electron acceptor and focused on three different study sites (see Section 2). Legend: GW = groundwater of the study site, ARF = agricultural runoff water of the study site, DIW = deionized water, Milli-Q = Milli-Q water.

Study site	Reactor type	Code	Water source	Sediment addition	Electron donor	Temp.
Sant Andreu de Llavaneres aquifer	Stimulated	B	GW (NO_3^-)	Yes	CH_3COOH	20ºC
	Control	C1	GW (NO_3^-)	Yes	No	
	Control	C2	Milli-Q	Yes	No	
	Control	C3	GW (NO_3^-)	No	CH_3COOH	
Matanza-Riachuelo basin aquifer	Stimulated	BioN	GW (NO_3^-)	Yes	C_2H_6O	24ºC
	Stimulated	BioCr	GW (Cr^{6+})	Yes	C_2H_6O	
	Stimulated	BioCrN	GW (NO_3^-+Cr^{6+})	Yes	C_2H_6O	
	Control	CtrlCrN	GW (NO_3^-+Cr^{6+})	Yes	No	
	Control	Blank	DIW	Yes	No	
CW in the Lerma basin	Stimulated	C-24	ARF (NO_3^-)	No	Animal compost	24ºC
	Control	C-24-blank	DIW	No	Animal compost	24ºC
	Stimulated	H-24	ARF (NO_3^-)	No	Wheat hay	24ºC
	Control	H-24-blank	DIW	No	Wheat hay	24ºC
	Stimulated	S-24	ARF (NO_3^-)	No	Corn stubble	24ºC
	Control	S-24-blank	DIW	No	Corn stubble	24ºC
	Stimulated	S-16	ARF (NO_3^-)	No	Corn stubble	16ºC
	Control	S-16-blank	DIW	No	Corn stubble	16ºC
	Stimulated	S-8	ARF (NO_3^-)	No	Corn stubble	8ºC
	Control	S-8-blank	DIW	No	Corn stubble	8ºC
	Stimulated	DS-24	ARF (NO_3^-)	No	Decomposed corn stubble	24ºC
	Control	DS-24-blank	DIW	No	Decomposed corn stubble	24ºC

In the flow-through experiment, synthetic water from the inflow reservoir flowed from the bottom to the top of a glass column (filled with silica balls) until discharging into the outflow reservoir at a flow rate of 0.2 mL/min (**Figure 3.1**). Eh and pH probes were installed between the column and the outflow container. Temperature was maintained at 14 °C. Eight sampling points were established: one at the inflow container, six along the glass column at 10 cm intervals (VP1 to VP6) and one at the outflow container. The biostimulation was performed through three injection points near the bottom of the column. An initial operation period with no electron donor injection was carried out to assess the system performance (Stage 0). After Stage 0, different biostimulation strategies were tested by injecting whey in varying C/N ratios and periodicities: I) injection every 4 days at a 3.0 C/N ratio from day 0 to 24; II) no injection from day 24 to 77; III) daily injection at a 2.0 C/N ratio from day 77 to 99; IV) daily injection at a 1.25 C/N ratio from day 99 to 114; V) daily injection at a 1.5 C/N ratio from day 114 to 144; and VI) no injection from day 144 to 170.

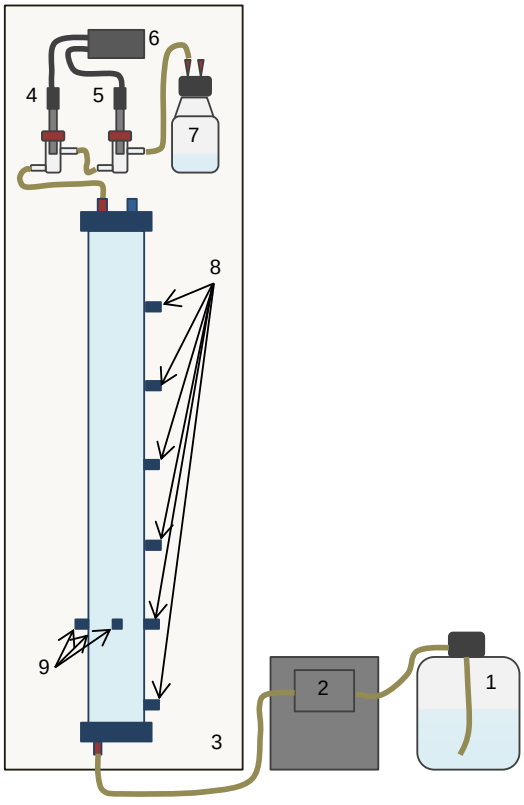

Figure 3.1. Column design. Scheme of the system. 1) inflow water, 2) peristaltic pump, 3) refrigerating chamber, 4) Eh probe, 5) pH probe, 6) multiparametric analyzer, 7) outflow water, 8) sampling points and 9) injection points.

3.2. Field-scale surveys

In the Sant Andreu de Llavaneres aquifer (see **section 2.1**), in-situ heterotrophic denitrification stimulation was induced by injecting CH_3COOH by pulses intro the aquifer. The total biostimulation period was 22 months (2015-2017). A total of forty-four samples were collected from two wells and three piezometers in the pilot-plant (EW, PZ1, PZ2, PZ3 and MW, **Figure 2.2**) to evaluate the induced NO_3^- attenuation. Nine sampling campaigns were performed during the twenty-two months of the pilot-plant operation (months 1, 2, 7, 10, 11, 12, 14, 17 and 19), and one was performed two months after the end of injections (month 24). Sediment for the batch experiments was obtained from the piezometer cores.

To evaluate the natural NO_3^- and Cr^{6+} attenuation in the Matanza-Riachuelo basin aquifer (see **section 2.2**), groundwater samples were collected on September 2017 from 12 wells (P13, P28 and P29, P15, P16, P21, P22, P26, P27, P31, P33 and P34, **Figure 2.3**). Soil samples for the batch experiments were collected from a drilling downstream of the chemical industry, near the P28 monitoring well (**Figure 2.3**).

The field survey in the CW at the Lerma basin (see **section 2.3**) involved 13 sampling campaigns consisting on the collection of six water samples (H1 to H6) along the CW flow line (**Figure 2.5**). In the first period, three surveys were performed to test two different operating conditions before the biostimulation: a flow rate of ~5.5 L/s and a flow rate of ~2.5 L/s. The second period involved the application of corn stubble on September 25, 2017, and the evaluation of the treatment (autumn-winter) with two surveys performed 7 and 14 days after the application. The third period involved a second application of corn stubble on May 11, 2018, and the evaluation of the treatment (spring-summer), with eight surveys performed from May 2018 to October 2018. Throughout the second and third periods, the CW was operated at a higher flow rate (~16 L/s).

3.3. Analytical techniques

Depending on the purpose of each experiment, different chemical parameters were determined in the collected samples, considering the following ones: concentration of dissolved major anions (NO_3^-, NO_2^-, Cl^- and SO_4^{2-}), NH_4^+, non-purgeable dissolved organic carbon (NPDOC), dissolved inorganic carbon (DIC), major cations and trace elements in water samples; concentration of N and C in solid materials; concentration of N_2O gas. Also, different isotopic parameters were determined: δ^{15}N-NO_3^-, δ^{18}O-NO_3^-, δ^{15}N-NO_2^-, δ^{18}O-NO_2^-, δ^{13}C-DIC, δ^{13}C-DOC, δ^{34}S-SO_4^{2-}, δ^{18}O-SO_4^{2-} and δ^{53}Cr in water samples, δ^{13}C-C_{bulk} and δ^{15}N-N_{bulk} in solid samples and δ^{15}N-N_2O, δ^{18}O-N_2O in gas samples.

The water samples collected from the field and laboratory batch experiments were immediately filtered through 0.2 µm Millipore® filters after being collected and were stored at 4 ºC until analysis. The aliquots for NH_4^+, δ^{15}N-NO_3^-, δ^{18}O-NO_3^-, δ^{15}N-NO_2^- and δ^{18}O-NO_2^- analysis were frozen. The aliquots for the DIC, δ^{13}C-DIC and δ^{13}C-DOC analyses were left with no headspace and stored at 4 ºC. The soil and sediment samples were preserved frozen. The dried vegetal and animal waste materials and the minerals were milled and stored at room temperature. The gas samples (headspace of batch experiments) were preserved at room temperature under an Ar atmosphere.

The methods employed for the analyses are summarized in **Table 3.3**. Chemical and isotopic analyses were prepared at the laboratory of the MAiMA-UB research group and analyzed at the Centres Científics i Tecnològics of the Universitat de Barcelona (CCiT-UB), except the δ^{53}Cr that was determined at the University of Copenhagen.

The stable isotopes are expressed using delta notation ($\delta = ((R_{sample}-R_{standard})/R_{standard})$, where R is the ratio between the heavy and the light isotopes). The considered international standards were: Atmospheric N_2 (AIR) for δ^{15}N, Vienna Standard Mean Oceanic Water (V-SMOW) for δ^{18}O, Vienna Peedee Belemnite (V-PDB) for δ^{13}C, Vienna Canyon Diablo Troillite (V-CDT) for δ^{34}S and NIST SRM 979 for δ^{53}Cr. Following Coplen (2011), several international and laboratory (CCiT) standards were interspersed among samples for the normalization of the isotopic results (**Table 3.4**).

Table 3.3. Analytical techniques. Methods and equipment employed for the samples analyses.

Parameter	Method	Equipment
Major anions (Cl^-, NO_2^-, NO_3^- and SO_4^{2-})	High-performance liquid chromatography (HPLC)	WATERS 515 pump and WATERS IC-PAK anions column with WATERS 432 and UV/V KONTRON detectors
NO_2^-	Spectrophotometry after Griess reaction (García-Robledo et al., 2014)	SP-830 PLUS (Metertech) and CARY 1E UV-visible
NH_4^+	Spectrophotometry after indophenol blue reaction (Bolleter et al., 1961)	CARY 1E UV-visible
NH_4^+	NH_4^+ ion selective electrode	ORION, Thermo Scientific
DIC	Titration	METROHM 702 SM Titrino
NPDOC	Organic matter combustion	TOC 500 SHIMADZU
Major cations (including Cr^{6+} and Fe^{2+}) and trace elements	Inductively coupled plasma optical emission spectroscopy (ICP-OES) and Inductively coupled plasma mass spectroscopy (ICP-MS)	Perkin Elmer Optima 8300, Perkin Elmer Optima 2300 and Perkin Elmer Elan 6000
N_2O	Gas chromatography (GC)	Thermo Scientific Trace 1300 with electron capture detector (ECD)
C and N % (solid samples)	Elemental analyzer (EA)	Carlo Erba1108 CHNS-O EA
$\delta^{15}N\text{-}NO_3^-$ $\delta^{18}O\text{-}NO_3^-$	Isotope Ratio Mass Spectrometry (IRMS) after sample preparation following the cadmium and azide reduction methods (McIlvin and Altabet, 2005; Ryabenko et al., 2009)	Pre-Con coupled to a Finnigan MAT 253 IRMS (Thermo Scientific)
$\delta^{15}N\text{-}NO_2^-$ $\delta^{18}O\text{-}NO_2^-$	IRMS after sample preparation following the azide reduction method (McIlvin and Altabet, 2005)	Pre-Con coupled to a Finnigan MAT 253 IRMS (Thermo Scientific)
$\delta^{15}N\text{-}N_2O$ $\delta^{18}O\text{-}N_2O$	IRMS	Pre-Con coupled to a Finnigan MAT 253 IRMS (Thermo Scientific)
$\delta^{53}Cr$	Thermal ionization mass spectrometry (TIMS) after sample preparation following an adapted method from Frei et al. (2009).	IsotopX “Phoenix” multicollector
$\delta^{34}S\text{-}SO_4^{2-}$ $\delta^{18}O\text{-}SO_4^{2-}$	IRMS after dissolved SO_4^{2-} was precipitated as $BaSO_4$ by adding $BaCl_2 \cdot 2H_2O$ after acidifying the sample with HCl and boiling to prevent $BaCO_3$ precipitation (Dogramaci et al., 2001)	Carlo Erba EA coupled in a continuous flow to a Finnigan Delta XP Plus IRMS and ThermoQuest high-temperature conversion EA coupled in a continuous flow with a Finnigan Matt Delta XP Plus IRMS
$\delta^{13}C\text{-}DIC$	IRMS after carbonate conversion to CO_2 gas by adding phosphoric acid	Gas-Bench II coupled to a MAT-253 IRMS (Thermo Scientific)
$\delta^{13}C\text{-}DOC$	HPLC-IRMS	Delta V ADVANTAGE (Thermo-Finnigan)
$\delta^{13}C\text{-}C_{bulk}$ $\delta^{15}N\text{-}N_{bulk}$	EA-IRMS	Carlo Erba EA coupled to a Finnigan Delta C IRMS

Table 3.4. Standards and reproducibility for isotopic analysis. International and laboratory (CCiT) standards used for normalization of the results.

Analysis	Standards	Reproducibility (1σ)
$\delta^{15}N\text{-}NO_3^-$	USGS-32, USGS-34, USGS-35 and CCiT-IWS ($\delta^{15}N$ = +16.9 ‰)	±1.0 ‰
$\delta^{18}O\text{-}NO_3^-$	USGS-32, USGS-34, USGS-35 and CCiT-IWS ($\delta^{18}O$ = +28.5 ‰)	±1.5 ‰
$\delta^{15}N\text{-}N_{bulk}$	USGS-40, IAEA-N1, IAEA-NO3, IAEA-N2	±0.2 ‰
$\delta^{13}C\text{-}C_{bulk}$	USGS-40, IAEA-CH7, IAEA-CH6	±0.2 ‰
$\delta^{13}C$-DIC	CCiT-$NaHCO_3$ ($\delta^{13}C$ = -4.4 ‰), CCiT-$NaKHCO_3$ ($\delta^{13}C$ = -18.7 ‰) and CCiT-$KHCO_3$ ($\delta^{13}C$ = +29.2 ‰)	±0.2 ‰
$\delta^{13}C$-DOC	IAEA-CH6, CCiT-Gly ($\delta^{13}C$ = -30.8 ‰) and CCiT-UCGEMA ($\delta^{13}C$ = -24.8 ‰)	±0.3 ‰
$\delta^{34}S\text{-}SO_4^{2-}$	NBS-127, SO5, SO6 and CCiT-YCEM ($\delta^{34}S$ = +12.8 ‰)	±0.2 ‰
$\delta^{18}O\text{-}SO_4^{2-}$	NBS-127, SO6, USGS-34, CCiT-YCEM ($\delta^{18}O$ = +17.6 ‰) and CCiT-ACID ($\delta^{18}O$ = +13.2 ‰)	±0.5 ‰
$\delta^{53}Cr$	NIST SRM 979 and NIST 3112a	±0.08 ‰

3.4. Calculations

Under closed system conditions, the isotopic fractionation was calculated by means of the Rayleigh distillation **Equation 3.1**. Thus, the $\varepsilon^{15}N_{NO3/N2}$ and $\varepsilon^{18}O_{NO3/N2}$ were obtained from the slope of the linear correlation between the natural logarithm of the substrate remaining fraction ($Ln(C_{residual}/C_{initial})$, where C refers to the analyte concentration) and the determined isotope ratios ($Ln(R_{residual}/R_{initial})$, where $R = \delta+1$).

$$Ln\left(\frac{R_{residual}}{R_{initial}}\right) = \varepsilon \times Ln\left(\frac{C_{residual}}{C_{initial}}\right) \quad \textbf{(Equation 3.1)}$$

The percentage of NO_3^- attenuation caused by denitrification at field-scale was estimated by using these $\varepsilon^{15}N_{NO3/N2}$ and $\varepsilon^{18}O_{NO3/N2}$ calculated under closed system conditions and **Equation 3.2**, which is derived from the Rayleigh fractionation model (**Equation 3.1**).

$$DEN\ \% = \left[1 - \left(\frac{C_{residual}}{C_{initial}}\right)\right] \times 100 = \left[1 - \left(\frac{R_{residual}}{R_{initial}}\right)^{\left(\frac{1}{\varepsilon}\right)}\right] \times 100 \quad \textbf{(Equation 3.2)}$$

REFERENCES

Bolleter, W.T., Bushman, C.J., Tidwell, P.W., 1961. Spectrophotometric Determination of Ammonia as Indophenol. Anal. Chem. 33, 592–594. https://doi.org/10.1021/ac60172a034

Coplen, T.B., 2011. Guidelines and recommended terms for expression of stable-isotope-ratio and gas-ratio measurement results. Rapid Commun. Mass Spectrom. 25, 2538–2560. https://doi.org/10.1002/rcm.5129

Dogramaci, S.., Herczeg, A.., Schiff, S.., Bone, Y., 2001. Controls on $\delta^{34}S$ and $\delta^{18}O$ of dissolved sulfate in aquifers of the Murray Basin, Australia and their use as indicators of flow processes. Appl. Geochemistry 16, 475–488. https://doi.org/10.1016/S0883-2927(00)00052-4

Frei, R., Gaucher, C., Poulton, S.W., Canfield, D.E., 2009. Fluctuations in Precambrian atmospheric oxygenation recorded by chromium isotopes. Nature 461, 250–253. https://doi.org/10.1038/nature08266

García-Robledo, E., Corzo, A., Papaspyrou, S., 2014. A fast and direct spectrophotometric method for the sequential determination of nitrate and nitrite at low concentrations in small volumes. Mar. Chem. 162, 30–36. https://doi.org/10.1016/j.marchem.2014.03.002

Hernández-del Amo, E., Menció, A., Gich, F., Mas-Pla, J., Bañeras, L., 2018. Isotope and microbiome data provide complementary information to identify natural nitrate attenuation processes in groundwater. Sci. Total Environ. 613–614, 579–591. https://doi.org/10.1016/j.scitotenv.2017.09.018

McIlvin, M.R., Altabet, M.A., 2005. Chemical conversion of nitrate and nitrite to nitrous oxide for nitrogen and oxygen isotopic analysis in freshwater and seawater. Anal Chem 77, 5589–5595. https://doi.org/10.1021/ac050528s

Otero, N., Torrentó, C., Soler, A., Menció, A., Mas-Pla, J., 2009. Monitoring groundwater nitrate attenuation in a regional system coupling hydrogeology with multi-isotopic methods: The case of Plana de Vic (Osona, Spain). Agric. Ecosyst. Environ. 133, 103–113. https://doi.org/10.1016/j.agee.2009.05.007

Ryabenko, E., Altabet, M. a., Wallace, D.W.R., 2009. Effect of chloride on the chemical conversion of nitrate to nitrous oxide for $\delta^{15}N$ analysis. Limnol. Oceanogr. Methods 7, 545–552. https://doi.org/10.4319/lom.2009.7.545

Vitòria, L., Soler, A., Canals, À., Otero, N., 2008. Environmental isotopes (N, S, C, O, D) to determine natural attenuation processes in nitrate contaminated waters: Example of Osona (NE Spain). Appl. Geochemistry 23, 3597–3611. https://doi.org/10.1016/j.apgeochem.2008.07.018

4. SUMMARY OF RESULTS AND GENERAL DISCUSSION

4.1. Evaluation of different low-cost materials to promote denitrification

The batch and flow-through laboratory experiments demonstrated that Mag-NP, corn stubble, wheat hay, animal compost and whey could efficiently promote the denitrification in polluted water bodies. The most remarkable results found for each series of experiments regarding the electron donor and acceptor consumption and the by-product accumulation are summarized in **sections 4.1.1** to **4.1.3**. The best electron donor to implement a specific biostimulation strategy must be chosen in accordance to the characteristics of the polluted site. For example, whey could be appropriate for being injected into polluted aquifers through wells, while wheat hay or corn stubble could be appropriate for being deposited in CWs and the Mag-NP could be applied through PRBs both in aquifers or CWs.

4.1.1. Potential use of ferrous iron minerals as electron donors

During the first week of incubation of the microcosms containing Fe minerals (BioSedGW), a 30-60 % NO_3^- concentration decrease was achieved due to heterotrophic bacteria that used the organic C from both sediment and groundwater as electron donor (**Figure 4.1**). After the first week, the NO_3^- continued to decrease only in the microcosms containing Mag-NP. About 96 % NO_3^- reduction was achieved in 91 days (**Figure 4.1**), showing transient NO_2^- accumulation up to 0.2 mM. The NH_4^+ concentration was below 0.04 mM, discarding a major contribution of DNRA. The low percentage of N_2O-N detected (up to 0.8 % from the initial N), suggested that the final product of the reduction was N_2, either during the initial heterotrophic activity and as a result of the denitrification promoted by the Mag-NP. According to these results, the Mag-NP allowed a higher Fe^{2+} availability with respect to the micro-sized minerals. Aquilina et al. (2018) and Yang et al. (2017) also related an increased autotrophic denitrification to a decreased grain size of Fe minerals. Smaller particles enhance the mineral solubility, which might accelerate microbial reduction rates (Aquilina et al., 2018; Braunschweig et al., 2013). The application of Fe^{2+} minerals could be advantageous due to the regeneration of Fe^{2+} from the reduction of precipitated Fe^{3+}

minerals if NO_3^- is completely removed and if an electron donor is present (Straub et al., 2004). However, excessive Fe^{3+} precipitation could produce clogging and therefore, a decreased NO_3^- reduction efficiency (Chen et al., 2018; Coby and Picardal, 2005; Cooper et al., 2003; Wang et al., 2017).

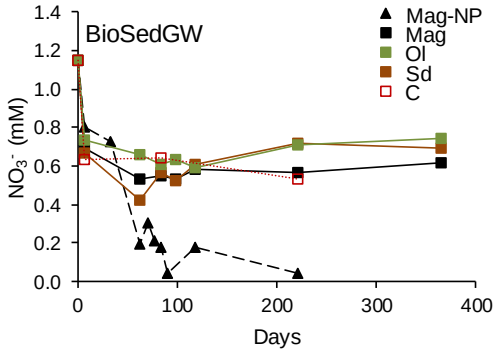

Figure 4.1. Nitrate attenuation in the BioSedGW experiments. The microcosms contained sediment, groundwater and one of the tested minerals (Mag-NP, Mag, Ol or Sd). C refers to the control without mineral.

No abiotic reactivity was observed between the Fe^{2+}-containing minerals and NO_3^- or NO_2^- ($AbFeNO_3$ and $AbNO_2$ experiments, **Figure 4.2A**). However, a rapid NO_2^- reduction was observed in the experiments with added aqueous Fe^{2+} ($AbFeNO_2$ experiments, **Figure 4.2B**). A faster reduction (~50 h) was observed in the experiments containing Sd compared to the experiments without mineral or with Mag or Ol (~175 h), possibly due to an increased dissolution rate of Sd, that increased the aqueous Fe^{2+} availability. The lack of differences on the NO_2^- reduction rate in the experiments without mineral or with Mag or Ol, could be explained by the aqueous Fe^{2+}/N ratio used, that was above the stoichiometric. Since the measured NH_4^+ was below 0.05 mM, NO_2^- was reduced to gaseous products. As previously observed by other authors, N_2O accumulated at the headspace of the batches due to the NO_2^- abiotic reduction by Fe^{2+} oxidation (Buchwald et al., 2016; Chen et al., 2018; Coby and Picardal, 2005; Wang et al., 2016). The sum of the remaining NO_2^- and the produced N_2O for each sample was close to the initial NO_2^- amount, demonstrating that N_2O was the end product of the reduction (**Figure 4.2C**). The aqueous Fe^{2+} decreased from 5 mM to approximately 2 mM in accordance to NO_2^- reduction, showing no significant differences between the four tested conditions (**Figure**

4.2D). When applying Fe^{2+}-containing minerals in polluted water bodies to promote denitrification, a decreased water quality due to NO_2^- accumulation could be avoided as a result of its abiotic reduction if Fe^{2+} is found in the aqueous form. However, the NO_2^- abiotic reduction would be beneficial only if the generated N_2O is further reduced to N_2 biotically.

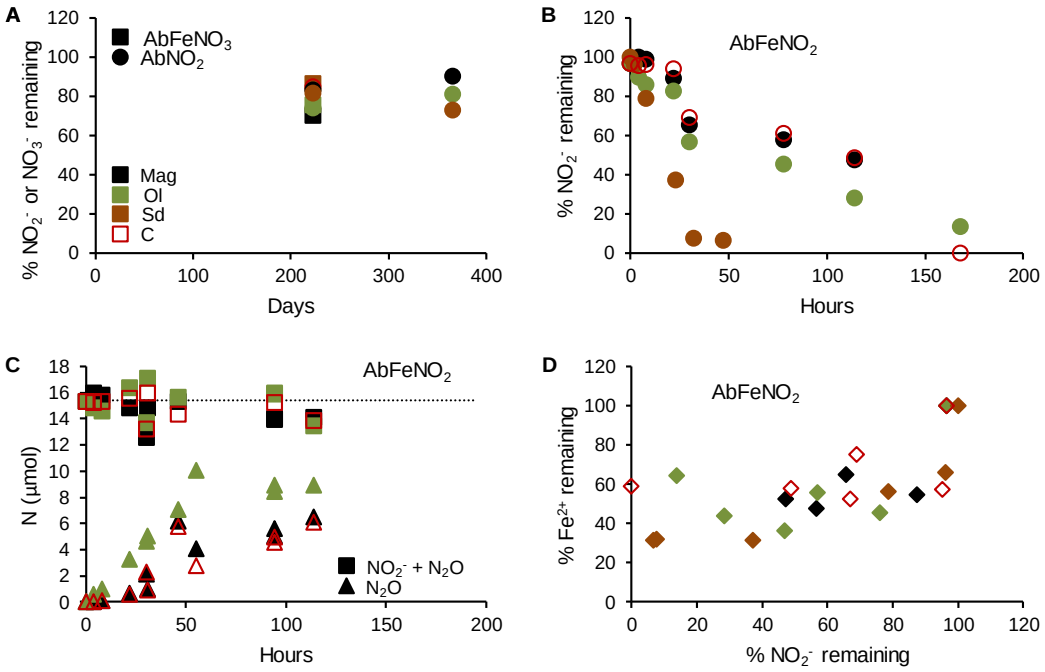

Figure 4.2. Abiotic reactivity between ferrous iron and nitrate or nitrite. The abiotic experiments contained deionized water with NO_3^- or NO_2^-, the tested Fe^{2+} minerals (Mag, Ol or Sd) and in some cases, aqueous Fe^{2+}. C refers to the control without mineral. For the $AbNO_2$ and $AbFeNO_3$ experiments, **A**) shows the remaining NO_2^- or NO_3^-, respectively. For the $AbFeNO_2$ experiments, **B**) shows the remaining NO_2^-, **C**) the generated N_2O-N and the sum of N_2O-N and NO_2^--N, in which the dotted line reflects the initial NO_2^- content, and **D**) the remaining Fe^{2+}.

In additional abiotic experiments with synthetic seawater ($AbSeaNO_2$), a higher reactivity was observed with a combination of synthetic Fe^{2+} aqueous and associated to minerals ($AbSeaNO_2$-$StFe_{aq+s}$) compared to when the synthetic Fe^{2+} was only found aqueous or associated to minerals ($AbSeaNO_2$-$StFe_{aq}$ or $AbSeaNO_2$-$StFe_s$) (**Figure 4.3**). This finding contrasted with the lack of differences in reactivity between the $AbFeNO_2$ experiments with and without added minerals (Mag, Ol or C). Two explanations could be: I) the effect of salinity upon reactivity or II) the use of a higher aqueous Fe^{2+}/NO_2^- ratio in the $AbFeNO_2$

experiments (approximately 3.3 compared to 1.5 in the $AbSeaNO_2$ experiments), that did not allow to reveal such difference. Furthermore, the $AbSeaNO_2$-$BioFe_{aq+s}$ experiments showed that the Fe^{2+} produced biotically is more reactive than when being from synthetic origin ($AbSeaNO_2$-$StFe_{aq+s}$) (**Figure 4.3**). This fact should be considered in future laboratory-scale studies aiming to evaluate the use of Fe^{2+} containing materials to promote the denitrification.

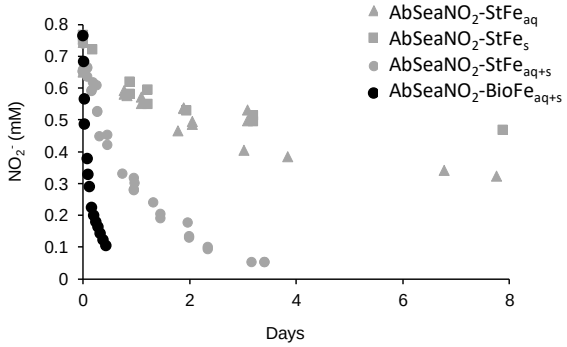

Figure 4.3. Abiotic nitrite reduction by ferrous iron produced biotically and synthetically. Comparison between biotically-produced and synthetic ferrous iron when found aqueous (aq), associated to minerals (s) or in a combination of both (aq+s). These experiments were performed with synthetic seawater.

4.1.2. Potential use of rural waste products as electron donors

Complete denitrification was reached in approximately 40 h in the microcosms containing corn stubble and wheat hay, and in approximately 95 h in those containing animal compost (**Figure 4.4.A**). Hence, these three carbon sources can promote the denitrification. NH_4^+ was detected in some of the samples (up to 1 mM), suggesting the possible coexistence of denitrification and DNRA and/or the input of NH_4^+-N supplied from the C sources tested (control microcosms with the C sources and DIW showed NO_3^- + NO_2^- + NH_4^+ below 0.12 mM). Transient NO_2^- accumulation was observed with the three materials. Higher NO_2^- accumulation was related to lower rates of NO_3^- reduction. The NPDOC concentration provided an approximation of the amount of added C present in dissolved form. Although the quantity of compost in the microcosms was only one-quarter of the quantity of vegetal materials, the measured NPDOC concentrations in the three types of microcosms were

similar (13.2-27.3 mM for stubble, 11.8-16.8 mM for hay, and 5.3-14.3 mM for compost). The intrinsic C concentrations of the three sources were similar, but the C bioavailability could differ between each product, and even between replicates, due to heterogeneity in the materials (Breulmann et al., 2014; Sobczak and Findlay, 2002; Warneke et al., 2011).

Additional experiments with stubble showed that denitrification reached completion from 8 to 24 ºC, but with different lag periods and NO_3^- reduction rates. Complete denitrification was achieved after 40 h at 24 ºC, 65 h at 16 ºC, and 140 h at 8 ºC (**Figure 4.4.B**). A decrease in NO_3^- reduction rate associated with lower temperatures following the Arrhenius relationship has been well documented (Dawson and Murphy, 1972). One of the main issues associated with biostimulation strategies is their effectiveness during long-term treatments. The denitrification induced by partially decomposed stubble (sampled 7.5 months after being in contact with water) was completed in less than 25 h (**Figure 4.4.B**), showing that the intrinsic capacity of the stubble to promote denitrification was still important, at least at lab-scale. However, the NPDOC content in the microcosms containing partially decomposed stubble (1.7-8.8 mM) was lower than that in the microcosms with fresh stubble incubated at 24 ºC (13.2-27.3 mM), pointing to a decreased availability of the electron donor over time. The maximum N_2O concentration detected in the headspace of the microcosms containing partially decomposed stubble incubated at 24 ºC (as well as that in the microcosms containing fresh stubble incubated at 16 and 8 ºC) accounted only for 0.015 % of the initial NO_3^--N content of the microcosms. Therefore, the GHG release at lab-scale was not significant.

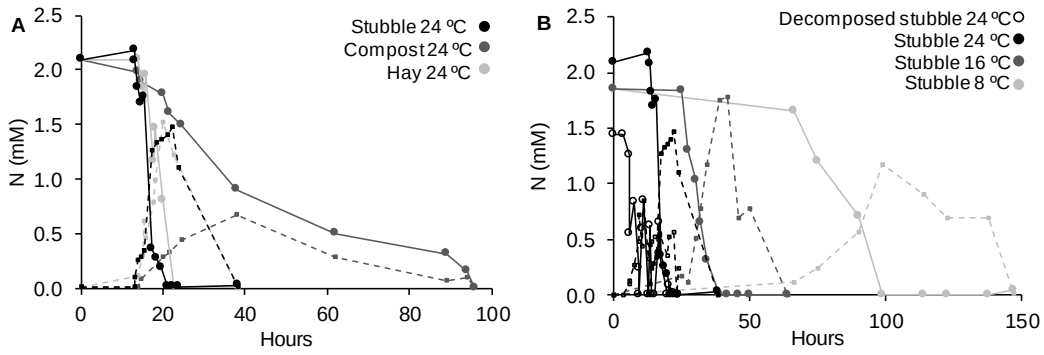

Figure 4.4. Evolution of denitrification in the biostimulated microcosms. NO_3^- (circles joined with a continuous line) and NO_2^- (squares joined with a dashed line) measured in (**A**) the batch experiments employing different carbon sources and (**B**) the experiments testing the effects of temperature and lifespan of the stubble.

4.1.3. Potential use of whey as electron donor

In the flow-through experiment, two days after the first whey injection in Stage I (injection every four days at a 3.0 C/N ratio), NO_3^- attenuation began and NO_2^- accumulated, reaching 1.5 mM (inflow NO_3^- was 1.9 mM). After the peak, NO_2^- started to decrease until both compounds were completely depleted in less than sixteen days from the beginning of the biostimulation strategy (**Figure 4.5**). After a period with no injection, where NO_3^- concentration progressively increased to the initial values (Stage II), the injection strategy was switched to a daily injection with a 2.0 C/N ratio (Stage III). During Stage III, NO_3^- was also rapidly and completely reduced but with no NO_2^- accumulation because the latent denitrifying community during the recovery period quickly adapted when the injections were resumed compared to the beginning of the biostimulation. Using a daily injection with a 1.25 (Stage IV) or 1.5 (Stage V) C/N ratios, NO_3^- in the outflow was maintained at approximately 0.5 and 0.4 mM, respectively. Therefore, whey injection at C/N ratios between 1.25 and 1.5 is enough to achieve NO_3^- concentrations below the threshold for consumption. The NH_4^+ was rarely detected during the test, with concentrations below 0.19 mM, suggesting that DNRA did not contribute significantly to NO_3^- attenuation.

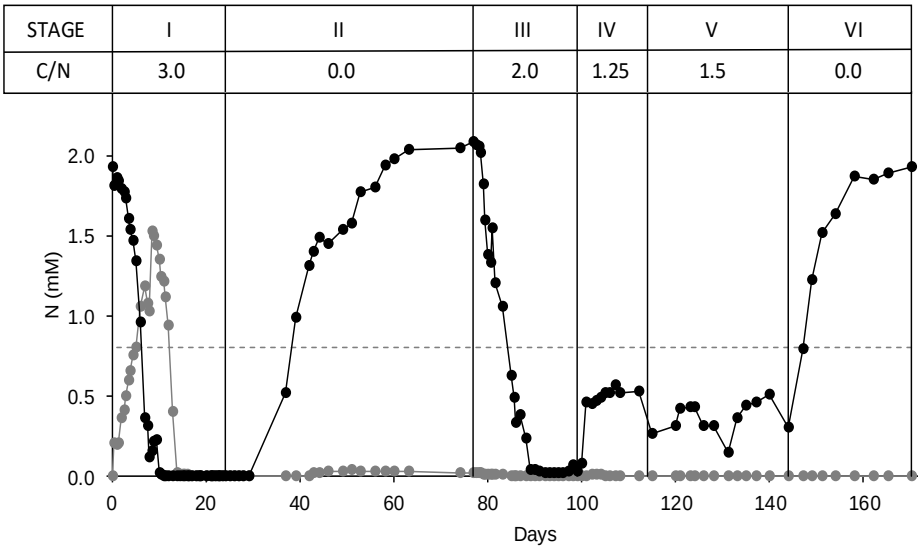

Figure 4.5. Induced nitrate attenuation by whey injections. NO_3^- (black) and NO_2^- (grey) concentration evolution during the different tested stages in the flow-through experiment. The dashed line depicts the threshold for human consumption.

During the recovery Stage II and VI (no injection), forty and eleven days, respectively, were needed to equal the inflow water NO_3^- concentration (**Figure 4.5**). The long time needed to recover the initial NO_3^- values during Stage II reinforces the excessive whey injection during the Stage I, which is undesired to avoid a decrease in the water quality.

At the outflow of the column, the NPDOC peaks derived from injections decreased progressively after the microbial acclimation period (**Figure 4.6**). For the bioremediation strategies design, it has to be considered that apart from the injected electron donor, the organic C compounds resulting from bacterial metabolism, biomass degradation and cellular lysis could also act as a secondary electron donor source, especially at low C/N ratios (Carrey et al., 2018). As expected from the denitrification by organic carbon oxidation, the product HCO_3^- showed an inverse trend compared to the NO_3^- concentration. The maximum HCO_3^- concentration coincided with complete NO_3^- depletion at Stages I and III and its production stopped during the recovery Stage II (**Figure 4.6**). The gap between C derived from injected whey and the sum of generated DIC and outflow NPDOC was attributed to biomass and CO_2 production.

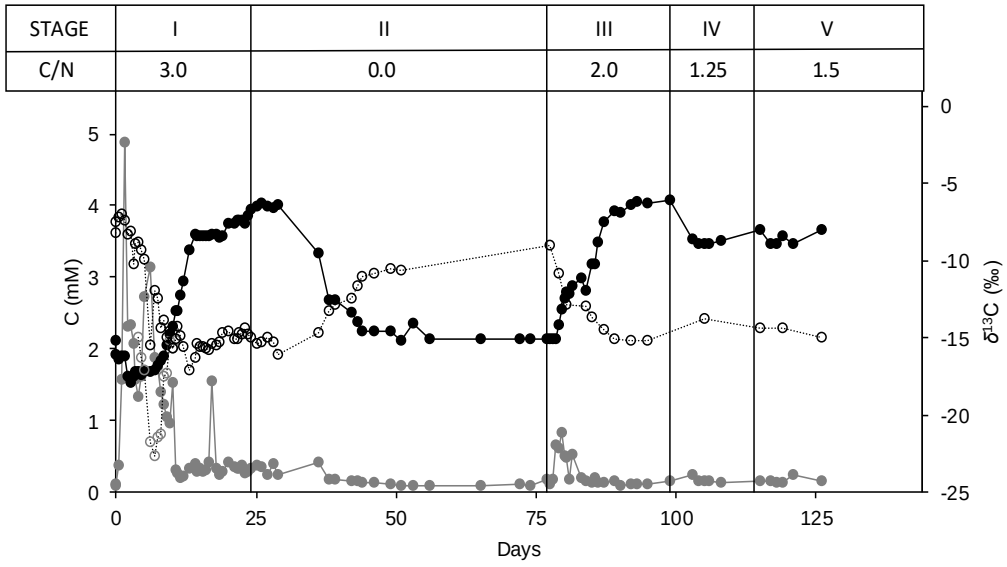

Figure 4.6. Organic carbon consumption and inorganic carbon production. Concentration (full circles) and isotopic composition (empty circles) evolution of dissolved organic (grey) and inorganic (black) carbon during the different tested stages in the flow-through experiment.

4.2. Isotope results from the laboratory experiments

The isotopic characterization of the different N species and other compounds involved in the denitrification reactions, provided valuable information concerning the NO_3^- attenuation mechanisms during the biostimulation treatments. The most relevant findings obtained from the laboratory experiments are summarized in **sections 4.2.1** to **4.2.4**. Not only the experiments focusing on the evaluation of different low-cost materials to promote denitrification but also the ones performed using the electron donors employed during the field-scale studies are discussed (see **section 3.1**).

4.2.1. Nitrate isotopic characterization

The $\varepsilon^{15}N_{NO3/N2}$ and $\varepsilon^{18}O_{NO3/N2}$ values calculated from the laboratory experiments (see **section 3.1**) are presented in **Table 4.1** and can be compared to those reported in the literature up to date for similar experiments (**Table 1.1**). These ε values were determined for all the batch experiments performed and also for the stages of the flow-through experiment that allowed a complete NO_3^- removal (Stages I and III). In the recovery and partial denitrification periods of the flow-through experiment, the NO_3^- isotopic characterization suggested a mix of denitrified and non-denitrified water at the outflow. During the partial denitrification stages (Stages IV and V), no correlation was observed between the isotopic composition and the natural logarithm (Ln) of the NO_3^- concentration or $1/[NO_3^-]$. The isotopic values during these stages were close to the inflow synthetic water isotopic composition. For the recovery stages (Stages II and VI), a correlation between the Ln of the remaining NO_3^- concentration and the isotopic composition was observed. However, the resulting trend from plotting $\delta^{15}N\text{-}NO_3^-$ and $\delta^{18}O\text{-}NO_3^-$ versus $1/[NO_3^-]$ was better adjusted to a linear correlation than to a logarithmic trend, which is indicative of mixing processes. For this reason, it is not appropriate to use the Rayleigh model (**Equation 3.1**) if the NO_3^- reduction is not complete in flow-through experiments.

The $\varepsilon^{15}N/\varepsilon^{18}O$ obtained for the induced NO_3^- reduction by Mag-NP (3.1), stand out among the typical calculated values for denitrification laboratory experiments of approximately 1.0.

Likely due to $\delta^{18}O\text{-}NO_2^-$ equilibration with $\delta^{18}O\text{-}H_2O$ and subsequent NO_2^- reoxidation to NO_3^-, Knöller et al. (2011) also found a $\varepsilon^{15}N/\varepsilon^{18}O$ of 3 ($\varepsilon^{15}N_{NO3}$ = -16.2 ‰ and $\varepsilon^{18}O_{NO3}$ = -5.5 ‰), using succinate as electron donor. These results might be coherent with our results after such a long incubation (approximately 200 days) and considering that NO_2^- accumulation was observed. After $\delta^{18}O\text{-}NO_2^-$ exchange with $\delta^{18}O\text{-}H_2O$, which ranges between -4 and -7 ‰ in the groundwater employed for the experiments, if NO_2^- reoxidates to NO_3^-, a decreased $\delta^{18}O\text{-}NO_3^-$ enrichment might be expected compared to the $\delta^{15}N\text{-}NO_2^-$ enrichment. Therefore, the resulting $\varepsilon^{15}N/\varepsilon^{18}O$ might be higher than those close to 1.0 usually resulting from NO_3^- reduction to NO_2^- and subsequent reduction to gaseous products.

Table 4.1. Range of $\varepsilon^{15}N_{NO3/N2}$, $\varepsilon^{18}O_{NO3/N2}$ and $\varepsilon^{15}N/\varepsilon^{18}O$ values determined in the laboratory experiments. The results include the batch and flow-through experiments. Legend: GW = groundwater, SGW = synthetic groundwater, ARW = agricultural runoff water, μ = microorganisms.

Catalyst	Electron acceptor	Electron donor	Medium	$\varepsilon^{15}N_{NO3/N2}$	$\varepsilon^{18}O_{NO3/N2}$	$\varepsilon^{15}N/\varepsilon^{18}O$
μ from sediment and GW	NO_3^-	C (sediment) + Fe^{2+} minerals	GW	-12.0	-10.9	1.1
μ from sediment and GW	NO_3^-	Mag-NP	GW	-33.1	-10.7	3.1
μ from sediment and GW	NO_3^-	$C_2H_4O_2$	GW	-12.6	-13.3	0.9
μ from sediment and GW	NO_3^- ± Cr^{6+}	C_2H_6O	GW	-23.9	-25.7	0.9
μ from corn stubble and ARW	NO_3^-	Corn stubble	ARW	-15.7 to -28.3	-9.7 to -30.4	0.8 to 1.6
μ from wheat hay and ARW	NO_3^-	Wheat hay	ARW	-31.9	-18.0	1.8
μ from animal compost and ARW	NO_3^-	Animal compost	ARW	-10.5	-12.6	0.8
μ from whey	NO_3^-	Whey	SGW	-8.6 to -10.9	-5.5 to -16.3	0.7 to 1.6

By using ε values determined at laboratory to estimate the natural or induced NO_3^- reduction at field-scale, interferences from processes other than denitrification that could also lead to a concentration decrease at field-scale (e.g., dilution due to water discharges

from rainfall) are avoided. Carrey et al. (2013), Torrentó et al. (2011) and Vidal-Gavilan et al. (2013) already applied the $\varepsilon^{15}N_{NO3/N2}$ and $\varepsilon^{18}O_{NO3/N2}$ values obtained from laboratory experiments under closed conditions, using either intrinsic or added electron donors, to quantify the extent of natural or induced denitrification in polluted groundwater. In a similar way, some of the values obtained in these laboratory experiments were later applied to calculate the denitrification efficiency in field-scale studies.

4.2.2. Nitrite and nitrous oxide isotopic characterization

In this section, only the experiments focusing on the evaluation of the use of Fe^{2+} minerals to promote the denitrification are discussed. It includes the results from the biotic experiments with NO_3^- and Mag-NP, the abiotic experiments with NO_2^- and Fe^{2+} (from minerals and/or aqueous), and a biotic experiment with NO_2^- and acetate that was performed as a control. The discussion addresses the usefulness of the isotopic characterization of the denitrification intermediates NO_2^- and N_2O to distinguish different biotic and abiotic reactions that could take place simultaneously if Fe^{2+}-containing minerals are applied to remediate NO_3^- polluted water bodies.

Focusing on the NO_2^- isotopic characterization in the experiments with synthetic seawater, no differences in the determined $\varepsilon^{18}O_{NO2/N2O}$ and $\varepsilon^{15}N_{NO2/N2O}$ were observed between the NO_2^- abiotic reduction by Fe^{2+} from biotic or synthetic origin and neither when using aqueous Fe^{2+} or aqueous plus mineral-associated Fe^{2+} (**Table 4.2**). In contrast, higher ε were found for the experiments with only mineral-associated Fe^{2+}. Furthermore, in these abiotic experiments, the $\varepsilon^{15}N/\varepsilon^{18}O$ ranged from 1.4 to 1.8, while for the NO_2^- biotic reduction by acetate in a pure culture of *Shewanella loihica*, the obtained $\varepsilon^{15}N/\varepsilon^{18}O$ (0.3) is one of the lowest values reported up to date (**Table 1.1**). Hence, in laboratory microcosms with *S. loihica* as the sole existing NO_2^--reducing microorganism, the $\varepsilon^{15}N/\varepsilon^{18}O$ calculated in the present experiment could be used to distinguish the biotic and abiotic NO_2^- reduction. However, a field-scale application of the $\varepsilon^{15}N/\varepsilon^{18}O$ ratio to distinguish the different mechanisms of NO_2^- reduction should be discarded since the values reported in the literature for the NO_2^- abiotic reduction by Fe^{2+} oxidation overlaps those of the NO_2^- reduction by other heterotrophic bacteria (**Table 1.1 and Table 4.2**). On the other hand,

observing a correlation between the $\delta^{15}N_{NO2}$ and the natural logarithm of the aqueous Fe^{2+} concentration could be useful to discard the occurrence of heterotrophic NO_2^- reduction at field-scale.

Table 4.2. Range of $\varepsilon^{15}N_{NO2/N2O}$, $\varepsilon^{18}O_{NO2/N2O}$ and $\varepsilon^{15}N/\varepsilon^{18}O$ values determined in the laboratory experiments. The results include biotic and abiotic batch experiments. Legend: DIW = deionized water with NO_2^-, SSW = synthetic seawater with NO_2^-, aq = aqueous, s = associated to minerals.

Catalyst	Electron acceptor	Electron donor	Medium	$\varepsilon^{15}N_{NO2/N2O}$	$\varepsilon^{18}O_{NO2/N2O}$	$\varepsilon^{15}N/\varepsilon^{18}O$
Shewanella loihica	NO_2^-	Acetate	SSW	-1.6	-5.3	0.3
Abiotic	NO_2^-	Synthetic Fe^{2+} (aq)	DIW	-14.1	-	-
Abiotic	NO_2^-	Synthetic Fe^{2+} (aq+s)	DIW	-14.1 to -17.8	-	-
Abiotic	NO_2^-	Synthetic Fe^{2+} (aq)	SSW	-8.6	-6.3	1.4
Abiotic	NO_2^-	Synthetic Fe^{2+} (s)	SSW	-19.7	-11.4	1.7
Abiotic	NO_2^-	Synthetic Fe^{2+} (aq+s)	SSW	-8.7	-5.2	1.7
Abiotic	NO_2^-	Biotic Fe^{2+} (aq+s)	SSW	-8.1	-4.6	1.8

Moving to the N_2O isotopic characterization, a much higher $\delta^{15}N$-N_2O variation was found for biotic experiments (NO_3^- reduction to N_2 by Mag-NP) compared to abiotic experiments (NO_2^- reduction to N_2O by aqueous Fe^{2+}). Hence, observing important $\delta^{15}N$-N_2O variations in denitrification studies could be indicative of biotic reactivity. Chen et al. (2018) also observed a higher increase of $\delta^{15}N$-N_2O in biotic compared to abiotic NO_2^- reduction experiments. Also, the measured $\delta^{15}N$ can be compared with the modelled substrate and product $\delta^{15}N$ composition by applying the calculated $\varepsilon^{15}N_{NO3/N2}$ and $\varepsilon^{15}N_{NO2/N2O}$ in the batch experiments (Mariotti et al., 1981). Since the N_2O is an intermediate of the NO_3^- biotic reduction but the final product of the abiotic NO_2^- reduction, the determined $\delta^{15}N$-N_2O should fit the initial $\delta^{15}N$ of the substrate at the end of the NO_2^- abiotic reduction but should be higher than that for the NO_3^- biotic reduction. In the Mag-NP biotic experiment, the $\delta^{15}N$-N_2O determined in most of the samples was above the modelled line (**Figure 4.7**), indicating a further reduction of N_2O to N_2. Contrarily, in the abiotic experiments (**Figure 4.7**), the $\delta^{15}N$-N_2O of the samples was initially below the modelled line but increased until approaching the substrate initial $\delta^{15}N$ at the end of the reaction, suggesting the generation of the intermediate NO and confirming that N_2O was the end product. Similarly to our

results, Chen et al. (2018) also found initial $\delta^{15}N\text{-}N_2O$ more negative than the starting $\delta^{15}N\text{-}NO_2^-$ due to NO generation, while Jones et al. (2015) also found a good correlation between the calculated $\varepsilon^{15}N_{NO2}$ and the measured $\delta^{15}N\text{-}N_2O$.

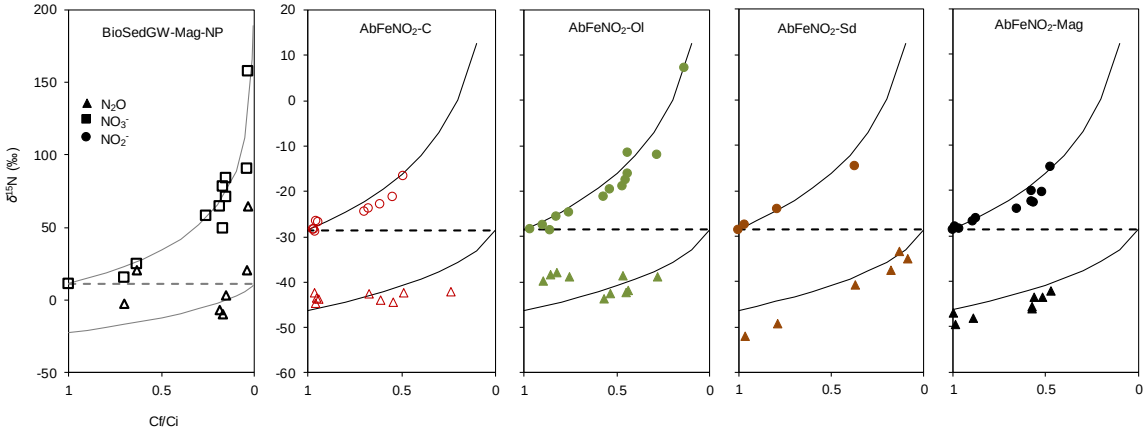

Figure 4.7. $\delta^{15}N$ evolution of substrate and nitrous oxide. Modelled and measured $\delta^{15}N$ of the N_2O and the substrate in the BioSedGW-Mag-NP (**A**) and AbFeNO$_2$ (**B**) experiments. This model was first described by Mariotti et al. (1981).

To assess the contributions of the biotic and abiotic NO_2^- reduction by Fe^{2+} oxidation, performing new experiments to determine the $\varepsilon^{15}N_{NO2/N2}$ and the $\varepsilon^{15}N_{N2O/N2}$ in the biotic experiments could be advantageous. Liu et al. (2018) assessed the contribution of each reaction by modelling the kinetics of each reaction tested separately. They found a major contribution of the abiotic compared to the biotic reaction for the Fe^{2+} oxidation, but a major contribution of the biotic compared to the abiotic reaction for the NO_2^- reduction. The use of models developed either by using isotope or chemical data might be limited at field-scale due to the complexity of the reactions. For example, the production of exopolymeric substances (EPS) could increase the NO_2^- abiotic reduction rate due to complexation with the Fe^{2+} (Jamieson et al., 2018), and as observed in our experiments with synthetic seawater, the biotically produced Fe^{2+} is more reactive than synthetic Fe^{2+}.

4.2.3. Chromium isotopic characterization

Since the Cr^{6+} could compete with NO_3^- for the available electron donors, the implications on the isotopic fractionation of these compounds if simultaneously found in polluted water bodies must be addressed, especially, if the ε values are intended to be used to trace its natural or induced reduction. This hypothesis is also valid for the simultaneous presence of other electron acceptors in contaminated sites.

Either in experiments with (BioCrN) or without (BioCr) NO_3^-, two slopes were observed for the $\varepsilon^{53}Cr$ calculations during the Cr^{6+} reduction (**Figure 4.8**). The first stage was defined by the samples with a higher Cr^{6+} content (0.21 to 0.06 mM) and showed higher $\varepsilon^{53}Cr$ (-1.4 and -1.8 ‰) compared to the second stage (-0.2 and -0.9 ‰), that corresponded to samples with lower Cr^{6+} concentration (0.002 to 0.05 mM). Chen et al. (2018) also found two-stage trends for the Cr^{6+} reduction under various conditions. They found $\varepsilon^{53}Cr$ ranging from -2.6 to -2.8 ‰, during the first stage and between -1.0 and -1.1 ‰ for the second stage. These authors suggested that the decreased Cr^{6+} bioavailability when the reduction progresses could mask the isotopic fractionation. However, in other biotic Cr^{6+} reduction experiments, such two-stage trends were not observed (Basu et al., 2014; Sikora et al., 2008). This two-stage pattern could have implications when using $\varepsilon^{53}Cr$ values calculated from laboratory experiments to quantify the natural or induced Cr^{6+} reduction, since different $\varepsilon^{53}Cr$ values should be used depending on the Cr^{6+} concentration in order to not underestimate or overestimate the extent of the reaction. On the other hand, when Cr^{6+} was concomitantly reduced with NO_3^-, a slightly higher $\varepsilon^{53}Cr$ (absolute value) was obtained compared to the absence of NO_3^-, although the reduction rate was similar. However, Han et al. (2012) found a much lower $\varepsilon^{53}Cr$ (–0.4 ‰) under denitrifying conditions compared to in the absence of NO_3^- (-2 ‰), while Chen et al. (2018) obtained similar $\varepsilon^{53}Cr$ values in the presence (-2.4 ‰ and -0.9 ‰) and absence (-2.7 ‰ and -1.1 ‰) of NO_3^-. Hence, the presence of NO_3^- might influence the $\varepsilon^{53}Cr$, and when calculating Cr^{6+} reduction efficiency from field-based data, the $\varepsilon^{53}Cr$ values employed should take into account the presence or absence of NO_3^-. In addition, since the $\varepsilon^{53}Cr$ (single stage) calculated for the Cr^{6+} biotic reduction range from -1.8 to -4.5 ‰ (Basu et al., 2014; Sikora et al., 2008) and for the abiotic reduction from -2.9 ‰ to -4.9 ‰ have been reported (Døssing et al., 2011; Ellis et

al., 2002; Kitchen et al., 2012), it is not likely possible to distinguish and abiotic reactivity from the biotic one.

In the case of NO_3^-, its attenuation was slower in the presence of Cr(VI) compared to absence. Nevertheless, we obtained equal $\varepsilon^{15}N_{NO3/N2}$ and $\varepsilon^{18}O_{NO3/N2}$ values (-23.9 ‰ and -25.7 ‰, respectively) for the experiments with or without Cr(VI) (**Table 4.1**).

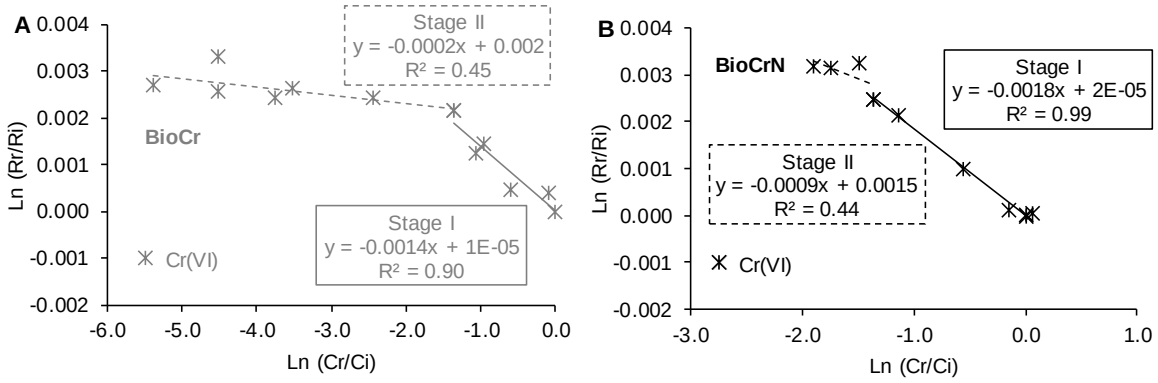

Figure 4.8. Hexavalent chromium isotopic fractionation during the batch experiments. $\varepsilon^{53}Cr$ calculated for the Cr^{6+} reduction experiments without (**A**) and with (**B**) NO_3^-.

4.2.4. Carbon compounds isotopic characterization

In this section, the usefulness of the $\delta^{13}C$ analysis both from organic and inorganic C compounds to get insight into the fate of the applied electron donor during biostimulation treatments to induce the heterotrophic denitrification is discussed. The results of the flow-through experiment testing whey and the batch experiments testing rural waste products as potential electron donors are presented as an example.

In the flow-through experiment, as NPDOC in the outflow decreased due to electron donor consumption (whey), the remaining DOC became enriched in $\delta^{13}C$ since bacteria preferentially consumed the lighter C molecules (**Figure 4.6**). The $\delta^{13}C$ results only covered the first ten days of the biostimulation strategy; therefore, it could be assumed that no biomass degradation or cell lysis events occurred, and bacterial biomass organic C pool contribution was negligible in this period. On the other hand, while the product DIC

concentration increased, it became depleted in $\delta^{13}C$, while during the recovery period, the $\delta^{13}C$-DIC was progressively enriched and coupled to a concentration decrease until both concentration and isotopic composition reached the initial synthetic water values (**Figure 4.6**). Both the $\delta^{13}C$-DIC and DIC concentration remained mainly constant at partial denitrification Stages IV and V. The measured $\delta^{13}C$-DIC at the outflow samples was found to depend on the $\delta^{13}C$ of the inflow water DIC (-9 ‰), the $\delta^{13}C$ of whey (-28 ‰), the isotopic fractionation produced during bacterial metabolism, and it might had been also influenced by the equilibrium between the CO_2(aq), HCO_3^- and CO_3^{2-} species (Blaser and Conrad, 2016; Mariotti, 1991).

The influence of the initial $\delta^{13}C$ of the electron donor on the product $\delta^{13}C$-DIC was also observed in the rural waste products batch experiments. The initial $\delta^{13}C$-DIC in water of -13.1 ‰ decreased to -15.5 ‰ and -20.0 ‰ in the microcosms containing hay and compost, respectively, but remained unchanged in the stubble experiment. The most significant change in the $\delta^{13}C$-DIC was observed for the experiment involving hay, which presented a lower $\delta^{13}C$-C_{bulk} (-27.8 ‰) compared to that of compost (-25.4‰); stubble did not produce any change because its $\delta^{13}C$-C_{bulk} (-13.6 ‰) is close to the $\delta^{13}C$-DIC of water (-13.1 ‰). Hay and stubble presented a different intrinsic $\delta^{13}C$-C_{bulk} as they are classified as C4 and C3 plants, respectively (Leary, 1988). An isotopic fractionation effect derived from the bacterial C metabolism did not seem to be significant under the tested conditions. These results showed that the $\delta^{13}C$-DIC analysis can be applied to assess the efficiency of biostimulation strategies at field-scale only when using C sources with an intrinsic $\delta^{13}C$-C_{bulk} differing from the $\delta^{13}C$-DIC of water (such as C4 plant materials).

4.3. Evaluation of the natural or induced denitrification at field-scale

During the field-scale studies (see **sections 3 and 3.2**), the ε values determined for NO_3^- from the laboratory experiments were applied by using the **Equation 3.2**, which is derived from the Rayleigh model, to evaluate the natural or induced denitrification in three different polluted sites.

4.3.1. Tracing induced denitrification in a polluted aquifer

As explained in **sections 2.1 and 3.2**, a pilot-plant was set up in Sant Andreu de Llavaneres to induce in-situ heterotrophic denitrification by injecting CH_3COOH by pulses for 22 months into an alluvial aquifer. Prior to the treatment, natural NO_3^- attenuation was not observed. The sampling campaigns in the pilot-plant began one month after the CH_3COOH injections started and continued for two years, with the last survey being performed two months after stopping the injections. The unaffected MW (n = 6) presented average values of 0.9 mM (SD = 0.04) for NO_3^- concentration, +6.3 ‰ (SD = 1.3) for δ^{15}N-NO_3^- and +4.2 ‰ (SD = 0.9) for δ^{18}O-NO_3^-, which were considered to be the groundwater NO_3^- background composition. These isotopic values suggested that NO_3^- pollution in the studied aquifer was derived from N inorganic fertilizer that had been volatilized and nitrified (**Figure 4.9**). Following the electron donor addition, the three monitoring piezometers showed a marked NO_3^- decrease. Contrarily, a flat trend in the NO_3^- evolution was observed at the EW (**Figure 4.10**), showing concentrations between 13 % and 33 % lower than the MW. In all the samples NO_2^- was below 0.02 mM and NH_4^+ was below 0.01 mM. Therefore, pollution swapping due to accumulation of these compounds was discarded. During the initial operation (1st month), the NO_3^- isotopic composition did not show a relevant δ^{15}N or δ^{18}O enrichment, indicating that the denitrification was not significant (**Figure 4.11A**). After seven operation months, and until the end of the monitoring period, a clear δ^{15}N-NO_3^- and δ^{18}O-NO_3^- enrichment evidenced the biological NO_3^- reduction at the pilot-plant. The degree of reduction depended on the specific point and sampling campaign. According to the concentration measured, more than 95 % NO_3^- was reduced at PZ1 in the 14th, 17th and 19th months, and at PZ2 in the 17th month. However, those

samples could not be isotopically analyzed, since the NO_3^- concentration was below the detection limit. The isotopic composition of the remnant samples determined that the denitrification at the pilot-plant piezometers reached a significance of approximately 50 %. Even two months after stopping the biostimulation (month 24th), more than a 50 % of the groundwater NO_3^- was still denitrified at PZ1.

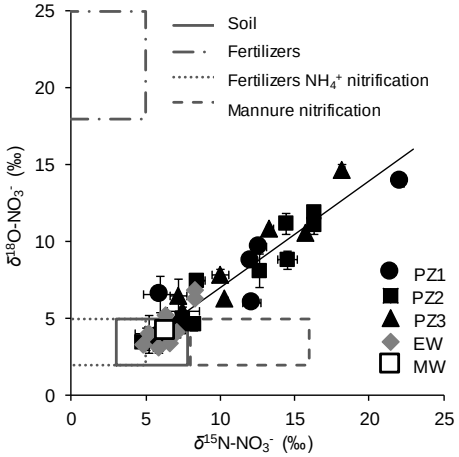

Figure 4.9. $\delta^{15}N$ vs $\delta^{18}O$ diagram from field samples. Results from the piezometers and the EW samples and mean value of the unaffected MW, including standard deviation. The regression line is presented as a continuous black line (slope = 0.7 (r^2 = 0.95)). The boxes (grey continuous and dashed lines) represent NO_3^- sources from Vitòria et al., (2004) and references therein.

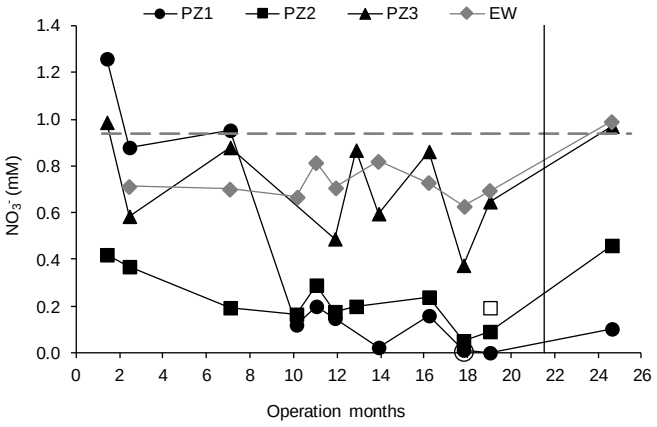

Figure 4.10. Nitrate evolution in the pilot-plant. The dashed grey line corresponds to the MW mean concentration. Empty symbols for PZ1 and PZ2 correspond to bottom samples (two-depth sampling). The vertical line corresponds to the last injection date.

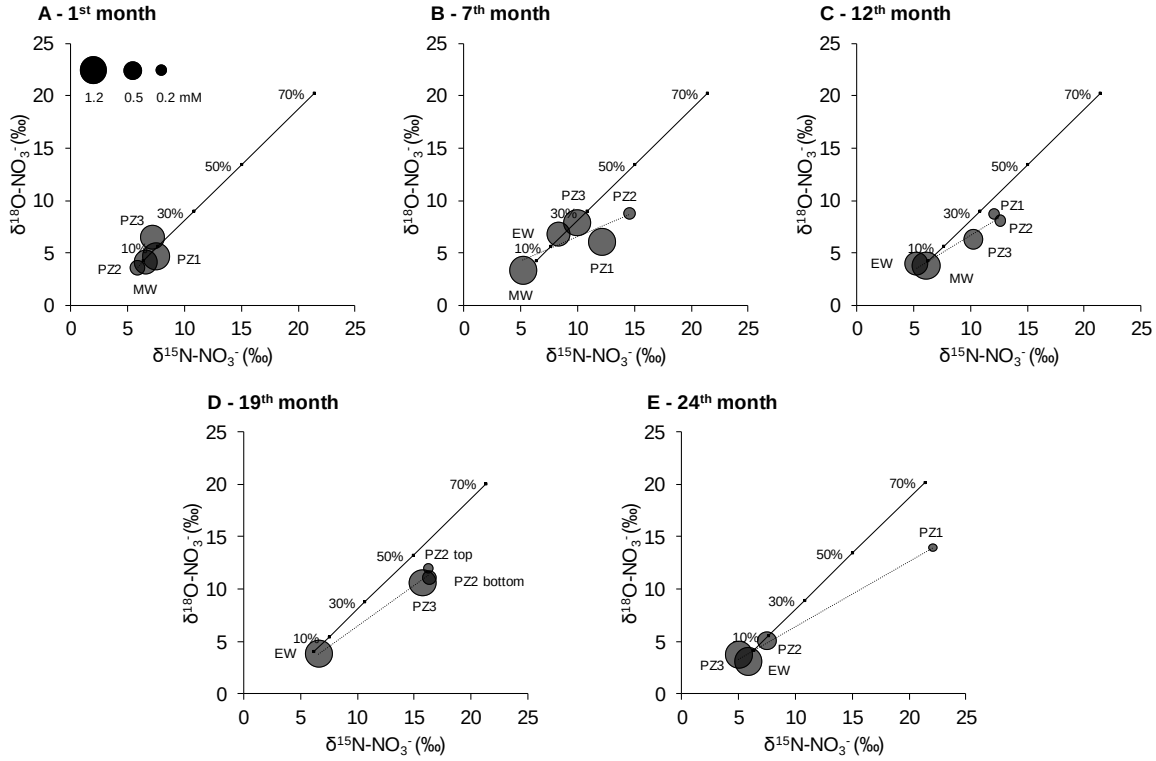

Figure 4.11. Representative sampling campaigns from the pilot-plant. A) 1st month, 1.2 slope (r^2 = 0.45); **B**) 7th month, 0.5 slope (r^2 = 0.8); **C**) 12th month, 0.6 slope (r^2 = 0.9); **D**) 19th month, 0.8 slope (r^2 = 1.0); **E**) 24th month, 0.6 slope (r^2 = 1.0). Regression line for each campaign is presented as a dashed line. The DEN % line (continuous line) was calculated using the isotopic fractionation values obtained in laboratory experiments and the average concentration and isotopic composition of the MW as initial values.

In the 7th month campaign, a slight isotopic enrichment and NO_3^- concentration decrease was observed at the EW with respect to the MW, being indicative of the denitrification occurrence (**Figure 4.11B**). However, from the 7th month onward, despite the lower NO_3^- concentration at the EW with respect to the MW, the isotopic data did not show significant differences (e.g., 12th or 19th month) (**Figure 4.11C-D**). The reason is that the groundwater extracted at the EW was a mix of denitrified groundwater from PZ1 and PZ2 located upstream and untreated water from the MW located downstream, due to a depression cone at EW forced by the water extraction (**Figure 2.2**). Furthermore, several samples from the field site showed lower $\delta^{18}O\text{-}NO_3^-$ values than expected, considering the denitrification slope calculated using the microcosm experiments (e.g., 7th, 12th and 19th month) (**Figure 4.11B-C-D**). This finding can be explained as the result of the NO_2^- reoxidation to NO_3^- throughout the remediation treatment (Wunderlich et al., 2013). The

shift in the slope throughout the induced denitrification treatment can provide information regarding the relevance of the NO_2^- reoxidation process at the field-scale. The $\delta^{15}N\text{-}NO_3^-$ and $\delta^{18}O\text{-}NO_3^-$ values close to the theoretical DEN % line might point to a direct NO_2^- reduction to gaseous N products, while lower $\delta^{18}O\text{-}NO_3^-$ values might point to the NO_2^- reoxidation. Slopes near 0.5 were generally observed during the initial biostimulation (e.g., 7th month) (**Figure 4.11B**), which became closer to 1.0 throughout the pilot-plant operation (e.g., 19th month) (**Figure 4.11D**). At the last sampling campaign, corresponding to the recovery period after stopping the CH_3COOH injections, the slope was again closer to 0.5 (24th month) (**Figure 4.11E**). An unsolved question is the effect of the biotic and abiotic NO_2^- oxidation to NO_3^- upon $\delta^{15}N\text{-}NO_3^-$ throughout denitrification in groundwater. It is expected that the possible effect upon $\delta^{15}N\text{-}NO_3^-$ would be lower than the observed for $\delta^{18}O\text{-}NO_3^-$ during the abiotic NO_2^- oxidation, enabling the $\delta^{18}O\text{-}NO_3^-$ versus $\delta^{15}N\text{-}NO_3^-$ slope to decrease.

The isotopic results for dissolved SO_4^{2-} from a subset of the pilot-plant samples showed a 0.4 (r^2 = 0.93) slope from the regression line between $\delta^{34}S\text{-}SO_4^{2-}$ and $\delta^{18}O\text{-}SO_4^{2-}$, which is in the range of the slopes from 0.25 to 1.4 reported in the literature for BSR (Aharon and Fu, 2000; Antler et al., 2013). However, the samples with the lowest SO_4^{2-} concentration were not the most enriched in $\delta^{18}O\text{-}SO_4^{2-}$ and $\delta^{34}S\text{-}SO_4^{2-}$ and vice versa. Since there was surplus NO_3^- in the groundwater and due to the lack of correlation between the SO_4^{2-} chemical and isotopic data, BSR did not likely play a significant role at the pilot-plant. In the same context of water quality, the presence of remaining CH_3COOH at a harmful level for consumption was also discarded due to the excess of electron acceptors such as NO_3^- or SO_4^{2-} in groundwater since denitrification was not complete at the EW.

4.3.2. Tracing the natural denitrification in a nitrate and chromium polluted aquifer

Groundwater in some areas within the MRB (Argentina) is affected by both Cr^{6+} and NO_3^- pollution (see **sections 2.2 and 3.2**). In groundwater samples collected in the San Ignacio neighbourhood, next and downstream of the chemical industry plant that leaded the Cr^{6+} contamination, Cr^{6+} concentrations ranged from below detection limit to 0.041 mM, NO_3^- from 0.5 to 3.9 mM and NPDOC from 0.08 to 0.2 mM. Near the industry, the $\delta^{53}Cr$ was

+1.2 ‰ but the values increased to +3.4 ‰ downstream, suggesting Cr^{6+} biotic reduction. The concomitant NO_3^- reduction was evidenced by an enrichment in the heavy isotopes from +10.6 to +22.8 ‰ for the $\delta^{15}N$ and from +6.1 to +12.7 ‰ for the $\delta^{18}O$. The samples with higher $\delta^{53}Cr$ also presented higher $\delta^{15}N_{NO3}$ and $\delta^{18}O_{NO3}$. In accordance to the NO_3^- isotope composition, the source of contamination was related to septic systems leakage (**Figure 4.12**), which could also be the source of NPDOC that allowed both the denitrification and Cr^{6+} reduction at the study site.

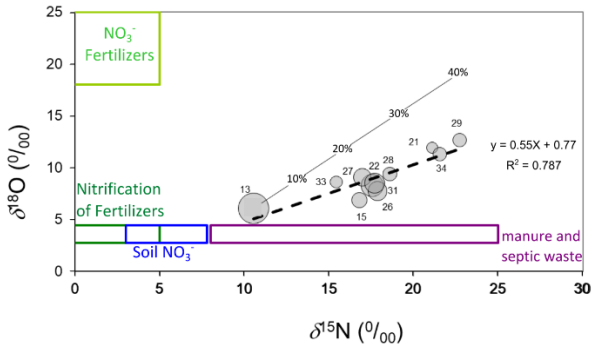

Figure 4.12. Estimated percentage of denitrification in the study site. The boxes of the NO_3^- sources have been obtained from Vitòria et al (2004) and references therein. The solid line represents the Rayleigh model used to calculate the denitrification percentage, while the dotted line is the linear regression of the field samples.

To calculate the percentage of Cr^{6+} attenuation, we used the sample P34 as initial value of Cr^{6+} concentration and isotope composition, because the well is located close to the source of contamination and it presented the highest Cr^{6+} content. Also, we used the $\varepsilon^{53}Cr$ values calculated for the two isotopic fractionation stages observed in the laboratory experiments containing both NO_3^- and Cr^{6+} to perform the Rayleigh model (see **section 4.2.3**). By using the $\varepsilon^{53}Cr$ from stage I, the attenuation was 60-70 %, while with the $\varepsilon^{53}Cr$ from stage II, the attenuation increased to 80-90 % (**Figure 4.13**). The sample with higher Cr^{6+} concentration (P28), fell in the theoretical line from applying the stage I $\varepsilon^{53}Cr$, the sample with medium Cr^{6+} concentration (P31), fell in the theoretical line from applying the stage II $\varepsilon^{53}Cr$, while samples with lowest Cr^{6+} concentrations (P33, P21, P22 and P29), fell in a theoretical line of dilution (**Figure 4.13**). The decrease in Cr^{6+} concentration in these samples would be partially linked to a process of mixing with uncontaminated groundwater and not only to reduction of Cr^{6+} to Cr^{3+}. With regards to NO_3^- attenuation, the sample with

the highest NO_3^- content was assumed as initial value (P13) and ε values calculated from the laboratory experiments were employed for the Rayleigh model. The samples collected in the field presented a NO_3^- attenuation between 20 and 30 % and showed a lower slope between $\delta^{18}O\text{-}NO_3^-$ and $\delta^{15}N\text{-}NO_3^-$ (0.5) with respect to the batch experiments (1.0) (**Figure 4.12**), which agrees with reported slopes of nearly 0.5 for field scale studies and nearly 1.0 for laboratory studies (Carrey et al., 2013; Critchley et al., 2014; Otero et al., 2009; Wunderlich et al., 2012). The main reason is the oxidation of the intermediates NO_2^- and/or NH_4^+ to NO_3^- at field-scale (Granger and Wankel, 2016; Wunderlich et al., 2013). Overall, according to the ε values calculated in laboratory experiments, for the studied groundwater samples, the natural attenuation of Cr^{6+} is considerably larger than the natural attenuation of NO_3^-. These high percentages of attenuation could explain the low concentrations of NPDOC detected in the groundwater samples at the study site.

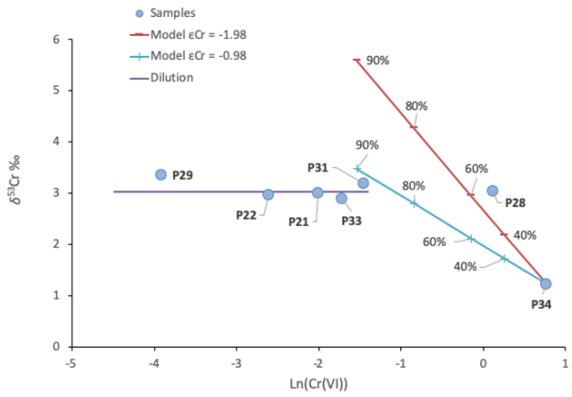

Figure 4.13. Isotopic characterization of the field samples. The red line represents the Rayleigh model calculated with the $\varepsilon^{53}Cr$ obtained from stage I, while the blue line represents the Rayleigh model calculated with the $\varepsilon^{53}Cr$ obtained from stage II, determined during the laboratory experiments. The purple line represents dilution with unpolluted groundwater.

4.3.3. Tracing nitrate natural and induced attenuation in a CW

As explained in **sections 2.3 and 3.2**, a surface flow CW was constructed in the Lerma Basin in order to diminish the release of NO_3^- to the Arba River. Previous to the application of an external electron donor, three field surveys were performed to test two different flow

rate operating conditions (~5.5 and ~2.5 L/s) to evaluate the natural NO_3^- attenuation. At the CW, NO_3^- was not reduced at ~5.5 L/s, but a slight attenuation (from 1.3 to 0.8 mM) occurred at ~2.5 L/s (**Figure 4.14**). In all samples, NO_2^- was below the detection limit and NH_4^+ below 0.01 mM. The decrease in NO_3^- was coupled to increases in $\delta^{15}N\text{-}NO_3^-$ and $\delta^{18}O\text{-}NO_3^-$ from the inlet to the outlet of the CW. The slope of the relation between $\delta^{18}O\text{-}NO_3^-$ and $\delta^{15}N\text{-}NO_3^-$ for these samples was 0.8 (r^2 = 0.91), which is indicative of denitrification activity (Aravena et al., 1998). The intrinsic denitrification activity in the CW did not support complete denitrification, likely due to the low NPDOC content of the water (0.4 – 0.6 mM).

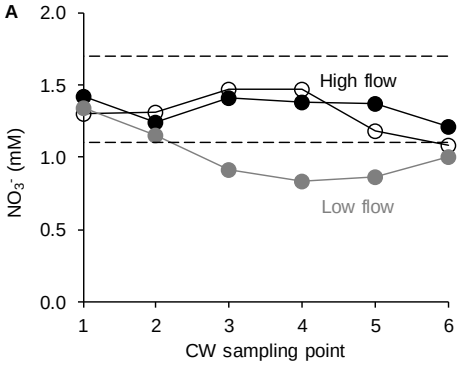

Figure 4.14. Nitrate evolution in the CW before biostimulation. Black or grey circles depict the sampling campaigns at ~5.5 L/s (full symbols for June 14, 2017 and empty symbols for September 5, 2017), or ~2.5 L/s (September 12, 2017), respectively. Dashed lines represent the range of NO_3^- concentrations measured at the inlet of the CW throughout the study period.

For this reason, the second and third periods of the study involved the application of corn stubble on September 25, 2017, and May 11, 2018, respectively. Throughout these two periods, the CW was operated at a higher flow rate (~16 L/s), and samples were collected to evaluate the induced denitrification. After 14 days following the application of stubble in autumn (September 25, 2017), denitrification was almost complete at the outlet (H6) (**Figure 4.15A**). The NO_2^- accumulation reached 0.2 mM at the outlet 7 days after the treatment, but decreased to 0.1 mM after 14 days. The maximum NH_4^+ concentration (0.01 mM) was measured at the outlet 7 days after treatment, pointing to a non-significant contribution of DNRA. The lifetime of the treatment in autumn was estimated to be between 2 and 4 weeks. Application of stubble in spring (May 5, 2018) also induced

denitrification, showing complete NO_3^- removal at the outlet 14 days after the stubble application. A decrease in NO_2^- and NH_4^+ accumulation with time was observed as during the previous treatment period. The NO_3^- concentration in the outlet then began to increase progressively until reaching a level similar to that at the inlet by approximately 100 days after treatment (**Figure 4.15B**). Thus, the treatment in spring-summer had a lifetime of approximately 12 weeks, which is approximately three times longer than that of the treatment in autumn. This is in accordance with laboratory results and with previous wetland studies reporting increased denitrification rates at higher temperatures (Bachand and Horne, 1999; Christensen and Srensen, 1986; Si et al., 2018). Therefore, stubble was considered effective in removing N compounds from agricultural runoff water. On the other hand, the NPDOC concentration at the outlet increased with respect to the background values for 14 days after stubble application, indicating a release of organic C to the gully (up to 1.1 mM compared to background NPDOC of 0.5 to 0.8 mM). Because the gully contained NO_3^--polluted water, it was considered that the surplus organic C could lead to NO_3^- attenuation downstream. Furthermore, occurrence of BSR was discarded since no correlation between SO_4^{2-} concentration and isotopic composition was observed.

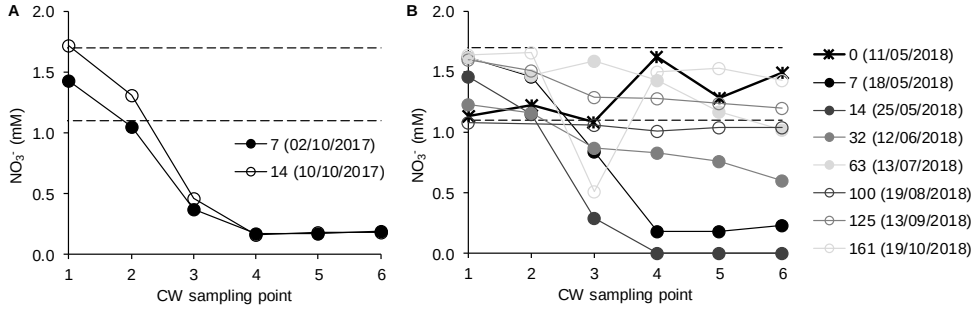

Figure 4.15. Nitrate attenuation in the CW after biostimulation. NO_3^- concentration along the CW, where dashed lines represent the range of NO_3^- concentrations measured at the inlet of the CW throughout the study period. In the legend the numbers correspond to days since the stubble application. The sampling campaigns are represented by shades of grey (from darker to lighter as time progressed). Application of stubble in autumn (**A**) and spring (**B**).

The $\varepsilon^{15}N_{NO3/N2}$ and $\varepsilon^{18}O_{NO3/N2}$ values obtained from lab-scale experiments in which fresh stubble was incubated at 24 and 16 ºC, and partially decomposed stubble was incubated at 24 ºC, were used to calculate three denitrification % lines that were plotted on a $\delta^{15}N$-NO_3^- versus $\delta^{18}O$-NO_3^- graph along with the isotopic results for the CW samples (**Figure**

4.16). These three laboratory conditions encompass the average temperatures recorded during the biostimulation periods tested at the CW. The slope of $\delta^{15}N\text{-}NO_3^-$ versus $\delta^{18}O\text{-}NO_3^-$ for the field samples collected after the biostimulation was 1.0 (r^2 = 0.98) (**Figure 4.16**). The similarity between the field-scale and lab-scale slopes, suggested that plant uptake did not likely contribute significantly to NO_3^- removal. The results showed that at least 60% of NO_3^- attenuation was achieved in the CW due to the induced denitrification. The largest contribution of denitrification was observed in the outlet samples (H6). By 14 days after the second stubble application, NO_3^- concentration in some samples was below the level required for the isotopic analysis. Therefore, the biostimulation achieved a NO_3^- attenuation percentage close to 100 %. The added stubble could have enhanced denitrification by increasing the organic C content of the water and by inhibiting O_2 production through photosynthesis, as previously hypothesized Jacobs and Harrison (2014) for floating vegetation in CWs. However, the denitrification efficiency was limited. The most likely explanations involve the high O_2 content of the inlet water and the vast surface available for O_2 diffusion, the high water flow rate tested in the CW (~16 L/s), and the possible generation of preferential flows within the CW (e.g., due to stubble accumulation in some points) that could have led to a lower degree of interaction between water and stubble.

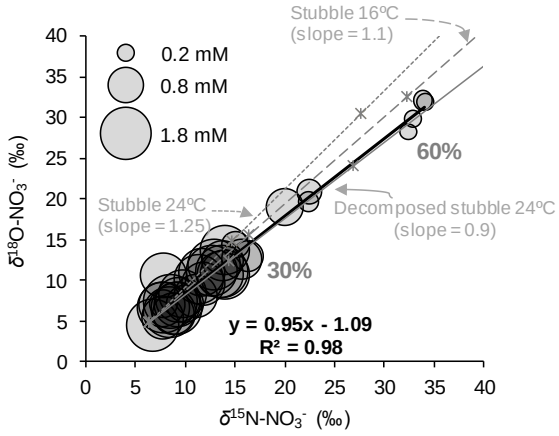

Figure 4.16. Denitrification efficiency in the CW determined from the laboratory-obtained *ε* values. Isotopic composition of the samples collected at the CW, including the regression line (black). The three denitrification % lines (grey) correspond to the three conditions tested in the laboratory that were closest to the CW conditions throughout the field-scale test.

REFERENCES

Aharon, P., Fu, B., 2000. Microbial sulfate reduction rates and sulfur and oxygen isotope fractionations at oil and gas seeps in deepwater Gulf of Mexico. Geochim. Cosmochim. Acta 64, 233–246. https://doi.org/10.1016/S0016-7037(99)00292-6

Antler, G., Turchyn, A. V., Rennie, V., Herut, B., Sivan, O., 2013. Coupled sulfur and oxygen isotope insight into bacterial sulfate reduction in the natural environment. Geochim. Cosmochim. Acta 118, 98–117. https://doi.org/10.1016/j.gca.2013.05.005

Aquilina, L., Roques, C., Boisson, A., Vergnaud-Ayraud, V., Labasque, T., Pauwels, H., Pételet-Giraud, E., Pettenati, M., Dufresne, A., Bethencourt, L., Bour, O., 2018. Autotrophic denitrification supported by biotite dissolution in crystalline aquifers (1): New insights from short-term batch experiments. Sci. Total Environ. 619–620, 842–853. https://doi.org/10.1016/j.scitotenv.2017.11.079

Aravena, R., Robertson, W.D., 1998. Use of multiple isotope tracers to evaluate denitrification in ground water: study of nitrate from a large-flux septic system plume. Ground Water 36, 975–982.

Bachand, P.A.M., Horne, A.J., 1999. Denitrification in constructed free-water surface wetlands: I. Very high nitrate removal rates in a macrocosm study. Ecol. Eng. 14, 9–15. https://doi.org/10.1016/S0925-8574(99)00016-6

Basu, A., Johnson, T.M., Sanford, R.A., 2014. Cr isotope fractionation factors for Cr(VI) reduction by a metabolically diverse group of bacteria. Geochim. Cosmochim. Acta 142, 349–361. https://doi.org/10.1016/j.gca.2014.07.024

Blaser, M., Conrad, R., 2016. Stable carbon isotope fractionation as tracer of carbon cycling in anoxic soil ecosystems. Curr. Opin. Biotechnol. 41, 122–129. https://doi.org/10.1016/j.copbio.2016.07.001

Braunschweig, J., Bosch, J., Meckenstock, R.U., 2013. Iron oxide nanoparticles in geomicrobiology: from biogeochemistry to bioremediation. N. Biotechnol. 30, 793–802. https://doi.org/10.1016/j.nbt.2013.03.008

Breulmann, M., Masyutenko, N.P., Kogut, B.M., Schroll, R., Dörfler, U., Buscot, F., Schulz, E., 2014. Short-term bioavailability of carbon in soil organic matter fractions of different particle sizes and densities in grassland ecosystems. Sci. Total Environ. 497–498, 29–37. https://doi.org/10.1016/j.scitotenv.2014.07.080

Buchwald, C., Grabb, K., Hansel, C.M., Wankel, S.D., 2016. Constraining the role of iron in environmental nitrogen transformations: Dual stable isotope systematics of abiotic NO_2^- reduction by Fe(II) and its production of N_2O. Geochim. Cosmochim. Acta. https://doi.org/10.1016/j.gca.2016.04.041

Carrey, R., Otero, N., Soler, A., Gómez-Alday, J.J., Ayora, C., 2013. The role of Lower Cretaceous sediments in groundwater nitrate attenuation in central Spain: Column experiments. Appl. Geochemistry 32, 142–152. https://doi.org/10.1016/j.apgeochem.2012.10.009

Carrey, R., Rodríguez-Escales, P., Soler, A., Otero, N., 2018. Tracing the role of endogenous carbon in denitrification using wine industry by-product as an external electron donor: Coupling isotopic tools with mathematical modeling. J. Environ. Manage. 207, 105–115. https://doi.org/10.1016/j.jenvman.2017.10.063

Chen, D., Liu, T., Li, X., Li, F., Luo, X., Wu, Y., Wang, Y., 2018. Biological and chemical processes of microbially mediated nitrate-reducing Fe(II) oxidation by Pseudogulbenkiania sp. strain 2002. Chem. Geol. 476, 59–69. https://doi.org/10.1016/j.chemgeo.2017.11.004

Chen, G., Qin, L., Han, J., Mu, Y., Yu, H., 2018. Two-stage chromium isotope fractionation during microbial Cr(VI) reduction. Water Res. 148, 10–18. https://doi.org/10.1016/j.watres.2018.09.034

Christensen, P.B., Srensen, J.A.N., 1986. Temporal Variation of Denitrification Activity in Plant-Covered , Littoral Sediment from Lake Hampen , Denmark 51, 1174–1179.

Coby, A.J., Picardal, F.W., 2005. Inhibition of NO_3^- and NO_2^- reduction by microbial Fe(III) reduction: Evidence of a reaction between NO_2^- and cell surface-bound Fe^{2+}. Appl. Environ. Microbiol. 71, 5267–5274.

https://doi.org/10.1128/AEM.71.9.5267-5274.2005

Cooper, D.C., Picardal, F.W., Schimmelmann, A., Coby, A.J., 2003. Chemical and Biological Interactions during Nitrate and Goethite Reduction by Shewanella putrefaciens 200 Chemical and Biological Interactions during Nitrate and Goethite Reduction by Shewanella putrefaciens 200. Appl. Environ. Microbiol. 69, 3517–3525. https://doi.org/10.1128/AEM.69.6.3517

Critchley, K., Rudolph, D.L., Devlin, J.F., Schillig, P.C., 2014. Stimulating in situ denitrification in an aerobic, highly permeable municipal drinking water aquifer. J. Contam. Hydrol. 171, 66–80. https://doi.org/10.1016/j.jconhyd.2014.10.008

Dawson, R.N., Murphy, K.L., 1972. The temperature dependency of biological denitrification. Water Res. 6, 71–83. https://doi.org/10.1016/0043-1354(72)90174-1

Døssing, L.N., Dideriksen, K., Stipp, S.L.S., Frei, R., 2011. Reduction of hexavalent chromium by ferrous iron: A process of chromium isotope fractionation and its relevance to natural environments. Chem. Geol. 285, 157–166. https://doi.org/10.1016/j.chemgeo.2011.04.005

Ellis, A.S., Johnson, T.M., Bullen, T.D., 2002. Chromium isotopes and the fate of hexavalent chromium in the environment. Science (80), 295, 2060–2062. https://doi.org/10.1126/science.1068368

Granger, J., Wankel, S.D., 2016. Isotopic overprinting of nitrification on denitrification as a ubiquitous and unifying feature of environmental nitrogen cycling. Proc. Natl. Acad. Sci. 113, E6391–E6400. https://doi.org/10.1073/pnas.1601383113

Han, R., Qin, L., Brown, S.T., Christensen, J.N., Beller, H.R., 2012. Differential isotopic fractionation during Cr(VI) reduction by an aquifer-derived bacterium under aerobic versus denitrifying conditions. Appl. Environ. Microbiol. 78, 2462–2464. https://doi.org/10.1128/AEM.07225-11

Jacobs, A.E., Harrison, J.A., 2014. Effects of floating vegetation on denitrification, nitrogen retention, and greenhouse gas production in wetland microcosms. Biogeochemistry 119, 51–66. https://doi.org/10.1007/s10533-013-9947-9

Jamieson, J., Prommer, H., Kaksonen, A.H., Sun, J., Siade, A.J., Yusov, A., Bostick, B., 2018. Identifying and Quantifying the Intermediate Processes during Nitrate-Dependent Iron(II) Oxidation. Environ. Sci. Technol. 52, 5771–5781. https://doi.org/10.1021/acs.est.8b01122

Jones, L.C., Peters, B., Lezama Pacheco, J.S., Casciotti, K.L., Fendorf, S., 2015. Stable Isotopes and Iron Oxide Mineral Products as Markers of Chemodenitrification. Environ. Sci. Technol. 49, 3444–3452. https://doi.org/10.1021/es504862x

Kitchen, J.W., Johnson, T.M., Bullen, T.D., Zhu, J., Raddatz, A., 2012. Chromium isotope fractionation factors for reduction of Cr(VI) by aqueous Fe(II) and organic molecules. Geochim. Cosmochim. Acta 89, 190–201. https://doi.org/10.1016/j.gca.2012.04.049

Leary, M.H.O., 1988. Carbon Isotopes in Photosynthesis. Bioscience 38, 328–336.

Liu, T., Chen, D., Luo, X., Li, X., Li, F., 2018. Microbially mediated nitrate-reducing Fe(II) oxidation: Quantification of chemodenitrification and biological reactions. Geochim. Cosmochim. Acta. https://doi.org/10.1016/j.gca.2018.06.040

Mariotti, A., 1991. Le carbone 13 en abondance naturelle, traceur de la dynamique de la matière organique des sols et de l'évolution des paléoenvironnements continentaux. Cah. Orstom, sér. Pédol. XXVI, 299–313.

Mariotti, A., Germon, J.C., Hubert, P., Kaiser, P., Letolle, R., Tardieux, A., Tardieux, P., 1981. Experimental determination of nitrogen kinetic isotope fractionation: Some principles; illustration for the denitrification and nitrification processes. Plant Soil 62, 413–430. https://doi.org/10.1007/BF02374138

Otero, N., Soler, A., Canals, À., 2004. Fertilizer Characterization: Isotopic Data (N, S, O, C, and Sr). Environ. Sci. Technol. 38, 3254–3262. https://doi.org/10.1021/es0348187

Otero, N., Torrentó, C., Soler, A., Menció, A., Mas-Pla, J., 2009. Monitoring groundwater nitrate attenuation in a regional system coupling hydrogeology with multi-isotopic methods: The case of Plana de Vic (Osona, Spain). Agric. Ecosyst. Environ. 133, 103–113. https://doi.org/10.1016/j.agee.2009.05.007

Si, Z., Song, X., Wang, Y., Cao, X., Zhao, Y., Wang, B., Chen, Y., Arefe, A., 2018. Intensified heterotrophic denitrification in constructed wetlands using four solid carbon sources: Denitrification efficiency and bacterial community structure. Bioresour. Technol. 267, 416–425. https://doi.org/10.1016/j.biortech.2018.07.029

Sikora, E.R., Johnson, T.M., Bullen, T.D., 2008. Microbial mass-dependent fractionation of chromium isotopes. Geochim. Cosmochim. Acta 72, 3631–3641. https://doi.org/10.1016/j.gca.2008.05.051

Sobczak, W. V., Findlay, S., 2002. Variation in Bioavailability of Dissolved Organic Carbon among Stream Hyporheic Flowpaths. Ecology 83, 3194–3209.

Straub, K.L., Schönhuber, W.A., Buchholz-Cleven, B.E.E., Schink, B., 2004. Diversity of ferrous iron-oxidizing, nitrate-reducing bacteria and their involvement in oxygen-independent iron cycling. Geomicrobiol. J. 21, 371–378. https://doi.org/10.1080/01490450490485854

Torrentó, C., Urmeneta, J., Otero, N., Soler, A., Viñas, M., Cama, J., 2011. Enhanced denitrification in groundwater and sediments from a nitrate-contaminated aquifer after addition of pyrite. Chem. Geol. 287, 90–101. https://doi.org/10.1016/j.chemgeo.2011.06.002

Vidal-Gavilan, G., Folch, A., Otero, N., Solanas, A.M., Soler, A., 2013. Isotope characterization of an in situ biodenitrification pilot-test in a fractured aquifer. Appl. Geochemistry 32, 153–163. https://doi.org/10.1016/j.apgeochem.2012.10.033

Wang, M., Hu, R., Zhao, J., Kuzyakov, Y., Liu, S., 2016. Iron oxidation affects nitrous oxide emissions via donating electrons to denitrification in paddy soils. Geoderma 271, 173–180. https://doi.org/10.1016/j.geoderma.2016.02.022

Wang, R., Yang, C., Zhang, M., Xu, S.Y., Dai, C.L., Liang, L.Y., Zhao, H.P., Zheng, P., 2017. Chemoautotrophic denitrification based on ferrous iron oxidation: Reactor performance and sludge characteristics. Chem. Eng. J. 313, 693–701. https://doi.org/10.1016/j.cej.2016.12.052

Warneke, S., Schipper, L.A., Matiasek, M.G., Scow, K.M., Cameron, S., Bruesewitz, D.A., McDonald, I.R., 2011. Nitrate removal, communities of denitrifiers and adverse effects in different carbon substrates for use in denitrification beds. Water Res. 45, 5463–5475. https://doi.org/10.1016/j.watres.2011.08.007

Wunderlich, A., Meckenstock, R., Einsiedl, F., 2012. Effect of different carbon substrates on nitrate stable isotope fractionation during microbial denitrification. Environ. Sci. Technol. 46, 4861–4868. https://doi.org/10.1021/es204075b

Wunderlich, A., Meckenstock, R.U., Einsiedl, F., 2013. A mixture of nitrite-oxidizing and denitrifying microorganisms affects the $\delta^{18}O$ of dissolved nitrate during anaerobic microbial denitrification depending on the $\delta^{18}O$ of ambient water. Geochim. Cosmochim. Acta 119, 31–45. https://doi.org/10.1016/j.gca.2013.05.028

Yang, Y., Chen, T., Morrison, L., Gerrity, S., Collins, G., Porca, E., Li, R., Zhan, X., 2017. Nanostructured pyrrhotite supports autotrophic denitrification for simultaneous nitrogen and phosphorus removal from secondary effluents. Chem. Eng. J. 328, 511–518. https://doi.org/10.1016/j.cej.2017.07.061

5. CONCLUSIONS

The results obtained from the present thesis allowed: I) to demonstrate the feasibility of using different low-cost electron donors to promote denitrification in polluted water bodies, II) to improve the knowledge on the parameters affecting the denitrification efficiency, III) to evaluate the occurrence of different reactions simultaneously to the biotic NO_3^- reduction during biostimulation treatments and IV) to trace the magnitude of natural and/or induced NO_3^- attenuation by using isotope tools in two aquifers and in a CW.

The laboratory experiments demonstrated that Mag-NP, corn stubble, wheat hay, animal compost and whey could promote denitrification in polluted water bodies. In these biotic experiments, complete NO_3^- reduction to N_2 was proved by transient NO_2^- accumulation, negligible N_2O release and insignificant contribution of DNRA on the NO_3^- attenuation. In the case of biostimulation strategies with Fe^{2+} compounds, it was found that NO_2^- could also be abiotically reduced giving N_2O as end-product, which can be further reduced to N_2 biotically. Furthermore, to avoid clogging issues during field-scale treatments due to electron donor or biomass release, the used ratio between electron donor and acceptor should be evaluated.

The $\varepsilon^{15}N_{NO3/N2}$ and $\varepsilon^{18}O_{NO3/N2}$ were calculated for all the batch experiments and for the stages of the flow-through experiment that allowed complete denitrification. For the recovery and partial denitrification stages, the NO_3^- isotopic characterization showed a mix of denitrified and non-denitrified water at the outflow. Other remarkable findings concerning the isotopic characterization of other compounds involved in denitrification in selected experiments are:

- For NO_2^-, the $\varepsilon^{15}N_{NO2/N2O}$ and $\varepsilon^{18}O_{NO2/N2O}$ allowed to distinguish the biotic from the abiotic NO_2^- reduction by Fe^{2+} at laboratory. However, application at field-scale might not be conclusive due to the wide range of values reported in the literature. Also, a correlation between the $\delta^{15}N_{NO2}$ and the natural logarithm of the Fe^{2+} concentration might allow to discard the heterotrophic NO_2^- reduction at laboratory and field-scale.
- For N_2O, a comparison between the measured and modelled $\delta^{15}N\text{-}N_2O$ using the ε value determined for the substrate, allowed distinguishing the biotic from the abiotic NO_2^- reduction. Large $\delta^{15}N\text{-}N_2O$ variations due to further reduction to N_2, might also denote biotic rather than abiotic NO_2^- reduction. These results are highly valuable since few isotopic data for N_2O has been reported in the literature up to date.
- The Cr^{6+}, a contaminant that can be reduced simultaneously to NO_3^- in the presence of an electron donor, presented a two-stage isotopic fractionation.
- The $\delta^{13}C$-DIC analysis might provide information on the fate of the applied electron donor only if using C sources with a $\delta^{13}C\text{-}C_{bulk}$ differing from the $\delta^{13}C$-DIC of water.

In the field-scale studies, the chemical and isotopic characterization allowed to evaluate the efficiency of the natural and/or induced denitrification. Using ε values determined at laboratory to estimate the extent of natural or induced NO_3^- reduction at field, allowed avoiding interferences from other processes that could also lead to a concentration decrease (e.g., dilution due to water discharges from rainfall). However, hydrogeological and biochemical effects could influence the results. Due to these effects, the percentages obtained from isotope data must be considered an estimation, not a precise calculation.

- During the in-situ groundwater remediation strategy by means of CH_3COOH injections in the Sant Andreu de Llavaneres aquifer, more than 50 % NO_3^- attenuation was achieved in the studied piezometers. However, since in a few samples NO_3^- was below the limit for isotopic analysis, the contribution could have been higher. The isotopic characterization of NO_3^- also evidenced a mixture between denitrified and non-denitrified groundwater at the extraction well.
- In groundwater samples collected from the Matanza-Riachuelo Basin, the isotopic characterization of NO_3^- and Cr^{6+} evidenced their concomitant natural biotic reduction due to NPDOC from septic system leakage (between 20 and 30 % for NO_3^- and between 60 and 90 % for Cr^{6+}). The attenuation of Cr^{6+} in a few samples was also due to dilution with uncontaminated groundwater.
- At the CW, a slight natural NO_3^- attenuation was only observed when the flow was decreased from 5.5 to 2.5 L/s. The subsequent biostimulation with corn stubble allowed at least a 60 % of NO_3^- removal (16 L/s). However, since in a few samples NO_3^- was below the limit for isotopic analysis, the contribution could have been higher. The treatment in autumn lasted in one month, while in spring the attenuation remained for three months. The effectivity of the treatment was limited due to high O_2 content of the inlet water, high water flow, and possible generation of preferential flows within the CW.

The results also allowed to evaluate the safety of the biostimulation treatments. The studied strategies were considered safe because the NO_2^- and NH_4^+ concentrations were low or decreased over time, the remaining NPDOC could maintain NO_3^- attenuation downstream, and the occurrence of BSR was discarded. Also in the case of the polluted aquifers, a lower slope between $\delta^{18}O\text{-}NO_3^-$ and $\delta^{15}N\text{-}NO_3^-$ observed in the field (0.5-0.7) compared to laboratory experiments (1.0-1.1) suggested the NO_2^- reoxidation to NO_3^- which is positive from a groundwater quality perspective.

6. FUTURE WORK

In the present thesis, different low-cost electron donors (vegetal waste products, organic C rich residue from dairy industry and Fe^{2+} containing minerals) demonstrated to be useful to promote denitrification at laboratory-scale. Given this finding, the use of other waste materials should be investigated, considering its availability in different regions facing groundwater NO_3^- pollution. Apart from the research performed at laboratory-scale, the efficacy of a biostimulation strategy by applying corn stubble in a CW treating agricultural runoff water to promote the denitrification was tested at field-scale. However, a field-scale application of the other low-cost electron donors that were found feasible to induce the NO_3^- reduction (wheat hay, whey and Mag-NPs) is still pending. Different remediation strategies using these compounds should be designed and implemented to evaluate its efficacy to remediate different NO_3^- polluted water bodies. Furthermore, in the case of surface flow CWs, methods to decrease the O_2 diffusion into water must be investigated to increase the efficacy and longevity of the biostimulation strategies based on the addition of external electron donors.

Concerning the possibility of pollution swapping during the implementation of remediation treatments, it is crucial to keep focusing on gaining knowledge on the mechanisms of generation, accumulation and reduction of the NO_3^- reduction intermediate products: NH_4^+, NO_2^-, NO and N_2O. Most of the studies reported in the literature up to date do not include an exhaustive characterization of the concentration variations of all of these compounds during the natural or induced denitrification. Future studies at laboratory and field-scale must include both chemical and isotopic characterization involving all the possible N compounds, either in the dissolved or gaseous forms or even solid-bound (if sediment is present), that could suffer transformation processes along with the NO_3^- reduction. In a study to assess N_2O emissions, a lower accumulation was found during the heterotrophic denitrification in laboratory incubations compared to the field (Weymann et al., 2010), pointing to a limited transferability of the laboratory results to field. Nevertheless, determining the GHG production in future laboratory studies aiming to find biostimulation with minimal GHG emissions should be considered. Furthermore, in field-scale denitrification tests, monitoring these GHG is essential to check the contribution to global climate change.

With regards to the use of ε values determined at laboratory-scale to evaluate the extent of denitrification at field-scale, exhaustive studies must be performed to disentangle all the possible causes of NO_2^- reoxidation at field-scale and which is the effect of NO_2^-

reoxidation on the $\delta^{15}N\text{-}NO_3^-$, to address the reliability of using this method. Also, the possible causes of the large variation in the $\varepsilon^{15}N/\varepsilon^{18}O$ ratio found for the NO_2^- biotic reduction must be investigated, especially, to address its influence on the isotopic composition of the produced and reduced N_2O during denitrification experiments.

Following on from the use of the isotopic characterization to evaluate the fate of different contaminants at field-scale, the possible isotopic fractionation occurring in two stages of other electron acceptors (apart from Cr^{6+}) that can be reduced simultaneously to NO_3^- in the presence of abundant electron donor, must be considered in future studies. The experiments to determine these ε values must be designed in order to achieve a wide range of samples with very low concentrations of the studied contaminant to ensure a correct interpretation of the results. The influence of the presence of other electron acceptors simultaneously to NO_3^- on the electron donor consumption and the NO_3^- reduction rates should also be considered.

Furthermore, reliable methods to detect at field-scale possible abiotic reactions between the electron donors and the intermediate N compounds of the denitrification must be investigated (e.g., NO_2^- reduction). Apart from the NO_3^-, NO_2^- and N_2O isotopic characterization, measuring the site preference (SP) of the generated N_2O (i.e. the intramolecular distribution of N isotopes, since the N_2O molecule has an asymmetric linear structure (N-N-O)) (Buchwald et al., 2016; Heil et al., 2014; Jones et al., 2015) could be helpful in assessing the contribution of each of the biotic and abiotic reactions. Also, determining the isotopic composition of the different possible electron donors found at the study site (e.g., Fe^{2+}) and characterizing the generated products, including the precipitation of secondary minerals could provide valuable information on the reaction mechanisms (Chen et al., 2018; Liu et al., 2018). In this context, the knowledge gained during the two stays abroad performed during the development of the present thesis that aimed to learn the analytical techniques for the isotopic characterization of the SP of the N_2O and of Fe^{2+}, could be applied to gain insight into the NO_3^- reduction mechanisms under different conditions.

Finally, the data obtained from the laboratory studies performed in the context of this thesis can be used in the future to develop numerical models. These models could help to predict the biogeochemical reactions involving the electron donor and acceptor of interest in different polluted areas to optimize the design of the bioremediation strategies before implementation.

REFERENCES

Buchwald, C., Grabb, K., Hansel, C.M., Wankel, S.D., 2016. Constraining the role of iron in environmental nitrogen transformations: Dual stable isotope systematics of abiotic NO_2^- reduction by Fe(II) and its production of N_2O. Geochim. Cosmochim. Acta 186, 1–12. https://doi.org/10.1016/j.gca.2016.04.041

Chen, D., Liu, T., Li, X., Li, F., Luo, X., Wu, Y., Wang, Y., 2018. Biological and chemical processes of microbially mediated nitrate-reducing Fe(II) oxidation by Pseudogulbenkiania sp. strain 2002. Chem. Geol. 476, 59–69. https://doi.org/10.1016/j.chemgeo.2017.11.004

Heil, J., Wolf, B., Brüggemann, N., Emmenegger, L., Tuzson, B., Vereecken, H., Mohn, J., 2014. Site-specific 15N isotopic signatures of abiotically produced N_2O. Geochim. Cosmochim. Acta 139, 72–82. https://doi.org/10.1016/j.gca.2014.04.037

Jones, L.C., Peters, B., Lezama Pacheco, J.S., Casciotti, K.L., Fendorf, S., 2015. Stable Isotopes and Iron Oxide Mineral Products as Markers of Chemodenitrification. Environ. Sci. Technol. 49, 3444–3452. https://doi.org/10.1021/es504862x

Liu, T., Chen, D., Luo, X., Li, X., Li, F., 2018. Microbially mediated nitrate-reducing Fe(II) oxidation: Quantification of chemodenitrification and biological reactions. Geochim. Cosmochim. Acta. https://doi.org/10.1016/j.gca.2018.06.040

Weymann, D., Geistlinger, H., Well, R., Von Der Heide, C., Flessa, H., 2010. Kinetics of N_2O production and reduction in a nitrate-contaminated aquifer inferred from laboratory incubation experiments. Biogeosciences 7, 1953–1972. https://doi.org/10.5194/bg-7-1953-2010

7. ANNEX

ANNEX 1

Induced nitrate attenuation by ferrous iron containing minerals.

Rosanna Margalef-Marti[1], Raúl Carrey[1], José Antonio Benito[2], Vicenç Marti[2], Albert Soler[1], Neus Otero[1,3]

[1] Grup MAiMA, SGR Mineralogia Aplicada, Geoquímica i Geomicrobiologia, Departament de Mineralogia, Petrologia i Geologia Aplicada, Facultat de Ciències de la Terra, Universitat de Barcelona (UB), Barcelona, C/Martí i Franquès s/n, 08028 Barcelona, Spain.

[2] Materials Science and Metallurgical Engineering Department and Barcelona Research Center in Multiscale Science and Engineering, EEBE, Technical University of Catalonia (UPC), Av. Eduard Maristany 16, 08019 Barcelona, Spain.

[3] Serra Húnter Fellowship, Generalitat de Catalunya, Spain.

Submitted to *Chemosphere*

Impact factor (JCR/WOS) = 5.1 (2018)

Q1, 32/251 Environmental sciences

Induced nitrate attenuation by ferrous iron containing minerals

Rosanna Margalef-Marti[1], Raúl Carrey[1], José Antonio Benito[2], Vicenç Marti[2], Albert Soler[1], Neus Otero[1,3]

[1] Grup MAiMA, SGR Mineralogia Aplicada, Geoquímica i Geomicrobiologia, Departament de Mineralogia, Petrologia i Geologia Aplicada, Facultat de Ciències de la Terra, Universitat de Barcelona (UB), C/Martí i Franquès s/n, 08028 Barcelona (Spain).

[2] Materials Science and Metallurgical Engineering Department and Barcelona Research Center in Multiscale Science and Engineering, EEBE, Technical University of Catalonia (UPC), Av. Eduard Maristany 16, 08019 Barcelona (Spain).

[3] Serra Húnter Fellowship, Generalitat de Catalunya (Spain).

ABSTRACT

Since nitrate (NO_3^-) has been related to human health and environmental problems, safe and sustainable strategies to remediate polluted water bodies must be investigated. This work aims to assess the feasibility of using ferrous iron (Fe^{2+})-containing minerals to promote denitrification while avoiding pollution swapping (e.g. accumulation of the by-products nitrite (NO_2^-) or nitrous oxide (N_2O)). Magnetite, siderite and olivine were tested micro-sized and magnetite was also tested nano-sized. To accomplish the objective, samples obtained from several biotic and abiotic batch experiments were characterized chemically and isotopically. The biotic NO_3^- reduction was only completed in microcosms containing magnetite nanoparticles, suggesting an increased Fe^{2+} availability from nano-sized minerals. No abiotic reactivity was observed between the Fe^{2+}-containing minerals and NO_3^- or NO_2^-. However, NO_2^- was abiotically reduced by dissolved Fe^{2+}, when added. Since the biotic NO_3^- reduction produces innocuous nitrogen gas (N_2) while the abiotic NO_2^- reduction produces the greenhouse gas N_2O, the latter one would be advantageous only if the N_2O is further reduced biotically. For the induced denitrification by magnetite nanoparticles, the calculated

$\varepsilon^{15}N_{NO3}$ was -33.1 ‰, $\varepsilon^{18}O_{NO3}$ was -10.7 ‰ and $\varepsilon^{15}N_{NO3}/\varepsilon^{18}O_{NO3}$ was 3.1. These values might be applied in future field studies to quantify the efficiency of bioremediation treatments. For the abiotic NO_2^- reduction, the $\varepsilon^{15}N_{NO2}$ ranged from -14.1 to -17.8 ‰. The NO_2^- isotopic characterization did not seem to be a useful tool to distinguish the abiotic from the biotic NO_2^- reduction at field-scale. Nevertheless, $\delta^{15}N\text{-}N_2O$ analysis could provide valuable information on the occurrence of these processes.

Keywords: abiotic nitrite reduction, denitrification, isotopic fractionation, magnetite nanoparticles, nitrous oxide

1. INTRODUCTION

Nitrate (NO_3^-) has been related to human health disorders such as cancer and blue baby syndrome and to environmental problems such as eutrophication of water bodies (Rivett et al., 2008; Vitousek et al., 1997; Ward et al., 2005). Due to decades of excessive crop fertilization and septic system leakage, NO_3^- is widely found in groundwater. Consequently, since 1991, European directives (2006/118/EC, 2006; 91/676/EEC, 1991; 98/83/EC, 1998) have arisen to face the NO_3^- pollution persistence. One of the measures that can be implemented to attenuate the NO_3^- concentration in water bodies is the addition of external electron donors to promote the denitrification, since these compounds are usually deficient at field-scale (Rivett et al., 2008). The NO_3^- is reduced to innocuous nitrogen gas (N_2) simultaneously to the oxidation of an electron donor by the denitrifying microorganisms (Borden et al., 2012; Böttcher et al., 1990; Otero et al., 2009; Smith et al., 2001). However, intermediate N compounds can be generated and accumulated since the denitrification occurs through a series of enzymatic reactions involving the conversion of NO_3^- to nitrite (NO_2^-), nitric oxide (NO), nitrous oxide (N_2O) and finally N_2 (Betlach and Tiedje, 1981; Knowles, 1982; Vidal-

Gavilan et al., 2013; Weymann et al., 2010). Not only NO_3^- but also these intermediate N compounds have been recognized to produce detrimental effects for the environment and human health (Badr and Probert, 1993; Vitousek et al., 1997; Ward et al., 2005). Therefore, pollution swapping should be avoided when inducing the denitrification at field-scale.

In the search of economical and sustainable electron donors, diverse industrial and agricultural waste products rich in organic carbon (C) have already proved to induce the heterotrophic denitrification at laboratory scale (Carrey et al., 2018; Gibert et al., 2008; Margalef-Marti et al., 2019b; Trois et al., 2010). Also, few laboratory studies testing minerals such as pyrite, pyrrhotite or biotite showed potential to promote the lithoautotrophic denitrification (Aquilina et al., 2018; Bosch et al., 2012; Torrentó et al., 2011; Yang et al., 2017). Furthermore, since the mineral nanoparticles (NP) (e.g. Fe oxides) are usually more reactive than macroparticles, their potential use to remediate polluted water bodies has gained attraction during the last years (Braunschweig et al., 2013). At laboratory-scale, materials such as Fe(0)-NP, magnetite-NP, Fe^{3+}oxide-NP or magnetite/maghemite-NP have been found to remove organic and inorganic contaminants such as uranium, chromium, arsenic, ethylene glycol and phenol (Chowdhury and Yanful, 2010; Crane et al., 2011; Zelmanov and Semiat, 2008). Regarding NO_3^-, pyrite-NP, zeolite supported Fe/Ni-NP and Fe(0)/magnetite-NP have been observed to attenuate the pollution (Bosch et al., 2012; Cho et al., 2015b, 2015a; He et al., 2018).

In the aforementioned denitrification studies, a transient NO_2^- accumulation was observed (Ge et al., 2012; Torrentó et al., 2011; Yang et al., 2017) and although the gas emissions were not measured, the N_2O accumulation cannot be discarded since this greenhouse gas (GHG) is usually detected during the NO_3^- reduction both at laboratory and field-scale (Jurado et al., 2017; Margalef-Marti et al., 2019a; Morley et al., 2008; Weymann et al., 2010). During the last years, numerous studies have pointed

that abiotic reactions involving the N and Fe biogeochemical cycles occur simultaneously to the biotic denitrification (Carlson et al., 2013; Klueglein and Kappler, 2013; Matocha and Coyne, 2007; Melton et al., 2014). The NO_2^- reduction by ferrous iron (Fe^{2+}) oxidation have been well documented (Buchwald et al., 2016; Dhakal et al., 2013; Grabb et al., 2017; Rakshit et al., 2016) and might be advantageous to avoid a water quality decrease due to NO_2^- accumulation. However, the N_2O has been proposed as the final product of this abiotic NO_2^- reduction by Fe^{2+} oxidation (Buchwald et al., 2016; Chen et al., 2018; Coby and Picardal, 2005; Wang et al., 2016). Hence, supplying NO_3^- polluted water bodies with Fe^{2+}-containing minerals to induce the lithoautotrophic denitrification might promote N_2O generation from both the biotic and the abiotic NO_2^- reduction. In fact, in laboratory experiments, Cooper et al. (2003) found a larger N_2O production during the denitrification in the presence of Fe compared to absence. Nevertheless, the accumulated N_2O by both the biotic and abiotic pathways could be further reduced biotically in the presence of electron donors. The relative contribution of the two pathways of N_2O production should be assessed since the GHG is currently a focus of attention in climate change research (Reay et al., 2012).

The analysis of stable isotopes coupled to hydrochemical investigations is a widely accepted approach to understand biogeochemical processes in water bodies. The enzymatic NO_3^- reduction provokes an enrichment in the heavy isotopes ^{15}N and ^{18}O of the unreacted substrate, unlike processes such as dilution that leads to a concentration decrease without influencing the isotopic signature (Böttcher et al., 1990; Fukada et al., 2003; Mariotti et al., 1981; Aravena and Robertson, 1998). The same pattern is expected throughout the enzymatic reduction of all N intermediate products (e.g. NO_2^- or N_2O), which will be initially depleted in ^{15}N and ^{18}O with respect to the substrate until the ultimate product will reach the substrate initial isotopic composition. Although the NO_3^- isotopic evolution through the heterotrophic denitrification has been widely studied (Carrey et al., 2014; Granger et al., 2008; Grau-Martínez et al., 2017; Wunderlich et al.,

2012), the characterization during the lithoautotrophic denitrification is scarce (Torrentó et al., 2011, 2010). Furthermore, the information on the dual isotope systematics of NO_2^- and N_2O throughout its abiotic reduction by Fe^{2+} is also limited (Buchwald et al., 2016; Chen et al., 2018; Grabb et al., 2017; Jones et al., 2015). Therefore, it is not clear in which extent the isotopic characterization of NO_3^-, NO_2^- and N_2O might help in distinguishing biotic and abiotic reactions involving the N and Fe biogeochemical cycles.

In this context, the aim of this work is to assess at laboratory-scale the suitability of using Fe^{2+}-containing minerals to promote the NO_3^- attenuation in polluted groundwater. The selected minerals were magnetite (Mag), siderite (Sd) and olivine (Ol), and were tested micro-sized and nano-sized (only Mag-NP) to quantify the changes in reactivity. Special attention was directed on the generation of the by-products NO_2^- and N_2O throughout the biotic process. The possible abiotic reactivity between the dissolved Fe^{2+} or the Fe^{2+}-containing minerals and NO_3^- or NO_2^- was also evaluated. To accomplish the objective, the samples obtained from several batch experiments were characterized chemically and isotopically.

2. METHODS

2.1. Batch experiments

Five series of batch experiments (described below) were set inside a glove box, using 20 mL serum bottles, crimp sealed with butyl rubber stoppers under an Ar atmosphere. Incubations were performed at 23 ºC and constant shaking in the darkness to avoid photodegradation processes. The bottles were sacrificed by turns at time intervals depending on the NO_3^- and NO_2^- reduction dynamics. The detailed composition of each batch experiment is shown in **Table 1**. The characterization of the different types of water employed is shown in the Supplementary Information **Table S1**. The micro-sized

minerals (Mag, Sd and Ol) preparation and Mag size reduction is detailed in Supplementary Information **Section S1**.

In the biotic experiments, the laboratory microcosms simulated aquifer conditions. Groundwater (1 mM NO_3^-) was obtained from well SMC-002 located in Roda de Ter (Barcelona, Spain). In this area, lithoautotrophic denitrification occurrence have been previously reported (Hernández-del Amo et al., 2018; Otero et al., 2009; Vitòria et al., 2008). Furthermore, in water collected from the SMC-002 well, genes encoding the NO_2^- and N_2O reductases (nirS, nirK, and nosZ1) have been detected and certain genus of denitrifying and Fe^{2+} oxidizing bacteria have been identified (Hernández-del Amo et al., 2018). In this biotic batch experiments, milled limestone was used as sediment to increase microbial diversity. Micro-sized Mag, Ol and Sd and Mag-NP were tested to assess its potential use to promote NO_3^- attenuation. The series of experiments BioSedGW contained sediment, groundwater (1 mM NO_3^-) and one of the selected minerals while the series BioSedDIW contained also sediment, deionized water with $NaNO_3$ (1 mM) and one of the selected minerals, to assess the contribution of the sediment on the induced denitrification. Both series included a control without mineral. Furthermore, three bottles containing sediment and MilliQ water were incubated to determine the possible leakage of organic C from the milled limestone that was used as sediment.

The micro-sized Mag, Ol and Sd were also tested to assess its potential abiotic reactivity with NO_3^- and NO_2^-. Three series of parallel anoxic incubations were performed. The series $AbFeNO_3$ contained NO_3^- rich synthetic water (1 mM), one of the three selected minerals and dissolved Fe^{2+}. The series $AbFeNO_2$ contained NO_2^- rich synthetic water (1 mM), one of the three selected minerals and dissolved Fe^{2+}. In both series dissolved Fe^{2+} was added to maximize Fe^{2+} availability from a filtered $FeCl_2 \cdot 4H_2O$ aqueous solution (5 mM). Finally, the series AbNO2 contained NO_2^- rich synthetic water (1 mM) and one of the three selected minerals.

Table 1. Biotic and abiotic experiments. Content of the batches. R stands for the number or replicates. DIW refers to deionized water. (*) The number of replicates is for each mineral (Min) used (Mag, Ol, Sd, Mag-NP). C refers to the control without mineral.

Experiment	Conditions	R	Code
Biotic NO_3^- attenuation (groundwater)	Sediment (2.5 g) + groundwater (15 mL, 1 mM NO_3^-)	3	BioSedGW-C
	Sediment (2.5 g) + groundwater (15 mL, 1 mM NO_3^-) + mineral (100 mg)	10 (*)	BioSedGW-Min
Biotic NO_3^- attenuation (DIW)	Sediment (2.5 g) + DIW (15 mL, 1 mM NO_3^-)	3	BioSedDIW-C
	Sediment (2.5 g) + DIW (15 mL, 1 mM NO_3^-) + mineral (100 mg)	3 (*)	BioSedDIW-Min
Blank	Sediment (2.5 g) + MilliQ water (15 mL)	3	Blank
Abiotic NO_3^- attenuation (synthetic water + Fe(II))	Synthetic water (10 mL, 1 mM NO_3^-) + $FeCl_2$ (5 mM)	3	Ab$FeNO_3$-C
	Synthetic water (10 mL, 1 mM NO_3^-) + $FeCl_2$ (5 mM) + mineral (50 mg)	3 (*)	Ab$FeNO_3$-Min
Abiotic NO_2^- attenuation (synthetic water)	Synthetic water (10 mL, 1 mM NO_2^-) + mineral (50 mg)	3 (*)	AbNO_2-Min
Abiotic NO_2^- attenuation (synthetic water + Fe(II))	Synthetic water (10 mL, 1 mM NO_2^-) + $FeCl_2$ (5 mM)	8	Ab$FeNO_2$-C
	Synthetic water (10 mL, 1 mM NO_2^-) + $FeCl_2$ (5 mM) + mineral (50 mg)	8 (*)	Ab$FeNO_2$-Min

2.2. Analytical techniques

All samples were filtered through 0.2 µm Millipore® filter immediately when obtained and stored at 4 ºC until analysis except aliquots for ammonium (NH_4^+) concentration and isotopic characterization of N and O from dissolved NO_3^- and NO_2^- that were preserved frozen at -20 ºC. Samples from the experiments $AbFeNO_3$ and $AbFeNO_2$ were analyzed immediately when obtained.

Concerning the chemical analyses, the concentrations of NO_3^- and NO_2^- were analyzed by high performance liquid chromatography (HPLC, WATERS 515 pump and WATERS IC-PAK ANIONS column with WATERS 432 and UV/V KONTRON detectors). Exceptionally, in the $AbFeNO_2$ experiments, the NO_2^- concentration was calculated from the isotope ratio mass spectrometer (IRMS) peak areas results. The NH_4^+ concentration was determined by spectrophotometry (CARY 1E UV-visible) using the indophenol blue method ($AbFeNO_2$ experiments) (Bolleter et al., 1961) or by ionic chromatography (BioSedGW and BIoSedDIW experiments). The N_2O accumulated at the head-space of the vials was measured by gas chromatography (GC) with an electron capture detector (ECD) (Thermo Scientific, Trace 1300). The NPDOC was analyzed by organic matter combustion (TOC 500 SHIMADZU). The dissolved Fe and trace elements were determined by inductively coupled plasma optical emission spectrometry (ICP-OES, Perkin Elmer Optima 8300 and Perkin Elmer Optima 3200 RL).

The δ^{15}N-NO_3^-, δ^{18}O-NO_3^- and δ^{15}N-NO_2^- compositions were determined following the cadmium and azide reduction method (McIlvin and Altabet, 2005; Ryabenko et al., 2009). N_2O was analyzed using a Pre-Con (Thermo Scientific) coupled to an IRMS (Finnigan MAT 253, Thermo Scientific). Notation is expressed in terms of δ (‰) relative to the international standards: Atmospheric N_2 (AIR) for δ^{15}N and Vienna Standard Mean Oceanic Water (V-SMOW) for δ^{18}O. Hence, $\delta = (R_{sample}-R_{standard})/R_{standard}$, where

R is the ratio between the heavy and the light isotopes. According to Coplen (2011), several international and laboratory (CCiT) standards were interspersed among samples for the normalization of the results: USGS-51, USGS-32, USGS-34, USGS-35, CCiT-$NaNO_3$ ($\delta^{15}N$ = +16.9 ‰, $\delta^{18}O$ = +28.5 ‰) and CCiT-KNO_2 ($\delta^{15}N$ = +28.5 ‰). The reproducibility (1σ) of the samples, calculated from the standards systematically interspersed in the analytical batches, was ±1.0 ‰ for $\delta^{15}N$-NO_3^-, ±1.5 ‰ for $\delta^{18}O$-NO_3^-, ±0.5 for $\delta^{15}N$-NO_2^- and ±0.1 for $\delta^{15}N$-NO_2^-. Chemical and isotopic analyses were prepared at the laboratory of the MAiMA-UB research group and analyzed at the Centres Científics i Tecnològics of the Universitat de Barcelona (CCiT-UB).

2.3. Isotopic fractionation calculation

Under closed system conditions, the isotopic fractionation ($\varepsilon^{18}O$ and $\varepsilon^{15}N$) can be calculated by means of a Rayleigh distillation equation (**Equation 1**) (Böttcher et al., 1990; Mariotti et al., 1988). Thus, the ε can be obtained from the slope of the linear correlation between the natural logarithm of the substrate remaining fraction ($Ln(C_{residual}/C_{initial})$, where C refers to analyte concentration) and the determined isotope ratios ($Ln(R_{residual}/R_{initial})$, where $R = (\delta+1)$).

$$Ln\left(\frac{R_{residual}}{R_{initial}}\right) = \varepsilon \times Ln\left(\frac{C_{residual}}{C_{initial}}\right) \quad \textbf{Equation 1}$$

3. RESULTS AND DISCUSSION

The mineral characterization is detailed in the Supplementary Information **Section S2**. All data obtained from the laboratory experiments is reported in the Supplementary Information **Table S2**.

3.1. Induced denitrification by Fe^{2+}-containing minerals

During the first week of incubation, in all BioSedGW-Min and BioSedDIW-Min microcosms, the NO_3^- concentration decreased between 30 % and 60 % (**Figures 1A and 1B**). The NO_3^- attenuation was also observed in the BioSedGW-C microcosms that lacked mineral (up to 40 % NO_3^- reduction). Therefore, the beginning of denitrification was likely caused by heterotrophic bacteria that used the organic C from both sediment and groundwater as electron donor. In the blank experiments containing only MilliQ water and sediment, 0.4 ± 0.03 mM NPDOC leaked from the used limestone, which has to be added to the 0.2 mM NPDOC already present in groundwater in the BioSedGW experiments. These results are consistent with the lower NO_2^- accumulation found in BioSedGW-Min microcosms (up to 0.2 mM) compared to the BioSedDIW-Min microcosms (up to 0.6 mM) (**Figures 1C and 1D**) and suggested that both groundwater and sediment were sources of denitrifying microorganisms.

After the first week, the NO_3^- or NO_2^- concentrations did not change significantly in the BioSedDIW experiments (**Figures 1B and 1D**). In the BioSedGW-Mag/Ol/Sd/C microcosms, significant differences in the NO_3^- concentration were not observed (**Figure 1A**), but from day 118 on, NO_2^- was no longer detected (**Figure 1C**). These results suggested that the organic C from sediment and groundwater and the Fe^{2+} available from the micro-sized minerals were insufficient to complete denitrification. Nevertheless, in the BioSedGW-Mag-NP microcosms, about 96 % NO_3^- reduction was achieved in 91 days (**Figure 1A**), showing transient NO_2^- accumulation (up to 0.2 mM) until day 91 (**Figure 1C**). In the BioSedGW microcosms, NH_4^+ concentration was below 0.04 mM, discarding a major contribution of the dissimilatory NO_3^- reduction to ammonium (DNRA) and suggesting that the end products of NO_3^- reduction were gaseous N compounds. The measured N_2O at the head-space of the BioSedGW vials was below 0.1 % of the initial N in the control, below 0.4 % in the micro-sized minerals microcosms, and below 0.8 % in the Mag-NP microcosms. The highest concentration

being detected in the BioSedGW-Mag-NP microcosms is consistent with the highest reduction being observed in these batches. The low percentage of N in the form of N_2O found in the BioSedGW experiments suggested that the final gaseous product of the biotic NO_3^- reduction was N_2, either during the initial heterotrophic activity and as a result of the denitrification promoted by the Mag-NP. Therefore, if during the denitrification promoted by the Mag-NP, an abiotic reactivity between NO_2^- and Fe^{2+} occurred, the produced N_2O seemed to be further reduced to N_2 biotically. Similarly, in a NO_3^- polluted aquifer in the presence of Fe^{2+} and low organic C, the results obtained by Smith et al. (2017) suggested that NO_3^- was reduced both heterotrophically and lithoautotrophically while NO_2^- was also reduced abiotically and the generated N_2O was biotically reduced to N_2 down-gradient.

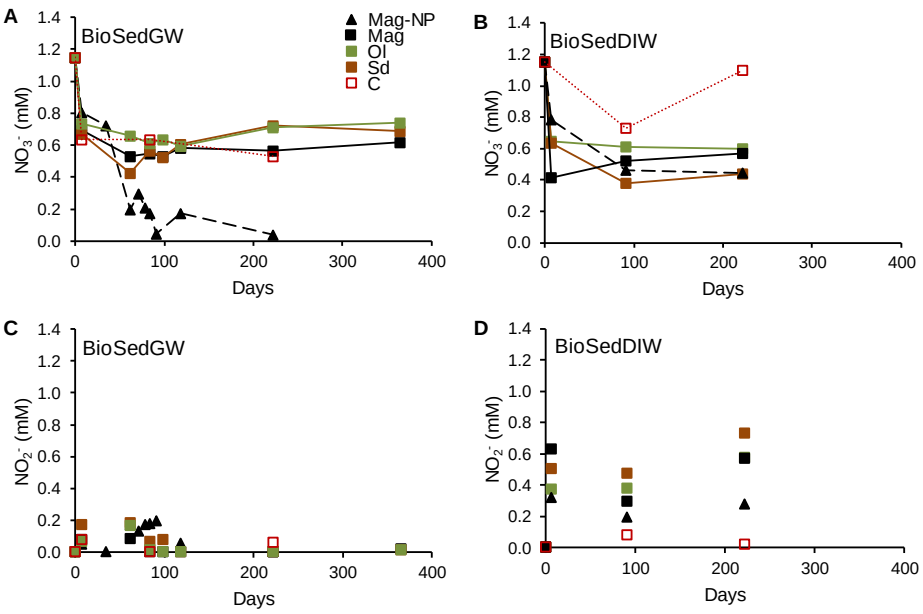

Figure 1. NO_3^- attenuation in the biotic experiments. NO_3^- (**A, C**) and NO_2^- (**B, D**) concentrations measured in the BioSedGW (**A, B**) and BioSedDIW (**C, D**) experiments.

Our results suggest that the Mag-NP allowed a higher Fe^{2+} availability with respect to micro-sized Mag. Possibly, in the micro-sized minerals experiments the available

Fe^{2+}/N molar ratio was too low to complete NO_3^- reduction, especially in the case of Sd and Ol (initial Fe^{2+}/N of 13 and 7, respectively compared to 24 calculated for Mag and Mag-NP). In a study with *Microbacterium*, 90 % NO_3^- removal was achieved when using a Fe^{2+}/N ratio of nearly 30, which is far above from the stoichiometric ratio of 5 (Zhou et al., 2016). Furthermore, the Mag Fe^{2+}/Fe^{3+} stoichiometry could influence the reactivity (Gorski et al., 2010). Similar to our results, Aquilina et al. (2018) and Yang et al. (2017) related an increased denitrification rate to a decreased grain size of minerals (granite-biotite and pyrrothithe, respectively). Smaller particles enhance the mineral solubility, which might accelerate microbial reduction rates. Braunschweig et al. (2013) even suggested that in case of nanoparticles precipitation, the solubility might be independent of the aggregate size. Therefore, the higher reactivity of Mag-NP compared to micro-sized Mag seem consistent with an increased dissolution leading an increased Fe^{2+} availability.

Dissolved Fe concentration was below detection limit in almost all samples of our biotic experiments. Possibly, bacteria oxidized the structural Fe^{2+} of the minerals or the Fe^{2+} adsorbed on the mineral surface. Alternatively, as Fe^{2+} was released from the mineral through dissolution, bacteria immediately oxidized it to Fe^{3+}, which precipitated and became unavailable for detection. The produced Fe^{3+} can precipitate on the microbial cells surface, which might decrease the denitrification activity due to blocking of NO_3^- transport into the cells (Chen et al., 2018; Coby and Picardal, 2005; Cooper et al., 2003; Wang et al., 2017). Therefore, the application of Fe^{2+} minerals could be advantageous due to the regeneration of Fe^{2+} from the reduction of precipitated Fe^{3+} minerals if NO_3^- is completely reduced and if an electron donor is present (Straub et al., 2004) but, excessive Fe^{3+} precipitation could produce clogging issues and a decreased NO_3^- reduction efficiency.

The NO_3^- dependent Fe^{2+} oxidation (NDFO) process, is still not well constrained (Bryce et al., 2018; Price et al., 2018; Straub et al., 1996). Among the microorganisms that

have been related to the NDFO, lithoautotrophs have been identified but most of them are mixotrophic, requiring an organic C co-substrate for growth, or even the NDFO could result from a synergistic activity between different NO_3^- reducing and Fe^{2+} oxidizing microorganisms (Bryce et al., 2018; Melton et al., 2014; Price et al., 2018; Weber et al., 2006). Both denitrifying and Fe^{2+} oxidizing bacteria were previously identified in the groundwater employed in the BioSedGW experiments (Hernández-del Amo et al., 2018). Some authors propose that the NDFO mixotrophic communities might need a lower organic C supply to reduce NO_3^- compared to the heterotrophic communities (Devlin et al., 2000; He et al., 2016).

3.2. NO_3^- and NO_2^- abiotic reactivity with Fe^{2+}

The experiments AbFeNO_3 and AbNO_2 showed a lack of abiotic reactivity between the Fe^{2+}-containing minerals and NO_3^- or NO_2^- (**Figure 2A**), which is opposed to the observed abiotic reduction promoted by Mag (10 % for NO_3^- and 20 % for NO_2^-, from initial 0.5 mM) in similar experiments performed by Dhakal et al. (2013). Hence, it was confirmed that in our BioSedGW and BioSedDIW experiments the observed NO_3^- reduction was caused by biological activity.

However, a rapid NO_2^- reduction was observed in the Ab$FeNO_2$ experiments (**Figure 2B**). The beginning of the reaction seemed to be immediate and the NO_2^- removal was completed in both the Ab$FeNO_2$-Min and Ab$FeNO_2$-C experiments, which is consistent with previous studies showing a significant NO_2^- reduction (approximately 60 % in 4 days) even at an equimolar dissolved Fe^{2+}/ NO_2^- molar ratio (Jones et al., 2015). A faster reduction (~ 50 hours) was observed in the Ab$FeNO_2$-Sd experiments compared to the Ab$FeNO_2$-Mag/Ol/C (~ 175 hours), possibly due to an increased dissolution rate of Sd that increased the dissolved Fe^{2+} availability, either by releasing it or by modifying the surface in which to be adsorbed. The lack of differences on the NO_2^- reduction rate in the Ab$FeNO_2$-Mag/Ol/C experiments, could be explained by the employed dissolved

Fe^{2+}/N ratio above the stoichiometric (see Supplementary Information **Section S2**). Since the measured NH_4^+ was below 0.05 mM, it was considered that NO_2^- was reduced to gaseous products.

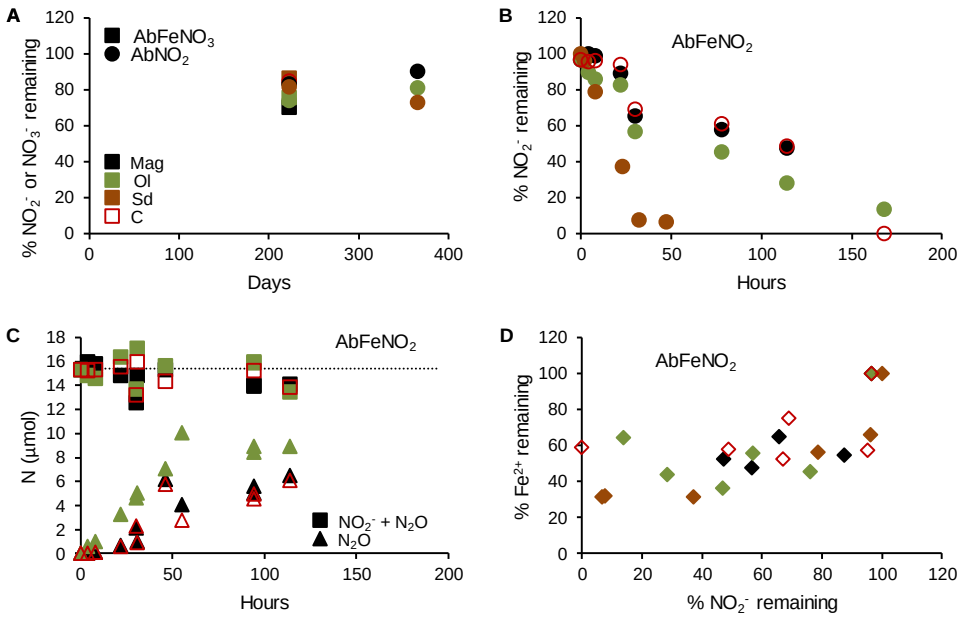

Figure 2. Abiotic reactivity between Fe^{2+} and N compounds. For the $AbNO_2$ and $AbFeNO_3$ experiments, **A**) shows the remaining NO_2^- (circles) or NO_3^- (squares), respectively. For the $AbFeNO_2$ experiments, **B**) show the remaining NO_2^-, **C**) the generated N-N_2O (triangles) including the sum of N-N_2O and N-NO_2^- (squares), in which the dotted line refers to the NO_2^- initial content, and **D**) the remaining Fe^{2+}.

As previously observed by other authors, N_2O accumulated at the headspace of the batches as a result of the NO_2^- abiotic reduction by Fe^{2+} oxidation (Buchwald et al., 2016; Chen et al., 2018; Coby and Picardal, 2005; Wang et al., 2016). Our results show that N_2O was the end product because a mass balance between the remaining NO_2^- in the solution and the accumulated N_2O in the headspace for each vial was close to the NO_2^- initial value (**Figure 2C**). Kampschreur et al. (2011) observed a complete

recovery of NO_2^- as NO and N_2O, suggesting that the missing mass balance complement to the N_2O is likely to be found as NO.

A Fe^{2+} decrease was observed in accordance to NO_2^- reduction from the initial 5 mM to approximately 2 mM, showing no significant differences between the four tested conditions (**Figure 2D**). Total dissolved Fe measured by ICP-OES was considered to be solely Fe^{2+} since Fe^{3+} was quickly precipitated and because the ICP-OES method have previously shown equal results compared with ferrozine analysis (Smith et al., 2017). In most of the publications focusing on the abiotic NO_2^- reduction coupled to Fe^{2+} oxidation, an homogeneous reaction produced by the oxidation of aqueous Fe^{2+} is distinguished from an heterogeneous reaction, in which the Fe^{2+} is associated to mineral or bacterial surfaces or found as structural Fe^{2+} within minerals. Some studies suggest that a faster NO_2^- reduction is produced through the heterogeneous reaction (Buchwald et al., 2016; Dhakal et al., 2013) but, NO_2^- reduction inhibition has been found for low or null dissolved Fe^{2+} concentrations even in the presence of mineral-associated Fe^{2+} (Tai and Dempsey, 2009). This is consistent with the lack of reactivity in the $AbNO_2$ experiments compared to the $AbFeNO_2$ batches. According to these results, if Fe^{2+}-containing minerals are applied in polluted water bodies to promote the denitrification, NO_2^- accumulation could be avoided after its abiotic reduction in the presence of dissolved Fe^{2+}. However, this NO_2^- abiotic reduction would be beneficial only if the generated N_2O is further reduced biotically.

3.3. Isotopic characterization

3.3.1. Isotopic fractionation of NO_3^- during the biotic reduction

The initial isotopic values measured in groundwater of +11.3 ‰ for $\delta^{15}N\text{-}NO_3^-$ and +10.1 ‰ for $\delta^{18}O\text{-}NO_3^-$ increased to +158.1 ‰ and +47.5 ‰, respectively, throughout the NO_3^- attenuation promoted by the Mag-NP. The calculated $\varepsilon^{15}N_{NO3}$ was -33.1 ‰ (R^2 = 0.86) and $\varepsilon^{18}O_{NO3}$ was -10.7 ‰ (R^2 = 0.74) (**Figure 3A**), giving a $\varepsilon^{15}N_{NO3}/\varepsilon^{18}O_{NO3}$ of

3.1. While this $\varepsilon^{18}O_{NO3}$ is within the range of values reported for biotic denitrification experiments at laboratory-scale, the $\varepsilon^{15}N_{NO3}$ and the $\varepsilon^{15}N_{NO3}/\varepsilon^{18}O_{NO3}$ are found in the highest extreme (absolute values) (see **Table 2**). Similar $\varepsilon^{15}N_{NO3}$ were reported by Torrentó et al. (2011) in batch experiments using aquifer material and pyrite (-27.6 ‰) and by Tsushima et al. (2006) in column experiments using riparian aquifer sediments (-34.1 ‰). However, Torrentó et al. (2011) obtained a $\varepsilon^{15}N_{NO3}/\varepsilon^{18}O_{NO3}$ close to 1 and Tsushima et al. (2006) did not report values for $\varepsilon^{18}O_{NO3}$. Likely due to $\delta^{18}O\text{-}NO_2^-$ equilibration with $\delta^{18}O\text{-}H_2O$ and subsequent NO_2^- reoxidation to NO_3^-, Knöller et al. (2011) found a $\varepsilon^{15}N_{NO3}/\varepsilon^{18}O_{NO3}$ of 3 ($\varepsilon^{15}N_{NO3}$ = -16.2 ‰ and $\varepsilon^{18}O_{NO3}$ = -5.5 ‰), using succinate as electron donor and *Pseudomonas pseudoalcaligenes*. These results might be coherent with our results after such a long incubation and important NO_2^- accumulation. After $\delta^{18}O\text{-}NO_2^-$ exchange with $\delta^{18}O\text{-}H_2O$, which ranges between -4 and -7 ‰ in the area where the SMC-002 well is placed, if NO_2^- reoxidates to NO_3^-, a decreased $\delta^{18}O\text{-}NO_3^-$ enrichment might be expected compared to the $\delta^{15}N\text{-}NO_2^-$ enrichment. Therefore, the resulting $\varepsilon^{15}N_{NO3}/\varepsilon^{18}O_{NO3}$ might be higher than those close to 1.0 usually resulting from NO_3^- reduction to NO_2^- and subsequent reduction to gaseous products. If a bioremediation strategy by using Mag-NP to promote denitrification is implemented, the calculated ε values in the present study could be applied to evaluate the efficiency of the treatment (Margalef-Marti et al., 2019c; Meckenstock et al., 2004; Vidal-Gavilan et al., 2013).

In the case of the BioSedGW-Mag/Ol/Sd experiments, an isotopic fractionation was also observed. These isotopic results are presented as a whole since a similar trend was found for the different tested conditions, which is explained by the use of the NPDOC released from sediment and groundwater as electron donor in all cases. Calculated $\varepsilon^{15}N_{NO3}$ was -12.0 ‰ (R^2 = 0.56) and $\varepsilon^{18}O_{NO3}$ was -10.9 ‰ (R^2 = 0.63) (**Figure 3B**), giving a $\varepsilon^{15}N_{NO3}/\varepsilon^{18}O_{NO3}$ of 1.1. These values are within the range reported

for biotic denitrification in laboratory-scale experiments (see **Table 2**) and point to a lack of NO_2^- reoxidation in contrast to the Mag-NP experiments.

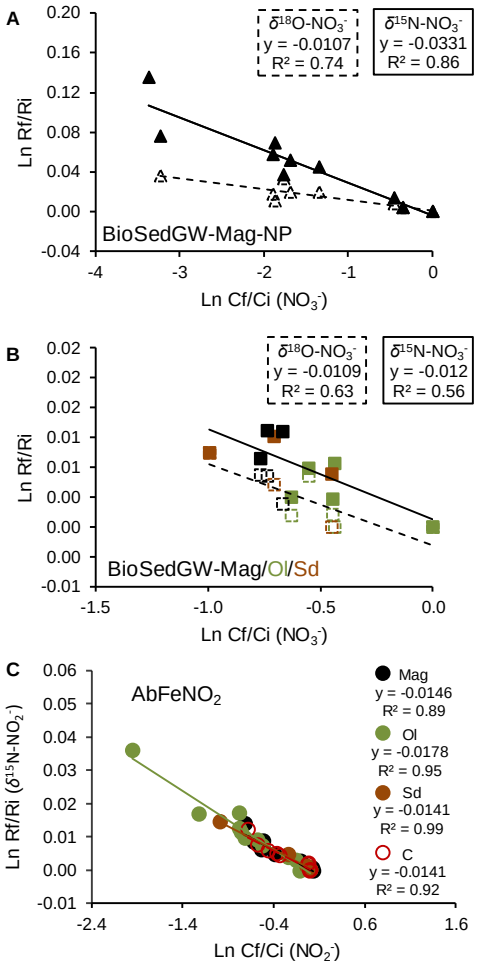

Figure 3. NO_3^- and NO_2^- ε calculation. For the biotic experiments, the plots **A** and **B** (BioSedGW-Mag-NP and BioSedGW-Mag/Ol/Sd/C, respectively), show the $\delta^{15}N\text{-}NO_3^-$ (black continuous line) and $\delta^{18}O\text{-}NO_3^-$ (black dotted line) fractionation. For the abiotic experiment $AbFeNO_2$, the plot **C** show the $\delta^{15}N\text{-}NO_2^-$ fractionation. The isotopic data is expressed in terms of δ (‰).

3.3.2. Isotopic fractionation of N-NO_2^- during the abiotic reduction

In the $AbFeNO_2$ experiments, the initial $\delta^{15}N\text{-}NO_2^-$ of -28.5 ‰ increased to -16.8 ‰, -14.9 ‰, -14.5 ‰ and +7.1 ‰ in the C, Mag, Sd and Ol batches, respectively. No

significant differences were observed in the calculated $\varepsilon^{15}N_{NO2}$ for these experiments (**Figure 3C**), suggesting that the observed NO_2^- abiotic reduction was mainly caused by the dissolved Fe^{2+} oxidation. The $\varepsilon^{15}N_{NO2}$ values were -14.1 ‰ (R^2 = 0.92) for the AbFeNO_2-C, -14.1 ‰ (R^2 = 0.99) for Sd, -14.6 ‰ (R^2 = 0.89) for Mag and -17.8 ‰ (R^2 = 0.95) for Ol. In these experiments, the $\varepsilon^{18}O_{NO2}$ was not calculated because no clear $\delta^{18}O$-NO_2^- enrichment coupled to the NO_2^- reduction was observed, pointing to $\delta^{18}O$-NO_2^- equilibration with $\delta^{18}O$-H_2O. In similar studies, a possible contribution from $\delta^{18}O$-NO_2^- equilibration with $\delta^{18}O$-H_2O could not be discarded (Buchwald et al., 2016; Grabb et al., 2017), and Jones et al. (2015) also found a weaker $\delta^{18}O$-NO_2^- enrichment compared to the $\delta^{15}N$-NO_2^- enrichment ($\varepsilon^{18}O_{NO2}$ = 10 ‰ vs $\varepsilon^{15}N_{NO2}$ = 13 ‰, respectively). These authors proposed an exchange between $\delta^{18}O$-NO_2^- and $\delta^{18}O$-H_2O since de $\delta^{18}O$-NO_2^- continued to variate after the abiotic NO_2^- reduction was stopped.

Testing the NO_2^- abiotic reduction with different incubation conditions, other authors have reported $\varepsilon^{15}N_{NO2}$ values ranging from -2.3 ‰ to -44.8 ‰, $\varepsilon^{18}O_{NO2}$ from -4.1 ‰ to -33.0 ‰, and $\varepsilon^{15}N_{NO2}/\varepsilon^{18}O_{NO2}$ between 0.5 and 1.6 (see **Table 2**). Our $\varepsilon^{15}N_{NO2}$ results fall within this wide range. Although different isotopic trends were found between NO_2^- reduction caused by structural Fe^{2+} or Fe^{2+} adsorbed onto mineral surfaces or dissolved Fe^{2+} in the laboratory studies performed by Buchwald et al. (2016) and Grabb et al. (2017), we did not observe such difference. Considering the wide range of reported ε values, it is not likely that the NO_2^- isotopic characterization could be useful at field-scale to distinguish the homogeneous and heterogeneous reactions. Furthermore, $\varepsilon^{15}N_{NO2}$ and $\varepsilon^{18}O_{NO2}$ within this range have also been reported for the biotic NO_2^- reduction, which resulted in $\varepsilon^{15}N_{NO2}/\varepsilon^{18}O_{NO2}$ between 0.7 and 22.0 (see **Table 2**). Therefore, the NO_2^- isotopic characterization may neither be useful at field-scale to distinguish the abiotic from the biotic NO_2^- reduction.

Table 2. Range of $\varepsilon^{15}N$, $\varepsilon^{18}O$ and $\varepsilon^{15}N/\varepsilon^{18}O$ values reported in the literature for NO_3^- and NO_2^- reduction laboratory experiments. Both the biotic and abiotic reductions are included. In the pure culture experiments, the enzymes are specified inside the parentheses (if reported). n.d. = no determined.

ELECTRON ACCEPTOR	ELECTRON DONOR	INVOLVED MICROORGANISMS	$\varepsilon^{15}N$	$\varepsilon^{18}O$	$\varepsilon^{15}N/\varepsilon^{18}O$	REFERENCE
NO_3^-	C_{org}	*Ochrobactrum* sp., *Paracoccus denitrificans, Pseudomonas stutzeri* (NAR)	-5.4 to -26.6	-4.8 to -22.8	1.0 to 1.2	(Granger et al., 2008)
NO_3^-	C_{org}	*Rhodobacter sphaeroides* (NAP)	-16	-8.9	1.8	
NO_3^-	C_{org}	*Pseudomonas pseudoalcaligenes*, *Azoarcus* sp.	-8.6 to -16.2	-4.0 to -7.3	1.3 to 3.0	(Knöller et al., 2011)
NO_3^-	C_{org}	*Thauera aromatica, Aromatoleum aromaticum*	-17.3 to -23.5	-15.9 to -23.7	1.0 to 1.2	(Wunderlich et al., 2012)
NO_3^-	Compounds from riparian sediments and groundwater	Microorganisms from riparian sediments and groundwater	-32.9 to -34.1	n.d.	n.d.	(Tsushima et al 2006)
NO_3^-	Pyrite	*Thiobacillus denitrificans*	-15.0 to -27.6	-13.5 to -21.3	1.1 to 1.3	(Torrentó et al. 2011, 2010)
NO_2^-	C_{org}	*Pseudomonas aeruginosa, Pseudomonas chlororaphis, Pseudomonas stutzeri* (Fe-NIR)	-3 to -11	-2 to -12	0.7 to 3.3	(Martin and Casciotti, 2016)
NO_2^-	C_{org}	*Achromobacter xylosoxidans, Ochrobactrum sp., Pseudomonas aureofaciens* (Cu-NIR)	-19 to -26	0 to -6	3.1 to 22.0	
NO_2^-	Nontronite	Abiotic	-11.1	-10.4	1.1	(Grabb et al., 2017)
NO_2^-	Aqueous + adsorbed Fe^{2+} (Nontronite)	Abiotic	-2.3	-4.5	0.5	
NO_2^-	Green rust	Abiotic	-4.2 to -9.4	-4.1 to -9.4	0.8 to 1.1	
NO_2^-	Aqueous Fe^{2+}	Abiotic	-6.1 to -33.9	-5.7 to -24.8	0.8 to 1.6	(Buchwald et al 2016)
NO_2^-	Aqueous + adsorbed Fe^{2+} (Goethite)	Abiotic	-5.9 to -44.8	-5.2 to -33.0	1.0 to 1.4	
NO_2^-	Aqueous Fe^{2+}	Abiotic	-12.9	-9.8	1.3	(Jones et al., 2015)

3.3.3. Isotopic evolution of N_2O during the biotic and abiotic experiments

The isotopic composition of the accumulated N_2O in the biotic NO_3^- reduction experiments showed variations. Neither N_2O nor NO_3^- concentrations presented a clear relationship with the determined $\delta^{15}N\text{-}N_2O$ or $\delta^{18}O\text{-}N_2O$ due to the simultaneous production and reduction of this intermediate product of the denitrification. However, a correlation was observed between $\delta^{18}O\text{-}N_2O$ and $\delta^{15}N\text{-}N_2O$, giving slopes ranging from -2.4 to +2.3 for the BioSedGW-Min experiments (**Figures 4A and 4B**). The $\delta^{15}N\text{-}N_2O$ ranged from -11.1 ‰ to +63.4 ‰ and the $\delta^{18}O\text{-}N_2O$ from -3.5 ‰ to +62.6 ‰ in the BioSedGw-Mag-NP experiments, while in the BioSedGW experiments containing micro-sized minerals, the $\delta^{15}N\text{-}N_2O$ ranged from -31.3 ‰ to +5.1 ‰ and the $\delta^{18}O\text{-}N_2O$ from -12.0 ‰ to +52.4 ‰. The increased variation of the $\delta^{15}N\text{-}N_2O$ in the BioSedGw-Mag-NP compared to the BioSedGW-Mag/Ol/Sd and the similar $\delta^{18}O\text{-}N_2O$ enrichment between the BioSedGw-Mag-NP and the BioSedGW-Mag/Ol/Sd, is consistent with the obtained ε values for the substrates. Moving to the abiotic experiments, a lower variation in the $\delta^{15}N\text{-}N_2O$ was observed compared to the biotic experiments (**Figure 4C**). It is likely that during the beginning of N_2O production the $\delta^{15}N\text{-}N_2O$ decreases and afterwards increases (e.g. initial N_2O produced in the $AbFeNO_2$-Mag experiments presents a $\delta^{15}N\text{-}N_2O$ of -48.4 ‰ that decreases to -53.8 ‰ and then increases to -43.4 ‰). Because the $\delta^{18}O\text{-}NO_2^-$ in these experiments presented equilibration with $\delta^{18}O\text{-}H_2O$, the $\delta^{18}O\text{-}N_2O$ results did not provide valuable information.

Since a much higher $\delta^{15}N\text{-}N_2O$ variation was observed for the biotic experiments compared to the abiotic experiments, observing important $\delta^{15}N\text{-}N_2O$ variations in denitrification studies could be indicative of biotic reactivity. Chen et al. (2018) also observed a higher increase of $\delta^{15}N\text{-}N_2O$ in biotic compared to abiotic NO_2^- reduction experiments.

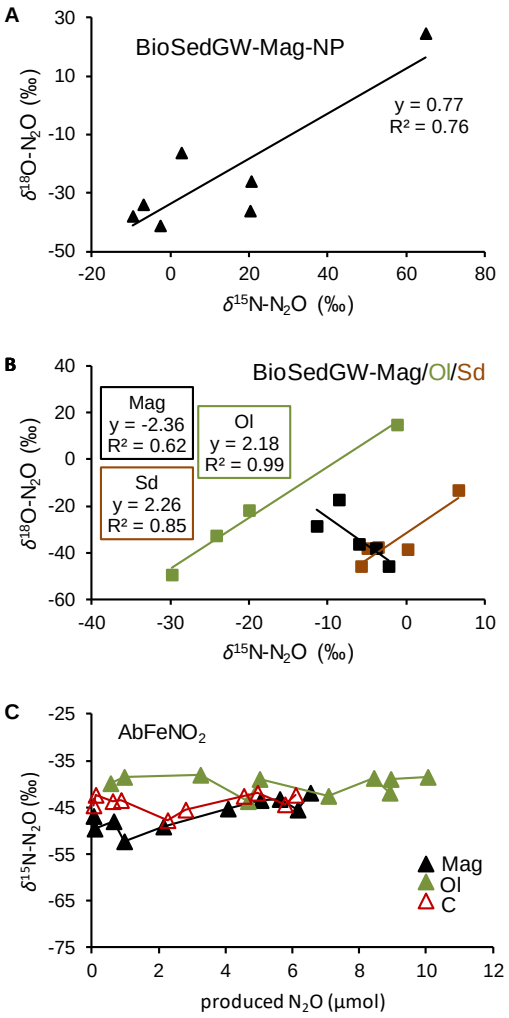

Figure 4. N_2O isotopic composition. $\delta^{15}N\text{-}N_2O$ versus $\delta^{18}O\text{-}N_2O$ plots for the experiments BioSedGW-Mag-NP (**A**) and BioSedGW-Mag/Ol/Sd (**B**), in which the substrate was NO_3^-; and $\delta^{15}N\text{-}N_2O$ versus N_2O plots for the $AbFeNO_2$ experiments (**C**), in which the substrate was NO_2^-.

An alternative way to use the $\delta^{15}N\text{-}N_2O$ data to distinguish biotic and abiotic reactions could be modelling the substrate (NO_3^- or NO_2^-) and product (N_2O) $\delta^{15}N$ composition by applying the calculated $\varepsilon^{15}N_{NO3}$ and $\varepsilon^{15}N_{NO2}$ in the batch experiments and to compare it with the determined $\delta^{15}N$ in the samples (Mariotti et al., 1981). Since the N_2O is an intermediate product of the NO_3^- biotic reduction but the end product of the abiotic NO_2^- reduction, at the end of the reaction, the determined $\delta^{15}N\text{-}N_2O$ of the samples should fit the initial $\delta^{15}N$ of the substrate in the case of the NO_2^- abiotic reduction but should be

higher than that in the case of the NO_3^- biotic reduction. In the BioSedGW-Mag-NP experiment plot (**Figure 5A**), the $\delta^{15}N\text{-}N_2O$ determined in most of the samples are above the modelled line, indicating a further reduction of the N_2O to N_2. Contrarily, in the AbFeNO_2 experiments (**Figure 5B**), the $\delta^{15}N\text{-}N_2O$ of the samples was initially below the modelled line but increased until reaching the substrate initial $\delta^{15}N$ at the end of the reaction, suggesting the generation of the intermediate product NO and confirming that N_2O was the end product of the NO_2^- abiotic reduction. Similar to our results, Chen et al. (2018) found initial $\delta^{15}N\text{-}N_2O$ more negative than the starting $\delta^{15}N\text{-}NO_3^-$ and $\delta^{15}N\text{-}NO_2^-$ due to NO generation. Also in another study, a good correlation was found between the calculated $\varepsilon^{15}N_{NO2}$ and the obtained $\delta^{15}N\text{-}N_2O$ values for the abiotic NO_2^- reduction by Fe^{2+} oxidation (Jones et al., 2015).

According to these results, the $\delta^{15}N\text{-}N_2O$ analysis could be useful to determine the occurrence of biotic and abiotic reactions involving N compounds and Fe. To quantify the contributions of the biotic and abiotic NO_2^- reduction by Fe^{2+} oxidation, performing new experiments to determine the $\varepsilon^{15}N_{NO2}$ and the $\varepsilon^{15}N_{N2O}$ in the biotic experiments could be advantageous after coupling this data to the already determined $\varepsilon^{15}N_{NO2}$ in the abiotic experiments and $\varepsilon^{15}N_{NO3}$ in the biotic experiments. Liu et al. (2018) assessed the contribution of each reaction by modelling the kinetics of each reaction tested separately. Concerning the Fe^{2+} oxidation, they found a major contribution of the abiotic compared to the biotic reaction while for the NO_2^- reduction, they found a major contribution of the biotic compared to the abiotic reaction. However, the use of models developed either by using isotopes or isotopic data could be limited at field-scale due to the complexity of the reactions. For example, Jamieson et al. (2018) suggest that the bacterial production of exopolymeric substances (EPS) could increase the NO_2^- abiotic reduction rate since Fe^{2+} can be complexed to the organic C from EPS. Other data that could be helpful in assessing the contribution of the biotic and abiotic reaction could be the analysis of the generated secondary minerals (Chen et al., 2018; Liu et al., 2018),

the site preference (SP) of the generated N_2O (i.e. the intramolecular distribution of N isotopes since the N_2O molecule has an asymmetric linear structure (N-N-O)) (Buchwald et al., 2016; Heil et al., 2014; Jones et al., 2015) and the Fe^{2+} isotopic composition.

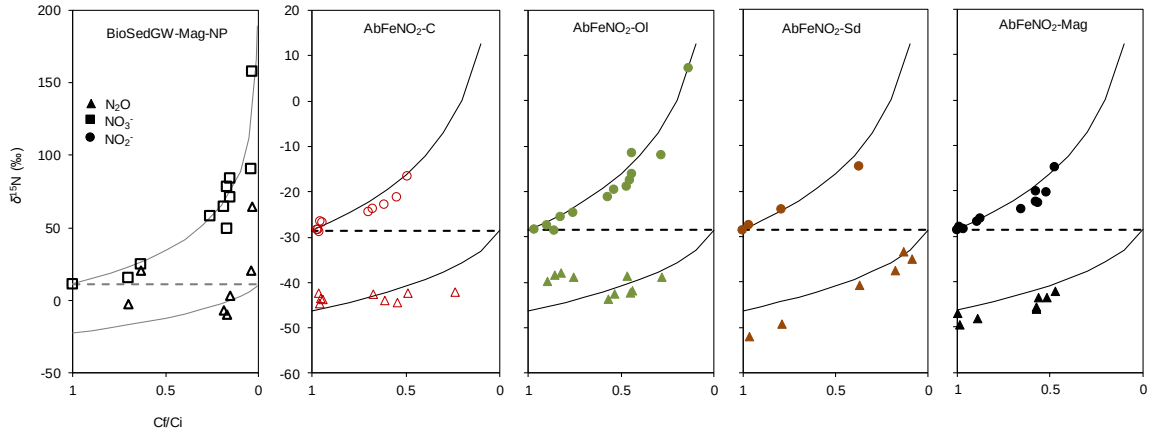

Figure 5. Relationship between the $\delta^{15}N$ of substrate and N_2O. Modelled and measured $\delta^{15}N$ of the N_2O and its initial substrates in the BioSedGW-Mag-NP and $AbFeNO_2$ experiments. Note that the substrate was NO_3^- for the BioSedGW-Mag-NP microcosms and NO_2^- for the $AbFeNO_2$ tests. This model was first described by Mariotti et al. (1981).

CONCLUSIONS

In the biotic experiments, the beginning of denitrification was caused by heterotrophic bacteria that used the organic C from sediment and groundwater. Afterwards, complete NO_3^- reduction was only achieved in the BioSedGW-Mag-NP microcosms, suggesting an increased Fe^{2+} availability for the Mag-NP compared to micro-sized Mag, Ol and Sd. Transient NO_2^- accumulation was observed but the final product of this biotic NO_3^- reduction was N_2. The lack of reactivity between the Fe^{2+}-containing minerals and NO_3^- or NO_2^-, confirmed that the NO_3^- reduction in the BioSedGW experiments was biotic. However, the abiotic NO_2^- reduction to N_2O by dissolved Fe^{2+} was demonstrated in the

AbFeNO$_2$ experiments. Therefore, if during the denitrification promoted by the Mag-NP, NO_2^- reacted abiotically with Fe^{2+}, the produced N_2O was further reduced to N_2. This abiotic reaction would be advantageous to avoid a water quality decrease due to NO_2^- accumulation only if the generated N_2O is further reduced biotically.

For the BioSedGW-Mag-NP, the calculated $\varepsilon^{15}N_{NO3}$ was -33.1 ‰, $\varepsilon^{18}O_{NO3}$ was -10.7 ‰ and $\varepsilon^{15}N_{NO3}/\varepsilon^{18}O_{NO3}$ was 3.1, suggesting $\delta^{18}O\text{-}NO_2^-$ equilibration with $\delta^{18}O\text{-}H_2O$ and subsequent NO_2^- reoxidation to NO_3^-. These ε values might be applied in future field studies to quantify the efficiency of bioremediation treatments. The isotopic results for the BioSedGW-Mag/Ol/Sd showed a similar trend since in all conditions the NPDOC released from sediment and groundwater was used as electron donor. Calculated $\varepsilon^{15}N_{NO3}$ was -12.0 ‰, $\varepsilon^{18}O_{NO3}$ was -10.9 ‰ and $\varepsilon^{15}N_{NO3}/\varepsilon^{18}O_{NO3}$ was 1.1, pointing to a lack of NO_2^- reoxidation. In the AbFeNO$_2$ experiments, the $\varepsilon^{15}N_{NO2}$ ranged from -14.1 ‰ to -17.8 ‰. Considering the wide range of reported $\varepsilon^{15}N_{NO2}$, it is not likely that the NO_2^- isotopic characterization could be useful at field-scale to distinguish the homogeneous from the heterogeneous abiotic reaction or the abiotic from the biotic NO_2^- reduction. Nevertheless, a high $\delta^{15}N\text{-}N_2O$ variation during the N compounds reduction could be indicative of biotic reactivity. Modelling the substrate (NO_3^- or NO_2^-) and product (N_2O) $\delta^{15}N$ composition by applying the calculated $\varepsilon^{15}N_{NO3}$ and $\varepsilon^{15}N_{NO2}$ in the batch experiments and comparing it with the determined $\delta^{15}N$ in the samples can be also useful to determine the occurrence of biotic and abiotic reactions.

ACKNOWLEDGMENTS

This work has been financed by the following projects: REMEDIATION (CGL2014-57215-C4), NANOREMOV (CGL2017-87216-C4-3-R) and ISOTEC (CGL2017-87216-C4-1-R), financed by the Spanish Government and AEI/FEDER from the UE, and MAG (2017-SGR-1733) from the Catalan Government. Margalef-Marti, R. is grateful to the Spanish Government for the Ph.D. grant BES-2015-072882. We would like to thank the

CCiT-UB for providing analytical support, Francesc Roca for his contribution on the Mag nanoparticles obtainment and Àngels Canals for her contribution on the XRD analysis and results interpretation.

REFERENCES

2006/118/EC, 2006. Groundwater Directive. Council Directive 2006/118/EC, of 12 December 2006, on the protection of groundwater against pollution and deterioration [WWW Document]. Off. J. Eur. Comm. URL http://ec.europa.eu/environment/index_en.htm (accessed 4.9.17).

91/676/EEC, 1991. Nitrates Directive. Council Directive 91/676/EEC of 12 December 1991, concerning the protection of waters against pollution caused by nitrates from agricultural sources. [WWW Document]. Off. J. Eur. Comm. URL http://ec.europa.eu/environment/index_en.htm (accessed 4.9.17).

98/83/EC, 1998. Drinking Water Directive. Council Directive 98/83/EC, of 3 November 1998, on the quality of water intended for human consumption. [WWW Document]. Off. J. Eur. Comm. URL http://ec.europa.eu/environment/index_en.htm (accessed 4.9.17).

Aquilina, L., Roques, C., Boisson, A., Vergnaud-Ayraud, V., Labasque, T., Pauwels, H., Pételet-Giraud, E., Pettenati, M., Dufresne, A., Bethencourt, L., Bour, O., 2018. Autotrophic denitrification supported by biotite dissolution in crystalline aquifers (1): New insights from short-term batch experiments. Sci. Total Environ. 619–620, 842–853. https://doi.org/10.1016/j.scitotenv.2017.11.079

Aravena, R., Robertson, W.D., 1998. Use of multiple isotope tracers to evaluate denitrification in ground water: study of nitrate from a large-flux septic system plume. Ground Water 36, 975–982.

Badr, O., Probert, S.D., 1993. Environmental impacts of atmospheric nitrous oxide. Appl. Energy 44, 197–231. https://doi.org/10.1016/0306-2619(93)90018-K

Betlach, M.R., Tiedje, J.M., 1981. Kinetic Explanation for Accumulation of Nitrite, Nitric Oxide, and Nitrous Oxide during Bacterial Denitrification. Appl. Environ. Microbiol. 42, 1074–1084. https://doi.org/Article

Bolleter, W.T., Bushman, C.J., Tidwell, P.W., 1961. Spectrophotometric Determination of Ammonia as Indophenol. Anal. Chem. 33, 592–594. https://doi.org/10.1021/ac60172a034

Borden, A.K., Brusseau, M.L., Carroll, K.C., McMillan, A., Akyol, N.H., Berkompas, J., Miao, Z., Jordan, F., Tick, G., Waugh, W.J., Glenn, E.P., 2012. Ethanol addition for enhancing denitrification at the uranium mill tailing site in Monument Valley, AZ. Water. Air. Soil Pollut. 223, 755–763. https://doi.org/10.1007/s11270-011-0899-1

Bosch, J., Lee, K.Y., Jordan, G., Kim, K.W., Meckenstock, R.U., 2012. Anaerobic, nitrate-dependent oxidation of pyrite nanoparticles by thiobacillus denitrificans. Environ. Sci. Technol. 46, 2095–2101. https://doi.org/10.1021/es2022329

Böttcher, J., Strebel, O., Voerkelius, S., Schmidt, H.-L., 1990. Using isotope fractionation of nitrate-nitrogen and nitrate-oxygen for evaluation of microbial denitrification in a sandy aquifer. J. Hydrol. 114, 413–424. https://doi.org/10.1016/0022-1694(90)90068-9

Braunschweig, J., Bosch, J., Meckenstock, R.U., 2013. Iron oxide nanoparticles in geomicrobiology: from biogeochemistry to bioremediation. N. Biotechnol. 30, 793–802. https://doi.org/10.1016/j.nbt.2013.03.008

Bryce, C., Blackwell, N., Schmidt, C., Otte, J., Huang, Y., Kleindienst, S., Tomaszewski, E., Schad, M., Warter, V., Peng, C., Byrne, J., Kappler, A., 2018. Microbial anaerobic Fe(II) oxidation - ecology, mechanisms and environmental implications. Environ. Microbiol. 20, 3462–3483. https://doi.org/10.1111/1462-2920.14328

Buchwald, C., Grabb, K., Hansel, C.M., Wankel, S.D., 2016. Constraining the role of iron in environmental nitrogen transformations: Dual stable isotope systematics of abiotic NO_2^- reduction by Fe(II) and its production of N_2O. Geochim. Cosmochim. Acta. https://doi.org/10.1016/j.gca.2016.04.041

Carlson, H.K., Clark, I.C., Blazewicz, S.J., Iavarone, A.T., Coates, J.D., 2013. Fe(II) oxidation is an innate capability of nitrate-reducing bacteria that involves abiotic and biotic reactions. J. Bacteriol. 195, 3260–3268. https://doi.org/10.1128/JB.00058-13

Carrey, R., Otero, N., Vidal-Gavilan, G., Ayora, C., Soler, A., Gómez-Alday, J.J., 2014. Induced nitrate attenuation by glucose in groundwater: Flow-through experiment.

Chem. Geol. 370, 19–28. https://doi.org/10.1016/j.chemgeo.2014.01.016

Carrey, R., Rodríguez-Escales, P., Soler, A., Otero, N., 2018. Tracing the role of endogenous carbon in denitrification using wine industry by-product as an external electron donor: Coupling isotopic tools with mathematical modeling. J. Environ. Manage. 207, 105–115. https://doi.org/10.1016/j.jenvman.2017.10.063

Chen, D., Liu, T., Li, X., Li, F., Luo, X., Wu, Y., Wang, Y., 2018. Biological and chemical processes of microbially mediated nitrate-reducing Fe(II) oxidation by Pseudogulbenkiania sp. strain 2002. Chem. Geol. 476, 59–69. https://doi.org/10.1016/j.chemgeo.2017.11.004

Cho, D.W., Song, H., Kim, B., Schwartz, F.W., Jeon, B.H., 2015a. Reduction of nitrate in groundwater by Fe(0)/Magnetite nanoparticles entrapped in Ca-Alginate beads. Water. Air. Soil Pollut. 226. https://doi.org/10.1007/s11270-015-2467-6

Cho, D.W., Song, H., Schwartz, F.W., Kim, B., Jeon, B.H., 2015b. The role of magnetite nanoparticles in the reduction of nitrate in groundwater by zero-valent iron. Chemosphere 125, 41–49. https://doi.org/10.1016/j.chemosphere.2015.01.019

Chowdhury, S.R., Yanful, E.K., 2010. Arsenic and chromium removal by mixed magnetite-maghemite nanoparticles and the effect of phosphate on removal. J. Environ. Manage. 91, 2238–2247. https://doi.org/10.1016/j.jenvman.2010.06.003

Coby, A.J., Picardal, F.W., 2005. Inhibition of NO_3^- and NO_2^- reduction by microbial Fe(III) reduction: Evidence of a reaction between NO_2^- and cell surface-bound Fe^{2+}. Appl. Environ. Microbiol. 71, 5267–5274. https://doi.org/10.1128/AEM.71.9.5267-5274.2005

Cooper, D.C., Picardal, F.W., Schimmelmann, A., Coby, A.J., 2003. Chemical and Biological Interactions during Nitrate and Goethite Reduction by Shewanella putrefaciens 200 Chemical and Biological Interactions during Nitrate and Goethite Reduction by Shewanella putrefaciens 200. Appl. Environ. Microbiol. 69, 3517–3525. https://doi.org/10.1128/AEM.69.6.3517

Coplen, T.B., 2011. Guidelines and recommended terms for expression of stable-isotope-ratio and gas-ratio measurement results. Rapid Commun. Mass Spectrom. 25, 2538–2560. https://doi.org/10.1002/rcm.5129

Crane, R.A., Dickinson, M., Popescu, I.C., Scott, T.B., 2011. Magnetite and zero-valent

iron nanoparticles for the remediation of uranium contaminated environmental water. Water Res. 45, 2931–2942. https://doi.org/10.1016/j.watres.2011.03.012

Devlin, J.F., Eedy, R., Butler, B.J., 2000. The effects of electron donor and granular iron on nitrate transformation rates in sediments from a municipal water supply aquifer. J. Contam. Hydrol. 46, 81–97. https://doi.org/10.1016/S0169-7722(00)00126-1

Dhakal, P., Matocha, C.J., Huggins, F.E., Vandiviere, M.M., 2013. Nitrite reactivity with magnetite. Environ. Sci. Technol. 47, 6206–6213. https://doi.org/10.1021/es304011w

Fukada, T., Hiscock, K.M., Dennis, P.F., Grischek, T., 2003. A dual isotope approach to identify denitrification in groundwater at a river-bank infiltration site. Water Res. 37, 3070–3078. https://doi.org/10.1016/S0043-1354(03)00176-3

Ge, S., Peng, Y., Wang, S., Lu, C., Cao, X., Zhu, Y., 2012. Nitrite accumulation under constant temperature in anoxic denitrification process: The effects of carbon sources and COD/NO_3-N. Bioresour. Technol. 114, 137–143. https://doi.org/10.1016/j.biortech.2012.03.016

Gibert, O., Pomierny, S., Rowe, I., Kalin, R.M., 2008. Selection of organic substrates as potential reactive materials for use in a denitrification permeable reactive barrier (PRB). Bioresour. Technol. 99, 7587–7596. https://doi.org/10.1016/j.biortech.2008.02.012

Gorski, C. a, Nurmi, J.T., Tratnyek, P.G., Hofstetter, T.B., Scherer, M.M., 2010. Redox Behavior of Magnetite : Reduction. Environ. Sci. Technol. 44, 55–60. https://doi.org/10.1021/es9016848

Grabb, K.C., Buchwald, C., Hansel, C.M., Wankel, S.D., 2017. A dual nitrite isotopic investigation of chemodenitrification by mineral-associated Fe(II) and its production of nitrous oxide. Geochim. Cosmochim. Acta 196, 388–402. https://doi.org/10.1016/j.gca.2016.10.026

Granger, J., Sigman, D.M., Lehmann, M.F., Tortell, P.D., 2008. Nitrogen and oxygen isotope fractionation during dissimilatory nitrate reduction by denitrifying bacteria. Limnol. Oceanogr. 53, 2533–2545. https://doi.org/10.4319/lo.2008.53.6.2533

Grau-Martínez, A., Torrentó, C., Carrey, R., Rodríguez-Escales, P., Domènech, C., Ghiglieri, G., Soler, A., Otero, N., 2017. Feasibility of two low-cost organic

substrates for inducing denitrification in artificial recharge ponds: Batch and flow-through experiments. J. Contam. Hydrol. 198, 48–58. https://doi.org/10.1016/j.jconhyd.2017.01.001

He, S., Tominski, C., Kappler, A., Behrens, S., Roden, E.E., 2016. Metagenomic analyses of the autotrophic Fe(II)-oxidizing, nitrate-reducing enrichment culture KS. Appl. Environ. Microbiol. 82, 2656–2668. https://doi.org/10.1128/AEM.03493-15

He, Y., Lin, H., Dong, Y., Li, B., Wang, L., Chu, S., Luo, M., Liu, J., 2018. Zeolite supported Fe/Ni bimetallic nanoparticles for simultaneous removal of nitrate and phosphate: Synergistic effect and mechanism. Chem. Eng. J. 347, 669–681. https://doi.org/10.1016/j.cej.2018.04.088

Heil, J., Wolf, B., Brüggemann, N., Emmenegger, L., Tuzson, B., Vereecken, H., Mohn, J., 2014. Site-specific ^{15}N isotopic signatures of abiotically produced N_2O. Geochim. Cosmochim. Acta 139, 72–82. https://doi.org/10.1016/j.gca.2014.04.037

Hernández-del Amo, E., Menció, A., Gich, F., Mas-Pla, J., Bañeras, L., 2018. Isotope and microbiome data provide complementary information to identify natural nitrate attenuation processes in groundwater. Sci. Total Environ. 613–614, 579–591. https://doi.org/10.1016/j.scitotenv.2017.09.018

Jamieson, J., Prommer, H., Kaksonen, A.H., Sun, J., Siade, A.J., Yusov, A., Bostick, B., 2018. Identifying and Quantifying the Intermediate Processes during Nitrate-Dependent Iron(II) Oxidation. Environ. Sci. Technol. 52, 5771–5781. https://doi.org/10.1021/acs.est.8b01122

Jones, L.C., Peters, B., Lezama Pacheco, J.S., Casciotti, K.L., Fendorf, S., 2015. Stable Isotopes and Iron Oxide Mineral Products as Markers of Chemodenitrification. Environ. Sci. Technol. 49, 3444–3452. https://doi.org/10.1021/es504862x

Jurado, A., Borges, A. V., Brouyère, S., 2017. Dynamics and emissions of N_2O in groundwater: A review. Sci. Total Environ. 584–585, 207–218. https://doi.org/10.1016/j.scitotenv.2017.01.127

Kampschreur, M.J., Kleerebezem, R., de Vet, W.W.J.M., Van Loosdrecht, M.C.M., 2011. Reduced iron induced nitric oxide and nitrous oxide emission. Water Res. 45, 5945–5952. https://doi.org/10.1016/j.watres.2011.08.056

Klueglein, N., Kappler, A., 2013. Abiotic oxidation of Fe(II) by reactive nitrogen species in cultures of the nitrate-reducing Fe(II) oxidizer *Acidovorax sp*. BoFeN1 - questioning the existence of enzymatic Fe(II) oxidation. Geobiology 11, 180–190. https://doi.org/10.1111/gbi.12019

Knöller, K., Vogt, C., Haupt, M., Feisthauer, S., Richnow, H.H., 2011. Experimental investigation of nitrogen and oxygen isotope fractionation in nitrate and nitrite during denitrification. Biogeochemistry 103, 371–384. https://doi.org/10.1007/s10533-010-9483-9

Knowles, R., 1982. Denitrification. Microbiol. Rev. 46, 43–70.

Liu, T., Chen, D., Luo, X., Li, X., Li, F., 2018. Microbially mediated nitrate-reducing Fe(II) oxidation: Quantification of chemodenitrification and biological reactions. Geochim. Cosmochim. Acta. https://doi.org/10.1016/j.gca.2018.06.040

Margalef-Marti, R., Carrey, R., Merchán, D., Soler, A., Causapé, J., Otero, N., 2019a. Feasibility of using rural waste products to increase the denitrification efficiency in a surface flow constructed wetland. J. Hydrol. 124035. https://doi.org/10.1016/j.jhydrol.2019.124035

Margalef-Marti, R., Carrey, R., Soler, A., Otero, N., 2019b. Evaluating the potential use of a dairy industry residue to induce denitri fi cation in polluted water bodies : A fl ow-through experiment. J. Environ. Manage. 245, 86–94. https://doi.org/10.1016/j.jenvman.2019.03.086

Margalef-Marti, R., Carrey, R., Viladés, M., Jubany, I., Vilanova, E., Grau, R., Soler, A., Otero, N., 2019c. Use of nitrogen and oxygen isotopes of dissolved nitrate to trace field-scale induced denitrification efficiency throughout an in-situ groundwater remediation strategy. Sci. Total Environ. https://doi.org/10.1016/j.scitotenv.2019.06.003

Mariotti, A., Germon, J.C., Hubert, P., Kaiser, P., Letolle, R., Tardieux, A., Tardieux, P., 1981. Experimental determination of nitrogen kinetic isotope fractionation: Some principles; illustration for the denitrification and nitrification processes. Plant Soil 62, 413–430. https://doi.org/10.1007/BF02374138

Mariotti, A., Landreau, A., Simon, B., 1988. ^{15}N isotope biogeochemistry and natural denitrification process in groundwater: Application to the chalk aquifer of northern France. Geochim. Cosmochim. Acta 52, 1869–1878. https://doi.org/10.1016/0016-7037(88)90010-5

Martin, T.S., Casciotti, K.L., 2016. Nitrogen and oxygen isotopic fractionation during microbial nitrite reduction. Limnol. Oceanogr. 61, 1134-1143. https://doi.org/10.1002/lno.10278

Matocha, C.J., Coyne, M.S., 2007. Short-term Response of Soil Iron to Nitrate Addition. Soil Sci. Soc. Am. J. 71, 108. https://doi.org/10.2136/sssaj2005.0170

McIlvin, M.R., Altabet, M.A., 2005. Chemical conversion of nitrate and nitrite to nitrous oxide for nitrogen and oxygen isotopic analysis in freshwater and seawater. Anal Chem 77, 5589–5595. https://doi.org/10.1021/ac050528s

Meckenstock, R.U., Morasch, B., Griebler, C., Richnow, H.H., 2004. Stable isotope fractionation analysis as a tool to monitor biodegradation in contaminated acquifers. J. Contam. Hydrol. 75, 215–255. https://doi.org/10.1016/j.jconhyd.2004.06.003

Melton, E.D., Swanner, E.D., Behrens, S., Schmidt, C., Kappler, A., 2014. The interplay of microbially mediated and abiotic reactions in the biogeochemical Fe cycle. Nat. Rev. Microbiol. 12, 797–808. https://doi.org/10.1038/nrmicro3347

Morley, N., Baggs, E.M., Dörsch, P., Bakken, L., 2008. Production of NO, N_2O and N_2 by extracted soil bacteria, regulation by NO_2^- and O_2 concentrations. FEMS Microbiol. Ecol. 65, 102–112. https://doi.org/10.1111/j.1574-6941.2008.00495.x

Otero, N., Torrentó, C., Soler, A., Menció, A., Mas-Pla, J., 2009. Monitoring groundwater nitrate attenuation in a regional system coupling hydrogeology with multi-isotopic methods: The case of Plana de Vic (Osona, Spain). Agric. Ecosyst. Environ. 133, 103–113. https://doi.org/10.1016/j.agee.2009.05.007

Price, A., Pearson, V.K., Schwenzer, S.P., Miot, J., Olsson-Francis, K., 2018. Nitrate-dependent iron oxidation: A potential Mars metabolism. Front. Microbiol. 9, 1–15. https://doi.org/10.3389/fmicb.2018.00513

Rakshit, S., Matocha, C.J., Coyne, M.S., Sarkar, D., 2016. Nitrite reduction by Fe(II) associated with kaolinite. Int. J. Environ. Sci. Technol. 13, 1329–1334. https://doi.org/10.1007/s13762-016-0971-x

Reay, D.S., Davidson, E.A., Smith, K.A., Smith, P., Melillo, J.M., Dentener, F., Crutzen, P.J., 2012. Global agriculture and nitrous oxide emissions. Nat. Clim. Chang. 2, 410–416. https://doi.org/10.1038/nclimate1458

Rivett, M.O., Buss, S.R., Morgan, P., Smith, J.W.N., Bemment, C.D., 2008. Nitrate attenuation in groundwater: A review of biogeochemical controlling processes. Water Res. 42, 4215–4232. https://doi.org/10.1016/j.watres.2008.07.020

Ryabenko, E., Altabet, M. a., Wallace, D.W.R., 2009. Effect of chloride on the chemical conversion of nitrate to nitrous oxide for $\delta^{15}N$ analysis. Limnol. Oceanogr. Methods 7, 545–552. https://doi.org/10.4319/lom.2009.7.545

Smith, R.L., Kent, D.B., Repert, D.A., Böhlke, J.K., 2017. Anoxic nitrate reduction coupled with iron oxidation and attenuation of dissolved arsenic and phosphate in a sand and gravel aquifer. Geochim. Cosmochim. Acta 196, 102–120. https://doi.org/10.1016/j.gca.2016.09.025

Smith, R.L., Miller, D.N., Brooks, M.H., Widdowson, M.A., Killingstad, M.W., 2001. In situ stimulation of groundwater denitrification with formate to remediate nitrate contamination. Environ. Sci. Technol. 35, 196–203. https://doi.org/10.1021/es001360p

Straub, K.L., Benz, M., Schink, B., Widdel, F., 1996. Anaerobic, nitrate-dependent microbial oxidation of ferrous iron. Appl. Environ. Microbiol. 62, 1458–1460.

Straub, K.L., Schönhuber, W.A., Buchholz-Cleven, B.E.E., Schink, B., 2004. Diversity of ferrous iron-oxidizing, nitrate-reducing bacteria and their involvement in oxygen-independent iron cycling. Geomicrobiol. J. 21, 371–378. https://doi.org/10.1080/01490450490485854

Tai, Y.L., Dempsey, B.A., 2009. Nitrite reduction with hydrous ferric oxide and Fe(II): Stoichiometry, rate, and mechanism. Water Res. 43, 546–552. https://doi.org/10.1016/j.watres.2008.10.055

Torrentó, C., Cama, J., Urmeneta, J., Otero, N., Soler, A., 2010. Denitrification of groundwater with pyrite and *Thiobacillus denitrificans*. Chem. Geol. 278, 80–91. https://doi.org/10.1016/j.chemgeo.2010.09.003

Torrentó, C., Urmeneta, J., Otero, N., Soler, A., Viñas, M., Cama, J., 2011. Enhanced denitrification in groundwater and sediments from a nitrate-contaminated aquifer after addition of pyrite. Chem. Geol. 287, 90–101. https://doi.org/10.1016/j.chemgeo.2011.06.002

Trois, C., Pisano, G., Oxarango, L., 2010. Alternative solutions for the bio-denitrification of landfill leachates using pine bark and compost. J. Hazard. Mater. 178, 1100–

1105. https://doi.org/10.1016/j.jhazmat.2010.01.054

Tsushima, K., Ueda, S., Ohno, H., Ogura, N., Katase, T., Watanabe, K., 2006. Nitrate decrease with isotopic fractionation in riverside sediment column during infiltration experiment. Water. Air. Soil Pollut. 174, 47–61. https://doi.org/10.1007/s11270-005-9024-7

Vidal-Gavilan, G., Folch, A., Otero, N., Solanas, A.M., Soler, A., 2013. Isotope characterization of an in situ biodenitrification pilot-test in a fractured aquifer. Appl. Geochemistry 32, 153–163. https://doi.org/10.1016/j.apgeochem.2012.10.033

Vitòria, L., Soler, A., Canals, À., Otero, N., 2008. Environmental isotopes (N, S, C, O, D) to determine natural attenuation processes in nitrate contaminated waters: Example of Osona (NE Spain). Appl. Geochemistry 23, 3597–3611. https://doi.org/10.1016/j.apgeochem.2008.07.018

Vitousek, P.M., Aber, J.D., Howarth, R.W., Likens, G.E., Matson, P.A., Schindler, D.W., Schlesinger, W.H., Tilman, D.G., 1997. Summary for Policymakers, in: Intergovernmental Panel on Climate Change (Ed.), Climate Change 2013 - The Physical Science Basis. Cambridge University Press, Cambridge, pp. 1–30. https://doi.org/10.1017/CBO9781107415324.004

Wang, M., Hu, R., Zhao, J., Kuzyakov, Y., Liu, S., 2016. Iron oxidation affects nitrous oxide emissions via donating electrons to denitrification in paddy soils. Geoderma 271, 173–180. https://doi.org/10.1016/j.geoderma.2016.02.022

Wang, R., Yang, C., Zhang, M., Xu, S.Y., Dai, C.L., Liang, L.Y., Zhao, H.P., Zheng, P., 2017. Chemoautotrophic denitrification based on ferrous iron oxidation: Reactor performance and sludge characteristics. Chem. Eng. J. 313, 693–701. https://doi.org/10.1016/j.cej.2016.12.052

Ward, M.H., DeKok, T.M., Levallois, P., Brender, J., Gulis, G., Nolan, B.T., VanDerslice, J., 2005. Workgroup Report: Drinking-Water Nitrate and Health—Recent Findings and Research Needs. Environ. Health Perspect. 113, 1607–1614. https://doi.org/10.1289/ehp.8043

Weber, K.A., Achenbach, L.A., Coates, J.D., 2006. Microorganisms pumping iron: Anaerobic microbial iron oxidation and reduction. Nat. Rev. Microbiol. 4, 752–764. https://doi.org/10.1038/nrmicro1490

Weymann, D., Geistlinger, H., Well, R., Von Der Heide, C., Flessa, H., 2010. Kinetics

of N_2O production and reduction in a nitrate-contaminated aquifer inferred from laboratory incubation experiments. Biogeosciences 7, 1953–1972. https://doi.org/10.5194/bg-7-1953-2010

Wunderlich, A., Meckenstock, R., Einsiedl, F., 2012. Effect of different carbon substrates on nitrate stable isotope fractionation during microbial denitrification. Environ. Sci. Technol. 46, 4861–4868. https://doi.org/10.1021/es204075b

Yang, Y., Chen, T., Morrison, L., Gerrity, S., Collins, G., Porca, E., Li, R., Zhan, X., 2017. Nanostructured pyrrhotite supports autotrophic denitrification for simultaneous nitrogen and phosphorus removal from secondary effluents. Chem. Eng. J. 328, 511–518. https://doi.org/10.1016/j.cej.2017.07.061

Zelmanov, G., Semiat, R., 2008. Iron(3) oxide-based nanoparticles as catalysts in advanced organic aqueous oxidation. Water Res. 42, 492–498. https://doi.org/10.1016/j.watres.2007.07.045

Zhou, J., Wang, H., Yang, K., Ji, B., Chen, D., Zhang, H., Sun, Y., Tian, J., 2016. Autotrophic denitrification by nitrate-dependent Fe(II) oxidation in a continuous up-flow biofilter. Bioprocess Biosyst. Eng. 39, 277–284. https://doi.org/10.1007/s00449-015-1511-7

SUPPLEMENTARY INFORMATION TO:

Induced nitrate attenuation by ferrous iron containing minerals.

Rosanna Margalef-Marti[1], Raúl Carrey[1], José Antonio Benito[2], Vicenç Marti[2], Albert Soler[1], Neus Otero[1,3]

[1] Grup MAiMA, SGR Mineralogia Aplicada, Geoquímica i Geomicrobiologia, Departament de Mineralogia, Petrologia i Geologia Aplicada, Facultat de Ciències de la Terra, Universitat de Barcelona (UB), Barcelona, C/Martí i Franquès s/n, 08028 Barcelona, Spain.

[2] Materials Science and Metallurgical Engineering Department and Barcelona Research Center in Multiscale Science and Engineering, EEBE, Technical University of Catalonia (UPC), Av. Eduard Maristany 16, 08019 Barcelona, Spain.

[3] Serra Húnter Fellowship, Generalitat de Catalunya, Spain.

Submitted to *Chemosphere*

Section S1. Micro-sized minerals preparation and magnetite size reduction

Magnetite (Mag) was obtained from “Mina Cala” (Huelva, Spain), siderite (Sd) from “El guarnón” (Güéjar Sierra, Granada, Spain) and olivine (Ol) from Canet d’Adri (Girona, Spain). The minerals were milled in a vibratory disc mill (RETSCH, RS 100) using a tungsten carbide bowl (WC 94%, Co 6%) and sieved to obtain the fraction with a particle size below 30 µm. An aliquot of Mag microparticles was then milled in a planetary ball mill (FRITSCH, PULVERISETTE P5) at 200 rpm during 15 h, using a stainless steel bowl, deionized water and 0.4 mm steel balls (S110) as grinding media to obtain nanoparticles.

Section S2. Mineral characterization

The main composition of the minerals was estimated by X-Ray Diffraction (XRD, PANalytical X'Pert PRO), the particle size of the Mag micro and nanoparticles was determined by Laser Diffraction Particle Size Analysis (LDPSA, LS13320, BeckmanCoulter) and morphology by Field Emission Scanning Electron Microscopy (FESEM, JSM-7610F, JEOL).

XRD analysis showed a purity of around 90% for Mag ($Fe^{2+}Fe^{3+}{}_2O_4$), 30% for Sd (Fe_2CO_3) and 80% for Ol (Forsterite ferroan, $Fe^{2+}{}_{0.2}Mg_{1.8}SiO_4$). Therefore, the given Fe^{2+}/N molar ratio of the minerals in the biotic experiments was approximately 24 for Mag, 13 for Sd and 7 for Ol. In the abiotic experiments ($AbFeNO_3$ and $AbFeNO_2$), the ratio was reduced by half, but dissolved Fe^{2+} was added at a Fe^{2+}/N of 5. Therefore, although using the same quantity of mineral, in the experiments containing Mag, the Fe^{2+} availability could be higher compared to Sd, and the Ol experiments could present the lowest electron donor availability. The stoichiometric Fe^{2+}/N reported for the NO_3^- and NO_2^- reductions are 5 and 2, respectively (**Equation 2** and **3**) (Melton et al., 2014; Tai and Dempsey, 2009).

$$10Fe^{2+} + 2NO_3^- + 24H_2O \rightarrow 10Fe(OH)_3 + N_2 + 18H^+ \qquad \textbf{Equation 2}$$

$$4Fe^{2+} + 2NO_2^- + 5H_2O \rightarrow 4FeOOH + N_2O + 6H^+ \qquad \textbf{Equation 3}$$

According to the LDPSA analysis, the first milling and sieving step gave solid particles with an average Mag particle diameter of 8.12 µm (between 0.07 and 36.24 µm) and the second milling step gave aggregates with an average of 1.16 µm (between 0.04 and 2.00 µm) (Supplementary information, **Figure S1A**). The % volume mode was used for calculations. Although the particle diameter range was wide, a 10 fold decrease in the mineral size was observed in the Mag-NP compared to the micro-sized Mag. Such decrease was confirmed by the FESEM images, in which was also observed that the

Mag-NP aggregates are formed by smaller nanoparticles with an average particle diameter around 100 nm (Supplementary information, **Figure S1B**).

REFERENCES

Melton, E.D., Swanner, E.D., Behrens, S., Schmidt, C., Kappler, A., 2014. The interplay of microbially mediated and abiotic reactions in the biogeochemical Fe cycle. Nat. Rev. Microbiol. 12, 797–808. https://doi.org/10.1038/nrmicro3347

Tai, Y.L., Dempsey, B.A., 2009. Nitrite reduction with hydrous ferric oxide and Fe(II): Stoichiometry, rate, and mechanism. Water Res. 43, 546–552. https://doi.org/10.1016/j.watres.2008.10.055

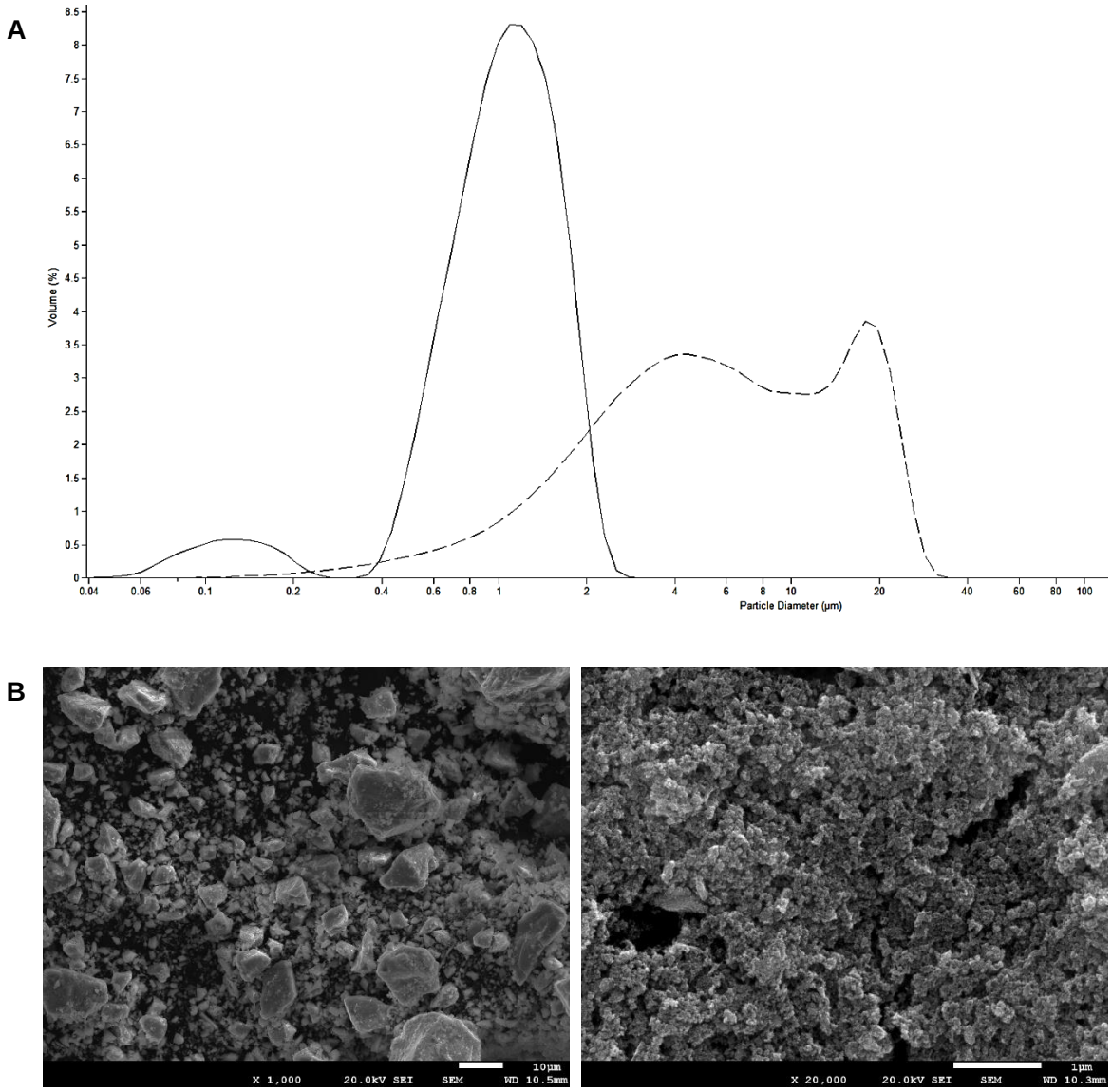

Figure S1. Mag particles characterization. A. Particle diameter before (dashed line) and after (continuous line) the second milling step. **B**. Particle morphology before (left) and after (right) the second milling step.

Table S1. Water composition for each series of experiments. Groundwater was used in the BioSedGW experiments, deionized water (DIW) in the BioSedDIW experiments and synthetic water (produced with DIW) in the $AbFeNO_3$, $AbFeNO_2$ and $AbNO_2$ experiments (see **Table 1**). The concentrations are expressed in ppm.

	BioSedGW	BioSedDIW	$AbFeNO_3$	$AbFeNO_2$ and $AbNO_2$
$NaHCO_3$	-	-	306.9	347.6
KH_2PO_4	-	-	4.9	7.0
$MgCl_2 \cdot 6H_2O$	-	-	259.9	275.6
KCl	-	-	107.3	116.0
$CaCl_2 \cdot 2H_2O$	-	-	124.8	99.3
Na_2SO_4	-	-	210.0	219.5
KNO_2	-	-	-	124.8
$NaNO_3$	-	97.7	0.1	-
Groundwater NO_3^-	71.3	-	-	-
Groundwater NPDOC	2.3	-	-	-

Table S2.1. Results for de BioSedGW experiments. Chemical and isotopic characterization. n.d. = no determined.

	Days	pH	NO_3^- (mM)	NO_2^- (mM)	NH_4^+ (mM)	N_2O (nmol)	$\delta^{15}N\text{-}NO_3^-$ (‰)	$\delta^{18}O\text{-}NO_3^-$ (‰)	$\delta^{15}N\text{-}N_2O$ (‰)	$\delta^{18}O\text{-}N_2O$ (‰)
Groundwater	0	7.6	1.15	0.00	n.d.	n.d.	+11.3	+10.1	n.d.	n.d.
BioSedGW-Mag-NP-1	7	5.8	0.80	0.05	0.00	7.08	+15.3	+14.3	-2.6	-41.2
BioSedGW-Mag-NP-2	34	n.d.	0.72	0.00	0.00	12.57	+24.8	+17.9	+20.4	-36.0
BioSedGW-Mag-NP-3	62	7.9	0.20	0.17	n.d.	0.89	+49.4	+44.0	-9.6	-37.7
BioSedGW-Mag-NP-4	71	7.1	0.30	0.13	n.d.	n.d.	+58.0	+30.2	n.d.	n.d.
BioSedGW-Mag-NP-5	78	7.1	0.21	0.17	0.00	38.18	+64.5	+29.8	-6.8	-33.9
BioSedGW-Mag-NP-6	84	7.2	0.17	0.18	n.d.	34.02	+71.0	+27.7	+2.9	-16.1
BioSedGW-Mag-NP-7	91	7.2	0.05	0.19	n.d.	43.29	+90.5	+47.5	+20.6	-26.1
BioSedGW-Mag-NP-8	118	7.1	0.18	0.05	0.00	0.00	+84.0	+20.9	n.d.	n.d.
BioSedGW-Mag-NP-9	222	7.0	0.04	0.00	0.03	63.84	+158.1	+25.0	+64.9	+24.9
BioSedGW-Ol-1	7	6.4	0.74	0.07	0.04	0.29	+15.1	+11.8	-29.8	-49.7
BioSedGW-Ol-2	62	8.1	0.66	0.16	0.04	0.59	+19.2	+17.1	n.d.	n.d.
BioSedGW-Ol-3	84	7.7	0.61	0.01	n.d.	0.56	+15.4	+11.6	-24.2	-32.8
BioSedGW-Ol-4	98	7.6	0.63	0.00	0.02	0.36	n.d.	n.d.	-19.9	-22.0
BioSedGW-Ol-5	118	7.6	0.59	0.00	n.d.	0.00	n.d.	n.d.	n.d.	n.d.
BioSedGW-Ol-6	222	7.6	0.71	0.00	0.01	0.38	+19.9	+10.1	-1.2	+14.7
BioSedGW-Ol-7	365	n.d.	0.74	0.01	0.01	n.d.	n.d.	n.d.	n.d.	n.d.

Table S2.1. Continued.

	Days	pH	NO_3^- (mM)	NO_2^- (mM)	NH_4^+ (mM)	N_2O (nmol)	$\delta^{15}N\text{-}NO_3^-$ (‰)	$\delta^{18}O\text{-}NO_3^-$ (‰)	$\delta^{15}N\text{-}N_2O$ (‰)	$\delta^{18}O\text{-}N_2O$ (‰)
BioSedGW-Sd-1	7	6.3	0.67	0.17	0.03	3.19	n.d.	n.d.	-4.9	-38.3
BioSedGW-Sd-2	62	7.6	0.43	0.18	0.04	7.43	+21.4	+20.2	-5.7	-45.9
BioSedGW-Sd-3	84	7.1	0.57	0.06	n.d.	11.06	+23.6	+15.8	-3.6	-38.0
BioSedGW-Sd-4	98	7.1	0.52	0.08	n.d.	14.19	n.d.	n.d.	+0.2	-38.9
BioSedGW-Sd-5	118	7.1	0.61	0.00	n.d.	0.00	n.d.	n.d.	n.d.	n.d.
BioSedGW-Sd-6	222	7.0	0.72	0.00	n.d.	6.55	+18.5	+10.1	+6.6	-13.5
BioSedGW-Sd-7	365	n.d.	0.69	0.02	0.01	n.d.	n.d.	n.d.	n.d.	n.d.
BioSedGW-Mag-1	7	6.3	0.69	0.08	0.04	2.42	n.d.	n.d.	-5.9	-36.5
BioSedGW-Mag-2	62	7.6	0.53	0.08	0.01	n.d.	+20.5	+17.1	n.d.	n.d.
BioSedGW-Mag-3	84	7.2	0.55	0.00	n.d.	35.51	+24.4	+17.0	-2.3	-46.0
BioSedGW-Mag-4	98	7.2	0.53	0.00	0.00	0.94	n.d.	n.d.	-8.5	-17.4
BioSedGW-Mag-5	118	7.2	0.58	0.00	n.d.	3.16	n.d.	n.d.	-3.8	-38.3
BioSedGW-Mag-6	222	7.0	0.57	0.00	0.01	11.88	+24.4	+13.3	-11.3	-28.6
BioSedGW-Mag-7	365	n.d.	0.62	0.02	0.01	n.d.	n.d.	n.d.	n.d.	n.d.

Table S2.1. Continued.

	Days	pH	NO_3^- (mM)	NO_2^- (mM)	NH_4^+ (mM)	N_2O (nmol)	$\delta^{15}N\text{-}NO_3^-$ (‰)	$\delta^{18}O\text{-}NO_3^-$ (‰)	$\delta^{15}N\text{-}N_2O$ (‰)	$\delta^{18}O\text{-}N_2O$ (‰)
BioSedGW-C-1	7	6.1	0.63	0.08	n.d.	6.87	+15.3	+13.7	-4.0	-42.0
BioSedGW-C-2	84	7.1	0.64	0.00	n.d.	0.00	n.d.	n.d.	n.d.	n.d.
BioSedGW-C-3	222	6.9	0.53	0.06	n.d.	n.d.	+29.2	+20.9	n.d.	n.d.

Table S2.2. ICP results for de BioSedGW-Mag-NP experiments. The results are expressed in ppm (semi-quantitative). Pb, Cd, Co, Cu, Zn, Al, Be, Li, Mo, Ni, Sb, Ti, Tl, V, As, Cr, P, Se were also analyzed but concentrations were below detection limit. <d.l. = below detection limit. These results are not reported in the manuscript.

	Groundwater	BioSedGW-Mag-NP-1	BioSedGW-Mag-NP-2	BioSedGW-Mag-NP-4	BioSedGW-Mag-NP-5	BioSedGW-Mag-NP-6	BioSedGW-Mag-NP-7	BioSedGW-Mag-NP-8
Ca	92.73	113.63	116.47	98.91	108.03	102.82	100.53	96.00
Na	28.07	31.17	31.47	29.68	31.40	30.77	30.50	29.94
Mg	25.86	28.10	28.90	24.96	26.71	26.13	25.71	25.27
S	23.93	27.81	28.15	25.87	29.00	27.71	27.09	26.16
Si	13.70	5.56	4.64	4.70	4.59	4.54	4.67	4.15
K	5.04	5.80	4.91	4.84	10.21	12.61	5.88	6.02
B	2.85	2.72	2.75	2.97	2.86	3.36	3.13	2.97
Sr	1.13	0.72	0.67	0.64	0.66	0.64	0.63	0.60
Ba	0.05	< d.l.	<d.l.	0.01	<d.l.	<d.l.	0.01	<d.l.
Fe	0.02	0.04	0.03	0.02	0.02	0.03	0.03	0.01
Mn	0.00	0.15	0.15	0.06	0.07	0.07	0.06	0.06

Table S2.3. Results for de BioSedDIW experiments. Chemical and isotopic characterization. n.d. = no determined.

	Days	pH	NO_3^- (mM)	NO_2^- (mM)	NH_4^+ (mM)	N_2O (nmol)	$\delta^{15}N\text{-}NO_3^-$ (‰)	$\delta^{18}O\text{-}NO_3^-$ (‰)	$\delta^{15}N\text{-}N_2O$ (‰)	$\delta^{18}O\text{-}N_2O$ (‰)
DIW	0	n.d.	1.15	0.00	n.d.	n.d.	+16.9	+28.5	n.d.	n.d.
BioSedDIW-Ol-1	7	6.4	0.65	0.37	n.d.	0.12	+28.7	+43.9	-36.1	-48.3
BioSedDIW-Ol-2	91	8.9	0.61	0.38	n.d.	0.18	n.d.	n.d.	-15.7	-40.8
BioSedDIW-Ol-3	222	8.6	0.60	0.57	n.d.	n.d.	n.d.	n.d.	n.d.	n.d.
BioSedDIW-Sd-1	7	6.3	0.63	0.50	n.d.	0.24	n.d.	n.d.	-18.8	-44.2
BioSedDIW-Sd-2	91	7.8	0.38	0.47	n.d.	0.14	+24.2	+49.2	-12.8	-45.2
BioSedDIW-Sd-3	222	7.5	0.44	0.73	n.d.	n.d.	n.d.	n.d.	n.d.	n.d.
BioSedDIW-Mag-1	7	5.6	0.42	0.63	n.d.	0.11	n.d.	n.d.	-29.8	-46.3
BioSedDIW-Mag-2	91	8.1	0.52	0.29	n.d.	0.11	n.d.	n.d.	-18.5	-43.2
BioSedDIW-Mag-3	222	7.8	0.57	0.57	n.d.	n.d.	+15.1	+22.6	n.d.	n.d.
BioSedDIW-Mag-NP-1	7	5.8	0.79	0.32	n.d.	0.21	+20.5	+35.9	-28.5	-45.2
BioSedDIW-Mag-NP-2	91	7.8	0.46	0.19	n.d.	0.24	+29.8	+39.2	-10.3	-61.0
BioSedDIW-Mag-NP-3	222	7.6	0.44	0.28	n.d.	n.d.	n.d.	n.d.	n.d.	n.d.
BioSedDIW-C-1	91	8.2	0.73	0.08	n.d.	0.00	n.d.	n.d.	n.d.	n.d.
BioSedDIW-C-2	222	n.d.	1.10	0.02	n.d.	n.d.	+16.3	+20.1	n.d.	n.d.

Table S2.4. Results for de $AbFeNO_3$ experiments. Chemical and isotopic characterization. n.d. = no determined.

	Days	pH	NO_3^- (mM)	NO_2^- (mM)	N_2O (nmol)	$\delta^{15}N\text{-}NO_3^-$ (‰)	$\delta^{18}O\text{-}NO_3^-$ (‰)
Synthetic water	0	n.d.	1.48	0.00	n.d.	+16.9	+28.5
$AbFeNO_3$-Mag-1	50	4.1	n.d.	n.d.	0.00	n.d.	n.d.
$AbFeNO_3$-Mag-2	222	n.d.	1.04	0.02	n.d.	n.d.	n.d.
$AbFeNO_3$-Ol-1	50	4.4	n.d.	n.d.	0.00	n.d.	n.d.
$AbFeNO_3$-Ol-2	222	n.d.	1.12	0.01	n.d.	n.d.	n.d.
$AbFeNO_3$-Sd-1	50	4	n.d.	n.d.	0.00	+16.7	+28.6
$AbFeNO_3$-Sd-2	222	n.d.	1.28	0.01	n.d.	n.d.	n.d.
$AbFeNO_3$-C-1	15	5.29	1.22	0.01	n.d.	n.d.	n.d.
$AbFeNO_3$-C-2	50	6.4	n.d.	n.d.	0.00	n.d.	n.d.
$AbFeNO_3$-C-3	222	n.d.	1.26	0.01	n.d.	n.d.	n.d.

Table S2.4. Results for de $AbNO_2$ experiments. Chemical characterization.

	Days	NO_3^- (mM)	NO_2^- (mM)
Synthetic water	0	0.00	1.52
$AbNO_2$-Mag-1	222	0.01	1.26
$AbNO_2$-Mag-2	365	0.01	1.38
$AbNO_2$-Ol-1	222	0.00	1.13
$AbNO_2$-Ol-2	365	0.02	1.23
$AbNO_2$-Sd-1	222	0.01	1.24
$AbNO_2$-Sd-2	365	0.11	1.11

Table S2.5. Results for de $AbFeNO_2$ experiments. Chemical and isotopic characterization. n.d. = no determined. The initial NO_2^- concentration of the synthetic water was slightly lower in the case of the $AbFeNO_2$-Sd experiments compared to the $AbFeNO_2$-Mag/Ol/C experiments.

	Hours	NO_2^- (mM)	NH_4^+ (mM)	$N\text{-}N_2O$ (µmol)	Fe (mM)	$\delta^{15}N\text{-}NO_2^-$ (‰)	$\delta^{15}N\text{-}N_2O$ (‰)
Synthetic water	0	1.10	n.d.	n.d.	5.00	-28.5	n.d.
$AbFeNO_2$-Sd-1	2	1.06	0.0	n.d.	3.30	-27.4	-51.8
$AbFeNO_2$-Sd-2	8	0.87	0.0	n.d.	2.81	-24.1	-49.2
$AbFeNO_2$-Sd-3	23	0.41	0.0	n.d.	1.58	-14.5	-40.6
$AbFeNO_2$-Sd-4	32	0.08	0.0	n.d.	1.60	n.d.	n.d.
$AbFeNO_2$-Sd-5	47	0.07	0.0	n.d.	1.56	n.d.	n.d.
Synthetic water	0	1.54	n.d.	n.d.	5.00	-28.5	n.d.
$AbFeNO_2$-Mag-1	4	1.59	n.d.	0.0	n.d.	-28.8	-46.9
$AbFeNO_2$-Mag-2	8	1.57	n.d.	0.1	n.d.	-28.1	-49.5
$AbFeNO_2$-Mag-3	22	1.42	n.d.	0.7	n.d.	-26.8	-48.1
$AbFeNO_2$-Mag-4	30	1.04	n.d.	2.1	3.26	-24.2	-49.1
$AbFeNO_2$-Mag-5	31	1.39	n.d.	1.0	2.74	-26.1	-52.3
$AbFeNO_2$-Mag-6	46	0.92	n.d.	6.2	n.d.	-20.1	-45.6

Table S2.5. Continued.

	Hours	NO_2^- (mM)	NH_4^+ (mM)	$N\text{-}N_2O$ (µmol)	Fe (mM)	$\delta^{15}N\text{-}NO_2^-$ (‰)	$\delta^{15}N\text{-}N_2O$ (‰)
$AbFeNO_2$-Mag-7	55	n.d.	n.d.	4.1	n.d.	n.d.	-45.2
$AbFeNO_2$-Mag-8	78	0.92	n.d.	n.d.	n.d.	-22.5	n.d.
$AbFeNO_2$-Mag-9	94	0.90	n.d.	5.1	2.38	-22.6	-43.4
$AbFeNO_2$-Mag-10	94	0.83	n.d.	5.6	n.d.	-20.3	-43.4
$AbFeNO_2$-Ol-1	114	0.75	n.d.	6.5	2.62	-14.9	-41.9
$AbFeNO_2$-Ol-2	4	1.43	n.d.	0.6	n.d.	-27.7	-39.9
$AbFeNO_2$-Ol-3	8	1.37	n.d.	1.0	n.d.	-28.8	-38.5
$AbFeNO_2$-Ol-4	22	1.32	n.d.	3.3	n.d.	-25.8	-38.1
$AbFeNO_2$-Ol-5	30	0.91	n.d.	4.7	2.80	-21.4	-43.7
$AbFeNO_2$-Ol-6	31	1.21	n.d.	5.0	2.28	-24.9	-39.0
$AbFeNO_2$-Ol-7	46	0.86	n.d.	7.1	n.d.	-19.7	-42.7
$AbFeNO_2$-Ol-8	55	n.d.	n.d.	10.1	n.d.	n.d.	-38.5
$AbFeNO_2$-Ol-9	78	0.72	n.d.	n.d.	n.d.	-17.6	-42.4
$AbFeNO_2$-Ol-10	94	0.75	n.d.	8.4	1.81	-19.2	-38.8

Table S2.5. Continued.

	Hours	NO_2^- (mM)	NH_4^+ (mM)	$N\text{-}N_2O$ (µmol)	Fe (mM)	$\delta^{15}N\text{-}NO_2^-$ (‰)	$\delta^{15}N\text{-}N_2O$ (‰)
$AbFeNO_2$-Ol-11	94	0.70	n.d.	8.9	n.d.	-16.4	-42.0
$AbFeNO_2$-Ol-12	114	0.45	n.d.	9.0	2.20	-12.2	-38.9
$AbFeNO_2$-Ol-13	168	0.71	n.d.	n.d.	n.d.	-11.8	n.d.
$AbFeNO_2$-Ol-14	168	0.22	n.d.	n.d.	3.23	7.1	n.d.
$AbFeNO_2$-C-1	4	1.52	n.d.	0.1	n.d.	-29.0	-44.6
$AbFeNO_2$-C-2	8	1.53	n.d.	0.1	n.d.	-28.5	-42.3
$AbFeNO_2$-C-3	22	1.49	n.d.	0.6	n.d.	-26.8	-43.6
$AbFeNO_2$-C-4	30	1.10	n.d.	2.3	3.77	-24.5	-47.8
$AbFeNO_2$-C-5	31	1.51	n.d.	0.9	2.86	-26.8	-43.5
$AbFeNO_2$-C-6	46	0.86	n.d.	5.8	n.d.	-21.3	-44.4
$AbFeNO_2$-C-7	55	n.d.	n.d.	2.8	n.d.	n.d.	-45.4
$AbFeNO_2$-C-8	78	0.97	n.d.	n.d.	n.d.	-22.9	n.d.
$AbFeNO_2$-C-9	94	1.07	n.d.	4.5	2.64	-23.9	-42.6

Table S2.5. Continued.

	Hours	NO_2^- (mM)	NH_4^+ (mM)	$N\text{-}N_2O$ (µmol)	Fe (mM)	$\delta^{15}N\text{-}NO_2^-$ (‰)	$\delta^{15}N\text{-}N_2O$ (‰)
$AbFeNO_2$-C-10	94	0.37	n.d.	5.0	n.d.	n.d.	-42.0
$AbFeNO_2$-C-11	114	0.78	n.d.	6.1	2.89	-16.8	-42.4
$AbFeNO_2$-C-12	168	0.00	n.d.	n.d.	2.96	n.d.	n.d.

Table S2.6. ICP results for de AbFeNO$_2$ experiments. The results are expressed in ppm. Pb, Al, Be, Li, Mo, Sb, Ti, Tl, V, As, Cr and Se were also analyzed but concentrations were below detection limit. <d.l. = below detection limit; h = hours. The employed instrument for the analysis was: Perkin Elmer Optima 8300. These results are not reported in the manuscript.

	h	Ca	Mg	Ba	Cd	Co	Cu	Mn	Sr	Zn	K	Ni	Na	B	P	S	Si
AbFeNO$_2$-Sd-1	2	38.05	30.71	0.11	<d.l.	0.03	0.06	10.93	0.06	0.06	95.81	<d.l.	150.06	0.20	<d.l.	45.04	0.65
AbFeNO$_2$-Sd-2	8	37.74	32.19	0.14	<d.l.	0.04	0.05	14.94	0.07	0.05	94.13	<d.l.	146.97	<d.l.	<d.l.	42.72	0.53
AbFeNO$_2$-Sd-3	23	38.77	32.33	0.17	<d.l.	0.04	0.06	22.07	0.08	0.06	93.14	<d.l.	148.32	1.12	<d.l.	37.70	1.43
AbFeNO$_2$-Sd-4	32	41.00	34.17	0.18	0.01	0.05	0.08	24.32	0.09	0.08	93.98	<d.l.	149.81	0.97	<d.l.	38.41	1.30
AbFeNO$_2$-Sd-5	47	39.89	32.74	0.18	<d.l.	0.05	0.08	25.42	0.09	0.09	92.96	<d.l.	152.08	1.96	<d.l.	38.41	1.70
AS	0	23.41	30.99	0.01	<d.l.	<d.l.	<d.l.	<d.l.	0.01	0.03	117.29	<d.l.	165.38	<d.l.	2.12	45.58	<d.l.
AbFeNO$_2$-Mag-4	30	23.85	32.97	0.04	0.02	0.03	<d.l.	0.24	0.02	0.07	114.72	<d.l.	161.23	<d.l.	<d.l.	44.17	2.17
AbFeNO$_2$-Mag-5	31	24.05	33.55	0.03	0.01	0.03	<d.l.	0.25	0.02	0.04	118.40	<d.l.	165.56	1.06	<d.l.	44.39	2.38
AbFeNO$_2$-Mag-9	94	26.74	34.82	0.04	0.01	0.03	<d.l.	0.42	0.02	0.09	118.26	<d.l.	164.49	1.95	<d.l.	44.74	3.88
AbFeNO$_2$-Ol-1	114	27.17	35.50	0.04	0.01	0.03	<d.l.	0.43	0.02	0.08	119.65	<d.l.	166.33	<d.l.	<d.l.	45.91	2.83
AbFeNO$_2$-Ol-5	30	22.11	46.48	0.02	0.01	0.13	<d.l.	0.12	0.02	0.06	116.82	0.11	165.71	1.06	<d.l.	44.72	4.52
AbFeNO$_2$-Ol-6	31	22.03	54.82	0.04	0.04	0.16	<d.l.	0.23	0.02	0.31	115.66	0.24	167.97	2.67	<d.l.	42.75	10.64
AbFeNO$_2$-Ol-10	94	21.94	50.31	0.03	0.01	0.15	<d.l.	0.13	0.02	0.04	116.04	0.11	157.48	<d.l.	<d.l.	43.74	5.57
AbFeNO$_2$-Ol-12	114	22.55	50.24	0.02	0.01	0.17	<d.l.	0.13	0.02	0.07	118.44	0.16	169.17	2.06	<d.l.	44.82	7.42
AbFeNO$_2$-Ol-14	168	24.34	45.69	0.03	0.01	0.11	<d.l.	0.12	0.02	0.09	120.15	0.13	168.44	<d.l.	<d.l.	45.92	5.22

Table S2.6. Continued.

	h	Ca	Mg	Ba	Cd	Co	Cu	Mn	Sr	Zn	K	Ni	Na	B	P	S	Si
AbFeNO$_2$-C-4	30	22.37	30.62	0.02	0.02	<d.l.	<d.l.	0.07	0.01	0.06	120.47	<d.l.	162.92	<d.l.	<d.l.	45.14	<d.l.
AbFeNO$_2$-C-5	31	21.76	30.92	0.02	0.01	<d.l.	<d.l.	0.06	0.01	0.03	118.66	<d.l.	166.36	1.38	<d.l.	44.71	1.38
AbFeNO$_2$-C-9	94	21.43	30.22	0.02	0.01	<d.l.	<d.l.	0.06	0.01	0.11	116.97	<d.l.	165.70	2.72	<d.l.	45.04	2.54
AbFeNO$_2$-C-11	114	22.31	31.08	0.02	0.02	<d.l.	<d.l.	0.07	0.01	0.13	118.32	<d.l.	166.67	<d.l.	<d.l.	45.93	<d.l.
AbFeNO$_2$-C-12	168	21.58	30.44	0.04	0.03	<d.l.	<d.l.	0.13	0.01	0.69	117.26	<d.l.	167.29	3.49	<d.l.	35.52	2.06

ANNEX 2

Geochemical and isotopic study of abiotic nitrite reduction coupled to bio-produced Fe(II) oxidation in marine environments.

Offeddu F.G.[1], Benaiges-Fernandez R.[1,2], Margalef-Marti R.[3], Palau J.[1,3], Urmeneta J.[2,4], Carrey R.[3], Otero N.[3,5] and Cama J.[1]

[1] Institute of Environmental Assessment and Water Research (IDAEA, CSIC), 08034 Barcelona, Spain.

[2] Departament de Genètica, Microbiologia i Estadística, Universitat de Barcelona, 08028 Barcelona, Spain.

[3] Grup MAiMA, SGR Mineralogia Aplicada, Geoquímica i Geomicrobiologia, Departament de Mineralogia, Petrologia i Geologia Aplicada, Facultat de Ciències de la Terra, Universitat de Barcelona (UB), 08028 Barcelona, Spain.

[4] Institut de Recerca de la Biodiversitat (IRBio), Universitat de Barcelona, 08028 Barcelona, Spain.

[5] Serra Húnter Fellowship. Generalitat de Catalunya, Spain.

In preparation

Geochemical and isotopic study of abiotic nitrite reduction coupled to bio-produced Fe(II) oxidation in marine environments

Offeddu F.G.[a], Benaiges-Fernandez R.[a,b], Margalef-Marti R.[c], Palau J.[a,c] , Urmeneta J.[b,d], Carrey R.[c], Otero N.[c,e] and Cama J.[a]

[a] Institute of Environmental Assessment and Water Research (IDAEA, CSIC), 08034 Barcelona, Spain

[b] Departament de Genètica, Microbiologia i Estadística, Universitat de Barcelona, 08028 Barcelona, Spain

[c] Grup MAiMA, SGR Mineralogia Aplicada, Geoquímica i Geomicrobiologia, Departament de Mineralogia, Petrologia i Geologia Aplicada, Facultat de Ciències de la Terra, Universitat de Barcelona (UB), 08028 Barcelona, Spain

[d] Institut de Recerca de la Biodiversitat (IRBio), Universitat de Barcelona, 08028 Barcelona, Spain

[e] Serra Húnter Fellowship. Generalitat de Catalunya, Spain

ABSTRACT

Estuarine sediments are often rich in iron oxides, organic matter and anthropogenic nitrogen compounds (e.g. nitrite) transported by continental waters. In these anoxic environments, dissimilatory iron reducing bacteria (e.g. *Shewanella loihica*) can catalyze the Fe(III)-oxide minerals reduction releasing Fe(II), which may interact with nitrite leading to its removal via formation of nitrous oxide and Fe(III). Since nitrous oxide is a potent greenhouse gas, the characteristics of this reaction must be investigated.

In this work, nitrite reduction coupled to oxidation of Fe(II), either bio-produced (aqueous and solid-bound) or synthetic (only aqueous, only solid-bound or both), was studied by

means of different sets of batch experiments simulating an anoxic marine medium. In addition, the biotic nitrite reduction by *S. loihica* with lactate or acetate were studied to assess its possible contribution in the abiotic experiments.

To obtain bio-produced Fe(II), ferrihydrite was reduced by *S. loihica* in the presence of lactate (pH ≈ 8.2). The released Fe(II) was found aqueous, adsorbed on the ferrihydrite surface and partially transformed to nanocrystalline magnetite, producing solid Fe(II). The results of the nitrite reduction experiments indicated that the bio-produced Fe(II) presents a higher reactivity than synthetic Fe(II). Also in the case of synthetic Fe(II), it was observed that the abiotic nitrite reduction is faster and more efficient in the presence of both aqueous and solid-bound Fe(II) compared to when only aqueous or solid-bound Fe(II) are found in the media. The possible contribution of the biotic nitrite reduction on the abiotic ones was found insignificant.

The isotopic characterization of the nitrite reduction at laboratory showed similar $\varepsilon^{15}N/\varepsilon^{18}O$ ratios for all abiotic experiments (1.4 to 1.8). In contrast, a lower $\varepsilon^{15}N/\varepsilon^{18}O$ ratio (0.3) was obtained for the heterotrophic nitrite reduction by *S. loihica*. Since these $\varepsilon^{15}N/\varepsilon^{18}O$ values are close to or within the wide range of reported values in the literature for the abiotic and biotic nitrite reduction, the use of the $\varepsilon^{15}N/\varepsilon^{18}O$ ratio to distinguish different mechanisms of nitrite reduction at field-scale might be limited. As an alternative, the correlation between $\delta^{15}N_{NO2}$ and the natural logarithm of the Fe(II) concentration could be useful to identify or discard the occurrence of heterotrophic NO_2^- reduction in field scenarios.

Keywords: iron reducing bacteria, ferrihydrite, abiotic nitrite reduction, ferrous iron oxidation, nitrite isotope fractionation

GRAPHICAL ABSTRACT

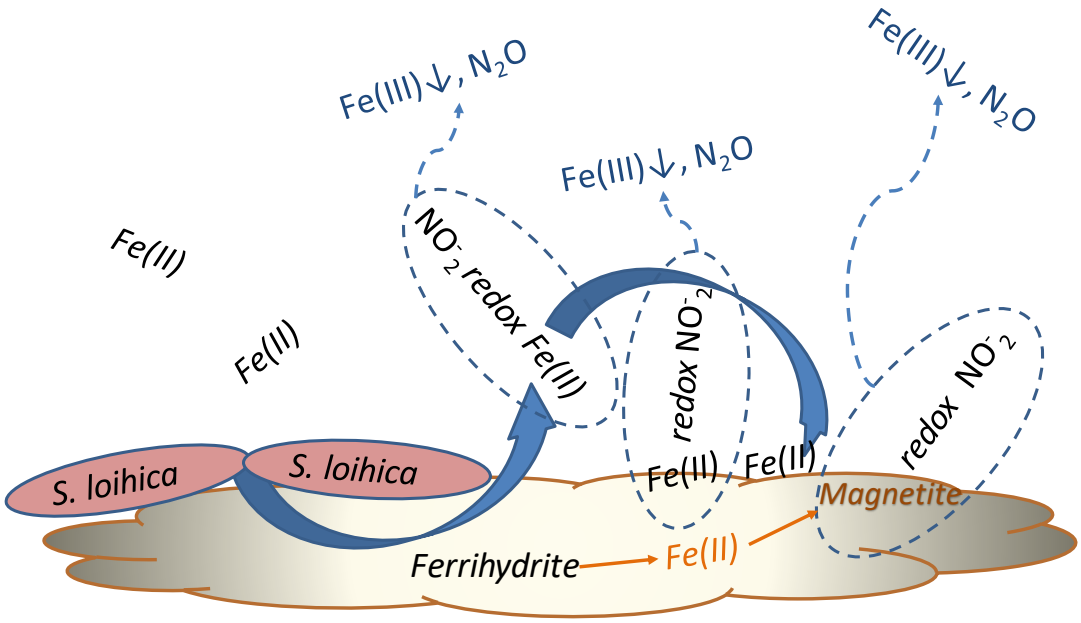

1 INTRODUCTION

The intensive use of organic and inorganic fertilizers and domestic or industrial wastewater are mainly responsible for nitrogen input and contamination of water resources (Guerbois et al., 2014). Marine sediments in estuarine and coastal areas often contain terrigenous organic matter and other constituents such as iron and anthropogenic nitrogen compounds (e.g., NO_x) due to riverine and submarine groundwater inputs (Jani and Toor, 2018). In such environments, marine dissimilatory iron reducing bacteria (e.g., *Shewanella loihica*) are able to reduce Fe(III)-oxide minerals under anoxic conditions producing aqueous and mineral-associated Fe(II) (**Equation 1**) (Melton et al., 2014; Lovley, 1991). This bio-produced Fe(II) can abiotically reduce nitrite (NO_2^-) via formation of nitrous oxide (N_2O) (**Equation 2**) (Kampschreur et al. 2011; Tai and Dempsey, 2009), which is a potent greenhouse gas and the single greatest ozone-depleting substance (Ravishankara et al.

2009). Consequently, in recent years, the NO_2^- reduction by Fe(II) oxidation, (i.e., chemodenitrification), has become a subject of investigation (Grabb et al. 2017; Lu et al. 2017; Buchwald et al., 2016; Tai and Dempsey, 2009).

$CH_3CHOHCOO^- + 4Fe(OH)_3 + 7H^+ \rightarrow CH_3COO^- + HCO_3^- + 4Fe(II) + 10H_2O$ (**Equation 1**)

$4Fe(II) + 2NO_2^- + 5H_2O \rightarrow 4FeOOH + N_2O + 6H^+$ (**Equation 2**)

The NO_2^- abiotic reduction can occur in the presence of aqueous Fe(II), Fe(II) associated to mineral surfaces or minerals containing Fe(II) (Rakshit et al. 2016; Wu et al., 2015; Dhakal et al., 2013; Tai and Dempsey, 2009), three forms of iron that might coexist in environments where the Fe(II) originates from the bio-reduction of Fe(III)-(hydr)oxides, such as ferrihydrite (Fh). Also, even in laboratory experiments with aqueous Fe(II), precipitation of Fe(III)-(hydr)oxides or mixed valence (Fe(II), Fe(III)) iron minerals will occur after the oxidation of aqueous Fe(II) coupled to the NO_2^- reduction (Chen et al., 2018; Lu et al., 2017). Therefore, the NO_2^- abiotic reduction by oxidation of Fe(II) usually takes place under heterogenous systems (i.e. presence of aqueous Fe(II) and Fe(II) associated to minerals), while if the Fe(II) was only found in the aqueous form it would be considered an homogeneous system.

Some studies have concluded that the abiotic NO_2^- reduction is faster through the heterogeneous reaction (Buchwald et al., 2016; Dhakal et al., 2013). Tai and Dempsey (2009) observed higher NO_2^- reduction rates when the ratio aqueous-Fe(II)/Fe(III)-(hydr)oxides was 0.3 compared to > 0.3, but the reduction stopped when the aqueous Fe(II) concentrations became low or null, even in the presence of mineral-associated

Fe(II). These authors also found that the NO_2^- reduction is negligible in the absence of Fe(III)-(hydr)oxides. Lu et al. (2017) also observed that magnetite was not able to reduce NO_2^- in the absence of aqueous Fe(II). In contrast, Dhakal et al. (2013) found that magnetite was able to abiotically reduce NO_2^- in the absence of aqueous Fe(II), although the reduction rate increased when aqueous Fe(II) was added.

To date, the evaluation of the NO_2^- abiotic reduction coupled to oxidation of Fe(II) in heterogenous systems at the laboratory scale has been performed through the addition of synthetic Fe(II) (e.g., $FeCl_2$) to aqueous solutions without or with different minerals (Lu et al., 2017; Robertson and Thamdrup, 2017; Rakshit et al. 2016; Robertson et al., 2016). However, in natural settings Fe(II) can originate from microbial reduction of Fe(III)-minerals and therefore, might present different properties compared to the synthetic one. The dissimilatory Fe(III) reduction might also alter the properties of the iron minerals surfaces or result in formation of secondary iron mineral phases such as magnetite or siderite (Roh et al., 2006), which might affect the Fe(II) reactivity. Therefore, evaluation of abiotic NO_2^- reduction by Fe(II) oxidation in systems closer to natural conditions is required.

Isotopic analysis is a powerful tool to trace NO_x transformation processes. The enzymatic NO_3^- reduction provokes an enrichment in the heavy isotopes ^{15}N and ^{18}O of the remaining substrate (Fukada et al., 2003; Aravena and Robertson, 1998; Böttcher et al., 1990; Mariotti et al., 1981), unlike processes such as dilution that could lead to a concentration decrease without influencing the isotopic signature. The same pattern is expected for the biotic reduction of other N species (e.g. NO_2^- or N_2O). Data on the dual N-O isotope systematics during the biotic NO_2^- reduction remain scarce (Martin and Casciotti, 2016; Bryan et al., 1983). For the abiotic NO_2^- reduction by Fe(II) oxidation, two recent isotopic studies found results similar to what is expected for the biotic reaction (Buchwald et al., 2016; Grabb et al., 2017). According to the isotopic data reported up to date for the NO_2^-

reduction, it is unclear to which degree the isotopic characterization might help in distinguishing biotic and abiotic NO_2^- reduction. Therefore, further studies on the potential of isotope data to elucidate the process controlling the fate of NO_2^- in the field are needed.

Ferrihydrite is ubiquitous in the environment and abundant in marine sediment (Canfield, 1989). Given its thermodynamic instability and large surface area, ferrihydrite presents a high reactivity in the presence of aqueous Fe(II), which may lead to mineral transformation to more crystalline phases containing Fe(II) such as magnetite (Tomaszevsky et al., 2016; Boland et al., 2014; Yang et al., 2010; Yee et al. 2006; Hansel et al., 2003). In this study, ferrihydrite was the Fe(III) mineral chosen to biotically produce Fe(II). *S. loihica* strain PV-4 was employed to induce the reductive dissolution of ferrihydrite after Benaiges-Fernandez et al. (2019). The reactivity of the bio-produced Fe(II) was compared to that of synthetic Fe(II) in batch experiments with synthetic seawater and NO_2^- under anoxic conditions. Furthermore, the abiotic NO_2^- reduction rate by oxidation of Fe(II) was compared to that of the biotic NO_2^- reduction by oxidation of organic carbon compounds (lactate and acetate). The aims of the study were: I) to elucidate the fate of bio-produced Fe(II) by the reductive dissolution of ferrihydrite mediated by *S. loihica*, II) to investigate the kinetics of NO_2^- reduction by Fe(II) oxidation in marine environments, III) to distinguish abiotic from biotic NO_2^- reduction by means of isotopic analysis.

2 METHODS

2.1 Bacterial culture and solutions preparation

S. loihica strain PV-4 was purchased from the German Collection of Microorganisms and Cell Cultures (DSMZ 17748). Bacteria was recovered and cultivated in M1 medium (Gao

et al., 2006) with 10 mM of lactate as electron donor and carbon source and 10 mM of Fe(III) citrate as electron acceptor.

Synthetic seawater (SSW) was prepared to simulate the marine sediment conditions following the standard protocol D1141-98 (ATSM International). To biotically produce Fe(II) from the reductive dissolution of ferrihydrite, 10 mM of sodium lactate and 10 mM of TRIS-HCl (Tris) as a buffer (pH ≈ 8.2) were added to SSW. Hereafter, this medium will be referred as M-SSW.

Stock solutions of synthetic Fe(II) and NO_2^- (12.8 and 2.8 g L^{-1} respectively) were freshly prepared inside an anoxic glove box by dissolving the convenient amounts of $FeSO_4$ and KNO_2, respectively, in ultrapure Milli-Q water (Merck Millipore) previously degassed with N_2. The Fe(II) solution was acidified to reach pH 1. Both solutions were subsequently filtered (0.22 µm) and stored.

All solutions and materials employed during the experiments were sterilized by autoclave (121 ºC, 20 min) unless otherwise stated.

2.2 Ferrihydrite synthesis

2L-ferrihydrite was synthesized according to a modified protocol of Schwertmann and Cornell (2007) (see **Section S1** in **SI** for more details). The specific surface area was measured by the Brunauer-Emmett-Teller (BET) method (Brunauer et al., 1938) using a Gemini 2370 surface area analyzer using 5-point N_2 adsorption isotherms. Sample degassing with nitrogen lasted for 2 h at 137 °C. The determined BET specific surface area was between 140 and 180 $m^2\,g^{-1}$.

2.3 Experimental setup and sampling procedure

Three sets of batch experiments were performed to investigate: I) the abiotic NO_2^- reduction by bio-produced Fe(II) (AbSeaNO_2-BioFe), II), the abiotic NO_2^- reduction by synthetic Fe(II) (AbSeaNO_2-StFe), III) the biotic NO_2^- reduction by *S. loihica* with acetate or lactate (BioSeaNO_2). The tested conditions are listed in **Table 1**. All batch experiments were run at least in duplicates. The experiments were performed in bottles capped with a screw cap, silicone o-ring and blue butyl rubber stopper and wrapped in aluminum foil to avoid light exposition. The experiments were performed inside a glove box purged with N_2 and equipped with UV germicidal light for periodical sterilization. Dissolved oxygen was checked by luminescent dissolved oxygen (LDO) probe (detection limit 0.01 mg L^{-1}). Incubations were performed at 22 ± 2 ºC.

For the abiotic NO_2^- reduction by bio-produced Fe(II), the batch experiments consisted of two stages. In the first stage (Ferr), the anaerobic reductive dissolution of ferrihydrite mediated by *S. loihica* strain PV-4 was performed with ferrihydrite powder in M-SSW medium (w/v ratio = 1:100). *S. loihica* was inoculated to reach a final concentration of $1 \cdot 10^7$ colony-forming units (cfu) mL^{-1}. To obtain the bacterial suspension, the cells were cultivated for 24 h, then harvested by centrifugation (5000 rpm for 10 min) and the pellet was re-suspended in SSW. This step was repeated three times as a washing protocol. When the ferrihydrite reduction stopped, NO_2^- was added to reach a concentration of 0.8 mM. In the second stage (AbSeaNO_2-BioFe$_{aq+s}$), NO_2^- abiotic reduction was promoted by the bio-produced Fe(II) that was found both aqueous and associated to the ferrihydrite.

For the abiotic NO_2^- reduction by synthetic Fe(II), three types of batch experiments were performed to investigate the role of solid-bound and aqueous Fe(II) on NO_2^- reduction. In these experiments, 10 mM of acetate and 10 mM of Tris-HCl buffer solution were added to the SSW to achieve similar initial conditions to the AbSeaNO_2-BioFe$_{aq+s}$ experiments after

the completion of the ferrihydrite reduction (Ferr). Experiment $\underline{AbSeaNO_2\text{-}StFe_{aq}}$ contained NO_2^- and aqueous Fe(II) (1.2 mM) but no ferrihydrite, whereas the experiment $\underline{AbSeaNO_2\text{-}StFe_s}$ contained NO_2^-, ferrihydrite and Fe(II) associated to the ferrihydrite but no aqueous Fe(II). This was achieved by adding the NO_2^- once all de added aqueous Fe(II) (1.2 mM) was depleted from the media due to ferrihydrite uptake. Finally, experiment $\underline{AbSeaNO_2\text{-}StFe_{aq+s}}$ contained NO_2^-, ferrihydrite and both aqueous Fe(II) and Fe(II) associated to ferrihydrite. As in the previous experiment, an initial amount of 1.2 mM Fe(II) was added to the media and it was depleted due to ferrihydrite uptake, but an extra amount of 1.2 mM aqueous Fe(II) was added to find it also in the aqueous form.

Table 1. Batch experiments content. In the codes of the experiments, "aq" refers to aqueous Fe(II) and "s" refers to solid-bound Fe(II). The Fe(II) concentration refers to the Fe(II) content in the batch experiments previous to the NO_2^- addition (for the $AbSeaNO_2\text{-}BioFe_{aq+s}$ experiments, it does not take into account the amount of solid-bound Fe(II)).

Code	Fh (g)	Vol. (mL)	Fe(II) (mM)	NO_2^- (mM)	Acetate (mM)	Lactate (mM)	*S. loihica*
Ferr	5	500	-	-	-	10	yes
$AbSeaNO_2\text{-}BioFe_{aq+s}$	3.8	380	1.2 (biotic)	0.65	8	-	-
$AbSeaNO_2\text{-}StFe_{aq}$	-	250	1.2 (synthetic)	0.65	10	-	-
$AbSeaNO_2\text{-}StFe_s$	2.5	250	1.2 (synthetic)	0.65	10	-	-
$AbSeaNO_2\text{-}StFe_{aq+s}$	2.5	250	2.4 (synthetic)	0.65	10	-	-
$BioSeaNO_2$-Lactate	-	250	-	0.65	-	10	yes
$BioSeaNO_2$-Acetate	-	250	-	0.65	10	-	yes

For the biotic NO_2^- reduction, two sets of batch experiments were performed using SSW inoculated with *S. loihica* and containing NO_2^-, 10 mM of buffer Tris-HCl and 10 mM of lactate (BioSeaNO_2-Lactate) or acetate (BioSeaNO_2-Acetate), in absence of ferrihydrite. These experiments were performed to investigate the possible interference of the NO_2^- biotic reduction during the abiotic NO_2^- reduction by bio-produced Fe(II).

During the batch experiments, samples were obtained periodically according to the Fe(II) reduction/oxidation and NO_2^- reduction dynamics. Samples were obtained after shaking the bottles for liquid-solid homogenization and immediately filtered (0.22 µm). The concentration of NO_2^- was immediately determined (1 mL aliquots). Aliquots of 1 mL were acidified with 6 M HCl solution for immediate Fe analysis. Aliquots of 4 mL were acidified with 6 M HCl solution and stored in the dark at 4 ºC for further lactate/acetate analysis. For the isotopic analysis (δ^{15}N-NO_2^- and δ^{18}O-NO_2^-), aliquots of 5 mL were immediately frozen and defrosted just before measurements.

Furthermore, control experiments were performed to examine the potential interferences between the compounds of the batch experiments: SSW, buffer, acetate, Fe(II) and NO_2^- (see **Section S2** in **SI** for details). Also, adsorption experiments were carried out to quantify the uptake of aqueous Fe(II) by ferrihydrite and a Fe(II) adsorption isotherm was performed to determine the mechanisms responsible for Fe(II) adsorption on ferrihydrite surface (see **Section S3** in **SI** for details).

2.4 Analytical techniques

Mineralogical inspections of reacted and unreacted samples were carried out by: I) scanning electron microscopy (SEM) using a Hitachi H-4100FE instrument under a 15–20 kV potential in a high vacuum and utilizing the backscattered electron detector (BSD) in field emission (FE) and coating the samples with carbon, II) X-ray diffraction (XRD) using a

PANalytical X'Pert PRO MPD θ/θ Bragg-Brentano powder diffractometer of 240 mm in radius and Cu Kα radiation (λ = 1.5418 Å), and III) Fourier transform infrared spectrometry (FTIR) utilizing a Perkin Elmer frontier / ATR diamond / detector DTGS, accumulation at 16 scans, spectral resolution 4 cm^{-1}, spectral range 4000 - 225 cm^{-1}.

Concentrations of iron and nitrite were both measured by spectrophotometry (SP-830 PLUS, Metertech Inc.) at wavelengths of 510 nm and 540 nm, respectively. Ferrous iron and total iron concentrations were measured immediately after sampling by the phenanthroline method (Stucki, 1981). Nitrite concentration was measured after adding sulphanilamide and the N-(1-naphthyl)-ethylenediamine dihydrochloride (NED) reagents and an incubation time of 20 min, following Garcia-Robledo et al. (2004). Total dissolved iron was also measured by Inductively Coupled Plasma Optical Emission Spectroscopy (ICP-OES, Perkin- Elmer 3000) to confirm that all dissolved iron was in the form of Fe(II). Uncertainty in Fe concentration measured between phenanthroline method and ICP-OES was better than 5 %. Concentrations of lactate and acetate were measured by High Performance Liquid Chromatography (Waters 600 HPLC pump controller equipped with an Aminex HPX-87H column (300 x 7.8 mm), BioRad, and a Waters 717plus autoinjector). Associated uncertainty was better than 3 %. The pH (± 0.02 pH units) of the initial medium was measured into the glove box using Thermo Orion pH electrodes and periodically calibrated with standard solutions of pH 2, 4 and 7.

$\delta^{15}N\text{-}NO_2^-$ and $\delta^{18}O\text{-}NO_2^-$ were determined following the azide reduction method (McIlvin and Altabet, 2005; Ryabenko et al., 2009). N_2O was analyzed using a Pre-Con (Thermo Scientific) coupled to a Finnigan MAT 253 Isotope Ratio Mass Spectrometer (IRMS, Thermo Scientific). Notation is expressed in terms of δ ‰ ($\delta = (R_{sample}\text{-}R_{standard})/R_{standard}$, where R is the ratio between the heavy and the light isotopes) (Coplen, 2011). Used international standards were atmospheric N_2 (AIR) for $\delta^{15}N$ and Vienna Standard Mean

Oceanic Water (V-SMOW) for $\delta^{18}O$. According to Coplen (2011), several international and laboratory (in-house) standards were interspersed among samples for normalization of analyses. Two international standards (USGS 34 and 35) and two internal laboratory standards (CCiT-$NaNO_3$ ($\delta^{15}N$ = +16.9 ‰ and $\delta^{18}O$ = +28.5 ‰) and CCiT-KNO_2 ($\delta^{15}N$ = -28.5 ‰)) were employed to correct the $\delta^{15}N$-NO_2^- and $\delta^{18}O$-NO_2^- values. The reproducibility (1σ) of the samples, calculated from the standards systematically interspersed in the analytical batches, was ±1.0 ‰ for $\delta^{15}N$-NO_2^- and ±1.5 ‰ for $\delta^{18}O$-NO_2. The isotopic analyses were prepared at the MAiMA-UB research group laboratory and analyzed at the Scientific and technical services of Barcelona University (CCiT-UB).

Under closed system conditions, the isotopic fractionation values (i.e., $\varepsilon^{15}N_{NO2}$ and $\varepsilon^{18}O_{NO2}$) are calculated according to the Rayleigh distillation equation: from which ε values can be obtained from the slope of the linear correlation between the natural logarithm of the substrate remaining fraction ($\ln(C_{residual}/C_{initial})$, where C refers to the analyte concentration), and the determined isotope ratios ($\ln(R_{residual}/R_{initial})$, where $R = (\delta+1)$).

$$\ln\left(\frac{R_{residual}}{R_{initial}}\right) = \varepsilon \times \ln\left(\frac{C_{residual}}{C_{initial}}\right) \qquad \textbf{(Equation 3)}$$

3 RESULTS AND DISCUSSION

3.1 Bio-reduction of ferrihydrite

Three different stages were distinguished during the reductive dissolution of ferrihydrite mediated by *S. loihica* (Ferr experiments, **Figure 1**). In the first stage, a dramatic drop of the initial concentration of lactate was accompanied by a sharp increase in acetate concentration while aqueous Fe(II) was not detected. Afterwards, a gradual decrease in

lactate and increase in acetate were observed together with a significant increase in aqueous Fe(II). In the final stage, lactate was totally depleted after about 60 days from the beginning of the experiment, and acetate and Fe(II) leveled off with respective concentrations of about 8 and 1.1 mM. Total consumption of lactate led to an unavailability of the electron donor, ceasing therefore bio-reduction and leaving the acetate and aqueous Fe(II) concentrations constant.

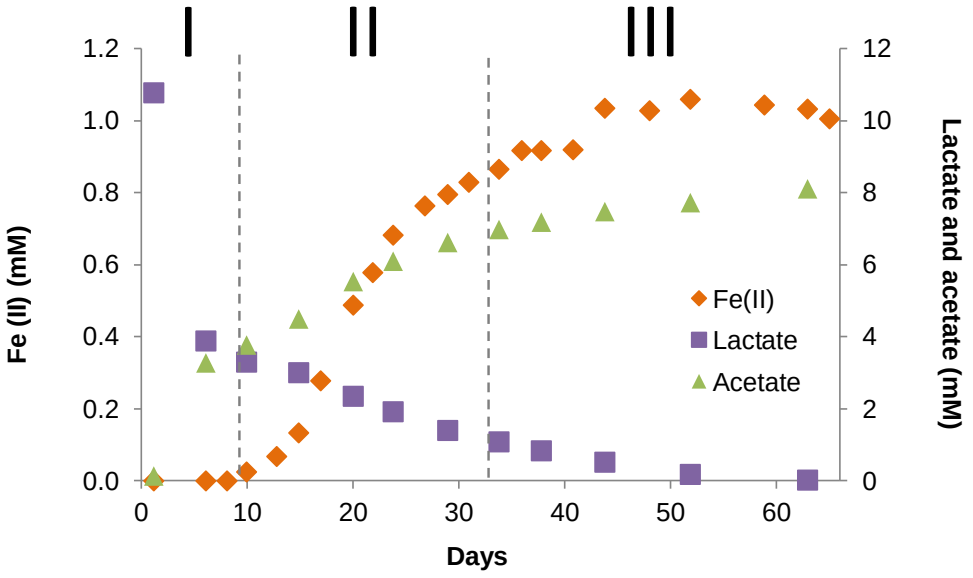

Figure 1. Reductive dissolution of ferrihydrite (Ferr experiments). Lactate consumption and acetate and Fe(II) production by *S. loihica* showed three stages (biomass production, maximum microbial activity and halt of microbial metabolism).

According to **Equation 1**, for the Fe(III) oxide minerals reduction, the stoichiometric molar ratio between the consumed lactate and produced acetate is 1. Nonetheless, a 20 % deficit of acetate (carbon loss) was observed throughout the experiments (**Figure 1**). This

non-stoichiometric behavior was mainly attributed to the use of lactate as a carbon source for biomass formation during microbial growth (Lanthier et al., 2008). On the other hand, since the stoichiometric Fe(II)/acetate molar ratio is 4 and the highest measured concentrations of aqueous Fe(II) and acetate were 1.1 and 8 mM, respectively, only 3.5 % of all the possible Fe(II) produced was detected in the media (aqueous). A plausible explanation for the observed aqueous Fe(II) deficit could be Fe(II) adsorption on the ferrihydrite surface. It is known that the high surface area combined with the poor crystalline organization of ferrihydrite at high pH (i.e. pH ≈ 8.2) can cause an exceptionally large sorption capacity of cations (Dzomback and Morel, 1990). The Fe(II)-adsorption and Fe(II)-isotherm assays allowed to confirm the occurrence of the Fe(II) adsorption process,. The results determined the maximum concentration of adsorbed Fe(II) on the ferrihydrite was ≈ 1.2 mM and revealed that the decrease of aqueous Fe(II) was not only due to Fe(II) adsorption but also to an additional process, such as formation of a Fe(II)-bearing phase (e.g. magnetite) (**Section S3** (**SI**)).

Earlier studies indicated that adsorption of Fe(II) on ferrihydrite can result in ferrihydrite transformation to goethite, magnetite or lepidocrocite (Xiao et al., 2018; Xiao et al. 2017; Dippon et al., 2015; Piepenbrock et al. 2011; Yang et al., 2010; Hansel et al., 2003). Factors as diverse as the thermodynamic properties of the mineral phases involved, the aqueous Fe(II) concentration and formation rates, biological and physical settings or the design of the experimental setup can influence the ferrihydrite transformation (Dippon et al. 2015). SEM, XRD and FTIR analyses of the solid samples before and after the Fe(III) bioreduction process showed that ferrihydrite was indeed transformed into magnetite ($Fe(II)Fe(III)_2O_4$) (**Figure 2**). Yang et al. (2010) pointed out that this transformation is caused by inclusion of the bio-produced Fe(II) into the mineral lattice. **Figure 2b** compares two XRD patterns of pristine and bio-reduced samples. In addition to initial ferrihydrite (75

wt% purity), two new phases (nanocrystalline magnetite and microcrystalline hematite) were present in the reacted sample (Ferr experiment) with estimated amounts of 23.5 wt% (magnetite) and 1.5 wt% (hematite). The minor content of the latter was likely formed during ferrihydrite autoclave process (Das et al., 2010).

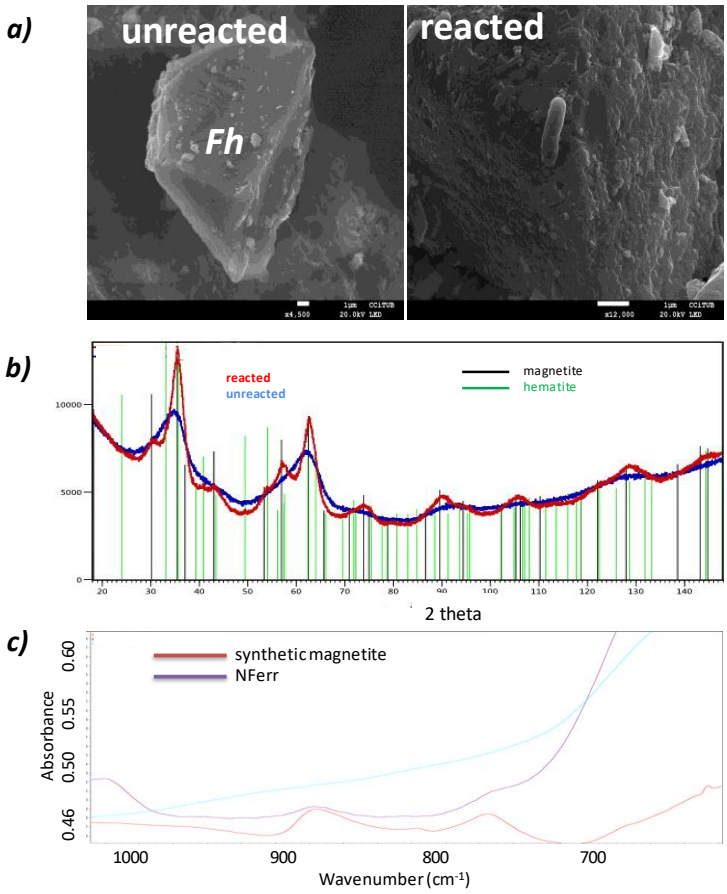

Figure 2. Characterization of ferrihydrite before and after reduction. a) SEM images show an unreacted (left) and a reacted ferrihydrite particle attached to a cell of *S.loihica* (right); b) XRD patterns of the unreacted (blue line) and reacted (red line) ferrihydrite samples; black and green vertical lines show the 2θ positions of peaks of magnetite and hematite, respectively; c) FTIR spectra of unreacted ferrihydrite (blue line), reacted ferrihydrite (purple line) and pure magnetite (red line).

3.2 Abiotic NO_2^- reduction coupled to Fe(II) oxidation

In the AbSeaNO_2-BioFe_{aq+s} experiments, a fast removal of both nitrite and aqueous Fe(II) was observed and achieved about 50% and 30% reduction, respectively, in 2 h (**Figure 3a**). After 10 h, almost total removal of NO_2^- (87%) and up to 38% removal of the initial aqueous Fe(II) were observed. The calculated NO_2^- reduction rate was 6.47 mM^{-1} d^{-1} ($t_{1/2}$ = 0.07 d) (**Section S4** (**SI**)). The dynamics of this abiotic NO_2^- reduction mediated by bio-produced Fe(II) was then compared to that of synthetic Fe(II).

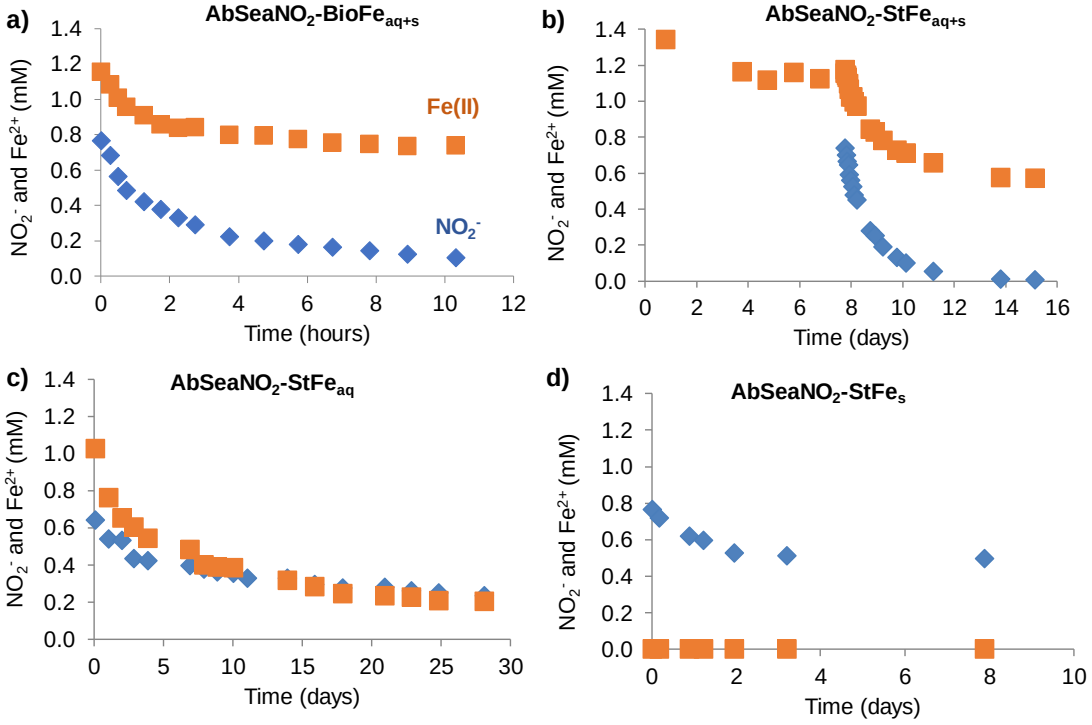

Figure 3. Variation of concentration of Fe(II) and NO_2^- throughout experiments: a) bio-produced Fe(II) in the presence of ferrihydrite (AbSeaNO_2-BioFe_{aq+s}); b) aqueous and solid-bound synthetic Fe(II) (AbSeaNO_2-StFe_{aq+s}); c) aqueous synthetic Fe(II) (AbSeaNO_2-StFe_{aq}); and d) solid-bond synthetic Fe(II) (AbSeaNO_2-StFe_s).

In the experiments AbSeaNO_2-StFe_{aq+s}, the NO_2^- and aqueous Fe(II) concentrations declined up to 87 % and 38 %, respectively, within about 2 days (**Figure 3b**). The estimated NO_2^- reduction rate was 0.75 mM^{-1} d^{-1} ($t_{1/2}$ = 0.47 d) (**Section S4** (**SI**)). Therefore, in the experiments with bio-produced Fe(II), the reduction of NO_2^- was faster compared to when using synthetic Fe(II) even though the Fe(II) was found both aqueous and associated to the ferrihydrite in the two types experiments. It has to be considered that although the initial aqueous Fe(II) concentration was similar in the two types of experiments, in the experiments with bio-produced Fe(II) the estimated concentration of Fe(II) associated to mineral was much higher (i.e., around 30 mM) compared to that of the experiments with synthetic Fe(II) (1.2 mM). These results suggest that in the AbSeaNO_2-BioFe_{aq+s} experiments, the Fe(II) that is reincorporated in the ferrihydrite and involved in magnetite transformation (during the Ferr experiments), is available to reduce NO_2^- (Tai and Dempsey, 2009; Rakshit et al., 2008). Similarly, Byrne et al. (2011) found that an enhanced Fe(II)-rich surface (e.g. magnetite) of bio-reduced Fe(III)-amorphous oxyhydroxides is able to reduce toxic hexavalent chromium to the less harmful trivalent form.

The abiotic NO_2^- reduction was also tested with synthetic Fe(II) when found only in the aqueous or solid-bound forms. In the AbSeaNO_2-StFe_{aq} experiments, after a week, Fe(II) depletion was approximately 50 % of the initial concentration and 35 % of NO_2^- was reduced (**Figure 3c**). After a month, 70 % Fe(II) had been reduced and 65% NO_2^-. The NO_2^- reduction rate (k_{obs}) was estimated to be 0.081 mM^{-1} d^{-1} with a half-life value ($t_{1/2}$) of 12.7 d (**Section S4** (**SI**)). In the AbSeaNO_2-StFe_s experiments, about 27% of NO_2^- reduction occurred within 2 days (**Figure 3d**), indicating that in the absence of aqueous Fe(II), the Fe(II) adsorbed on the ferrihydrite surface was able to reduce NO_2^-. After these 2 days, the reaction stopped, and NO_2^- concentration remained constant. A nitrite reduction

rate of 0.21 mM^{-1} d^{-1} was calculated (**Section S4** (**SI**)). Therefore, the fastest abiotic NO_2^- reduction was achieved when the Fe(II) was bound both in the aqueous form and associated to the ferrihydrite while the lowest rate was found for aqueous Fe(II) in the absence of ferrihydrite. When Fe(II) was only solid-bound, an intermediate rate and extent was obtained.

3.3 Biotic (heterotrophic) NO_2^- reduction by *S. loihica*

Biotic experiments showed a lag of microbial activity before NO_2^- reduction commenced. In the cultures amended with either lactate or acetate, the lag period lasted about 24 h and 10 d respectively (**Figure 4**). Yoon et al. (2013) reported a similar behavior for *Shewanella* spp. In the AbSeaNO_2 experiments, the NO_2^- reduction was completed in approximately 30 hours and 60 days when using lactate or acetate as electron donors, respectively (**Figure 4**). In contrast, NO_2^- was consumed in 10 h due to the abiotic reduction by oxidation of the bio-produced Fe(II) (**Figure 3a**).

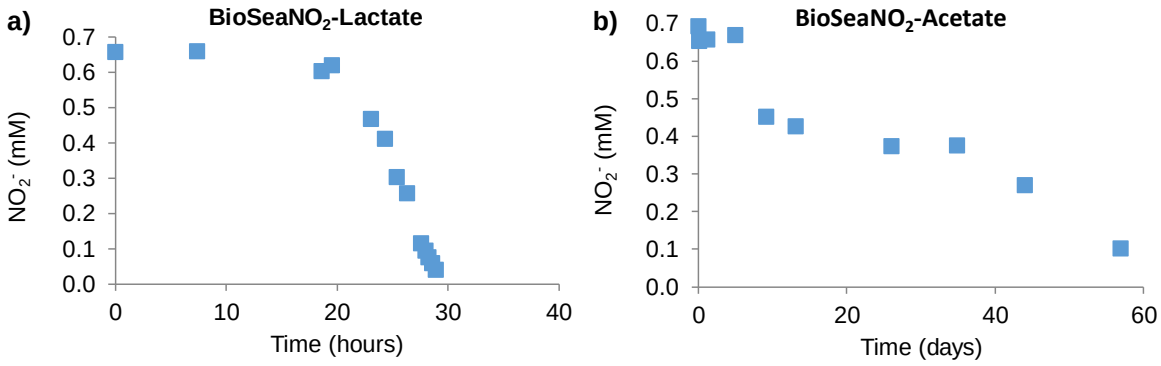

Figure 4. Heterotrophic nitrite reduction mediated by *S.loihica* in absence of Fe(II) and ferrihydrite. Two sets of batch experiments were performed by using lactate (a) or acetate (b) as electron donors.

These results allowed to discard a significant contribution of microbial NO_2^- reduction in the abiotic experiments with bio-produced Fe(II), that contained acetate as a result of the ferrihydrite reduction by *S. loihica* coupled to the oxidation of lactate.

3.4 Isotopic fractionation during abiotic NO_2^- reduction

In the abiotic NO_2^- reduction experiments, as the NO_2^- concentration decreased, the unreacted substrate became enriched in the heavy isotopes (^{15}N and ^{18}O), as it is commonly observed for denitrification. The plots showing the $\varepsilon^{15}N_{NO2}$ and $\varepsilon^{18}O_{NO2}$ calculations are presented in **Section S6** (**SI**) and the obtained values along with the $\varepsilon^{15}N/\varepsilon^{18}O$ are summarized in **Table 2**. The $\varepsilon^{15}N_{NO2}$ ranged from -8.1 ‰ to -19.7 ‰, the $\varepsilon^{18}O_{NO2}$ from -4.6 ‰ to -11.4 ‰ and the $\varepsilon^{15}N/\varepsilon^{18}O$ from 1.4 to 1.8. These values are in the range of reported values in the literature for both, the biotic (heterotrophic) and abiotic NO_2^- reduction (**Table 3**).

Table 2. NO_2^- reduction rate, $\varepsilon^{15}N_{NO2}$, $\varepsilon^{18}O_{NO2}$ and $\varepsilon^{15}N/\varepsilon^{18}O$ results. The calculations of the isotopic fractionation values are shown in **Section S5** (**SI**). n.c. = non calculated.

Code	NO_2^- reduction rate ($mM^{-1}\ d^{-1}$)	$\varepsilon^{15}N_{NO2}$ (‰)	$\varepsilon^{18}O_{NO2}$ (‰)	$\varepsilon^{15}N/\varepsilon^{18}O$
$AbSeaNO_2$-$StFe_{aq}$	0.081	-8.6	-6.3	1.4
$AbSeaNO_2$-$StFe_s$	0.21	-19.7	-11.4	1.7
$AbSeaNO_2$-$StFe_{aq+s}$	0.75	-8.7	-5.2	1.7
$AbSeaNO_2$-$BioFe_{aq+s}$	6.47	-8.1	-4.6	1.8
$BioSeaNO_2$-Acetate	n.c.	-1.6	-5.3	0.3

Table 3. $\varepsilon^{15}N$, $\varepsilon^{18}O$ and $\varepsilon^{15}N/\varepsilon^{18}O$ reported in the literature for the NO_2^- reduction. For NO_2^- biotic reduction, ε is calculated for conversion to N_2, whereas for NO_2^- abiotic reduction, the final product is assumed to be N_2O. * References: (1) Martin and Casciotti (2016); (2) Bryan et al., 1983; (3) Brunner et al., 2013; (4) (Jacob et al., 2016); (5) (Grabb et al., 2017); (6) (Buchwald et al., 2016).

bacteria	Electron donor	$\varepsilon^{15}N$ (‰)	$\varepsilon^{18}O$ (‰)	$\varepsilon^{15}N/\varepsilon^{18}O$	Reference
Pseudomonas aeruginosa (Fe-NIR)	C_{org} (medium)	-9.5	-4.2	2.3	(1) *
Pseudomonas chlororaphis (Fe-NIR)	C_{org} (medium)	-8.25	-9.75	0.8	(1) *
Pseudomonas stutzeri (Fe-NIR)	C_{org} (medium)	-7.0	-5.0	1.4	(1) *
Pseudomonas aureofaciens (Cu-NIR)	C_{org} (medium)	-20.5	-3.5	5.9	(1) *
Achromobacter xylosoxidans (Cu-NIR)	C_{org} (medium)	-21.0	-1.0	21.0	(1) *
Ochrobactrum sp. (Cu-NIR)	C_{org} (medium)	-23.5	-2.5	9.4	(1) *
Pseudomonas stutzeri (Fe-NIR)	C_{org} (medium)	-1.0	n.a.	n.a.	(2) *
Kuenenia stuttgartiensis (Fe-NIR)	C_{org} (medium)	-16.0	n.a.	n.a.	(3) *
Environmental community	-	-10	n.a.	n.a.	(4) *
Abiotic	Nontronite	-11.1	-10.4	1.1	(5) *
Abiotic	Nontronite + Fe(II) synth	-2.3	-4.5	0.5	(5) *
Abiotic	Green rust	-4.2 to -9.4	-4.1 to -9.4	0.8 to 1.1	(5) *
Abiotic	Fe(II) synth	-6.1 to -33.9	-5.7 to -24.8	0.8 to 1.6	(6) *
Abiotic	Goethite + Fe(II) synth	-5.9 to 44.8	-5.2 to 33.0	1.0 to 1.4	(6) *

In the experiments testing the NO_2^- abiotic reduction by synthetic Fe(II), no differences in the NO_2^- isotopic fractionation were observed in experiments with aqueous plus solid-bound Fe(II) when comparing biotic (AbSeaNO_2-BioFe$_{aq+s}$) or synthetic (AbSeaNO_2-StFe$_{aq+s}$) origin of Fe(II) (**Table 2**). Similarly no significant differences were found between experiments with aqueous plus solid-bound Fe(II) (AbSeaNO_2-StFe$_{aq+s}$), and only aqueous Fe(II) (AbSeaNO_2-StFe$_{aq}$) (**Table 2**). In contrast, higher $\varepsilon^{15}N_{NO2}$ and $\varepsilon^{18}O_{NO2}$ (absolute values) were observed in experiments with only solid-bound Fe(II) (AbSeaNO_2-StFe$_s$) (**Table 2**).

In **Figure 5**, the isotopic composition expected at a hypothetical 25 % NO_2^- reduction for each tested condition was modelled by means of the Rayleigh equation (Eq.1) (note that the final percentage of NO_2^- reduction in each experiment was different). The ε values obtained for the AbSeaNO_2-BioFe$_{aq+s}$ and AbSeaNO_2-StFe$_{aq+s}$ experiments were similar to those obtained for the AbSeaNO_2-StFe$_{aq}$ experiments. Therefore, it was assumed that the aqueous Fe(II) played an important role on the NO_2^- isotopic fractionation during its abiotic reduction in the presence of ferrihydrite. However, the AbSeaNO_2-StFe$_{aq+s}$ and especially the AbSeaNO_2-BioFe$_{aq+s}$ experiments showed a higher reduction rate than AbSeaNO_2-StFe$_{aq}$.

Since biotic factors can be excluded in these NO_2^- abiotic reduction experiments, the observed $\varepsilon^{15}N_{NO2}$ and $\varepsilon^{18}O_{NO2}$ variability between the AbSeaNO_2-StFe$_s$ and the rest of experiments, could have been caused by the different NO_2^- reduction rates presented by each condition or by possible differences in the reduction mechanism: oxidation of aqueous or solid-bound Fe(II). In previous studies, lower ε values have been associated to higher NO_2^- reduction rates both during biotic and abiotic reactions (Bryan et al., 1983; Buchwald et al., 2016). Concerning the NO_2^- abiotic reduction, the reaction kinetics might be influenced by the initial concentration and proportion of the reactants (NO_2^- and Fe(II)),

the solution pH, and the presence of minerals either added externally or precipitated during the reaction (Buchwald et al., 2016; Grabb et al., 2017). In the case of minerals, parameters such as quantity, composition (including the Fe oxidation state) and mineral specific surface could influence the reaction. Therefore, it is difficult to unravel if the observed ε variability is uniquely due to the different reduction rates or if it is also influenced by a possible different reaction mechanism (oxidation of aqueous or solid-bound Fe(II) coupled to NO_2^- reduction). Differences on the ε and the NO_2^- removal rate have been observed when using aqueous Fe(II) as electron donor compared to Fe(II) associated to mineral surfaces (Buchwald et al., 2016). From our results, an effect of the NO_2^- reduction rate on the isotopic fractionation is not likely relevant since similar $\varepsilon^{15}N_{NO2}$ and $\varepsilon^{18}O_{NO2}$ were obtained for the $AbSeaNO_2$-$StFe_{aq+s}$ and $AbSeaNO_2$-$BioFe_{aq+s}$ experiments that presented different NO_2^- reduction rates (hours compared to days). In this kind of experiments, even when studying the reaction mediated by aqueous Fe(II), the production of different Fe-bearing oxides and hydroxides throughout the Fe(II) oxidation might hinder a comparison between the conditions tested in the present study and other studies reported in the literature.

In NO_2^- reduction experiments it is important to consider a possible effect on the $\varepsilon^{15}N/\varepsilon^{18}O$ due to a $\delta^{18}O$-NO_2^- equilibration with $\delta^{18}O$-H_2O that might depend on the tested salinity, temperature and/or pH conditions (Buchwald and Casciotti, 2013). Moreover, if the intermediate NO accumulates and the reaction is reversible, it could reoxidate to NO_2^- by incorporating an O atom from water, which might also influence the $\varepsilon^{15}N/\varepsilon^{18}O$ (Buchwald et al., 2016). In a study conducted at room temperature and pH 7.6, over the 2 hours between sampling and the azide reaction, an isotopic effect due to O equilibration was considered negligible (0.0035‰) (Martin and Casciotti, 2016). Since our samples (pH between 7.8 and 8.2) were immediately freezed when obtained and immediately analyzed

after unfreezing, we did not expect an O equilibration effect. The similar slopes observed in the abiotic NO_2^- reduction tests for the short ($AbSeaNO_2$-$BioFe_{aq+s}$) and long ($AbSeaNO_2$-$StFe_{aq+s}$) incubation periods (**Table 2, Figure 4**) reinforced the lack of $\delta^{18}O$-NO_2^- equilibration with $\delta^{18}O$-H_2O.

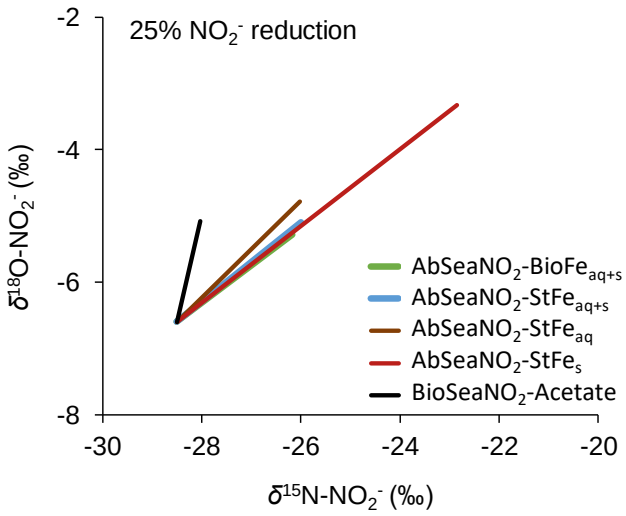

Figure 5. NO_2^- isotopic fractionation when nitrite reduction achieves a 25%. The lines were drawn by using the Rayleigh model and the ε values reported in **Table 2**, for each tested condition.

3.5 Use of isotopic tools to distinguish abiotic from biotic NO_2^- reduction at field-scale

As in the abiotic reduction, in the biotic NO_2^- reduction, a concentration decrease yielded an enrichment in the heavy isotopes (^{15}N and ^{18}O) of the unreacted substrate. The isotopic fractionation calculations are shown in **Section S5** (**SI**) and summarized in **Table 2**. The NO_2^- reduction by *S. loihica* using acetate as electron donor yielded a $\varepsilon^{15}N_{NO2}$ of -1.6 ‰, $\varepsilon^{18}O_{NO2}$ of -5.3 ‰, and $\varepsilon^{15}N/\varepsilon^{18}O$ of 0.3. The $\varepsilon^{15}N_{NO2}$ and $\varepsilon^{18}O_{NO2}$ obtained are within the range of reported values in literature for both, the biotic (heterotrophic) and abiotic NO_2^-

reduction (**Table 3**). Nevertheless, they are slightly lower (absolute values) than those from our abiotic experiments. Moreover, the obtained $\varepsilon^{15}N/\varepsilon^{18}O$ in these biotic experiments (0.3) highly differs from the values obtained for the abiotic experiments and is one of the lowest $\varepsilon^{15}N/\varepsilon^{18}O$ values reported in the literature.

During the biotic NO_2^- reduction experiments, the $\varepsilon^{15}N_{NO2}$ and $\varepsilon^{18}O_{NO2}$ might depend on the enzymes involved in the NO_2^- reduction, the NO_2^- transport across the cell and the NO_2^- reduction rate, while factors such as the pH or salinity might not provoke significant effects, as it has been observed for the NO_3^- biotic reduction (Granger et al., 2008; Wunderlich et al., 2012). The bacterial NO_2^- reduction can be catalyzed by two enzymes located in the periplasm (Cu containing NO_2^- reductase encoded by *nirK* (Cu-NIR) and Fe-containing NO_2^- reductase encoded by *nirS* (Fe-NIR) (Kuypers et al. (2018) and references therein). The obtained $\varepsilon^{15}N/\varepsilon^{18}O$ ratio of 0.3 for the biotic NO_2^- reduction by *S. loihica* lacks resemblance with those reported in a study on NO_2^- reduction with different bacterial species (Martin and Casciotti, 2016). Martin and Casciotti (2016) attributed the variations in the $\varepsilon^{15}N/\varepsilon^{18}O$ ratio to the use of different enzymes since the species containing Fe-NIR yielded lower $\varepsilon^{15}N/\varepsilon^{18}O$ ratios (from 0.7 to 3.3) than the species containing Cu-NIR (from 3.1 to 22.0). These authors suggested that Fe-NIR could produce a higher NO_2^--O isotopic fractionation because it allows cleavage of both N-O bounds, since the Fe-NIR catalytic site might bind NO_2^--N (Fülöp et al., 1995; Maia and Moura, 2014). In contrast, the Cu-NIR catalytic site might bind both the NO_2^--O atoms and the N-O bond closest to the Asp98 residue is cleaved (Li et al., 2015; Murphy et al., 1997), independently of the isotopic composition. However, since the reported NO_2^- reductase for *S. loihica* is the Cu-NIR (Simpson et al., 2010), our results do not fit this hypothesis. We observed a by far higher $\varepsilon^{18}O_{NO2}$ compared to the $\varepsilon^{15}N_{NO2}$ in contrast to the low $\varepsilon^{18}O$ reported by Martin and Casciotti (2016), for microorganisms containing the Cu-NIR.

The $\varepsilon^{15}N/\varepsilon^{18}O$ of 0.3 obtained for the NO_2^- reduction by *S. loihica* significantly differs from the range of $\varepsilon^{15}N/\varepsilon^{18}O$ obtained for the NO_2^- abiotic reduction from 1.4 to 1.8 (**Table 2**). Hence, considering that *S. loihica* is the only NO_2^- reducing microorganism in controlled laboratory experiments, the $\varepsilon^{15}N/\varepsilon^{18}O$ values calculated in the present study could allow to distinguish the contribution of the biotic (heterotrophic) and abiotic NO_2^- reductions. However, taking into account the large variability of the $\varepsilon^{15}N/\varepsilon^{18}O$ values (0.3 to 22.0) found in this study and in the literature for the biotic NO_2^- reduction (**Table 2** and **Table 3**), it might be difficult to distinguish between biotic and abiotic reactions in real marine environments by using isotope tools. One reason is the existence of complex bacterial communities with various NO_2^- reducing enzymes. A second one is the overlap of these $\varepsilon^{15}N/\varepsilon^{18}O$ values obtained for the biotic reduction with those related to the abiotic reduction (0.5 to 1.8; **Table 2** and **Table 3**).

Alternatively, the correlation between the $\delta^{15}N_{NO2}$ and the natural logarithm of the Fe(II) concentration could be useful to identify or discard the occurrence of heterotrophic NO_2^- reduction at field-scale. In our abiotic tests, the Fe(II) concentration decrease coupled to the $\delta^{15}N_{NO2}$ and the $\delta^{18}O_{NO2}$ increase (**Figure 6**). Both for the $\delta^{15}N_{NO2}$ and the $\delta^{18}O_{NO2}$, the AbSeaNO_2-StFe_{aq} experiment showed a lower slope (-5.8 and -4.1, respectively) than the AbSeaNO_2-StFe_{aq+s} (-33.8 and -23.3, respectively) and AbSeaNO_2-BioFe_{aq+s} (-33.2 and -20.0, respectively) experiments, likely due to the lower reduction rate. Since at field scale the possible equilibration between the $\delta^{18}O$-NO_2^- and the $\delta^{18}O$-H_2O and the occurrence of N cycling processes such as NO_2^- oxidation to NO_3^-, NO_2^- reduction to NH_4^+ or NH_4^+ oxidation to NO_2^- could have an influence on the $\delta^{18}O$-NO_2^-, the use of the $\delta^{15}N_{NO2}$ versus the natural logarithm of the Fe(II) concentration plot is preferred. Therefore, when assessing the fate of NO_2^- and Fe at field-scale, if a good correlation is observed between the $\delta^{15}N_{NO2}$ and Fe(II) concentration, that could be used as an indicative of NO_2^- reduction

by Fe(II) oxidation either abiotically or biotically (autotrophic), while no correlation could be indicative of heterotrophic NO_2^- reduction.

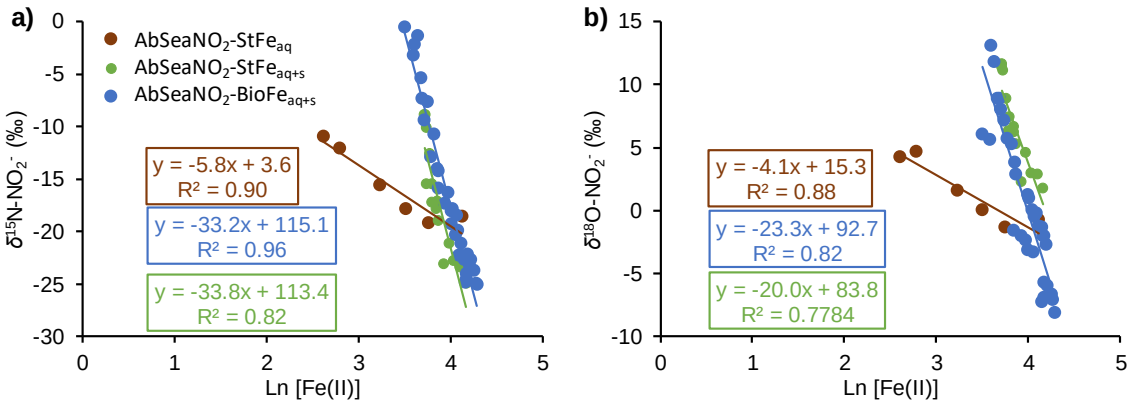

Figure 6. Correlation between the nitrite isotopic composition and Ln Fe(II) concentration. For the abiotic experiments containing aqueous Fe(II), the evolution of the $\delta^{15}N\text{-}NO_2^-$ and the $\delta^{18}O\text{-}NO_2^-$ is presented against the natural logarithm of the Fe(II) concentration.

4 CONCLUSIONS

Batch experiments simulating an anoxic marine medium were carried out to study nitrite reduction coupled to (bio-produced and synthetic) Fe(II) oxidation. Fe(II) bio-production was driven by ferrihydrite reduction mediated by *S. loihica* using lactate as electron donor. The released Fe(II) was found aqueous, adsorbed on the ferrihydrite surface and partially transformed to nanocrystalline magnetite, producing solid Fe(II).

Efficiency in nitrite reduction was strictly related to the availability of Fe(II). Experiments with bio-produced Fe(II) (aqueous and solid-bound) and with synthetic Fe(II) (aqueous and solid-bound) indicated that the bio-produced Fe(II) presents a higher reactivity than

synthetic Fe(II). In further experiments with synthetic Fe(II) (only aqueous, only solid-bound or both) it was found that the abiotic nitrite reduction is faster and more efficient in the presence of both aqueous and solid-bound Fe(II) compared to when only aqueous or solid-bound Fe(II) are found.

No differences in the NO_2^- isotopic fractionation were observed for the abiotic NO_2^- reduction regarding the biotic or synthetic source of Fe(II). In addition, no significant differences in $\varepsilon^{15}N_{NO2}$ and $\varepsilon^{18}O_{NO2}$ were observed for the abiotic NO_2^- reduction by aqueous Fe(II) or aqueous and solid-bound Fe(II). In contrast, the isotopic fractionation was larger in the experiments with only solid-bound Fe(II). For the biotic (heterotrophic) experiments, a higher $\varepsilon^{18}O_{NO2}$ was observed compared to $\varepsilon^{15}N_{NO2}$. The obtained $\varepsilon^{15}N/\varepsilon^{18}O$ ratio (0.3) is one of the lowest values reported in the literature. Hence, in laboratory microcosms mimicking marine environments with *S. loihica* as the only existing NO_2^- reducing microorganism, the $\varepsilon^{15}N/\varepsilon^{18}O$ ratio calculated could be used to distinguish between biotic and abiotic NO_2^- reduction. However, as the obtained $\varepsilon^{15}N/\varepsilon^{18}O$ values were close to or within the wide range of reported values in the literature for the abiotic NO_2^- reduction by Fe(II) oxidation and the NO_2^- reduction by other heterotrophic bacteria, the use of the $\varepsilon^{15}N/\varepsilon^{18}O$ ratio to distinguish different mechanisms of NO_2^- reduction in field cases should be prevented. As an alternative, the correlation between $\delta^{15}N_{NO2}$ and the natural logarithm of the Fe(II) concentration could be useful to identify or discard the occurrence of heterotrophic NO_2^- reduction in field scenarios.

ACKNOWLEDGEMENTS

This study was financially supported by projects PACE-ISOTEC (CGL2017-87216-C4-1-R) financed by the Spanish Government and EI/FEDER financed by the European Union, and

by MAG (2017 SGR 1733) financed by the Catalan Government. R. Margalef-Marti thanks the Spanish Government for the Ph.D. grant BES-2015-072882. Jordi Bellés (IDAEA-CSIC), Natàlia Moreno (IDAEA-CSIC) and Xavier Alcové (SCTT-Barcelona University) are thanked for laboratory assistance and XRD analyses, respectively.

REFERENCES

Aravena, R., Robertson, W.D., 1998. Use of multiple isotope tracers to evaluate denitrification in ground water: study of nitrate from a large-flux septic system plume. Groundwater 36, 975-982.

Benaiges-Fernandez R., Palau J., Offeddu F.G., Cama J., Urmeneta J., Soler J., Dold B., 2019. Dissimilatory bioreduction of iron(III) oxides by *Shewanella loihica* under marine sediment conditions. Marine Environmental Research.

Boland, D.D., Collins, R.N., Miller, C.J., Glover, C.J., Waite, T.D., 2014. Effect of solution and solid-phase conditions on the Fe (II)-accelerated transformation of ferrihydrite to lepidocrocite and goethite. Environmental science & technology 48, 5477-5485.

Böttcher, J., Strebel, O., Voerkelius, S., Schmidt, H.L., 1990. Using isotope fractionation of nitrate-nitrogen and nitrate-oxygen for evaluation of microbial denitrification in a sandy aquifer. Journal of Hydrology 114, 413-424.

Brunauer, S., Emmett, P.H., Teller, E., 1938. Adsorption of gases in multimolecular layers. Journal of the American chemical society 60, 309-319.

Bryan, B.A., Shearer, G., Skeeters, J.L., Kohl, D.H., 1983. Variable expression of the nitrogen isotope effect associated with denitrification of nitrite. Journal of Biological Chemistry 258, 8613-8617.

Buchwald C., Casciotti, K.L. 2013. Isotopic ratios of nitrite as tracers of the sources and age of oceanic nitrite. Nature Geoscience 6 (4), 308

Buchwald, C., Grabb, K., Hansel, C.M., Wankel, S.D., 2016. Constraining the role of iron in environmental nitrogen transformations: Dual stable isotope systematics of abiotic

NO_2^- reduction by Fe(II) and its production of N_2O. Geochimica et Cosmochimica Acta 186, 1-12.

Byrne, J., Telling, N., Coker, V., Pattrick, R., Van Der Laan, G., Arenholz, E., Tuna, F., Lloyd, J., 2011. Control of nanoparticle size, reactivity and magnetic properties during the bioproduction of magnetite by *Geobacter sulfurreducens*. Nanotechnology 22, 455709.

Canfield, D.E., 1989. Reactive iron in marine sediments. Geochimica et Cosmochimica Acta 53, 619-632.

Chen, D., Liu, T., Li, X., Li, F., Luo, X., Wu, Y., Wang, Y., 2018. Biological and chemical processes of microbially mediated nitrate-reducing Fe(II) oxidation by *Pseudogulbenkiania sp*. strain 2002. Chemical Geology 476, 59-69.

Coplen, T.B., 2011. Guidelines and recommended terms for expression of sTable-isotope-ratio and gas-ratio measurement results. Rapid communications in mass spectrometry 25, 2538-2560.

Das, S., Hendry, M.J., Essilfie-Dughan, J., 2010. Transformation of two-line ferrihydrite to goethite and hematite as a function of pH and temperature. Environmental science & technology 45, 268-275.

Dhakal, P., Matocha, C., Huggins, F., Vandiviere, M., 2013. Nitrite reactivity with magnetite. Environmental science & technology 47, 6206-6213.

Dippon, U., Schmidt, C., Behrens, S., Kappler, A., 2015. Secondary mineral formation during ferrihydrite reduction by *Shewanella oneidensis* MR-1 depends on incubation vessel orientation and resulting gradients of cells, Fe(II) and Fe minerals. Geomicrobiology Journal 32, 878-889.

Dong, H., Fredrickson, J.K., Kennedy, Zachara, J.M., D.W., Kukkadapu, R.K., Onstott, T.C., 2000. Mineral transformations associated with the microbial reduction of magnetite. Chemical Geology, 169, 299-318

Dzombak, D.A., Morel, F., 1990. Surface complexation modeling: hydrous ferric oxide. John Wiley & Sons.

Fukada, T., Hiscock, K.M., Dennis, P.F., Grischek, T., 2003. A dual isotope approach to identify denitrification in groundwater at a river-bank infiltration site. Water Research 37, 3070-3078.

Fülöp, V., Moir, J.W., Ferguson, S.J., Hajdu, J., 1995. The anatomy of a bifunctional enzyme: structural basis for reduction of oxygen to water and synthesis of nitric oxide by cytochrome cd1. Cell 81, 369-377.

Gao, H., Obraztova, A., Stewart, N., Popa, R., Fredrickson, J.K., Tiedje, J.M., Nealson, K.H., Zhou, J., 2006. Shewanella loihica sp. nov., isolated from iron-rich microbial mats in the Pacific Ocean. International Journal of Systematic and Evolutionary Microbiology 56, 1911-1916.

García-Robledo E., Corzo A., Papaspyrou S., 2014. A fast and direct spectrophotometric method for the sequential determination of nitrate and nitrite at low concentrations in small volumes. Marine Chemistry 162, 30-36.

Grabb, K.C., Buchwald, C., Hansel, C.M., Wankel, S.D., 2017. A dual nitrite isotopic investigation of chemodenitrification by mineral-associated Fe(II) and its production of nitrous oxide. Geochimica et Cosmochimica Acta 196, 388-402.

Granger, J., Sigman, D.M., Lehmann, M.F., Tortell, P.D., 2008. Nitrogen and oxygen isotope fractionation during dissimilatory nitrate reduction by denitrifying bacteria. Limnology and Oceanography 53, 2533-2545.

Guerbois, D., Ona-Nguema, G., Morin, G., Abdelmoula, M., Laverman, A.M., Mouchel, J.-M., Barthelemy, K., Maillot, F., Brest, J., 2014. Nitrite reduction by biogenic hydroxycarbonate green rusts: Evidence for hydroxy-nitrite green rust formation as an intermediate reaction product. Environmental science & technology 48, 4505-4514.

Hansel, C.M., Benner, S.G., Neiss, J., Dohnalkova, A., Kukkadapu, R.K., Fendorf, S., 2003. Secondary mineralization pathways induced by dissimilatory iron reduction of ferrihydrite under advective flow. Geochimica et Cosmochimica Acta 67, 2977-2992.

Jani J., Toor G.S., 2016. Composition, sources, and bioavailability of nitrogen in a longitudinal gradient from freshwater to estuarine waters. Water Research,137, 344-354

Kampschreur, M.J., Kleerebezem, R., de Vet, W.W., van Loosdrecht, M.C., 2011. Reduced iron induced nitric oxide and nitrous oxide emission. Water Research 45, 5945-5952.

Kuypers, M.M., Marchant, H.K., Kartal, B., 2018. The microbial nitrogen-cycling network. Nature Reviews Microbiology 16, 263.

Lanthier, M., Gregory, K.B., Lovley, D.R., 2008. Growth with high planktonic biomass in Shewanella oneidensis fuel cells. FEMS microbiology letters 278, 29-35.

Li, Y., Hodak, M., Bernholc, J., 2015. Enzymatic mechanism of copper-containing nitrite reductase. Biochemistry 54, 1233-1242.

Lovley, D.R., 1991. Dissimilatory Fe(III) and Mn(IV) reduction. Microbiology and Molecular Biology Reviews 55, 259-287.

Lu, Y., Xu, L., Shu, W., Zhou, J., Chen, X., Xu, Y., Qian, G., 2017. Microbial mediated iron redox cycling in Fe(hydr)oxides for nitrite removal. Bioresource technology 224, 34-40.

Maia, L.B., Moura, J.J., 2014. How biology handles nitrite. Chemical reviews 114, 97.

Mariotti, A., Germon, J., Hubert, P., Kaiser, P., Letolle, R., Tardieux, A., Tardieux, P., 1981. Experimental determination of nitrogen kinetic isotope fractionation: some principles; illustration for the denitrification and nitrification processes. Plant and soil 62, 413-430.

Martin, T.S., Casciotti, K.L., 2016. Nitrogen and oxygen isotopic fractionation during microbial nitrite reduction. Limnology and Oceanography 61, 1134-1143.

McIlvin, M.R., Altabet, M.A., 2005. Chemical conversion of nitrate and nitrite to nitrous oxide for nitrogen and oxygen isotopic analysis in freshwater and seawater. Analytical Chemistry 77, 5589-5595.

Melton, E.D., Swanner, E.D., Behrens, S., Schmidt, C., Kappler, A., 2014. The interplay of microbially mediated and abiotic reactions in the biogeochemical Fe cycle. Nature Reviews Microbiology 12, 797.

Murphy, M.E., Turley, S., Adman, E.T., 1997. Structure of Nitrite Bound to Copper-containing Nitrite Reductase from *Alcaligenes faecalis* mechanistic implications. Journal of Biological Chemistry 272, 28455-28460.

Piepenbrock, A., Dippon, U., Porsch, K., Appel, E., Kappler, A., 2011. Dependence of microbial magnetite formation on humic substance and ferrihydrite concentrations. Geochimica et Cosmochimica Acta 75, 6844-6858.

Rakshit, S., Matocha, C.J., Coyne, M.S., Sarkar, D., 2016. Nitrite reduction by Fe(II) associated with kaolinite. Environmental science & technology, 13, 1329-1334.

Rakshit, S., Matocha, C.J., Coyne, M.S., 2008. Nitrite reduction by siderite. Soil Science Society of America Journal 72, 1070-1077.

Ravishankara A. R., Daniel J. S., Portman R.W., 2009. Nitrous Oxide (N_2O): The Dominant Ozone-Depleting Substance Emitted in the 21st Century.Science , Vol. 326, Issue 5949,123-125

Robertson, E.K., Roberts, K.L., Burdorf, L.D., Cook, P., Thamdrup, B., 2016. Dissimilatory nitrate reduction to ammonium coupled to Fe(II) oxidation in sediments of a periodically hypoxic estuary. Limnology and Oceanography 61, 365-381.

Robertson, E.K., Thamdrup, B., 2017. The fate of nitrogen is linked to iron(II) availability in a freshwater lake sediment. Geochimica et Cosmochimica Acta 205, 84-99.

Roh, Y., Gao, H., Vali, H., Kennedy, D.W., Yang, Z.K., Gao, W., Dohnalkova, A.C., Stapleton, R.D., Moon, J.-W., Phelps, T.J., Fredrickson, J.K., Zhou, J., 2006. Metal Reduction and Iron Biomineralization by a Psychrotolerant Fe(III)-Reducing Bacterium, *Shewanella sp*. Strain PV-4. Applied Environmental Microbiology, 72, 3236 – 3244.

Ryabenko, E., Altabet, M.A., Wallace, D.W., 2009. Effect of chloride on the chemical conversion of nitrate to nitrous oxide for $\delta^{15}N$ analysis. Limnology and Oceanography: Methods 7, 545-552.

Schwertmann U. and Cornell R. M., Iron Oxides in the Laboratory: Preparation and Characterization, Wiley-VCH Verlag GmbH, Weinheim, Germany, 2007.

Simpson, P.J., Richardson, D.J., Codd, R., 2010. The periplasmic nitrate reductase in Shewanella: the resolution, distribution and functional implications of two NAP isoforms, NapEDABC and NapDAGHB. Microbiology 156, 302-312.

Stucki, J., 1981. The quantitative assay of minerals for Fe(II) and Fe(III) using 1, 10-phenanthroline: II. A photochemical method 1. Soil Science Society of America Journal 45, 638-641.

Tai, Y.-L., Dempsey, B.A., 2009. Nitrite reduction with hydrous ferric oxide and Fe (II): stoichiometry, rate, and mechanism. Water research 43, 546-552.

Tomaszewski, E.J., Cronk, S.S., Gorski, C.A., Ginder-Vogel, M., 2016. The role of dissolved Fe (II) concentration in the mineralogical evolution of Fe(hydr)oxides during redox cycling. Chemical Geology 438, 163-170.

Wunderlich, A., Meckenstock, R., Einsiedl, F., 2012. Effect of different carbon substrates on nitrate stable isotope fractionation during microbial denitrification. Environmental science & technology 46, 4861-4868.

Wu D., Shao B., Fu M., Luo C., Liu Z., 2015. Denitrification of nitrite by ferrous hydroxy complex: Effects on nitrous oxide and ammonium formation. Chemical Engineering Journal 279, 149-155.

Xiao, W., Jones, A.M., Collins, R.N., Bligh, M.W., Waite, T.D., 2017a. Use of fourier transform infrared spectroscopy to examine the Fe (II)-Catalyzed transformation of ferrihydrite. Talanta 175, 30-37.

Xiao, W., Jones, A.M., Li, X., Collins, R.N., Waite, T.D., 2018. Effect of Shewanella oneidensis on the kinetics of Fe(II)-catalyzed transformation of ferrihydrite to crystalline iron oxides. Environmental science & technology 52, 114-123.

Yang, L., Steefel, C.I., Marcus, M.A., Bargar, J.R., 2010. Kinetics of Fe(II)-catalyzed transformation of 6-line ferrihydrite under anaerobic flow conditions. Environmental science & technology 44, 5469-5475.

Yee, N., Shaw, S., Benning, L.G., Nguyen, T.H., 2006. The rate of ferrihydrite transformation to goethite via the Fe(II) pathway. American Mineralogist 91, 92-96.

Yoon, S., Sanford, R.A., Löffler, F.E., 2013. *Shewanella spp*. use acetate as an electron donor for denitrification but not ferric iron or fumarate reduction. Appl. Environ. Microbiol. 79, 2818-2822.

SUPPLEMENTARY INFORMATION TO:

Geochemical and isotopic study of abiotic nitrite reduction coupled to bio-produced Fe(II) oxidation in marine environments.

Offeddu F.G.[1], Benaiges-Fernandez R.[1,2], Margalef-Marti R.[3], Palau J.[1,3], Urmeneta J.[2,4], Carrey R.[3], Otero N.[3,5] and Cama J.[1]

[1] Institute of Environmental Assessment and Water Research (IDAEA, CSIC), 08034 Barcelona, Spain.

[2] Departament de Genètica, Microbiologia i Estadística, Universitat de Barcelona, 08028 Barcelona, Spain.

[3] Grup MAiMA, SGR Mineralogia Aplicada, Geoquímica i Geomicrobiologia, Departament de Mineralogia, Petrologia i Geologia Aplicada, Facultat de Ciències de la Terra, Universitat de Barcelona (UB), 08028 Barcelona, Spain.

[4] Institut de Recerca de la Biodiversitat (IRBio), Universitat de Barcelona, 08028 Barcelona, Spain.

[5] Serra Húnter Fellowship. Generalitat de Catalunya, Spain.

In preparation

S1. Ferrihydrite (Fh) synthesis description

For preparation of approximately 10 g of 2L-ferrihydrite a modified procedure based on Schwertmann and Cornell (2007) was followed. 40 g of $Fe(NO_3)\cdot 9H_2O$ were dissolved in MiliQ water. 1 M KOH solution was used to bring pH of the previous solution to 7.5. Afterwards solution was centrifuged at 4500 rpm for 10 min. After removing the clean water in excess, dialysis cellulose tubular membranes were filled with the denser portion, hermetically closed and submerged in 5 liters of Milli-Q water. Electric conductivity was periodically checked, and water was renewed every 12 hours approximately until conductivity reached the value of ~ 5 µS cm^{-1}. The tubular membrane was then settled in *falcon* vials and centrifuged at 4500 rpm during 10 min to eliminate excessive water. In a final step, solid was congealed with liquid nitrogen, and immediately freeze-dried for 48 h. Solid was retrieved and grinded in a mortar (final fraction size < 5µm in diameter).

S2. Control experiments description

Control experiments (**Table S1**) were performed to test possible interferences of SSW, acetate, lactate and ferrihydrite on Fe(II) or nitrite. The evolution of nitrite concentration was checked in the presence of ferrihydrite and acetate (C1), only acetate (C2) and only SSW (C3). The evolution of synthetic Fe(II) concentration was checked in the presence of acetate (C4) and with SSW (C5). Nitrite and Fe(II) concentrations were periodically measured during a month, and no changes were observed.

Table S1. Control experiments content. All the experiments were performed with SSW and Tris-HCl buffer solution. Fe(II) concentration refers to aqueous Fe(II).

Code	Fh (g)	Volume (mL)	Aqueous synthetic Fe(II) (mM)	NO_2^- (mM)	Acetate (mM)
C1	2.5	250	-	0.65	10
C2	-	250	-	0.65	10
C3	-	250	-	0.65	-
C4	-	250	0.75	-	10
C5	-	250	1.00	-	-

S3. Adsorption experiments description

Non-stirred adsorption experiments were carried out by means of sequential injections of 0.2 mM Fe(II) in anoxic SSW with acetate and TRIS buffer, to quantify the amount of aqueous Fe(II) adsorbed on de ferrihydrite surface. **Figure S1** shows the results of this experiment. The injected aqueous Fe(II) decreased to very low concentrations (0.09 mM) after 100 min, reaching 90-95 % removal in approximately 2 h. Therefore, a rapid adsorption of the injected Fe(II) (1.2 mM) on the ferrihydrite surface was demonstrated.

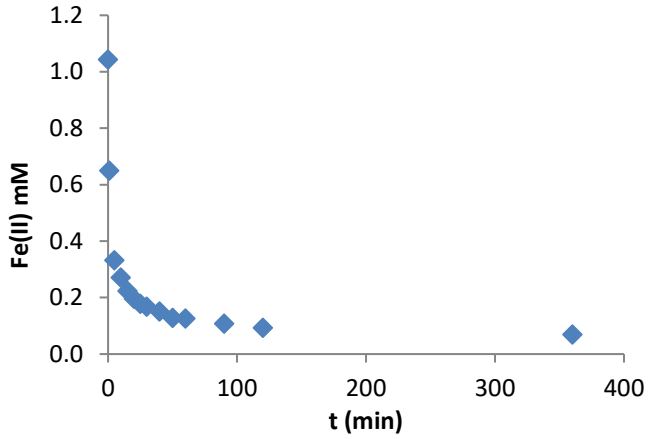

Figure S1. Fe(II) adsorption onto ferrihydrite. The initial concentrations were: Fe(II) = 1.2 mM; acetate = 10 mM; Tris-HCl = 10 mM and pH = 8.2. Volume of synthetic seawater (SSW) = 250 mL and initial mass of ferrihydrite = 2.5 g.

A Fe(II) adsorption isotherm was carried out by means of stirred batch experiments with anoxic SSW, acetate, buffer and ferrihydrite as absorbent and aqueous Fe(II) as adsorptive. The concentration of the latter was increased from 0.4 to 40 mM. In all batches, equilibrium was reached within 4 h, and Fe(II) was measured. The difference between the initial and equilibrium Fe(II) concentrations corresponded to adsorbed Fe(II) (**Figure S2**). Considering that the mean number of available sites for sorption in ferrihydrite is 2.2 - 2.5 sites nm^{-2} (Hiemstra and Van Riemsdijk, 2009; Dzombak and Morel, 1990), the measured specific surface area (160 m^2g^{-1}) and the amount of

ferrihydrite added in the experiments (2.5 g in 250 mL), the calculated available sites were 5.8 x 10^{-3} mol sites L^{-1}. The typical shape of site-limited adsorption isotherm in which Fe(II) adsorption rapidly occurs before reaching a maximum adsorption was not observed. This behavior indicated that the decrease of aqueous Fe(II) was not only due to Fe(II) adsorption but also to an additional process, such as formation of a Fe(II)-bearing phase (e.g. magnetite).

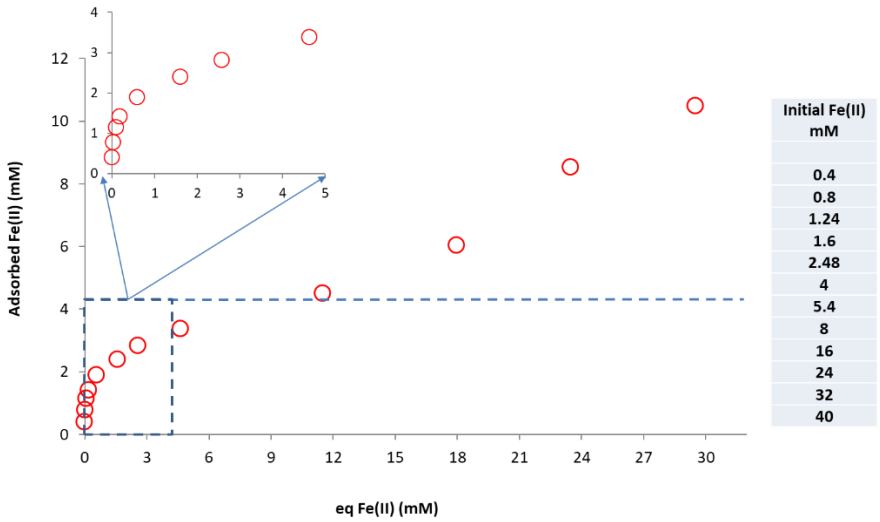

Figure S2. Isotherm adsorption of Fe(II) onto ferrihydrite. Each point represents a 50 mL batch reactor filled with SSW, 10 mM of acetate and buffer, 0.5 g of ferrihydrite and Fe(II). All reactors were shaken overnight. Values on the right column are the Fe(II) initial concentrations. The horizontal dashed line represents a theoretical maximum for absorbable iron; the left inset shows the initial stage of adsorbed Fe(II) concentration as a function of Fe(II) at equilibrium (from 0 to 5 mM).

S4. Nitrite reduction calculations

Rates of nitrite reduction were obtained using a second-order rate expression:

$$\frac{d[NO_2^-]}{dt} = -k_{obs}\,[Fe(II)]\,[NO_2^-] \qquad \textbf{(Equation S1)}$$

where k_{obs} is the nitrite reduction rate constant. The values for k_{obs} were determined for each experiment using the integrated form:

$$\frac{1}{[Fe(II)]_0 - \alpha[NO_2^-]_0} \cdot ln\frac{[NO_2^-]_0([Fe(II)]_0 - \alpha X)}{[Fe(II)]_0([NO_2^-]_0 - X)} = k_{obs} \cdot t \qquad \textbf{(Equation S2)}$$

where $[NO_2^-]_0$ and $[Fe(II)]_0$ are the initial concentrations of nitrite and total ferrous iron, respectively, X denotes the disappearance of nitrite and α corresponds to the mols of Fe(II) reacted per mol of nitrite reduced.

For each experiment, the rate constant (k_{obs}) was derived from the slope of the right-hand side of **equation S2** versus time (t). The calculations are presented in the **Figure S3** and results obtained are summarized in **Table S2**. The second-order fitting of nitrite concentration data derived from **equations S1** and **S2** is presented in **Figure S4**.

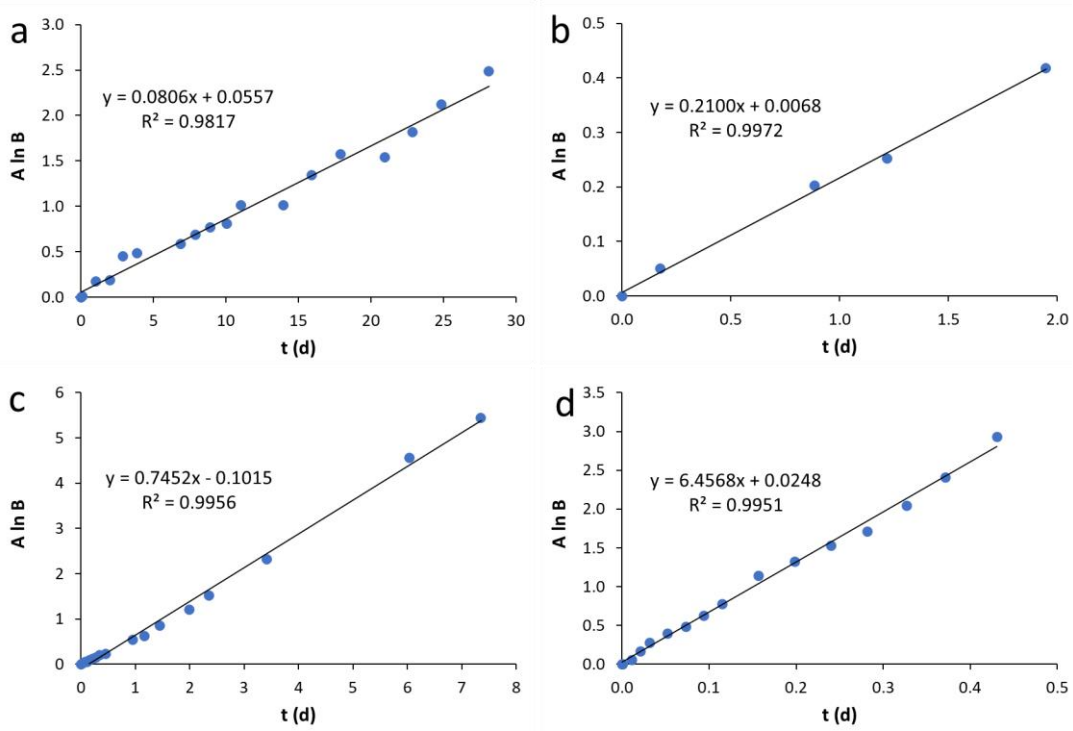

Figure S3. **Linear regressions based on equation S2.** $A = 1/[Fe(II)]_0 - \alpha[NO_2^-]_0$ and $B = [NO_2^-]_0([Fe(II)]_0 - \alpha X)/[Fe(II)]_0([NO_2^-]_0 - X)$. Each plot correspond to a different experiment: A) AbSeaNO$_2$-StFe$_{aq}$; B) AbSeaNO$_2$-StFe$_s$; C) AbSeaNO$_2$-StFe$_{aq+s}$; D) AbSeaNO$_2$-BioFe$_{aq+s}$.

Table S2. Parameter values used in equation S2 and calculated half-life values of NO_2^-. α was a fitting parameter. Concentrations of initial NO_2^-, dissolved Fe(II) and total Fe(II) are also indicated. <dl = below detection limit, * = fitted value.

Experiment	α	Initial NO_2^- (mM)	Initial aqueous Fe(II) (mM)	Initial total Fe(II) (mM)	k_{obs} (mM^{-1} d^{-1})	R^2	Half-life NO_2^- (d)
AbSeaNO$_2$-StFe$_{aq}$	2.7	0.65	1.25	1.25	0.081	0.982	12.7
AbSeaNO$_2$-StFe$_s$	2.7	0.76	< dl	1.26	0.21	0.997	*
AbSeaNO$_2$-StFe$_{aq+s}$	2.7	0.74	1.15	2.60	0.75	0.996	0.47
AbSeaNO$_2$-BioFe$_{aq+s}$	2.7	0.77	1.18	2.10	6.47	0.995	0.07

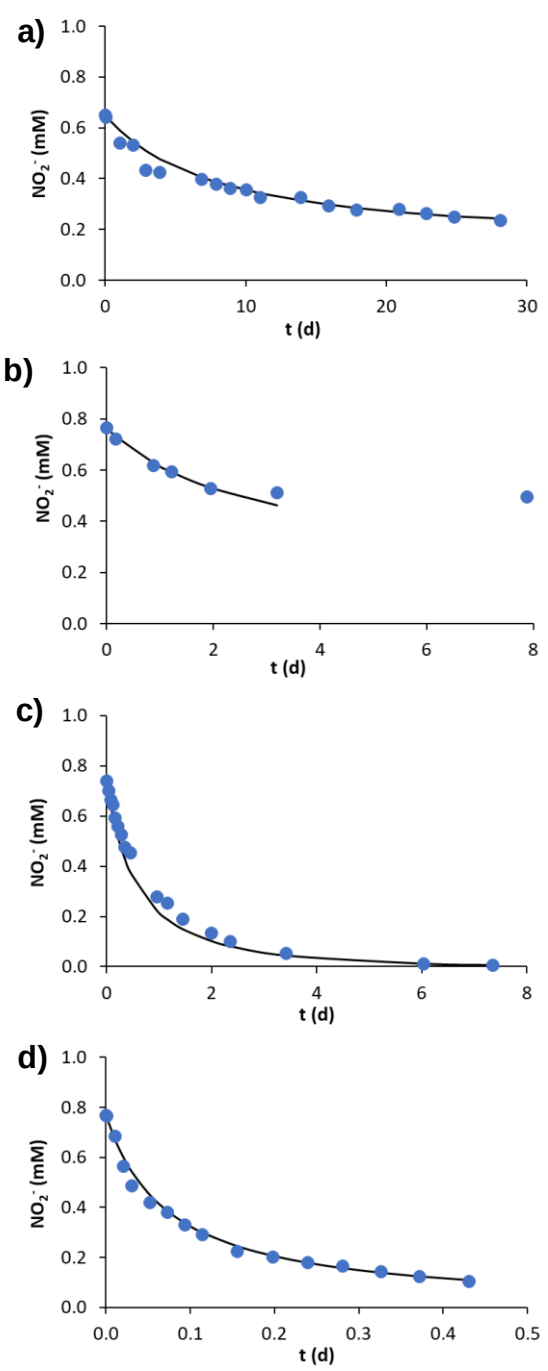

Figure S4. Abiotic NO_2^- reduction by oxidation of Fe(II). Evolution of Fe(II) and NO_2^- over time in the abiotic NO_2^- reduction experiments (left), corresponding to **Figure 3** in the manuscript, including the second-order fitting of nitrite concentration data derived from **equations S1** and **S2** (right). a) AbSeaNO_2-StFe_{aq}, b) AbSeaNO_2-StFe_s, c) AbSeaNO_2-StFe_{aq+s}, d) AbSeaNO_2-BioFe_{aq+s}.

S5. Nitrite isotopic fractionation calculations

The $\varepsilon^{15}N_{NO2}$ and $\varepsilon^{18}O_{NO2}$ are calculated by means of a Rayleigh distillation model (**equation 3** in the manuscript). Linear correlations between the natural logarithm of the substrate remaining fraction and the determined isotope ratios for all the replicates of the batch experiments performed to investigate the abiotic NO_2^- reduction by oxidation of synthetic Fe(II) are shown in **Figure S5**.

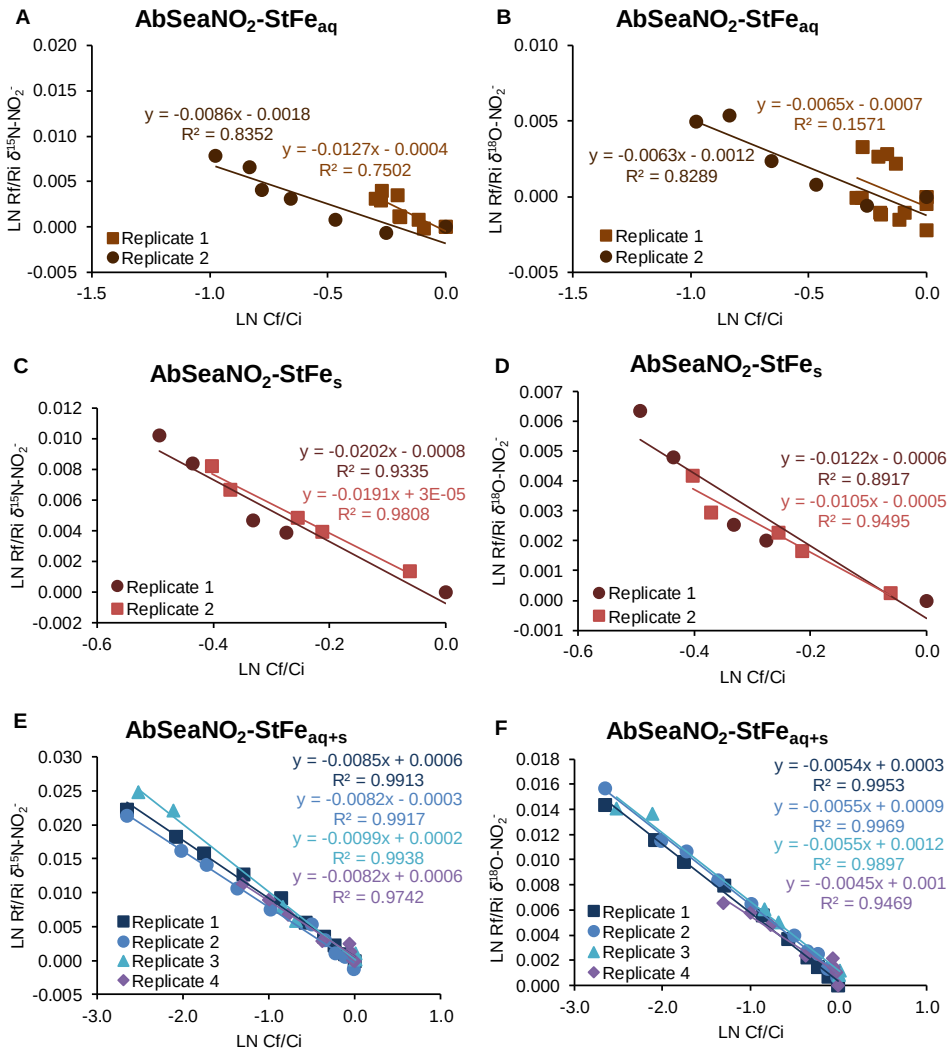

Figure S5. $\varepsilon^{15}N_{NO2}$ and $\varepsilon^{18}O_{NO2}$ calculations for the AbSeaNO$_2$-StFe experiments. The $\varepsilon^{15}N_{NO2}$ are presented in the left and $\varepsilon^{18}O_{NO}$ in the right. A+B) AbSeaNO$_2$-StFe$_{aq}$, C+D) AbSeaNO$_2$-StFe$_s$, E+F) AbSeaNO$_2$-StFe$_{aq+s}$.

Linear correlations between the natural logarithm of the substrate remaining fraction and the determined isotope ratios for all the replicates of the batch experiments performed to investigate the abiotic NO_2^- reduction by oxidation of bio-produced Fe(II) are presented in the **Figure S6**.

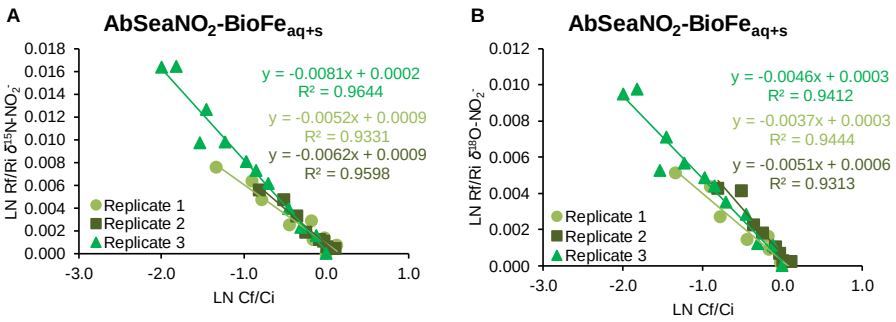

Figure S6. $\varepsilon^{15}N_{NO2}$ and $\varepsilon^{18}O_{NO2}$ calculations for the AbSeaNO$_2$-StFe$_{aq+s}$ experiments. The $\varepsilon^{15}N_{NO2}$ are presented in the left and $\varepsilon^{18}O_{NO}$ in the right.

Linear correlations between the natural logarithm of the substrate remaining fraction and the determined isotope ratios for all the replicates of the batch experiments performed to investigate the biotic NO_2^- reduction are presented in the **Figure S7**.

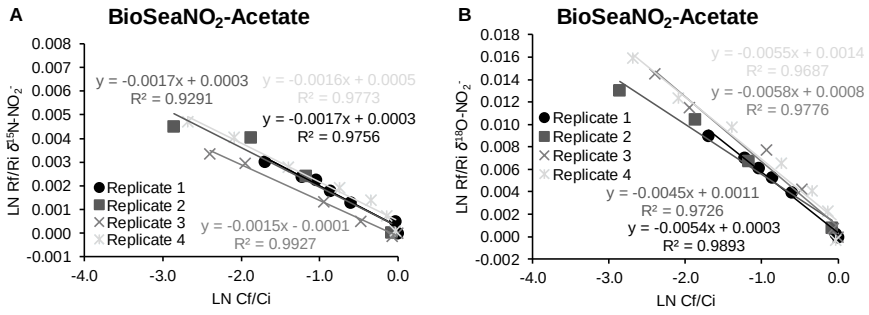

Figure S7. $\varepsilon^{15}N_{NO2}$ and $\varepsilon^{18}O_{NO2}$ calculations for the BioSeaNO$_2$-Acetate experiments. The $\varepsilon^{15}N_{NO2}$ are presented in the left and $\varepsilon^{18}O_{NO}$ in the right.

REFERENCES

Dzombak, D.A., Morel, F., 1990. Surface complexation modeling: hydrous ferric oxide. John Wiley & Sons.

Hiemstra, T., Van Riemsdijk, W.H., 2009. A surface structural model for ferrihydrite I: Sites related to primary charge, molar mass, and mass density. Geochimica et Cosmochimica Acta 73, 4423-4436.

Schwertmann U. and Cornell R. M., Iron Oxides in the Laboratory: Preparation and Characterization, Wiley-VCH Verlag GmbH, Weinheim, Germany, 2007.

ANNEX 3

Evaluating the potential use of a dairy industry residue to induce denitrification in polluted water bodies: a flow-through experiment.

Rosanna Margalef-Marti[1], Raúl Carrey[1], Albert Soler[1], Neus Otero[1,2]

[1] Grup MAiMA, SGR Mineralogia Aplicada, Geoquímica i Geomicrobiologia, Departament de Mineralogia, Petrologia i Geologia Aplicada, Facultat de Ciències de la Terra, Universitat de Barcelona (UB), Barcelona, Spain.

[2] Serra Húnter Fellowship, Generalitat de Catalunya, Spain.

Journal of Environmental Management, Volume 245, 1 September 2019, Pages 86-94
https://doi.org/10.1016/j.jenvman.2019.03.086

Impact factor (JCR/WOS) = 4.9 (2018)
Q1, 37/250 Environmental sciences

Journal of Environmental Management 245 (2019) 86–94

Contents lists available at ScienceDirect

Journal of Environmental Management

journal homepage: www.elsevier.com/locate/jenvman

Research article

Evaluating the potential use of a dairy industry residue to induce denitrification in polluted water bodies: A flow-through experiment

Rosanna Margalef-Marti[a,*], Raúl Carrey[a], Albert Soler[a], Neus Otero[a,b]

[a] Grup MAiMA, SGR Mineralogia Aplicada, Geoquímica I Geomicrobiologia, Departament de Mineralogia, Petrologia I Geologia Aplicada, Facultat de Ciències de la Terra, Universitat de Barcelona (UB), Barcelona, Spain
[b] Serra Húnter Fellowship, Generalitat de Catalunya, Spain

ARTICLE INFO

Keywords:
Groundwater
Isotopic fractionation
Nitrate
Remediation
Whey

ABSTRACT

Improving the effectiveness and economics of strategies to remediate groundwater nitrate pollution is a matter of concern. In this context, the addition of whey into aquifers could provide a feasible solution to attenuate nitrate contamination by inducing heterotrophic denitrification, while recycling an industry residue. Before its application, the efficacy of the treatment must be studied at laboratory-scale to optimize the application strategy in order to avoid the generation of harmful intermediate compounds. To do this, a flow-through denitrification experiment using whey as organic C source was performed, and different C/N ratios and injection periodicities were tested. The collected samples were analyzed to determine the chemical and isotopic composition of N and C compounds. The results proved that whey could promote denitrification. Nitrate was completely removed when using either a 3.0 or 2.0 C/N ratio. However, daily injection with C/N ratios from 1.25 to 1.5 seemed advantageous, since this strategy decreased nitrate concentration to values below the threshold for water consumption while avoiding nitrite accumulation and whey release with the outflow. The isotopic results confirmed that nitrate attenuation was due to denitrification and that the production of DIC was related to bacterial whey oxidation. Furthermore, the isotopic data suggested that when denitrification was not complete, the outflow could present a mix of denitrified and nondenitrified water. The calculated isotopic fractionation values ($\varepsilon^{15}N_{NO3/N2}$ and $\varepsilon^{18}O_{NO3/N2}$) might be applied in the future to quantify the efficiency of the bioremediation treatments by whey application at field-scale.

1. Introduction

Nitrogen is essential for life, but many compounds such as the oxidized forms nitrate (NO_3^-), nitrite (NO_2^-) and nitrogen oxide (N_2O) have been recognized to produce detrimental effects on human health and the environment (Rivett et al., 2008; Vitousek et al., 1997; Ward et al., 2005). A concentration of 0.8 mM NO_3^- is the threshold value for consumption set in the World Health Organization guidelines for drinking water (WHO, 2011) and the European Drinking Water Directive (98/83/EC, 1998) and the threshold established by the Groundwater Framework Directive (2006/118/EC, 2006) as a goal to achieve good groundwater quality status. At the European level, measures aiming to reduce and prevent NO_3^- pollution from agricultural sources have been applied since 1991, following the Nitrates Directive (91/676/EEC, 1991). However, the last available report from the European Environmental Agency shows, for the period 1992–2012, an overall diminution in NO_3^- content in surface water but a flat trend in groundwater (European Environment Agency (EEA), 2015). Sebilo et al. (2013) performed a long-term lysimeter study and found that N is retained in soils for up to 30 years and that due to past fertilizer applications, NO_3^- can continue leaching into groundwater for an additional five decades. Consequently, developing remediation strategies and improving their effectiveness and economics is fundamental.

One of the most studied remediation treatments for removing NO_3^- from water is based on the enhancement of denitrification (Khan and Spalding, 2004; Vidal-Gavilan et al., 2013). Denitrification is the oxidation of an electron donor and subsequent reduction of NO_3^- to harmless gaseous N_2 through a series of enzymatic reactions involving diverse N compounds: $NO_3^- \rightarrow NO_2^- \rightarrow NO \rightarrow N_2O \rightarrow N_2$ (Knowles, 1982). It occurs naturally in the environment if an electron donor is available, if intrinsic denitrifying bacteria are present and if dissolved oxygen concentration is low (Korom, 1992). However, NO_3^- usually persists in groundwater due to electron donor deficiency (Rivett et al., 2008). To overcome this natural limitation, promotion of heterotrophic

* Corresponding author.
E-mail address: rosannamargalef@ub.edu (R. Margalef-Marti).

https://doi.org/10.1016/j.jenvman.2019.03.086
Received 30 January 2019; Received in revised form 15 March 2019; Accepted 16 March 2019

denitrification based on the addition of external carbon (C) sources within the aquifers has already been implemented and demonstrated to be effective (Borden et al., 2012; Critchley et al., 2014; Leverenz et al., 2010; Smith et al., 2001). The specific electron donor compound employed, as well as the feeding strategy, play a critical role in the resulting efficiency (Vidal-Gavilan et al., 2014).

Pure organic C compounds, such as glucose, acetate, ethanol or methanol, effectively promote heterotrophic denitrification (Akunna et al., 1993; Carrey et al., 2014a; Peng et al., 2007). However, since the use of pure compounds might become expensive in long-term treatments, there has been an increasing interest in using alternative organic C sources. The potential use of animal or vegetal waste has already been verified (Grau-Martínez et al., 2017; Trois et al., 2010). However, to promote groundwater remediation within the aquifer, liquid compounds are preferable as they could be easily applied by injection through already constructed wells. In this context, a wine industry residue was recently tested to promote heterotrophic denitrification (Carrey et al., 2018). The use of whey may also be an economically feasible solution to attenuate NO_3^- pollution, while providing waste recycling. To the authors' knowledge, although a few previous studies focused on N removal by lactic acid derived products (Fernández-Nava et al., 2010; Safonov et al., 2018; Sage et al., 2006; Tang et al., 2018), an assessment of whey recycling to promote denitrification by means of isotopic tools has not yet been reported. The dairy industry byproduct has already been demonstrated to be a feasible electron donor to remove other water contaminants, such as Cr^{6+}, trichloroethylene (TCE) or 2,4,6-trinitrotoluene (TNT) (Innemanová et al., 2015; Mclean et al., 2015; Němeček et al., 2015; Orozco et al., 2010). Furthermore, as whey is considered one of the most important pollutants in dairy industry wastewaters, its reuse would decrease the treatment cost (Carvalho et al., 2013). Before field-scale application, laboratory experiments must be performed to assess the viability of using whey to promote denitrification and to assess the occurrence of adverse effects, such as the accumulation of undesirable intermediates or clogging due to a biomass increase (Rodríguez-Escales et al., 2016; Vidal-Gavilan et al., 2014).

Chemical and isotopic characterization has been widely applied to trace natural and induced NO_3^- transformation processes (Aravena and Robertson, 1998; Vidal-Gavilan et al., 2013). In the course of denitrification, unreacted residual NO_3^- becomes enriched in the heavy isotopes ^{15}N and ^{18}O, permitting the differentiation of biological attenuation from other processes, such as dilution, that have no influence on the isotopic signature (Böttcher et al., 1990). The observed isotopic fractionation (ε) of N and O from dissolved NO_3^- can be used to estimate the efficacy of induced denitrification (Mariotti et al., 1988). Furthermore, the isotopic characterization ($\delta^{13}C$) of dissolved organic and inorganic carbon (DOC and DIC) during denitrification might provide knowledge on the fate of the added organic C source (Carrey et al., 2018; Nascimento and Krishnamurthy, 1997).

This work aims to evaluate the suitability of whey to promote heterotrophic denitrification if injected into NO_3^- polluted aquifers. The present study investigates the best strategy to reduce NO_3^- values below the threshold fixed by European Directives, as well as the best strategy to achieve complete whey consumption while preventing the generation of adverse compounds, such as NO_2^-, or excessive biomass. To reach the goal, the response to modifications to the C/N ratio or injection periodicity were assessed by means of a laboratory flow-through experiment. The isotopic composition of N and O from dissolved NO_3^- and C from DOC and DIC were determined throughout the experiment and were discussed along with the chemical characterization.

2. Materials and methods

2.1. Experimental setup

The flow-through experiment was performed simulating aquifer conditions. Synthetic water was prepared with an approximate NO_3^- concentration of 1.9 mM, which was maintained throughout the experiment. The specific chemical composition of the inflow water is shown as supporting information (Table S1).

Synthetic water from the inflow reservoir (2000 mL) flowed from the bottom to the top of a glass column (70 cm long, 8 cm diameter) and was discharged into the outflow reservoir (500 mL). Flow rate was maintained at a constant rate of 0.2 mL/min by using a peristaltic pump (Micropump Reglo digital, 4 channels, ISMATEC). The glass column was filled with silica balls (5 mm diameter) to provide a homogenous porous medium; the total volume was 3.5 L and the water volume was 1.2 L. To monitor the Eh and pH evolution, probes were installed between the column and the outflow container, and values were recorded hourly. All components of the experimental system were connected by Tygon tubes and were installed inside a temperature-regulated chamber set at 14 °C, except the inflow container. Eight sampling points were established: one at the inflow container, six along the glass column at 10 cm intervals (VP1 to VP6) and one at the outflow container. The injection was performed through three injection points located at the same height as the sampling point VP2, near the bottom of the column (Fig. 1).

Before biostimulation (described in section 2.2), an initial operation period with no electron donor injection was carried out in order to assess the system performance (Stage 0). During this initial operation period, a bromide tracer test was conducted to determine the hydraulic parameters of the column. The average water residence time in the column was estimated to be approximately 4 days.

2.2. Electron donor supply

Whey (from ecological stockbreeding) was used as the unique electron donor source to promote heterotrophic denitrifying bacterial growth. The determined nonpurgeable dissolved organic C (NPDOC) and total organic C (TOC) in whey were 2.15 M and 2.48 M, respectively. As whey is known to usually contain a certain amount of NO_3^- (Oliveira et al., 1995), it was assumed that it would also serve as the denitrifying bacteria inoculum. The used whey had NO_3^- and NO_2^- concentrations (determined by high-performance liquid chromatography (HPLC)) of 0.03 mM and 0.14 mM, respectively. Its contribution was considered insignificant in the experiment compared to the synthetic water's initial NO_3^- concentration (1.9 mM) and considering the low volume injected (between 0.25 and 3 mL).

After Stage 0, different feeding strategies (Stages I to VI) were tested by injecting whey in varying C/N ratios and periodicities. The molar C/N ratio was calculated according to the total NPDOC measured in whey. The initial parameters were set according to the literature data and then optimized based on the obtained results. Throughout Stage I, the injection was carried out every 4 days at a 3.0 C/N ratio. Throughout Stages III, IV and V, a daily injection was tested with 2.0, 1.5 and 1.25 C/N ratios, respectively. Stages II and VI, which had no injection, were used to assess the running period of the treatment. The experiment ran for almost 5 months, and samples were periodically obtained according to each stage's purpose. All stages are summarized in Table 1.

2.3. Analytical methods

All samples were immediately filtered when obtained through a 0.2 μm Millipore® filter and stored at 4 °C until analysis, except aliquots for isotopic characterization of N and O of dissolved NO_3^- that were preserved frozen at −20 °C. Aliquots with no headspace were stored for organic and inorganic C concentration and isotopic composition

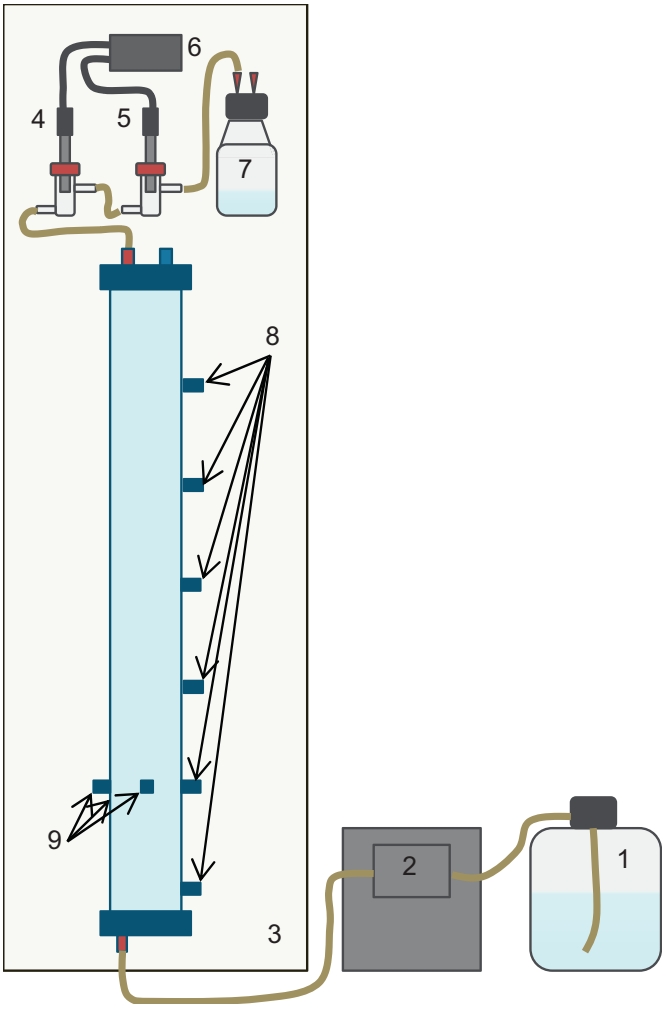

Fig. 1. Scheme of the flow-through experimental design. Components: 1) inflow water, 2) peristaltic pump, 3) refrigerating chamber, 4) Eh probe, 5) pH probe, 6) multiparametric analyzer, 7) outflow water, 8) sampling points (VP1 to VP6) and 9) injection points.

Table 1
Experimental stages during the flow-through experiment. Tested C/N ratios and injection periodicities (IP).

STAGE	DAYS	C/N	IP
0	previous	0.0	NONE
I	0 to 24	3.0	4 days
II	24 to 77	0.0	NONE
III	77 to 99	2.0	1 day
IV	99 to 114	1.25	1 day
V	114 to 144	1.5	1 day
VI	144 to 170	0.0	NONE

determination.

Major anions (Cl^-, NO_2^-, NO_3^- and SO_4^{2-}) were analyzed by HPLC (WATERS 515 pump and WATERS IC-PAK ANIONS column with WATERS 432 and UV/V KONTRON detectors); NH_4^+ was determined by spectrophotometry using the indophenol blue method (CARY 1E UV–visible); DIC was measured by titration (METROHM 702 SM Titrino); NPDOC was analyzed by the organic matter combustion method (TOC 500 SHIMADZU); major cations were determined by ICP-OES (PerkinElmer Optima 8300) and trace elements by ICP-MS (PerkinElmer Elan 6000).

The δ^{15}N-NO_3^- and δ^{18}O-NO_3^- were determined following the cadmium reduction method (McIlvin and Altabet, 2005; Ryabenko et al., 2009). The N_2O was analyzed using a Pre-Con (Thermo Scientific) coupled to a Finnigan MAT 253 Isotope Ratio Mass Spectrometer (IRMS, Thermo Scientific). The δ^{13}C-DIC was analyzed by carbonate conversion to CO_2 gas by adding a phosphoric acid solution and measurement using a Gas-Bench II coupled to a MAT-253 IRMS (Thermo Scientific). The δ^{13}C-DOC was determined by HPLC-IRMS (Delta V ADVANTAGE, Thermo-Finnigan). Notation is expressed in terms of δ ‰ ($\delta = ((R_{sample}-R_{standard})/R_{standard})$, where R is the ratio between the heavy and the light isotopes). The international standards used in this study were: AIR (Atmospheric N_2) for δ^{15}N, V-SMOW (Vienna Standard Mean Oceanic Water) for δ^{18}O and V-PDB (Vienna Peedee Belemnite) for δ^{13}C. According to (Coplen, 2011), several international and laboratory standards were interspersed among samples for normalization of analyses. Three international standards (USGS 32, 34 and 35) and one internal laboratory standard (CCIT-IWS ($\delta^{15}N = +16.9$‰ and $\delta^{18}O = +28.5$‰)) were employed to correct δ^{15}N-NO_3^- and δ^{18}O-NO_3^- values; three internal laboratory standards (CCIT-NaHCO3 ($\delta^{13}C = -4.4$‰), CCIT-NaKHCO3 ($\delta^{13}C = -18.7$‰) and CCIT-KHCO3 ($\delta^{13}C = +29.2$‰)) to correct δ^{13}C-DIC analyses; and one international standard (IAEA-CH6) and two internal laboratory standards (CCIT-Gly ($\delta^{13}C = -30.8$‰) and CCIT-UCGEMA ($\delta^{13}C = -24.8$‰)) to correct δ^{13}C-DOC results. The reproducibility (1σ) of the samples, calculated from the standards systematically interspersed in the analytical batches, was ± 1.0‰ for δ^{15}N-NO_3^-, ± 1.5‰ for δ^{18}O-NO_3^-, ± 0.2‰ for δ^{13}C-DIC and ± 0.3‰ for δ^{13}C-DOC.

Chemical and isotopic analyses were prepared at the laboratory of the MAiMA-UB research group and analyzed at the Centres Científics i Tecnològics of the Universitat de Barcelona (CCiT-UB).

3. Results and discussion

3.1. NO_3^- attenuation promoted by whey injections

The chemical and isotopic composition of N and C compounds from the samples collected throughout the experiment are reported in supporting information, Table S2. The pH and Eh recorded hourly from Stage I to V are presented in supporting information, Fig. S1. While the pH values averaged 7.4 and did not show significant variations along the experiment, the Eh fluctuated from +515 to −345 mV, demonstrating that the whey injections promoted the reducing conditions needed for denitrification. Two days after the first injection in Stage I (injection every four days at a 3.0 C/N ratio), NO_3^- attenuation began and NO_2^- accumulated, reaching 1.5 mM (NO_3^- in the inflow along the experiment was 1.9 ± 0.2 mM). After the peak, NO_2^- started to decrease until both compounds were completely depleted in less than sixteen days from the beginning of the biostimulation strategy (Fig. 2). The lag-phase was short, possibly because significant denitrifying bacterial species were intrinsically present in whey, as it usually contains traces of N compounds (Oliveira et al., 1995). Tang et al. (2018) after inducing denitrification by addition of lactate observed a high microbial diversity encompassed by a diversification on metabolic pathways which even increased when using a complex C source rich in lactic acid. The stimulated bacterial community in the present experiment was not determined since it was not a main goal in the paper, on future field-scale applications, the bacterial community might vary from site to site. In addition to denitrification, the observed NO_3^- reduction could have been promoted by the dissimilatory NO_3^- reduction to ammonium (DNRA). However, during the experiment, NH_4^+ was rarely detected during Stages I, II and III, with concentrations below 0.19 mM. This suggests that denitrification was the main NO_3^- removal process and that DNRA did not contribute significantly to NO_3^- attenuation. After a period with no injection, where NO_3^- concentration progressively increased to the initial values (Stage II), the injection strategy was switched to a daily injection with a 2.0 C/N ratio (Stage III). During Stage III, NO_3^- was also rapidly and completely reduced but with no NO_2^- accumulation. In a similar study, no NO_2^- accumulated during a daily

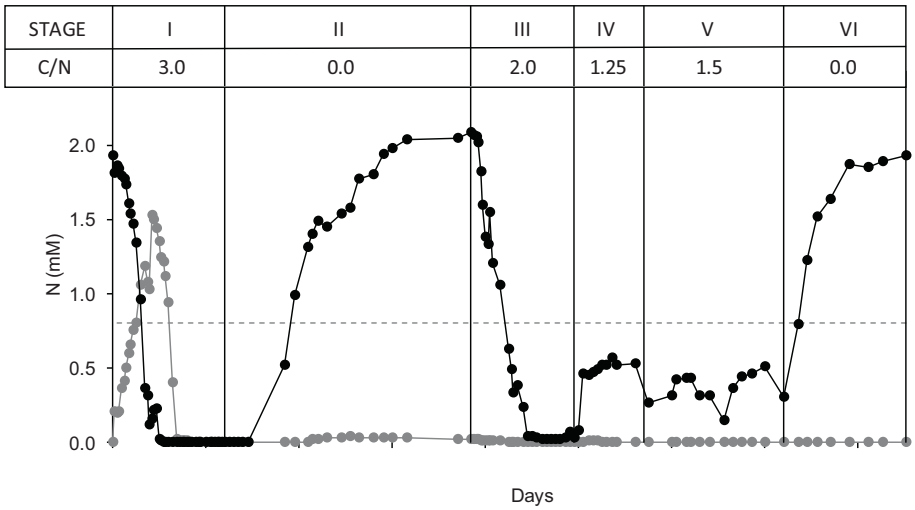

Fig. 2. NO_3^- and NO_2^- evolution. NO_3^- (black dots) and NO_2^- (gray dots) concentration evolution throughout the biostimulation and recovery periods of the flow-through experiment (Stages I to VI). The black vertical lines depict the beginning and the end of each stage, while the gray dashed horizontal line depicts the NO_3^- threshold for water consumption.

injection strategy using a 2.5 C/N ratio tested after a weekly injection strategy that presented NO_2^- values up to 0.7 mM (initial NO_3^- was 1.6 mM) (Vidal-Gavilan et al., 2014). The lack of NO_2^- accumulation during the daily injection strategy was likely due to the latent denitrifying community during the recovery period that quickly adapted when the injections were resumed compared to the beginning of the biostimulation.

During Stages I and III, complete NO_3^- reduction was achieved since the electron donor was in excess. In the following injection periods, lower C/N ratios were tested with a daily injection strategy. With a 1.25 C/N ratio (Stage IV), NO_3^- in the outflow was maintained at approximately 0.5 mM, and with a 1.5 C/N ratio (Stage V), NO_3^- decreased to approximately 0.4 mM. The slight NO_3^- concentration fluctuations observed during Stages IV and V were due to system instability caused by clogging derived from biomass accumulation inside the tubes. Biomass accumulation began at the end of Stage I but increased significantly during the following stages. In a wastewater treatment study, lowering the C/N ratio from 20 to 4 favored a poor flocculation and settleability, which resulted in a higher effluent turbidity and suspended solids (Ye et al., 2011). These results are in accordance with the observed biomass migration across the column and tubes in our experiment and in a similar laboratory biostimulation study performed by (Carrey et al., 2018). The long persistence of denitrification during the recovery Stage II was a demonstration of the excessive organic C supplied during Stage I and suggested the possible use of biomass as a secondary organic C pool, since biomass was observed to be the main electron donor source at low C/N ratios in a similar flow-through experiment (Carrey et al., 2018). After the last whey injection in Stage I, five days were needed to reach NO_3^- levels above the detection limit, and forty days were needed to equal the inflow water NO_3^- concentration. In contrast, the recovery period in Stage VI lasted just eleven days due to the higher initial NO_3^- concentration (approximately 0.5 mM) and the lower C/N ratio. The lower C/N ratio could have also decreased the availability of biomass as a secondary C source during Stage VI compared to Stage II due to the aforementioned promotion of biomass migration and loss with the outflow.

Vertical profile samples were useful in assessing the denitrification process along the column. After biostimulation, both in the case of complete (Stage I) and partial (Stage V) denitrification, a sharp NO_3^- decrease was observed at the bottom of the column, near and below the injection point (16 cm) (Fig. 3A and C). Following the redox sequence, dissolved oxygen from the inflow water should be consumed before NO_3^- is used as an electron acceptor. Therefore, NO_3^- attenuation was expected to be observed above the injection points rather than below. Possibly because whey is denser than water, part of the whey might have accumulated at the bottom of the column, thereby increasing the C/N ratio in the first centimeters of the column, which may have led to strong reducing conditions and, consequently, made the NO_3^- attenuation start below the injection points. This fact should be taken into account in future field-scale applications since whey could flow down to the bottom part of the aquifer due to these density differences. Contrarily, during the recovery period (Stage II), NO_3^- was progressively reduced along the column (Fig. 3B). Conclusions concerning the NO_2^- distribution within the column could not be made since no NO_2^- accumulation was detected when the vertical profile samples were obtained.

3.2. NO_3^- isotopic characterization

Under closed system conditions, the ε can be modeled using a Rayleigh distillation Equation (1). In this way, the ε is obtained from the slope of the linear correlation between the natural logarithm of the substrate remaining fraction ($Ln(C_{residual}/C_{initial})$, where C refers to analyte concentration) and the determined isotope ratios ($Ln(R_{residual}/R_{initial})$, where $R = (\delta+1)$). Despite the column being an open system, as the electron donor and acceptor were replenished, it was assumed that during the injection periods with excess C/N ratios (Stages I and III), the isotopic composition of outflow NO_3^- was solely influenced by the NO_3^- bacterial reduction. The treatment homogeneity was demonstrated by the vertical profile results, showing complete denitrification at the bottom of the column that allowed to discard a mix of treated and nontreated synthetic water at the outflow container. Therefore, we considered it appropriate to use the Rayleigh model to calculate the ε during the biostimulation Stages I and III. Previous studies have demonstrated equal isotopic fractionation between batches and similar flow-through induced denitrification experiments (Carrey et al., 2014b; Grau-Martínez et al., 2017). However, for the recovery (II, VI) and partial denitrification stages (IV, V), a possible mix between denitrified and nondenitrified water could not be discarded and for this reason, the Rayleigh equation was not applied.

$$Ln\left(\frac{R_{residual}}{R_{initial}}\right) = \varepsilon \times Ln\left(\frac{C_{residual}}{C_{initial}}\right) \quad (1)$$

As expected for the NO_3^- biological reduction, a linear correlation between the $\delta^{15}N\text{-}NO_3^-$ and $\delta^{18}O\text{-}NO_3^-$ and the Ln of the remaining NO_3^- concentration was observed in the stages that achieved complete NO_3^- removal (Stages I and III). During both stages, the isotopic composition increased from values of the synthetic water ($\delta^{15}N\text{-}NO_3^- = +16.7‰$ and $\delta^{18}O\text{-}NO_3^- = +28.4‰$) to values up to $\delta^{15}N\text{-}NO_3^- = +45.8‰$ and $\delta^{18}O\text{-}NO_3^- = +77.3‰$ during Stage I and up to $\delta^{15}N$-

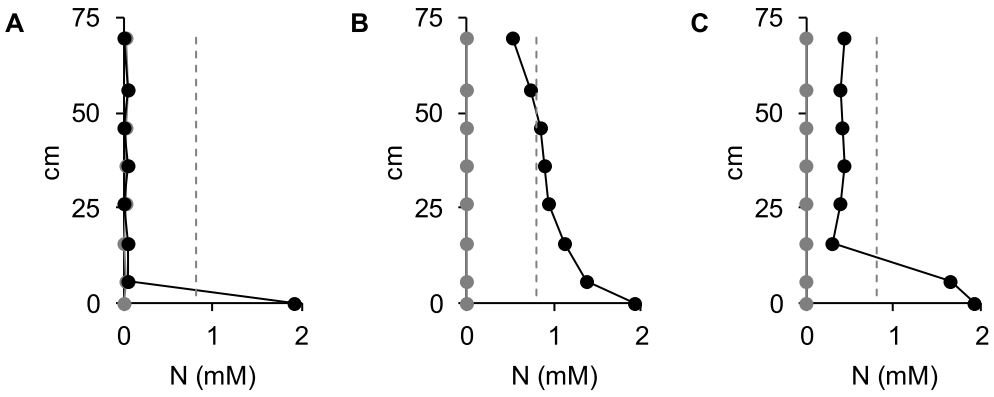

Fig. 3. NO_3^- and NO_2^- vertical profile. NO_3^- (black dots) and NO_2^- (gray dots) concentration along the column. A) Stage I (C/N = 3.0, day 16), B) Stage II (recovery, day 36) and C) Stage V (C/N = 1.5, day 136). The Y axis depicts the height of each sampling point with respect to the bottom of the column (Fig. 1). The gray dashed line depicts the NO_3^- threshold for water consumption.

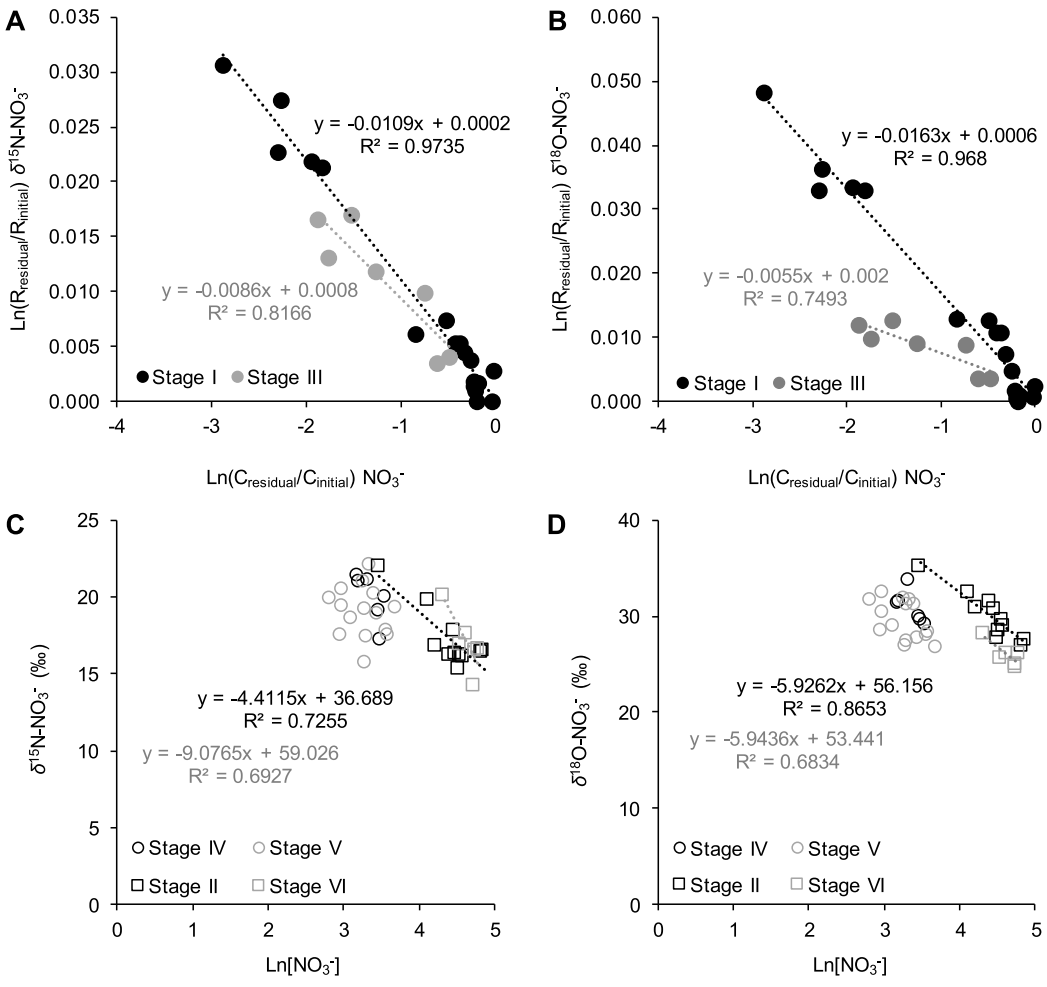

Fig. 4. NO_3^- isotopic results. δ^{15}N-NO_3^- and δ^{18}O-NO_3^- composition versus concentration plots, including the regression line for complete denitrification stages (A and B) and partial denitrification and recovery stages (C and D). For plots A and B, the Rayleigh equation is used (Equation (1)). No regression line is presented for the partial denitrification periods.

NO_3^- = +31.7‰ and δ^{18}O-NO_3^- = +39.6‰ during Stage III. The calculated $\varepsilon^{15}N_{NO3/N2}$ and $\varepsilon^{18}O_{NO3/N2}$ were −10.9‰ and −16.3‰, respectively, for Stage I and −8.6‰ and −5.5‰, respectively, for Stage III (Fig. 4A and B). The resulting $\varepsilon^{15}N/\varepsilon^{18}O$ was 0.7 for Stage I and 1.6 for Stage III. Nevertheless, during the partial denitrification stages (Stages IV and V), no correlation was observed between the isotopic composition and the Ln of the NO_3^- concentration (Fig. 4C and D) or 1/[NO_3^-] (supporting information, Fig. S2). The isotopic values during these stages were close to the synthetic water isotopic composition. For the recovery stages (Stages II and VI), a correlation between the Ln of the remaining NO_3^- concentration and the isotopic composition was again observed (Fig. 4C and D). However, the resulting trend from plotting δ^{15}N-NO_3^- and δ^{18}O-NO_3^- versus 1/[NO_3^-] was better adjusted to a linear correlation than to a logarithmic trend (supporting information, Fig. S2), which is indicative of mixing processes. These results suggested a mix of denitrified and nondenitrified water at the outflow during the recovery and partial denitrification periods.

During the experiment, the NO_3^- isotopic fractionation could have been influenced by several factors. The $\varepsilon^{15}N_{NO3/N2}$ and $\varepsilon^{18}O_{NO3/N2}$ might depend on the enzymes involved in the NO_3^- reduction, the

NO_3^- transport across the cell and the NO_3^- reduction rate, while factors such as the pH or salinity do not seem to provoke significant effects (Granger et al., 2008; Wunderlich et al., 2012). Due to the use of different initial electron donor and acceptor concentrations among the tested stages, the ratio of cellular NO_3^- uptake and efflux before the enzymatic reaction and the NO_3^- reduction rate was expected to play a role in the variability in the $\varepsilon^{15}N_{NO3/N2}$ and $\varepsilon^{18}O_{NO3/N2}$ results. Furthermore, a shift in the $\varepsilon^{15}N/\varepsilon^{18}O$ ratio with respect to 1, the typical recognized value for denitrification, can be attributed to (I) NO_2^- re-oxidation to NO_3^- (Buchwald and Casciotti, 2010; Granger and Wankel, 2016; Wunderlich et al., 2013); (II) NH_4^+ oxidation to NO_3^- (Bourbonnais et al., 2013; Dähnke and Thamdrup, 2016; Granger and Wankel, 2016) and (III) major activity of bacteria containing the periplasmic NO_3^- reductase (NAP) instead of the membrane-bound NO_3^- reductase (NAR) (Granger et al., 2008). For this reason, $\varepsilon^{15}N/\varepsilon^{18}O$ values close to 2 are usually found in field-scale freshwater denitrification studies (Critchley et al., 2014; Otero et al., 2009), while values remain close to 1 in laboratory experiments performed under controlled closed conditions (Carrey et al., 2013; Grau-Martínez et al., 2017). NAP is not expected to be of great significance, since it is not a respiratory enzyme and it is not associated with energy production (Granger et al., 2008 and references therein), and NH_4^+ was rarely detected throughout all the experimental stages. Hence, the most likely explanation for the higher calculated $\varepsilon^{15}N/\varepsilon^{18}O$ value for Stage III (1.6, $r^2 = 0.87$) compared to Stage I (0.7, $r^2 = 0.96$) is the occurrence of NO_2^- reoxidation, since a higher O_2 diffusion into the system was expected during Stage III due to daily injections compared to the decreased periodicity in Stage I. However, other explanations cannot be completely ruled out. The influence of the important N assimilation that took place in Stage I because of the initial biostimulation also needs to be considered and the mix between denitrified and nondenitrified groundwater that occurred during the recovery and partial denitrification stages.

3.3. Whey consumption

NPDOC results showed organic C consumption coupled with NO_3^- reduction. The highest NPDOC concentration at the outflow was observed at the beginning of Stage I but was also significant at the beginning of Stage III (4.9 and 1.6 mM C, respectively, while injected whey was 5.1 and 3.4 mM C, respectively). The initial lack of organic C decrease at the outflow with respect to the injected whey can be explained by the time needed for the establishment of the bacterial community. After the acclimation period of 2 days, NPDOC peaks in the outflow of the column derived from injections decreased progressively (Fig. 5). Apart from the injected electron donor, the organic C resulting from bacterial metabolism, biomass degradation and cellular lysis could also act as a secondary electron donor source, especially at low C/N ratios (Carrey et al., 2018).

The HCO_3^- showed an inverse trend compared to the NO_3^- concentration as expected from heterotrophic denitrification (Equation (2)). The DIC concentration started to increase 5 days after the beginning of injections, with maximum values coinciding with complete NO_3^- depletion at Stages I and III (4.0 and 4.1 mM C, respectively, compared to the background C of 1.8 mM), and its production stopping during the recovery Stage II (Fig. 5). The gap between C derived from injected whey and the sum of the outflow DIC and NPDOC was attributed to biomass and CO_2 production.

$$4NO_3^- + 5C_{org} + 2H_2O \rightarrow 2N_2 + 4HCO_3^- + CO_2 \quad (2)$$

Denitrification studies that include C isotopic characterization are still scarce, likely because it is difficult to separate all the intricate pathways involved in the process. At the beginning of this study (between the second and third injections), as NPDOC in the outflow decreased due to electron donor consumption, the remaining DOC became enriched in $\delta^{13}C$ (Fig. 5). The isotopic fractionation was likely caused because bacteria preferentially consumed the lighter C molecules, leading to an isotopic increase from $\delta^{13}C$-DOC values close to the isotopic composition of whey (−28‰) to $\delta^{13}C$-DOC values in the outflow up to −15‰ (Fig. 5). It must be considered that not only whey and its enzymatic oxidation influence the $\delta^{13}C$-DOC results, since the organic C resulting from bacterial metabolism, biomass degradation or cell lysis events introduces variations in the global $\delta^{13}C$-DOC (Carrey et al., 2018). The $\delta^{13}C$ results only covered the first ten days of Stage I; therefore, it could be assumed that no biomass degradation or cell lysis events occurred, and bacterial biomass organic C pool contribution was negligible in this period. Thus, the observed C isotopic fractionation was related to the enzymatic oxidation of whey. The slope of the regression line between $\delta^{13}C$-DOC and Ln[NPDOC] was −7‰ ($r^2 = 0.66$) (Fig. 6A).

Regarding HCO_3^- production during Stage I, as DIC concentration increased, it became depleted in $\delta^{13}C$ (−17‰), while during Stage II (recovery period), the $\delta^{13}C$-DIC was progressively enriched and coupled to a concentration decrease until both concentration and isotopic composition reached the initial synthetic water values (−8‰) (Fig. 5). Both the $\delta^{13}C$-DIC and DIC concentration remained mainly constant at partial denitrification Stages IV and V. The measured $\delta^{13}C$-DIC at the outflow samples is a mix between the $\delta^{13}C$ of the inflow water DIC (−9‰) and the DIC produced from whey oxidation. For this reason, $\delta^{13}C$-DIC is influenced by the $\delta^{13}C$ of whey (−28‰), the isotopic fractionation produced during bacterial metabolism, and could be affected by the equilibrium between the CO_2(aq), HCO_3^- and CO_3^{2-} species (Blaser and Conrad, 2016; Mariotti, 1991). Observing the isotopic results obtained at each period, a nearly linear correlation

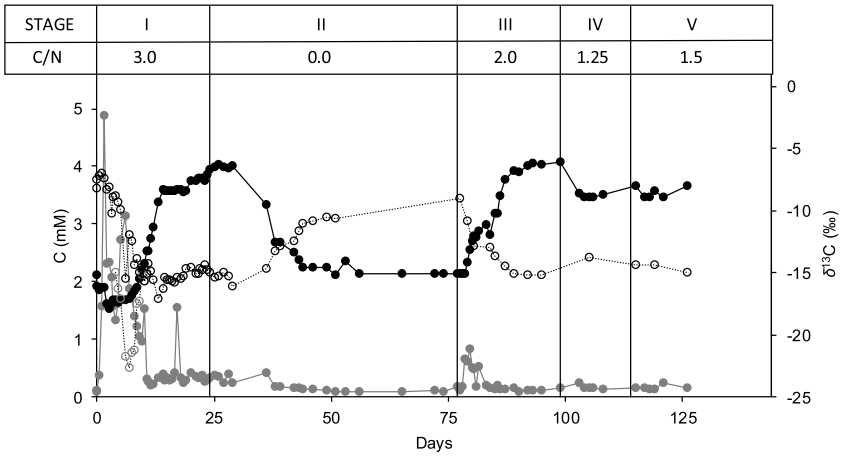

Fig. 5. DIC and NPDOC concentration and isotopic composition evolution. Concentration (full circles) and $\delta^{13}C$ (empty circles) evolution of NPDOC (gray) and DIC (black) throughout the biostimulation and recovery periods of the flow-through experiment (Stages I to V). The black vertical lines depict the beginning and the end of each stage.

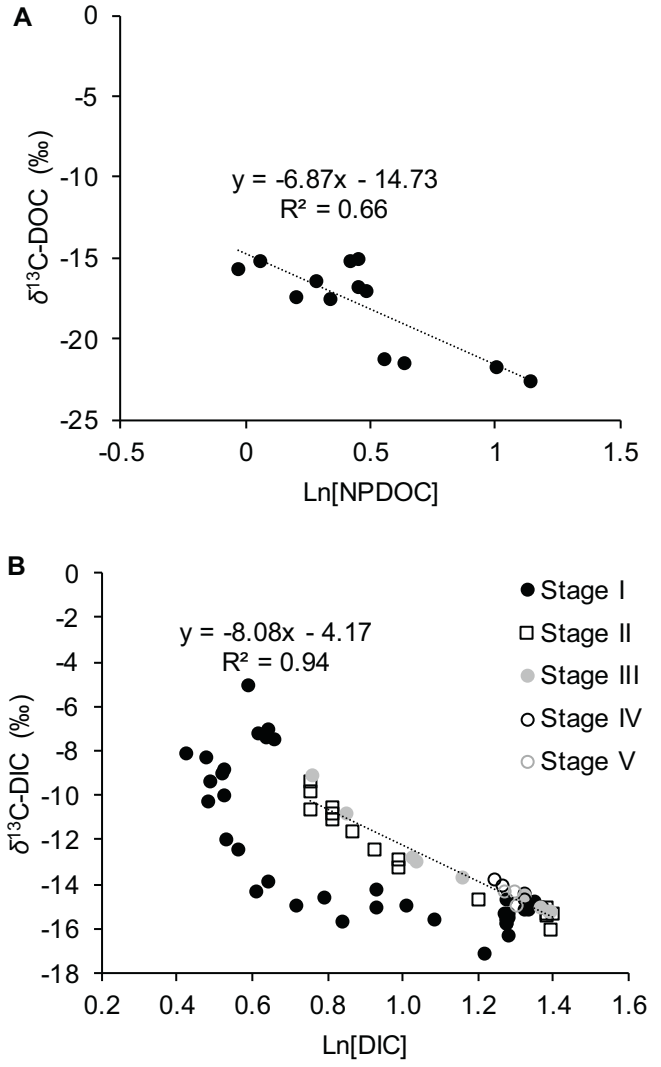

Fig. 6. NPDOC and DIC isotopic composition versus concentration. A) For NPDOC, only results for Stage I were available. B) For DIC, samples from Stages I to V were analyzed.

between δ^{13}C-DIC and Ln[DIC] was observed during Stages II (recovery) and III (complete denitrification period), giving a slope of −8‰ (r^2 = 0.94) (Fig. 6B). However, a nonlinear trend was found for Stage I. The reason could be a higher isotopic fractionation produced during the beginning of Stage I that accounted for most of the biomass generation throughout the study compared to the following stages. In fact, from the middle to the end of Stage I, a line with a parallel trend to the linear correlation obtained for Stages II and III was observed. The results obtained for the few samples collected throughout the partial denitrification Stages IV and V fell at the lower extreme of the regression line plotted for Stages II and III. This can be explained by a higher influence of the inflow water δ^{13}C-DIC on the outflow δ^{13}C-DIC, since during the partial denitrification stages, a lower amount of DIC was produced compared to Stages I and III.

3.4. Suitability for field-scale application

Thinking about this experiment in terms of achieving safe drinking water, semiquantitative ICP analysis in selected outflow water samples was performed to discard possible trace elements released from whey injections (supporting information, Table S3). As no toxic elements were observed to be released and given the results discussed above, whey was considered to be a safe electron donor to promote denitrification in polluted aquifers. For field-scale application, it is recommended to use whey from ecological stockbreeding to avoid the release of antibiotic and hormone residues to the aquifer. Promotion of bacterial metabolic pathways such as DNRA (discussed in section 3.1) or bacterial SO_4^{2-} reduction (BSR), that could also decrease the water quality by generating hydrogen sulphide, were also discarded. Denitrification and BSR can occur simultaneously, especially at high C/N ratios (Laverman et al., 2012), and whey has already been reported to promote BSR (Christensen et al., 1996). Throughout the present experiment, the SO_4^{2-} concentration did not show significant variations, suggesting that the excess of organic C did not lead to BSR. Therefore, the C/N ratios and injection strategies tested in the present study are considered appropriate in terms of being applied in future field-scale projects aiming to remediate NO_3^- polluted groundwater. Furthermore, the release of the greenhouse gases (GHG) CO_2, CH_4 and N_2O during N and C cycling processes has become a matter of concern. In denitrification strategies, parameters such as the water O_2 concentration, the C/N ratio and the temperature might play an important role in GHG emissions (Miettinen et al., 2015; Spoelstra et al., 2010; Teiter and Mander, 2005). In a study to assess N_2O emissions during the heterotrophic denitrification, a lower accumulation was found in laboratory incubations compared to field (Weymann et al., 2010). These authors attributed the discrepancy to sampling and storage procedures and to differences in the dissolved O_2 concentration and the spatial scale. Although the transferability of the laboratory results to field seems to be limited, determining the GHG production in future laboratory studies should be considered aiming to find biostimulation strategies that lowers GHG emissions. Furthermore, in future field-scale induced denitrification tests, monitoring these GHG is needed to check the contribution to global climate change.

Whey could be easily injected through already constructed wells to promote in situ groundwater denitrification in contaminated aquifers, in contrast to solid compounds that might require application through passive systems, such as permeable reactive barriers (Gibert et al., 2008; Huang et al., 2015; Robertson et al., 2008). The following studies of in situ biostimulation by different electron donor supply strategies could be taken as references and could be improved upon: injection through wells placed across the path of the contaminant plume (Tartakovsky et al., 2002); injection through a daisy-like well system (Khan and Spalding, 2004); cross-injection through wells perpendicular to the flow direction (Critchley et al., 2014; Gierczak et al., 2007); injection through infiltration galleries (Salminen et al., 2014); or even pumping groundwater, mixing it with an electron donor in a tank and reinjecting it through wells (Vidal-Gavilan et al., 2013). Another option could be the supply of electron donor at the inlet of a constructed wetland to enhance denitrification (Lin et al., 2002). The advantages and disadvantages of each strategy must be carefully evaluated, and previous hydrogeochemical characterization at the field-scale is crucial to succeed in the operational design. Once a strategy is implemented, the calculated $\varepsilon^{15}N_{NO3/N2}$ and $\varepsilon^{18}O_{NO3/N2}$ in the present experiment could be applied to evaluate the efficiency of the bioremediation treatment, as has been done in previous studies (Vidal-Gavilan et al., 2013). However, attention must be focused on hydrogeochemical effects, such as mixing, dilution or rainfall events, which could influence the results and, thus, hinder the evaluation of the remediation strategy performance. For this reason, coupling isotopic approximation with all possible data obtained throughout the characterization process will provide a more accurate evaluation.

4. Conclusions

Whey can be used as a sustainable electron donor source for groundwater remediation, as it has been demonstrated to effectively promote denitrification. Thus, manufacturing waste could be transformed into profit. A daily injection strategy seems to avoid NO_2^- accumulation, and C/N ratios of approximately 1.25 or 1.5 are enough to

reach NO_3^- concentrations below the threshold for water consumption, while avoiding excess organic C in the effluent, which is advantageous from the perspective of achieving complete whey consumption. However, biomass presence in the water flow due to a decreased settleability at low C/N ratios must be controlled if applied at the field-scale to avoid clogging issues. The NO_3^- isotopic characterization confirmed that complete NO_3^- removal achieved at Stages I and III was due to denitrification and suggested that at partial denitrification stages (IV and V) and at recovery stages (II and VI), the outflow could contain a mix of denitrified and nondenitrified water. The calculated $\varepsilon^{15}N_{NO3/N2}$ and $\varepsilon^{18}O_{NO3/N2}$ of NO_3^- might be applied in future field studies to quantify the efficiency of bioremediation treatments. Using $\delta^{13}C$ analyses might help in assessing the fate of electron donor consumption, as C isotopic composition of products, such as DIC or biomass, is clearly influenced by substrate $\delta^{13}C$ and the isotopic fractionation produced throughout the enzymatic activity. From our results, we observed the bacterial preferential consumption of lighter C molecules, as observed for NO_3^-, and a trend of the produced $\delta^{13}C$-DIC towards the $\delta^{13}C$-DOC of the injected whey. However, the complexity of the bacterial metabolism that can involve diverse pathways of catabolic and anabolic processes and the lack of continuity of the $\delta^{13}C$-DOC analysis hindered the interpretation of the $\delta^{13}C$ results.

Acknowledgements

This work was financed by the projects: REMEDIATION (CGL2014-57215-C4) and PACE-ISOTEC (CGL2017-87216-C4-1-R), both financed by the Spanish Government and the AEI/FEDER from the EU, and MAG (2017 SGR 1733) from the Catalan Government. Margalef-Marti, R. would like to thank the Spanish Government for the Ph.D. grant BES-2015-072882. We would also like to thank the CCiT of the Universitat de Barcelona for the analytical support.

Appendix A. Supplementary data

Supplementary data to this article can be found online at https://doi.org/10.1016/j.jenvman.2019.03.086.

References

2006/118/EC, 2006. Groundwater Directive. Council Directive 2006/118/EC, of 12 December 2006, on the protection of groundwater against pollution and deterioration. [WWW Document]. Off. J. Eur. Comm accessed 4.9.17. http://ec.europa.eu/environment/index_en.htm.

91/676/EEC, 1991. Nitrates Directive. Council Directive 91/676/EEC of 12 December 1991, concerning the protection of waters against pollution caused by nitrates from agricultural sources. [WWW Document]. Off. J. Eur. Comm. http://ec.europa.eu/environment/index_en.htm, Accessed date: 4 September 2017.

98/83/EC, 1998. Drinking Water Directive. Council Directive 98/83/EC, of 3 November 1998, on the quality of water intended for human consumption. [WWW Document]. Off. J. Eur. Comm. http://ec.europa.eu/environment/index_en.htm, Accessed date: 4 September 2017.

Akunna, J.C., Bizeau, C., Moletta, R., 1993. Nitrate and nitrite reductions with anaerobic sludge using various carbon sources: glucose, glycerol, acetic acid, lactic acid and methanol. Water Res. 27, 1303–1312. https://doi.org/10.1016/0043-1354(93)90217-6.

Aravena, R., Robertson, W.D., 1998. Use of multiple isotope tracers to evaluate denitrification in ground water: study of nitrate from a large-flux septic system plume. Gr. Water 36, 975–982.

Blaser, M., Conrad, R., 2016. Stable carbon isotope fractionation as tracer of carbon cycling in anoxic soil ecosystems. Curr. Opin. Biotechnol. 41, 122–129. https://doi.org/10.1016/j.copbio.2016.07.001.

Borden, A.K., Brusseau, M.L., Carroll, K.C., McMillan, A., Akyol, N.H., Berkompas, J., Miao, Z., Jordan, F., Tick, G., Waugh, W.J., Glenn, E.P., 2012. Ethanol addition for enhancing denitrification at the uranium mill tailing site in Monument Valley, AZ. Water Air Soil Pollut. 223, 755–763. https://doi.org/10.1007/s11270-011-0899-1.

Böttcher, J., Strebel, O., Voerkelius, S., Schmidt, H.-L., 1990. Using isotope fractionation of nitrate-nitrogen and nitrate-oxygen for evaluation of microbial denitrification in a sandy aquifer. J. Hydrol. 114, 413–424. https://doi.org/10.1016/0022-1694(90)90068-9.

Bourbonnais, A., Lehmann, M.F., Hamme, R.C., Manning, C.C., Juniper, S.K., 2013. Nitrate elimination and regeneration as evidenced by dissolved inorganic nitrogen isotopes in Saanich Inlet, a seasonally anoxic fjord. Mar. Chem. 157, 194–207. https://doi.org/10.1016/j.marchem.2013.09.006.

Buchwald, C., Casciotti, K.L., 2010. Oxygen isotopic fractionation and exchange during bacterial nitrite oxidation. Limnol. Oceanogr. 55, 1064–1074. https://doi.org/10.4319/lo.2010.55.3.1064.

Carrey, R., Otero, N., Soler, A., Gómez-Alday, J.J., Ayora, C., 2013. The role of Lower Cretaceous sediments in groundwater nitrate attenuation in central Spain: column experiments. Appl. Geochem. 32, 142–152. https://doi.org/10.1016/j.apgeochem.2012.10.009.

Carrey, R., Otero, N., Vidal-Gavilan, G., Ayora, C., Soler, A., Gómez-Alday, J.J., 2014a. Induced nitrate attenuation by glucose in groundwater: flow-through experiment. Chem. Geol. 370, 19–28. https://doi.org/10.1016/j.chemgeo.2014.01.016.

Carrey, R., Rodríguez-Escales, P., Otero, N., Ayora, C., Soler, a., Gómez-Alday, J.J., 2014b. Nitrate attenuation potential of hypersaline lake sediments in central Spain: flow-through and batch experiments. J. Contam. Hydrol. 164, 323–337. https://doi.org/10.1016/j.jconhyd.2014.06.017.

Carrey, R., Rodríguez-Escales, P., Soler, A., Otero, N., 2018. Tracing the role of endogenous carbon in denitrification using wine industry by-product as an external electron donor: coupling isotopic tools with mathematical modeling. J. Environ. Manag. 207, 105–115. https://doi.org/10.1016/j.jenvman.2017.10.063.

Carvalho, F., Prazeres, A.R., Rivas, J., 2013. Cheese whey wastewater: characterization and treatment. Sci. Total Environ. 445–446, 385–396. https://doi.org/10.1016/j.scitotenv.2012.12.038.

Christensen, B., Laake, M., Lien, T., 1996. Treatment of acid mine water by sulfate-reducing bacteria. Results from a bench scale experiment. Water Res. 30, 1617–1624. https://doi.org/10.1016/0043-1354(96)00049-8.

Coplen, T.B., 2011. Guidelines and recommended terms for expression of stable-isotope-ratio and gas-ratio measurement results. Rapid Commun. Mass Spectrom. 25, 2538–2560. https://doi.org/10.1002/rcm.5129.

Critchley, K., Rudolph, D.L., Devlin, J.F., Schillig, P.C., 2014. Stimulating in situ denitrification in an aerobic, highly permeable municipal drinking water aquifer. J. Contam. Hydrol. 171, 66–80. https://doi.org/10.1016/j.jconhyd.2014.10.008.

Dähnke, K., Thamdrup, B., 2016. Isotope fractionation and isotope decoupling during anammox and denitrification in marine sediments. Limnol. Oceanogr. 61, 610–624. https://doi.org/10.1002/lno.10237.

European Environment Agency (EEA), 2015. Nutrient Trend [WWW Document]. https://www.eea.europa.eu/, Accessed date: 2 May 2018.

Fernández-Nava, Y., Marañón, E., Soons, J., Castrillón, L., 2010. Denitrification of high nitrate concentration wastewater using alternative carbon sources. J. Hazard Mater. 173, 682–688. https://doi.org/10.1016/j.jhazmat.2009.08.140.

Gibert, O., Pomierny, S., Rowe, I., Kalin, R.M., 2008. Selection of organic substrates as potential reactive materials for use in a denitrification permeable reactive barrier (PRB). Bioresour. Technol. 99, 7587–7596. https://doi.org/10.1016/j.biortech.2008.02.012.

Gierczak, R., Devlin, J.F., Rudolph, D.L., 2007. Field test of a cross-injection scheme for stimulating in situ denitrification near a municipal water supply well. J. Contam. Hydrol. 89, 48–70. https://doi.org/10.1016/j.jconhyd.2006.08.001.

Granger, J., Wankel, S.D., 2016. Isotopic overprinting of nitrification on denitrification as a ubiquitous and unifying feature of environmental nitrogen cycling. Proc. Natl. Acad. Sci. 113, E6391–E6400. https://doi.org/10.1073/pnas.1601383113.

Granger, J., Sigman, D.M., Lehmann, M.F., Tortell, P.D., 2008. Nitrogen and oxygen isotope fractionation during dissimilatory nitrate reduction by denitrifying bacteria. Limnol. Oceanogr. 53, 2533–2545. https://doi.org/10.4319/lo.2008.53.6.2533.

Grau-Martínez, A., Torrentó, C., Carrey, R., Rodríguez-Escales, P., Domènech, C., Ghiglieri, G., Soler, A., Otero, N., 2017. Feasibility of two low-cost organic substrates for inducing denitrification in artificial recharge ponds: batch and flow-through experiments. J. Contam. Hydrol. 198, 48–58. https://doi.org/10.1016/j.jconhyd.2017.01.001.

Huang, G., Huang, Y., Hu, H., Liu, F., Zhang, Y., Deng, R., 2015. Remediation of nitrate-nitrogen contaminated groundwater using a pilot-scale two-layer heterotrophic-autotrophic denitrification permeable reactive barrier with spongy iron/pine bark. Chemosphere 130, 8–16. https://doi.org/10.1016/j.chemosphere.2015.02.029.

Innemanová, P., Velebová, R., Filipová, A., Čvančarová, M., Pokorný, P., Němeček, J., Cajthaml, T., 2015. Anaerobic in situ biodegradation of TNT using whey as an electron donor: a case study. N. Biotech. 32, 701–709. https://doi.org/10.1016/j.nbt.2015.03.014.

Khan, I.A., Spalding, R.F., 2004. Enhanced in situ denitrification for a municipal well. Water Res. 38, 3382–3388. https://doi.org/10.1016/j.watres.2004.04.052.

Knowles, R., 1982. Denitrification. Microbiol. Rev. 46, 43–70.

Korom, S.F., 1992. Natural denitrification in the saturated zone: a review. Water Resour. Res. 28, 1657–1668. https://doi.org/10.1029/92WR00252.

Laverman, A.M., Pallud, C., Abell, J., Van Cappellen, P., 2012. Comparative survey of potential nitrate and sulfate reduction rates in aquatic sediments. Geochim. Cosmochim. Acta 77, 474–488. https://doi.org/10.1016/j.gca.2011.10.033.

Leverenz, H.L., Haunschild, K., Hopes, G., Tchobanoglous, G., Darby, J.L., 2010. Anoxic treatment wetlands for denitrification. Ecol. Eng. 36, 1544–1551. https://doi.org/10.1016/j.ecoleng.2010.03.014.

Lin, Y.F., Jing, S.R., Wang, T.W., Lee, D.Y., 2002. Effects of macrophytes and external carbon sources on nitrate removal from groundwater in constructed wetlands. Environ. Pollut. 119, 413–420. https://doi.org/10.1016/S0269-7491(01)00299-8.

Mariotti, A., 1991. Le carbone 13 en abondance naturelle, traceur de la dynamique de la matière organique des sols et de l'évolution des paléoenvironnements continentaux. Cah. Orstom, sér. Pédol. XXVI, 299–313.

Mariotti, A., Landreau, A., Simon, B., 1988. ^{15}N isotope biogeochemistry and natural denitrification process in groundwater: application to the chalk aquifer of northern France. Geochim. Cosmochim. Acta 52, 1869–1878. https://doi.org/10.1016/0016-7037(88)90010-5.

McIlvin, M.R., Altabet, M.A., 2005. Chemical conversion of nitrate and nitrite to nitrous oxide for nitrogen and oxygen isotopic analysis in freshwater and seawater. Anal. Chem. 77, 5589–5595. https://doi.org/10.1021/ac050528s.

Mclean, J.E., Ervin, J., Zhou, J., Sorensen, D.L., Dupont, R.R., 2015. Biostimulation and bioaugmentation to enhance reductive dechlorination of TCE in a long-term flow through column study. Groundw. Monit. Remediat. 35, 76–88. https://doi.org/10.1111/gwmr.12113.

Miettinen, H., Pumpanen, J., Heiskanen, J.J., 2015. Towards a more comprehensive understanding of lacustrine greenhouse gas dynamics — two-year measurements of concentrations and fluxes of CO_2, CH_4 and N_2O in a typical boreal lake surrounded by managed forests. Boreal Environ. Res. 20, 75–89.

Nascimento, C., Krishnamurthy, R.V., 1997. Inorganic carbon in denitrifying environments investigation. Geophys. Res. Lett. 24, 1511–1514.

Němeček, J., Pokorný, P., Lacinová, L., Černík, M., Masopustová, Z., Lhotský, O., Filipová, A., Cajthaml, T., 2015. Combined abiotic and biotic in-situ reduction of hexavalent chromium in groundwater using nZVI and whey: a remedial pilot test. J. Hazard Mater. 300, 670–679. https://doi.org/10.1016/j.jhazmat.2015.07.056.

Oliveira, C.P., Gloria, M.B.A., Barbour, J.F., Scanlan, R.A., 1995. Nitrate, nitrite, and volatile nitrosamines in whey-containing food products. J. Agric. Food Chem. 43, 967–969. https://doi.org/10.1021/jf00052a023.

Orozco, A.M.F., Contreras, E.M., Zaritzky, N.E., 2010. Cr(VI) reduction capacity of activated sludge as affected by nitrogen and carbon sources, microbial acclimation and cell multiplication. J. Hazard Mater. 176, 657–665. https://doi.org/10.1016/j.jhazmat.2009.11.082.

Otero, N., Torrentó, C., Soler, A., Menció, A., Mas-Pla, J., 2009. Monitoring groundwater nitrate attenuation in a regional system coupling hydrogeology with multi-isotopic methods: the case of Plana de Vic (Osona, Spain). Agric. Ecosyst. Environ. 133, 103–113. https://doi.org/10.1016/j.agee.2009.05.007.

Peng, Y.Z., Ma, Y., Wang, S.Y., 2007. Denitrification potential enhancement by addition of external carbon sources in a pre-denitrification process. J. Environ. Sci. 19, 284–289. https://doi.org/10.1016/S1001-0742(07)60046-1.

Rivett, M.O., Buss, S.R., Morgan, P., Smith, J.W.N., Bemment, C.D., 2008. Nitrate attenuation in groundwater: a review of biogeochemical controlling processes. Water Res. 42, 4215–4232. https://doi.org/10.1016/j.watres.2008.07.020.

Robertson, W.D., Vogan, J.L., Lombardo, P.S., 2008. Nitrate removal rates in a 15 Year old permeable reactive barrier treating septic system nitrate. Gr. Water Monit. Remediat. 28, 65–72.

Rodríguez-Escales, P., Folch, A., Vidal-Gavilan, G., van Breukelen, B.M., 2016. Modeling biogeochemical processes and isotope fractionation of enhanced in situ biodenitrification in a fractured aquifer. Chem. Geol. 425, 52–64. https://doi.org/10.1016/j.chemgeo.2016.01.019.

Ryabenko, E., Altabet, M. a., Wallace, D.W.R., 2009. Effect of chloride on the chemical conversion of nitrate to nitrous oxide for $\delta^{15}N$ analysis. Limnol Oceanogr. Methods 7, 545–552. https://doi.org/10.4319/lom.2009.7.545.

Safonov, A.V., Babich, T.L., Sokolova, D.S., Grouzdev, D.S., Tourova, T.P., Poltaraus, A.B., Zakharova, E.V., Merkel, A.Y., Novikov, A.P., Nazina, T.N., 2018. Microbial community and in situ bioremediation of groundwater by nitrate removal in the zone of a radioactive waste surface repository. Front. Microbiol. 9, 1–17. https://doi.org/10.3389/fmicb.2018.01985.

Sage, M., Daufin, G., Gésan-Guiziou, G., 2006. Denitrification potential and rates of complex carbon source from dairy effluents in activated sludge system. Water Res. 40, 2747–2755. https://doi.org/10.1016/j.watres.2006.04.005.

Salminen, J.M., Petäjäjärvi, S.J., Tuominen, S.M., Nystén, T.H., 2014. Ethanol-based in situ bioremediation of acidified, nitrate-contaminated groundwater. Water Res. 63, 306–315. https://doi.org/10.1016/j.watres.2014.06.013.

Sebilo, M., Mayer, B., Nicolardot, B., Pinay, G., Mariotti, A., 2013. Long-term fate of nitrate fertilizer in agricultural soils. Proc. Natl. Acad. Sci. U. S. A 110 18185–9. https://doi.org/10.1073/pnas.1305372110.

Smith, R.L., Miller, D.N., Brooks, M.H., Widdowson, M.A., Killingstad, M.W., 2001. In situ stimulation of groundwater denitrification with formate to remediate nitrate contamination. Environ. Sci. Technol. 35, 196–203. https://doi.org/10.1021/es001360p.

Spoelstra, J., Schiff, S.L., Semkin, R.G., Jeffries, D.S., Elgood, R.J., 2010. Nitrate attenuation in a small temperate wetland following forest harvest. For. Ecol. Manage. 259, 2333–2341. https://doi.org/10.1016/j.foreco.2010.03.006.

Tang, J., Wang, X.C., Hu, Y., Pu, Y., Huang, J., Hao Ngo, H., Zeng, Y., Li, Y., 2018. Nitrogen removal enhancement using lactic acid fermentation products from food waste as external carbon sources: performance and microbial communities. Bioresour. Technol. 256, 259–268. https://doi.org/10.1016/j.biortech.2018.02.033.

Tartakovsky, B., Millette, D., Del Isle, S., Guiot, S.R., 2002. Ethanol-stimulated bioremediation of nitrate-contaminated ground water. Gr. Water Monit. Remediat. https://doi.org/10.1111/j.1745-6592.2002.tb00656.x.

Teiter, S., Mander, Ü., 2005. Emission of N_2O, N_2, CH_4, and CO_2 from constructed wetlands for wastewater treatment and from riparian buffer zones. Ecol. Eng. 25, 528–541. https://doi.org/10.1016/j.ecoleng.2005.07.011.

Trois, C., Pisano, G., Oxarango, L., 2010. Alternative solutions for the bio-denitrification of landfill leachates using pine bark and compost. J. Hazard Mater. 178, 1100–1105. https://doi.org/10.1016/j.jhazmat.2010.01.054.

Vidal-Gavilan, G., Folch, A., Otero, N., Solanas, A.M., Soler, A., 2013. Isotope characterization of an in situ biodenitrification pilot-test in a fractured aquifer. Appl. Geochem. 32, 153–163. https://doi.org/10.1016/j.apgeochem.2012.10.033.

Vidal-Gavilan, G., Carrey, R., Solanas, A., Soler, A., 2014. Feeding strategies for groundwater enhanced biodenitrification in an alluvial aquifer: chemical, microbial and isotope assessment of a 1D flow-through experiment. Sci. Total Environ. 494–495, 241–251. https://doi.org/10.1016/j.scitotenv.2014.06.100.

Vitousek, P.M., Aber, J.D., Howarth, R.W., Likens, G.E., Matson, P.A., Schindler, D.W., Schlesinger, W.H., Tilman, D.G., 1997. Human alteration of the global nitrogen cycle: sources and consequences. Ecol. Appl. 7, 737–750. https://doi.org/10.1017/CBO9781107415324.004.

Ward, M.H., deKok, T.M., Levallois, P., Brender, J., Gulis, G., Nolan, B.T., VanDerslice, J., 2005. Workgroup report: drinking-water nitrate and health - recent findings and research needs. Environ. Health Perspect. 113, 1607–1614. https://doi.org/10.1289/ehp.8043.

Weymann, D., Geistlinger, H., Well, R., Von Der Heide, C., Flessa, H., 2010. Kinetics of N_2O production and reduction in a nitrate-contaminated aquifer inferred from laboratory incubation experiments. Biogeosciences 7, 1953–1972. https://doi.org/10.5194/bg-7-1953-2010.

WHO, 2011. Guidelines for Drinking-Water Quality, fourth ed. WHO, Geneva, pp. 340. World Heal. Organ. https://doi.org/10.1016/S1462-0758(00)00006-6.

Wunderlich, A., Meckenstock, R., Einsiedl, F., 2012. Effect of different carbon substrates on nitrate stable isotope fractionation during microbial denitrification. Environ. Sci. Technol. 46, 4861–4868. https://doi.org/10.1021/es204075b.

Wunderlich, A., Meckenstock, R.U., Einsiedl, F., 2013. A mixture of nitrite-oxidizing and denitrifying microorganisms affects the $\delta^{18}O$ of dissolved nitrate during anaerobic microbial denitrification depending on the $\delta^{18}O$ of ambient water. Geochim. Cosmochim. Acta 119, 31–45. https://doi.org/10.1016/j.gca.2013.05.028.

Ye, F., Ye, Y., Li, Y., 2011. Effect of C/N ratio on extracellular polymeric substances (EPS) and physicochemical properties of activated sludge flocs. J. Hazard Mater. 188, 37–43. https://doi.org/10.1016/j.jhazmat.2011.01.043.

Journal of Environmental Management 247 (2019) 877

Contents lists available at ScienceDirect

Journal of Environmental Management

journal homepage: www.elsevier.com/locate/jenvman

Corrigendum

Corrigendum to "Evaluating the potential use of a dairy industry residue to induce denitrification in polluted water bodies: A flow-through experiment" [J. Environ. Manag. 245, 2019, 86–94]

Rosanna Margalef-Marti[a,*], Raúl Carrey[a], Albert Soler[a], Neus Otero[a,b]

[a] Grup MAiMA, SGR Mineralogia Aplicada, Geoquímica i Geomicrobiologia, Departament de Mineralogia, Petrologia i Geologia Aplicada, Facultat de Ciències de la Terra, Universitat de Barcelona (UB), Barcelona, Spain
[b] Serra Húnter Fellowship, Generalitat de Catalunya, Spain

In the original article, the X axis numbering in Figure 2 is missing. The correct Figure 2 appears below.

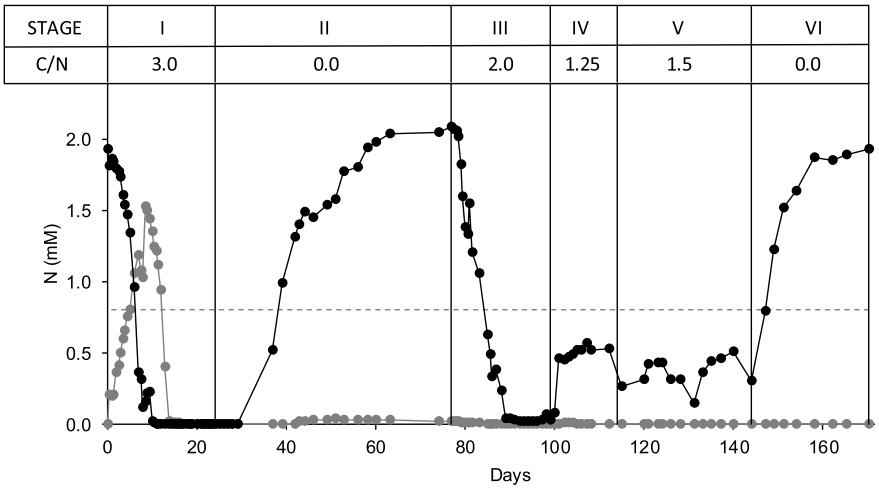

DOI of original article: https://doi.org/10.1016/j.jenvman.2019.03.086
* Corresponding author. Departament de Mineralogia, Petrologia i Geologia Aplicada, Facultat de Ciències de la Terra, Universitat de Barcelona, Spain.
E-mail address: rosannamargalef@ub.edu (R. Margalef-Marti).

https://doi.org/10.1016/j.jenvman.2019.06.065

Available online 21 June 2019

SUPPLEMENTARY INFORMATION TO:

Evaluating the potential use of a dairy industry residue to induce denitrification in polluted water bodies: a flow-through experiment.

Rosanna Margalef-Marti[1], Raúl Carrey[1], Albert Soler[1], Neus Otero[1,2]

[1] Grup MAiMA, SGR Mineralogia Aplicada, Geoquímica i Geomicrobiologia, Departament de Mineralogia, Petrologia i Geologia Aplicada, Facultat de Ciències de la Terra, Universitat de Barcelona (UB), Barcelona (Spain).

[2] Serra Húnter Fellowship, Generalitat de Catalunya, Spain.

Journal of Environmental Management

Volume 245, 1 September 2019, Pages 86-94

https://doi.org/10.1016/j.jenvman.2019.03.086

Figure S1. Eh and pH evolution. Eh (black dots) and pH (gray dots) values from the beginning of biostimulation at Stage I until the middle of Stage V. The black vertical lines depict the beginning and the end of each stage.

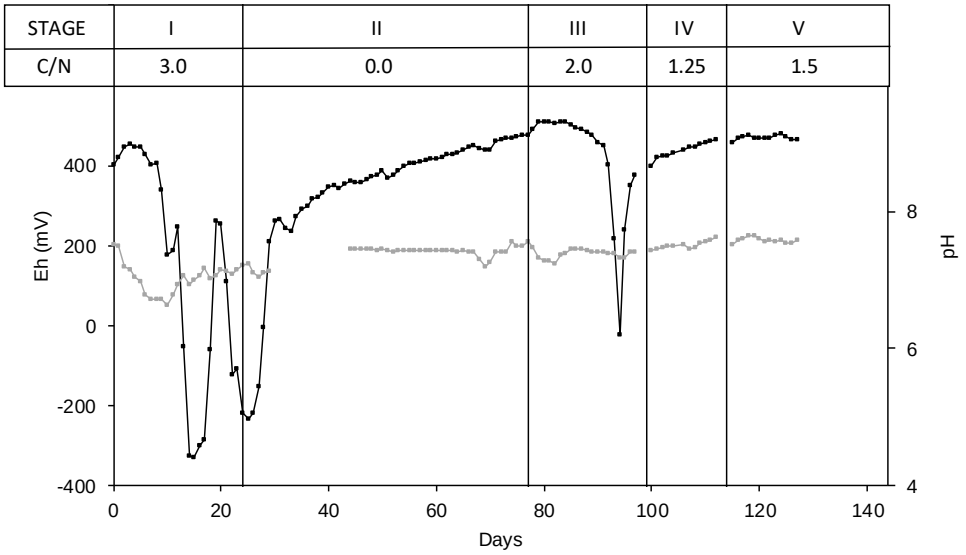

Figure S2. NO_3^- isotopic composition versus 1/[NO_3^-] plots. δ^{15}N-NO_3^- (A) and δ^{18}O-NO_3^- (B) for each stage against 1/[NO_3^-]. Stage I and III correspond to complete denitrification periods, Stage IV and V to partial denitrification periods and Stage II and VI to recovery periods. The correlation for the logarithmic trend obtained for Stage I and III is presented as dashed lines, while the linear trend for Stage II and VI is presented as continuous lines.

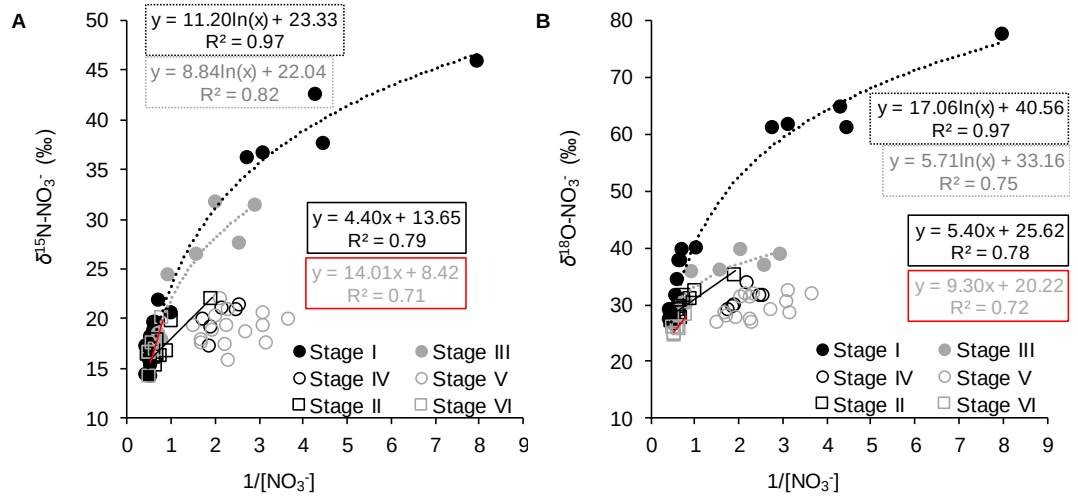

Table S1. Inflow water composition. Concentration of the reagents employed in the preparation of the synthetic water.

Chemical	mM
$CHNaO_3$	1.80
KH_2PO_4	0.03
$MgCl_2 \cdot 6H_2O$	1.25
KCl	1.45
$CaCl_2 \cdot 2H_2O$	0.85
Na_2SO_4	1.45
$NaNO_3$	1.90

Table S2. N and C compounds chemical and isotopic results. Measured concentration and isotopic composition of the N and C compounds from the samples collected throughout the flow-through experiment. “n.a.” refers to samples that were not analyzed.

		NO_3^- (mM)	NO_2^- (mM)	NH_4^+ (mM)	$\delta^{15}N\text{-}NO_3^-$ (‰)	SD ($\delta^{15}N\text{-}NO_3^-$)	$\delta^{18}O\text{-}NO_3^-$ (‰)	SD ($\delta^{18}O\text{-}NO_3^-$)	DIC (mM)	NPDOC (mM)	$\delta^{13}C$-DIC (‰)	$\delta^{13}C$-DOC (‰)
	DAY	SAMPLES COLLECTED AT THE OUTLET										
STAGE I	0.0	1.9	0.0	n.a.	14.4	0.1	27.2	1.5	1.9	0.1	-7.5	n.a.
	0.5	1.8	0.2	n.a.	15.3	0.1	27.2	0.2	1.8	0.1	-7.2	n.a.
	1.0	1.9	0.2	n.a.	16.0	0.1	27.5	0.0	1.9	0.4	-7.0	n.a.
	1.5	1.8	0.2	n.a.	14.3	0.1	26.5	0.1	1.9	1.6	-7.4	n.a.
	2.0	1.8	0.4	n.a.	15.7	0.0	27.7	0.0	1.6	4.9	-8.3	n.a.
	2.5	1.8	0.4	n.a.	16.1	0.0	28.4	0.5	1.5	2.3	-8.1	n.a.
	3.0	1.7	0.5	n.a.	18.2	0.4	31.4	0.7	1.6	2.3	-10.2	n.a.
	3.5	1.6	0.6	0.1	18.8	0.0	34.2	0.6	1.7	2.1	-8.9	n.a.
	4.0	1.5	0.7	n.a.	19.7	0.1	37.6	0.6	1.7	1.6	-8.8	-15.0
	4.5	1.5	0.8	n.a.	19.6	0.2	37.7	0.4	1.6	1.3	-9.3	-16.3
	5.0	1.3	0.8	n.a.	21.8	0.1	39.6	0.3	1.7	1.6	-9.9	-17.0
	6.0	1.0	1.1	0.0	20.5	0.2	40.0	0.2	1.7	2.7	-15.4	-21.7
	7.0	0.4	1.2	n.a.	36.1	0.1	60.9	0.9	1.7	3.1	-12.0	-22.6
	7.5	0.3	1.1	0.0	36.7	0.3	61.5	0.3	1.8	1.9	-12.4	-21.4
	8.0	0.1	1.0	n.a.	45.8	0.5	77.3	0.0	1.8	1.7	-14.3	-21.2
	8.5	0.2	1.5	n.a.	n.a.	n.a.	n.a.	n.a.	1.9	1.4	-13.9	-17.5
	9.0	0.2	1.5	n.a.	37.6	0.3	61.1	0.2	2.1	1.2	-14.9	-17.3
	9.5	0.2	1.4	n.a.	42.5	0.2	64.5	0.1	2.2	1.1	-14.6	-15.2
	10.0	0.0	1.4	n.a.	n.a.	n.a.	n.a.	n.a.	2.3	1.0	-15.7	-15.6
	10.5	0.0	1.2	n.a.	n.a.	n.a.	n.a.	n.a.	2.5	1.5	-15.0	-15.1

Table S2. Continued.

		NO_3^- (mM)	NO_2^- (mM)	NH_4^+ (mM)	$\delta^{15}N\text{-}NO_3^-$ (‰)	SD ($\delta^{15}N\text{-}NO_3^-$)	$\delta^{18}O\text{-}NO_3^-$ (‰)	SD ($\delta^{18}O\text{-}NO_3^-$)	DIC (mM)	NPDOC (mM)	$\delta^{13}C$-DIC (‰)	$\delta^{13}C$-DOC (‰)
	DAY	SAMPLES COLLECTED AT THE OUTLET										
STAGE I	11.0	0.0	1.2	n.a.	n.a.	n.a.	n.a.	n.a.	2.5	0.3	-14.2	n.a.
	11.5	0.0	1.1	0.0	n.a.	n.a.	n.a.	n.a.	2.7	0.3	-14.9	n.a.
	12.0	0.0	0.9	n.a.	n.a.	n.a.	n.a.	n.a.	3.0	0.2	-15.5	n.a.
	13.0	0.0	0.4	n.a.	n.a.	n.a.	n.a.	n.a.	3.4	0.2	-17.1	n.a.
	14.0	0.0	0.0	n.a.	n.a.	n.a.	n.a.	n.a.	3.6	0.3	-16.3	n.a.
	14.5	0.0	0.0	n.a.	n.a.	n.a.	n.a.	n.a.	3.6	0.4	-15.4	n.a.
	15.0	0.0	0.0	n.a.	n.a.	n.a.	n.a.	n.a.	3.6	0.3	-15.5	n.a.
	15.5	0.0	0.0	n.a.	n.a.	n.a.	n.a.	n.a.	3.6	0.3	-15.5	n.a.
	16.0	0.0	0.0	0.1	n.a.	n.a.	n.a.	n.a.	3.6	0.3	-15.7	n.a.
	16.5	0.0	0.0	n.a.	n.a.	n.a.	n.a.	n.a.	3.6	0.3	-15.8	n.a.
	17.0	0.0	0.0	n.a.	n.a.	n.a.	n.a.	n.a.	3.6	n.a.	-15.3	n.a.
	18.0	0.0	0.0	n.a.	n.a.	n.a.	n.a.	n.a.	3.6	0.4	-15.5	n.a.
	18.5	0.0	0.0	n.a.	n.a.	n.a.	n.a.	n.a.	3.6	1.6	-15.3	-16.7
	19.0	0.0	0.0	n.a.	n.a.	n.a.	n.a.	n.a.	3.6	0.3	-14.7	n.a.
	20.0	0.0	0.0	0.0	n.a.	n.a.	n.a.	n.a.	3.8	0.3	-14.6	n.a.
	21.0	0.0	0.0	n.a.	n.a.	n.a.	n.a.	n.a.	3.8	0.3	-15.1	n.a.
	21.5	0.0	0.0	n.a.	n.a.	n.a.	n.a.	n.a.	3.8	0.4	-15.1	n.a.
	22.0	0.0	0.0	n.a.	n.a.	n.a.	n.a.	n.a.	3.8	0.3	-14.7	n.a.
	22.5	0.0	0.0	n.a.	n.a.	n.a.	n.a.	n.a.	3.8	0.3	-14.7	n.a.
	23.0	0.0	0.0	n.a.	n.a.	n.a.	n.a.	n.a.	3.8	0.3	-14.4	n.a.
	23.5	0.0	0.0	n.a.	n.a.	n.a.	n.a.	n.a.	3.8	0.4	-14.8	n.a.
	24.0	0.0	0.0	n.a.	n.a.	n.a.	n.a.	n.a.	3.9	0.3	-15.0	n.a.

Table S2. Continued.

		NO_3^- (mM)	NO_2^- (mM)	NH_4^+ (mM)	$\delta^{15}N\text{-}NO_3^-$ (‰)	SD ($\delta^{15}N\text{-}NO_3^-$)	$\delta^{18}O\text{-}NO_3^-$ (‰)	SD ($\delta^{18}O\text{-}NO_3^-$)	DIC (mM)	NPDOC (mM)	$\delta^{13}C$-DIC (‰)	$\delta^{13}C$-DOC (‰)
	DAY	SAMPLES COLLECTED AT THE OUTLET										
STAGE II	25.0	0.0	0.0	n.a.	n.a.	n.a.	n.a.	n.a.	4.0	0.3	-15.4	n.a.
	26.0	0.0	0.0	n.a.	n.a.	n.a.	n.a.	n.a.	4.0	0.3	-15.3	n.a.
	27.0	0.0	0.0	n.a.	n.a.	n.a.	n.a.	n.a.	4.0	0.4	-15.0	n.a.
	28.0	0.0	0.0	n.a.	n.a.	n.a.	n.a.	n.a.	4.0	0.4	-15.2	n.a.
	29.0	0.0	0.0	0.0	n.a.	n.a.	n.a.	n.a.	4.0	0.2	-16.0	n.a.
	36.0	0.5	0.0	0.2	22.0	0.2	35.1	0.1	3.3	0.4	-14.7	n.a.
	38.0	1.1	0.0	n.a.	16.8	0.0	30.9	0.1	2.7	0.3	-13.2	n.a.
	39.0	1.0	0.0	n.a.	19.8	0.1	32.4	1.0	2.7	0.4	-12.9	n.a.
	42.0	1.3	0.0	n.a.	16.3	0.7	31.5	0.3	2.5	0.2	-12.4	n.a.
	43.0	1.4	0.0	n.a.	17.8	0.5	30.7	0.5	2.4	0.2	-11.6	n.a.
	44.0	1.5	0.0	0.1	15.3	0.2	28.5	0.3	2.3	0.2	-11.0	n.a.
	46.0	1.4	0.0	n.a.	16.3	0.1	27.7	0.2	2.3	0.2	-10.8	n.a.
	49.0	1.5	0.0	n.a.	16.3	0.6	29.6	1.0	2.3	0.1	-10.5	n.a.
	51.0	1.6	0.0	n.a.	16.1	0.2	29.0	0.8	2.1	0.1	-10.6	n.a.
	53.0	1.8	0.0	n.a.	n.a.	n.a.	n.a.	n.a.	2.3	0.1	n.a.	n.a.
	56.0	1.8	0.0	n.a.	n.a.	n.a.	n.a.	n.a.	2.1	0.1	n.a.	n.a.
	58.0	1.9	0.0	n.a.	n.a.	n.a.	n.a.	n.a.	2.1	0.1	-9.8	n.a.
	60.0	2.0	0.0	n.a.	n.a.	n.a.	n.a.	n.a.	n.a.	0.1	n.a.	n.a.
	63.0	2.0	0.0	0.0	16.4	0.2	27.0	1.0	2.1	0.1	-9.3	n.a.
	65.0	1.7	0.0	n.a.	n.a.	n.a.	n.a.	n.a.	2.1	0.1	n.a.	n.a.
	72.0	1.4	0.0	n.a.	n.a.	n.a.	n.a.	n.a.	2.1	0.1	n.a.	n.a.
	74.0	2.1	0.0	n.a.	n.a.	n.a.	n.a.	n.a.	2.1	0.2	n.a.	n.a.

Table S2. Continued.

		NO_3^- (mM)	NO_2^- (mM)	NH_4^+ (mM)	$\delta^{15}N\text{-}NO_3^-$ (‰)	SD ($\delta^{15}N\text{-}NO_3^-$)	$\delta^{18}O\text{-}NO_3^-$ (‰)	SD ($\delta^{18}O\text{-}NO_3^-$)	DIC (mM)	NPDOC (mM)	$\delta^{13}C$-DIC (‰)	$\delta^{13}C$-DOC (‰)
	DAY	SAMPLES COLLECTED AT THE OUTLET										
STAGE II	77.0	2.1	0.0	n.a.	16.5	1.0	27.5	0.2	2.1	n.a.	n.a.	n.a.
STAGE III	77.5	2.1	0.0	n.a.	n.a.	n.a.	n.a.	n.a.	2.1	0.1	-9.0	n.a.
	78.0	2.1	0.0	0.0	n.a.	n.a.	n.a.	n.a.	2.1	0.2	n.a.	n.a.
	78.5	2.0	0.0	0.0	n.a.	n.a.	n.a.	n.a.	2.1	0.7	n.a.	n.a.
	79.0	1.8	0.0	n.a.	n.a.	n.a.	n.a.	n.a.	2.3	0.6	-10.8	n.a.
	79.5	1.6	0.0	n.a.	n.a.	n.a.	n.a.	n.a.	2.5	0.8	n.a.	n.a.
	80.0	1.4	0.0	0.0	18.4	0.6	30.3	0.2	2.7	0.5	n.a.	n.a.
	80.5	1.3	0.0	n.a.	n.a.	n.a.	n.a.	n.a.	2.8	0.5	-12.8	n.a.
	81.0	1.5	0.0	n.a.	n.a.	n.a.	n.a.	n.a.	2.8	0.2	n.a.	n.a.
	81.5	1.2	0.0	n.a.	17.9	0.3	30.2	0.2	2.9	0.5	n.a.	n.a.
	83.0	1.1	0.0	n.a.	24.4	0.1	35.6	0.8	3.0	0.2	n.a.	n.a.
	84.0	1.2	0.0	n.a.	n.a.	n.a.	n.a.	n.a.	2.8	0.2	-12.9	n.a.
	85.0	0.6	0.0	n.a.	26.4	0.9	35.9	0.8	3.2	0.1	-13.6	n.a.
	85.5	0.5	0.0	n.a.	31.7	0.3	39.6	0.4	3.2	0.2	n.a.	n.a.
	86.0	0.3	0.0	n.a.	31.3	0.9	38.9	1.1	3.5	0.1	n.a.	n.a.
	87.0	0.4	0.0	0.0	27.6	0.1	36.8	0.5	3.8	0.1	-14.5	n.a.
	88.0	0.2	0.0	n.a.	n.a.	n.a.	n.a.	n.a.	n.a.	0.2	n.a.	n.a.
	89.0	0.0	0.0	n.a.	n.a.	n.a.	n.a.	n.a.	3.9	0.1	-15.1	n.a.
	90.0	0.0	0.0	0.0	n.a.	n.a.	n.a.	n.a.	3.9	0.1	n.a.	n.a.
	91.0	0.0	0.0	n.a.	n.a.	n.a.	n.a.	n.a.	n.a.	0.1	n.a.	n.a.
	92.0	0.0	0.0	n.a.	n.a.	n.a.	n.a.	n.a.	4.0	0.1	-15.2	n.a.
	93.0	0.0	0.0	n.a.	n.a.	n.a.	n.a.	n.a.	4.1	0.2	n.a.	n.a.

Table S2. Continued.

		NO_3^- (mM)	NO_2^- (mM)	NH_4^+ (mM)	$\delta^{15}N\text{-}NO_3^-$ (‰)	SD ($\delta^{15}N\text{-}NO_3^-$)	$\delta^{18}O\text{-}NO_3^-$ (‰)	SD ($\delta^{18}O\text{-}NO_3^-$)	DIC (mM)	NPDOC (mM)	$\delta^{13}C$-DIC (‰)	$\delta^{13}C$-DOC (‰)
	DAY	SAMPLES COLLECTED AT THE OUTLET										
STAGE III	94.0	0.0	0.0	n.a.	n.a.	n.a.	n.a.	n.a.	n.a.	n.a.	n.a.	n.a.
	95.0	0.0	0.0	n.a.	n.a.	n.a.	n.a.	n.a.	4.0	0.2	-15.2	n.a.
	96.0	0.0	0.0	n.a.	n.a.	n.a.	n.a.	n.a.	n.a.	n.a.	n.a.	n.a.
	97.0	0.0	0.0	n.a.	n.a.	n.a.	n.a.	n.a.	n.a.	n.a.	n.a.	n.a.
	98.0	0.1	0.0	n.a.	n.a.	n.a.	n.a.	n.a.	n.a.	0.2	n.a.	n.a.
	99.0	0.0	0.0	n.a.	n.a.	n.a.	n.a.	n.a.	4.1	n.a.	n.a.	n.a.
STAGE IV	100.0	0.1	0.0	n.a.	n.a.	n.a.	n.a.	n.a.	3.8	n.a.	-14.6	n.a.
	101.0	0.5	0.0	n.a.	n.a.	n.a.	n.a.	n.a.	3.5	0.2	-14.0	n.a.
	102.0	0.4	0.0	0.0	n.a.	n.a.	n.a.	n.a.	n.a.	n.a.	n.a.	n.a.
	103.0	0.5	0.0	n.a.	n.a.	n.a.	n.a.	n.a.	3.5	0.2	n.a.	n.a.
	104.0	0.5	0.0	n.a.	n.a.	n.a.	n.a.	n.a.	3.5	0.1	n.a.	n.a.
	105.0	0.5	0.0	n.a.	n.a.	n.a.	n.a.	n.a.	3.5	0.2	-13.8	n.a.
	106.0	0.5	0.0	n.a.	n.a.	n.a.	n.a.	n.a.	3.5	0.2	n.a.	n.a.
	107.0	0.6	0.0	n.a.	20.0	0.2	29.1	0.6	n.a.	n.a.	n.a.	n.a.
	108.0	0.5	0.0	n.a.	19.1	0.2	29.9	0.4	3.5	n.a.	n.a.	n.a.
	109.0	0.4	0.0	n.a.	21.3	0.0	31.4	0.2	n.a.	0.1	n.a.	n.a.
	110.0	0.4	0.0	n.a.	21.0	0.2	31.5	0.5	n.a.	n.a.	n.a.	n.a.
	111.0	0.5	0.0	n.a.	21.1	0.5	33.7	0.4	n.a.	n.a.	n.a.	n.a.
	112.0	0.5	0.0	n.a.	17.2	n.a.	29.6	n.a.	n.a.	0.1	n.a.	n.a.
STAGE V	115.0	0.3	0.0	n.a.	19.9	0.3	31.7	0.2	3.7	n.a.	-14.3	n.a.
	116.0	0.6	0.0	n.a.	17.8	0.1	28.0	0.3	n.a.	n.a.	n.a.	n.a.
	117.0	0.6	0.0	n.a.	17.5	0.1	28.4	0.4	3.5	0.3	n.a.	n.a.

Table S2. Continued.

		NO_3^- (mM)	NO_2^- (mM)	NH_4^+ (mM)	$\delta^{15}N\text{-}NO_3^-$ (‰)	SD ($\delta^{15}N\text{-}NO_3^-$)	$\delta^{18}O\text{-}NO_3^-$ (‰)	SD ($\delta^{18}O\text{-}NO_3^-$)	DIC (mM)	NPDOC (mM)	$\delta^{13}C$-DIC (‰)	$\delta^{13}C$-DOC (‰)
	DAY	SAMPLES COLLECTED AT THE OUTLET										
STAGE V	118.0	0.7	0.0	n.a.	n.a.	n.a.	n.a.	n.a.	3.5	0.2	n.a.	n.a.
	119.0	0.5	0.0	n.a.	20.2	0.0	31.2	0.0	3.6	0.2	-14.3	n.a.
	120.0	0.3	0.0	n.a.	20.5	0.2	32.4	0.4	n.a.	n.a.	n.a.	n.a.
	121.0	0.4	0.0	n.a.	20.9	0.4	31.9	0.2	3.5	n.a.	n.a.	n.a.
	123.0	0.4	0.0	n.a.	15.7	0.8	26.9	0.0	n.a.	n.a.	n.a.	n.a.
	124.0	0.4	0.0	n.a.	19.2	0.4	31.2	0.0	n.a.	n.a.	n.a.	n.a.
	126.0	0.3	0.0	n.a.	19.4	0.9	30.4	0.6	3.7	n.a.	-14.9	n.a.
	128.0	0.3	0.0	n.a.	17.5	0.1	28.4	0.4	n.a.	n.a.	n.a.	n.a.
	131.0	0.2	0.0	n.a.	n.a.	n.a.	n.a.	n.a.	n.a.	n.a.	n.a.	n.a.
	133.0	0.4	0.0	n.a.	18.6	0.4	29.0	0.5	n.a.	n.a.	n.a.	n.a.
	135.0	0.4	0.0	n.a.	17.4	0.1	27.3	0.3	n.a.	n.a.	n.a.	n.a.
	137.0	0.5	0.0	n.a.	22.1	0.0	31.7	0.2	n.a.	n.a.	n.a.	n.a.
	140.0	0.5	0.0	n.a.	18.9	0.9	27.7	0.5	n.a.	n.a.	n.a.	n.a.
	141.0	0.7	0.0	n.a.	19.3	0.2	26.8	0.4	n.a.	n.a.	n.a.	n.a.
	144.0	0.3	0.0	n.a.	n.a.	n.a.	n.a.	n.a.	n.a.	n.a.	n.a.	n.a.
STAGE VI	147.0	0.8	0.0	n.a.	n.a.	n.a.	n.a.	n.a.	n.a.	n.a.	n.a.	n.a.
	149.0	1.2	0.0	n.a.	20.1	0.3	28.2	0.5	n.a.	n.a.	n.a.	n.a.
	151.0	1.5	0.0	n.a.	16.9	0.3	25.6	0.0	n.a.	n.a.	n.a.	n.a.
	154.0	1.6	0.0	n.a.	17.6	0.6	26.1	0.1	n.a.	n.a.	n.a.	n.a.
	158.0	1.9	0.0	n.a.	16.5	0.2	24.9	0.5	n.a.	n.a.	n.a.	n.a.
	162.0	1.8	0.0	n.a.	14.3	0.3	24.7	0.0	n.a.	n.a.	n.a.	n.a.
	165.0	1.9	0.0	n.a.	n.a.	n.a.	n.a.	n.a.	n.a.	n.a.	n.a.	n.a.

Table S2. Continued.

		NO_3^- (mM)	NO_2^- (mM)	NH_4^+ (mM)	$\delta^{15}N\text{-}NO_3^-$ (‰)	SD ($\delta^{15}N\text{-}NO_3^-$)	$\delta^{18}O\text{-}NO_3^-$ (‰)	SD ($\delta^{18}O\text{-}NO_3^-$)	DIC (mM)	NPDOC (mM)	$\delta^{13}C$-DIC (‰)	$\delta^{13}C$-DOC (‰)
	DAY	SAMPLES COLLECTED AT THE OUTLET										
STAGE VI	170.0	1.9	0.0	n.a.	16.6	0.3	26.1	0.1	n.a.	n.a.	n.a.	n.a.
	cm	SAMPLES FROM THE VERTICAL PROFILES										
STAGE I (day 16)	06.0	0.0	0.0	n.a.	n.a.	n.a.	n.a.	n.a.	n.a.	n.a.	n.a.	n.a.
	16.0	0.1	0.0	n.a.	n.a.	n.a.	n.a.	n.a.	n.a.	n.a.	n.a.	n.a.
	26.0	0.0	0.0	n.a.	n.a.	n.a.	n.a.	n.a.	n.a.	n.a.	n.a.	n.a.
	36.0	0.0	0.0	n.a.	n.a.	n.a.	n.a.	n.a.	n.a.	n.a.	n.a.	n.a.
	46.0	0.0	0.0	n.a.	n.a.	n.a.	n.a.	n.a.	n.a.	n.a.	n.a.	n.a.
	56.0	0.0	0.0	n.a.	n.a.	n.a.	n.a.	n.a.	n.a.	n.a.	n.a.	n.a.
STAGE II (day 36)	06.0	1.4	0.0	n.a.	n.a.	n.a.	n.a.	n.a.	n.a.	n.a.	n.a.	n.a.
	16.0	1.1	0.0	n.a.	n.a.	n.a.	n.a.	n.a.	n.a.	n.a.	n.a.	n.a.
	26.0	0.9	0.0	n.a.	n.a.	n.a.	n.a.	n.a.	n.a.	n.a.	n.a.	n.a.
	36.0	0.9	0.0	n.a.	n.a.	n.a.	n.a.	n.a.	n.a.	n.a.	n.a.	n.a.
	46.0	0.8	0.0	n.a.	n.a.	n.a.	n.a.	n.a.	n.a.	n.a.	n.a.	n.a.
	56.0	0.7	0.0	n.a.	n.a.	n.a.	n.a.	n.a.	n.a.	n.a.	n.a.	n.a.
STAGE V (day 136)	06.0	1.7	0.0	n.a.	n.a.	n.a.	n.a.	n.a.	n.a.	n.a.	n.a.	n.a.
	16.0	0.3	0.0	n.a.	n.a.	n.a.	n.a.	n.a.	n.a.	n.a.	n.a.	n.a.
	26.0	0.4	0.0	n.a.	n.a.	n.a.	n.a.	n.a.	n.a.	n.a.	n.a.	n.a.
	36.0	0.4	0.0	n.a.	n.a.	n.a.	n.a.	n.a.	n.a.	n.a.	n.a.	n.a.
	46.0	0.4	0.0	n.a.	n.a.	n.a.	n.a.	n.a.	n.a.	n.a.	n.a.	n.a.
	56.0	0.4	0.0	n.a.	n.a.	n.a.	n.a.	n.a.	n.a.	n.a.	n.a.	n.a.

Table S3. ICP results. Concentration of cations and trace elements measured by ICP-OES (ppm) and ICP-MS (ppb), respectively.

		STAGE I										STAGE II		
	DAY	0.0	2.0	4.0	7.0	8.0	9.5	12.0	16.0	21.0	24.0	36.0	49.0	63.0
ICP-OES (ppm)	K	176.4	100.1	96.9	83.7	92.2	85.7	80.6	76.9	73.5	72.8	66.8	71.1	66.5
	Ca	40.0	39.1	39.0	39.1	42.6	42.5	39.8	38.5	38.8	37.1	37.4	36.0	37.1
	Mg	33.8	33.5	33.4	32.8	35.8	35.3	34.0	32.4	33.2	31.9	32.5	31.9	33.2
	S	58.1	56.6	55.7	57.0	59.9	58.9	57.2	56.8	51.1	48.0	47.2	46.3	46.9
	P	0.4	1.1	0.5	0.7	0.7	0.5	0.4	0.5	0.7	0.7	0.8	0.7	1.2
	Si	4.4	3.2	3.8	3.6	4.1	4.9	3.8	3.3	2.7	2.3	2.2	1.5	1.2
	B	0.2	0.1	0.1	0.1	0.1	0.1	0.1	0.1	0.1	0.0	0.0	0.0	0.0
	Zn	0.5	1.8	1.9	2.4	2.2	2.8	1.7	0.7	0.3	0.1	0.4	0.1	0.1
	Na	178.4	173.2	171.7	174.2	183.3	176.3	176.5	175.2	177.2	176.6	263.1	179.9	175.3
	Sr	0.1	0.0	0.0	0.0	0.0	0.0	0.0	0.0	0.0	0.0	0.0	0.0	0.0
ICP-MS (ppb)	Mn	7.3	14.0	12.7	32.5	33.9	55.1	42.6	21.4	22.6	2.1	3.2	3.0	0.7
	Fe	122.4	124.5	112.7	142.1	116.5	116.5	137.4	163.9	155.4	133.3	119.2	119.9	133.9
	Al	3.8	3.0	1.1	1.6	1.9	1.6	2.6	2.0	2.1	3.0	3.0	2.3	8.1
	Cu	4.1	5.2	3.9	7.3	6.3	7.1	14.9	10.7	3.1	4.1	20.7	2.5	2.0
	Tl	0.1	0.1	0.0	0.0	0.0	0.0	0.0	0.0	0.0	0.0	0.0	0.0	0.0
	Co	0.6	0.8	0.8	1.1	1.0	1.6	1.2	0.7	0.5	0.2	0.2	0.1	0.1
	Pb	0.4	0.1	0.4	0.1	0.1	0.1	0.7	0.2	0.2	0.1	0.7	0.1	0.1
	Sr	57.2	41.3	47.3	45.6	45.2	49.4	43.0	40.3	30.9	29.4	25.0	24.2	24.1
	Li	0.4	0.4	0.3	0.3	0.3	0.3	0.4	0.3	0.2	0.2	0.1	0.2	0.2
	Be	0.0	0.0	0.0	0.0	0.0	0.0	0.0	0.0	0.0	0.0	0.0	0.0	0.0
	Sc	1.4	1.0	1.2	1.2	1.1	1.3	1.2	1.1	0.7	0.7	0.6	0.4	0.3
	Ti	2.9	4.6	2.9	3.7	2.8	2.6	2.6	3.2	2.6	3.0	3.4	3.4	4.5
	V	1.0	1.1	1.2	1.4	1.5	1.5	1.5	1.5	1.5	1.5	1.4	1.3	1.4

Table S3. Continued.

		STAGE I										STAGE II		
	DAY	0.0	2.0	4.0	7.0	8.0	9.5	12.0	16.0	21.0	24.0	36.0	49.0	63.0
ICP-MS (ppb)	Cr	1.9	2.5	2.2	1.7	1.4	1.2	1.2	0.8	0.9	0.7	0.7	0.8	0.6
	Ni	3.7	4.4	4.3	4.7	5.3	6.6	5.5	4.8	2.2	1.2	4.6	1.4	1.0
	Ga	0.0	0.0	0.0	0.0	0.0	0.0	0.0	0.0	0.0	0.0	0.0	0.0	0.0
	Ge	0.0	0.0	0.0	0.0	0.0	0.0	0.0	0.0	0.0	0.0	0.0	0.0	0.0
	As	0.5	0.5	0.6	0.6	0.6	2.4	0.6	0.5	0.4	0.6	0.4	0.5	0.3
	Se	9.3	3.3	2.9	2.9	3.3	2.1	3.1	0.0	1.0	3.1	8.7	1.5	0.5
	Rb	5.0	5.9	4.6	6.4	5.3	5.5	6.0	6.6	5.5	5.9	4.1	2.4	2.0
	Y	0.0	0.0	0.0	0.1	0.1	0.1	0.1	0.0	0.0	0.0	0.0	0.0	0.0
	Zr	0.9	1.7	0.7	0.6	0.6	0.7	0.8	1.1	0.8	0.9	0.8	0.3	0.2
	Nb	0.0	0.0	0.0	0.0	0.0	0.0	0.0	0.0	0.0	0.0	0.0	0.0	0.0
	Mo	0.3	0.2	0.2	0.2	0.1	0.1	0.1	0.1	0.1	0.0	0.2	0.2	0.1
	Ru	0.0	0.0	0.0	0.0	0.0	0.0	0.0	0.0	0.0	0.0	0.0	0.0	0.0
	Rh	0.0	0.0	0.0	0.0	0.0	0.0	0.0	0.0	0.0	0.0	0.0	0.0	0.0
	Pd	0.1	0.0	0.0	0.0	0.0	0.0	0.0	0.0	0.0	0.0	0.0	0.0	0.0
	Ag	0.2	0.1	0.1	0.1	0.1	0.1	0.1	0.1	0.1	0.1	0.3	0.1	0.0
	Cd	0.9	1.1	1.0	1.4	1.5	1.2	0.6	0.2	0.1	0.1	0.1	0.1	0.0
	In	0.0	0.0	0.0	0.0	0.0	0.0	0.0	0.0	0.0	0.0	0.0	0.0	0.0
	Sn	0.5	0.1	0.0	0.0	0.0	0.1	0.1	0.1	0.0	0.1	0.5	0.0	0.0
	Sb	31.1	22.6	29.6	32.3	36.7	48.1	36.5	26.6	6.5	3.9	5.2	11.4	11.2
	Te	0.0	0.0	0.0	0.0	0.0	0.0	0.0	0.0	0.0	0.0	0.0	0.0	0.0
	Cs	0.1	0.0	0.0	0.0	0.0	0.0	0.0	0.0	0.0	0.0	0.0	0.0	0.0
	Ba	39.6	18.9	36.6	38.4	33.7	45.8	31.8	22.3	18.3	25.2	299.4	10.3	5.8
	La	0.0	0.0	0.0	0.0	0.0	0.0	0.0	0.0	0.0	0.0	0.0	0.0	0.0

Table S3. Continued.

		STAGE I										STAGE II		
	DAY	0.0	2.0	4.0	7.0	8.0	9.5	12.0	16.0	21.0	24.0	36.0	49.0	63.0
ICP-MS (ppb)	Ce	0.0	0.0	0.0	0.0	0.0	0.0	0.0	0.0	0.0	0.0	0.0	0.0	0.0
	Pr	0.0	0.0	0.0	0.0	0.0	0.0	0.0	0.0	0.0	0.0	0.0	0.0	0.0
	Nd	0.0	0.0	0.0	0.0	0.0	0.0	0.0	0.0	0.0	0.0	0.0	0.0	0.0
	Sm	0.0	0.0	0.0	0.0	0.0	0.0	0.0	0.0	0.0	0.0	0.0	0.0	0.0
	Eu	0.0	0.0	0.0	0.0	0.0	0.0	0.0	0.0	0.0	0.0	0.0	0.0	0.0
	Gd	0.0	0.0	0.0	0.0	0.0	0.0	0.0	0.0	0.0	0.0	0.0	0.0	0.0
	Tb	0.0	0.0	0.0	0.0	0.0	0.0	0.0	0.0	0.0	0.0	0.0	0.0	0.0
	Dy	0.0	0.0	0.0	0.0	0.0	0.0	0.0	0.0	0.0	0.0	0.0	0.0	0.0
	Ho	0.0	0.0	0.0	0.0	0.0	0.0	0.0	0.0	0.0	0.0	0.0	0.0	0.0
	Er	0.0	0.0	0.0	0.0	0.0	0.0	0.0	0.0	0.0	0.0	0.0	0.0	0.0
	Tm	0.0	0.0	0.0	0.0	0.0	0.0	0.0	0.0	0.0	0.0	0.0	0.0	0.0
	Yb	0.0	0.0	0.0	0.0	0.0	0.0	0.0	0.0	0.0	0.0	0.0	0.0	0.0
	Lu	0.0	0.0	0.0	0.0	0.0	0.0	0.0	0.0	0.0	0.0	0.0	0.0	0.0
	Hf	0.0	0.0	0.0	0.0	0.0	0.0	0.0	0.0	0.0	0.0	0.0	0.0	0.0
	Ta	0.0	0.0	0.0	0.0	0.0	0.0	0.0	0.0	0.0	0.0	0.0	0.0	0.0
	W	0.0	0.0	0.0	0.0	0.0	0.0	0.0	0.0	0.0	0.0	0.0	0.0	0.0
	Re	0.0	0.0	0.0	0.0	0.0	0.0	0.0	0.0	0.0	0.0	0.0	0.0	0.0
	Os	0.0	0.0	0.0	0.0	0.0	0.0	0.0	0.0	0.0	0.0	0.0	0.0	0.0
	Ir	0.0	0.0	0.0	0.0	0.0	0.0	0.0	0.0	0.0	0.0	0.0	0.0	0.0
	Pt	0.0	0.0	0.0	0.0	0.0	0.0	0.0	0.0	0.0	0.0	0.0	0.0	0.0
	Au	0.1	0.0	0.1	0.0	0.1	0.0	0.1	0.0	0.0	0.0	0.1	0.0	0.0
	Hg	0.3	0.2	0.2	0.1	0.1	0.2	0.1	0.0	0.0	0.0	0.2	0.0	0.0
	Bi	0.3	0.1	0.1	0.0	0.0	0.0	0.0	0.0	0.0	0.0	0.1	0.1	0.0

Table S3. Continued.

		STAGE I										STAGE II		
	DAY	0.0	2.0	4.0	7.0	8.0	9.5	12.0	16.0	21.0	24.0	36.0	49.0	63.0
ICP-MS	Th	0.6	0.2	0.2	0.1	0.1	0.1	0.1	0.0	0.0	0.0	0.0	0.0	0.0
(ppb)	U	0.1	0.1	0.1	0.1	0.0	0.0	0.1	0.1	0.1	0.1	0.1	0.0	0.0

ANNEX 4

Feasibility of using rural waste products to increase the denitrification efficiency in a surface flow constructed wetland.

Rosanna Margalef-Marti[1], Raúl Carrey[1], Daniel Merchán[2], Albert Soler[1], Jesús Causapé[3], Neus Otero[1,4]

[1] Grup MAiMA, SGR Mineralogia Aplicada, Geoquímica i Geomicrobiologia, Departament de Mineralogia, Petrologia i Geologia Aplicada, Facultat de Ciències de la Terra, Universitat de Barcelona (UB), C/Martí i Franquès s/n, 08028 Barcelona (Spain).

[2]Department of Engineering, IS-FOOD Institute (Innovation & Sustainable Development in Food Chain), Public University of Navarre, Campus de Arrosadia, 31006 Pamplona, Navarra, Spain.

[3] Geological Survey of Spain (IGME), C/Manuel Lasala 44 9◦B, 50006 Zaragoza, Spain.

[4] Serra Húnter Fellowship, Generalitat de Catalunya, Spain.

Journal of Hydrology, Volume 578, November 2019, 124035

https://doi.org/10.1016/j.jhydrol.2019.124035

Impact factor (JCR/WOS) = 4.4 (2018)

Q1, 6/91 Water resources, 15/196 Geosciences multidispiplinary , 6/132 Civil engineering

Journal of Hydrology 578 (2019) 124035

Contents lists available at ScienceDirect

Journal of Hydrology

journal homepage: www.elsevier.com/locate/jhydrol

Research papers

Feasibility of using rural waste products to increase the denitrification efficiency in a surface flow constructed wetland

Rosanna Margalef-Marti[a,*], Raúl Carrey[a], Daniel Merchán[b], Albert Soler[a], Jesús Causapé[c], Neus Otero[a,d]

[a] Grup MAiMA, SGR Mineralogia Aplicada, Geoquímica i Geomicrobiologia, Departament de Mineralogia, Petrologia i Geologia Aplicada, Facultat de Ciències de la Terra, Universitat de Barcelona (UB), C/Martí i Franquès s/n, 08028 Barcelona, Spain
[b] Department of Engineering, IS-FOOD Institute (Innovation & Sustainable Development in Food Chain), Public University of Navarre, Campus de Arrosadia, 31006 Pamplona, Navarra, Spain
[c] Geological Survey of Spain—IGME, C/Manuel Lasala 44 9°B, 50006 Zaragoza, Spain
[d] Serra Húnter Fellowship, Generalitat de Catalunya, Spain

ARTICLE INFO

This manuscript was handled by Huaming Guo, Editor-in-Chief

Keywords:
Denitrification
Constructed wetland
Electron donor
Isotopic fractionation
Remediation

ABSTRACT

A surface flow constructed wetland (CW) was set in the Lerma gully to decrease nitrate (NO_3^-) pollution from agricultural runoff water. The water flow rate and NO_3^- concentration were monitored at the inlet and the outlet, and sampling campaigns were performed which consisted of collecting six water samples along the CW flow line. After two years of operation, the NO_3^- attenuation was limited at a flow rate of ~2.5 L/s and became negligible at ~5.5 L/s. The present work aimed to assess the feasibility of using rural waste products (wheat hay, corn stubble, and animal compost) to induce denitrification in the CW, to assess the effect of temperature on this process, and to trace the efficiency of the treatment by using isotopic tools. In the first stage, microcosm experiments were performed. Afterwards, the selected waste material was applied in the CW, and the treatment efficiency was evaluated by means of a chemical and isotopic characterization and using the isotopic fractionation (ε) values calculated from laboratory experiments to avoid field-scale interference. The microcosms results showed that the stubble was the most appropriate material for application in the CW, but the denitrification rate was found to decrease with temperature. In the CW, biostimulation in autumn-winter promoted NO_3^- attenuation between two weeks and one month (a reduction in NO_3^- between 1.2 and 1.5 mM was achieved). After the biostimulation in spring-summer, the attenuation was maintained for approximately three months (NO_3^- reduction between 0.1 and 1.5 mM). The $\varepsilon^{15}N_{NO3/N2}$ and $\varepsilon^{18}O_{NO3/N2}$ values obtained from the laboratory experiments allowed to estimate the induced denitrification percentage. At an approximate average flow rate of 16 L/s, at least 60% of NO_3^- attenuation was achieved in the CW. The field samples exhibited a slope of 1.0 for $\delta^{18}O\text{-}NO_3^-$ versus $\delta^{15}N\text{-}NO_3^-$, similar to those of the laboratory experiments (0.9–1.2). Plant uptake seemed to play a minor role in NO_3^- attenuation in the CW. Hence, the application of stubble in the CW allowed the removal of large amounts of NO_3^- from the Lerma gully, especially when applied during the warm months, but its efficacy was limited to a short time period (up to three months).

1. Introduction

Since nitrate (NO_3^-) is known to cause ecological and human health problems (Vitousek et al., 1997; Ward et al., 2005), the presence of this nutrient in water bodies worldwide is a matter of concern. The extensive application of synthetic and organic fertilizers is a major source of NO_3^- pollution. Therefore, agricultural runoff water should be treated before it is drained into larger water bodies such as aquifers, rivers, and/or lakes. Constructed wetlands (CWs) are considered promising, low cost systems for the remediation of diverse water pollutants, are simple to operate, and have low energy requirements (Wu et al., 2015). Hence, directing agricultural runoff water through a CW could be useful for removing NO_3^- to minimize pollution.

The surface flow CWs consists of free surface water flowing horizontally through an artificial pond containing floating and/or emergent rooted vegetation and a high diversity of microorganisms (Ilyas and Masih, 2017; Sirivedhin and Gray, 2006; Vymazal, 2007). The main processes that might contribute to NO_3^- pollution mitigation in surface

* Corresponding author.
E-mail address: rosannamargalef@ub.edu (R. Margalef-Marti).

https://doi.org/10.1016/j.jhydrol.2019.124035
Received 23 April 2019; Received in revised form 7 August 2019; Accepted 9 August 2019
Available online 13 August 2019

flow CWs are plant uptake, assimilation by microorganisms, and denitrification (Rogers et al., 1991). The latter refers to the reduction of NO_3^- by microorganisms through a series of enzymatic reactions involving the intermediates NO_2^-, NO, and N_2O, before finally being reduced to N_2 (Knowles, 1982). Parameters such as temperature, dissolved oxygen (O_2), NO_3^- loading, the source and amount of organic carbon (C), microbial species, the type and density of macrophytes, wetland age, and hydraulic conditions play key roles in the NO_3^- removal efficiency (Bachand and Horne, 1999; Beutel et al., 2009; Kong et al., 2009; Sirivedhin and Gray, 2006). Different approaches can be implemented to enhance water remediation, but strategies directed toward the induction of bacterial NO_3^- respiration are preferred since denitrification is an authentic N sink in water, unlike biomass sequestration (Scott et al., 2008). N storage by plants is generally considered temporary, because organic N returns to the system after the death and decay of plants if they are not harvested (Cooper and Cooke, 1984; Gumbricht, 1993).

In CWs, macrophytes are able not only to assimilate NO_3^-, but also to promote denitrification efficiency. Plants exert an influence on the diversity of microbial species and their enzymatic activities by releasing exudates and oxygen to the rhizosphere (Kong et al., 2009, and references therein), and decomposed plant material can be used by microbes as a source of organic C. For this reason, increased NO_3^- removal is usually found in vegetated CWs relative to that in non-vegetated systems (Jacobs and Harrison, 2014; Soana et al., 2017). If the CW cannot provide enough organic C to support complete denitrification (e.g., from inlet water, soil, plant root exudates, and decomposed vegetal material), the addition of an external organic C source as an electron donor could enhance the heterotrophic denitrification efficiency (Lu et al., 2009; Si et al., 2018). Since the use of pure reagents such as glucose, acetate, or ethanol may be expensive in long-term treatments, the use of industrial or agricultural residues that are rich in organic C could represent a more sustainable solution. Solid products such as animal or vegetal waste (Grau-Martínez et al., 2017; Si et al., 2018; Trois et al., 2010), as well as industrial liquid by-products (Carrey et al., 2018; Margalef-Marti et al., 2019), have already been reported as being useful for promoting denitrification.

The pollutant removal efficiency in CWs can be estimated by monitoring the inlet and outlet concentrations of the pollutant (Kovacic et al., 2000; Tanner et al., 2005; Uusheimo et al., 2018). However, this method does not reveal the specific processes involved in the attenuation, making it challenging to focus on the improvement of the wetland design and operation. Stable isotope analyses can provide information on the NO_3^- transformation pathways. In the course of denitrification, the unreacted residual NO_3^- becomes enriched in the heavy isotopes ^{15}N and ^{18}O, permitting the distinction between biological attenuation and other processes such as dilution which could also lead to decreases in concentration without influencing the isotopic signature (Böttcher et al., 1990; Fukada et al., 2003; Mariotti et al., 1981; Aravena and Robertson, 1998). In plants, significant enrichment in both ^{15}N and ^{18}O is observed in the NO_3^- extracted from leaves after uptake relative to the NO_3^- from water, but the changes in the NO_3^- isotopic composition in the water are minor (Estrada et al., 2017; Spoelstra et al., 2010). Therefore, the NO_3^- isotopic characterization of water samples collected at the CW might improve the understanding and support the evaluation of the performance of the remediation strategy.

In this context, the present work was developed to assess the feasibility of using rural waste products (wheat hay, corn stubble, and animal compost) to induce denitrification in a surface flow CW, and to trace the treatment efficiency in the autumn–winter and spring-summer seasons. In the first stage, lab-scale experiments were performed to identify the most appropriate electron donor to be applied in the CW, and to evaluate the effect of temperature on NO_3^- reduction. The isotopic fractionations (ε) of N and O of dissolved NO_3^- under each condition were also determined. In the second stage, the selected material was applied in the CW and the treatment efficiency was evaluated by means of a chemical and isotopic characterization using the ε values calculated from the laboratory experiments.

2. Methods

2.1. Laboratory experiments

Six types of batch experiments were performed in 150 mL crystal Pyrex® bottles crimp-sealed with butyl rubber stoppers under an argon (Ar) headspace. Each microcosm contained 100 mL of water (2 mM NO_3^-) collected from the inlet of the studied CW (see Section 2.2) and a specific C source: corn stubble (1 g); wheat hay (1 g); or animal compost (0.25 g). The six series of parallel experiments were determined according to the waste product employed and the incubation temperature. Series I (C-24) and II (H-24) contained animal compost and wheat hay, respectively, and were incubated at 24 °C; series III (S-24), IV (S-16), and V (S-8) contained corn stubble and were incubated at 24 °C, 16 °C, and 8 °C, respectively; series VI (DS-24) contained partially decomposed corn stubble and was incubated at 24 °C. The partially decomposed stubble was obtained from the CW 7.5 months after its application on September 25, 2017 (see Section 2.2). All series included at least eight replicates of the biostimulated microcosms. Control microcosms for each tested material were prepared using deionized water (DIW) to discard the potential supply of N from the waste products. The detailed content of each microcosm is described in Table 1. During incubation, all microcosms were maintained in darkness and under constant vibratory shaking. The biostimulated microcosms were sacrificed at time intervals depending on the denitrification dynamics until complete NO_3^- and NO_2^- removals were achieved. The control microcosms were sacrificed at the end of the biostimulation experiments. Water samples from batch experiments were analyzed for major anions (NO_3^-, NO_2^-, Cl^-, and SO_4^{2-}), ammonium (NH_4^+), non-purgeable dissolved organic C (NPDOC), dissolved inorganic C (DIC), major cations, trace elements, $\delta^{15}N\text{-}NO_3^-$, $\delta^{18}O\text{-}NO_3^-$, and $\delta^{13}C\text{-}DIC$. Samples from control microcosms

Table 1
Series of experiments. Tested conditions and composition of microcosms. DIW = deionized water.

Series	Condition	Code	C source	Material (g)	C (g/L)	Water source (100 mL)	Temperature (°C)
I	Biostimulated	C-24	Animal compost	0.25	0.8	Wetland	24
	Control	C-24-blank	Animal compost	0.25	0.8	DIW	24
II	Biostimulated	H-24	Wheat hay	1	4.2	Wetland	24
	Control	H-24-blank	Wheat hay	1	4.2	DIW	24
III	Biostimulated	S-24	Corn stubble	1	3.6	Wetland	24
	Control	S-24-blank	Corn stubble	1	3.6	DIW	24
IV	Biostimulated	S-16	Corn stubble	1	3.6	Wetland	16
	Control	S-16-blank	Corn stubble	1	3.6	DIW	16
V	Biostimulated	S-8	Corn stubble	1	3.6	Wetland	8
	Control	S-8-blank	Corn stubble	1	3.6	DIW	8
VI	Biostimulated	DS-24	Decomposed stubble	1	3.6	Wetland	24
	Control	DS-24-blank	Decomposed stubble	1	3.6	DIW	24

were analyzed for major anions and NPDOC. The gas accumulated in the headspace of the vials was collected and analyzed for nitrous oxide (N_2O) concentration. The three organic C sources were analyzed for C and N concentrations and $\delta^{13}C\text{-}C_{bulk}$ and $\delta^{15}N\text{-}N_{bulk}$.

2.2. CW test

In the 2000s, approximately 20,000 ha of rainfed croplands were transformed into irrigated agricultural land in the Arba River Basin (Zaragoza, Spain). A small watershed representative of the area (Lerma basin, 733 ha) was monitored to assess the effects of this transformation on the water balance and the salt and NO_3^--N exports (Merchán et al., 2015, 2014, 2013). In general, the implementation of irrigation implied a three-fold increase in N export to the receiving water bodies, in this case the Arba River, which was the first surface water body in the Ebro River Basin to be declared affected by NO_3^- pollution according to the Nitrates Directive 91/676/EEC. In order to diminish the release of NO_3^- from the Lerma Basin to the Arba River, a surface flow CW was constructed in October 2015, initially covering an area of ~1500 m^2, and was enlarged in June 2017, covering a final area of ~2500 m^2 with a depth of ~40 cm. The surface water of the Lerma gully can be partially diverted towards the CW. Water flow in the Lerma gully varies between 15 and 60 L/s. Temperature and precipitation data collected monthly in the area are reported in Supporting information (Table S1).

The CW is fully automated, with high-frequency monitoring (every 10 min) of the water flow rate and NO_3^- concentration at both the inlet and the outlet. Emergent macrophytes (*Typha* and *Phragmites*) started growing since its construction, and occupied approximately 75% of the CW surface at the time the present study began, since the enlarged part was still unvegetated. The field survey was performed in three periods and involved 13 sampling campaigns, each consisting of the collection of six water samples (H1 to H6) from along the wetland flow line (Fig. 1). In the first period (June to September 2017), two different operating conditions were tested before the biostimulation by modifying the inlet opening; three sampling campaigns were performed at two different flow rates (~5.5 L/s and ~2.5 L/s). The second period involved the application of corn stubble obtained from the surrounding crops (~8000 kg) on September 25, 2017, and the evaluation of treatment efficiency by performing two sampling campaigns 7 and 14 d after the application. The third period involved a second application of corn stubble (~6000 kg) on May 11, 2018, and the evaluation of treatment efficiency by performing eight sampling campaigns from May 2018 to October 2018. In the two biostimulation periods, the corn stubble was applied over all the CW surface between H1 and H3. Throughout these second and third periods, the CW was operated at a higher flow rate (~16 L/s). The given flow rate for the CW test periods is that measured at the outlet. The calculated residence time of NO_3^- in the CW was 21, 51 and 112 h for the tested flow rates of 16, 5.5 and 2.5 L/s, respectively. Detailed information about the sampling campaigns is shown in Table 2. Water samples collected at the CW were analyzed for major anions (NO_3^-, NO_2^-, Cl^-, and SO_4^{2-}), NH_4^+, NPDOC, DIC, major cations, trace elements, $\delta^{15}N\text{-}NO_3^-$, $\delta^{18}O\text{-}NO_3^-$, $\delta^{34}S\text{-}SO_4^{2-}$, $\delta^{18}O\text{-}SO_4^{2-}$, and $\delta^{13}C$-DIC.

2.3. Analytical methods

Water samples for the field and laboratory batch experiments were immediately filtered through 0.2 µm Millipore® filters after being collected, and were stored at 4 °C until analysis. The aliquots for NH_4^+, $\delta^{15}N\text{-}NO_3^-$, and $\delta^{18}O\text{-}NO_3^-$ analysis were frozen, and the aliquots for the DIC and $\delta^{13}C$-DIC analyses were left with no headspace and stored at 4 °C.

Anions (Cl^-, NO_2^-, NO_3^-, and SO_4^{2-}) were analyzed by high-performance liquid chromatography (HPLC) (Waters 515 pump and Waters IC-Pak anion column with Waters 432 and KONTRON UV/Vis detectors). NH_4^+ was analyzed by three techniques due to equipment availability issues: I) spectrophotometry using the indophenol blue method (CARY 1E UV–visible), II) ion chromatography or III) ammonia ion selective electrode (ORION, Thermo Scientific). DIC was analyzed by titration (METROHM 702 SM Titrino), NPDOC by organic matter combustion (TOC 500 SHIMADZU), and major cations and trace elements by ICP-OES (Perkin Elmer Optima 8300). The concentration of N_2O accumulated at the headspace of the vials was analyzed by gas chromatography (GC) (Thermo Scientific Trace 1300 with ECD detector), and C and N concentrations in the waste materials employed as C sources were analyzed with an elemental analyzer (EA) (Carlo Erba1108 CHNS-O EA). The $\delta^{15}N\text{-}NO_3^-$ and $\delta^{18}O\text{-}NO_3^-$ were determined following the cadmium and azide reduction method (McIlvin and Altabet, 2005; Ryabenko et al., 2009). The isotopic composition of the N_2O obtained from the NO_3^- reduction was analyzed using a PreCon coupled to a Finnigan MAT 253 isotope ratio mass spectrometer (IRMS) (Thermo Scientific). For the SO_4^{2-} isotopic analysis, the dissolved SO_4^{2-} was precipitated as $BaSO_4$ by adding $BaCl_2{\cdot}2H_2O$ after acidifying the sample with HCl and boiling it in order to prevent precipitation of $BaCO_3$ (Dogramaci et al., 2001). The $\delta^{34}S\text{-}SO_4^{2-}$ was analyzed with a Carlo Erba EA coupled in continuous flow to a Finnigan Delta XP Plus IRMS, whereas the $\delta^{18}O\text{-}SO_4^{2-}$ was analyzed with a ThermoQuest high-temperature conversion analyzer (TC/EA) coupled in continuous flow to a Finnigan Matt Delta XP Plus IRMS. The $\delta^{13}C$-DIC was analyzed via carbonate conversion to CO_2 gas by adding a phosphoric acid solution and measuring the gas evolved with a Gas-Bench II coupled to a MAT-253 IRMS (Thermo Scientific). The $\delta^{13}C\text{-}C_{bulk}$ and $\delta^{15}N\text{-}N_{bulk}$ of the waste materials employed as C sources were determined with a Carlo Erba EA coupled to a Finnigan Delta C IRMS.

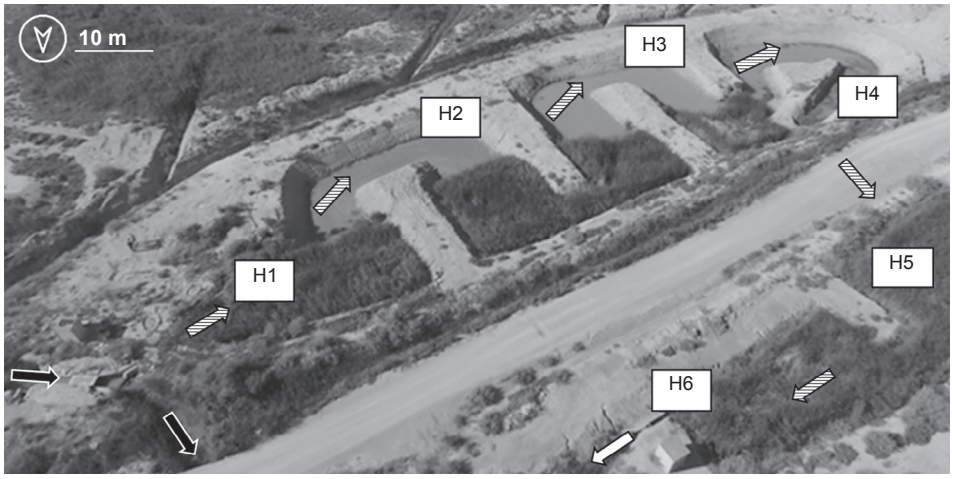

Fig. 1. CW design. Photograph of the surface flow CW with emergent macrophytes. The sampling points are depicted with white squares (H1 to H6), and the water flow within the CW with striped arrows. Non-treated water flow discharging to the Lerma gully is depicted with black arrows, and that of treated water with a white arrow.

Table 2
Sampling campaigns. Sampling dates and operation mode of the CW for all sampling campaigns (six samples each).

Test period	Date	Days since stubble addition	Operation mode	Observations
I	14/06/2017	–	5.5 L/s	No external organic C addition
	05/09/2017	–	5.5 L/s	
	12/09/2017	–	2.5 L/s	
II	02/10/2017	7	16 L/s	First organic C source addition on 25/09/2017
	10/10/2017	14		
III	11/05/2018	0	16 L/s	Second organic C source addition on 11/05/2018
	18/05/2018	7		
	25/05/2018	14		
	12/06/2018	32		
	13/07/2018	63		
	19/08/2018	100		
	13/09/2018	125		
	19/10/2018	161		

The isotopic notation is expressed in terms of δ (‰) relative to the international standards: atmospheric N_2 (AIR) for $\delta^{15}N$, Vienna Standard Mean Oceanic Water (V-SMOW) for $\delta^{18}O$, Vienna Pee Dee Belemnite (V-PDB) for $\delta^{13}C$, and Vienna Canyon Diablo Troillite (V-CDT) for $\delta^{34}S$. Hence, $\delta = ((R_{sample}-R_{standard})/R_{standard})$, where R is the ratio between the heavy and the light isotopes. Following Coplen (2011), several international and laboratory (CCiT) standards were interspersed among the samples for normalization of the results (Supporting Information Table S2). The reproducibilities (1 σ) of the samples, calculated from the standards systematically interspersed in the analytical batches, were ± 1.0‰ for $\delta^{15}N$-NO_3^-, ± 1.5‰ for $\delta^{18}O$-NO_3^-, ± 0.2‰ for $\delta^{15}N$-N_{bulk}, ± 0.2‰ for $\delta^{13}C$-C_{bulk}, ± 0.2‰ for $\delta^{13}C$-DIC, ± 0.2‰ for $\delta^{34}S$-SO_4^{2-}, and ± 0.5‰ for $\delta^{18}O$-SO_4^{2-}. Samples for chemical and isotopic analyses were prepared at the laboratory of the MAiMA-UB research group, and analyzed at the Centres Científics i Tecnològics of the Universitat de Barcelona (CCiT-UB).

3. Results and discussion

3.1. Lab-scale evaluation of the nitrate removal capacities of compost, hay, and stubble at 24 °C

The chemical and isotopic characterization of the samples obtained from the laboratory experiments are presented in the Supporting Information (Table S3). Although the intrinsic N content measured in the three waste products (stubble, hay, and compost) were low (Table 3), it was not possible to disregard a certain supply of N from these materials throughout the incubations. The control microcosms containing the three C sources and DIW showed NO_3^-, NO_2^-, and NH_4^+ concentrations below 0.09 mM, 0.02 mM, and 0.12 mM, respectively.

The biostimulation experiments showed that the three tested C sources were able to promote NO_3^- removal. Complete denitrification (total NO_3^- and NO_2^- removal) was reached in approximately 40 h in the microcosms containing stubble and hay, and in approximately 95 h in that containing compost (Fig. 2A). NH_4^+ was detected in some of the samples (in concentrations of up to 1 mM), but with no clear pattern, suggesting the possible coexistence of denitrification and dissimilatory NO_3^- reduction to NH_4^+ (DNRA) and/or the input of NH_4^+-N supplied from the C sources tested. Transient NO_2^- accumulation of up to 1.5 mM (stubble and hay) and 0.7 mM (compost) were observed. The highest concentration of NO_2^- in the stubble and hay microcosms were detected after complete NO_3^- reduction, and subsequently decreased to below the detectable limit in less than 40 h from the beginning of the experiment. Contrarily, in the microcosms containing compost, the highest NO_2^- concentration was observed after 40 h, and thereafter decreased along with NO_3^- concentration until both compounds were below the detectable limits, after 96 h. The differences in NO_2^- accumulation between the compost, stubble, and hay experiments were likely related to the rate of NO_3^- reduction. NO_2^- accumulation has been reported to depend on the relative rates of NO_3^- and NO_2^- reduction (Betlach and Tiedje, 1981), as well as on the type of C source and C/N ratios employed (Akunna et al., 1993; Ge et al., 2012). The slower reduction observed with compost could be due to the lower amount of material used in the experiments (0.25 g instead of the 1 g used for stubble and hay). Although the intrinsic C concentrations of the three sources were similar (Table 3), the C bioavailability could differ between each product, and even between replicates, due to heterogeneity in the materials (Breulmann et al., 2014; Sobczak and Findlay, 2002; Warneke et al., 2011). Consequently, the NPDOC concentration did not show a clear correlation with NO_3^- reduction, but provided an approximation of the amount of added C present in dissolved form. Although the quantity of compost in the microcosms was only one-quarter of the quantity of vegetal materials used, the measured NPDOC concentrations in the three types of microcosms were similar (13.2–27.3 mM for stubble, 11.8–16.8 mM for hay, and 5.3–14.3 mM for compost). The $\delta^{13}C$-DIC provided information about the transformation of organic C from the waste materials to inorganic C; a brief discussion is presented in the Supporting Information (Section S1).

Concerning the safety of the materials, the ICP-OES analyses showed that there was no release of toxic trace elements from any of the tested compounds (Supporting Information Table S4). Hay and stubble seemed to be more feasible than compost for application in the CW. Compost resulted in a lower denitrification rate, the NO_2^- accumulation lasted longer, and it was highly soluble and could be rapidly removed from the CW via the water flow. In this study, stubble was selected for application in the studied CW due to a higher availability in the area. Therefore, further experiments were only performed with stubble.

Table 3
Waste products composition. C and N concentrations and isotopic composition of the corn stubble, wheat hay, and animal compost employed to promote denitrification.

Source	C (%)	N (%)	$\delta^{13}C$ (‰)	$\delta^{15}N$ (‰)
Animal compost	32.1	3.1	−25.4	10.8
Wheat hay	40.9	0.4	−27.8	3.0
Corn stubble	36.1	1.0	−13.6	6.7

3.2. Lab-scale evaluation of the effect of temperature on denitrification induction by stubble

The denitrification activity of microorganisms is usually increased with higher temperatures, and therefore higher NO_3^- attenuation from water can be observed during warm periods (Rivett et al., 2008; Spieles and Mitsch, 1999). To assess the effect of temperature on the induced denitrification strategy, additional experiments were performed. A comparison between different incubation temperatures in corn stubble experiments showed that denitrification reached completion across the

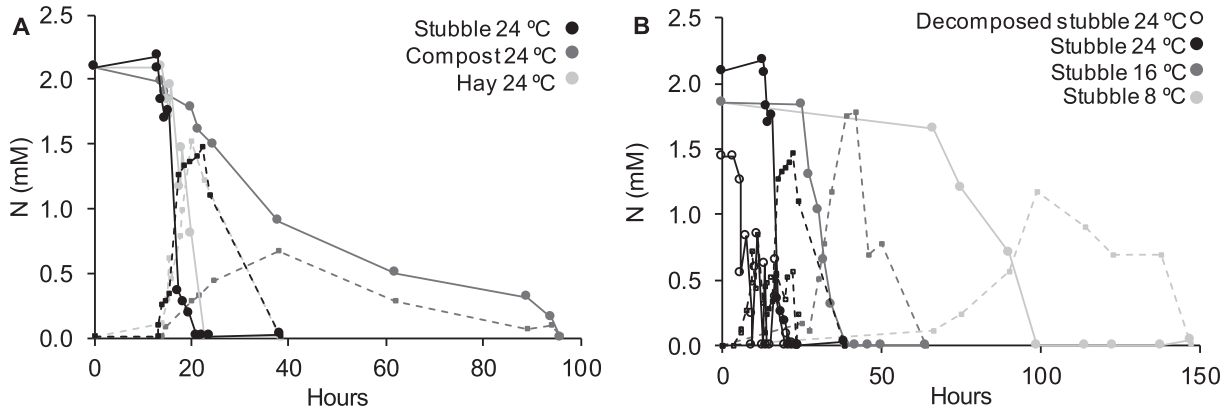

Fig. 2. Evolution of denitrification in the biostimulated microcosms. NO_3^- (circles joined by a continuous line) and NO_2^- (squares joined by a dashed line) measured in (A) the batch experiments employing different C sources and (B) the experiments testing the effects of temperature and lifespan of the stubble.

whole temperature range studied (from 8 to 24 °C), but with different lag periods and NO_3^- reduction rates. Complete denitrification was achieved after 40 h at 24 °C, 65 h at 16 °C, and 140 h at 8 °C (Fig. 2B). The decrease in NO_3^- began after 10 h at 24 °C, whereas at 16 °C and 8 °C lag periods of 45 h and 79 h, respectively, were observed. A decrease in NO_3^- reduction rate associated with lower temperatures following the Arrhenius relationship has been well documented (Dawson and Murphy, 1972). Therefore, the denitrification efficiency might decrease during the winter months or low-temperature periods in comparison to that during the summer months, and thus application of the carbon source throughout the spring months might be advantageous. Significant transient NO_2^- accumulation (up to 1.5 mM at 24 °C, 1.8 mM at 16 °C, and 1.0 mM at 8 °C) was observed in all the experiments. As discussed in the previous section, NO_2^- accumulation was less significant in the experiment with a lower denitrification rate (8 °C).

3.3. Lab-scale assessment of the lifespan of the denitrification induced by stubble

One of the main issues associated with biostimulation strategies is their effectiveness during long-term treatments. It is thus important to consider the lifespan of the material to be employed in the CW. In another laboratory experiment with vegetable materials (palm leaves and compost), induced NO_3^- degradation was shown to be maintained for more than 220 d (Grau-Martínez et al., 2017). In this context, microcosms containing partially decomposed stubble (sampled in the CW 7.5 months after its application) were incubated and compared to microcosms containing fresh stubble. The denitrification induced by the partially decomposed stubble proceeded at a higher rate than that induced by the fresh stubble; complete NO_3^- reduction was achieved in less than 25 h with the former, instead of 40 h with the latter (Fig. 2B). In the partially decomposed stubble microcosms, transient NO_2^- accumulation was below 0.8 mM. Due to the increased heterogeneity of the material after being in the field and in contact with water for months, high variabilities in both NO_3^- and NO_2^- concentrations were observed between replicates. Therefore, the reduction rates obtained from these experiments must be considered approximations. These results showed that the intrinsic capacity of the stubble to promote denitrification after 7.5 months being in contact with water was still important, at least at lab-scale. However, the NPDOC content in the microcosms containing partially decomposed stubble (1.7–8.8 mM) were lower than those in the microcosms with fresh stubble incubated at 24 °C (13.2–27.3 mM), pointing to a decreased availability of the electron donor over time. In the CW, the specific lifespan of the treatment might be shorter, since the organic C also typically consumes O_2 before using NO_3^- as an electron donor. The N_2O accumulated in the headspace of the microcosms containing partially decomposed stubble incubated at 24 °C (as well as that in the microcosms containing fresh stubble incubated at 16 and 8 °C) was also measured since the release of greenhouse gases during N transformation processes is a matter of concern. The maximum N_2O concentration detected accounted for 0.015% of the initial N-NO_3^- content of the microcosms (Supporting Information (Table S3)).

3.4. Lab-scale: NO_3^- isotopic fractionation calculation.

Under closed-system conditions, the isotopic fractionation (ε) for a determined element (e.g., N and O from dissolved NO_3^-) can be calculated by means of a Rayleigh distillation equation (Equation (1)). Thus, ε can be obtained from the slope of the linear correlation between the natural logarithm of the remaining substrate fraction ($Ln(C_{residual}/C_{initial})$, where C refers to analyte concentration) and the determined isotope ratios ($Ln(R_{residual}/R_{initial})$, where $R = \delta + 1$). These $\varepsilon^{15}N_{NO3/N2}$ and $\varepsilon^{18}O_{NO3/N2}$ values, determined at lab-scale under controlled conditions, can be later applied at field-scale to estimate the contribution of denitrification to the NO_3^- attenuation, while avoiding field-scale interference such as dilution due to rainfall (Böttcher et al., 1990; Mariotti et al., 1988). We calculated $\varepsilon^{15}N_{NO3/N2}$ and $\varepsilon^{18}O_{NO3/N2}$ under all tested conditions at lab-scale (Fig. 3) to appropriately evaluate the efficacy of the induced denitrification strategy tested at the CW. A summary of the calculated $\varepsilon^{15}N_{NO3/N2}$, $\varepsilon^{18}O_{NO3/N2}$, and $\varepsilon^{15}N/\varepsilon^{18}O$ values is shown in (Table 4); $\varepsilon^{15}N_{NO3/N2}$ ranged from −31.9 to −10.5‰, $\varepsilon^{18}O_{NO3/N2}$ from −30.4 to −9.7‰, and $\varepsilon^{15}N/\varepsilon^{18}O$ from 0.8 to 1.8. These values fall within the reported range for heterotrophic denitrification (see Table 4;Grau-Martínez et al., (2017)). The lowest $\varepsilon^{15}N_{NO3/N2}$ and $\varepsilon^{18}O_{NO3/N2}$ values were found for the microcosms containing compost incubated at 24 °C and stubble incubated at 8 °C, which were the two experiments that presented lower NO_3^- reduction rates. Apart from the microcosms containing stubble incubated at 8 °C, the other microcosms containing stubble (both fresh and partially decomposed and incubated at 16 or 24 °C) presented narrower ranges of $\varepsilon^{15}N_{NO3/N2}$ (from −28.3 to –22.5‰), $\varepsilon^{18}O_{NO3/N2}$ (from −30.4 to −21.2‰) and $\varepsilon^{15}N/\varepsilon^{18}O$ (from 0.8 to 1.1). These values were employed to assess the efficiency of the biostimulation strategy at the studied CW.

$$\mathrm{Ln}\left(\frac{R_{residual}}{R_{initial}}\right) = \varepsilon \times \mathrm{Ln}\left(\frac{C_{residual}}{C_{initial}}\right) \quad (1)$$

3.5. Performance of the CW before application of stubble

The chemical and isotopic characterization of the samples obtained from the CW both before and after application of the electron donor are presented in Supporting Information (Table S5). Three sampling campaigns were performed at the CW before stubble application. While

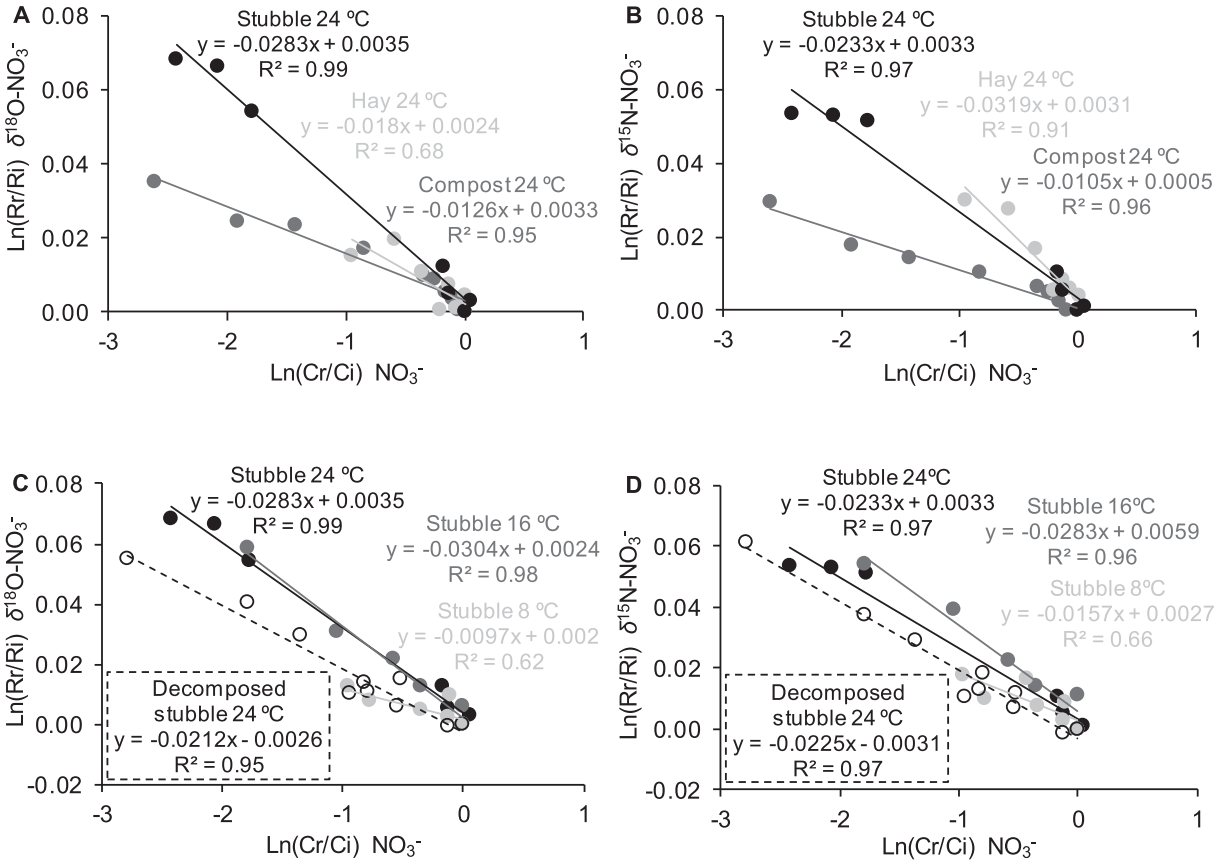

Fig. 3. NO_3^--O and NO_3^--N isotopic fractionation throughout denitrification in the biostimulated microcosms. Results from the batch experiments testing (A, B) different C sources and (C, D) the effects of temperature and lifespan of the stubble.

Table 4
Calculated ε values from the laboratory microcosms. $\varepsilon^{18}O_{NO3/N2}$, $\varepsilon^{15}N_{NO3/N2}$, and $\varepsilon^{15}N_{NO3/N2}/\varepsilon^{18}O_{NO3/N2}$ for each condition tested at laboratory-scale.

Experiment	$\varepsilon^{18}O_{NO3/N2}$	$\varepsilon^{15}N_{NO3/N2}$	$\varepsilon^{15}N/\varepsilon^{18}O$
Compost 24 °C	−12.6	−10.5	0.8
Hay 24 °C	−18.0	−31.9	1.8
Stubble 24 °C	−28.3	–23.3	0.8
Stubble 16 °C	−30.4	−28.3	0.9
Stubble 8 °C	−9.7	−15.7	1.6
Decomposed stubble 24 °C	−21.2	–22.5	1.1

NO_3^- was not significantly reduced during the two sampling campaigns performed at a ~5.5 L/s flow rate (June and September 2017), a slight attenuation (from 1.3 to 0.8 mM) occurred under operation at ~ 2.5 L/s (September 2017) (Fig. 4A). In all samples, NO_2^- was below the detection limit and NH_4^+ was below 0.01 mM, suggesting that NO_3^- had been either transformed to gaseous N products through denitrification or assimilated by plants or microorganisms (Supporting information (Table S5)). Whereas no increase in δ^{15}N-NO_3^- nor δ^{18}O-NO_3^- was observed in the samples collected during the first campaign at ~ 5.5 L/s (June 14, 2017), an increase was observed at the middle section of the CW (H3) during the second survey at ~5.5 L/s (September 5, 2017). In this latter campaign, the inlet (H1) presented δ^{15}N-NO_3^- and δ^{18}O-NO_3^- values of +11.6‰ and +8.7‰, respectively, which increased at the middle point (H3) up to +19.2‰ and +18.2‰, respectively, and decreased at the outlet (H6) to +9.6‰ and +7.1‰, respectively (Fig. 4B). A proposed explanation is that the occurrence of preferential flows within the wetland (e.g., heterogeneous flow rate between surface and bottom water or between lateral and central water) could have led to an increased hydraulic retention time and/or stagnant water at the H3 sampling site. In the campaign performed at a ~ 2.5 L/s flow rate (September 12, 2017), the decrease in NO_3^- concentration was coupled to increases in δ^{15}N-NO_3^- and δ^{18}O-NO_3^- from the inlet (+7.0‰ and + 4.7‰, respectively, at H1) to the outlet (+17.1‰ and + 13.0‰, respectively, at H6) of the CW (Fig. 4B). The slope of the relation between δ^{18}O-NO_3^- and δ^{15}N-NO_3^- for the samples collected in these three campaigns was 0.8 (r^2 = 0.91) (Fig. 4B), which is indicative of denitrification activity (Aravena and Robertson, 1998). These results are in agreement with previous results reporting the occurrence of denitrification in CWs even in the presence of dissolved O_2 (Sirivedhin and Gray, 2006). The intrinsic denitrification activity in the CW did not support complete denitrification, likely due to the low NPDOC content of the water (0.4–0.6 mM). Therefore, it was decided to evaluate the feasibility of adding an external electron donor source to promote NO_3^- attenuation when operating at a ~16 L/s flow rate.

3.6. Performance of the CW after application of stubble

Application of stubble in autumn (September 25, 2017) induced denitrification in the CW approximately 2 d after the application (Fig. 5B). Denitrification was almost complete at the outlet (H6) by 14 d following the application (0.2 mM NO_3^- remaining of the initial 1.4–1.7 mM) (Fig. 5A). In the two sampling campaigns, NO_2^- accumulated beginning at H2 and reached a concentration of 0.2 mM by the outlet (H6) by 7 d after treatment, but decreased to 0.1 mM by 14 d. Such a decrease in NO_2^- accumulation over time has been previously observed in laboratory experiments and other denitrification studies (Carrey et al., 2014; Margalef-Marti et al., 2019; Vidal-Gavilan et al., 2013). The maximum NH_4^+ concentration of 0.02 mM was measured at H3 after 7 d, while it decreased by the outlet (H6) to 0.01 mM in both campaigns, pointing to a non-significant contribution of DNRA. Due to

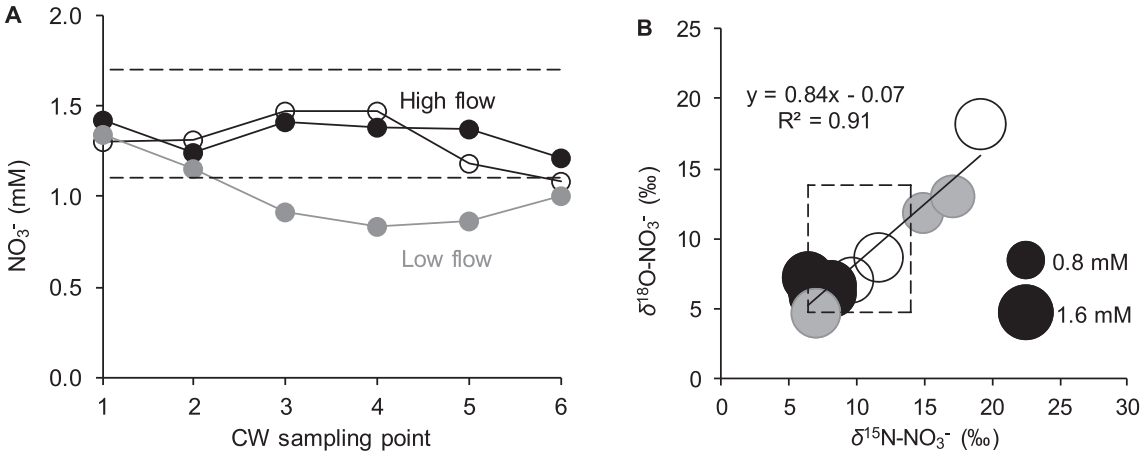

Fig. 4. NO_3^- attenuation in the CW before the application of stubble. Black circles depict the sampling campaigns performed at a ~5.5 L/s flow rate (full symbols for the campaign of June 14, 2017 and empty symbols for that of September 5, 2017), and grey circles depict the sampling campaigns performed at a ~2.5 L/s flow rate (September 12, 2017). (A) NO_3^- concentration along the CW flow direction, where dashed lines represent the range of NO_3^- concentrations measured at the inlet of the CW throughout the study period. (B) Isotopic characterization including the regression line, where the dashed square represents the range of isotopic compositions measured at the inlet of the CW throughout the study period.

the application of stubble, the outlet flow rate decreased until the system became partially blocked, leaving the monitoring probes exposed to the air. When the problem was solved (October 17, 2017) and the outlet flow was stabilized at approximately 16 L/s, the NO_3^- concentration monitored at the outlet showed fluctuations, pointing to a slight denitrification activity until October 24, 2017 (Fig. 5C). Thus, the lifetime of the treatment in autumn (recorded temperatures in October 2017 ranged from 10.3 °C to 20.4 °C, averaging 16.0 °C) was estimated to be between 2 weeks and 1 month.

Application of stubble in spring (May 5, 2018) also induced denitrification and underwent a shorter acclimation time (1 d) with respect to the first application, likely due to faster acclimation by the previously stimulated bacterial community (Fig. 6A). By 7 d after the stubble application, the NO_3^- concentration at the outlet (H6) was 0.2 mM, and denitrification was complete after 14 d. The NO_3^- concentration in the outlet then began to increase progressively until reaching a level similar to that at the inlet by approximately 100 d after treatment (Fig. 6B). A lower NO_3^- concentration measured in H3 during the last sampling campaign (+161 d) was attributed to stagnant water near the sampling point due to the accumulation of partially decomposed stubble. Thus, the treatment in spring-summer (temperatures recorded from May to October 2018 presented monthly minimums from 9.6 to 19.9 °C, monthly maximums from 20.0 to 28.4 °C, and monthly averages from 15.8 to 24.6 °C) induced significant denitrification for approximately three months, which is three times longer than that induced by the treatment in autumn. The NO_3^- concentration decrease at the outlet compared to inlet during these three months ranged from 0.1 to 1.5 mM (highest attenuation corresponded to the first month after stubble application). All the monitored NO_3^- concentrations at the inlet and outlet of the CW during this study period are presented in the Supporting Information Figure S1. The increased efficiency of the treatment in spring-summer compared to that of the treatment in autumn is in accordance with laboratory results (incubation at 8, 16, and 24 °C) and with previous wetland studies reporting increased denitrification rates at higher temperatures (Bachand and Horne, 1999; Christensen and Srensen, 1986; Si et al., 2018). The faster acclimation by the previously stimulated bacterial community could have been also responsible for this increased attenuation activity.

After the second stubble application, 0.1 mM of NO_2^- was detected at the outlet (H6) for 63 d. Afterwards, it was no longer detected (except at the aforementioned point H3 where water stagnated), confirming a decreased NO_2^- accumulation with time as observed during the previous treatment period. The maximum NH_4^+ concentration detected, 0.3 mM, was recorded at H4 7 d after application, while at the outlet (H6), the concentration was 0.05 mM. At 14 d and one month after application, NH_4^+ at the outlet decreased to 0.02 mM and 0.01 mM, respectively. These results suggest that transient DNRA activity could have arisen between H2 and H4 following the stubble application. NO_3^- is reduced to NH_4^+ through DNRA, depending on parameters such as microbial growth rate, NO_2^- accumulation, and the C:N ratio (Kraft et al., 2014). It is generally accepted that DNRA is favored at high C:N ratios, when NO_3^- is limited (rather than the electron donor being limited), or when high NO_3^- levels inhibit NO_2^- reductase (Giles et al., 2012; Kelso et al., 1997). This hypothesis is consistent with the higher degree of NH_4^+ accumulation observed in laboratory experiments compared to that observed in the field, since higher C:N ratios with a more homogeneous distribution were found in the batch experiments. It is also necessary to account for the possible input of N from the applied stubble. NO_2^- and NH_4^+ have a lower threshold for human consumption (0.01 and 0.03 mM, respectively) with respect to that of NO_3^- (0.8 mM) (98/83/EC, 1998). However, since NH_4^+ accumulation decreased before the outlet and fell to insignificant levels by 14 d after treatment, and the NO_2^- accumulation also decreased over time, stubble was considered effective in removing N compounds from agricultural runoff water.

A few authors have previously attempted to calculate the denitrification efficiency in CWs by means of isotopic assessment, but using ε values available in the literature and only for N-NO_3^- (Lund et al., 1999; Søvik and Mørkved, 2008). The $\varepsilon^{15}N_{NO3/N2}$ and $\varepsilon^{18}O_{NO3/N2}$ values obtained from our lab-scale experiments in which fresh stubble was incubated at 24 and 16 °C, and partially decomposed stubble was incubated at 24 °C, were used to calculate three denitrification % lines (Eq. (2), derived from Eq. (1)) that were plotted on a graph of δ^{18}O-NO_3^- versus δ^{15}N-NO_3^- along with the isotopic results for the CW samples (Fig. 7). These three laboratory conditions encompass the average temperatures recorded during the biostimulation periods tested at the CW. The slope of δ^{18}O-NO_3^- versus δ^{15}N-NO_3^- for the field samples collected after the biostimulation treatment was 1.0 (r^2 = 0.98) (Fig. 7), which is slightly higher than that obtained for the intrinsic denitrification before the stubble addition (0.8 (r^2 = 0.91)), which is likely due to the use of a different C source and the promotion of a different bacterial community. Also, the slope obtained after the biostimulation (1.0) was similar to the slopes obtained in the lab-scale experiments using partially decomposed stubble incubated at 24 °C (0.9) and those using fresh stubble incubated at 24 and 16 °C (1.25 and 1.1, respectively). This is consistent with the temperatures registered in

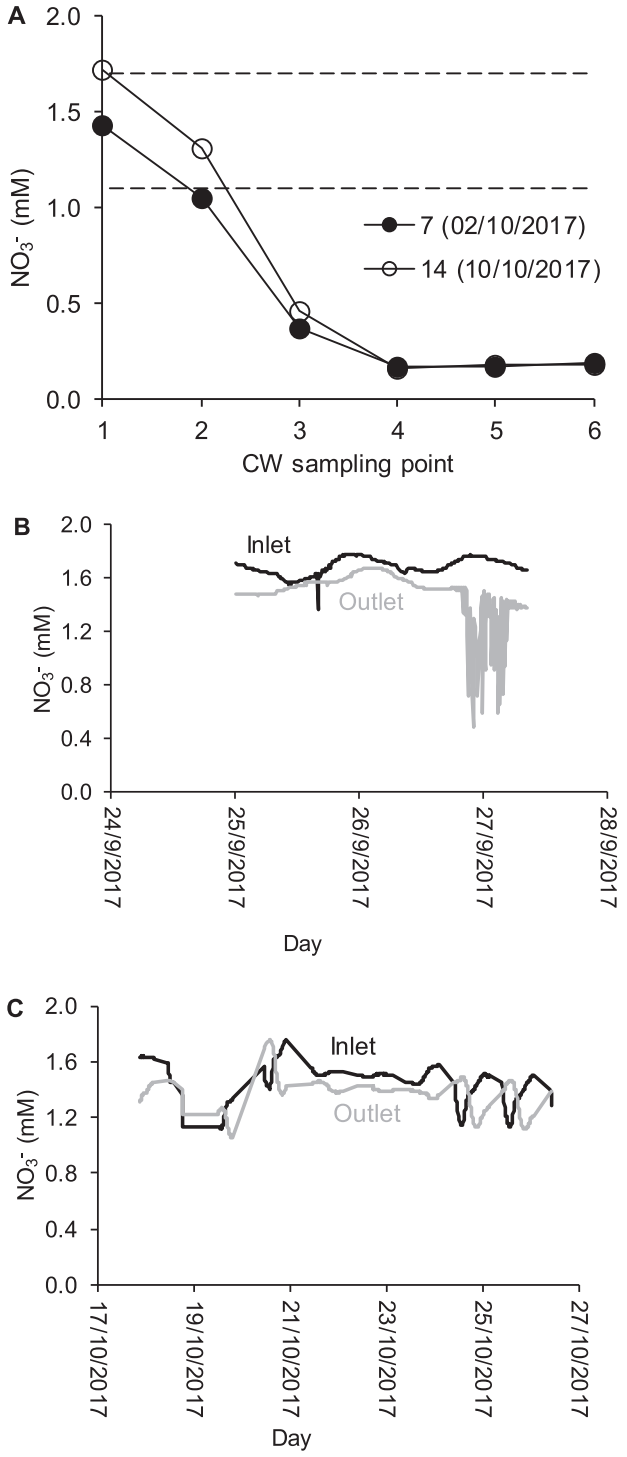

Fig. 5. NO_3^- attenuation in the CW after the first application of stubble in autumn. (A) NO_3^- concentration along the CW, where dashed lines represent the range of NO_3^- concentrations measured at the inlet of the CW throughout the study period. Full symbols depict the sampling campaign conducted on October 2, 2017, and empty symbols depict that conducted on October 10, 2017 (seven and fourteen days after the application of the stubble, respectively). (B, C) NO_3^- concentrations monitored at the inlet (black) and outlet (grey) in the days before and after the sampling campaigns, respectively.

the area throughout the test period, and with the stubble being in contact with water. This similarity between the field-scale and lab-scale slopes, together with the observed isotopic fractionation in the CW suggested that plant uptake did not likely contribute significantly to the NO_3^- removal.

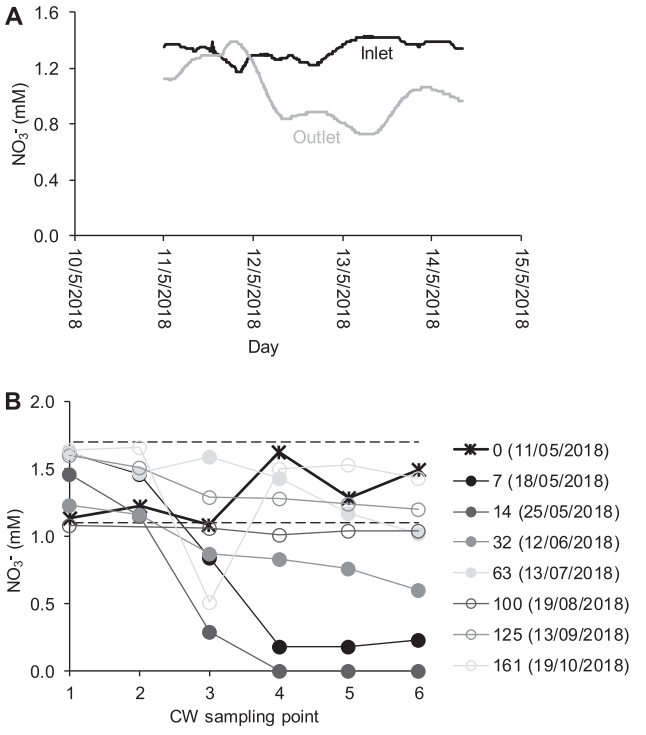

Fig. 6. NO_3^- attenuation in the CW after the second application of stubble in spring. (A) NO_3^- concentrations monitored at the inlet (black) and outlet (grey) of the CW throughout the first days of treatment. (B) NO_3^- concentrations along the CW flow direction, for each sampling campaign. Dashed lines represent the range of NO_3^- concentrations measured at the inlet of the CW throughout the study period. The 7 sampling campaigns performed throughout the 100 days after stubble application are represented by shades of grey (from darker to lighter as time progressed), with the last represented by the empty symbols. The campaign performed before application is represented by asterisks.

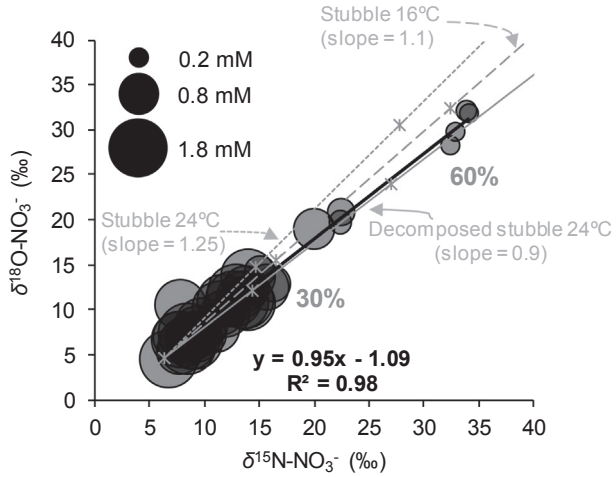

Fig. 7. Denitrification efficiency in the CW determined from the laboratory-obtained ε values. Isotopic values obtained from the samples collected at the CW, including the regression line (black). The three denitrification % lines (grey) presented correspond to the three conditions tested in the laboratory that were closest to the CW conditions throughout the field-scale test.

$$\text{Denitrification\%} = \left[1 - \left(\frac{C_{residual}}{C_{initial}}\right)\right] \times 100 = \left[1 - e^{\left(\frac{\delta_{residual} - \delta_{initial}}{\varepsilon}\right)}\right] \times 100 \quad (2)$$

The results showed that at least 60% of NO_3^- attenuation was

achieved in the CW due to the induced denitrification, although this value was obtained from the less-favorable situation (where the denitrification % was calculated from the experiments using stubble incubated at 24 °C). If the denitrification % is instead calculated based on the experiment using partially decomposed stubble incubated at 24 °C, which presents the slope most similar to that of the field samples (0.9 compared to 1.0), then denitrification accounted for a 70% NO_3^- removal. The largest contribution of denitrification, as determined by isotopic data, was observed in the outlet samples (H6) taken 7 and 14 d after the first stubble application, and 7 d after the second stubble application. By 14 d after the second stubble application, NO_3^- concentration in some samples was below the level required for the isotopic analysis. Therefore, the induced denitrification allowed a NO_3^- attenuation close to 100%. After two weeks of treatment, the contribution of the induced denitrification at the outlet (H6) began to decrease, from 30% in June 2018 to 5% in September 2018, and slightly increased to 20% by the last survey in October 2018. Considering an average flow rate of 16 L/s (the application of stubble led to fluctuations in the flow rate due to partial blockages at some points caused by stubble accumulation) and these results, in the studied CW, at least 80 kg of NO_3^- were removed per day over the first two weeks after the stubble application in May 2018 and 30 kg/d were removed from 14 to 63 d after the supply, after which time the removal decreased. A comparison between the denitrification percentages calculated using chemical and isotopic data revealed that using concentration values always resulted in a higher value. Since the contribution calculated from the isotopic data was considered to be linked to NO_3^- attenuation due to denitrification, the difference could be due to a decrease in NO_3^- concentration provoked by dilution due to precipitation, or the contribution of plant uptake to NO_3^- attenuation.

3.7. Effect and evolution of NPDOC in the CW

Since the amount of organic C released from the CW to the Lerma gully, and from there to the Arba River was a matter of concern, the NPDOC concentration in the field samples were measured. Only the results obtained from the second stubble application are discussed (the first application gave similar results). The NPDOC concentration at the outlet increased with respect to the background values by 7 d after application, and the increased level was maintained for 14 d in total (Fig. 8). The increase began at H3, reached a maximum between H4 and H5 (1.6–1.7 mM), and decreased to approximately 1.0–1.1 mM by the outlet (H6), indicating a release of organic C to the gully (background NPDOC concentrations ranged from 0.5 to 0.8 mM). Because the gully contained NO_3^--polluted water, it was considered that the surplus organic C could lead to NO_3^- attenuation downstream. The high NPDOC concentration detected between H3 and H5 could have provoked a decrease in water quality within the CW due to the promotion of processes such as DNRA (previously discussed) and bacterial SO_4^{2-} reduction (BSR), through which NH_4^+ and H_2S are produced, respectively. Although BSR is usually induced when NO_3^- is completely removed from the environment, the coexistence of denitrification and BSR in the presence of an abundance of an electron donor has also been demonstrated (Laverman et al., 2012). The isotopic characterization of SO_4^{2-} can provide information to assess its transformation processes because the decrease in SO_4^{2-} concentration is coupled to increases in δ^{34}S-SO_4^{2-} and δ^{18}O-SO_4^{2-} through the BSR (Strebel et al., 1990). Correlation between SO_4^{2-} concentration and isotopic composition was not identified in the samples collected at the CW, suggesting that BSR was not occurring in the CW. Therefore, the possibility of a decrease in water quality in the CW due to H_2S production as a result of excess organic C was discarded.

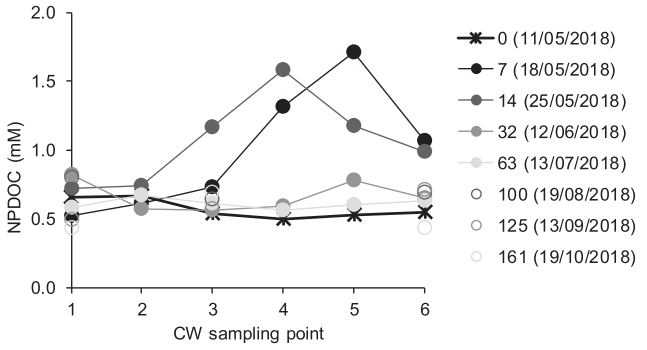

Fig. 8. Dissolved organic C in the CW before and after application of stubble. NPDOC concentration along the CW flow. The 5 sampling campaigns conducted within the 63 days after stubble application are presented in shades of grey, from darkest to lightest as time progressed. The campaign performed before application is represented by asterisks.

3.8. Suitability of the strategy and future improvements

The remediation strategy tested in the CW allowed the induction of the removal of NO_3^- from agricultural runoff water. The NO_3^- attenuation was primarily related to denitrification. Previous studies also found that denitrification was an important N sink in CWs in comparison to plant uptake (Lin et al., 2002; Soana et al., 2017). It has to be considered that denitrification can only be considered a N sink if intermediate products such as NO_2^- or N_2O are not accumulated during the NO_3^- reduction. The added stubble could have enhanced denitrification not only by increasing the organic C content of the water but also by inhibiting O_2 production through photosynthesis by shading the water column, as previously hypothesized by Jacobs and Harrison (2014) for floating vegetation in CWs. However, the denitrification efficiency was limited. The most likely explanation involves the high O_2 content of the inlet water (near saturation, approximately 0.28 and 0.34 mM in summer and winter, respectively) (Merchán et al., 2014) and the vast surface available for O_2 diffusion. Other parameters that could have also contributed to the limited denitrification efficiency include the high water flow rate tested in the CW (~16 L/s), and the possible generation of preferential flows within the CW (e.g., due to stubble accumulation in some points) that could led to a low degree of interaction between water and stubble.

Although application of solid residues such as maize stubble in surface flow CWs might have advantages over the application of liquid organic C sources, which face the problems of greater loss by bacterial oxidation (Lin et al., 2002) and greater release with the water flow, new strategies for increasing the lifespan and efficacy of the induced denitrification must be investigated. In addition, increased intrinsic denitrification capacity of the CW is expected after plant growth covers the entire surface. Previous studies have reported increased denitrification activity in vegetated CWs relative to the levels in non-vegetated systems (Lin et al., 2002; Soana et al., 2017), with efficacy varying among plants of different species or age (Lin et al., 2002; Lund et al., 1999). The organic C pool released after plant senescence has also been demonstrated to increase the bacterial activity, as this C can also be used as electron donor (Peralta et al., 2012; Soana et al., 2017). In this direction, Kang et al. (2018) proposed the use of plants whose growth season is winter. Therefore, the organic C supply from senescence would occur throughout the summer months, when temperatures are higher and more appropriate conditions are established for the promotion of significant denitrification activity.

N_2O production was not assessed in our field-scale tests. At lab-scale, limited N_2O production was observed. However, at field-scale, higher N_2O emissions could occur as a result of denitrification induced by the stubble addition because the high O_2 content of the inlet water and the free surface water flow might allow more extensive O_2 diffusion in water. Since N_2O emissions are detrimental for air quality, the production of this greenhouse gas should also be monitored in treatments aiming to induce denitrification. Isotopic characterization of the N_2O

emitted from a given CW could also provide further information about the N transformation processes that led to the decrease in NO_3^- concentration.

4. Conclusions

At laboratory-scale, maize stubble, wheat hay, and animal compost were able to induce complete denitrification. Stubble was selected for field-scale application due to its better local availability. In the following incubations, stubble sampled from the CW 7.5 months after its application was still able to support complete NO_3^- attenuation. Complete NO_3^- attenuation was achieved over the temperature range of 8 to 24 °C, although lower temperatures resulted in lower reduction rates. The $\varepsilon^{15}N_{NO3/N2}$ and $\varepsilon^{18}O_{NO3/N2}$ values obtained from the laboratory experiments allowed evaluation of the performance of the remediation strategy at the CW.

Before the application of the stubble, NO_3^- attenuation at the CW (from 1.3 to 0.8 mM) was only observed when the flow was decreased from approximately 5.5 to 2.5 L/s. The biostimulation in autumn–winter promoted NO_3^- attenuation lasting between 2 weeks and one month, while in spring-summer the attenuation capacity remained for approximately three months (~16 L/s flow rate). The isotopic characterization of the CW samples indicated that at least 60% of the initial NO_3^- was removed in the CW due to the induced denitrification. However, since in a few samples NO_3^- was below the limit necessary for isotopic analysis, the contribution could have been higher. The slope of $\delta^{18}O\text{-}NO_3^-$ versus $\delta^{15}N\text{-}NO_3^-$ obtained in the CW after the stubble application (1.0) was close to that obtained in the experiments involving partially decomposed stubble incubated at 24 °C (1.1). Plant uptake seemed to play only a minor role in NO_3^- attenuation in the CW. The treatment was considered safe because NO_2^- and NH_4^+ accumulation (below 0.2 and 0.1 mM, respectively) decreased over time, surplus NPDOC (below 2.3 mM) released from the CW could maintain NO_3^- attenuation downstream, and because the occurrence of BSR was discarded. However, the longevity and effectivity of the treatment were limited due to the high O_2 content of the inlet water, high water flow, and the possible generation of preferential flows within the CW.

Declaration of Competing Interest

The authors declare that they have no known competing financial interests or personal relationships that could have appeared to influence the work reported in this paper.

Acknowledgements

This work was financed by the projects REMEDIATION (CGL2014-57215-C4), AGRO-SOS (CGL2015-66016-R) and PACE-ISOTEC (CGL2017-87216-C4-1-R) financed by the Spanish Government and AEI/FEDER financed by the European Union, and by MAG (2017 SGR 1733) financed by the Catalan Government. R. Margalef-Marti thanks the Spanish Government for the Ph.D. grant BES-2015-072882. D. Merchán was supported by the "Juan de la Cierva – Formación" program (FJCI-2018-24920). We would also like to thank the CCiT of the Universitat the Barcelona for the analytical support, and A. Fernández for his contribution to the study.

Appendix A. Supplementary data

Supplementary data to this article can be found online at https://doi.org/10.1016/j.jhydrol.2019.124035.

References

91/676/EEC, 1991. Nitrates Directive. Council Directive 91/676/EEC of 12 December 1991, concerning the protection of waters against pollution caused by nitrates from agricultural sources. [WWW Document]. Off. J. Eur. Comm. URL http://ec.europa.eu/environment/index_en.htm (accessed 4.9.17).

98/83/EC, 1998. Drinking Water Directive. Council Directive 98/83/EC, of 3 November 1998, on the quality of water intended for human consumption. [WWW Document]. Off. J. Eur. Comm. URL http://ec.europa.eu/environment/index_en.htm (accessed 4.9.17).

Akunna, J.C., Bizeau, C., Moletta, R., 1993. Nitrate and nitrite reductions with anaerobic sludge using various carbon sources: glucose, glycerol, acetic acid, lactic acid and methanol. Water Res. 27, 1303–1312. https://doi.org/10.1016/0043-1354(93)90217-6.

Aravena, R., Robertson, W.D., 1998. Use of multiple isotope tracers to evaluate denitrification in ground water: study of nitrate from a large-flux septic system plume. Ground Water 36, 975–982.

Bachand, P.A.M., Horne, A.J., 1999. Denitrification in constructed free-water surface wetlands: I. Very high nitrate removal rates in a macrocosm study. Ecol. Eng. 14, 9–15. https://doi.org/10.1016/S0925-8574(99)00016-6.

Betlach, M.R., Tiedje, J.M., 1981. Kinetic Explanation for Accumulation of Nitrite, Nitric Oxide, and Nitrous Oxide during Bacterial Denitrification. Appl. Environ. Microbiol. 42, 1074–1084 https://doi.org/Article.

Beutel, M.W., Newton, C.D., Brouillard, E.S., Watts, R.J., 2009. Nitrate removal in surface-flow constructed wetlands treating dilute agricultural runoff in the lower Yakima Basin. Washington. Ecol. Eng. 35, 1538–1546. https://doi.org/10.1016/j.ecoleng.2009.07.005.

Böttcher, J., Strebel, O., Voerkelius, S., Schmidt, H.L., 1990. Using isotope fractionation of nitrate-nitrogen and nitrate-oxygen for evaluation of microbial denitrification in a sandy aquifer. J. Hydrol. 114, 413–424. https://doi.org/10.1016/0022-1694(90)90068-9.

Breulmann, M., Masyutenko, N.P., Kogut, B.M., Schroll, R., Dörfler, U., Buscot, F., Schulz, E., 2014. Short-term bioavailability of carbon in soil organic matter fractions of different particle sizes and densities in grassland ecosystems. Sci. Total Environ. 497–498, 29–37. https://doi.org/10.1016/j.scitotenv.2014.07.080.

Carrey, R., Otero, N., Vidal-Gavilan, G., Ayora, C., Soler, A., Gómez-Alday, J.J., 2014. Induced nitrate attenuation by glucose in groundwater: Flow-through experiment. Chem. Geol. 370, 19–28. https://doi.org/10.1016/j.chemgeo.2014.01.016.

Carrey, R., Rodríguez-Escales, P., Soler, A., Otero, N., 2018. Tracing the role of endogenous carbon in denitrification using wine industry by-product as an external electron donor: coupling isotopic tools with mathematical modeling. J. Environ. Manage. 207, 105–115. https://doi.org/10.1016/j.jenvman.2017.10.063.

Christensen, P.B., Srensen, J.A.N., 1986. Temporal Variation of Denitrification Activity in Plant-Covered, Littoral Sediment from Lake Hampen. Denmark 51, 1174–1179.

Cooper, A.B., Cooke, J.G., 1984. Nitrate loss and transformation in 2 vegetated headwater streams. New Zeal. J. Mar. Freshw. Res. 18, 441–450. https://doi.org/10.1080/00288330.1984.9516065.

Coplen, T.B., 2011. Guidelines and recommended terms for expression of stable-isotope-ratio and gas-ratio measurement results. Rapid Commun. Mass Spectrom. 25, 2538–2560. https://doi.org/10.1002/rcm.5129.

Dawson, R.N., Murphy, K.L., 1972. The temperature dependency of biological denitrification. Water Res. 6, 71–83. https://doi.org/10.1016/0043-1354(72)90174-1.

Dogramaci, S., Herczeg, A., Schiff, S., Bone, Y., 2001. Controls on $\delta^{34}S$ and $\delta^{18}O$ of dissolved sulfate in aquifers of the Murray Basin, Australia and their use as indicators of flow processes. Appl. Geochemistry 16, 475–488. https://doi.org/10.1016/S0883-2927(00)00052-4.

Estrada, N.L., Böhlke, J.K., Sturchio, N.C., Gu, B., Harvey, G., Burkey, K.O., Grantz, D.A., McGrath, M.T., Anderson, T.A., Rao, B., Sevanthi, R., Hatzinger, P.B., Jackson, W.A., 2017. Stable isotopic composition of perchlorate and nitrate accumulated in plants: Hydroponic experiments and field data. Sci. Total Environ. 595, 556–566. https://doi.org/10.1016/j.scitotenv.2017.03.223.

Fukada, T., Hiscock, K.M., Dennis, P.F., Grischek, T., 2003. A dual isotope approach to identify denitrification in groundwater at a river-bank infiltration site. Water Res. 37, 3070–3078. https://doi.org/10.1016/S0043-1354(03)00176-3.

Ge, S., Peng, Y., Wang, S., Lu, C., Cao, X., Zhu, Y., 2012. Nitrite accumulation under constant temperature in anoxic denitrification process: the effects of carbon sources and COD/NO3-N. Bioresour. Technol. 114, 137–143. https://doi.org/10.1016/j.biortech.2012.03.016.

Giles, M., Morley, N., Baggs, E.M., Daniell, T.J., 2012. Soil nitrate reducing processes - drivers, mechanisms for spatial variation, and significance for nitrous oxide production. Front. Microbiol. 3, 1–16. https://doi.org/10.3389/fmicb.2012.00407.

Grau-Martínez, A., Torrentó, C., Carrey, R., Rodríguez-Escales, P., Domènech, C., Ghiglieri, G., Soler, A., Otero, N., 2017. Feasibility of two low-cost organic substrates for inducing denitrification in artificial recharge ponds: batch and flow-through experiments. J. Contam. Hydrol. 198, 48–58. https://doi.org/10.1016/j.jconhyd.2017.01.001.

Gumbricht, T., 1993. Nutrient removal capacity in submersed macrophyte pond systems in a temperature climate. Ecol. Eng. 2, 49–61. https://doi.org/10.1016/0925-8574(93)90026-C.

Ilyas, H., Masih, I., 2017. The performance of the intensified constructed wetlands for organic matter and nitrogen removal: a review. J. Environ. Manage. 198, 372–383. https://doi.org/10.1016/j.jenvman.2017.04.098.

Jacobs, A.E., Harrison, J.A., 2014. Effects of floating vegetation on denitrification, nitrogen retention, and greenhouse gas production in wetland microcosms. Biogeochemistry 119, 51–66. https://doi.org/10.1007/s10533-013-9947-9.

Kang, Y., Zhang, J., Li, B., Zhang, Y., Sun, H., Hao Ngo, H., Guo, W., Xie, H., Hu, Z., Zhao, C., 2018. Improvement of bioavailable carbon source and microbial structure toward enhanced nitrate removal by Tubifex tubifex. Chem. Eng. J. 353, 699–707. https://doi.org/10.1016/j.cej.2018.07.182.

Kelso, B.H.L., Smith, R.V., Laughlin, R.J., Lennox, S.D., 1997. Dissimilatory nitrate

reduction in anaerobic sediments leading to river nitrite accumulation. Appl. Environ. Microbiol. 63, 4679–4685.
Knowles, R., 1982. Denitrification. Microbiol. Rev. 46, 43–70.
Kong, L., Wang, Y. Bin, Zhao, L.N., Chen, Z.H., 2009. Enzyme and root activities in surface-flow constructed wetlands. Chemosphere 76, 601–608. https://doi.org/10.1016/j.chemosphere.2009.04.056.
Kovacic, D.A., David, M.B., Gentry, L.E., Starks, K.M., Cooke, R.A., 2000. Effectiveness of Constructed Wetlands in Reducing Nitrogen and Phosphorus Export from Agricultural Tile Drainage. J. Environ. Qual. 29, 1262. https://doi.org/10.2134/jeq2000.00472425002900040033x.
Kraft, B., Tegetmeyer, H.E., Sharma, R., Klotz, M.G., Ferdelman, T.G., Hettich, R.L., Geelhoed, J.S., Strous, M., 2014. The environmental controls that govern the end product of bacterial nitrate respiration. Science 345 (6197), 676–679. https://doi.org/10.1126/science:1254070.
Laverman, A.M., Pallud, C., Abell, J., Cappellen, P. Van, 2012. Comparative survey of potential nitrate and sulfate reduction rates in aquatic sediments. Geochim. Cosmochim. Acta 77, 474–488. https://doi.org/10.1016/j.gca.2011.10.033.
Lin, Y.F., Jing, S.R., Wang, T.W., Lee, D.Y., 2002. Effects of macrophytes and external carbon sources on nitrate removal from groundwater in constructed wetlands. Environ. Pollut. 119, 413–420. https://doi.org/10.1016/S0269-7491(01)00299-8.
Lu, S., Hu, H., Sun, Y., Yang, J., 2009. Effect of carbon source on the denitrification in constructed wetlands. J. Environ. Sci. 21, 1036–1043. https://doi.org/10.1016/S1001-0742(08)62379-7.
Lund, L., Horne, A., Williams, A., 1999. Estimating denitrification in a large constructed wetland using stable nitrogen isotope ratios. Ecol. Eng. 14, 67–76. https://doi.org/10.1016/S0925-8574(99)00020-8.
Margalef-Marti, R., Carrey, R., Soler, A., Otero, N., 2019. Evaluating the potential use of a dairy industry residue to induce denitrification in polluted water bodies: a flow-through experiment. J. Environ. Manage. 245. https://doi.org/10.1016/j.jenvman.2019.03.086.
Mariotti, A., Germon, J.C., Hubert, P., Kaiser, P., Letolle, R., Tardieux, A., Tardieux, P., 1981. Experimental determination of nitrogen kinetic isotope fractionation: some principles; illustration for the denitrification and nitrification processes. Plant Soil 62, 413–430. https://doi.org/10.1007/BF02374138.
Mariotti, A., Landreau, A., Simon, B., 1988. ^{15}N isotope biogeochemistry and natural denitrification process in groundwater: application to the chalk aquifer of northern France. Geochim. Cosmochim. Acta 52, 1869–1878. https://doi.org/10.1016/0016-7037(88)90010-5.
McIlvin, M.R., Altabet, M.A., 2005. Chemical conversion of nitrate and nitrite to nitrous oxide for nitrogen and oxygen isotopic analysis in freshwater and seawater. Anal Chem 77, 5589–5595. https://doi.org/10.1021/ac050528s.
Merchán, D., Causapé, J., Abrahão, R., 2013. Impact of irrigation implementation on hydrology and water quality in a small agricultural basin in Spain. Hydrol. Sci. J. 58, 1400–1413. https://doi.org/10.1080/02626667.2013.829576.
Merchán, D., Causapé, J., Abrahão, R., García-Garizábal, I., 2015. Assessment of a newly implemented irrigated area (Lerma Basin, Spain) over a 10-year period. II: salts and nitrate exported. Agric. Water Manag. https://doi.org/10.1016/j.agwat.2015.04.019.
Merchán, D., Otero, N., Soler, A., Causapé, J., 2014. Main sources and processes affecting dissolved sulphates and nitrates in a small irrigated basin (Lerma Basin, Zaragoza, Spain): isotopic characterization. Agric. Ecosyst. Environ. 195, 127–138. https://doi.org/10.1016/j.agee.2014.05.011.
Peralta, A.L., Matthews, J.W., Flanagan, D.N., Kent, A.D., 2012. Environmental factors at dissimilar spatial scales influence plant and microbial communities in restored wetlands. Wetlands 32, 1125–1134. https://doi.org/10.1007/s13157-012-0343-3.
Rivett, M.O., Buss, S.R., Morgan, P., Smith, J.W.N., Bemment, C.D., 2008. Nitrate attenuation in groundwater: a review of biogeochemical controlling processes. Water Res. 42, 4215–4232. https://doi.org/10.1016/j.watres.2008.07.020.
Rogers, K.H., Breen, P.F., Chick, A.J., 1991. Nitrogen Removal in Experimental Wetland Treatment Systems: Evidence for the Role of Aquatic Plants. Res. J. Water Pollut. Control Fed. 63, 934–941.
Ryabenko, E., Altabet, M.a., Wallace, D.W.R., 2009. Effect of chloride on the chemical conversion of nitrate to nitrous oxide for $\delta^{15}N$ analysis. Limnol. Oceanogr. Methods 7, 545–552. https://doi.org/10.4319/lom.2009.7.545.
Scott, J.T., McCarthy, M.J., Gardner, W.S., Doyle, R.D., 2008. Denitrification, dissimilatory nitrate reduction to ammonium, and nitrogen fixation along a nitrate concentration gradient in a created freshwater wetland. Biogeochemistry 87, 99–111. https://doi.org/10.1007/s10533-007-9171-6.
Si, Z., Song, X., Wang, Y., Cao, X., Zhao, Y., Wang, B., Chen, Y., Arefe, A., 2018. Intensified heterotrophic denitrification in constructed wetlands using four solid carbon sources: denitrification efficiency and bacterial community structure. Bioresour. Technol. 267, 416–425. https://doi.org/10.1016/j.biortech.2018.07.029.
Sirivedhin, T., Gray, K.A., 2006. Factors affecting denitrification rates in experimental wetlands: field and laboratory studies. Ecol. Eng. 26, 167–181. https://doi.org/10.1016/j.ecoleng.2005.09.001.
Soana, E., Balestrini, R., Vincenzi, F., Bartoli, M., Castaldelli, G., 2017. Mitigation of nitrogen pollution in vegetated ditches fed by nitrate-rich spring waters. Agric. Ecosyst. Environ. 243, 74–82. https://doi.org/10.1016/j.agee.2017.04.004.
Sobczak, W.V., Findlay, S., 2002. Variation in Bioavailability of Dissolved Organic Carbon among Stream Hyporheic Flowpaths. Ecology 83, 3194–3209.
Søvik, A.K., Mørkved, P.T., 2008. Use of stable nitrogen isotope fractionation to estimate denitrification in small constructed wetlands treating agricultural runoff. Sci. Total Environ. 392, 157–165. https://doi.org/10.1016/j.scitotenv.2007.11.014.
Spieles, D.J., Mitsch, W.J., 1999. The effects of season and hydrologic and chemical loading on nitrate retention in constructed wetlands: a comparison of low- and high-nutrient riverine systems. Ecol. Eng. 14, 77–91. https://doi.org/10.1016/S0925-8574(99)00021-X.
Spoelstra, J., Schiff, S.L., Semkin, R.G., Jeffries, D.S., Elgood, R.J., 2010. Nitrate attenuation in a small temperate wetland following forest harvest. For. Ecol. Manage. 259, 2333–2341. https://doi.org/10.1016/j.foreco.2010.03.006.
Strebel, O., Böttcher, J., Fritz, P., 1990. Use of isotope fractionation of sulfate-sulfur and sulfate-oxygen to assess bacterial desulfurication in a sandy aquifer. J. Hydrol. 121, 155–172. https://doi.org/10.1016/0022-1694(90)90230-U.
Tanner, C.C., Nguyen, M.L., Sukias, J.P.S., 2005. Nutrient removal by a constructed wetland treating subsurface drainage from grazed dairy pasture. Agric. Ecosyst. Environ. 105, 145–162. https://doi.org/10.1016/j.agee.2004.05.008.
Trois, C., Coulon, F., de Combret, C.P., Martins, J.M.F., Oxarango, L., 2010. Effect of pine bark and compost on the biological denitrification process of non-hazardous landfill leachate: focus on the microbiology. J. Hazard. Mater. 181, 1163–1169. https://doi.org/10.1016/j.jhazmat.2010.05.077.
Uusheimo, S., Tulonen, T., Aalto, S.L., Arvola, L., 2018. Mitigating agricultural nitrogen load with constructed ponds in northern latitudes: a field study on sedimental denitrification rates. Agric. Ecosyst. Environ. 261, 71–79. https://doi.org/10.1016/j.agee.2018.04.002.
Vidal-Gavilan, G., Folch, A., Otero, N., Solanas, A.M., Soler, A., 2013. Isotope characterization of an in situ biodenitrification pilot-test in a fractured aquifer. Appl. Geochemistry 32, 153–163. https://doi.org/10.1016/j.apgeochem.2012.10.033.
Vitousek, P.M., Aber, J.D., Howarth, R.W., Likens, G.E., Matson, P.A., Schindler, D.W., Schlesinger, W.H., Tilman, D.G., 1997. Summary for Policymakers, in: Intergovernmental Panel on Climate Change (Ed.), Climate Change 2013 - The Physical Science Basis. Cambridge University Press, Cambridge, pp. 1–30. https://doi.org/10.1017/CBO9781107415324.004.
Vymazal, J., 2007. Removal of nutrients in various types of constructed wetlands. Sci. Total Environ. 380, 48–65. https://doi.org/10.1016/j.scitotenv.2006.09.014.
Ward, M.H., DeKok, T.M., Levallois, P., Brender, J., Gulis, G., Nolan, B.T., VanDerslice, J., 2005. Workgroup Report: Drinking-Water Nitrate and Health—Recent Findings and Research Needs. Environ. Health Perspect. 113, 1607–1614. https://doi.org/10.1289/ehp.8043.
Warneke, S., Schipper, L.A., Matiasek, M.G., Scow, K.M., Cameron, S., Bruesewitz, D.A., McDonald, I.R., 2011. Nitrate removal, communities of denitrifiers and adverse effects in different carbon substrates for use in denitrification beds. Water Res. 45, 5463–5475. https://doi.org/10.1016/j.watres.2011.08.007.
Wu, H., Zhang, J., Ngo, H.H., Guo, W., Hu, Z., Liang, S., Fan, J., Liu, H., 2015. A review on the sustainability of constructed wetlands for wastewater treatment: design and operation. Bioresour. Technol. 175, 594–601. https://doi.org/10.1016/j.biortech.2014.10.068.

SUPPLEMENTARY INFORMATION TO:

Feasibility of using rural waste products to increase the denitrification efficiency in a surface flow constructed wetland.

Rosanna Margalef-Marti[1], Raúl Carrey[1], Daniel Merchán[2], Albert Soler[1], Jesús Causapé[3], Neus Otero[1,4]

[1] Grup MAiMA, SGR Mineralogia Aplicada, Geoquímica i Geomicrobiologia, Departament de Mineralogia, Petrologia i Geologia Aplicada, Facultat de Ciències de la Terra, Universitat de Barcelona (UB), C/Martí i Franquès s/n, 08028 Barcelona (Spain).

[2]Department of Engineering, IS-FOOD Institute (Innovation & Sustainable Development in Food Chain), Public University of Navarre, Campus de Arrosadia, 31006 Pamplona, Navarra, Spain.

[3] Geological Survey of Spain—IGME, C/Manuel Lasala 44 9◦B, 50006 Zaragoza, Spain.

[4] Serra Húnter Fellowship, Generalitat de Catalunya, Spain.

Journal of Hydrology,

Volume 578, November 2019, 124035

https://doi.org/10.1016/j.jhydrol.2019.124035

Supporting Information, section S1: δ^{13}C-DIC results

The δ^{13}C-DIC results provided information about the transformation of organic C from the waste materials to inorganic C (**Equation S1**). These results are presented in Supporting Information **Table S2**. As DIC concentration increased, the initial δ^{13}C-DIC in water of -13.1 ‰ decreased to -15.5 ‰ and -20.0 ‰ in the microcosms containing hay and compost, respectively, but remained unchanged in the stubble experiment (**Figure S2**). The flat trend observed in the experiments with stubble, in contrast to the correlations obtained with the experiments employing hay and compost, was attributed to the intrinsic δ^{13}C-C_{bulk} of each material (**Table 3**). The most significant change in the δ^{13}C-DIC was observed for the experiment involving hay, which presented a lower δ^{13}C-C_{bulk} (-27.8 ‰) compared to that of compost (-25.4‰); stubble did not produce any change because its δ^{13}C-C_{bulk} (-13.6 ‰) is close to the δ^{13}C-DIC of water (-13.1 ‰). Hay and stubble presented a different intrinsic δ^{13}C-C_{bulk} as they are classified as C4 and C3 plants, respectively (Leary, 1988). An isotopic fractionation effect derived from the bacterial C metabolism did not seem to be significant under the tested conditions. These results show that the δ^{13}C-DIC analysis can be applied to assess the efficiency of biostimulation strategies at field-scale when C sources with an intrinsic δ^{13}C-C_{bulk} differing from the δ^{13}C-DIC of water (such as C4 plant materials) are used.

$$5\ CH_2O + 4\ NO_3^- + 4\ H^+ \rightarrow 2\ N_2 + 5\ CO_2 + 7\ H_2O$$

Equation S1

References:

Leary, M.H.O., 1988. Carbon Isotopes in Photosynthesis. Bioscience 38, 328–336.

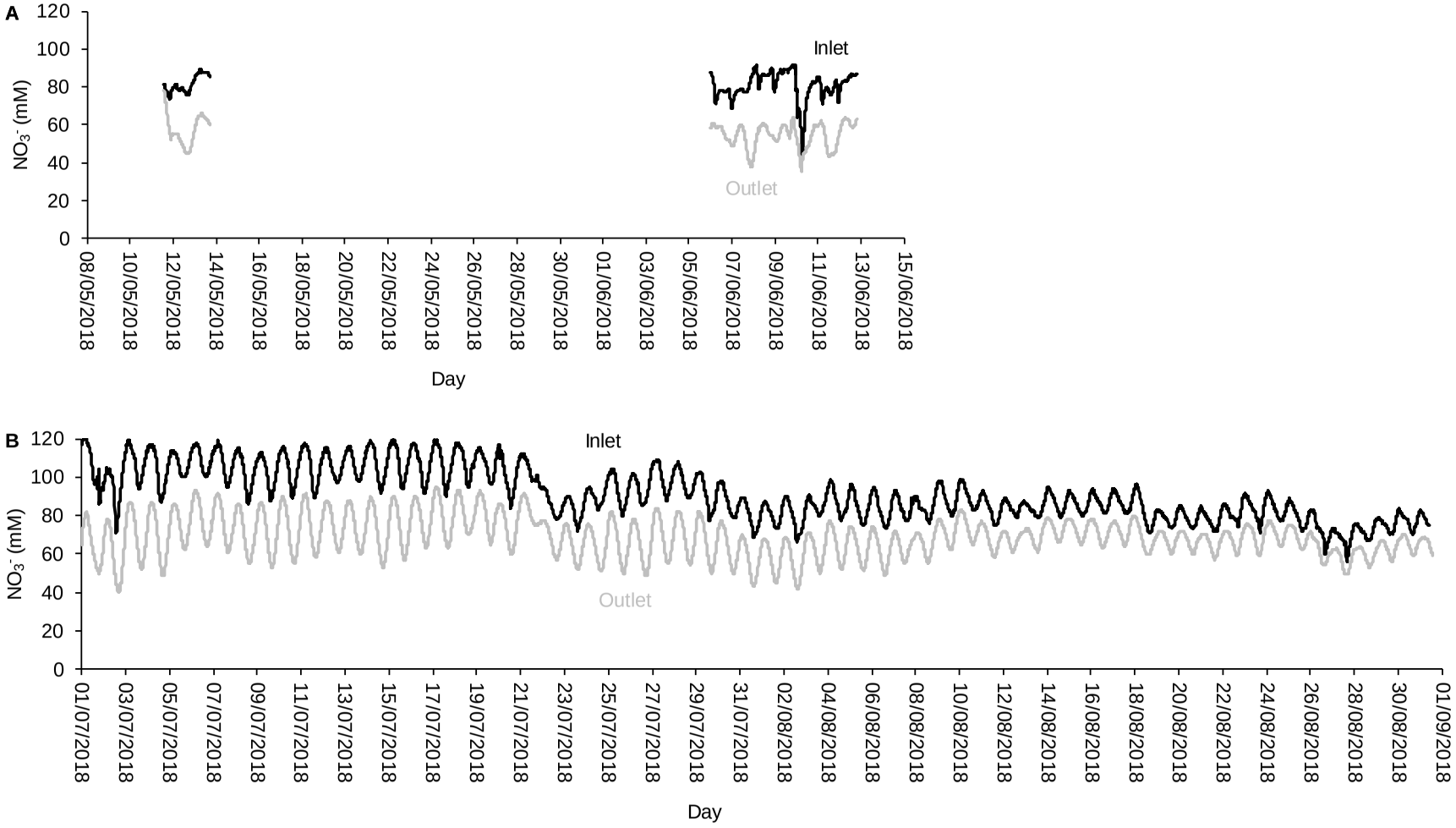

Figure S1. Monitored NO_3^- concentrations at the inlet and outlet of the CW during the third period of the test. The NO_3^- retention time in the CW was considered for the outlet data. (**A**) May-June 2018 and (**B**) July-August 2018. The data between 10/05/2018 and 06/06/2018 and between 13/06/2018 and 01/07/2018 is lacking due to technical issues.

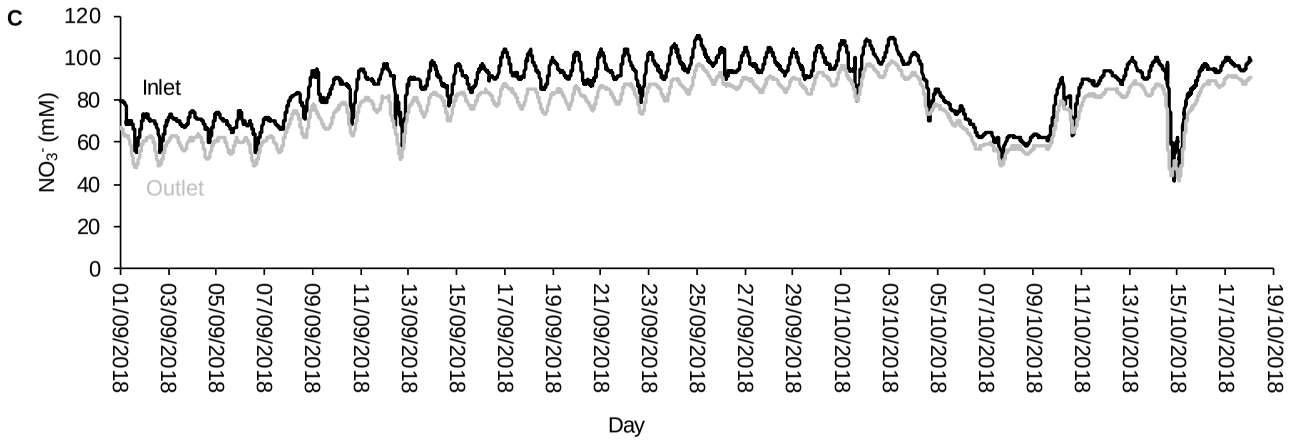

Figure S1. Monitored NO_3^- concentrations at the inlet and outlet of the CW during the third period of the test. The NO_3^- retention time in the CW was considered for the outlet data. (**C**) September-October 2018.

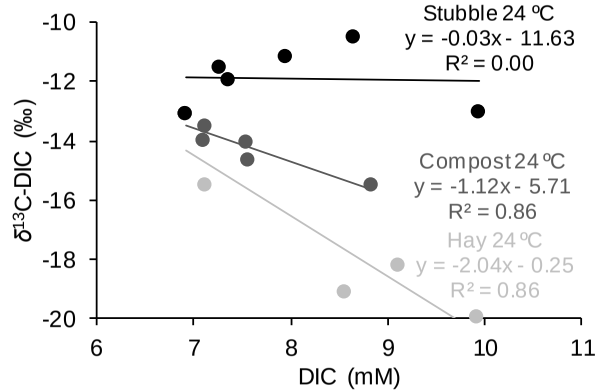

Figure S2. Relationship between δ^{13}C-DIC and DIC concentration throughout denitrification. Correlation between δ^{13}C-DIC and DIC concentration in the samples collected from laboratory batch experiments testing different C sources for the induction of the bacterial NO_3^- reduction.

Table S1. Precipitation and temperature records. Data collected from a meteorological station near the CW (coordinates X = 649168.18 and Y = 4662201.55).

Month	Precipitation (mm)	Average temperature (ºC)	Minimum temperature (ºC)	Maximum temperature (ºC)
June-17	80.2	23.2	13.2	30.2
July-17	46.6	23.6	15.1	28.3
August-17	79.4	23.2	16.5	29.1
September-17	47.2	17.6	12.5	23.3
October-17	11.1	16.0	10.3	20.4
November-17	13.1	8.6	2.5	15.3
December-17	17.3	5.1	0.3	9.4
January-18	64.5	6.8	2.0	12.7
February-18	37.6	4.9	0.9	10.0
March-18	82.8	8.5	3.8	12.3
April-18	173.9	12.8	5.8	16.8
May-18	54.7	15.8	9.6	20.0
June-18	17.3	20.9	15.8	26.2
July-18	44.2	24.6	19.9	28.4
August-18	4.4	23.8	19.1	28.2
September-18	19.7	21.2	15.9	23.9
October-18	0.0	16.3	13.1	18.8

Table S2. Standards for isotopic analysis. International and laboratory (CCiT) standards used for normalization of the results.

Analysis	Standards
$\delta^{15}N\text{-}NO_3^-$	USGS-32, USGS-34, USGS-35 and CCiT-IWS ($\delta^{15}N$ = +16.9 ‰)
$\delta^{18}O\text{-}NO_3^-$	USGS-32, USGS-34, USGS-35 and CCiT-IWS ($\delta^{18}O$ = +28.5 ‰)
$\delta^{15}N\text{-}N_{bulk}$	USGS-40, IAEA-N1, IAEA-NO3, IAEA-N2
$\delta^{13}C\text{-}C_{bulk}$	USGS-40, IAEA-CH7, IAEA-CH6
$\delta^{13}C$-DIC	CCiT-$NaHCO_3$ ($\delta^{13}C$ = -4.4 ‰), CCiT-$NaKHCO_3$ ($\delta^{13}C$ = -18.7 ‰) and CCiT-$KHCO_3$ ($\delta^{13}C$ = +29.2 ‰)
$\delta^{34}S\text{-}SO_4^{2-}$	NBS-127, SO5, SO6 and CCiT-YCEM ($\delta^{34}S$ = +12.8 ‰)
$\delta^{18}O\text{-}SO_4^{2-}$	NBS-127, SO6, USGS-34, CCiT-YCEM ($\delta^{18}O$ = +17.6 ‰) and CCiT-ACID ($\delta^{18}O$ = +13.2 ‰)

Table S3. Batch experiments results. N and C compounds concentration and isotopic composition. NH_4^+ in the DS-24 experiment was analyzed by ion selective electrode while in the others by spectrophotometry. * % of initial NO_3^-–N found as N_2O-N, n.d. = non determined.

Code	Hour	NO_3^- (mM)	NO_2^- (mM)	NH_4^+ (mM)	N_2O (nmol)	N_2O (%)*	NPDOC (mM)	DIC (mM)	$\delta^{15}N\text{-}NO_3^-$ (‰)	$\delta^{18}O\text{-}NO_3^-$ (‰)	$\delta^{13}C\text{-}DIC$ (‰)
CW water	0.0	2.1	0.0	0.0	n.d.	n.d.	0.5	6.9	6.4	4.9	-13.1
C-24-1	14.0	2.0	0.0	0.1	n.d.	n.d.	10.2	7.1	4.6	5.7	-13.5
C-24-2	14.5	1.9	0.1	0.1	n.d.	n.d.	n.d.	n.d.	6.7	8.5	n.d.
C-24-3	20.0	1.8	0.3	0.1	n.d.	n.d.	9.0	7.1	9.3	10.6	-14.0
C-24-4	21.5	1.6	0.3	0.1	n.d.	n.d.	n.d.	n.d.	11.6	13.8	n.d.
C-24-5	24.5	1.5	0.4	0.1	n.d.	n.d.	10.6	7.5	13.1	15.2	-14.1
C-24-6	38.0	0.9	0.7	0.1	n.d.	n.d.	8.8	7.6	17.0	22.6	-14.7
C-24-7	62.0	0.5	0.3	0.1	n.d.	n.d.	n.d.	n.d.	21.2	28.9	n.d.
C-24-8	89.0	0.3	0.1	n.d.	n.d.	n.d.	5.3	8.8	24.5	30.0	-15.5
C-24-9	94.0	0.2	0.1	n.d.	n.d.	n.d.	n.d.	n.d.	36.4	41.0	n.d.
C-24-10	96.0	0.0	0.0	n.d.	n.d.	n.d.	7.8	n.d.	n.d.	n.d.	n.d.
C-24-blank	188.0	0.0	0.0	n.d.	n.d.	n.d.	14.3	n.d.	n.d.	n.d.	n.d.
H-24-1	13.8	2.1	0.1	0.1	n.d.	n.d.	14.7	n.d.	10.3	9.5	-18.3
H-24-2	15.0	1.8	0.3	0.1	n.d.	n.d.	13.4	9.1	15.2	12.7	-18.3
H-24-3	15.5	1.7	0.6	n.d.	n.d.	n.d.	n.d.	n.d.	12.3	5.8	n.d.
H-24-4	15.8	1.9	0.5	n.d.	n.d.	n.d.	n.d.	n.d.	12.4	6.3	n.d.
H-24-5	17.8	1.2	0.8	0.0	n.d.	n.d.	11.8	n.d.	34.5	25.1	-17.7
H-24-6	18.0	1.5	1.0	n.d.	n.d.	n.d.	n.d.	n.d.	23.3	15.9	n.d.
H-24-7	20.0	0.8	1.5	n.d.	n.d.	n.d.	n.d.	n.d.	37.0	20.7	n.d.
H-24-8	22.5	0.0	1.2	0.0	n.d.	n.d.	12.5	8.6	n.d.	n.d.	-19.2
H-24-9	38.5	0.0	0.0	0.2	n.d.	n.d.	14.7	9.9	n.d.	n.d.	-20.0
H-24-blank-1	4.0	0.1	0.0	0.0	n.d.	n.d.	n.d.	n.d.	n.d.	n.d.	n.d.
H-24-blank-2	38.5	0.0	0.0	n.d.	n.d.	n.d.	16.9	1.8	n.d.	n.d.	n.d.
S-24-1	13.0	2.2	0.0	0.2	n.d.	n.d.	14.7	9.9	7.8	8.0	-13.0
S-24-2	13.3	2.1	0.1	n.d.	n.d.	n.d.	n.d.	n.d.	n.d.	n.d.	-11.4
S-24-3	14.0	1.8	0.3	n.d.	n.d.	n.d.	15.7	7.3	11.9	10.3	-11.6
S-24-4	14.8	1.7	0.3	n.d.	n.d.	n.d.	n.d.	n.d.	n.d.	n.d.	n.d.
S-24-5	15.5	1.8	0.3	0.3	n.d.	n.d.	18.2	7.4	17.2	17.5	-12.0
S-24-6	17.5	0.3	1.3	n.d.	n.d.	n.d.	13.2	n.d.	59.4	60.8	n.d.
S-24-7	18.5	0.3	1.3	0.1	n.d.	n.d.	n.d.	n.d.	61.1	73.8	n.d.
S-24-8	19.5	0.2	1.4	n.d.	n.d.	n.d.	n.d.	n.d.	62.0	76.1	n.d.
S-24-9	21.0	0.0	1.4	0.1	n.d.	n.d.	n.d.	n.d.	n.d.	n.d.	n.d.
S-24-10	22.3	0.0	1.5	n.d.	n.d.	n.d.	15.9	8.0	n.d.	n.d.	-11.2
S-24-11	23.8	0.0	1.1	n.d.	n.d.	n.d.	n.d.	n.d.	n.d.	n.d.	n.d.
S-24-12	38.5	0.0	0.0	1.0	n.d.	n.d.	18.5	8.7	n.d.	n.d.	-10.5
S-24-blank-1	38.5	0.1	0.0	0.0	n.d.	n.d.	27.3	n.d.	n.d.	n.d.	n.d.
CW water	0.0	1.9	0.0	n.d.	n.d.	n.d.	n.d.	n.d.	5.9	8.0	n.d.
S-16-1	25.0	1.8	0.2	n.d.	0.8	0.001	n.d.	n.d.	17.4	14.3	n.d.
S-16-2	27.0	1.3	0.1	n.d.	0.6	0.001	n.d.	n.d.	20.5	20.5	n.d.
S-16-3	30.0	1.0	0.5	n.d.	n.d.	n.d.	n.d.	n.d.	28.7	29.8	n.d.

Table S3. Continued.

Code	Hour	NO_3^- (mM)	NO_2^- (mM)	NH_4^+ (mM)	N_2O (nmol)	N_2O (%)*	NPDOC (mM)	DIC (mM)	$\delta^{15}N\text{-}NO_3^-$ (‰)	$\delta^{18}O\text{-}NO_3^-$ (‰)	$\delta^{13}C\text{-}DIC$ (‰)
CW water	0.0	2.1	0.0	0.0	n.d.	n.d.	0.5	6.9	6.4	4.9	-13.1
S-16-4	32.0	0.6	0.8	n.d.	2.5	0.002	n.d.	n.d.	46.2	39.7	n.d.
S-16-5	34.0	0.3	1.2	n.d.	n.d.	n.d.	n.d.	n.d.	62.1	68.6	n.d.
S-16-6	39.0	0.0	1.7	n.d.	8.7	0.009	n.d.	n.d.	n.d.	n.d.	n.d.
S-16-7	42.0	0.0	1.8	n.d.	1.9	0.002	n.d.	n.d.	n.d.	n.d.	n.d.
S-16-8	46.0	0.0	0.7	n.d.	0.4	0.000	n.d.	n.d.	n.d.	n.d.	n.d.
S-16-9	50.0	0.0	0.8	n.d.	1.1	0.001	n.d.	n.d.	n.d.	n.d.	n.d.
S-16-10	64.0	0.0	0.0	n.d.	n.d.	n.d.	n.d.	n.d.	n.d.	n.d.	n.d.
S-8'-1	66.0	1.6	0.0	n.d.	n.d.	n.d.	n.d.	n.d.	9.0	10.1	n.d.
S-8'-2	99.0	1.3	0.3	n.d.	n.d.	n.d.	n.d.	n.d.	13.6	13.0	n.d.
S-8'-3	114.0	0.9	0.3	n.d.	n.d.	n.d.	n.d.	n.d.	16.4	15.7	n.d.
S-8-1	66.0	1.7	0.1	n.d.	1.5	0.001	n.d.	n.d.	15.0	17.4	n.d.
S-8-2	75.0	1.2	0.2	n.d.	1.8	0.002	n.d.	n.d.	22.9	n.d.	n.d.
S-8-3	90.0	0.7	0.6	n.d.	2.0	0.002	n.d.	n.d.	24.3	20.6	n.d.
S-8-4	99.0	0.0	1.2	n.d.	5.1	0.005	n.d.	n.d.	n.d.	n.d.	n.d.
S-8-5	114.0	0.0	0.9	n.d.	2.8	0.003	n.d.	n.d.	n.d.	n.d.	n.d.
S-8-6	123.0	0.0	0.7	n.d.	0.0	0.000	n.d.	n.d.	n.d.	n.d.	n.d.
S-8-7	138.0	0.0	0.7	n.d.	3.4	0.003	n.d.	n.d.	n.d.	n.d.	n.d.
S-8-8	147.0	0.0	0.0	n.d.	0.6	0.001	n.d.	n.d.	n.d.	n.d.	n.d.
CW water	0.0	1.4	0.0	n.d.	n.d.	n.d.	0.5	n.d.	14.5	13.4	n.d.
DS-24-1	3.5	1.4	0.0	n.d.	n.d.	n.d.	n.d.	n.d.	n.d.	n.d.	n.d.
DS-24-2	5.5	1.3	0.1	0.1	n.d.	n.d.	2.2	n.d.	13.5	12.8	n.d.
DS-24-3	6.0	0.6	0.1	0.0	2.9	0.003	1.7	n.d.	25.2	23.9	n.d.
DS-24-4	7.5	0.8	0.3	n.d.	n.d.	n.d.	n.d.	n.d.	21.5	19.3	n.d.
DS-24-5	9.0	0.2	0.5	n.d.	1.6	0.002	1.9	n.d.	53.1	55.0	n.d.
DS-24-6	9.5	0.0	0.7	1.3	n.d.	n.d.	2.5	n.d.	n.d.	n.d.	n.d.
DS-24-7	10.5	0.6	0.4	n.d.	n.d.	n.d.	n.d.	n.d.	n.d.	n.d.	n.d.
DS-24-8	11.0	0.9	0.8	n.d.	5.4	0.005	n.d.	n.d.	26.7	28.6	n.d.
DS-24-9	12.5	0.0	0.3	n.d.	n.d.	n.d.	n.d.	n.d.	n.d.	n.d.	n.d.
DS-24-10	13.3	0.6	0.5	1.0	n.d.	n.d.	n.d.	n.d.	28.1	27.6	n.d.
DS-24-11	14.0	0.0	0.5	n.d.	n.d.	n.d.	1.7	n.d.	n.d.	n.d.	n.d.
DS-24-12	15.0	0.0	0.5	n.d.	n.d.	n.d.	n.d.	n.d.	n.d.	n.d.	n.d.
DS-24-13	17.0	0.6	0.5	n.d.	15.1	0.015	n.d.	n.d.	33.3	24.2	n.d.
DS-24-14	17.0	0.4	0.6	0.9	11.7	0.012	n.d.	n.d.	44.3	43.6	n.d.
DS-24-15	20.0	0.0	0.4	0.3	n.d.	n.d.	n.d.	n.d.	n.d.	n.d.	n.d.
DS-24-16	20.3	0.1	0.5	n.d.	12.7	0.013	n.d.	n.d.	78.5	70.7	n.d.
DS-24-17	22.0	0.0	0.6	n.d.	n.d.	n.d.	n.d.	n.d.	n.d.	n.d.	n.d.
DS-24-18	23.0	0.0	0.0	0.5	n.d.	n.d.	8.8	n.d.	n.d.	n.d.	n.d.
DS-24-19	24.0	0.0	0.2	n.d.	n.d.	n.d.	1.7	n.d.	n.d.	n.d.	n.d.

Table S4. ICP data. Major cations and trace elements concentration measured in the samples from the laboratory experiments (semiquantitative). All data is expressed as ppm. Hyphen = below detection limit. The Al, As, Be, Mo, Ni, Pb, Sb, Se and Ti were below detection limit in all analyzed samples.

Code	Hour	Na	S	Ca	Mg	K	Si	Sr	P	B	Li	Mn	Zn	Cu	Fe	Ba	V	Co	Tl	Cd	Cr
CW water	0.0	326.8	146.3	130.7	99.3	6.2	10.9	4.2	-	0.35	0.12	-	-	0.08	0.01	0.06	0.06	0.01	0.14	-	0.01
C-24-1	14.0	345.0	163.0	125.8	103.4	65.4	11.4	3.9	1.4	0.42	0.13	0.05	0.09	0.04	0.10	0.05	0.07	-	-	-	-
C-24-2	14.5	334.6	151.1	125.4	101.2	43.3	11.1	3.9	0.8	0.39	0.13	0.05	0.06	0.04	0.07	0.05	0.07	0.01	-	-	-
C-24-3	20.0	321.8	151.8	124.0	100.4	58.2	10.9	3.8	1.0	0.40	0.12	0.06	0.07	0.03	0.08	0.05	0.07	-	0.15	-	-
C-24-5	24.5	328.7	160.1	123.2	102.8	68.7	11.3	3.8	1.2	0.42	0.13	0.08	0.11	0.04	0.11	0.05	0.07	-	-	-	-
C-24-6	38.0	325.2	152.3	123.1	104.6	51.6	11.4	3.6	1.4	0.41	0.13	0.11	0.11	0.04	0.12	0.04	0.07	-	-	-	-
C-24-8	89.0	334.2	151.7	125.6	104.5	41.5	12.1	3.6	1.4	0.40	0.13	0.12	0.05	0.05	0.07	0.04	0.07	-	-	0.01	-
H-24-1	13.8	360.3	168.3	139.4	102.3	160.1	22.8	4.3	0.6	0.38	0.13	0.04	0.04	0.03	0.02	0.11	0.07	0.02	-	0.01	-
H-24-2	15.0	362.0	165.3	139.5	105.0	130.8	22.2	4.2	2.3	0.38	0.13	0.05	0.04	0.03	0.02	0.24	0.06	-	-	-	-
H-24-5	17.8	371.4	170.9	141.4	103.0	142.1	22.1	4.3	-	0.38	0.13	0.06	0.05	0.03	0.01	0.11	0.06	-	-	-	-
H-24-8	22.5	365.1	169.0	140.9	103.4	180.9	25.1	4.3	-	0.37	0.13	0.06	0.06	0.03	0.02	0.16	0.07	0.01	-	-	-
H-24-9	38.5	355.7	164.3	140.4	104.1	167.2	31.2	4.4	0.8	0.37	0.13	0.04	0.06	0.03	0.01	0.13	0.06	-	-	-	-
S-24-1	13.0	318.9	155.5	136.2	108.1	130.8	13.4	4.0	1.2	0.48	0.12	0.10	0.09	0.07	0.06	0.08	0.07	-	-	-	-
S-24-2	13.3	324.5	146.8	128.6	101.5	75.5	13.6	3.8	1.6	0.36	0.12	0.11	0.05	0.05	0.04	0.07	0.06	0.01	-	-	-
S-24-3	14.0	325.3	148.8	126.4	101.4	118.2	13.0	3.7	2.2	0.38	0.12	0.13	0.03	0.04	0.04	0.07	0.06	-	0.15	-	-
S-24-5	15.5	329.9	151.8	130.2	103.2	78.9	14.4	3.8	1.4	0.39	0.12	0.17	0.03	0.04	0.04	0.08	0.06	-	-	-	-
S-24-10	22.3	318.4	149.4	130.9	104.5	108.7	13.9	3.8	0.8	0.39	0.13	0.12	0.04	0.05	0.04	0.12	0.07	-	-	-	-
S-24-12	38.5	329.2	150.0	139.0	109.9	99.5	14.4	4.0	1.1	0.39	0.13	0.16	0.04	0.06	0.05	0.10	0.07	0.03	-	-	0.01

Table S5. CW test results. Chemical and isotopic characterization of the samples collected in the CW previous and after the implementation of the bioremediation strategy. X^1 is calculated from concentration data while X2 is calculated from isotopic data, n.d. = non determined, NH_4^+ in the 2017 campaigns was analyzed by ion chromatography while in the 2018 campaigns by ion selective electrode.

Date	Point	NO_2^- (mM)	NO_3^- (mM)	NH_4^+ (mM)	DIC (mM)	NPDOC (mM)	SO_4^{2-} (mM)	δ^{13}C-DIC (‰)	δ^{15}N-NO_3^- (‰)	δ^{18}O-NO_3^- (‰)	δ^{34}S-SO_4^{2-} (‰)	δ^{18}O-SO_4^{2-} (‰)	NO_3^- attenuation		
													%[1]	%[2]	kg/d
14/06/17	H1	0.0	1.4	n.d.	7.1	n.d.	n.d.	n.d.	6.4	7.2	0.8	12.5	n.d.	n.d.	n.d.
	H2	0.0	1.2	n.d.	6.9	n.d.	n.d.	n.d.	6.8	5.9	n.d.	n.d.	n.d.	n.d.	n.d.
	H3	0.0	1.4	n.d.	6.8	n.d.	n.d.	n.d.	6.8	6.5	1.8	12.7	n.d.	n.d.	n.d.
	H4	0.0	1.4	n.d.	n.d.	n.d.	n.d.	n.d.	8.1	6.7	n.d.	n.d.	n.d.	n.d.	n.d.
	H5	0.0	1.4	n.d.	6.9	n.d.	n.d.	n.d.	7.5	6.6	n.d.	n.d.	n.d.	n.d.	n.d.
	H6	0.0	1.2	n.d.	7.0	n.d.	n.d.	n.d.	8.3	6.1	2.5	12.4	n.d.	n.d.	n.d.
05/09/17	H1	0.0	1.3	0.0	7.5	0.6	n.d.	-12.9	11.6	8.7	n.d.	n.d.	n.d.	n.d.	n.d.
	H2	0.0	1.3	n.d.	7.3	0.5	n.d.	-12.7	n.d.	n.d.	n.d.	n.d.	n.d.	n.d.	n.d.
	H3	0.0	1.5	0.0	7.4	0.4	n.d.	-12.7	19.2	18.2	n.d.	n.d.	n.d.	n.d.	n.d.
	H4	0.0	1.5	n.d.	7.5	0.6	n.d.	-12.2	n.d.	n.d.	n.d.	n.d.	n.d.	n.d.	n.d.
	H5	0.0	1.2	n.d.	7.3	0.5	n.d.	-12.8	n.d.	n.d.	n.d.	n.d.	n.d.	n.d.	n.d.
	H6	0.0	1.1	0.0	7.3	0.5	n.d.	-12.4	9.6	7.1	n.d.	n.d.	n.d.	n.d.	n.d.
12/09/17	H1	0.0	1.3	0.0	7.1	0.4	n.d.	-12.4	7.0	4.7	3.4	13.5	n.d.	n.d.	n.d.
	H2	0.0	1.2	n.d.	7.5	0.5	n.d.	-12.8	n.d.	n.d.	n.d.	n.d.	n.d.	n.d.	n.d.
	H3	0.0	0.9	0.0	7.1	0.5	n.d.	-12.5	14.9	11.8	3.6	13.8	n.d.	n.d.	n.d.
	H4	0.0	0.8	n.d.	6.5	0.6	n.d.	-12.1	n.d.	n.d.	n.d.	n.d.	n.d.	n.d.	n.d.
	H5	0.0	0.9	n.d.	6.4	0.6	n.d.	-11.8	n.d.	n.d.	n.d.	n.d.	n.d.	n.d.	n.d.
	H6	0.0	1.0	0.0	6.6	0.5	n.d.	-12.0	17.1	13.0	3.1	13.1	n.d.	n.d.	n.d.
02/10/17	H1	0.0	1.4	0.0	7.0	0.4	4.2	-12.7	9.7	8.4	n.d.	n.d.	0.0	0.0	n.d.
	H2	0.1	1.1	n.d.	7.5	0.8	4.2	-11.8	13.7	12.4	n.d.	n.d.	26.5	16.8	n.d.
	H3	0.1	0.4	0.0	8.2	1.3	3.7	-12.1	22.4	20.9	n.d.	n.d.	73.8	43.9	n.d.

Table S5. Continued.

Date	Point	NO_2^- (mM)	NO_3^- (mM)	NH_4^+ (mM)	DIC (mM)	NPDOC (mM)	SO_4^{2-} (mM)	δ^{13}C-DIC (‰)	δ^{15}N-NO_3^- (‰)	δ^{18}O-NO_3^- (‰)	δ^{34}S-SO_4^{2-} (‰)	δ^{18}O-SO_4^{2-} (‰)	NO_3^- attenuation		
													%[1]	%[2]	kg/d
02/10/17	H4	0.2	0.2	n.d.	8.9	1.9	4.5	-11.7	n.d.	n.d.	n.d.	n.d.	87.8	n.d.	n.d.
	H5	0.2	0.2	n.d.	9.1	1.3	4.7	-12.0	n.d.	n.d.	n.d.	n.d.	87.8	n.d.	n.d.
	H6	0.2	0.2	0.0	9.1	2.3	4.4	-13.1	32.9	29.9	n.d.	n.d.	86.3	64.0	78.4
10/10/17	H1	0.0	1.7	0.0	n.d.	0.4	3.7	-12.6	8.5	7.4	3.9	13.9	0.0	0.0	n.d.
	H2	0.0	1.3	n.d.	7.6	0.6	3.7	-12.0	11.7	11.0	n.d.	n.d.	23.8	14.2	n.d.
	H3	0.1	0.5	0.0	8.1	0.9	3.0	-11.4	15.1	14.4	4.3	12.9	72.9	26.6	n.d.
	H4	0.1	0.2	n.d.	8.7	1.6	3.0	-11.1	n.d.	n.d.	n.d.	n.d.	90.7	n.d.	n.d.
	H5	0.1	0.2	n.d.	8.8	1.1	3.9	-11.5	n.d.	n.d.	n.d.	n.d.	89.1	n.d.	n.d.
	H6	0.1	0.2	0.0	n.d.	1.1	3.9	-11.5	34.1	31.9	4.4	12.6	89.5	68.1	100.3
11/05/18	H1	0.0	1.1	0.0	6.9	0.7	3.9	n.d.	11.1	8.0	4.2	12.4	n.d.	n.d.	n.d.
	H2	0.0	1.2	n.d.	7.0	0.7	4.3	n.d.	n.d.	n.d.	n.d.	n.d.	n.d.	n.d.	n.d.
	H3	0.0	1.1	0.0	6.8	0.5	4.2	n.d.	n.d.	n.d.	4.3	12.1	n.d.	n.d.	n.d.
	H4	0.0	1.6	n.d.	0.0	0.5	5.2	n.d.	13.7	11.1	n.d.	n.d.	n.d.	n.d.	n.d.
	H5	0.0	1.3	n.d.	6.9	0.5	5.4	n.d.	13.5	10.7	4.4	12.1	n.d.	n.d.	n.d.
	H6	0.0	1.5	0.0	6.9	0.5	5.4	n.d.	12.7	11.2	n.d.	n.d.	n.d.	n.d.	n.d.
18/05/18	H1	0.0	1.6	0.0	7.1	0.5	5.7	n.d.	12.9	11.9	3.9	12.2	0.0	0.0	n.d.
	H2	0.0	1.5	0.0	7.2	0.6	5.6	n.d.	13.9	10.7	n.d.	n.d.	9.9	0.0	n.d.
	H3	0.1	0.8	0.1	0.0	0.7	5.7	n.d.	20.1	19.0	3.7	12.1	48.0	27.8	n.d.
	H4	0.1	0.2	0.3	8.0	1.3	5.5	n.d.	n.d.	n.d.	n.d.	n.d.	88.8	n.d.	n.d.
	H5	0.1	0.2	0.3	7.9	1.7	5.7	n.d.	32.4	28.2	n.d.	n.d.	88.8	55.8	n.d.
	H6	0.1	0.2	0.1	7.9	1.1	5.5	n.d.	33.9	32.1	3.9	12.2	85.7	61.0	84.5
25/05/18	H1	0.0	1.5	0.0	7.2	0.7	5.8	n.d.	14.0	13.8	3.6	12.4	0.0	0.0	n.d.
	H2	0.0	1.2	0.1	7.5	0.7	5.7	n.d.	11.9	9.5	n.d.	n.d.	21.3	0.0	n.d.
	H3	0.1	0.3	0.0	8.1	1.2	5.3	n.d.	22.4	19.7	4.2	11.8	79.9	27.7	28.1

Table S5. Continued.

Date	Point	NO_2^- (mM)	NO_3^- (mM)	NH_4^+ (mM)	DIC (mM)	NPDOC (mM)	SO_4^{2-} (mM)	δ^{13}C-DIC (‰)	δ^{15}N-NO_3^- (‰)	δ^{18}O-NO_3^- (‰)	δ^{34}S-SO_4^{2-} (‰)	δ^{18}O-SO_4^{2-} (‰)	NO_3^- attenuation		
													%[1]	%[2]	kg/d
25/05/18	H4	0.0	0.0	0.1	9.4	1.6	4.4	n.d.	n.d.	n.d.	n.d.	n.d.	100.0	n.d.	n.d.
	H5	0.1	0.0	0.1	8.1	1.2	5.4	n.d.	n.d.	n.d.	3.9	11.8	100.0	n.d.	n.d.
	H6	0.1	0.0	0.0	8.3	1.0	5.2	n.d.	n.d.	n.d.	n.d.	n.d.	100.0	n.d.	n.d.
12/06/18	H1	0.0	1.2	0.0	0.0	0.8	4.2	n.d.	9.2	7.0	3.9	12.6	0.0	0.0	n.d.
	H2	0.0	1.2	0.0	7.4	0.6	4.3	n.d.	n.d.	n.d.	n.d.	n.d.	5.9	n.d.	n.d.
	H3	0.0	0.9	n.d.	7.3	0.6	4.2	n.d.	10.0	7.1	3.8	12.5	29.4	2.1	n.d.
	H4	0.0	0.8	0.0	0.0	0.6	4.2	n.d.	n.d.	n.d.	n.d.	n.d.	32.1	n.d.	n.d.
	H5	0.1	0.8	n.d.	0.0	0.8	4.3	n.d.	n.d.	n.d.	n.d.	n.d.	37.7	n.d.	n.d.
	H6	0.1	0.6	0.0	7.6	0.7	4.3	n.d.	16.3	12.9	3.9	12.4	51.2	25.8	27.1
13/07/18	H1	0.0	1.6	0.0	6.9	0.6	3.5	n.d.	8.4	6.1	n.d.	n.d.	0.0	0.0	n.d.
	H2	0.0	1.5	0.0	6.7	0.7	3.6	n.d.	n.d.	n.d.	n.d.	n.d.	9.7	n.d.	n.d.
	H3	0.0	1.6	0.0	7.1	0.6	3.4	n.d.	9.2	6.6	n.d.	n.d.	2.2	n.d.	n.d.
	H4	0.0	1.4	0.0	0.0	0.6	3.3	n.d.	n.d.	n.d.	n.d.	n.d.	12.0	n.d.	n.d.
	H5	0.1	1.2	n.d.	7.6	0.6	3.3	n.d.	n.d.	n.d.	n.d.	n.d.	27.8	n.d.	n.d.
	H6	0.1	1.0	0.0	0.0	0.6	3.3	n.d.	15.7	12.6	n.d.	n.d.	36.8	26.9	37.4
19/08/18	H1	0.0	1.1	n.d.	0.0	0.8	2.2	n.d.	7.7	5.4	4.7	12.2	0.0	0.0	n.d.
	H3	0.0	1.1	n.d.	0.0	0.6	2.2	n.d.	n.d.	n.d.	4.6	11.9	1.8	n.d.	n.d.
	H4	0.0	1.0	n.d.	7.8	n.d.	2.2	n.d.	n.d.	n.d.	n.d.	n.d.	7.0	n.d.	n.d.
	H5	0.0	1.0	n.d.	n.d.	n.d.	2.1	n.d.	n.d.	n.d.	n.d.	n.d.	4.5	n.d.	n.d.
	H6	0.0	1.0	n.d.	n.d.	0.7	2.1	n.d.	8.8	5.8	4.0	11.8	4.1	3.3	3.1
13/09/18	H1	0.0	1.6	n.d.	n.d.	0.5	2.4	n.d.	7.8	6.7	n.d.	n.d.	0.0	0.0	n.d.
	H2	0.0	1.5	n.d.	n.d.	n.d.	2.5	n.d.	n.d.	n.d.	n.d.	n.d.	5.7	n.d.	n.d.
	H3	0.0	1.3	n.d.	n.d.	0.6	2.5	n.d.	7.6	7.0	n.d.	n.d.	19.0	0.3	n.d.
	H4	0.0	1.3	n.d.	n.d.	n.d.	2.5	n.d.	7.9	10.6	n.d.	n.d.	19.7	8.5	n.d.

Table S5. Continued.

Date	Point	NO_2^- (mM)	NO_3^- (mM)	NH_4^+ (mM)	DIC (mM)	NPDOC (mM)	SO_4^{2-} (mM)	δ^{13}C-DIC (‰)	δ^{15}N-NO_3^- (‰)	δ^{18}O-NO_3^- (‰)	δ^{34}S-SO_4^{2-} (‰)	δ^{18}O-SO_4^{2-} (‰)	NO_3^- attenuation		
													%[1]	%[2]	kg/d
13/09/18	H5	0.0	1.2	n.d.	n.d.	n.d.	2.5	n.d.	n.d.	n.d.	n.d.	n.d.	22.3	n.d.	n.d.
	H6	0.0	1.2	n.d.	n.d.	0.7	2.5	n.d.	9.2	7.6	n.d.	n.d.	24.7	5.0	6.9
19/10/18	H1	0.0	1.6	n.d.	n.d.	0.4	2.6	n.d.	6.7	4.5	n.d.	n.d.	0.0	0.0	n.d.
	H2	0.0	1.7	n.d.	n.d.	n.d.	2.5	n.d.	n.d.	n.d.	n.d.	n.d.	-1.4	n.d.	n.d.
	H3	0.0	0.5	n.d.	n.d.	0.7	2.6	n.d.	7.8	7.1	n.d.	n.d.	68.6	8.3	n.d.
	H4	0.0	1.5	n.d.	n.d.	n.d.	2.6	n.d.	n.d.	n.d.	n.d.	n.d.	8.7	n.d.	n.d.
	H5	0.0	1.5	n.d.	n.d.	n.d.	2.6	n.d.	n.d.	n.d.	n.d.	n.d.	6.6	n.d.	n.d.
	H6	0.0	1.4	n.d.	n.d.	0.4	2.6	n.d.	11.4	10.1	n.d.	n.d.	12.6	21.0	29.4

ANNEX 5

Use of nitrogen and oxygen isotopes of dissolved nitrate to trace field-scale induced denitrification efficiency throughout an in-situ groundwater remediation strategy.

Rosanna Margalef-Marti[1], Raúl Carrey[1], Marta Viladés[2], Irene Jubany[3], Ester Vilanova[4], Roser Grau[5], Albert Soler[1], Neus Otero[1,6]

[1] Grup MAiMA, SGR Mineralogia Aplicada, Geoquímica i Geomicrobiologia, Departament de Mineralogia, Petrologia i Geologia Aplicada, Facultat de Ciències de la Terra, Universitat de Barcelona (UB), C/Martí i Franquès s/n, 08028 Barcelona (Spain).

[2] Sustainability Department, Fundació CTM Centre Tecnològic, Spain.

[3] Sustainability Area, Eurecat, Centre Tecnològic de Catalunya, Spain.

[4] Amphos 21 Consulting SL, Spain.

[5] Catalana de Perforacions, Spain.

[6] Serra Húnter Fellowship, Generalitat de Catalunya, Spain.

Science of the Total Environment, Volume 686, 10 October 2019, Pages 709-718

https://doi.org/10.1016/j.scitotenv.2019.06.003

Impact factor (JCR/WOS) = 5.6 (2018)

Q1, 27/250 Environmental sciences

Science of the Total Environment 686 (2019) 709–718

Contents lists available at ScienceDirect

Science of the Total Environment

journal homepage: www.elsevier.com/locate/scitotenv

Use of nitrogen and oxygen isotopes of dissolved nitrate to trace field-scale induced denitrification efficiency throughout an in-situ groundwater remediation strategy

Rosanna Margalef-Marti [a,*], Raúl Carrey [a], Marta Viladés [b], Irene Jubany [c], Ester Vilanova [d], Roser Grau [e], Albert Soler [a], Neus Otero [a,f]

[a] Grup MAiMA, SGR Mineralogia Aplicada, Geoquímica i Geomicrobiologia, Departament de Mineralogia, Petrologia i Geologia Aplicada, Facultat de Ciències de la Terra, Universitat de Barcelona (UB), Barcelona, Spain
[b] Sustainability Department, Fundació CTM Centre Tecnològic, Spain
[c] Sustainability Area, Eurecat, Centre Tecnològic de Catalunya, Spain
[d] Amphos 21 Consulting SL, Spain
[e] Catalana de Perforacions, Spain
[f] Serra Húnter Fellow, Generalitat de Catalunya, Spain

HIGHLIGHTS

- Laboratory calculated $\varepsilon^{15}N$ and $\varepsilon^{18}O$ allowed estimating field-scale denitrification.
- The induced nitrate reduction at the pilot-plant was higher than 50%.
- Lower $\delta^{18}O\text{-}NO_3^-$ values at field compared to laboratory suggested NO_2^- re-oxidation.
- Denitrified and non-denitrified water mixing at the EW was proven isotopically.

GRAPHICAL ABSTRACT

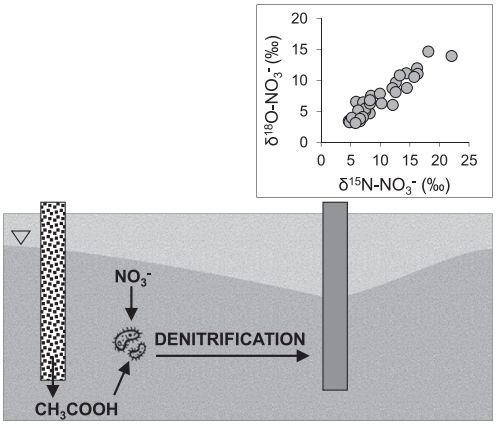

ARTICLE INFO

Article history:
Received 7 March 2019
Received in revised form 31 May 2019
Accepted 1 June 2019
Available online 5 June 2019

Editor: José Virgílio Cruz

Keywords:
Denitrification

ABSTRACT

In the framework of the Life+ InSiTrate project, a pilot-plant was established to demonstrate the viability of inducing in-situ heterotrophic denitrification to remediate nitrate (NO_3^-)-polluted groundwater. Two injection wells supplied acetic acid by pulses to an alluvial aquifer for 22 months. The monitoring was performed by regular sampling at three piezometers and two wells located downstream. In the present work, the pilot-plant monitoring samples were used to test the usefulness of the isotopic tools to evaluate the efficiency of the treatment. The laboratory microcosm experiments determined an isotopic fractionation (ε) for $N\text{-}NO_3^-$ of −12.6‰ and for $O\text{-}NO_3^-$ of −13.3‰. These $\varepsilon^{15}N_{NO3/N2}$ and $\varepsilon^{18}O_{NO3/N2}$ values were modelled by using a Rayleigh distillation equation to estimate the percentage of the induced denitrification at the pilot-plant while avoiding a possible interference from dilution due to non-polluted water inputs. In some of the field samples, the induced NO_3^- reduction

* Corresponding author.
E-mail address: rosannamargalef@ub.edu (R. Margalef-Marti).

https://doi.org/10.1016/j.scitotenv.2019.06.003

Electron donor
Groundwater
Isotopic fractionation
Pilot-plant
Remediation

was higher than 50% with respect to the background concentration. The field samples showed a reduced slope between δ^{18}O-NO_3^- and δ^{15}N-NO_3^- (0.7) compared to the laboratory experiments (1.1). This finding was attributed to the reoxidation of NO_2^- to NO_3^- during the treatment. The NO_3^- isotopic characterization also permitted the recognition of a mixture between the denitrified and partially or non-denitrified groundwater in one of the sampling points. Therefore, the isotopic tools demonstrated usefulness in assessing the implementation of the field-scale induced denitrification strategy.

1. Introduction

The scope of the anthropogenic disturbance of the nitrogen (N) cycle is conspicuous. Nitrate (NO_3^-) pollution is a current concern, as it has been related to ecological and human health disorders (Vitousek et al., 1997; Ward et al., 2005), and its presence in the groundwater is still increasingly large in many countries. The main sources of groundwater NO_3^- are linked to intensive use of synthetic and organic fertilizers and septic system leakage (Vitòria et al., 2008; Wassenaar, 1995). Some of the European directives that have arisen to mitigate the NO_3^- pollution (e.g., (2000/60/EC, 2000; 2006/118/EC, 2006; 91/676/EEC, 1991)) have focused on reducing the N inputs into the soil. However, due to the long residence time of N in the soil organic matter pool, the outcome of the agricultural management practices influencing the NO_3^- loading to the hydrosphere may be delayed for more than three decades (Sebilo et al., 2013). Therefore, water treatment is required to avoid the NO_3^- contamination impacts.

Denitrification has been shown to occur intrinsically throughout many environments, including aquifers, due to the ubiquity of the denitrifying microorganisms (Kraft et al., 2011; Philippot et al., 2007; Richardson and Watmough, 1999). While oxidizing an electron donor, these microorganisms are able to reduce NO_3^- (electron acceptor) to gaseous N_2 through a series of enzyme-mediated reactions: $NO_3^- \rightarrow NO_2^- \rightarrow NO \rightarrow N_2O \rightarrow N_2$ (Knowles, 1982). The mandatory conditions, such as electron acceptor availability and low oxygen concentration, are commonly encountered in the contaminated aquifers, but the electron donor presence is usually a limiting factor (Rivett et al., 2008). Hence, one of the feasible treatments for NO_3^- removal involves inducing in-situ heterotrophic denitrification by supplying an organic carbon (C) source as an external electron donor. The specific organic C compound employed and its supply strategy plays a critical role in the resulting execution efficiency. Among other parameters, this compound influences the NO_3^- reduction rates and the by-product accumulation (Hallin and Pell, 1998; Wilderer et al., 1987), which is undesirable, given that intermediates, such as nitrite (NO_2^-) or nitrous oxide (N_2O), could be even more harmful than NO_3^- itself (Badr and Probert, 1993; De Beer et al., 1997; Rivett et al., 2008). Therefore, the remediation approach must avoid pollution swapping to ensure the safety of the treatment. Several strategies to induce the heterotrophic denitrification have already been implemented at the field-scale (e.g., by ethanol or formate injection (Borden et al., 2012; Smith et al., 2001)). Over the treatment period, it is crucial to control the induced NO_3^- reduction efficiency.

Chemical and isotopic characterization has been applied to calculate the efficiency of the field-scale bioremediation strategies (Vidal-Gavilan et al., 2013), as well as to trace the natural NO_3^- transformation processes (Aravena and Robertson, 1998; Otero et al., 2009). In the course of denitrification, the unreacted residual NO_3^- becomes enriched in the heavy isotopes ^{15}N and ^{18}O (Aravena and Robertson, 1998; Böttcher et al., 1990; Mariotti et al., 1981), distinguishing the biological attenuation from other processes, such as dilution due to non-polluted water inputs (e.g., from rainfall), that could also lead to a concentration decrease without influencing the isotopic signature. The isotopic fractionation of N and O from dissolved NO_3^- ($\varepsilon^{15}N_{NO3/N2}$ and $\varepsilon^{18}O_{NO3/N2}$) determined at laboratory-scale, in denitrification experiments performed under controlled conditions, can be later applied at field-scale to estimate the NO_3^- attenuation significance during the intrinsic or induced denitrification (Böttcher et al., 1990; Mariotti et al., 1988). The isotopic characterization can also be used to determine the existence of undesired concurring processes, such as sulfate (SO_4^{2-}) reduction. Similarly to the case of NO_3^-, the isotopic composition of S and O from dissolved SO_4^{2-} allows to identify the occurrence of bacterial SO_4^{2-} reduction (BSR) by oxidation of an organic C electron donor, that could occur simultaneously to denitrification (Laverman et al., 2012; Strebel et al., 1990).

During the last decade, >50% of the wells monitored by the Catalan Water Agency in the Maresme area (north-east Spain) presented NO_3^- concentrations above 50 mg/L (ACA, 2018), the threshold value set by the directive (98/83/EC, 1998). Despite the Maresme was designated a nitrogen vulnerable zone in 1998 and good agricultural practices were implemented, NO_3^- is still exceeding 200 mg/L in a number of wells (DECRET 136/2009; DECRET 283/1998). In the framework of the Life+ InSiTrate project, a pilot-plant was set up in Sant Andreu de Llavaneres (Maresme) to produce safe drinking water from NO_3^--polluted groundwater by inducing in-situ denitrification. The present study aims to test the usefulness of the isotopic tools to determine the denitrification efficiency during a long-term induced attenuation strategy at the pilot-plant. An intrinsic prior goal is to determine the $\varepsilon^{15}N_{NO3/N2}$ and $\varepsilon^{18}O_{NO3/N2}$ values at laboratory-scale by using the selected electron donor, as well as the sediment and groundwater from the polluted alluvial aquifer. Afterwards, the suitability of using ε values calculated from the laboratory-scale assays to evaluate the field-scale denitrification treatment efficiency will be discussed.

2. Pilot-plant description

The project site is located 10 m nearby the San Andreu de Llavaneres Creek. The pilot plant is placed in an alluvial aquifer, formed by Quaternary (Holocene) coarse sand and silt sediments overlying an altered Paleozoic granite formation located at 40 m depth (IGC, 2011). Before the biostimulation, the area was characterized by means of pumping and tracing assays. The obtained permeability was between 70 and 100 m/d, transmissivity was between 800 and 1000 m^2/d and the average porosity was 0.5. The average aquifer temperature was 20.3 °C (SD = 1.4). Prior to the treatment, the aquifer showed aerobic conditions and natural NO_3^- attenuation was not observed, discarding the availability of electron donors in the aquifer that could promote denitrification intrinsically. The pilot-plant consisted of two electron donor injection wells (I1 and I2), one treated water extraction well (EW) at an approximate distance of 30 m from the two injection wells, three monitoring piezometers (PZ1, PZ2 and PZ3) between the injection and the extraction wells, and one monitoring well (MW) downstream, located out of the area affected by the biostimulation (Fig. 1).

The in-situ heterotrophic denitrification stimulation was performed by adding acetic acid (CH_3COOH) as an external electron donor. A variety of organic C compounds have been tested at the laboratory-scale to identify suitable electron donor sources (Carrey et al., 2018; Grau-Martínez et al., 2017; Peng et al., 2007). The CH_3COOH was selected by considering the technical (previous column experiments), environmental (life cycle assessment) and economic criteria (cost assessment) in the InSiTrate project. The addition of this compound through the injection wells was performed by pulses to avoid a high biomass accumulation that could lead to clogging issues, rather than a continuous supply

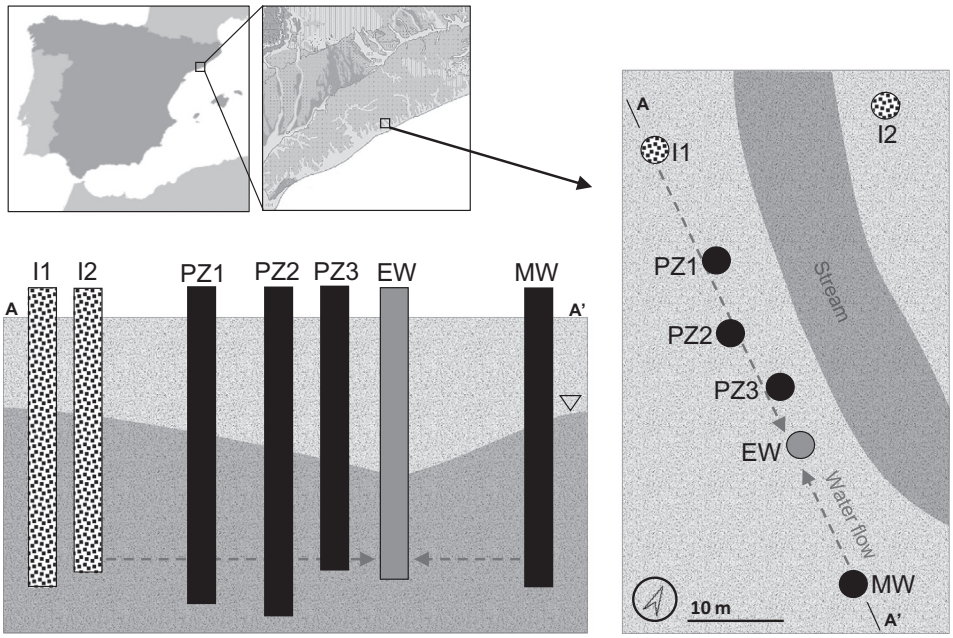

Fig. 1. Pilot-plant scheme. Location, schematic map and cross-section of the pilot-plant. I1 and I2 are the injection wells; PZ1, PZ2 and PZ3 the monitoring piezometers; EW the extraction well and MW the monitoring well. I2 is projected on the cross-section. Arrows depict the flow direction when the EW is operating. Natural flow direction is from I1 to MW.

(Khan and Spalding, 2004). The total biostimulation period was 22 months.

3. Methods

3.1. Laboratory experiments

The laboratory batch experiments simulated the aquifer conditions by using sediment and groundwater from the pilot-plant site. The groundwater was obtained from the MW and stored at 4 °C, whereas the sediment was obtained from the piezometer cores and stored frozen until use.

A total of 13 microcosms were settled by using 250 mL sealed glass flasks. The biostimulated microcosms (B1 to B10) were performed by adding CH_3COOH to the groundwater and sediment. Three types of control experiments were also performed. An untreated control (C1), to discard the intrinsic denitrification activity of the aquifer, contained groundwater and sediment from the study site with no CH_3COOH addition. Control C2, designed to discard the NO_3^- lixiviation from the sediment, contained MilliQ water and sediment with no CH_3COOH addition. Control C3 contained groundwater and CH_3COOH with no sediment, and was used to assess by comparison the contribution of the sediment on denitrification with respect to the groundwater. To attain the microbial stimulation, the CH_3COOH was injected at a 6.3C/N ratio (w/w) according to previous laboratory experiments (data not shown) and results reported by other authors (Elefsiniotis and Li, 2006; Her and Huang, 1995). Also because this amount is representative of the CH_3COOH expected at the pilot-plant. However, the C/N ratio might not be totally homogeneous at field-scale due to dilution within the aquifer. Both at laboratory and field-scale, the total C employed for the overall NO_3^- removal process might be higher than expected from the stoichiometric C/N ratio (e.g., Eq. (1) proposed by Elefsiniotis and Li, 2006), as the CH_3COOH is also required for the water deoxygenation by heterotrophic bacteria before using NO_3^- as the electron acceptor. A detailed composition of the microcosms is shown in Table 1.

$$\frac{33}{140}NO_3^- + \frac{1}{4}CH_3COO^- + \frac{23}{140}H_2CO_3 \rightarrow \frac{1}{28}C_5H_7O_2N + \frac{1}{10}N_2 + \frac{6}{35}H_2O + \frac{34}{70}HCO_3^- \quad (1)$$

The head-space was purged with Ar after filling and sealing the flasks with GL45 caps holding silicone rubber PTFE-protected septa. All of the microcosms were maintained at 20 °C in the darkness and with constant vibratory shaking throughout the experiment. The biostimulated microcosms were sacrificed by turns at time intervals depending on the denitrification dynamics until a complete NO_3^- and NO_2^- removal was achieved. The samples from C3 were regularly obtained using a 1 mL syringe with a 25 G needle (BD). The control microcosms were sacrificed at the end of the experiment.

3.2. Field survey

A total of forty-four samples were collected from five points in the pilot-plant (EW, PZ1, PZ2, PZ3 and MW) in ten sampling campaigns, 9 performed during the twenty-two months of the pilot-plant operation, and one performed two months after the end of injections. The sampling intervals were established according to the pilot-plant operation dynamics. In two of the sampling campaigns, two different depths (top and bottom) were sampled for PZ1 and PZ2 to check differences in the treatment along the water column. The monitoring wells and piezometers were purged prior to the sample collection by removing three well volumes.

Table 1
Batch experiments set-up. Composition for each microcosm.

Reactor	Code	Water source	Water volume (mL)	Flask volume (mL)	Sediment (g)	CH_3COOH 85% (μL)
Stimulated	B1-B10	MW	150	250	20	33
Control 1	C1	MW	150	250	20	0
Control 2	C2	Milli-Q	150	250	20	0
Control 3	C3	MW	300	500	0	66

3.3. Analyses

Both the field survey and laboratory assays samples were filtered (0.2 μm Millipore®) immediately when obtained and stored at 4 °C until analysis, except for aliquots for the isotopic characterization of N and O from NO_3^- that were preserved frozen at −20 °C.

The determined chemical parameters were major anions (NO_2^-, NO_3^- and SO_4^{2-}), analyzed by high-performance liquid chromatography (HPLC) (WATERS 515 pump and WATERS IC-PAK ANIONS column with WATERS 432 and UV/V KONTRON detectors) and ammonium (NH_4^+), analyzed by spectrophotometry (CARY 1E UV–visible) using the indophenol blue method (Bolleter et al., 1961).

The analyzed isotopes were N and O of the dissolved NO_3^- (δ^{15}N-NO_3^- and δ^{18}O-NO_3^-), and S and O of the dissolved SO_4^{2-} (δ^{34}S-SO_4^{2-} and δ^{18}O-SO_4^{2-}). The stable isotopes are expressed using delta notation ($\delta = ((R_{sample}\text{-}R_{standard})/R_{standard})$, where R is the ratio between the heavy and the light isotopes). The considered international standards were: Atmospheric N_2 (AIR) for δ^{15}N, Vienna Standard Mean Oceanic Water (V-SMOW) for δ^{18}O and Vienna Canyon Diablo Troillite (V-CDT) for δ^{34}S. The δ^{15}N-NO_3^- and δ^{18}O-NO_3^- composition was determined following the cadmium reduction method (McIlvin and Altabet, 2005; Ryabenko et al., 2009). Next, the N_2O was analyzed by using a Pre-Con (Thermo Scientific) coupled to a Finnigan MAT 253 Isotope Ratio Mass Spectrometer (IRMS, Thermo Scientific). For the SO_4^{2-} isotopic analysis, the dissolved SO_4^{2-} was precipitated as $BaSO_4$ (Dogramaci et al., 2001). The δ^{34}S-SO_4^{2-} was analyzed with a Carlo Erba Elemental Analyzer (EA) coupled in a continuous flow to a Finnigan Delta XP Plus IRMS, whereas the δ^{18}O-SO_4^{2-} was analyzed with a ThermoQuest high-temperature conversion analyzer (TC/EA) coupled in a continuous flow with a Finnigan Matt Delta XP Plus IRMS. According to Coplen (2011), several international and laboratory (CCiT) standards were interspersed among samples for the normalization of the isotopic results. For the δ^{15}N-NO_3^- and δ^{18}O-NO_3^- analysis the employed standards were USGS-32, USGS-34, USGS-35 and CCiT-IWS ($\delta^{15}N = +16.9‰$, $\delta^{18}O = +28.5‰$); for the δ^{34}S-SO_4^{2-} analyses, NBS-127, IAEA-SO-5, IAEA-SO-6, and CCiT-YCEM ($\delta^{34}S = +12.8‰$); and for the δ^{18}O-SO_4^{2-} analysis, NBS-127, CCiT-YCEM ($\delta^{18}O = +17.6‰$) and CCIT-ACID ($\delta^{18}O = +13.2‰$). The reproducibility (1σ) of the samples, calculated from the standards systematically interspersed in the analytical batches, was ± 1.0‰ for δ^{15}N-NO_3^-, ±1.5‰ for δ^{18}O-NO_3^-, ±0.2‰ for δ^{34}S-SO_4^{2-} and ± 0.5‰ for δ^{18}O-SO_4^{2-}.

The chemical and isotopic analyses were prepared in the MAiMA-UB research group laboratory and performed at the Centres Científics i Tecnològics of the Universitat de Barcelona (CCiT-UB).

3.4. Isotope data calculations

In the batch experiments, the isotopic fractionation was calculated by means of the Rayleigh distillation Eq. (2). Thus, the $\varepsilon^{15}N_{NO3/N2}$ and $\varepsilon^{18}O_{NO3/N2}$ were obtained from the slope of the linear correlation between the natural logarithm of the substrate remaining fraction (Ln ($C_{residual}/C_{initial}$), where C refers to the analyte concentration) and the determined isotope ratios (Ln($R_{residual}/R_{initial}$), where $R = \delta + 1$).

$$\mathrm{Ln}\left(\frac{R_{residual}}{R_{initial}}\right) = \varepsilon \times \mathrm{Ln}\left(\frac{C_{residual}}{C_{initial}}\right) \quad (2)$$

The percentage of NO_3^- attenuation caused by denitrification at field-scale was estimated by using these $\varepsilon^{15}N_{NO3/N2}$ and $\varepsilon^{18}O_{NO3/N2}$ calculated under closed system conditions and Eq. (3), which is derived from the Rayleigh fractionation model (Eq. (2)). The quantification of pollutants degradation by using Rayleigh derived equations has been applied elsewhere (Meckenstock et al., 2004; Otero et al., 2009; Schmidt et al., 2004; Vidal-Gavilan et al., 2013).

$$\mathrm{DEN}\% = \left[1-\left(\frac{\mathrm{Cresidual}}{\mathrm{Cinitial}}\right)\right] \times 100 = \left[1-\left(\frac{\mathrm{Rresidual}}{\mathrm{Rinitial}}\right)^{\left(\frac{1}{\varepsilon}\right)}\right] \times 100 \quad (3)$$

4. Results and discussion

4.1. Laboratory-scale experiments

4.1.1. NO_3^- reduction by CH_3COOH

The NO_3^- and NO_2^- lixiviation from the sediment was discarded, since the concentration of both compounds was below the detection limit in the C2 microcosm (Milli-Q water + sediment) after 102 h of incubation. The C1 microcosm (groundwater + sediment) showed no depletion of the initial NO_3^- concentration, thereby ruling out intrinsic denitrification activity from the aquifer groundwater or sediment in the microcosms due to the presence of trace electron donors. Thus, the observed NO_3^- reduction in the biostimulated microcosms (B1-B10) was considered to be caused by the CH_3COOH injection (Fig. 2). All data obtained from the laboratory-scale experiments is presented in the Supporting Information Table S1.

The bacterial NO_3^- reduction in the biostimulated experiments (B1-B10) was initiated between 32 and 47 h after the electron donor injection. The initial lag period was the acclimation time for the establishment of a heterotrophic bacterial community after unfreezing the sediment and merging it with the groundwater. Also, all of the oxygen present in the groundwater had to be consumed before using NO_3^- as the electron acceptor. The concentration analysis showed that after the onset, NO_3^- reduction proceeded rapidly until NO_3^- was completely consumed 70 h after biostimulation, yielding an average NO_3^- removal rate of 0.30 mmol/(dm^3·day) (calculated for the total length of the experiment including the acclimation period). As the NO_3^- concentration started to decrease, NO_2^- progressively accumulated, reaching a 0.26 mM maximum peak, which is 30% of the initial N-NO_3^- concentration, approximately 50 h after the injection. The transient NO_2^- accumulation has been widely reported to occur during the laboratory (Calderer et al., 2010; Carrey et al., 2013; Her and Huang, 1995) and field-scale (Critchley et al., 2014; Gierczak et al., 2007; Vidal-Gavilan et al., 2013) denitrification studies. The NO_2^- usually accumulates until the bacterial communities adapt to the new redox conditions caused by the electron donor addition. One of the reasons is an earlier induction of the NO_3^- reductases with respect to the NO_2^- reductases (Zumft, 1997 and references therein). After 50 h, the NO_2^- progressively decreased and was completely consumed when the NO_3^- removal was also accomplished. The NO_3^- reduction and NO_2^- accumulation observed can also be produced by dissimilatory NO_3^- reduction to NH_4^+ (DNRA). However, the NH_4^+ detected in the microcosms was low (up to 0.04 mM). Therefore, DNRA did not contribute significantly to the NO_3^- concentration decrease in the microcosms, pointing out denitrification as the main reaction.

In the biostimulated microcosm lacking sediment (C3), a complete NO_3^- reduction was also achieved, but the NO_2^- accumulation increased significantly. A 0.76 mM NO_2^- peak, which is 86% of the initial N-NO_3^-, was reached after 84 h and decreased rapidly until depletion was complete (Fig. 2). After 95 h, the NO_3^- and NO_2^- levels were below the detection limit. The average NO_3^- removal rate was 0.22 mmol/(dm^3·day), which is lower than the obtained from the biostimulated microcosms containing sediment. Although the groundwater alone provided the needed conditions to achieve a complete denitrification in the CH_3COOH amended microcosms, the sediment increased significantly the attenuation efficiency. The lowered NO_3^- removal rate and the increased magnitude of the NO_2^- peak in the microcosms lacking sediment might be attributed to a diminished initial bacterial content that

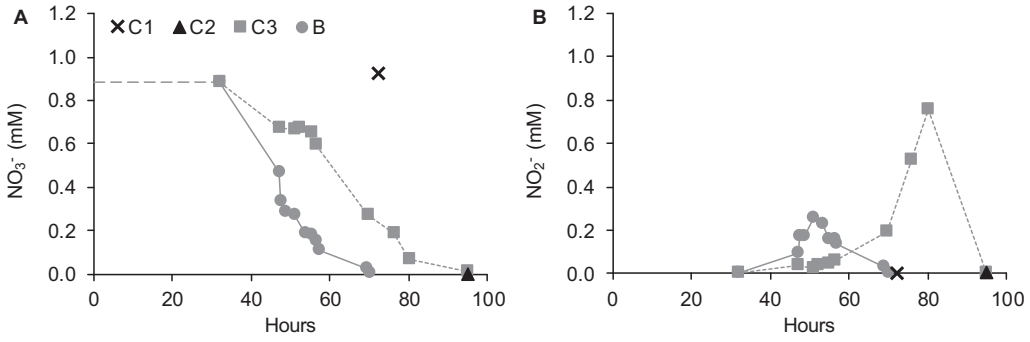

Fig. 2. NO_3^- and NO_2^- evolution in the microcosms. NO_3^- (**A**) and NO_2^- (**B**) concentration in the biostimulated and control microcosms. C1 (black cross): groundwater + sediment, C2 (black triangles): MilliQ water + sediment, C3 (grey squares): groundwater + CH_3COOH, B (grey circles): groundwater + sediment + CH_3COOH.

might result in lower and/or different bacterial species growth stimulation. Other reasons could include a buffering effect promoted by the sediment or the influence of the sediment surface upon reactivity.

4.1.2. Isotopic fractionation calculation

While being progressively reduced, the isotopic composition of the residual NO_3^- in the biostimulated microcosms became higher in both ^{15}N and ^{18}O. The initial groundwater values for $\delta^{15}N\text{-}NO_3^-$ and $\delta^{18}O\text{-}NO_3^-$ of +5.1‰ and +3.6‰, respectively, increased over the experimental period to +29.9‰ and +30.8‰, respectively. The calculated ε values, were −12.6‰ ($r^2 = 0.99$) for $\varepsilon^{15}N_{NO3/N2}$ and −13.3‰ ($r^2 = 0.96$) for $\varepsilon^{18}O_{NO3/N2}$, resulting in a $\varepsilon^{15}N/\varepsilon^{18}O$ of 0.95 (Fig. 3). These values fall within the reported range for the heterotrophic denitrification (from −5.4‰ to −26.6‰ for $\varepsilon^{15}N_{NO3/N2}$, from −4.8‰ to −23.7‰ for $\varepsilon^{18}O_{NO3/N2}$, and from 0.6 to 1.0 for $\varepsilon^{15}N/\varepsilon^{18}O$ (Granger et al., 2008; Wunderlich et al., 2012)).

Carrey et al. (2013), Torrentó et al. (2011) and Vidal-Gavilan et al. (2013) applied the $\varepsilon^{15}N_{NO3/N2}$ and $\varepsilon^{18}O_{NO3/N2}$ values obtained from laboratory batch experiments, using either intrinsic or added electron donors, to quantify the extent of natural or induced groundwater denitrification. By using the laboratory derived ε values to estimate the induced NO_3^- reduction, interferences from processes other than denitrification that could also lead to a concentration decrease (e.g., dilution due to water discharges from rainfall) are avoided. For the pilot-plant study, we considered it appropriate to apply the $\varepsilon^{15}N_{NO3/N2}$ and $\varepsilon^{18}O_{NO3/N2}$ calculated from the laboratory experiments because groundwater and sediment from the aquifer were used and consequently, a similar electron acceptor availability and stimulated bacterial community with respect to the field was expected.

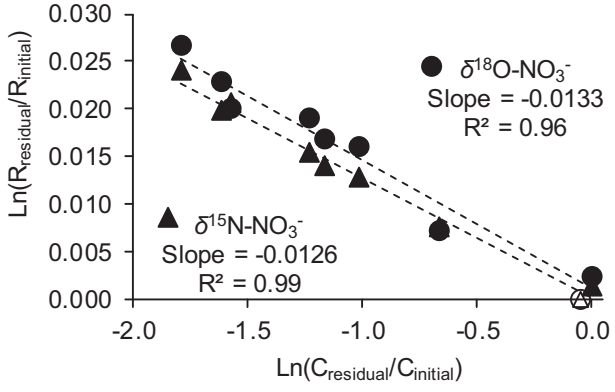

Fig. 3. NO_3^- isotopic fractionation in the microcosms. Samples from the biostimulated microcosms (black) and initial MW groundwater (empty) isotopic composition.

4.2. Field survey

4.2.1. Isotopic dynamic in the pilot-plant

The sampling campaigns began one month after the CH_3COOH injections started and continued for two years, with the last survey being performed two months after stopping the injections. All data obtained from the pilot-plant are presented in the Supporting Information Table S2. The unaffected MW ($n = 6$) presented average values of 0.9 mM (SD = 0.04) for NO_3^- concentration, +6.3‰ (SD = 1.3) for $\delta^{15}N\text{-}NO_3^-$ and +4.2‰ (SD = 0.9) for $\delta^{18}O\text{-}NO_3^-$, which were considered to be the groundwater NO_3^- background composition. The isotopic values of the MW fall in the soil NO_3^- area (Fig. 4) reported by Vitòria et al. (2004) and references therein. However, the high NO_3^- concentration suggested an anthropogenic origin. In a previous study located in a nearby area with intensive application of chemical fertilizers, Vitòria et al. (2005) demonstrated that the combined occurrence of volatilization and nitrification resulted in groundwater NO_3^- with $\delta^{15}N\text{-}NO_3^-$ and $\delta^{18}O\text{-}NO_3^-$ in the range of soil NO_3^-. Therefore, the isotopic values of the MW suggested that the NO_3^- pollution in the studied aquifer was derived from N inorganic fertilizer that had been volatilized and nitrified (Fig. 4).

Following the electron donor addition, the three monitoring piezometers showed a marked NO_3^- decrease. PZ1 and PZ2 reached NO_3^- concentrations below 0.3 mM from the 10th operation month and until the last injection. PZ3 also showed a decreasing trend but with a NO_3^- concentration higher than PZ1 and PZ2 and a temporal trend showing fluctuations (Fig. 5). Contrarily, a flat trend in the NO_3^- evolution was observed at the EW (Fig. 5), showing concentrations between 13% and 33% lower than the MW. In the two-depth sampling at PZ1 in the 17th month, no significant NO_3^- concentration differences were observed between the bottom and the top samples, and in both cases, NO_3^- was almost completely denitrified. However, at PZ2 in the 19th month, the bottom sample showed a doubled NO_3^- concentration compared to the top sample. In all the samples NO_2^- was below 0.02 mM (Supporting Information Fig. S1) and NH_4^+ was below 0.01 mM. Therefore, pollution swapping due to accumulation of these compounds was discarded in the pilot-plant.

In response to the NO_3^- attenuation in the piezometers, the $\delta^{15}N\text{-}NO_3^-$ and $\delta^{18}O\text{-}NO_3^-$ increased. The temporal dynamics of the NO_3^- isotopic composition in the pilot-plant is shown in the Supporting Information Fig. S2. The highest values were measured at PZ1, showing a $\delta^{15}N\text{-}NO_3^-$ and $\delta^{18}O\text{-}NO_3^-$ of +22.1‰ and +14.7‰, respectively (Fig. 4). Note that four samples were below the limit of concentration necessary for the isotopic analysis (0.05 mM), and could have even shown higher isotopic values. The $\delta^{15}N\text{-}NO_3^-$ and $\delta^{18}O\text{-}NO_3^-$ in the EW samples were close to the MW average values (Fig. 4). Two months after the end of the treatment, the EW and PZ3 recovered to NO_3^- background concentrations and isotopic values, but PZ1 and PZ2 still showed evidence of denitrification (Fig. 5).

When NO_3^- is completely removed from the environment, the excess organic C can trigger BSR, provoking a decrease in the treated water quality due to the production of H_2S. However, the coexistence of denitrification and BSR in the presence of an electron donor has also been demonstrated. Laverman et al. (2012) observed that the ratio between the BSR rate and the denitrification rate tends to increase at high organic matter concentrations. As in the studied pilot-plant, organic matter was available, BSR could occur simultaneously to denitrification. The isotopic results from a subset of the pilot-plant samples showed a 0.4 ($r^2 = 0.93$) slope from the regression line between $\delta^{18}O\text{-}SO_4^{2-}$ and $\delta^{34}S\text{-}SO_4^{2-}$ (Fig. 6), which is in the range of the slopes from 0.25 to 0.7 reported in the literature for BSR (Aharon and Fu, 2000). However, the samples with the lowest SO_4^{2-} concentration (~1 mM) were not the most enriched in $\delta^{18}O\text{-}SO_4^{2-}$ and $\delta^{34}S\text{-}SO_4^{2-}$ and vice versa (maximum measured SO_4^{2-} was ~5 mM). Since there was surplus NO_3^- in the groundwater and due to the lack of correlation between the SO_4^{2-} chemical and isotopic data, BSR did not likely play a significant role at the pilot-plant. In the same context of water quality, the presence of remaining CH_3COOH at a harmful level for consumption was also discarded due to the excess of electron acceptors such as NO_3^- or SO_4^{2-} in groundwater since denitrification was never completed at the EW.

4.2.2. Isotopic fractionation from the laboratory to field-scale

A subset of the campaigns considered to be representative of the treatment efficiency evaluation is discussed. As previously stated, the average NO_3^- concentration, $\delta^{15}N\text{-}NO_3^-$ and $\delta^{18}O\text{-}NO_3^-$ of the MW were used as the initial composition, since the MW was considered to be unaffected by the treatment. During the initial operation (1st month), the NO_3^- isotopic composition did not show a relevant $\delta^{15}N$ or $\delta^{18}O$ enrichment, indicating that the denitrification was not significant (Fig. 7A). After seven operation months, and until the end of the monitoring period, a clear $\delta^{15}N\text{-}NO_3^-$ and $\delta^{18}O\text{-}NO_3^-$ enrichment evidenced the biological NO_3^- reduction at the pilot-plant. The degree of reduction depended on the specific point and sampling campaign. According to the concentration measured, >95% NO_3^- was reduced at PZ1 in the 14th, 17th and 19th months, and at PZ2 in the 17th month. However, those samples could not be isotopically analyzed, since the NO_3^- concentration was below the detection limit (0.05 mM). The isotopic composition of the remnant samples determined that the denitrification at the pilot-plant piezometers reached a significance of approximately 50% (e.g., 19th month (Fig. 7D)). Even two months after stopping the biostimulation (month 24th), more than a 50% of the groundwater NO_3^- was still denitrified at PZ1 (Fig. 7E).

For each of the pilot-plant samples, the denitrification % calculated by using the isotopic data was compared to the % calculated by using the NO_3^- concentration (Supporting Information Table S2). For most of the pilot-plant samples (e.g., 2nd, 11th, 12th and 24th month campaigns), the calculated % from the chemical data was higher than the % obtained from the isotopic data, as expected from the influence of dilution due to non-polluted water inputs from rainfall (Supporting information Fig. S3). Four of the samples showed highly similar % values (<5% difference), suggesting that in these cases dilution did not occur. Contrarily, in five samples, the % calculated from the NO_3^- concentration was lower compared to the % from the isotopic data. This variation might be produced by different reasons, depending on the characteristics of the samples involved. For PZ1 and PZ3 from the 1st month campaign, the denitrification had not still begun, and the lower % could be derived from the intrinsic aquifer variability due to the use of an average value for the MW to draw the DEN % line instead of the specific MW value for each of the sampling campaigns. For PZ1 and PZ3 from the 7th month campaign and PZ3 from the 19th month campaign, the reason could be a mixing effect between treated and non-treated groundwater.

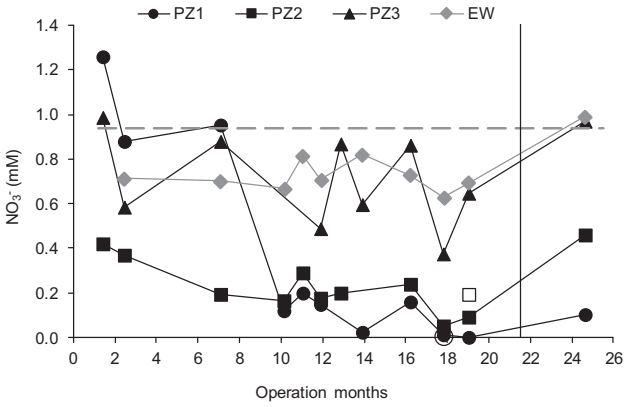

Fig. 5. NO_3^- evolution in the pilot-plant. The dashed grey line corresponds to the MW mean concentration. Empty symbols for PZ1 and PZ2 correspond to bottom samples (two-depth sampling). The vertical line corresponds to the last injection date.

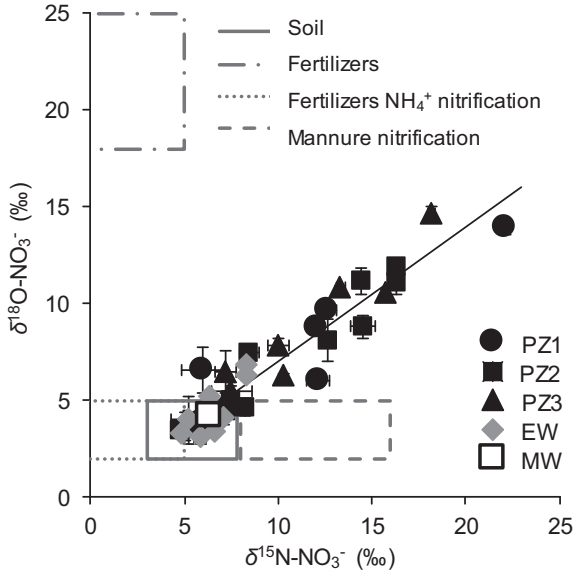

Fig. 4. $\delta^{15}N$ vs $\delta^{18}O$ diagram from field samples. Isotopic results from the piezometers and the EW (circles) samples and mean value of the unaffected MW (square), including standard deviation. The regression line is presented as a continuous black line (slope = 0.7 ($r^2 = 0.95$)). The boxes (grey continuous and dashed lines) represent NO_3^- sources from Vitòria et al., 2004 and references therein.

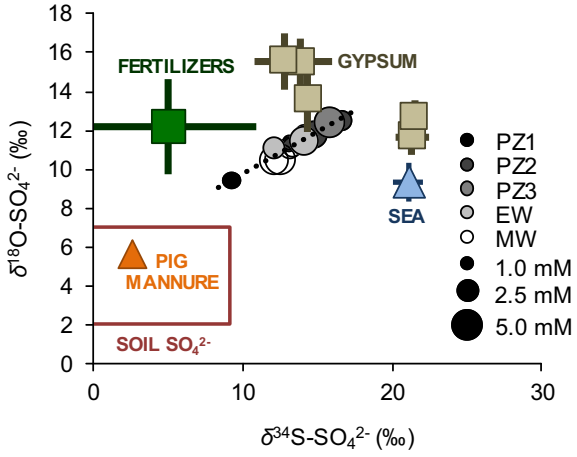

Fig. 6. Pilot-plant SO_4^{2-} concentration and isotopic composition. The regression line is presented as a dashed black line (slope = 0.4 ($r^2 = 0.93$)). The boxes, including standard deviation, represent SO_4^{2-} sources from Otero et al. (2007); Vitòria et al. (2004) and references therein.

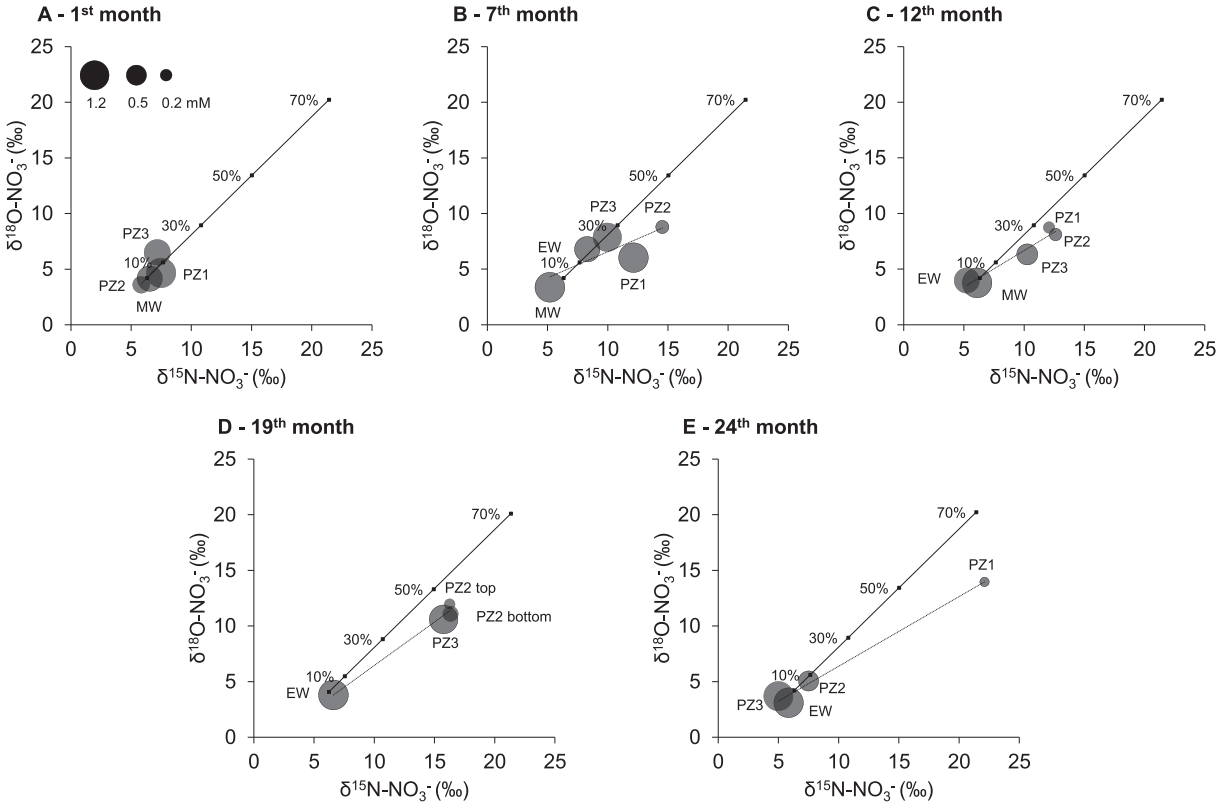

Fig. 7. Representative sampling campaigns from the pilot-plant. **A)** 1st month (1.2 slope ($r^2 = 0.45$)); **B)** 7th month, 0.5 slope ($r^2 = 0.8$); **C)** 12th month, 0.6 slope ($r^2 = 0.9$); **D)** 19th month, 0.8 slope ($r^2 = 1.0$); **E)** 24th month, 0.6 slope ($r^2 = 1.0$). Regression line for each campaign is presented as a dashed line. The DEN % line (continuous line) was calculated using the isotopic fractionation values obtained in the laboratory experiments, and the average concentration and isotopic composition of the MW as initial values.

Chemical and isotopic data of the EW evidenced a mixing between treated and non-treated groundwater. In the 7th month campaign, a slight isotopic enrichment and NO_3^- concentration decrease was observed at the EW with respect to the MW, being indicative of the denitrification occurrence (Fig. 7B). However, from the 7th month onward, despite the lower NO_3^- concentration at the EW with respect to the MW, the isotopic data did not show significant differences (e.g., 12th or 19th month) (Fig. 7C and D). The reason is that the groundwater extracted at the EW was a mix of denitrified groundwater from PZ1 and PZ2 located upstream and untreated water from the MW located downstream, due to a depression cone at EW forced by the water extraction (Fig. 1). To determine the contribution to EW, a theoretical mixing between 30% of PZ2 and 70% of MW was estimated using chemical and isotopic data, and was compared with the measured values (Table 2). Measured results are fairly in agreement with the estimated ones throughout the monitoring period. This mixing between treated and non-treated groundwater was also observed along the water column. During the two-depth sampling at PZ2 (19th month), no significant isotopic composition differences were observed, although the measured NO_3^- concentrations were 0.2 and 0.1 mM in the bottom and top samples, respectively (Fig. 7D). In these two samples, the denitrification % obtained with the isotopic data (~50%) might also result from mixing between the partially and non-denitrified groundwater. Therefore, the attenuation in the water column might be heterogeneous with reactive microsites where NO_3^- can be completely removed. In the same campaign (19th month), PZ3 showed a similar isotopic composition to the two samples from PZ2, but presented a remarkably higher NO_3^- concentration, reinforcing the idea of the groundwater mixing between the partially and non-denitrified groundwater. In PZ3, the denitrified water had a lesser contribution compared to PZ2. Due to the effect produced by this mixing, the obtained field-scale denitrification % from the laboratory determined $\varepsilon^{15}N_{NO3/N2}$ and $\varepsilon^{18}O_{NO3/N2}$ must be considered an estimation, and not a precise calculation.

Table 2
Groundwater mixing at EW. Theoretical mixing calculation between 30% of PZ2 and 70% of MW using chemical and isotopic data (E), compared with the measured (M) NO_3^- concentration and isotopic composition at the EW. Standard deviation (SD) is included.

	NO_3^- (mM)			$\delta^{15}N\text{-}NO_3^-$ (‰)			$\delta^{18}O\text{-}NO_3^-$ (‰)		
Month	E	M	SD	E	M	SD	E	M	SD
1	0.78	–	–	6.2	–	–	4.0	–	–
2	0.77	0.71	0.04	5.8	8.3	1.7	4.0	6.7	1.6
7	0.72	0.70	0.01	8.8	8.3	0.3	5.6	6.8	0.9
10	0.71	0.67	0.03	6.9	4.9	1.4	4.3	3.3	0.8
11	0.74	0.82	0.05	7.0	6.3	0.5	5.2	5.2	0.0
12	0.71	0.71	0.00	8.2	5.2	2.1	5.4	4.0	1.0
14	0.66	0.82	0.12	4.4	6.6	1.6	3.0	3.4	0.3
17	0.67	0.63	0.03	8.8	7.1	1.2	6.3	4.1	1.6
19	0.69	0.69	0.01	9.3	6.6	2.0	6.5	3.8	1.9
24	0.80	0.99	0.14	6.7	5.8	0.6	4.5	3.1	1.0

4.2.3. NO_2^- reoxidation evidence from the isotopic results

The determined slope between $\delta^{18}O\text{-}NO_3^-$ and $\delta^{15}N\text{-}NO_3^-$ from the field samples (0.7 ($r^2 = 0.95$)) and the slope from the batch experiments (1.1 ($r^2 = 0.99$)) agree with the already reported slopes of nearly 0.5 for groundwater denitrification studies at field-scale (Chen and MacQuarrie, 2005; Critchley et al., 2014; Otero et al., 2009), and nearly 1.0 for laboratory studies (Carrey et al., 2013; Grau-Martínez et al., 2017; Wunderlich et al., 2012). However, the slopes around 0.5 have also been found in pure culture laboratory experiments. The lower $\varepsilon^{18}O_{NO3/N2}$ compared to $\varepsilon^{15}N_{NO3/N2}$ can be caused by the use of the periplasmic NO_3^- reductase (NAP) instead of the membrane bound NO_3^- reductase (NAR) (Granger et al., 2008), or by the oxidation of the intermediates NO_2^- and NH_4^+ to NO_3^- (Granger and Wankel, 2016;

Wunderlich et al., 2013). It is widely assumed that NAP has an insignificant role in the aquifer environments where anaerobic conditions are prevalent, and because it does not involve a metabolic energy generation process (Moreno-Vivián et al., 1999). The denitrification and the DNRA coupled to the anaerobic ammonium oxidation (anammox) can occur concomitantly in freshwater environments (Castro-Barros et al., 2017; Jones et al., 2017). However, the DNRA in the pilot-plant was rather unimportant since NO_3^- did not achieve complete reduction. The DNRA is favored at high C/N ratios, when NO_3^- is limited instead of the electron donor (Giles et al., 2012; Jones et al., 2017; Kelso et al., 1997). Therefore, the lower slope observed at the field-scale is likely related to the NO_2^- reoxidation which is consistent with the possibility of oxygen diffusion in groundwater compared to the laboratory microcosms.

The $\delta^{18}O$ of some dissolved oxygenated compounds, such as NO_2^-, can be equilibrated with the $\delta^{18}O$-H_2O (Granger and Wankel, 2016; Kool et al., 2007). If the intermediate NO_2^- reoxidates to NO_3^-, the resulting $\delta^{18}O$-NO_3^- will be dependent on the $\delta^{18}O$ of the NO_3^- source, the $\delta^{18}O$ of the groundwater, the kinetic isotopic effects produced during the denitrification and during the water atom incorporation by the oxidoreductase throughout the NO_2^- oxidation. Considering a $\delta^{18}O$-H_2O ranging from −7 to −4‰ in the studied area and the $\delta^{18}O$-NO_3^- average composition of the samples obtained from the unaffected MW being +4.2‰ (SD = 0.9), a decreased $\varepsilon^{18}O_{NO3/N2}$ is expected in the pilot-plant if the intermediate NO_2^- reoxidates to NO_3^-.

Several samples from the field site showed lower $\delta^{18}O$-NO_3^- values than expected, considering the denitrification slope calculated using the microcosm experiments (e.g., 7th, 12th and 19th month) (Fig. 7B, C and D). This finding can be explained as the result of the NO_2^- reoxidation to NO_3^- throughout the remediation treatment. The low or null NO_2^- detection throughout the pilot-plant operation (Supporting Information, Fig. S2) seemed consistent with the NO_2^- reoxidation, which is positive from a groundwater quality perspective. The shift in the slope throughout the induced denitrification treatment can provide information regarding the relevance of the NO_2^- reoxidation process at the field-scale. The $\delta^{15}N$-NO_3^- and $\delta^{18}O$-NO_3^- values close to the theoretical DEN % line might point to a direct NO_2^- reduction to gaseous N products, while lower $\delta^{18}O$-NO_3^- values might point to the NO_2^- reoxidation. By checking each of the sampling campaigns separately, slopes near 0.5 were generally observed during the initial biostimulation (e.g., 7th month, 0.5 slope (r^2 = 0.8)) (Fig. 7B), which became closer to 1.0 throughout the pilot-plant operation (e.g., 19th month, 0.8 slope (r^2 = 1.0)) (Fig. 7D). At the last sampling campaign, corresponding to the recovery period after stopping the CH_3COOH injections, the slope was again closer to 0.5 (24th month, 0.6 slope (r^2 = 1.0)) (Fig. 7E).

An unsolved question is the effect of the biotic and abiotic NO_2^- oxidation to NO_3^- upon $\delta^{15}N$-NO_3^- throughout denitrification in groundwater. It is expected that the possible effect upon $\delta^{15}N$-NO_3^- would be lower than the observed for $\delta^{18}O$-NO_3^- during the abiotic NO_2^- oxidation, enabling the $\delta^{18}O$-NO_3^- versus $\delta^{15}N$-NO_3^- slope to decrease. For the biotic NO_2^- oxidation, an inverse isotopic fractionation for the $\delta^{15}N$ (and also for the $\delta^{18}O$) was observed during the NO_2^- oxidation to NO_3^- mediated by the marine species *Nitrococcus mobilis* (Buchwald and Casciotti, 2010; Casciotti, 2009). Consequently, when the NO_2^- reoxidation is observed during the in-situ groundwater remediation strategies, the denitrification significance might be biased if estimated by using the laboratory isotopic fractionation data.

5. Conclusions

After the implementation of an in-situ groundwater remediation strategy by CH_3COOH injections (InSiTrate project), the induced denitrifying activity reached NO_3^- concentrations below the threshold for water consumption. The $\varepsilon^{15}N_{NO3/N2}$ and $\varepsilon^{18}O_{NO3/N2}$ values obtained from the microcosm experiments allowed assessing the denitrification efficacy at the pilot-plant while avoiding the interference derived from dilution due to non-polluted water inputs. At the pilot-plant, more than a 50% of the background NO_3^- was reduced due to the induced heterotrophic denitrification. The isotopic results allowed to detect a mixture between the denitrified and non-denitrified groundwater at the EW. However, a limitation of the application of the isotopes to evaluate the treatment efficacy is that the denitrification significance could be underestimated due to the effect provoked by the mixing of non-denitrified groundwater with partially denitrified groundwater. The lower slope between $\delta^{18}O$-NO_3^- and $\delta^{15}N$-NO_3^- observed in the field (0.7) compared to the laboratory (1.1) was attributed to the NO_2^- reoxidation to NO_3^-. However, the effect of the NO_2^- reoxidation upon $\delta^{15}N$-NO_3^- is still unclear, and it is unknown in which measure the $\delta^{18}O$-NO_3^- values resulting from the NO_2^- reoxidation can be firmly extrapolated to the calculated DEN % line. In summary, the $\delta^{15}N$-NO_3^- and $\delta^{18}O$-NO_3^- analysis provides a valuable tool to assess the induced denitrification strategies at the field-scale by means of the laboratory calculated $\varepsilon^{15}N_{NO3/N2}$ and $\varepsilon^{18}O_{NO3/N2}$. However, attention must be focused on the hydrogeological and biochemical effects that could influence the results and thus the remediation strategies evaluation.

Supplementary data to this article can be found online at https://doi.org/10.1016/j.scitotenv.2019.06.003.

Acknowledgments

This work has been financed by the following projects: REMEDIATION (CGL2014-57215-C4) and PACE-ISOTEC (CGL2017-87216-C4-1-R), financed by the Spanish Government and AEI/FEDER from the UE; MAG (2017-SGR-1733) from the Catalan Government and LIFE Project InSiTrate (LIFE12 ENV/ES/000651). R. Margalef-Marti is grateful to the Spanish Government for the Ph.D. grant BES-2015-072882. We would like to thank the CCiT-UB for providing analytical support.

References

2000/60/EC, 2000. Water framework directive [WWW document]. Off. J. Eur. Comm. http://ec.europa.eu/environment/index_en.htm, Accessed date: 9 April 2017

2006/118/EC, 2006. Groundwater directive. Council directive 2006/118/EC, of 12 December 2006, on the protection of groundwater against pollution and deterioration [WWW document]. Off. J. Eur. Comm. http://ec.europa.eu/environment/index_en.htm, Accessed date: 9 April 2017

91/676/EEC, 1991. Nitrates directive. Council directive 91/676/EEC of 12 December 1991, concerning the protection of waters against pollution caused by nitrates from agricultural sources. [WWW document]. Off. J. Eur. Comm. http://ec.europa.eu/environment/index_en.htm, Accessed date: 9 April 2017

98/83/EC, 1998. Drinking water directive. Council directive 98/83/EC, of 3 November 1998, on the quality of water intended for human consumption. [WWW document]. Off. J. Eur. Comm. http://ec.europa.eu/environment/index_en.htm, Accessed date: 9 April 2017

ACA, 2018. Consulta de dades de control de la qualitat i la quantitat de l'aigua al medi de l'Agència Catalana de l'Aigua (ACA). [(WWW Document)].

Aharon, P., Fu, B., 2000. Microbial sulfate reduction rates and sulfur and oxygen isotope fractionations at oil and gas seeps in deepwater Gulf of Mexico. Geochim. Cosmochim. Acta 64, 233–246. https://doi.org/10.1016/S0016-7037(99)00292-6.

Aravena, R., Robertson, W.D., 1998. Use of multiple isotope tracers to evaluate denitrification in ground water: study of nitrate from a large-flux septic system plume. Ground Water 36, 975–982.

Badr, O., Probert, S.D., 1993. Environmental impacts of atmospheric nitrous oxide. Appl. Energy https://doi.org/10.1016/0306-2619(93)90018-K.

Bolleter, W.T., Bushman, C.J., Tidwell, P.W., 1961. Spectrophotometric determination of ammonia as indophenol. Anal. Chem. 33, 592–594. https://doi.org/10.1021/ac60172a034.

Borden, A.K., Brusseau, M.L., Carroll, K.C., McMillan, A., Akyol, N.H., Berkompas, J., Miao, Z., Jordan, F., Tick, G., Waugh, W.J., Glenn, E.P., 2012. Ethanol addition for enhancing denitrification at the uranium mill tailing site in Monument Valley, AZ. Water Air Soil Pollut. 223, 755–763. https://doi.org/10.1007/s11270-011-0899-1.

Böttcher, J., Strebel, O., Voerkelius, S., Schmidt, H.-L., 1990. Using isotope fractionation of nitrate-nitrogen and nitrate-oxygen for evaluation of microbial denitrification in a sandy aquifer. J. Hydrol. 114, 413–424. https://doi.org/10.1016/0022-1694(90)90068-9.

Buchwald, C., Casciotti, K.L., 2010. Oxygen isotopic fractionation and exchange during bacterial nitrite oxidation. Limnol. Oceanogr. 55, 1064–1074. https://doi.org/10.4319/lo.2010.55.3.1064.

Calderer, M., Gibert, O., Martí, V., Rovira, M., De Pablo, J., Jordana, S., Duro, L., Guimerá, J., Bruno, J., 2010. Denitrification in presence of acetate and glucose for bioremediation of nitrate-contaminated groundwater. Environ. Technol. 31, 799–814. https://doi.org/10.1080/09593331003667741.

Carrey, R., Otero, N., Soler, A., Gómez-Alday, J.J., Ayora, C., 2013. The role of Lower Cretaceous sediments in groundwater nitrate attenuation in central Spain: column experiments. Appl. Geochem. 32, 142–152. https://doi.org/10.1016/j.apgeochem.2012.10.009.

Carrey, R., Rodríguez-Escales, P., Soler, A., Otero, N., 2018. Tracing the role of endogenous carbon in denitrification using wine industry by-product as an external electron donor: coupling isotopic tools with mathematical modeling. J. Environ. Manag. 207, 105–115. https://doi.org/10.1016/j.jenvman.2017.10.063.

Casciotti, K.L., 2009. Inverse kinetic isotope fractionation during bacterial nitrite oxidation. Geochim. Cosmochim. Acta 73, 2061–2076. https://doi.org/10.1016/j.gca.2008.12.022.

Castro-Barros, C.M., Jia, M., van Loosdrecht, M.C.M., Volcke, E.I.P., Winkler, M.K.H., 2017. Evaluating the potential for dissimilatory nitrate reduction by anammox bacteria for municipal wastewater treatment. Bioresour. Technol. 233, 363–372. https://doi.org/10.1016/j.biortech.2017.02.063.

Chen, D.J.Z., MacQuarrie, K.T.B., 2005. Correlation of delta N-15 and delta O-18 in NO_3^- during denitrification in groundwater. J. Environ. Eng. Sci. 4, 221–226.

Coplen, T.B., 2011. Guidelines and recommended terms for expression of stable-isotope-ratio and gas-ratio measurement results. Rapid Commun. Mass Spectrom. 25, 2538–2560. https://doi.org/10.1002/rcm.5129.

Critchley, K., Rudolph, D.L., Devlin, J.F., Schillig, P.C., 2014. Stimulating in situ denitrification in an aerobic, highly permeable municipal drinking water aquifer. J. Contam. Hydrol. 171, 66–80. https://doi.org/10.1016/j.jconhyd.2014.10.008.

De Beer, D., Schramm, A., Santegoeds, C.M., Kühl, M., 1997. A nitrite microsensor for profiling environmental biofilms. Appl. Environ. Microbiol. 63, 973–977.

DECRET 136/2009, 2009. DECRET 136/2009, d'1 de setembre, d'aprovació del programa d'actuació aplicable a les zones vulnerables en relació amb la contaminació de nitrats que procedeixen de fonts agràries i de gestió de les dejeccions ramaderes [WWW Document]. URL. https://portaljuridic.gencat.cat/ca/pjur_ocults/pjur_resultats_fitxa/?action=fitxa&documentId=478701&language=ca_ES.

DECRET 283/1998, 1998. DECRET 283/1998, de 21 d'octubre, de designació de les zones vulnerables en relació amb la contaminació de nitrats procedents de fonts agràries. [WWW Document]. URL https://dogc.gencat.cat/ca/pdogc_canals_interns/pdogc_resultats_fitxa/?documentId=179342&language=ca_ES&action=fitxa (accessed 2.5.19).

Dogramaci, S., Herczeg, A., Schiff, S., Bone, Y., 2001. Controls on $\delta^{34}S$ and $\delta^{18}O$ of dissolved sulfate in aquifers of the Murray Basin, Australia and their use as indicators of flow processes. Appl. Geochem. 16, 475–488. https://doi.org/10.1016/S0883-2927(00)00052-4.

Elefsiniotis, P., Li, D., 2006. The effect of temperature and carbon source on denitrification using volatile fatty acids. Biochem. Eng. J. 28, 148–155. https://doi.org/10.1016/j.bej.2005.10.004.

Gierczak, R., Devlin, J.F., Rudolph, D.L., 2007. Field test of a cross-injection scheme for stimulating in situ denitrification near a municipal water supply well. J. Contam. Hydrol. 89, 48–70. https://doi.org/10.1016/j.jconhyd.2006.08.001.

Giles, M., Morley, N., Baggs, E.M., Daniell, T.J., 2012. Soil nitrate reducing processes - drivers, mechanisms for spatial variation, and significance for nitrous oxide production. Front. Microbiol. 3, 1–16. https://doi.org/10.3389/fmicb.2012.00407.

Granger, J., Wankel, S.D., 2016. Isotopic overprinting of nitrification on denitrification as a ubiquitous and unifying feature of environmental nitrogen cycling. Proc. Natl. Acad. Sci. 113, E6391–E6400. https://doi.org/10.1073/pnas.1601383113.

Granger, J., Sigman, D.M., Lehmann, M.F., Tortell, P.D., 2008. Nitrogen and oxygen isotope fractionation during dissimilatory nitrate reduction by denitrifying bacteria. Limnol. Oceanogr. 53, 2533–2545. https://doi.org/10.4319/lo.2008.53.6.2533.

Grau-Martínez, A., Torrentó, C., Carrey, R., Rodríguez-Escales, P., Domènech, C., Ghiglieri, G., Soler, A., Otero, N., 2017. Feasibility of two low-cost organic substrates for inducing denitrification in artificial recharge ponds: batch and flow-through experiments. J. Contam. Hydrol. 198, 48–58. https://doi.org/10.1016/j.jconhyd.2017.01.001.

Hallin, S., Pell, M., 1998. Metabolic properties of denitrifying bacteria adapting to methanol and ethanol in activated sludge. Water Res. 32, 13–18. https://doi.org/10.1016/S0043-1354(97)00199-1.

Her, J.J., Huang, J.S., 1995. Influences of carbon source and C/N ratio on nitrate/nitrite denitrification and carbon breakthrough. Bioresour. Technol. 54, 45–51. https://doi.org/10.1016/0960-8524(95)00113-1.

ICG, 2011. Memòria de l'institut Geològic de Catalunya 2011. [WWW Document]. https://icgc.cat/igcweb/files/igc_memoria2011.pdf, Accessed date: 5 February 2019.

Jones, Z.L., Jasper, J.T., Sedlak, D.L., Sharp, J.O., 2017. Sulfide-induced dissimilatory nitrate reduction to ammonium supports anaerobic ammonium oxidation (Anammox) in an open-water unit process wetland. 83, 1–14.

Kelso, B.H.L., Smith, R.V., Laughlin, R.J., Lennox, S.D., 1997. Dissimilatory nitrate reduction in anaerobic sediments leading to river nitrite accumulation. Appl. Environ. Microbiol. 63, 4679–4685.

Khan, I.A., Spalding, R.F., 2004. Enhanced in situ denitrification for a municipal well. Water Res. 38, 3382–3388. https://doi.org/10.1016/j.watres.2004.04.052.

Knowles, R., 1982. Denitrification. Microbiol. Rev. 46, 43–70.

Kool, D.M., Wrage, N., Oenema, O., Dolfing, J., Van Groenigen, J.W., 2007. Oxygen exchange between (de)nitrification intermediates and H_2O and its implications for source determination of NO_3^- and N_2O: a review. Rapid Commun. Mass Spectrom. 21, 3569–3578. https://doi.org/10.1002/rcm.3249.

Kraft, B., Strous, M., Tegetmeyer, H.E., 2011. Microbial nitrate respiration - genes, enzymes and environmental distribution. J. Biotechnol. 155, 104–117. https://doi.org/10.1016/j.jbiotec.2010.12.025.

Laverman, A.M., Pallud, C., Abell, J., Cappellen, P. Van, 2012. Comparative survey of potential nitrate and sulfate reduction rates in aquatic sediments. Geochim. Cosmochim. Acta 77, 474–488. https://doi.org/10.1016/j.gca.2011.10.033.

Mariotti, A., Germon, J.C., Hubert, P., Kaiser, P., Letolle, R., Tardieux, A., Tardieux, P., 1981. Experimental determination of nitrogen kinetic isotope fractionation: some principles; illustration for the denitrification and nitrification processes. Plant Soil 62, 413–430. https://doi.org/10.1007/BF02374138.

Mariotti, A., Landreau, A., Simon, B., 1988. ^{15}N isotope biogeochemistry and natural denitrification process in groundwater: application to the chalk aquifer of northern France. Geochim. Cosmochim. Acta 52, 1869–1878. https://doi.org/10.1016/0016-7037(88)90010-5.

McIlvin, M.R., Altabet, M.A., 2005. Chemical conversion of nitrate and nitrite to nitrous oxide for nitrogen and oxygen isotopic analysis in freshwater and seawater. Anal. Chem. 77, 5589–5595. https://doi.org/10.1021/ac050528s.

Meckenstock, R.U., Morasch, B., Griebler, C., Richnow, H.H., 2004. Stable isotope fractionation analysis as a tool to monitor biodegradation in contaminated acquifers. J. Contam. Hydrol. 75, 215–255. https://doi.org/10.1016/j.jconhyd.2004.06.003.

Moreno-vivián, C., Cabello, P., Blasco, R., Castillo, F., Cabello, N., Marti, M., 1999. Prokaryotic Nitrate Reduction : Molecular Properties and Functional Distinction among Bacterial Nitrate Reductases. vol. 181 pp. 6573–6584.

Otero, N., Canals, À., Soler, A., 2007. Using dual-isotope data to trace the origin and processes of dissolved sulphate: a case study in Calders stream (Llobregat basin, Spain). Aquat. Geochemistry 13, 109–126. https://doi.org/10.1007/s10498-007-9010-3.

Otero, N., Torrentó, C., Soler, A., Menció, A., Mas-Pla, J., 2009. Monitoring groundwater nitrate attenuation in a regional system coupling hydrogeology with multi-isotopic methods: the case of Plana de Vic (Osona, Spain). Agric. Ecosyst. Environ. 133, 103–113. https://doi.org/10.1016/j.agee.2009.05.007.

Peng, Y.Z., Ma, Y., Wang, S.Y., 2007. Denitrification potential enhancement by addition of external carbon sources in a pre-denitrification process. J. Environ. Sci. 19, 284–289. https://doi.org/10.1016/S1001-0742(07)60046-1.

Philippot, L., Hallin, S., Schloter, M., 2007. Ecology of denitrifying prokaryotes in agricultural soil. Adv. Agron., 249–305 https://doi.org/10.1016/S0065-2113(07)96003-4.

Richardson, D.J., Watmough, N.J., 1999. Inorganic nitrogen metabolism in bacteria. Curr. Opin. Chem. Biol. 3, 207–219. https://doi.org/10.1016/S1367-5931(99)80034-9.

Rivett, M.O., Buss, S.R., Morgan, P., Smith, J.W.N., Bemment, C.D., 2008. Nitrate attenuation in groundwater: a review of biogeochemical controlling processes. Water Res. 42, 4215–4232. https://doi.org/10.1016/j.watres.2008.07.020.

Ryabenko, E., Altabet, M.a., Wallace, D.W.R., 2009. Effect of chloride on the chemical conversion of nitrate to nitrous oxide for $\delta^{15}N$ analysis. Limnol. Oceanogr. Methods 7, 545–552. https://doi.org/10.4319/lom.2009.7.545.

Schmidt, T.C., Zwank, L., Elsner, M., Berg, M., Meckenstock, R.U., Haderlein, S.B., 2004. Compound-specific stable isotope analysis of organic contaminants in natural environments: a critical review of the state of the art, prospects, and future challenges. Anal. Bioanal. Chem. 378, 283–300. https://doi.org/10.1007/s00216-003-2350-y.

Sebilo, M., Mayer, B., Nicolardot, B., Pinay, G., Mariotti, A., 2013. Long-term fate of nitrate fertilizer in agricultural soils. Proc. Natl. Acad. Sci. U. S. A. 110, 18185–18189. https://doi.org/10.1073/pnas.1305372110.

Smith, R.L., Miller, D.N., Brooks, M.H., Widdowson, M.A., Killingstad, M.W., 2001. In situ stimulation of groundwater denitrification with formate to remediate nitrate contamination. Environ. Sci. Technol. 35, 196–203. https://doi.org/10.1021/es001360p.

Strebel, O., Böttcher, J., Fritz, P., 1990. Use of isotope fractionation of sulfate-sulfur and sulfate-oxygen to assess bacterial desulfurication in a sandy aquifer. J. Hydrol. 121, 155–172. https://doi.org/10.1016/0022-1694(90)90230-U.

Torrentó, C., Urmeneta, J., Otero, N., Soler, A., Viñas, M., Cama, J., 2011. Enhanced denitrification in groundwater and sediments from a nitrate-contaminated aquifer after addition of pyrite. Chem. Geol. 287, 90–101. https://doi.org/10.1016/j.chemgeo.2011.06.002.

Vidal-Gavilan, G., Folch, A., Otero, N., Solanas, A.M., Soler, A., 2013. Isotope characterization of an in situ biodenitrification pilot-test in a fractured aquifer. Appl. Geochem. 32, 153–163. https://doi.org/10.1016/j.apgeochem.2012.10.033.

Vitòria, L., Otero, N., Soler, A., Canals, A., 2004. Fertilizer characterization: isotopic data (N, S, O, C, and Sr). Environ. Sci. Technol. https://doi.org/10.1021/es0348187.

Vitòria, L., Soler, A., Aravena, R., Canals, À., 2005. Multi-isotopic approach (^{15}N, ^{13}C, ^{34}S, ^{18}O and D) for tracing agriculture contamination in groundwater. Environmental Chemistry: Green Chemistry and Pollutants in Ecosystems https://doi.org/10.1007/3-540-26531-7_5.

Vitòria, L., Soler, A., Canals, À., Otero, N., 2008. Environmental isotopes (N, S, C, O, D) to determine natural attenuation processes in nitrate contaminated waters: example of Osona (NE Spain). Appl. Geochem. 23, 3597–3611. https://doi.org/10.1016/j.apgeochem.2008.07.018.

Vitousek, P.M., Aber, J.D., Howarth, R.W., Likens, G.E., Matson, P.A., Schindler, D.W., Schlesinger, W.H., Tilman, D.G., 1997. Human alteration of the global nitrogen cycle: sources and consequences. Ecol. Appl. 7, 737–750. https://doi.org/10.1017/CBO9781107415324.004.

Ward, M.H., DeKok, T.M., Levallois, P., Brender, J., Gulis, G., Nolan, B.T., VanDerslice, J., 2005. Workgroup report: drinking-water nitrate and health—recent findings and research needs. Environ. Health Perspect. 113, 1607–1614. https://doi.org/10.1289/ehp.8043.

Wassenaar, L.I., 1995. Evaluation of the origin and fate of nitrate in the Abbotsford aquifer using the isotopes of ^{15}N and ^{18}O in NO_3^-. Appl. Geochem. 10, 391–405. https://doi.org/10.1016/0883-2927(95)00013-A.

Wilderer, P.A., Jones, W.L., Dau, U., 1987. Competition in denitrification systems affecting reduction rate and accumulation of nitrite. Water Res. 21, 239–245. https://doi.org/10.1016/0043-1354(87)90056-X.

Wunderlich, A., Meckenstock, R., Einsiedl, F., 2012. Effect of different carbon substrates on nitrate stable isotope fractionation during microbial denitrification. Environ. Sci. Technol. 46, 4861–4868. https://doi.org/10.1021/es204075b.

Wunderlich, A., Meckenstock, R.U., Einsiedl, F., 2013. A mixture of nitrite-oxidizing and denitrifying microorganisms affects the $\delta^{18}O$ of dissolved nitrate during anaerobic microbial denitrification depending on the $\delta^{18}O$ of ambient water. Geochim. Cosmochim. Acta 119, 31–45. https://doi.org/10.1016/j.gca.2013.05.028.

Zumft, W.G., 1997. Cell biology and molecular basis of denitrification. Microbiol. Mol. Biol. Rev. 61, 533–616.

SUPPLEMENTARY INFORMATION TO:

Use of nitrogen and oxygen isotopes of dissolved nitrate to trace field-scale induced denitrification efficiency throughout an in-situ groundwater remediation strategy.

Rosanna Margalef-Marti[1], Raúl Carrey[1], Marta Viladés[2], Irene Jubany[3], Ester Vilanova[4], Roser Grau[5], Albert Soler[1], Neus Otero[1,6]

[1] Grup MAiMA, SGR Mineralogia Aplicada, Geoquímica i Geomicrobiologia, Departament de Mineralogia, Petrologia i Geologia Aplicada, Facultat de Ciències de la Terra, Universitat de Barcelona (UB), C/Martí i Franquès s/n, 08028 Barcelona (Spain).

[2] Sustainability Department, Fundació CTM Centre Tecnològic, Spain.

[3] Sustainability Area, Eurecat, Centre Tecnològic de Catalunya, Spain.

[4] Amphos 21 Consulting SL, Spain.

[5] Catalana de Perforacions, Spain.

[6] Serra Húnter Fellowship, Generalitat de Catalunya, Spain.

Science of the Total Environment,

Volume 686, 10 October 2019, Pages 709-718

https://doi.org/10.1016/j.scitotenv.2019.06.003

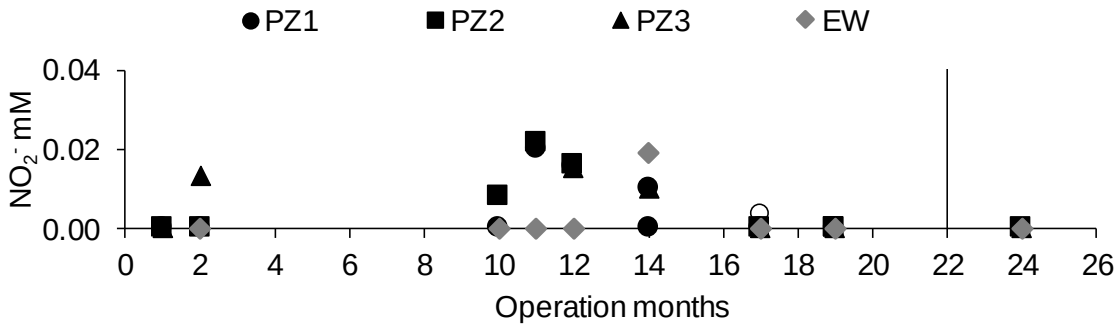

Figure S1. NO_2^- evolution during the pilot plant operation. NO_2^- concentration of the pilot plant samples. Empty symbols for PZ1 and PZ2 correspond to bottom samples (two-depth sampling). The vertical line corresponds to the last injection date.

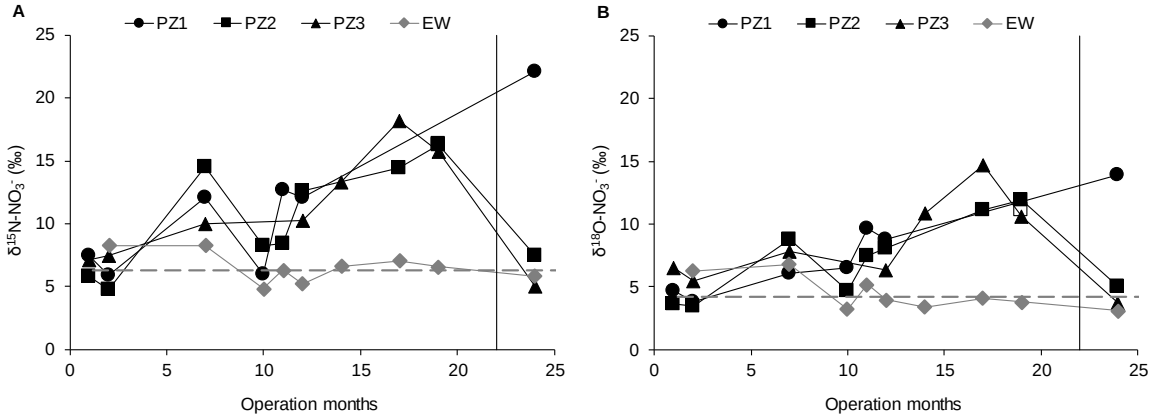

Figure S2. Temporal dynamics of the NO_3^- isotopic composition. A) $\delta^{15}N\text{-}NO_3^-$ and **B**) $\delta^{18}O\text{-}NO_3^-$ measured in the samples collected in the pilot-plant. The dashed grey line corresponds to the MW average composition. The vertical line corresponds to the last injection date. Empty symbols for PZ2 correspond to bottom samples (two-depth sampling).

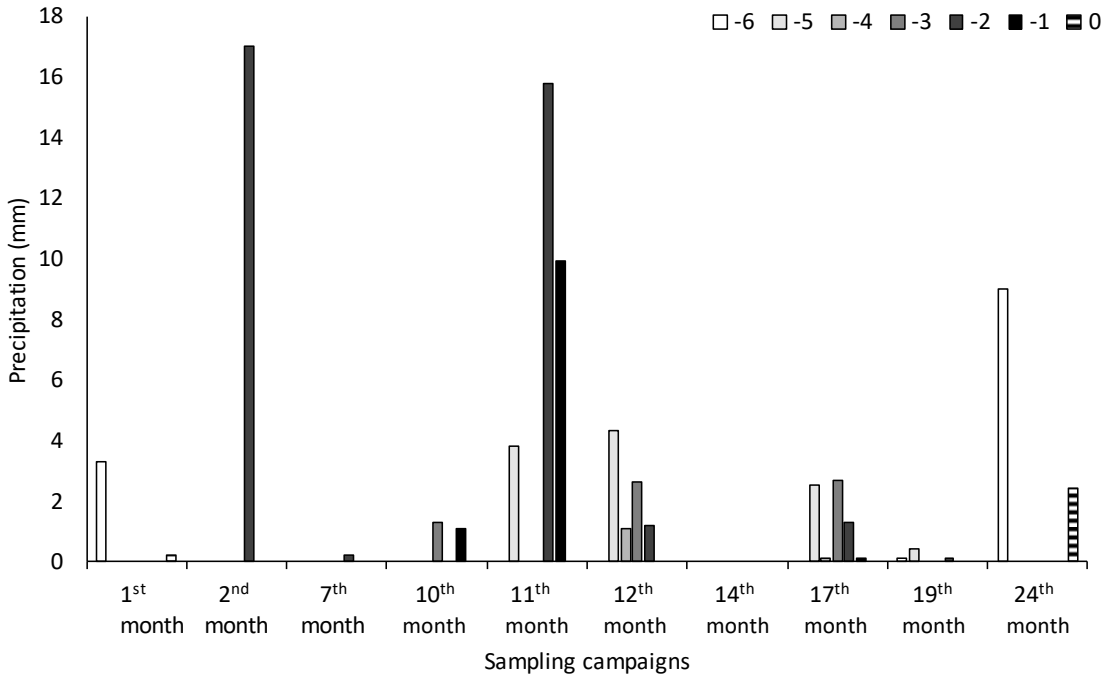

Figure S3. Rainfall data. Rainfall (mm) registered each sampling campaign day (striped bar) and the previous six days (dark to light grey colour). The data was recorded by station 0252D from the Spanish national meteorological agency (AEMET, Ministry of Agriculture, Food and Environment of Spain).

Table S1. Batch experiments results. Chemical and isotopic characterization of the samples obtained from the sacrificed microcosms. “n.d.” refers to parameters that were not determined.

CODE	HOUR	NO_3^- (mM)	NO_2^- (mM)	$\delta^{15}N\text{-}NO_3^-$ (‰)	$\delta^{18}O\text{-}NO_3^-$ (‰)	SD $\delta^{15}N\text{-}NO_3^-$	SD $\delta^{18}O\text{-}NO_3^-$	NH_4^+ (mM)
GW	0.0	0.89	0.01	5.0	3.6	0.3	1.4	n.d.
B-1	47.0	0.47	0.09	12.6	10.8	0.3	0.1	0.00
B-2	47.5	0.33	0.17	17.9	19.9	1.1	0.9	0.00
B-3	48.5	0.29	0.17	19.2	20.7	1.1	0.3	0.03
B-4	51.0	0.27	0.26	20.7	23.0	1.7	0.5	0.03
B-5	53.5	0.19	0.23	26.0	24.0	n.d.	n.d.	0.03
B-6	55.0	0.18	0.16	25.1	26.7	0.3	1.4	0.01
B-7	56.5	0.15	0.16	29.7	30.7	0.3	1.9	0.02
B-8	57.0	0.11	0.14	n.d.	n.d.	n.d.	n.d.	0.01
B-9	69.0	0.03	0.03	n.d.	n.d.	n.d.	n.d.	0.02
B-10	70.0	0.01	0.00	n.d.	n.d.	n.d.	n.d.	0.02
C1	72.0	0.92	0.00	6.5	6.0	0.9	0.3	0.04
C2	72.0	0.00	0.00	n.d.	n.d.	n.d.	n.d.	n.d.
C3-1	32.0	0.89	0.00	n.d.	n.d.	n.d.	n.d.	n.d.
C3-2	47.0	0.67	0.04	n.d.	n.d.	n.d.	n.d.	n.d.
C3-3	51.0	0.67	0.03	n.d.	n.d.	n.d.	n.d.	n.d.
C3-4	52.3	0.67	0.04	n.d.	n.d.	n.d.	n.d.	n.d.
C3-5	55.0	0.65	0.05	n.d.	n.d.	n.d.	n.d.	n.d.
C3-6	56.5	0.60	0.06	n.d.	n.d.	n.d.	n.d.	n.d.
C3-7	69.5	0.27	0.19	n.d.	n.d.	n.d.	n.d.	n.d.
C3-8	76.0	0.19	0.53	n.d.	n.d.	n.d.	n.d.	n.d.
C3-9	80.0	0.07	0.76	n.d.	n.d.	n.d.	n.d.	n.d.
C3-10	95.0	0.01	0.00	n.d.	n.d.	n.d.	n.d.	n.d.

Table S2. Pilot-plant results. Chemical and isotopic characterization of the samples obtained from the pilot-plant. "n.d." refers to parameters that were not determined.

Code	Month	NO_3^- (mM)	NO_2^- (mM)	$\delta^{15}N\text{-}NO_3^-$ (‰)	$\delta^{18}O\text{-}NO_3^-$ (‰)	SD $\delta^{15}N\text{-}NO_3^-$	SD $\delta^{18}O\text{-}NO_3^-$	SO_4^{2-} (mM)	$\delta^{34}S\text{-}SO_4^{2-}$ (‰)	$\delta^{18}O\text{-}SO_4^{2-}$ (‰)	SD $\delta^{18}O\text{-}SO_4^{2-}$	Denitrif. % (concentration)	Denitrif. % (isotopes)
PZ1	1	1.26	0.00	7.5	4.7	0.6	0.0	1.72	9.2	9.4	0.3	0	7
PZ2		0.42	0.00	5.8	3.6	0.6	0.8	1.04	13.1	11.3	0.1	55	0
PZ3		0.98	0.00	7.2	6.5	0.5	1.1	2.79	n.d.	n.d.	n.d.	0	5
W2		0.92	0.00	6.5	4.2	0.6	1.5	2.43	13.3	11.2	0.1	0	0
PZ1	2	0.88	0.00	5.9	3.8	0.1	0.5	1.40	n.d.	n.d.	n.d.	6	0
PZ2		0.37	0.00	4.7	3.5	0.5	0.1	1.13	13.1	11.4	0.1	61	0
PZ3		0.58	0.01	7.5	5.5	1.1	0.5	2.56	n.d.	n.d.	n.d.	38	0
W1		0.71	0.00	8.3	6.3	0.3	0.2	2.04	14.1	11.8	0.3	24	0
W2		0.97	0.00	8.7	5.7	0.3	0.1	2.34	13.1	11.1	0.2	0	0
PZ1	7	0.95	n.d.	12.1	6.0	0.6	0.0	0.00	n.d.	n.d.	n.d.	0	42
PZ2		0.19	n.d.	14.5	8.8	0.6	0.6	0.00	n.d.	n.d.	n.d.	79	52
PZ3		0.88	n.d.	10.0	7.9	0.6	0.3	0.00	n.d.	n.d.	n.d.	6	31
W1		0.70	n.d.	8.3	6.8	0.1	0.3	0.00	n.d.	n.d.	n.d.	25	22
W2		0.96	n.d.	5.2	3.4	0.5	1.2	0.00	n.d.	n.d.	n.d.	0	0
PZ1	10	0.12	0.00	6.0	6.5	1.1	1.2	1.58	n.d.	n.d.	n.d.	87	7
PZ2		0.16	0.01	8.2	4.7	0.2	0.5	1.90	n.d.	n.d.	n.d.	82	22
W1		0.67	0.00	4.9	3.2	0.3	0.1	2.41	n.d.	n.d.	n.d.	29	0
W2		0.88	0.00	5.0	3.6	0.3	1.4	2.45	n.d.	n.d.	n.d.	0	0

Table S2. Continued.

Code	Month	NO_3^- (mM)	NO_2^- (mM)	$\delta^{15}N\text{-}NO_3^-$ (‰)	$\delta^{18}O\text{-}NO_3^-$ (‰)	SD $\delta^{15}N\text{-}NO_3^-$	SD $\delta^{18}O\text{-}NO_3^-$	SO_4^{2-} (mM)	$\delta^{34}S\text{-}SO_4^{2-}$ (‰)	$\delta^{18}O\text{-}SO_4^{2-}$ (‰)	SD $\delta^{18}O\text{-}SO_4^{2-}$	Denitrif. % (concentration)	Denitrif. % (isotopes)
PZ1	11	0.20	0.02	12.7	9.7	0.4	0.1	2.80	14.1	11.4	n.d.	79	40
PZ2		0.29	0.02	8.5	7.5	0.5	0.2	4.07	14.7	11.8	n.d.	69	16
W1		0.82	0.00	6.3	5.2	0.3	0.1	4.24	14.1	11.5	0.1	13	0
W2		0.93	0.00	6.3	4.6	0.1	0.2	4.12	12.0	10.5	0.1	0	0
PZ1	12	0.15	0.02	12.1	8.7	0.3	0.2	0.66	n.d.	n.d.	n.d.	84	38
PZ2		0.18	0.02	12.6	8.1	0.2	1.1	2.46	16.6	12.5	0.2	81	40
PZ3		0.49	0.02	10.3	6.3	0.0	0.1	5.07	15.8	12.4	0.0	48	28
W1		0.71	0.00	5.2	4.0	1.0	1.3	2.82	12.1	11.1	0.2	25	0
W2		0.97	0.00	6.1	3.8	0.2	0.9	4.89	12.5	10.5	0.0	0	0
PZ1	14	0.02	0.01	n.d.	n.d.	n.d.	n.d.	2.42	n.d.	n.d.	n.d.	98	100
PZ3		0.59	0.01	13.3	10.8	0.2	0.1	3.37	n.d.	n.d.	n.d.	37	41
W1		0.82	0.02	6.6	3.4	0.2	0.2	2.61	n.d.	n.d.	n.d.	13	0
PZ145	17	0.00	0.00	n.d.	n.d.	n.d.	n.d.	1.12	n.d.	n.d.	n.d.	100	100
PZ139		0.01	0.00	n.d.	n.d.	n.d.	n.d.	1.15	n.d.	n.d.	n.d.	99	100
PZ237		0.05	0.00	14.4	11.2	0.2	0.7	1.66	n.d.	n.d.	n.d.	95	44
PZ3		0.37	0.00	18.2	14.7	0.1	0.4	2.28	n.d.	n.d.	n.d.	60	58
W1		0.63	0.00	7.1	4.1	0.2	0.4	2.11	n.d.	n.d.	n.d.	33	0

Table S2. Continued.

Code	Month	NO_3^- (mM)	NO_2^- (mM)	$\delta^{15}N\text{-}NO_3^-$ (‰)	$\delta^{18}O\text{-}NO_3^-$ (‰)	SD $\delta^{15}N\text{-}NO_3^-$	SD $\delta^{18}O\text{-}NO_3^-$	SO_4^{2-} (mM)	$\delta^{34}S\text{-}SO_4^{2-}$ (‰)	$\delta^{18}O\text{-}SO_4^{2-}$ (‰)	SD $\delta^{18}O\text{-}SO_4^{2-}$	Denitrif. % (concentration)	Denitrif. % (isotopes)
PZ1	19	0.00	0.01	n.d.	n.d.	n.d.	n.d.	n.d.	n.d.	n.d.	n.d.	100	100
PZ2 45		0.19	0.02	16.3	11.1	0.1	0.6	n.d.	n.d.	n.d.	n.d.	79	54
PZ2 38		0.09	0.01	16.3	12.0	0.1	0.1	n.d.	n.d.	n.d.	n.d.	90	53
PZ3		0.64	0.06	15.8	10.6	0.1	0.1	n.d.	n.d.	n.d.	n.d.	31	51
W1		0.69	0.00	6.6	3.8	0.3	0.5	n.d.	n.d.	n.d.	n.d.	26	0
PZ1	24	0.10	0.01	22.1	14.0	0.1	0.3	n.d.	n.d.	n.d.	n.d.	89	72
PZ2 45		0.46	0.02	7.5	5.1	0.0	0.7	n.d.	n.d.	n.d.	n.d.	51	12
PZ3		0.97	0.00	5.0	3.7	0.2	0.7	n.d.	n.d.	n.d.	n.d.	0	0
W1		0.99	0.00	5.8	3.1	0.3	0.0	n.d.	n.d.	n.d.	n.d.	0	0

ANNEX 6

Characterisation of the natural attenuation of chromium contamination in the presence of nitrate using isotopic methods. A case study from the Matanza-Riachuelo River basin, Argentina.

Elina Ceballos[1], Rosanna Margalef-Marti[2], Raúl Carrey[2], Robert Frei[3], Neus Otero[2,4], Albert Soler[2], Carlos Ayora[5]

[1] Instituto de Hidrología de Llanuras ‘‘Dr. Eduardo J. Usunoff”, CONICET-UNCPBA-CIC, República de Italia 780, 47 (B7300), Azul, Buenos Aires, Argentina.

[2] Grup MAiMA, SGR Mineralogia Aplicada, Geoquímica i Geomicrobiologia, Departament de Mineralogia, Petrologia i Geologia Aplicada, Facultat de Ciències de la Terra, Universitat de Barcelona (UB), C/Martí i Franquès s/n, 08028 Barcelona, Spain.

[3] Department of Geosciences and Natural Resource Management, University of Copenhagen, Copenhagen, Denmark.

[4] Serra Húnter Fellowship, Generalitat de Catalunya, Spain.

[5] Department of Geoscience, Institute of Environmental Assessment and Water Research, IDAEA-CSIC, C/Jordi Girona, 18, 08028 Barcelona, Spain.

Science of the Total Environment, Volume 699, 10 January 2020, 134331

https://doi.org/10.1016/j.scitotenv.2019.134331

Impact factor (JCR/WOS) = 5.6 (2018)

Q1, 27/250 Environmental sciences

Science of the Total Environment 699 (2020) 134331

Contents lists available at ScienceDirect

Science of the Total Environment

journal homepage: www.elsevier.com/locate/scitotenv

Characterisation of the natural attenuation of chromium contamination in the presence of nitrate using isotopic methods. A case study from the Matanza-Riachuelo River basin, Argentina

Elina Ceballos [a,*], Rosanna Margalef-Martí [b], Raul Carrey [b], Robert Frei [c], Neus Otero [b,d], Albert Soler [b], Carlos Ayora [e]

[a] Instituto de Hidrología de Llanuras "Dr. Eduardo J. Usunoff", CONICET-UNCPBA-CIC, República de Italia 780, 47 (B7300), Azul, Buenos Aires, Argentina
[b] Grup MAiMA, SGR Mineralogia Aplicada, Geoquímica i Geomicrobiologia, Departament de Mineralogia, Petrologia i Geologia Aplicada, Facultat de Ciències de la Terra, Universitat de Barcelona, UB, C/Martí i Franquès, s/n, 08028 Barcelona, Spain
[c] Department of Geosciences and Natural Resource Management, University of Copenhagen, Copenhagen, Denmark
[d] Serra Húnter Fellow, Generalitat de Catalunya, Spain
[e] Department of Geoscience, Institute of Environmental Assessment and Water Research, IDAEA-CSIC, C/Jordi Girona, 18, 08028 Barcelona, Spain

HIGHLIGHTS

- Cr(VI) reduction rate is not affected by the NO_3^- presence in laboratory tests.
- Cr(VI) isotopic fractionation shows a two-stage trend in batch experiments.
- Cr(VI) and NO_3^- reduction can occur concomitantly in groundwater.
- Isotope analyses can prove natural attenuation of Cr(VI) and NO_3^- in groundwater.
- Isotope tools allow distinguishing Cr (VI) reduction from dilution in groundwater.

GRAPHICAL ABSTRACT

Unlabelled Image

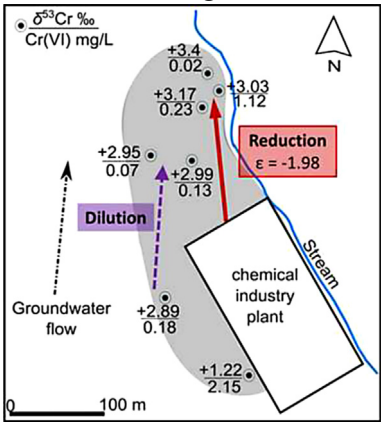

ARTICLE INFO

Article history:
Received 27 May 2019
Received in revised form 10 August 2019
Accepted 5 September 2019
Available online 9 September 2019

Editor: José Virgílio Cruz

Keywords:
Cr(VI) reduction
Denitrification
Isotopic fractionation

ABSTRACT

The groundwater contamination by hexavalent chromium (Cr(VI)) in a site of the Matanza-Riachuelo River basin (MRB), Argentina, has been evaluated by determining the processes that control the natural mobility and attenuation of Cr(VI) in the presence of high nitrate (NO_3^-) contents. The groundwater Cr(VI) concentrations ranged between 1.9E-5 mM and 0.04 mM, while the NO_3^- concentrations ranged between 0.5 mM and 3.9 mM.

In order to evaluate the natural attenuation of Cr(VI) and NO_3^- in the MRB groundwater, Cr and N isotopes were measured in these contaminants. In addition, laboratory batch experiments were performed to determine the isotope fractionation (ε) during the reduction of Cr(VI) under denitrifying conditions. While the Cr(VI) reduction rate is not affected by the presence of NO_3^-, the NO_3^- attenuation is slower in the presence of Cr(VI). Nevertheless, no significant differences on ε values were observed when testing the absence or presence of each contaminant. The ε^{53}Cr determined in the batch experiments describe a

* Corresponding author.
E-mail address: eceballos@ihlla.org.ar (E. Ceballos).

https://doi.org/10.1016/j.scitotenv.2019.134331

Groundwater
Matanza-Riachuelo basin

two- stage trend, in which Stage I is characterized by $\varepsilon^{53}Cr \sim -1.8‰$ and Stage II by $\varepsilon^{53}Cr \sim -0.9‰$. The respective $\varepsilon^{15}N_{NO3}$ obtained is $-23.9‰$ whereas $\varepsilon^{18}O_{NO3}$ amount to $-25.7‰$. Using these ε values and a Rayleigh fractionation model we estimate that an average of 60% of the original Cr(VI) is removed from the groundwater of the contaminated site. Moreover, the average degree of NO_3^- attenuation by denitrification is found to be about 20%. This study provides valuable information about the dynamics of a complex system that can serve as a basis for efficient management of contaminated groundwater in the most populated and industrialized basin of Argentina.

1. Introduction

Chromium (Cr) is a toxic contaminant in groundwater derived mostly from anthropogenic activities such as metallurgic, refractory, chemical, and tannery industries. In aquatic environments, Cr exists in two main oxidation states, Cr(VI) and Cr(III). Cr(VI) is more toxic and generally more mobile than Cr(III). The oxidized form, Cr(VI), can cause cancer and dermatitis (Kotas and Stasicka, 2000). In contrast, the reduced form, Cr(III), is an essential nutrient, it is less soluble, adsorbs strongly on solid surfaces and co-precipitates with Fe(III) hydroxides (Rai et al., 1989; Davis and Olsen, 1995). Furthermore, Cr(VI) can be naturally reduced through biotic or abiotic oxidation of electron donors such as aqueous Fe (II), Fe(II)-bearing minerals, reduced sulfur species and organic compounds (Palmer and Wittbrodt, 1991). Reduction of toxic Cr (VI) to less toxic Cr(III) is an important process for attenuating Cr (VI) contamination in groundwater by immobilization as Cr(III) (Palmer and Puls, 1994; Davis and Olsen, 1995). This natural process can be enhanced or induced by adding an external electron donor to promote biotic and/or abiotic reduction (Blowes et al., 2000; Mayer et al., 2001; Ellis et al., 2002; Wilkin et al., 2005; Wanner et al., 2012b; Jamieson-Hanes et al., 2012a, 2012b; Han et al., 2012; Basu et al., 2014).

Nitrate (NO_3^-) is another contaminant commonly found in groundwater (Rivett et al., 2008). Nitrate can also be reduced to N_2 gas through biotic or abiotic reactions (Korom, 1992). Denitrification is the main natural process to attenuate NO_3^- contamination in groundwater. Denitrification occurs under anaerobic conditions or dissolved oxygen concentrations below 2 mg/L (Korom, 1992; Cey et al., 1999). This process irreversibly eliminates NO_3^- from groundwater by reduction to N_2 through several intermediate steps ($NO_3^- \rightarrow NO_2^- \rightarrow NO \rightarrow N_2O \rightarrow N_2$) (Knowles, 1982). This chain of reactions can be interrupted at each step depending on biological and kinetic factors (Carrey et al., 2013).

Both processes, the biotic Cr(VI) reduction and the denitrification can be heterotrophic or autotrophic depending on the use of an organic C or inorganic compound (e.g., sulphide or Fe(II)), respectively as electron donors. Therefore, since both reactions compete for the supply of the electron donors, the presence of NO_3^- can decrease the effectiveness of microbial Cr(VI) reduction (Middleton et al., 2003).

Isotope studies have been applied to discriminate between processes that imply an attenuation of Cr(VI) and NO_3^- concentrations by reduction processes and transport processes in the porous medium (dilution/dispersion) (Aravena et al., 1993; Blowes, 2002; Berna et al., 2010; Wanner et al., 2012a; Margalef-Marti et al., 2019a). During the biotic or abiotic reduction of Cr(VI) to Cr(III), a kinetic isotope effect occurs since the lighter isotope, ^{52}Cr, reacts preferentially and therefore, the remaining dissolved Cr(VI) becomes enriched in the heavier isotope, ^{53}Cr (Ellis et al., 2002; Sikora et al., 2008; Kitchen et al., 2012; Basu et al., 2014). Additionally, the Cr(III) species do not undergo rapid isotopic exchange with Cr(VI) species (Zink et al., 2010). Therefore, the calculation of this change in the isotope ratios, or isotope fractionation (ε), can be used to assess the natural or induced attenuation of Cr(VI) in contaminated groundwater (Izbicki et al., 2008; Berna et al., 2010; Raddatz et al., 2011; Wanner et al., 2012a; Heikoop et al., 2014). Likewise, during denitrification, as NO_3^- concentration decreases, the residual NO_3^- becomes enriched in the heavy isotopes (^{15}N and ^{18}O) (Aravena and Robertson, 1998; Fukada et al., 2003; Kendall et al., 2007; Mariotti et al., 1988). Experimental studies show that NO_3^- reduction occurring simultaneously with Cr(VI) reduction can have a significant influence on the Cr(VI) isotope fractionation (Ishibashi et al., 1990; Dichristina, 1992; Garbisu et al., 1998; Viamajala et al., 2002; Vatsouria et al., 2005; Han et al., 2010, 2012). Moreover, isotope tracers have proven to be a powerful tool in identifying NO_3^- and Cr(VI) sources in groundwater (Ellis et al., 2002; Otero et al., 2009).

At present, no case studies evaluate, through laboratory and field scale studies, the coupled natural attenuation of hexavalent chromium and nitrates in groundwater. The Matanza-Riachuelo River basin (MRB) is the most populated (>4 million people), industrialized and contaminated basin in Argentina (Zabala et al., 2016). In several areas of the basin, the main source of water for human and industrial supply is groundwater. Ceballos et al. (2018) detected that groundwater, in some areas within MRB, is affected by both Cr(VI) (up to 5 mg/L) and NO_3^- (>100 mg/L) contamination. The main source of Cr(VI) contamination is related to a chemical industry plant that operated from 1968 to 1990, producing bichromates, chromic acid, sulfuric acid and tannery products (Salvador, 2013). During the operation period, the processing residues containing Cr(VI) salts were disposed untreated into nearby unlined piles where the dissolution of these waste salts promoted the migration of Cr(VI) through the vadose zone into groundwater. The aim of the present study is to combine Cr isotopes and N and O isotopes of dissolved nitrate for the purpose of identifying natural attenuation processes of Cr(VI) and NO_3^- in groundwater. An implicit primary goal is to determine, in laboratory experiments, using groundwater and sediment from the studied area, the degree of isotope fractionation of Cr ($\varepsilon^{53}Cr$) and of N ($\varepsilon^{15}N_{NO3}$) and O ($\varepsilon^{18}O_{NO3}$) during the simultaneous Cr(VI) and NO_3^- reduction. The final goal is to assess the usefulness of the isotope approach to study natural attenuation at field scale. The use of isotope tools to determine the extent of natural attenuation of Cr (VI) and NO_3^- in groundwater, serve as the basis for designing effective remediation strategies in the most exploited and contaminated aquifers in Argentina.

2. Study area

The MRB is located to the NE of the Buenos Aires province, Argentina (Fig. 1A). The MRB is a hydrographic basin that covers an area of approximately 2065 km^2 with very low slopes, forming a typical plain landscape. It consists of preferably continental sedimentary deposits. The main course is the Matanza River, which flows to the NE for 70 km before to be renamed Riachuelo about 15 km before discharging into the Río de la Plata. The area has a temperate climate with warm summers and cool winters. Average

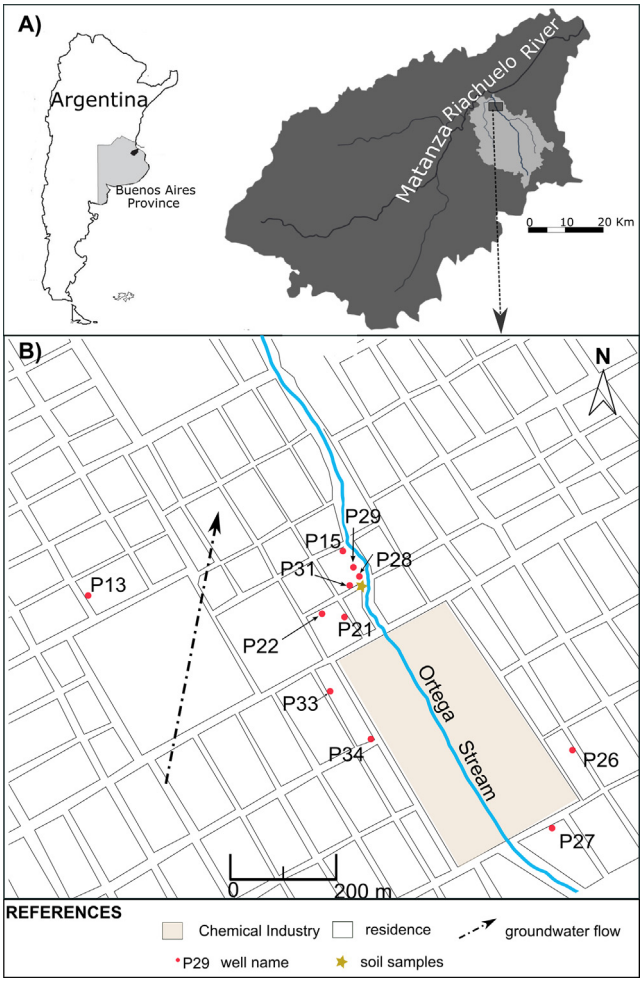

Fig. 1. A) Location of the Matanza-Riachuelo River basin (MRB), and Ortega stream sub basin. B) Site of study, San Ignacio neighbourhood.

rainfall for the period 1906–2014 was 1100 mm/year (Scioli and Burgos, 2015).

The MRB has its main source of water supply and industrial in two aquifer systems, the Upper aquifer of medium to low productivity with a variable water quality, and the Puelche Aquifer, of medium to high productivity and good water quality (Zabala et al., 2016). The Upper Aquifer holds the water table and receives natural recharge by infiltration of rainfall. Its thickness is around 40 m (Mancino et al., 2013) and consists of sandy-clayey-silts loess (Holocene), of homogeneous fine-grained loess and sandy loess (Pleistocene), and of interbedded carbonate (tosca). The Puelche Aquifer has a maximum thickness of 60 m consisting of quartz sands in the lower sandy section and silts and clays that are interbedded towards the top (Upper Pliocene to Pleistocene). These silty clay sediments behave as an aquitard of heterogeneous thickness but in some sectors of the lower basin this aquitard does not exist because the sediments of the Upper Aquifer are in direct contact with the sands of the Puelche Aquifer. Due to the Puelche Aquifer not outcropping in the MRB, its recharge occurs directly from the Upper Aquifer by vertical filtration (Vives et al., 2013). The average annual recharge to the Upper Aquifer for the period 1906–2014 was 133 mm/year (Scioli and Burgos 2015). The groundwater discharges to surface water (streams, rivers) including to Río de la Plata. The two aquifers show similar piezometric patterns, in both of them regional groundwater flow is SW to NE (Vives et al., 2013). In the upper and middle parts of the basin, the water table surface reflects a strong relationship with the streams. The piezometric levels of the Upper and Puelche Aquifer respond simultaneously to seasonal recharge elevations and dry-season drawdowns, showing a strong connection of both aquifers (Zabala et al., 2016). Groundwater of the Upper Aquifer and the Puelche Aquifer has a similar chemical composition, generally of a Na-HCO_3 type in the area of study (Ceballos et al., 2018). The study area is located in San Ignacio neighbourhood, Jagüel town, at the lowest stretch of the Ortega Stream sub basin, in a tributary of the Matanza-Riachuelo River (Fig. 1B). In this sector, the local flow direction of the Upper Aquifer would be conditioned by the Ortega stream, with a flow direction mainly of S-N/NW (Melián, 2014). A downward vertical hydraulic gradient from the Upper to the Puelche Aquifer has also been observed in the site of study (Ceballos et al., 2018). In the San Ignacio neighbourhood, the population does not have access to water supply and sanitation services. The residents have their own on-site solutions through septic tanks or pits. The drinking water supply is obtained from the municipal water trailer or purchased individually.

3. Methodology

3.1. Sampling of groundwater and soil

Groundwater samples were collected (September 2017) from three monitoring wells belonging to the basin authority ACUMAR (samples P13, P28 and P29) and nine private supply wells (samples P15, P21, P22, P26, P27, P31, P33 and P34) (Fig. 1B). Sample P28 was obtained from the Puelche Aquifer (well depth of 40 m) while the rest of the samples were obtained from the Upper aquifer (well depths from 15 to 20 m). The wells were purged three times the volume of water in the column. Parameters such as electrical conductivity (EC), temperature, pH and dissolved O_2 were measured in situ with a Multiparameter PCS Testr 35 Series tester, using a flow cell to avoid contact with the atmosphere. The samples were collected in polyethylene bottles after the wells had been continuously pumped until the EC values became stabilised. A volume of 30 mL was collected for non-purgeable dissolved organic carbon (NPDOC) analysis in glass bottles previously combusted. These samples were passed through a 0.45 μm nylon filter and acidified with 1 mL of HCl (2 N); the bottles were sealed with Parafilm® to minimise any contact with air. A volume of 200 mL was collected for Cr(VI) analysis in polyethylene bottles. These samples were filtered with a 0.45 μm membrane filter, then the pH was adjusted to 9 with NaOH (1 N) and stored at +4 °C. Samples for the Cr isotope analyses were collected in polyethylene bottles and stored at +4 °C until analysis. Samples for the NO_3^- isotope analyses were filtered with a 0.22 μm filter (PTFE Teflon filter), transferred into in 10 mL plastic vials and stored at −20 °C.

Soil samples were collected from a drilling downstream of the chemical industry site near the ACUMAR P28 monitoring well (see Fig. 1B). The drilling reached 4 m whereas the water table was detected at 3 m depth. The sediment was sampled between depths of 3 m and 4 m below the ground surface. These soil samples were isolated from the atmosphere with polypropylene and stored in the refrigerator at +4 °C, until used in the batch experiments.

3.2. Batch experiments

The batch experiments aimed to determine the isotope fractionation of Cr(VI), N-NO_3^- and O-NO_3^- during their reduction by organic carbon under different scenarios. Three types of biostimulated microcosms were set up in 125 mL crystal bottles sealed with butyl rubber septa and aluminium crimp under an argon (Ar) head-

space. The experiments were set up inside a glove box to avoid any trace of dissolved O_2 and N_2. Each bottle contained sediment and groundwater from the Upper aquifer. We used 75 mL of groundwater collected from the P13 monitoring well, 15 g of sediment collected near the P28 monitoring well and added ethanol as external carbon source. Organic carbon was selected to enhance Cr(VI) and NO_3^- reduction due to it is the main source of electrons at field. Three series of parallel experiments were performed according to Cr(VI) content (additional $K_2Cr_2O_7$ salt was added) and NO_3^- concentration (groundwater NO_3^- concentration was 4.2 mM, no additional NO_3^- was added). The experiment "BioCr" only contained Cr(VI) (0.2 mM), the experiment "BioN" only contained NO_3^- (4.2 mM) and the experiment "BioCrN" contained both species. For the "BioCr" experiment, the NO_3^- from groundwater was previously removed by inducing denitrification through the addition of ethanol as electron donor. All series included at least 10 replicates of biostimulated microcosms. Control microcosms without ethanol "CtrlCrN" were carried out for the BioCrN experiments to check the contribution of the sediment on the Cr(VI) and NO_3^- reduction. Moreover, a set of blank microcosms containing only sediment and deionized water (DIW) was also performed to evaluate sediment leaching. The detailed content of each microcosm is shown in Table 1. For incubation, the bottles were wrapped with aluminium foil to avoid photodegradation processes and were maintained at room temperature (~+24 °C) with continuous orbital agitation. The biostimulated microcosms were sacrificed after fixed time spans according to previous laboratory tests (data not shown). The control microcosms were sacrificed at the end of the biostimulated experiment. The samples were immediately filtered with 0.22 μm nylon filters and stored at +4 °C for further analysis. An aliquot for the NO_3^- isotopic analysis was stored at −20 °C.

3.3. Analytical techniques

The Cr(VI), NO_3^-, nitrite (NO_2^-), ammonium (NH_4^+) and non-purgeable dissolved organic carbon (NPDOC) concentration was determined in all samples. The $\delta^{53}Cr$, the $\delta^{15}N_{NO3}$ and $\delta^{18}O_{NO3}$ were determined in all samples collected in the field and in a subset of samples of the laboratory experiments considered representative based on the Cr(VI) and NO_3^- concentrations.

Main anions (NO_3^-, SO_4^{2-}, Cl^- and NO_2^-) were analysed by high-performance liquid chromatography (HPLC) using a WATERS 515 HPLC pump with IC-PAC Anion columns and WESCAN and UV/VIS KONTRON detectors. The NH_4^+ was determined by colorimetry, Indophenol blue method (SP-830 plus Metertech). The NPDOC was measured by organic matter combustion (TOC 500 SHIMADZU). The dissolved Cr(VI) was determined within 24 h of sample collection by using the diphenylcarbazide, SM 3500-Cr B method and a UV–Vis spectrophotometer (SP-830 plus Metertech). Total dissolved Cr and trace elements were determined by inductively coupled plasma mass spectrometry analyses (ICP-MS, Perkin-Elmer Elan 6000) and inductively coupled plasma optical emission spectrometry (ICP–OES, Perkin-Elmer Optima 3200 RL), respectively, after acidifying the filtered samples (1% HNO_3).

The $\delta^{53}Cr$ analyses were performed following a slightly modified method from Frei et al. (2009). An amount of water sample which would yield about 1 μg of total Cr was pipetted into 23 mL Teflon beakers (Savillex ™) together with an amount of a ^{50}Cr-^{54}Cr double spike so that a sample to spike ratio of ~3:1 (total Cr concentrations) was achieved. The mixture was totally evaporated and 3 mL of concentrated *aqua regia* was subsequently added. After 3 h with *aqua regia* on a hot plate at 100 °C, the sample was again dried down. Then, the sample was dissolved into 20 mL of ultrapure water (Milli Q®) and 0.5 mL of 1 N HCl, to which 0.5 mL of a 0.5 M ammonium peroxydisulfate solution (puratronic® quality) was added. The samples were then boiled for 1 h with beaker lids closed on a hot plate at 130 °C. This enabled the total oxidation of Cr to Cr(VI). The solution was then passed over 2 mL pre-cleaned anion exchange resin (DOWEX AG1X8; BioRad™). After rinsing with 5 mL of 0.1 N HCl, Cr(VI) was reduced during 30 min on the columns, with 1 mL of 2 N HNO_3 to which three drops of hydrogen peroxide were added. Cr(III) was then extracted with another 5 mL of the same 2 N HNO_3 hydrogen peroxide mixture into the 23 mL Savillex™ beaker and subsequently dried down. The produced chromium fraction was then purified, by passing the sample in 0.5 N HCl over a miniaturized disposable pipette-tip extraction column, fitted with a bottom and a top disposable PVC frit, which was charged with 300 μL of 200–400 mesh cation resin (AGW-X12, BioRad™), thus employing the slightly modified extraction procedure, published by Trinquier et al. (2009) and Bonnand et al. (2011). The yield of this mini-column extraction and purification step is usually ~70%. Samples were loaded onto Re filaments with a mixture of 3 μL silica gel, 0.5 μL 0.5 mol/L H_3BO_3 and 0.5 μL 0.5 mol/L of H_3PO_4. The samples were statically measured on an IsotopX "Phoenix" multicollector thermal ionization mass spectrometer (TIMS) at the Department of Geoscience and Natural Resource Management, University of Copenhagen, at temperatures between 1050 and 1200 °C, aiming at beam intensity at atomic mass unit (AMU) 52.9407 of 30–60 mV. Each load was analysed 2–4 times. Titanium, vanadium and iron interferences with Cr isotopes were corrected by comparing with $^{49}Ti/^{50}Ti$, $^{50}V/^{51}V$ and $^{54}Fe/^{56}Fe$ ratios. The final isotope composition of each sample was determined as the average value of repeated analyses and reported, relatively to the certified SRM 979.

The $\delta^{15}N_{NO3}$ and $\delta^{18}O_{NO3}$ were determined following the cadmium reduction method (McIlvin and Altabet, 2005; Ryabenko et al., 2009). Then, the N_2O was analysed using a Pre-Con (Thermo Scientific) coupled to a Finnigan MAT 253 Isotope Ratio Mass Spectrometer (IRMS, Thermo Scientific). Isotopic analyses of NO_3^- were prepared at the laboratory of the MAiMA-UB research group and analysed at the Centres Científics i Tècnològics of the Universitat de Barcelona (CCiT-UB).

The isotopic notation is expressed in terms of δ per mil relative to the international standards (Eq. (1)):

$$\delta = \frac{R_{sample} - R_{standard}}{R_{standard}} \quad (1)$$

where R = $^{53}Cr/^{52}Cr$ and $^{15}N/^{14}N$, respectively.

Table 1
Series of laboratory experiments. Tested conditions and microcosms composition. Cr(VI) was added as $K_2Cr_2O_7$ salt and NPDOC as ethanol, NO_3^- was already present in groundwater. The blank microcosms contained only sediment and deionized water (DIW).

Series	Condition	Replicates	NO_3^- (mM)	Cr(VI) (mM)	NPDOC (mM)
BioCr	Biostimulated	12	0.0	0.2	8.4
BioN	Biostimulated	12	4.2	0.0	11.8
BioCrN	Biostimulated	23	4.2	0.2	11.8
CtrlCrN	Control	3	4.2	0.2	0.0
Blank	DIW	3	0.0	0.0	0.0

Table 2
Standards used for the isotopic analysis. According to Coplen (2011), several international and laboratory (CCiT) standards were interspersed among samples for the normalisation of the results.

Analysis	International standards	Laboratory standards
$\delta^{53}Cr$	NIST SRM 979 and NIST 3112a	
$\delta^{15}N_{NO3}$	USGS-32, USGS-34, USGS-35	CCiT-IWS ($\delta^{15}N$ = +16.9‰)
$\delta^{18}O_{NO3}$	USGS-32, USGS-34, USGS-35	CCiT-IWS ($\delta^{18}O$ = +28.5 ‰).

NIST SRM 979 for $\delta^{53}Cr$, Vienna Standard Mean Oceanic Water (V-SMOW) for $\delta^{18}O$ and Atmospheric N_2 (AIR) for $\delta^{15}N$. According to Coplen (2011), several international and laboratory (CCiT) standards were interspersed among samples for the normalisation of the results (Table 2). The standard deviation reproducibility of the samples was ±0.08‰ for $\delta^{53}Cr$, ±1.0‰ for $\delta^{15}N_{NO3}$, ±1.5‰ for $\delta^{18}O_{NO3}$.

3.4. Isotope data calculations

The isotope fractionation (ε), under closed system conditions, can be calculated using the Rayleigh distillation equation (Eq. (2)). Thus, ε can be obtained from the slope of the linear correlation between the natural logarithm of the substrate remaining fraction ($Ln(C_{residual}/C_{initial})$, where C refers to the analyte concentration) and the determined isotope ratios ($Ln(R_{residual}/R_{initial})$, where R = ($\delta$ + 1).

$$Ln\left(\frac{R_{residual}}{R_{initial}}\right) = \varepsilon \times Ln\left(\frac{C_{residual}}{C_{initial}}\right) \quad (2)$$

The percentages of the Cr(VI) reduction and denitrification at field scale can be determined by using the isotopic composition of the samples and the ε values obtained at laboratory scale using Eq. 3 (Ellis et al., 2002; Berna et al., 2010; Raddatz et al., 2011; Torrentó et al., 2011; Carrey et al., 2013).

$$(\%) = \left[1 - e^{((\delta residual - \delta initial)/\varepsilon)}\right] \times 100 \quad (3)$$

4. Results and discussion

The chemical and isotopic data of the samples obtained from the laboratory batch experiments and the samples collected at field are summarised in Tables 3 and 4, respectively.

4.1. Batch experiments: Cr(VI) and NO_3^- reduction by organic matter

In the blank experiments uniquely containing sediment and DIW, 0.01 mM NO_3^- was detected, NO_2^- was below 0.006 mM, NH_4^+ below 0.03 mM and NPDOC reached up to 0.87 mM. These results suggest a possible lixiviation of N compounds and organic C from the sediment. However, since the NO_3^- concentration in groundwater was much higher (4.2 mM), the amount of lixiviated N was considered negligible. Control experiments without ethanol (CtrlCrN) showed no significant variation in the Cr(VI) and NO_3^- concentrations when incubated (38 to 263 h) with groundwater and sediment collected at the study site (Table 3). The NO_2^- and NH_4^+ concentration in these microcosms were below 0.005 mM, while NPDOC reached up to 0.33 mM. Therefore, despite NPDOC lixiviated from the sediment, it was not able to trigger neither NO_3^- nor Cr(VI) attenuation.

In the BioCr experiment, the initial Cr(VI) content of 0.19 mM started to decrease after approximately 50 h from the beginning of the experiment and was completely reduced during approximately 130 h (Fig. 2A). The $\delta^{53}Cr$ increased from +0.05‰ to +3.4‰. This increase coincides with the decrease in Cr(VI) concentration, which would indicate that Cr reduction was occurring (Table 3). In the BioN experiment, NO_3^- started to decrease after approximately 18 h from the beginning of the experiment and was completely eliminated within 31 h (Fig. 2B). After the onset of NO_3^- attenuation, NO_2^- started to accumulate reaching 1.7 mM at 28 h and then decreased until being completely reduced in approximately 40 h. Transient NO_2^- accumulation is commonly observed in denitrification experiments and is usually influenced by the initial growth of denitrifying bacteria and the induction of the nitrite reductase (Betlach and Tiedje, 1981; Carrey et al., 2013; Margalef-Martí et al., 2019b). The measured NH_4^+ concentration was below 0.02 mM. The amount of NH_4^+ detected could be derived from the sediment leaching and allowed to discard other reactions such as the dissimilatory NO_3^- reduction to NH_4^+ (DNRA) as responsible for NO_3^- reduction. The $\delta^{15}N_{NO3}$ increased from +11.2‰ to +56.5‰ and $\delta^{18}O_{NO3}$ from +7.1‰ to +65.7‰ as NO_3^- concentration decreased (Table 3). The enrichment in the heavy isotopes in the remaining substrate, both in the case of Cr(VI) and NO_3^- attenuation mediated by the ethanol addition, is consistent with bacterial heterotrophic activity.

In the BioCrN experiment, the initial content of Cr(VI) (0.2 mM) started to decrease after approximately 48 h from the beginning of the experiment and was completely reduced in approximately 130 h (Fig. 2A). In combination with the Cr(VI) reduction, the $\delta^{53}Cr$ of the remaining substrate increased from +0.05‰ to +3.3‰ (Table 3). Simultaneously, the initial NO_3^- content started to decrease after approximately 48 h from the beginning of the experiment and was completely eliminated in <100 h (Fig. 2B). After the onset of NO_3^- attenuation, NO_2^- started to accumulate reaching 2.0 mM at about 70 h and then decreased until being completely reduced in approximately 120 h. The measured NH_4^+ concentration was below 0.01 mM. As in the case of the BioN experiment, NH_4^+ observed could be derived from the sediment leaching and allowed to discard other NO_3^- reducing reactions such as DNRA. Under these conditions, the $\delta^{15}N_{NO3}$ increased from +11.2‰ to +64.8‰ and $\delta^{18}O_{NO3}$ from +7.1‰ to +72.2‰ (Table 3). The enrichment in the heavy isotopes of the remaining Cr(VI) and NO_3^- during its concomitant reduction by ethanol is again consistent with the bacterial heterotrophic activity.

The comparison of the BioCr and BioN experiments with the BioCrN experiments shows that while Cr(VI) reduction rate was not affected by denitrification, NO_3^- attenuation was slower in the presence of Cr(VI). Compared to the BioN experiments, in the BioCrN experiments the NO_3^- concentration decrease started 30 h later (48 h instead of 18) and the reduction of both NO_3^- and NO_2^- was completed 80 h later (120 h instead of 40). Therefore, the presence of Cr(VI) slowed down denitrification, but did not completely inhibit it. The most likely explanation is that the presence of Cr(VI) promotes a certain toxicity to the denitrifying bacterial species stimulated from the groundwater and sediment collected at the study site, while NO_3^- seems to have no effect on the stimulated Cr(VI) reducing species. The inhibition of NO_3^- reduction by Cr(VI) was previously observed by Kourtev et al. (2009). These authors found a decrease in NO_3^- reduction coupled with an increase of Cr(VI) content when using lactate as organic C source. The authors also observed a decreased bacterial growth yield when increasing the Cr(VI) concentration. These results suggest that Cr(VI) toxicity to NO_3^- reducing microorganisms might be dependent on its concentration, the specific species involved, and the electron donors employed.

4.2. Batch experiments: isotopic fractionation

Batch experiments were performed to determine the $\varepsilon^{53}Cr$, $\varepsilon^{15}N_{NO3}$ and $\varepsilon^{18}O_{NO3}$ under the three different conditions tested (BioCr, BioN and BioCrN). The calculations are shown in Fig. 3

Table 3
Chemical and isotopic data of the samples extracted in the batch experiments (n.d. = not determined, <LD = below the detection limit).

Experiment	Time	NPDOC	Cr(VI)	NH_4^+	NO_2^-	NO_3^-	$\delta^{53}Cr$	$\delta^{15}N\text{-}NO_3^-$	$\delta^{18}O\text{-}NO_3^-$
	(Hours)	(mM)	(mM)	(mM)	(mM)	(mM)	(‰)	(‰)	(‰)
BioCr	0	8.4	0.19	n.d	n.d.	n.d.	n.d	n.d.	n.d.
	71	24.5	0.106	n.d.	n.d.	n.d.	+0.5	n.d.	n.d.
	73	7.9	0.177	n.d.	n.d.	n.d.	+0.4	n.d.	n.d.
	96	21.1	0.067	n.d.	n.d.	n.d.	+1.3	n.d.	n.d.
	103	20.7	0.001	n.d.	n.d.	n.d.	+2.8	n.d.	n.d.
	103	20.1	0.058	n.d.	n.d.	n.d.	+1.5	n.d.	n.d.
	120	17.2	0.018	n.d.	n.d.	n.d.	n.d.	n.d.	n.d.
	120	14.1	0.004	n.d.	n.d.	n.d.	+2.5	n.d.	n.d.
	122	13.0	0.003	n.d.	n.d.	n.d.	+3.4	n.d.	n.d.
	122	12.6	0.014	n.d.	n.d.	n.d.	+2.5	n.d.	n.d.
	126	18.6	0.003	n.d.	n.d.	n.d.	+2.7	n.d.	n.d.
	126	21.4	0.003	n.d.	n.d.	n.d.	+2.6	n.d.	n.d.
BioN	0	11.8	n.d.	<LD	<LD	4.2	n.d.	+11.2	+7.1
	18	9.0	n.d.	<LD	0.2	3.8	n.d.	+21.3	+15.1
	19	8.9	n.d.	<LD	0.3	3.7	n.d.	+20.6	+14.2
	20	9.1	n.d.	<LD	0.4	3.4	n.d.	+29.4	+24.5
	22	8.5	n.d.	<LD	1	2.7	n.d.	+32.2	+30.8
	24	7.5	n.d.	<LD	1.6	1.9	n.d.	+46.0	+42.4
	26	6.9	n.d.	<LD	1.4	1	n.d.	+58.3	+56.3
	28	7.2	n.d.	<LD	1.7	0.9	n.d.	+56.5	+65.7
	31	5.8	n.d.	<LD	1.1	<LD	n.d.	n.d.	n.d.
	36	4.0	n.d.	<LD	0.1	<LD	n.d.	n.d.	n.d.
	39	6.8	n.d.	<LD	0	<LD	n.d.	n.d.	n.d.
	40	3.4	n.d.	<LD	0.1	<LD	n.d.	n.d.	n.d.
BioCrN	0	11.8	0.192	<LD	<LD	4.2	n.d.	+11.2	+7.1
	18	8.9	0.205	<LD	<LD	4.1	n.d.	n.d.	n.d.
	19	9.8	0.2	<LD	<LD	4.2	+0.1	n.d.	n.d.
	20	8.8	0.208	<LD	0.1	3.9	n.d.	n.d.	n.d.
	22	8.9	0.209	<LD	0.1	4	n.d.	9.9	6.9
	26	9.3	0.203	<LD	<LD	4	n.d.	n.d.	n.d.
	31	9.3	0.2	<LD	0.1	3.9	n.d.	n.d.	n.d.
	39	9.2	0.188	<LD	0.05	3.8	n.d.	n.d.	n.d.
	46	8.5	0.192	<LD	0.1	3.8	+0.1	n.d.	n.d.
	52	5.4	0.165	<LD	0.8	3.2	+0.2	n.d.	n.d.
	56	6.3	0.190	<LD	0.4	3.7	n.d.	+18.2	+13.7
	60	7.2	0.200	<LD	1	2.8	n.d.	+33.6	+28.5
	62	6.6	0.049	<LD	1.3	1.1	+2.6	+29.0	+28.1
	64	5.8	0.2	<LD	0.6	1.7	n.d.	+36.7	+34.2
	68	5.2	0.061	<LD	1.1	0.4	+2.2	+77.4	+63.7
	71	5.7	0.043	<LD	1.1	0.4	+3.3	n.d.	n.d.
	71	7.1	0.110	<LD	2	0	+1.1	n.d.	n.d.
	80	7.5	n.d.	<LD	1.9	0.5	n.d.	+64.8	+72.2
	96	5.6	0.029	<LD	<LD	0	+3.3	n.d.	n.d.
	103	0	0.002	<LD	<LD	0	n.d.	n.d.	n.d.
	108	6.8	0	<LD	0.9	0	+3.2	n.d.	n.d.
	120	6.8	0.033	<LD	0	0	n.d.	n.d.	n.d.
	132	6.5	0.0004	<LD	0	0	n.d.	n.d.	n.d.
CtrlCrN-0	38	n.d.	n.d.	n.d.	0	4.2	n.d.	n.d.	n.d.
CtrlCrN-1	71	0.3	0.2	0	0	4.6	0	n.d.	n.d.
CtrlCrN-2	263	0.3	n.d.	0	0	4.5	n.d.	n.d.	n.d.
Blank-0	38	0.9	n.d.	0	0	0	n.d.	n.d.	n.d.
Blank-1	38	0.5	n.d.	0	0	0	n.d.	n.d.	n.d.
Blank-2	71	n.d.	n.d.	0	0	0	n.d.	n.d.	n.d.

Table 4
Chemical and isotopic data from groundwater samples taken from the San Ignacio neighbourhood (n.d. = not determined, <LD = below the detection limit).

Sample	Well depth	Aquifer	pH	OD	EC	DOC	Ca^{2+}	Mg^{2+}	K^+	Na^+	NH_4^+	SO_4^{2-}	Cl^-	NO_2^-	NO_3^-	Cr(VI)	$\delta^{53}Cr$	$\delta^{15}N\text{-}NO_3^-$	$\delta^{18}O\text{-}NO_3^-$
N°	(m)			(mM)	(μm s/cm)	(mM)	(mM)	(mM)	(mM)	(mM)	(mM)	(mM)	(mM)	(mM)	(mM)	(mM)	(‰)	(‰)	(‰)
P13	20	Upper	7.1	0.14	1386	0.08	1.0	1.3	0.4	9.5	0.002	0.4	3.1	<0.002	3.9	1.9E−05	<LD	+10.6	+6.1
P14	15	Upper	7.9	n.d.	2000	0.14	1.1	2.1	0.6	15.7	0.001	0.9	6.5	<0.002	1.0	1.9E−05	<LD	+16.8	+6.9
P21	15	Upper	7.9	n.d.	1727	0.14	1.0	1.7	0.4	12.0	0.003	1.1	5.0	<0.002	0.5	0.003	+2.9	+21.1	+11.9
P22	15	Upper	8.0	n.d.	1085	0.17	0.8	1.3	0.4	13.0	0.002	0.9	3.5	<0.002	2.1	0.001	+2.9	+17.6	+8.3
P26	15	Upper	8.1	n.d.	1755	0.08	1.0	1.5	0.5	13.2	0.002	0.4	2.8	<0.002	1.5	1.9E−05	<LD	+17.9	+7.9
P27	15	Upper	8.0	n.d.	992	0.12	1.1	1.3	0.4	5.2	0.013	0.4	2.6	<0.002	1.3	1.9E−05	<LD	+17.0	+9.1
P28	40	Puelche	7.3	0.22	1803	0.07	0.5	0.6	0.2	6.2	0.004	0.9	5.3	<0.002	0.8	0.022	+3.0	+18.6	+9.4
P29	15	Upper	6.9	0.02	1696	0.20	1.1	0.9	0.3	4.7	0.004	0.3	1.6	<0.002	0.8	0.0004	+3.4	+22.8	+12.7
P31	15	Upper	n.d.	n.d.	n.d.	0.08	1.0	0.9	0.3	8.7	0.004	0.9	4.2	<0.002	1.7	0.005	+3.2	+17.7	+8.5
P33	15	Upper	7.9	n.d.	2060	0.07	2.7	2.5	0.4	11.3	0.004	4.4	1.7	<0.002	0.6	0.003	+2.9	+15.5	+8.7
P34	15	Upper	n.d.	n.d.	1424	0.12	1.1	1.1	0.3	8.7	0.004	0.2	1.8	<0.002	0.8	0.041	+1.2	+21.6	+11.4

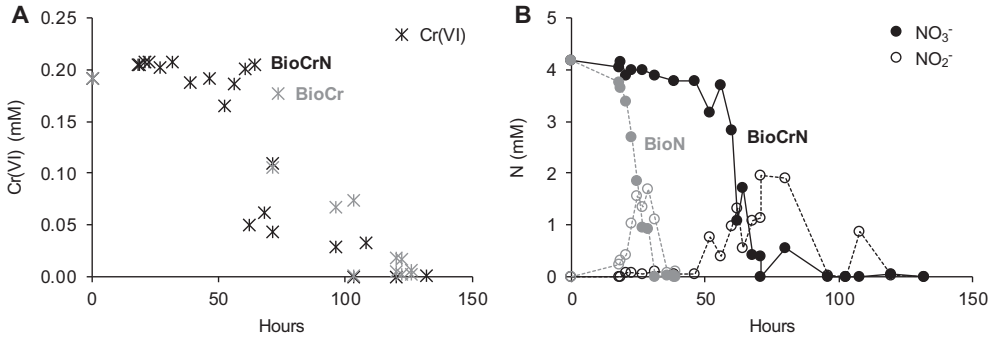

Fig. 2. Cr(VI) and NO_3^- concentration evolution during the laboratory experiments. A) Cr(VI) reduction by ethanol in the presence (black) and absence (grey) of NO_3^- and B) NO_3^- reduction by ethanol in the presence (black) and absence (grey) of Cr(VI).

and a summary of the obtained values including the $\varepsilon^{15}N/\varepsilon^{18}O$ calculation is presented in Table 5.

In both the BioCr and BioCrN experiments (Fig. 3A and B, respectively), two different slopes were observed, and consequently two $\varepsilon^{53}Cr$ values were calculated. During the Cr(VI) reduction in the absence of NO_3^- (BioCr), the first stage is defined by the samples with a higher Cr(VI) content (0.21 to 0.07 mM) and shows a $\varepsilon^{53}Cr$ of −1.4‰ ($r^2 = 0.90$), while the second stage applies to samples with lower Cr(VI) concentrations (0.05 to 0.002 mM) and reveals a $\varepsilon^{53}Cr$ of −0.2‰ ($r^2 = 0.45$). During the Cr(VI) reduction in the presence of denitrification (BioCrN), a similar pattern is observed. The first stage is defined by the samples with a higher Cr(VI) content (0.21 to 0.06 mM) and implies a $\varepsilon^{53}Cr$ of −1.8‰ ($r^2 = 0.99$), while the second stage applies to samples with lower Cr(VI) concentrations (0.05 to 0.03 mM) and reveals a $\varepsilon^{53}Cr$ of −0.9‰ ($r^2 = 0.44$). Likewise, Chen et al. (2019) assessed the $\varepsilon^{53}Cr$ during the Cr(VI) reduction under various conditions (temperatures from 18 to 34 °C and pH from 6.0 to 7.2, presence and absence of nitrate) and also found two-stage trends. These authors, upon the tested conditions, obtained a $\varepsilon^{53}Cr$ during the first stage ranging from −2.6‰ to −2.8‰, while in the second stage the values were between −1.0‰ and −1.1‰. Hence, a lower isotope fractionation (in absolute ε values) was found for the second stage, when Cr(VI) concentrations were lower, and yielded values similar to the isotope fractionation obtained in the present BioCr and BioCrN experiments. Furthermore, these authors, suggested that the decreased Cr(VI) bioavailability when the reduction progresses could mask the isotopic fractionation. However, in other biotic Cr (VI) reduction experiments, such two-stage trends were not observed (Basu et al., 2014; Sikora et al., 2008). If indeed, the Cr (VI) isotope fractionation occurs in two stages, the use of a $\varepsilon^{53}Cr$ for a single stage to estimate the Cr(VI) reduction at field-scale, could underestimate or overestimate the extent of the reaction. Therefore, two-stage pattern could have implications when using $\varepsilon^{53}Cr$ values calculated from laboratory experiments to quantify the natural or induced Cr(VI) reduction, since different $\varepsilon^{53}Cr$ values should be used depending on Cr(VI) concentration.

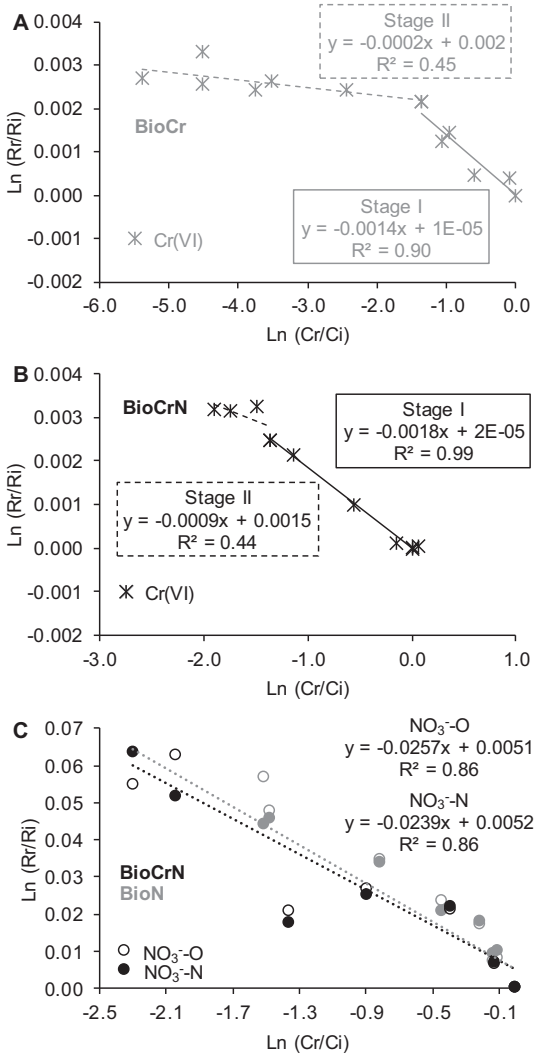

Fig. 3. Cr(VI) and NO_3^- isotopic fractionation during the batch experiments. A) $\varepsilon^{53}Cr$ calculated for the BioCr experiments, B) $\varepsilon^{53}Cr$ calculated for the BioCrN experiments and C) $\varepsilon^{15}N_{NO3}$ (full circles) and $\varepsilon^{18}O_{NO3}$ (empty circles) calculated for the BioN (grey) and BioCrN (black) experiments.

In the present study, when Cr(VI) was concomitantly reduced with NO_3^- (BioCrN), a slightly higher $\varepsilon^{53}Cr$ (absolute value) was obtained compared to the BioCr batch (Cr(VI) reduced in the absence of NO_3^-), although the reduction rate was similar. However, these results differ from those reported by Han et al. (2012). These authors found a lower $\varepsilon^{53}Cr$ value (−0.4‰) under denitrifying conditions compared to the value obtained in the absence of NO_3^- (−2‰). On the other hand, Chen et al. (2019) obtained similar $\varepsilon^{53}Cr$ values with presence (−2.4‰ and −0.9‰) and absence (−2.7‰ and −1.1‰) of NO_3^-. Therefore, it is clear that the presence of NO_3^- has an influence on the Cr(VI) isotope fractionation, and when calculating Cr(VI) reduction rates from field-based data, the $\varepsilon^{53}Cr$ values employed should take into account the presence or absence of NO_3^-.

As to the biotic Cr(VI) reduction in absence of NO_3^-, Basu et al. (2014) reported $\varepsilon^{53}Cr$ in a range of −2.2‰ a −3.1‰ for pure culture experiments using different bacterial species and Sikora et al.

Table 5
Calculated ε for the tested conditions at the laboratory. ε values obtained for the Cr(VI) and NO_3^- reduction by ethanol under different conditions (n.d.=not determined)

Series	Composition	$\varepsilon^{53}Cr$ (‰)	$\varepsilon^{15}N_{NO3}$ (‰)	$\varepsilon^{18}O_{NO3}$ (‰)	$\varepsilon^{15}N/\varepsilon^{18}O$
BioCr	Groundwater + sediment + Cr(VI) + ethanol	−1.4 (stage I) −0.2 (stage II)	n.d.	n.d.	n.d.
BioN	Groundwater (NO_3^-) + sediment + ethanol	n.d.	−23.9	−25.7	0.9
BioCrN	Groundwater (NO_3^-) + sediment + Cr(VI) + ethanol	−1.8 (stage I) −0.9 (stage II)	−23.9	−25.7	0.9

(2008) found a $\varepsilon^{53}Cr$ of −1.8‰ when testing 10 mM lactate and between −4.1 and −4.5‰ when testing lactate below 100 μM for the reduction. These results suggest that the microbial species and electron donor concentration involved in the Cr(VI) reduction could have an influence on the resulting isotope fractionation. For the abiotic Cr(VI) reduction, Ellis et al. (2002) found a $\varepsilon^{53}Cr = -3.5$‰ when using magnetite as the electron donor and Kitchen et al. (2012) and Døssing et al. (2011) found $\varepsilon^{53}Cr$ in a range of −2.9‰ and −4.9‰ when using Fe(II) or organic acids at different pH. These results suggest that no significant isotopic fractionation differences are found between biotic and abiotic Cr(VI) reactions.

The $\varepsilon^{15}N_{NO3}$ and $\varepsilon^{18}O_{NO3}$ values for the BioN and BioCrN experiments were calculated together. Despite the BioN experiment showing a higher NO_3^- reduction rate, a similar slope with a good correlation is obtained for both experiments (Fig. 3C). The $\varepsilon^{15}N_{NO3}$ and $\varepsilon^{18}O_{NO3}$ values are −23.9‰ and −25.7‰, respectively (Fig. 3C). These values and the resulting $\varepsilon^{15}N/\varepsilon^{18}O$ (0.9) are within the data range reported in the literature for denitrifying processes (Granger et al., 2008; Knöller et al., 2011; Grau-Martínez et al., 2017 and references therein). The obtained $\varepsilon^{15}N_{NO3}$ and $\varepsilon^{18}O_{NO3}$ values in the present experiments can be employed to quantify the natural attenuation of NO_3^- at the study site.

4.3. Natural attenuation of Cr(VI) and NO_3^- in the study area

Hydrochemical data for the 11 groundwater samples collected in the San Ignacio neighbourhood show pH values between 7.1 and 8.1, and electric conductivity (EC) varied from 992 μS/cm to 2060 μS/cm (Table 4). The Cr(VI) concentrations range from below detection limit to 0.041 mM, next and downstream of the chemical industry plant. The NO_3^- was detected in all samples from the studied area and concentrations vary between 0.5 mM and 3.9 mM, with an average of 1.4 mM. Likewise, the NPDOC varies between 0.08 mM and 0.2 mM. The presence of both contaminants in the deeper aquifer is linked to the hydraulic conductivity of the aquitard, because it controls the hydraulic connectivity between the Upper and the Puelche Aquifer.

The $\delta^{53}Cr$ in groundwater varies between +1.2‰ and +3.4‰, with an average value of +2.8‰. The spatial distribution of the $\delta^{53}Cr$ values indicates a downstream increase along the axis of the plume, following the groundwater flow line (Fig. 4). Near the source of Cr(VI), the $\delta^{53}Cr$ value is +1.2‰ and values increase to +3.4‰ 200 m downstream. The observed increase in $\delta^{53}Cr$ values downstream from the Cr(VI) source suggests that Cr(VI) attenuation is occurring due to biotic reduction.

The isotope values of dissolved nitrate indicate the occurrence of NO_3^- reduction, evidenced by an enrichment in the heavy isotopes that ranged from +10.6‰ to +22.8‰ for the $\delta^{15}N$ and from +6.1‰ to +12.7‰ for the $\delta^{18}O$ (Table 4). A positive linear correlation between $\delta^{15}N_{NO3}$ and $\delta^{18}O_{NO3}$ with a slope of 0.51 ($r^2 = 0.79$) is exhibited by the analysed samples (Fig. 6). These results are in the range of values reported in the literature for denitrification processes in groundwater (Aravena and Robertson, 1998; Kendall et al., 2007). In the samples obtained from the monitoring wells, dissolved O_2 concentrations vary between 0.02 and 0.2 mM, which would indicate inadequate conditions for denitrification according to the required O_2 concentration below 0.1 mM reported by Cey et al. (1999). However, denitrification has also been found at higher dissolved O_2 concentrations (Otero et al., 2009). On the other hand, the samples collected at the study site with higher $\delta^{53}Cr$ also are characterized by higher values of $\delta^{15}N_{NO3}$ and $\delta^{18}O_{NO3}$. For example, sample P29 yielded a $\delta^{53}Cr$ of +3.4‰, $\delta^{15}N_{NO3}$ of +22.8‰ and $\delta^{18}O_{NO3}$ of +12.7‰, which are the highest measured isotope values for these compounds (see also samples P31, P21 and P22 in Table 4). Therefore, we confirmed that Cr(VI) reduction can occur simultaneously with denitrifying processes. Furthermore, since the NO_3^- isotope composition of the samples collected in the field are within the defined range for wastewater NO_3^- (Fig. 6), we also identify that the source of NO_3^- is potentially related with septic systems leakage. On the other hand, septic systems leakage could be a source of NPDOC in groundwater and therefore, denitrification and Cr(VI) reduction could be related to the oxidation of organic matter.

4.4. Estimation of Cr(VI) and NO_3^- reduction percentage in contaminated groundwater

In the calculation of the percentage of Cr(VI) attenuation, we used the sample P34 as representative for the initial value of Cr (VI) concentration and isotope composition (Table 4), because it is the sample with the highest Cr(VI) content and because the well is located very close to the source of contamination. The $\varepsilon^{53}Cr$ values we used are those calculated in the BioCrN experiments (stage

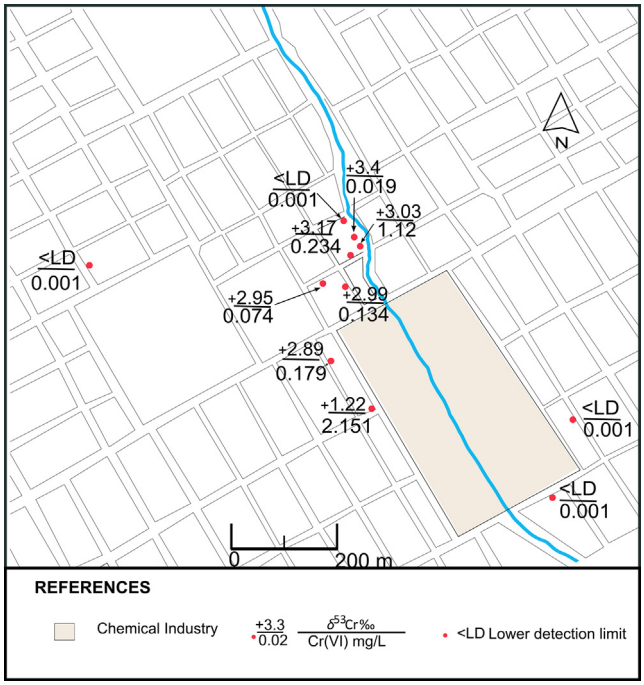

Fig. 4. Spatial distribution of $\delta^{53}Cr$ and Cr(VI) in San Ignacio neighbourhood.

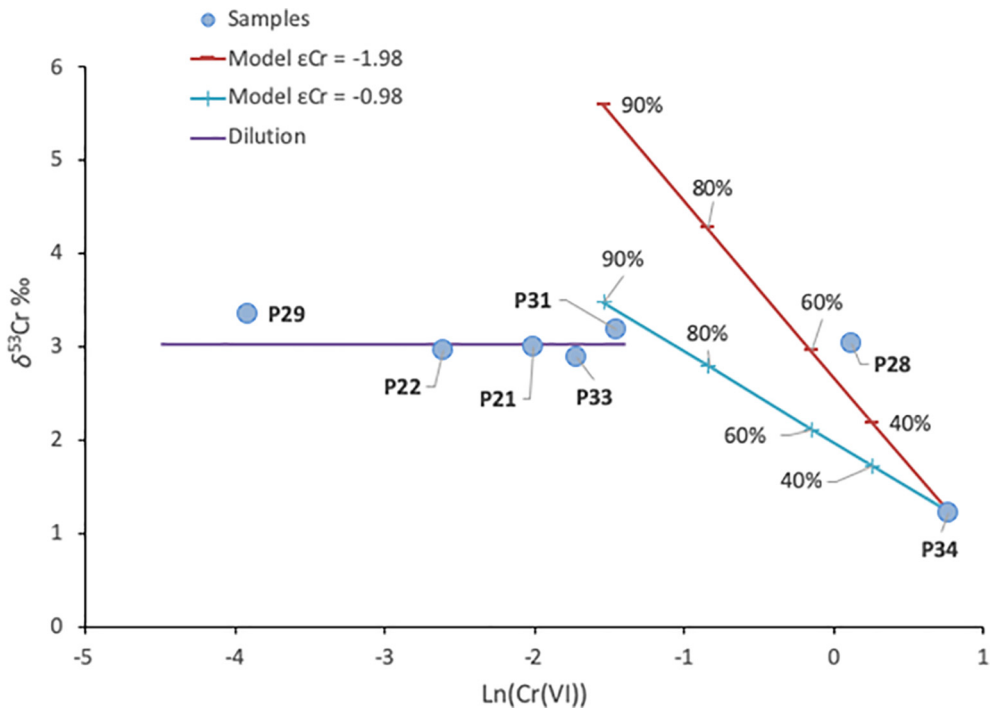

Fig. 5. Values of ε^{53}Cr vs. Ln Cr(VI). The red line represents a Rayleigh model calculated with stage I ε^{53}Cr and the blue line represents a Rayleigh model calculated with stage II ε^{53}Cr, obtained from BioCrN experiment. The purple line represents dilution with unpolluted groundwater. (For interpretation of the references to colour in this figure legend, the reader is referred to the web version of this article.)

$I = -1.8‰$ and stage II = $-0.98‰$), since we observed the simultaneous Cr(VI) and NO_3^- reduction at field. Calculated Cr(VI) attenuation percentages in groundwater samples by using the ε^{53}Cr from stage I vary between 60% and 70%, but when using the ε^{53}Cr value from stage II, the attenuation of Cr(VI) is calculated at much higher percentages (80% and 90%). Using the ε^{53}Cr values from stage I, in sample P33, extracted from the well located closest to the source (see Fig. 1), we calculate that ~60% of the original Cr (VI) was eliminated by reduction. In samples P21 and P22, located in the central part of the plume axis, these values are 63% and 62%, respectively. For samples P28, P29 and P31, located in the distal part of the plume, the reduction percentage is 64%, 69% and 66%, respectively. On the other hand, applying the ε^{53}Cr value from stage II, for sample P33, the Cr(VI) attenuation is 84%. For samples P21 and P22 the attenuation is 86% and 85%, respectively, and values for samples P28, P29 and P31 imply an attenuation percentage of 87%, 91% and 89%, respectively. Fig. 5 shows the δ^{53}Cr vs the Ln (Cr(VI)) of the studied samples together with two Cr reduction models calculated applying the Rayleigh equation. Sample P28, located downstream of the source, and with high Cr (V) concentration is located in the theoretical denitrification line obtained from applying stage I. However, sample P31 with a lower Cr (VI) concentration is located in the theoretical line obtained by applying the slope II model, showing a higher percentage of degradation. On the other hand, samples P33, P21, P22 and P29 have much lower Cr (VI) concentrations but similar isotopic composition. These samples are located in the theoretical line of dilution, starting from a sample with δ^{53}Cr and Cr (VI) concentration similar to P28 or P31, suggesting that the attenuation of Cr (VI) in these samples would be partially linked to a process of mixing with uncontaminated groundwater and not only to reduction of Cr(VI) to Cr(III).

With regards to NO_3^- attenuation, the sample with the highest NO_3^- content is assumed as initial value (P13) and ε values calculated from the BioN and BioCrN experiments ($-24.1‰$ for ε^{15}N and $-24.3‰$ for ε^{18}O) were selected. The lower slope between δ^{18}O-NO_3^- and δ^{15}N-NO_3^- obtained for the field samples (0.5 ($r^2 = 0.82$)) with respect to the batch experiments (1.0 ($r^2 = 0.95$)) (Fig. 6) agrees with reported slopes of nearly 0.5 for field scale studies and nearly 1.0 for laboratory studies (Carrey et al., 2013; Critchley et al., 2014; Otero et al., 2009; Wunderlich et al., 2012). The main reason that could cause this flatter slope in field-based data sets, is the oxidation of the intermediates NO_2^- and/or NH_4^+ to NO_3^- (Granger and Wankel, 2016; Wunderlich et al., 2013; Margalef-Marti et al., 2019a). According to the denitrification percentage line drawn from the laboratory results, most of the samples collected in the field imply an approximate NO_3^- attenuation of 20%, while three samples (P21, P34 and P29) yield a higher attenuation (approximately 30%) (Fig. 6). Overall, denitrification is taking place in the basin, but it cannot remove NO_3^- completely from groundwater. It should be noted that, according to the ε values calculated in laboratory experiments, for the studied groundwater samples, the natural attenuation of Cr(VI) is considerably larger than the natural attenuation of NO_3^-. These high percentages

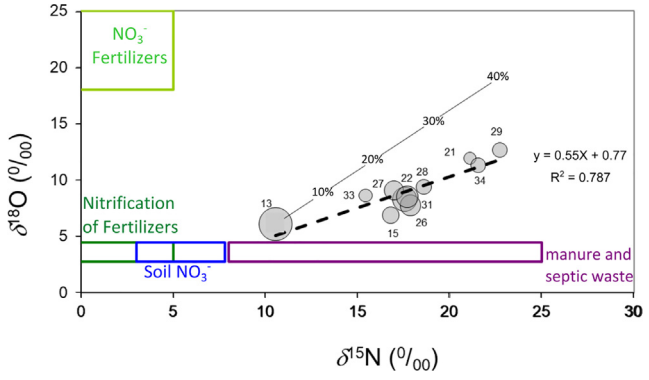

Fig. 6. Estimated percentage of denitrification in the study site, quantified by using the Rayleigh equation and the ε values obtained in the BioCrN experiments. The boxes of the nitrate sources are from Vitòria et al. (2004, and references therein). The solid line represents the model used to calculate the denitrification percentage, and the dotted line is the linear regression of the field samples.

of attenuation could explain the low concentrations of NPDOC detected in the groundwater samples at the study site.

The results obtained in the present study can be useful for future studies aiming to evaluate the Cr(VI) and NO_3^- degradation by using isotope tools in contaminated groundwater with these two compounds. Previous studies applied isotopes to evaluate the natural or induced attenuation of Cr(VI) (Novak et al., 2017; Economou-Eliopoulos et al., 2014; Heikoop et al., 20,104; Berna et al., 2010) and NO_3^- (Critchley et al., 2014; Margalef-Marti et al., 2019a; Otero et al., 2009; Vidal-Gavilan et al., 2013) at field. However, to the best of our knowledge no studies have reported an estimation of the percentage of degradation Cr(VI) and NO_3^- when found simultaneously in contaminated aquifers and none of the aforementioned studies considered the two-stage isotopic fractionation of Cr(VI). To avoid over or underestimation of the percentage of degradation of the two contaminants at field, this two stages Cr(VI) isotopic fractionation and the NO_3^- reduction rate decreases in the presence of Cr(VI) must be considered when designing laboratory experiments to calculate ε values. Furthermore, hydrogeological and biochemical effects such as mixing of water from different sources or NO_2^- reoxidation to NO_3^-, among many others, have to be taken into account to interpret field-scale results. Due to these effects, the percentages obtained from isotope data must be considered estimation, not a precise calculation (Margalef-Marti et al., 2019a).

5. Conclusions

The isotope analyses of Cr(VI) and NO_3^- allowed to evaluate the contribution of the natural attenuation processes in the evolution of these pollutants' concentrations in the groundwater at the studied site of the MRB. The results of our laboratory experiments evidence a concomitant Cr(VI) reduction with denitrification. The Cr (VI) reduction rate is not affected by the presence of NO_3^-, but NO_3^- attenuation is slower in the presence of Cr(VI). The ε^{53}Cr produced by the reduction of Cr(VI) to Cr(III) follows a two stage trend. A higher isotope fractionation (−1.4‰ and −1.8‰ in absence/presence of NO_3^- respectively) was found for the first stage compared to the second stage (−0.2‰ and −0.9‰ in absence/presence of NO_3^- respectively). The presence of NO_3^- did not affect notably the ε^{53}Cr, although the reduction rate was different. On the other hand, we obtained equal $\varepsilon^{15}N_{NO3}$ and $\varepsilon^{18}O_{NO3}$ values (−23.9‰ and −25.7‰, respectively) for the experiments with or without Cr(VI).

In a site of MRB, the δ^{53}Cr values of the studied samples increase downstream of the Cr(VI) source following a flow line, suggesting that isotope fractionation occurs along the plume. Using the ε^{53}Cr obtained at the laboratory, the calculated Cr(VI) attenuation at the study site varies between 60 and 70%, or between 85 and 90% when ε^{53}Cr from stage I or II are respectively applied. Besides, the isotope results allowed identifying dilution in those samples with lower Cr concentration. On the other hand, the percentage of NO_3^- attenuation in groundwater samples varies between approximately 20% and 30%. Hence, although Cr(VI) and NO_3^- are reduced concomitantly from the groundwater of the San Ignacio neighbourhood, the natural attenuation of Cr(VI) is considerably larger than that of NO_3^-.

The isotope methods used have made it possible to determine the degradation of contaminants and confirmed that concentration changes of contaminants are not exclusively due to dilution. Although with some uncertainty, we were able to calculate attenuation percentages of these contaminants in the contaminated basin studied which indicate a rather effective neutralization of otherwise toxic Cr(VI) in the groundwaters. These results provided a basis for planning an efficient management of the contaminated aquifer in the most populated and industrialized basin of Argentina.

Declaration of Competing Interest

The authors declare that they have no known competing financial interests or personal relationships that could have appeared to influence the work reported in this paper.

Acknowledgements

This research was supported by the Instituto de Hidrología de Llanura "Dr. Eduardo J. Usunoff" (IHLLA) and by IDAEA-CSIC as part of the programme EMHE "Enhancing Mobility between Latin-American and Caribbean countries and Europe". We thank the IHLLA technic staff for their assistance in water sampling and Ms. M. F. Altolaguirre, B.S., and Ms. O. Floriani, B.S., for assisting in the logistics of manipulation and conservation of samples. This research is also supported by the project PACE-ISOTEC (CGL2017-87216-C4-1-R), financed by the Spanish Government and AEI/FEDER from the UE, and the project MAG (2017 SGR 1733) from the Catalan Government. We also thank the Centres Científics i Tecnològics of the Universitat de Barcelona for its analytical support.

References

Aravena, R., Robertson, W.D., 1998. Use of multiple isotope tracers to evaluate denitrification in ground water: study of nitrate from a large flux septic system plume. Ground Water 36, 975–982.
Aravena, R., Evans, M.L., Cherry, J.A., 1993. Stable isotopes of oxygen and nitrogen in source identification of nitrate from septic systems. Groundwater 31 (2), 180–186.
Basu, A., Johnson, T.M., Sanford, R.A., 2014. Cr isotope fractionation factors for Cr (VI) reduction by a metabolically diverse group of bacteria. Geochim. Cosmochim. Acta 142, 349–361.
Berna, E.C., Johnson, T.M., Makdisi, R.S., Basu, A., 2010. Cr stable isotopes as indicators of Cr (VI) reduction in groundwater: a detailed time-series study of a point-source plume. Environ. Sci. Technol. 44 (3), 1043–1048.
Betlach, M.R., Tiedje, J.M., 1981. Kinetic explanation for accumulation of nitrite, nitric oxide, and nitrous oxide during bacterial denitrification. Appl. Environ. Microbiol. 42, 1074–1084. https://doi.org/Article.
Blowes, D., 2002. Tracking hexavalent Cr in groundwater. Science 295, 2024–2025.
Blowes, D.W., Ptacek, C.J., Benner, S.G., McRae, C.W., Bennett, T.A., Puls, R.W., 2000. Treatment of inorganic contaminants using permeable reactive barriers. J. Contam. Hydrol. 45 (1-2), 123–137.
Bonnand, P., Parkinson, I.J., James, R.H., Karjalainen, A.-M., Fehr, M.A., 2011. Accurate and precise determination of stable Cr isotope compositions in carbonates by double spike MC-ICP-MS. J. Anal. At. Spectrom. 26, 528. https://doi.org/10.1039/c0ja00167h.
Carrey, R., Otero, N., Soler, A., Gómez-Alday, J.J., Ayora, C., 2013. The role of lower Cretaceous sediments in groundwater nitrate attenuation in central Spain: column experiments. Appl. Geochem. 32, 142–152.
Ceballos, E., Bea, S.A., Sanci, R., 2018. Applying reactive transport modeling in a chromium contaminated site in the Matanza-Riachuelo Basin, Buenos Aires, Argentina. Int. J. Environ. Health 9 (1).
Cey, E.E., Rudolph, D.L., Aravena, R., Parkin, G., 1999. Role of the riparian zone in controlling the distribution and fate of agricultural nitrogen near a small stream in southern Ontario. J. Contam. Hydrol. 37 (1-2), 45–67.
Chen, G., Han, J., Mu, Y., Yu, H., Qin, L., 2019. Two-stage chromium isotope fractionation during microbial Cr (VI) reduction. Water Res. 148, 10–18.
Coplen, T.B., 2011. Guidelines and recommended terms for expression of stable-isotope-ratio and gas-ratio measurement results. Rapid Commun. Mass Spectrom. 25, 2538–2560. https://doi.org/10.1002/rcm.5129.
Critchley, K., Rudolph, D.L., Devlin, J.F., Schillig, P.C., 2014. Stimulating in situ denitrification in an aerobic, highly permeable municipal drinking water aquifer. J. Contam. Hydrol. 171, 66–80.
Davis, A., Olsen, R.L., 1995. The geochemistry of chromium migration and remediation in the subsurface. Groundwater 33 (5), 759–768.
Dichristina, T.J., 1992. Effects of nitrate and nitrite on dissimilatory iron reduction by Shewanella putrefaciens 200. J. Bacteriol. 174 (6), 1891–1896.
Døssing, L.N., Dideriksen, K., Stipp, S.L.S., Frei, R., 2011. Reduction of hexavalent chromium by ferrous iron: a process of chromium isotope fractionation and its relevance to natural environments. Chem. Geol. 285 (1–4), 157–166.
Economou-Eliopoulos, M., Frei, R., Atsarou, C., 2014. Application of chromium stable isotopes to the evaluation of Cr(VI) contamination in groundwater and rock leachates from central Euboea and the Assopos basin (Greece). Catena 122, 216–228.

Ellis, A., Johnson, T., Bullen, T.D., 2002. Chromium isotopes ratios and the fate of Chromium in the environment. Science 295, 2060–2062.
Frei, R., Gaucher, C., Poulton, S.W., Canfield, D.E., 2009. Fluctuations in Precambrian atmospheric oxygenation recorded by chromium isotopes. Nature 461, 250–253.
Fukada, T., Hiscock, K., Dennis, P.F., Grischek, T., 2003. A dual isotope approach to identify denitrification in groundwater at a river-bank infiltration site. Water Res. 37, 3070–3078.
Garbisu, C., Alkorta, I., Llama, M.J., Serra, J.L., 1998. Aerobic chromate reduction by Bacillus subtilis. Biodegradation 9 (2), 133–141.
Granger, J., Wankel, S.D., 2016. Isotopic overprinting of nitrification on denitrification as a ubiquitous and unifying feature of environmental nitrogen cycling. Proc. Natl. Acad. Sci. 113, E6391–E6400. https://doi.org/10.1073/pnas.1601383113.
Granger, J., Sigman, D.M., Lehmann, M.F., Tortell, P.D., 2008. Nitrogen and oxygen isotope fractionation during dissimilatory nitrate reduction by denitrifying bacteria. Limnol. Oceanogr. 53, 2533–2545. https://doi.org/10.4319/lo.2008.53.6.2533.
Grau-Martínez, A., Torrentó, C., Carrey, R., Rodríguez-Escales, P., Domènech, C., Ghiglieri, G., Soler, A., Otero, N., 2017. Feasibility of two low-cost organic substrates for inducing denitrification in artificial recharge ponds: batch and flow-through experiments. J. Contam. Hydrol. 198, 48–58. https://doi.org/10.1016/j.jconhyd.2017.01.001.
Han, R., Geller, J.T., Yang, L., Brodie, E.L., Chakraborty, R., Larsen, J.T., Beller, H.R., 2010. Physiological and transcriptional studies of Cr(VI) reduction under aerobic and denitrifying conditions by an aquifer-derived pseudomonad. Environ. Sci. Technol. 44 (19), 7491–7497.
Han, R., Qin, L., Brown, S.T., Christensen, J.N., Beller, H.R., 2012. Differential isotopic fractionation during Cr(VI) reduction by an aquifer-derived bacterium under aerobic versus denitrifying conditions. Appl. Environ. Microbiol. 78 (7), 2462–2464.
Heikoop, J.M., Johnson, T.M., Birdsell, K.H., Longmire, P., Hickmott, D.D., Jacobs, E.P., Vaniman, D.T., 2014. Isotopic evidence for reduction of anthropogenic hexavalent chromium in Los Alamos National Laboratory groundwater. Chem. Geol. 373, 1–9.
Ishibashi, Y., Cervantes, C., Silver, S., 1990. Chromium reduction in Pseudomonas putida. Appl. Environ. Microbiol. 56 (7), 2268–2270.
Izbicki, J.A., Ball, J.W., Bullen, T.D., Sutley, S.J., 2008. Chromium, chromium isotopes and selected trace elements, western Mojave Desert, USA. Appl. Geochem. 23 (5), 1325–1352.
Jamieson-Hanes, J., Gibson, B., Lindsay, M., Kim, Y., Ptacek, C., Blowes, D., 2012a. Chromium isotope fractionation during reduction of Cr (VI) under saturated flow conditions. Environ. Sci. Technol. 46, 6783–6789.
Jamieson-Hanes, J.H., Amos, R.T., Blowes, D.W., 2012b. Reactive transport modeling of chromium isotope fractionation during Cr(VI) reduction. Environ. Sci. Technol. 46 (24), 13311–13316.
Kendall, C., Elliott, E.M., Wankel, S.D., 2007. Tracing anthropogenic inputs of nitrogen to ecosystems (Chapter 12). In: Michener, R.H., Lajtha, K. (Eds.), Stable Isotopes in Ecology and Environmental Science. second ed. Blackwell Publishing, pp. 375–449.
Kitchen, J.W., Johnson, T.M., Bullen, T.D., Zhu, J., Raddatz, A., 2012. Chromium isotope fractionation factors for reduction of Cr (VI) by aqueous Fe (II) and organic molecules. Geochim. Cosmochim. Acta 89, 190–201.
Knöller, K., Vogt, C., Haupt, M., Feisthauer, S., Richnow, H.H., 2011. Experimental investigation of nitrogen and oxygen isotope fractionation in nitrate and nitrite during denitrification. Biogeochemistry 103, 371–384. https://doi.org/10.1007/s10533-010-9483-9.
Knowles, R., 1982. Denitrification. Microbiol. Rev. 46 (1), 43.
Korom, S.F., 1992. Natural denitrification in the saturated zone: a review. Water Resour. Res. 28 (6), 1657–1668.
Kotas, J., Stasicka, Z., 2000. Chromium occurrence in the environment and methods of its speciation. Environ. Pollut. 107, 263–283.
Kourtev, P.S., Nakatsu, C.H., Konopka, A., 2009. Inhibition of nitrate reduction by chromium(VI) in anaerobic soil microcosms. Appl. Environ. Microbiol. 75, 6249–6257. https://doi.org/10.1128/AEM.00347-09.
Mancino, C., Vives, L., Funes, A., Zarate, M., Martínez, S., 2013. Modelación del flujo subterráneo en la cuenca Matanza-Riachuelo, provincia de Buenos Aires. 1. Geología y geometría del subsuelo. Temas Actuales de la Hidrología Subterránea. Editorial EDULP, La Plata, pp. 85–92.
Margalef-Marti, R., Carrey, R., Viladés, M., Jubany, I., Vilanova, E., Grau, R., Soler, A., Otero, N., 2019a. Use of nitrogen and oxygen isotopes of dissolved nitrate to trace field-scale induced denitrification efficiency throughout an in-situ groundwater remediation strategy. Sci. Total Environ. 686, 709–718.
Margalef-Marti, R., Carrey, R., Soler, A., Otero, N., 2019b. Evaluating the potential use of a dairy industry residue to induce denitrification in polluted water bodies: a flow-through experiment. J. Environ. Manag. 245, 86–94.
Mariotti, A., Landreau, A., Simon, B., 1988. 15N isotope biogeochemistry and natural denitrification process in groundwater: application to the chalk aquifer of northern France. Geochim. Cosmochim. Acta 52, 1869–1878.
Mayer, K.U., Blowes, D.W., Frind, E.O., 2001. Reactive transport modeling of an in situ reactive barrier for the treatment of hexavalent chromium and trichloroethylene in groundwater. Water Resour. Res. 37, 3091–3103.
McIlvin, M.R., Altabet, M.A., 2005. Chemical conversion of nitrate and nitrite to nitrous oxide for nitrogen and oxygen isotopic analysis in freshwater and seawater. Anal. Chem. 77, 5589–5595. https://doi.org/10.1021/ac050528s.
Melián, A.F., 2014. Actualización del modelo numérico de flujo de agua subterránea en la cuenca Matanza-Riachuelo (Buenos Aires, Argentina) (M.Sc thesis) Fundación Centro Internacional de Hidrología Subterránea; Universitat Politècnica de Catalunya. p. 149. Unpublished.
Middleton, S.S., Latmani, R.B., Mackey, M.R., Ellisman, M.H., Tebo, B.M., Criddle, C.S., 2003. Cometabolism of Cr(VI) by Shewanella oneidensis MR-1 produces cell-associated reduced chromium and inhibits growth. Biotechnol. Bioeng. 83 (6), 627–637.
Novak, M., Martinkova, E., Chrastny, V., Stepanova, M., Sebek, O., Andronikov, A., Curik, J., Veselovsky, F., Prechova, E., Houskova, M., Buzek, F., Farkas, J., Komarek, A., 2017. The fate of Cr(VI) in contaminated aquifers 65 years after the first spillage of plating solutions: a δ^{53}Cr study at four Central European sites. Catena 158, 371–380.
Otero, N., Torrentó, C., Soler, A., Menció, A., Mas-Pla, J., 2009. Monitoring groundwater nitrate attenuation in a regional system coupling hydrogeology with multi-isotopic methods: the case of Plana de Vic (Osona, Spain). Agric. Ecosyst. Environ. 133, 103–113.
Palmer, C.D., Wittbrodt, P.R., 1991. Processes affecting the remediation of chromium contaminated sites. Environ. Health Perspect. 92, 25–40.
Palmer, C.D., Puls, R.W., 1994. Natural attenuation of hexavalent chromium in groundwater and soils. In EPA Environmental Assessment Sourcebook. Ann Arbor Press, INC. Chelsea, Michigan, pp. 57–72..
Raddatz, A.L., Johnson, T.M., McLing, T.L., 2011. Cr stable isotopes in Snake River Plain aquifer groundwater: evidence for natural reduction of dissolved Cr(VI). Environ. Sci. Technol. 45 (2), 502–507.
Rai, D., Eary, L.E., Zachara, J.M., 1989. Environmental chemistry of chromium. Sci. Total Environ. 86, 15–23.
Rivett, M.O., Buss, S.R., Morgan, P., Smith, J.W.N., Bemment, C.D., 2008. Nitrate attenuation in groundwater: a review of biogeochemical controlling processes. Water Res. 42, 4215–4232.
Ryabenko, E., Altabet, M.a., Wallace, D.W.R., 2009. Effect of chloride on the chemical conversion of nitrate to nitrous oxide for δ^{15}N analysis. Limnol. Oceanogr. Methods 7, 545–552. https://doi.org/10.4319/lom.2009.7.545.
Salvador, C., 2013. Historia de la Industria Curtidora Argentina. Ed. Dunken 320p.
Scioli C., Burgos G. 2015. Determinación de la Recarga Natural y Antrópica en la cuenca del río Matanza-Riachuelo. Informe Final del Proyecto de Aguas Subterráneas en la Cuenca Matanza Riachuelo. Convenio entre la Autoridad de Cuenca Matanza- Riachuelo y Comisión de Investigaciones Científicas de la Provincia de Buenos Aires, Segunda Etapa. 43 p..
Sikora, E.R., Johnson, T.M., Bullen, T.D., 2008. Microbial mass-dependent fractionation of chromium isotopes. Geochim. Cosmochim. Acta 72 (15), 3631–3641.
Torrentó, C., Urmeneta, J., Otero, N., Soler, A., Viñas, M., Cama, J., 2011. Enhanced denitrification in groundwater and sediments from a nitrate contaminated aquifer after addition of pyrite. Chem. Geol. 287, 90–101.
Trinquier, A., Elliott, T., Ulfbeck, D., Coath, C., Krot, A.N., Bizzarro, M., 2009. Origin of nucleosynthetic isotope heterogeneity in the solar protoplanetary disk. Science 324, 374–376. https://doi.org/10.1126/science.1168221.
Vatsouria, A., Vainshtein, M., Kuschk, P., Wiessner, A., D, Kosolapov, Kaestner, M., 2005. Anaerobic co-reduction of chromate and nitrate by bacterial cultures of Staphylococcus epidermidis L-02. J. Ind. Microbiol. Biotechnol. 32 (9), 409–414.
Viamajala, S., Peyton, B.M., Apel, W.A., Petersen, J.N., 2002. Chromate/nitrite interactions in Shewanella oneidensis MR-695 1: Evidence for multiple hexavalent chromium [Cr(VI)] reduction mechanisms dependent on physiological growth conditions. Biotechnol. Bioeng. 78 (7), 770–778.
Vidal-Gavilan, G., Folch, A., Otero, N., Solanas, A.M., Soler, A., 2013. Isotope characterization of an in situ biodenitrification pilot-test in a fractured aquifer. Appl. Geochem. 32, 153–163.
Vitòria, L., Otero, N., Canals, A., Soler, A., 2004. Fertilizer characterization: isotopic data (N, S, O, C and Sr). Environ. Sci. Technol. 38, 3254–3262.
Vives, L., Scioli, C., Mancino, C., Martínez, S., 2013. Modelación del flujo subterráneo en la cuenca Matanza Riachuelo, Provincia de Buenos Aires. 3. Modelo numérico de flujo. In: González, N., Kruse, E., Trovatto, M., Laurencena, P. (Eds.), Temas actuales de la hidrología subterránea. Editorial EDULP, La Plata, pp. 101–108.
Wanner, C., Eggenberger, U., Kurz, D., Zink, S., Mäder, U., 2012a. A chromate-contaminated site in southern Switzerland–Part 1: Site characterization and the use of Cr isotopes to delineate fate and transport. Appl. Geochem. 27 (3), 644–654.
Wanner, C., Zink, S., Eggenberger, U., Mäder, U., 2012b. Assessing the Cr (VI) reduction efficiency of a permeable reactive barrier using Cr isotope measurements and 2D reactive transport modeling. J. Contam. Hydrol. 131, 54–63.
Wilkin, R.T., Su, C., Ford, R.G., Paul, C.J., 2005. Chromium-removal processes during groundwater remediation by a zerovalent iron permeable reactive barrier. Environ. Sci. Technol. 39 (12), 4599–4605.
Wunderlich, A., Meckenstock, R., Einsiedl, F., 2012. Effect of different carbon substrates on nitrate stable isotope fractionation during microbial denitrification. Environ. Sci. Technol. 46, 4861–4868. https://doi.org/10.1021/es204075b.
Wunderlich, A., Meckenstock, R.U., Einsiedl, F., 2013. A mixture of nitrite-oxidizing and denitrifying microorganisms affects the δ^{18}O of dissolved nitrate during anaerobic microbial denitrification depending on the δ^{18}O of ambient water. Geochim. Cosmochim. Acta 119, 31–45. https://doi.org/10.1016/j.gca.2013.05.028.
Zabala, M.E., Manzano, M., Vives, L., 2016. Groundwater chemical baseline values to assess the recovery plan in the Matanza-Riachuelo River basin Argentina. Sci. Total Environ. 541, 1516–1530.
Zink, S., Schoenberg, R., Staubwasser, M., 2010. Isotopic fractionation and reaction kinetics between Cr(III) and Cr(VI) in aqueous media. Geochim. Cosmochim. Acta 74, 5729–5745.